

IN SILICO DYNAMIC OPTIMISATION STUDIES
FOR
BATCH/FED-BATCH MAMMALIAN CELL SUSPENSION
CULTURES PRODUCING BIOPHARMACEUTICALS

By
Ming-Chi Lam

SUBMITTED IN PARTIAL FULFILLMENT OF THE
REQUIREMENTS FOR THE DEGREE OF
DOCTOR OF PHILOSOPHY
AT
IMPERIAL COLLEGE LONDON
DEPARTMENT OF CHEMICAL ENGINEERING

© 2008

To my parents and sister: Man-kuk, Cheung-yin, and Lilian

Abstract

Mammalian cell cultures are valuable for synthesis of therapeutic proteins and antibodies. They are commonly cultivated in bioindustry in form of large-scale suspension fed-batch cultures. The structure and regulatory responses of mammalian cells are complex, making it challenging to model them for practical process optimisation. The adjustable degrees of freedom in the cell cultures can be continuous variables as well as binary-type variables. The binary-type variables may be irreversible in cases such as cell-cycle arrest. The main aim of this study was to develop a general model for mammalian cell cultures using extracellular variables and capturing major changes in cellular responses between batch and fed-batch cultures. The model development started with a simple model for a hybridoma cell culture using first-principle equations. The growth kinetics was only linked to glucose and glutamine and the cell population was divided into three cell-cycle phases to study the phenomenon of cell-cycle arrest. But there were certain deficiencies in predicting growth rates in the death phase in fed-batch cultures although it was successful to simultaneously optimise a combination of continuous and binary-irreversible degrees of freedom. Thus, the growth kinetics was further related to amino acids concentration and cellular responses to high versus low concentration of glutamine and glucose based on a Chinese hamster ovary cell-line where amino acids data were available. The model contained 192 parameters with 26 measured cell culture variables. Most of the sensitive parameters were able to be identified using the Sobol' method of Global Sensitivity Analysis. The model could capture the main trends of key variables and be used to search for the optimal working range of the controllable variables. But uncertainties in the sensitive model parameters caused non-negligible variations in the model-based optimisation results. It is recommended to couple such off-line optimisation with on-line measurements of a few major variables to tackle the real-time uncertain nature of the complex cell culture system.

Acknowledgment

During the last three and a half years I was glad to be able to work in a field that I enjoyed and be part of a research team in which most members were eager and devoted. There had been many people whom I came across and received much influence from. I would like to thank them all here as much as I can because without them I might not have reached this far. First of all, I highly appreciate my supervisors Dr. Mantalaris and Prof. Pistikopoulos who gave me chances to be challenged and to develop a strong sense of responsibility, confidence as well as enthusiasm towards my research. They were often supportive towards what had to be done. My research was funded by the Dorothy Hodgkin Postgraduate Awards from the Research Council UK (Hutchinson-Whampoa-BBSRC). It provided me with an opportunity to fully focus on my work. Amongst all lab-mates, I need to thank Dr. Ying-Swan Ho who taught me ELISA analysis and cell culture skills; Dr. Mayasari Lim as I learned much equipment maintenance from her; and Dr. Siti Ismail who helped me understand the complex nature of different types of mammalian cells. I was working under Dr. Cleo Kontoravdi at the beginning of my research and she provided me the low-serum suspension CRL-1606 hybridoma cells for experiments. I worked with an MSc student Kansuporn Sriyudthsak in my second year and she had contributed to the early stage of the cell-cycle model. Dr. Michalis Koutinas had given many insightful comments for my papers and, as the first bio-system modelling post-doc of my group, had given me much guidance upon project administration matters. Also, I need to thank Dr. Sergei Kucherenco for providing the C++/gPROMS codes for global sensitivity analysis.

Lastly, I must thank Dr. Danny Wong (BTI-A*Star, Singapore) for the CHO cell data and Dr. Yih Yean Lee (BTI-A*Star) for advices on the amino acid interconversions. My thanks also go to everyone in the lab/CPSE who had put up with me for so long.

Braunschweig, Germany
September 25, 2008.

Carolyn Ming-Chi Lam

Table of Contents

1 Introduction and Objectives	1
1.1 Mammalian Cell Cultures in Bioindustry	1
1.2 Current Limitations in Cell Culture Simulations	2
1.3 Thesis Aim and Objectives	4
1.4 Chapters Outline	5
2 Background and Literature Review	6
2.1 Background	6
2.1.1 Structure of the Mammalian Cell	6
2.1.2 Nutritional Requirement of Mammalian Cells	8
2.1.3 Cell-Cycle	9
2.1.4 Apoptosis	10
2.1.5 Antibodies & Recombinant Proteins	11
2.2 Literature Review	13
2.2.1 Cell Hosts and Bioreactors for Synthesis of Biopharmaceuticals	13
2.2.2 Modelling Mammalian, Yeast, and Microbial Cell Cultures	15
2.2.2.1 Modelling Bacterial and Yeast Cells	15
2.2.2.1.1 Genetic Network Inference.	17
2.2.2.1.2 Metabolic Modelling of Bacterial/Yeast Cells.	23
2.2.2.1.3 Mathematical Classification of Cell Culture Models	29
2.2.2.1.4 <i>In Silico</i> Cells.	31
2.2.2.2 Mammalian Cell Culture Modelling	32
2.2.2.2.1 Monod-Type Kinetics	32
2.2.2.2.2 Single-Cell Models.	34
2.2.2.2.3 Population Balance Models	35
2.2.2.2.4 Multiple Steady-State Models	36
2.2.2.2.5 Other Types of Mammalian Cell Culture Models	37
2.2.3 Applications of Model-Based Optimisation in Cell Cultures & Bioindustrial Processes	38
2.2.4 The Dynamic Nature of Biological Cell Cultures.	40

3 Hybridoma Culture Cell-Cycle Modelling & Optimisation	47
3.1 Cell-Cycle & Productivity Modelling	48
3.1.1 Relationship between Cell-Cycle & Productivity	48
3.1.2 Cell-Cycle Modelling	49
3.2 Development of Cell-Cycle Model for Hybridoma CRL-1606	51
3.2.1 Model Structure	51
3.2.1.1 Development of Model Equations.	51
3.2.1.2 Cell-Cycle Arrest Simulation	55
3.2.2 Materials and Methods	56
3.2.2.1 Batch and Fed-batch Cultures.	56
3.2.2.2 Cell Culture Analyses.	56
3.2.2.3 Parameter Estimation	58
3.2.3 Productivity Optimisation.	59
3.2.3.1 Model Transformation for Optimisation	59
3.2.4 Results and Discussion	62
3.2.4.1 Deviations in the Original Model	62
3.2.4.2 Results of the Adjusted Model	70
3.2.4.2.1 Growth and Cell-Cycle Distribution.	70
3.2.4.2.2 Metabolism.	72
3.2.4.2.3 Antibody Productivity	73
3.2.4.2.4 MIDO Optimisation	84
3.2.5 Conclusions of the Cell-Cycle Model.	87
3.2.6 Notations for the Cell-Cycle Model of Hybridoma Culture.	88
4 Model Development for CHO-IFNγ Cell Culture Including Amino Acids & Cellular Regulations	90
4.1 A Simple Amino Acid Model for CHO-IFN γ Culture	91
4.1.1 Cell-Line & Experiment Setup	91
4.1.2 Model Development.	92
4.1.2.1 Essential Amino Acids for Mammalian Cell Cultures	92
4.1.2.2 Structure of Model Equations.	94
4.1.3 Model Parameter Estimation	102
4.1.4 Parameter Sensitivity Analysis	112
4.1.4.1 Sensitivity Analysis Methods & the Method of Sobol'	112
4.1.4.2 GSA for the Simple Amino Acid CHO-IFN γ Model	116
4.1.5 Conclusions of the Simple Amino Acid Model	119
4.1.6 Notations for the Simple CHO-IFN γ Amino Acid Model	120

4.2	A CHO-IFN γ Model including Amino Acids & Cellular Regulations	123
4.2.1	Development of Model Equations.	123
4.2.1.1	Alterations in Cell Culture Dynamics	123
4.2.1.2	Growth/Death Rate & Cell Lysis	128
4.2.1.3	IFN γ Production	135
4.2.1.4	Consumption of Nutrients	136
4.2.1.5	Metabolic Byproducts	147
4.2.2	Model Equations Summary	151
4.2.3	Notations for the Complex CHO-IFN γ Model with Amino Acids	155
5	Parameter Estimation for the Complex CHO-IFNγ Model	163
5.1	Parameter Estimation Strategy.	163
5.1.1	Framework of Parameter Estimation for Highly Underspecified Model . . .	164
5.1.1.1	Response Factor Parameters.	165
5.1.1.2	Engineering, Stoichiometric, and Literature-Based Parameters. . . .	166
5.1.1.3	Directly Measurable Parameter	167
5.1.1.4	Isolation of Parameters	168
5.1.1.5	Regression of the Remaining Parameters	172
5.1.1.6	Identification of Sensitive Parameters via GSA.	172
5.1.1.7	Parameter Values for the Complex CHO-IFN γ Model	187
5.3	R-Square Analysis of Model Performance	192
5.3.1	Analysis of Experiment Data	192
5.3.2	Model Performance	194
6	Optimisation of the Nonlinear Complex CHO-IFNγ Model with Secondary-Binary Variables	246
6.1	Dynamic Optimisation Methods	246
6.1.1	Common Approaches for Continuous Dynamic Optimisation.	247
6.1.2	Dynamic Optimisation with/without Integer Variables in <i>gPROMS</i>	249
6.2	Model-Based Optimisation of CHO-IFN γ Culture	252
6.2.1	Formulation of the Optimisation Problem	252
6.2.2	Dynamic Optimisation Results and Discussion	257
6.3	Evaluation of Effects of Parameter Uncertainty	264
6.3.1	Numerical Uncertainty Analysis Using Random Sampling	264
6.3.2	Statistical Results	268

7 Conclusions & Future Work	277
7.1 Overall Conclusions	277
7.2 Recommended Future Work	280
Bibliography	282
Appendices	313
1 ELISA Protocol for Hybridoma CRL-1606 Antibody Analysis	313
2 Protocol for Cell-Cycle Analysis	315
3 Lineage Relationship between the Animal Sources of CHO and Hybridoma Cells	317
4 Molecular Structure of the 20 Amino Acids Modelled in CHO.	319
5 Calculation of Glutamine Degradation Rate, Maximum Specific Growth Rates, and Minimum Specific Death Rate.	321
6 Estimation of Measurement Error for Amino Acids & Identification of Outlying Initial Amino Acid Concentrations Using Fed-Batch Culture Simulation with Zero Growth Rate	324

List of Figures

1.1	Major steps involved in production of biopharmaceuticals using mammalian cell host.	2
2.1	A eukaryotic cell showing major typical structures. (Source: Bergin 2008)	6
2.2	Illustration of the major phases in mammalian cell-cycle	9
2.3	An overview of cellular pathways regulating apoptosis (Rowe and Chuang, 2004)	10
2.4	Schematic diagram for different types of models of cell cultures	29
2.5	Data of global-scale gene response of a yeast cell culture exposed to low, medium, and high concentration of glucose (Yin et al., 2003)	40
2.6	Simplified glucose-response pathways in yeast (Geladé et al., 2003)	41
2.7	Level of <i>HXT</i> gene expression for different hexose transporters in yeast at different glucose concentrations (Ozcan and Johnston 1995)	42
3.1	Illustration of the major phases in mammalian cell-cycle (same as Figure 2.2)	49
3.2	Schematic diagram of the proposed mixed-integer dynamic simulation and optimisation framework.	61
3.3	Viable cell concentration in batch and test fed-batch hybridoma cell cultures. Symbols represent experiment data and lines represent model simulation	63
3.4	Cell-cycle distribution in batch hybridoma cell cultures. Symbols represent experiment data and lines represent model simulation	63
3.5	Cell-cycle distribution in test fed-batch hybridoma cell culture. Symbols represent experiment data and lines represent model simulation	64
3.6	Monoclonal antibody (MAb) concentration in batch and test fed-batch hybridoma cell cultures. Symbols represent experiment data and lines represent model simulation.	65
3.7	Glucose and lactate concentration in batch hybridoma cell cultures. Symbols represent experiment data and lines represent model simulation.	65
3.8	Glutamine and ammonium concentration in batch hybridoma cell cultures. Symbols represent experiment data and lines represent model simulation.	66
3.9	Glucose and lactate concentration in test fed-batch hybridoma cell culture. Symbols represent experiment data and lines represent model simulation.	66

3.10 Glutamine and ammonium concentration in **test fed-batch** hybridoma cell culture.
 Symbols represent experiment data and lines represent model simulation. 67

3.11 Viable cell concentration in **optimised arrested fed-batch** hybridoma cell culture
 showing 3 different cell-cycle-arrest time (t_a). Symbols represent experiment data and
 lines represent model simulation. 67

3.12 Monoclonal antibody (MAb) concentration in **optimised arrested fed-batch** hybridoma
 cell culture showing three different cell-cycle-arrest time (t_a). Symbols represent
 experiment data and lines represent model simulation. 68

3.13 Ammonium concentration in **batch, test fed-batch, and optimised arrested fed-batch**
 hybridoma cell cultures. 68

3.14 Viable and total cell concentration in **batch** and **test fed-batch** hybridoma cell cultures
 with simulation from the *adjusted model*. 74

3.15 Monoclonal antibody (MAb) concentration in **batch** and **test fed-batch** hybridoma cell
 cultures with simulation from the *adjusted model*. 75

3.16 Specific monoclonal antibody productivity (Q_{MAb}) in **batch** and **test fed-batch**
 hybridoma cell cultures with simulation from the *adjusted model*. 75

3.17 Cell-cycle distribution in **batch** hybridoma cell cultures with simulation from the
adjusted model. 76

3.18 Cell-cycle distribution in **test fed-batch** hybridoma cell culture with simulation from
 the *adjusted model*. 77

3.19 Total cell concentration in batch and test fed-batch hybridoma cell cultures using
 simulation from the old model. There was overprediction in the test fed-batch culture
 although the cell-cycle simulation in figure 3.4. 77

3.20 Cell-cycle distribution in **optimised arrested fed-batch** hybridoma cell with simulation
 from the *adjusted model*. Three different cell-cycle-arrest time (t_a) are illustrated . . . 78

3.21 Viable and total cell concentration in **optimised arrested fed-batch** hybridoma cell
 cultures with simulation from the *adjusted model*. Three different cell-cycle-arrest
 time (t_a) are illustrated 79

3.22 Monoclonal antibody (MAb) concentration in **optimised arrested fed-batch** hybridoma
 cell cultures with simulation from the *adjusted model*. Three different cell-cycle-arrest
 time (t_a) are illustrated 79

3.23 Glucose and lactate concentration in **batch** hybridoma cell cultures with simulation from
 the *adjusted model*. 80

3.24	Glucose and lactate concentration in test fed-batch hybridoma cell culture with simulation from the <i>adjusted model</i>	80
3.25	Glucose concentration in optimised arrested fed-batch hybridoma cell cultures with simulation from the <i>adjusted model</i> . Three different cell-cycle-arrest time (t_a) are illustrated.	81
3.26	Lactate concentration in optimised arrested fed-batch hybridoma cell cultures with simulation from the <i>adjusted model</i> . Three different cell-cycle-arrest time (t_a) are illustrated.	81
3.27	Glutamine and ammonium concentration in batch hybridoma cell cultures with simulation from the <i>adjusted model</i>	82
3.28	Glutamine and ammonium concentration in test fed-batch hybridoma cell cultures with simulation from the <i>adjusted model</i>	82
3.29	Glutamine concentration in optimised arrested fed-batch hybridoma cell cultures with simulation from the <i>adjusted model</i> . Three different cell-cycle-arrest time (t_a) are illustrated.	83
3.30	Ammonium concentration in optimised arrested fed-batch hybridoma cell cultures with simulation from the <i>adjusted model</i> . Three different cell-cycle-arrest time (t_a) are illustrated.	83
3.31	Optimisation results for nutrient supplementation profile (top), $F_{in}(t)$, and cell-cycle arrest time indicated by y_2 (bottom) switching from 0 to 1	85
4.1	Simulations of the simple amino acid CHO-IFN γ model for batch culture and comparison with the corresponding experiment data.	105
4.2	Simulations of the simple amino acid CHO-IFN γ model for fed-batch culture with glutamine set-point at 0.1mM using parameter values from batch culture versus adjusted new parameter values. Circles represent experiment data	106
4.3	Simulations of the simple amino acid CHO-IFN γ model for fed-batch culture with glutamine set-point at 0.3mM (1st experiment) using parameter values from batch culture versus adjusted new parameter values. Circles represent experiment data.	107
4.4	Simulations of the simple amino acid CHO-IFN γ model for fed-batch culture with glutamine set-point at 0.3mM (2nd experiment) using parameter values from batch culture versus adjusted new parameter values. Circles represent experiment data.	108

4.5 Simulations of the simple amino acid CHO-IFN γ model for fed-batch culture with **glutamine set-point at 0.5mM** using parameter values from batch culture versus adjusted new parameter values. Circles represent experiment data. 109

4.6 Simulations of the simple amino acid CHO-IFN γ model for fed-batch culture with **glutamine set-point at 0.3mM and glucose set-point at 0.7mM** using parameter values from batch culture versus adjusted new parameter values. Circles represent experiment data 110

4.7 Simulations of the simple amino acid CHO-IFN γ model for fed-batch culture with **glutamine set-point at 0.3mM and glucose set-point at 0.35mM** using parameter values from batch culture versus adjusted new parameter values. Circles represent experiment data 111

4.8 The *Snf3/Rgt2* glucose sensing pathway in yeast by Geladé et al. (2003). 124

4.9 Conceptual representation of the response factor. 126

4.10 Amino acid network for the general model of CHO-IFN γ cell culture 140

5.1 Schematic diagram showing the involvement of Global Sensitivity Analysis (GSA) in the estimation of model parameter values. 165

5.2 Specific threonine uptake rate vs. threonine concentration in CHO-IFN γ batch culture. Solid line represents initial estimation of the relationship between the two variables. . 168

5.3 Specific glucose uptake rate versus glucose concentration in CHO-IFN γ batch culture. Solid line represents initial estimation of the relationship between the two variables. . 169

5.4 Specific aspartic acid uptake rate versus aspartic acid concentration in CHO-IFN γ batch culture. Solid line represents initial estimation of the relationship between the two variables. 170

5.5 Specific production rate of IFN γ in CHO-IFN γ batch culture. The shaded region represents the possible range for maximum specific production rate in batch condition. 171

5.6 Intrinsic specific growth rate in CHO-IFN γ batch culture where glucose and glutamine were exhausted at ~68 h. The difference in specific growth rate before and after exhaustion of glucose & glutamine was used for estimation of the max. specific growth rates . . . 171

5.7 Concentration of dead cells in CHO-IFN γ batch culture. The dotted line represents linearization of dead cell concentration up to mid-exponential phase for estimation of minimum death rate. 172

5.8	Normalised sensitivity index values for different parameter groups classified according to biological functions.	179
5.9	Comparison of S and S_{tot} for all sensitive parameter groups from GSA.	180
5.10	Normalised sensitivity index values for individual parameters that are related to the production of $IFN\gamma$	183
5.11	Normalised sensitivity index values for individual parameters that are related to the specific growth rate.	183
5.12	Normalised sensitivity index values for individual parameters that are related to the specific uptake rate of essential amino acids.	184
5.13	Normalised sensitivity index values for individual parameters that are related to the specific uptake rate of glutamine.	184
5.14	Normalised sensitivity index values for individual parameters that are related to the specific death rate.	185
5.15	Normalised sensitivity index values for individual parameters that are related to the specific uptake rate of glucose.	185
5.16	Normalised sensitivity index values for individual parameters that are related to the specific uptake rate of non-essential amino acids.	186
5.17	Normalised sensitivity index values for individual parameters that are related to the formation of byproducts.	186
5.18a-e	Simulation of CHO- $IFN\gamma$ batch culture and comparison with corresponding experiment data.	207
5.19a-e	Simulation of CHO- $IFN\gamma$ fed-batch culture with glutamine set-point at 0.1mM and comparison with corresponding experiment data.	212
5.20a-e	Simulation of CHO- $IFN\gamma$ fed-batch culture with glutamine set-point at 0.3mM (1st experiment) and comparison with corresponding experiment data.	217
5.21a-e	Simulation of CHO- $IFN\gamma$ fed-batch culture with glutamine set-point at 0.3mM (2nd experiment) and comparison with corresponding experiment data.	222
5.22a-e	Simulation of CHO- $IFN\gamma$ fed-batch culture with glutamine set-point at 0.5mM and comparison with corresponding experiment data.	227
5.23a-e	Simulation of CHO- $IFN\gamma$ fed-batch culture with glutamine set-point at 0.3mM and glucose set-point at 0.7mM and comparison with corresponding experiment data.	232

5.24a-e	Simulation of CHO-IFN γ fed-batch culture with glutamine set-point at 0.3mM and glucose set-point at 0.35mM & comparison with corresponding experiment data .	237
5.25i-vii	Time-profiles of the hypothetical response variable for glutamine concentration ($x_{res,Gln}$)	242
5.26i-vii	Time-profiles of the hypothetical response variable for glucose concentration ($x_{res,Glc}$)	244
6.1	IFN γ concentration profile of the optimised fed-batch CHO-IFN γ cell culture.	259
6.2	Viable and total cell concentration profiles of the optimised fed-batch CHO-IFN γ cell culture.	259
6.3	Glutamine concentration profile of the optimised fed-batch CHO-IFN γ cell culture . . .	260
6.4	Glucose concentration profile of the optimised fed-batch CHO-IFN γ cell culture. . . .	260
6.5	$F_{in}(t)$ supplementation profile of the optimised fed-batch CHO-IFN γ cell culture with $\Delta t = 1h$. The stream contained 100mM glutamine, other amino acids, and basic components of the DMEM medium. The height of each pulse in $L h^{-1}$ is equivalent to volume in ml. . .	261
6.6	Glucose supplementation profile of the optimised fed-batch CHO-IFN γ cell culture with $\Delta t = 1h$. The stream contained 40g/L(222mM) glucose. The height of each pulse in $L h^{-1}$ is equivalent to volume in ml.	261
6.7	Ammonium concentration profile of the optimised fed-batch CHO-IFN γ cell culture. . .	262
6.8	Lactate concentration profile of the optimised fed-batch CHO-IFN γ cell culture. . . .	262
6.9	Optimised profiles of the hypothetical response variables for glutamine ($x_{res,Gln}$) and glucose ($x_{res,Glc}$) concentrations	263
6.10	Convergence of the mean value of optimised IFN γ yield against number of parameter sets tested. The lines represent best-fit curves showing the trends of the mean values. . . .	269
6.11	Convergence of the standard deviation of optimised IFN γ yield against number of parameter sets tested. The lines represent best-fit curves showing the trends of the standard deviation.	269
6.12	Distribution of optimised IFN γ yield among 60 different sets of parameter values when the sensitive parameters were varied $\pm 10\%$	270
6.13	Distribution of optimised IFN γ yield among 60 different sets of parameter values when the sensitive parameters were varied $\pm 25\%$	270

6.14	Distribution of optimised IFN γ yield among 60 different sets of parameter values when the sensitive parameters were varied $\pm 50\%$	271
6.15	Mean (black circle) and standard deviation (grey area) of $F_{in}(t)$, $F_{in_glc}(t)$, glutamine, and glucose concentrations among the 60 optimised results of $\pm 10\%$ sensitive parameters .	273
6.16	Mean (black circle) and standard deviation (grey area) of $F_{in}(t)$, $F_{in_glc}(t)$, glutamine, and glucose concentrations among the 60 optimised results of $\pm 25\%$ sensitive parameters .	274
6.17	Mean (black circle) and standard deviation (grey area) of $F_{in}(t)$, $F_{in_glc}(t)$, glutamine, and glucose concentrations among the 60 optimised results of $\pm 50\%$ sensitive parameters .	275
A3.1	Linage relationship between Chinese hamster and mouse which are sources of CHO and hybridoma cells respectively.	317
A5.1	Glutamine concentration data for degradation rate estimation.	320
A5.2	Estimation of glutamine degradation rate in DMEM medium	321
A6.1	Mass balance testing of amino acids data in fed-batch CHO-IFN γ culture with glutamine set-point at 0.1mM	325
A6.2	Mass balance testing of amino acids data in fed-batch CHO-IFN γ culture with glutamine set-point at 0.3mM (1 st experiment)	328
A6.3	Mass balance testing of amino acids data in fed-batch CHO-IFN γ culture with glutamine set-point at 0.3mM (2 nd experiment)	331
A6.4	Mass balance testing of amino acids data in fed-batch CHO-IFN γ culture with glutamine set-point at 0.5mM	334
A6.5	Mass balance testing of amino acids data in fed-batch CHO-IFN γ culture with glutamine set-point at 0.3mM and glucose set-point at 0.7mM	337
A6.6	Mass balance testing of amino acids data in fed-batch CHO-IFN γ culture with glutamine set-point at 0.3mM and glucose set-point at 0.35mM	340

List of Tables

3.1	Degrees of freedom in the simulation of the hybridoma cell culture.	86
3.2	Parameter values for the cell-cycle model of the hybridoma cell culture	86
3.3	Notations for the cell-cycle model of the hybridoma culture.	88
4.1	Comparison of essential versus non-essential amino acids for different mammalian cells reported by Morgan (1958) and Simpson et al. (1998).	93
4.2	Parameter values of the simple amino acid model for batch culture of CHO-IFN γ cells.	102
4.3	Parameter groups for Global Sensitivity Analysis (GSA) of the simple amino acid model for the CHO-IFN γ culture	116
4.4	List of sensitive parameters of the simple amino acid CHO-IFN γ model identified by GSA.	118
4.5	Notations for the simple amino acid model of the CHO-IFN γ culture.	120
4.6	Chemical decomposition of glutamine to ammonia and pyrrolidone carboxylic acid studied at 37°C and pH 6.8 – 7.8 with different media containing foetal bovine serum (Ozturk and Palsson, 1990).	139
4.7	Notation of parameters for the complex CHO-IFN γ model.	155
4.8	Notations for major variables in the complex CHO-IFN γ model	161
4.9	Concentration of glucose, glutamine and other amino acids in the inlet streams.	162
5.1	List of grouped parameters of the complex CHO-IFN γ model for Global Sensitivity Analysis (GSA).	174
5.2	List of sensitive parameters out of 179 parameters analysed with GSA.	181
5.3	List of estimated values of all 192 parameters in the complex CHO-IFN γ model.	187
5.4	List of degrees of freedom in the CHO-IFN γ cell cultures.	191
5.5	Summary of R-square and modified-R-square values for batch and fed-batch CHO-IFN γ cell cultures.	195
6.1	Initial guesses of control profiles of $F_{in}(t)$ and $F_{in_glc}(t)$ used in dynamic optimisation of fed-batch CHO-IFN γ cell culture.	255

6.2	List of parameters that were varied to test the effect of parameter value uncertainty on dynamic optimisation output.	265
6.3	List of fed-batch parameters of which the values were fixed due to insensitivity, inactive (zero value), not affecting growth or productivity, or being at theoretical limit.	266
6.4	12 Initial guesses of control profiles of $F_{in}(t)$ and $F_{in_glc}(t)$ used in evaluation of the effects of uncertainty of sensitive model parameters.	267
6.5	Computational time spent on dynamic optimisation of the original parameter set of the CHO model and evaluation of the effects of uncertainty of sensitive parameters.	267
6.6	Lower and upper ranges of the ratio of standard deviation versus mean values of $F_{in}(t)$, $F_{in_glc}(t)$, $Gln(t)$, and $Glc(t)$	272
A4.1	Amino acid structure of the 20 amino acids	319
A5.1	Calculation of the average glutamine degradation rate in DMEM medium	321
A5.2	Calculation of the average specific growth rate before and after exhaustion of glucose and glutamine in CHO-IFN γ batch culture.	322
A5.3	Calculation of the minimum specific death rate in CHO-IFN γ batch culture	323
A6.1	Estimation of measurement error of glutamine in CHO-IFN γ fed-batch cultures.	324

Chapter 1

— Introduction and Objectives

1.1 Mammalian Cell Cultures in Bioindustry

Mammalian cell cultures take a wide range of forms depending on the cell types and culturing methods. Some examples include adhesive tissue cells grown on 2-dimensional plates or 3-dimensional scaffolds, cells encased in gel-like beads grown in nutrient-rich solution, and suspension individual cells grown in well-mixed stirred-tank reactors. The last method is commonly used in the bio-pharmaceutical industry to produce antibodies and recombinant proteins from mammalian cell hosts on a large scale.

A typical series of processes involved in the development of a new biological drug is shown in Figure 0.1. Cells which have been made to be capable of producing the product of interest (procedure dependent on products) are screened to select high producers. Then the nutrient composition, i.e. media, of the cell culture is optimised to enhance productivity by testing a wide selection of combinations. After that, the cell culture is grown in larger bioreactors and further degrees of freedom, e.g. nutrient supplementation time-profile, reactor operation mode (batch/fed-batch/continuous/perfusion) etc., are decided. Finally, the bioreaction is scaled-up to produce the drug in large quantity.

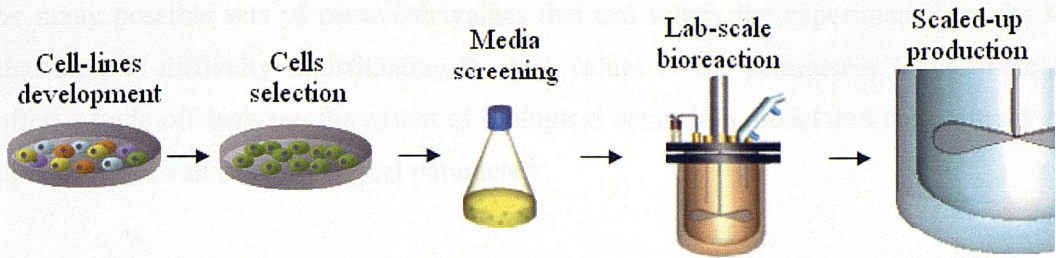


Fig.1.1: Major steps involved in production of biopharmaceuticals using mammalian cell host.

The decisions made for most of the degrees of freedom are often fully dependent on experiment results. For mammalian cell cultures which are expensive and grow much slower than bacteria, heavy experimentation can significantly increase cost and time to market. The overall market of recombinant DNA therapeutics, for example, is projected to grow from US\$41.7 billion in 2006 to US\$52.2 billion in 2010 (Pavlou and Reichert, 2004). With such a valuable market, there is much benefit in terms of profit and efficiency if some of the selection steps can be done more rapidly at a lower cost. The lab-scale bioreaction stage is a suitable candidate for computational simulations since the well-agitated cell culture can be considered homogeneous and no major changes in media composition is involved at this process development stage. However, simulations are rarely used to model the biological dynamics of cell cultures in bioindustry. The main reason is a lack of suitable mathematical models, which is discussed in the next section.

1.2 Current Limitations in Cell Culture Simulations

Many mathematical models have been developed to describe a single biological cell or an entire cell culture. The majority of the models are for bacterial systems due to their simple nutritional demand, ease of growth, and less complex cellular structures. Among those mammalian cell culture models, assumptions of sufficient availability of essential amino acids are often made for model simplification purposes, so the models cannot accurately predict cell culture dynamics when amino acids, which are excluded in most of the models, are exhausted in the media. However, when a mammalian cell model is trying to represent the biological complexity in great detail but the number of model parameters far exceeds the number of practically measurable variables, there will

be many possible sets of parameter values that can satisfy the experimental results so that there is difficulty in estimating the true values of the parameters. Thus, there is often a trade-off between the extent of biological detail in a model and the accuracy of the estimated values of the model parameters.

Although modelling of biological systems has a long history, the development of biological models applicable to real industrial processes is still in its infancy. Current computational involvements in biological processes are in the areas of physical or chemical property analysis, especially during scale-up of bioreactors. There is significant potential for simulations of the biological properties of cell cultures to assist understanding the cellular system and even to optimise it more efficiently. It is hoped that the work from this thesis can provide a small contribution towards achieving such a goal.

1.3 Thesis Aim and Objectives

The aim of this study is to develop an *in silico* modelling platform to simulate and optimise a lab-scale mammalian cell suspension culture producing biological drug. In particular, the fact that some degrees of freedom encountered in mammalian cell cultures are not continuous but are binary-irreversible or switch-like has been taken into account during development of model structures and optimisation strategies. The detailed objectives are as follows:

- (1) To develop a simple first-principle dynamic mammalian (hybridoma cells) suspension culture model which includes cell cycle distribution, and a strategy to optimise two common degrees of freedom: nutrient supplementation time-profile and cell cycle arresting time where the former is continuous and the latter is binary-irreversible.
- (2) To construct a tractable batch and fed-batch mammalian (CHO cells) suspension culture model which includes amino acids essential for cell growth, which has so far been neglected in most mammalian culture models due to the difficulty of amino acids measurement and parameter values estimation. Secondary switch-like variables will be introduced to model an 'alternation' in cell culture behaviours observed between batch and fed-batch cultures.
- (3) To develop a strategy for systematic estimation of model parameter values of a complex non-linear biological model (CHO cells) with large degrees of freedom for parameter values.
- (4) To computationally optimise the supplementation time-profiles of two dominating nutrients, glutamine and glucose, which affect the secondary switch-like variables in the CHO cell suspension culture model developed in order to maximise drug yield. The significance of parameter values uncertainty will also be analysed.

1.4 Chapters Outline

This thesis is divided into seven chapters. Chapter 2 presents certain fundamental biological features related to this study and provides a literature review of the practical concerns in biological drug production and existing mathematical cell culture models. Chapter 3 develops a simple first-principle model for hybridoma cells suspension culture producing monoclonal antibodies (MAbs) and applies a mixed-integer dynamic optimisation (MIDO) algorithm to simultaneously optimise the nutrient supplementation time-profile and cell cycle arresting time of fed-batch cultures. Chapter 4 attempts to expand the first-principle model to include amino acids which significantly affect growth of mammalian cells. Chinese Hamster Ovary (CHO) cells producing interferon-gamma ($\text{IFN}\gamma$) were used to provide experiment data. The CHO cell culture exhibited an alteration in growth pattern when cultured under controlled low concentrations of glutamine and glucose. This behaviour was simulated using two secondary switch-like variables. In Chapter 5, the large number of model parameters of the CHO cells model developed at the end Chapter 4 was estimated using a combination of parameter isolation, parameter estimation using gPROMS (Process Systems Enterprise Ltd., 2008), and Global Sensitivity Analysis (GSA). Optimisation of the supplementation time-profiles of glutamine and glucose to maximise $\text{IFN}\gamma$ yield using this model is presented in Chapter 6 with analysis of the possible effects of uncertainty in sensitive parameters. Finally, overall conclusions and possible future work are discussed in Chapter 7.

Chapter 2

— Background & Literature Review

2.1 Background

This section aims to provide an introduction for mammalian cells that is important for the understanding of some biological concepts in subsequent chapters. The cells involved in this work are only individual suspension cells that are non-adherent to any surface or other cells, thus they do not form clusters. The internal structure of mammalian cells is highly organised and the nutritional requirement is more complex than other simpler organisms such as bacteria. In the following paragraphs, the basic cell structure, growth requirements, cell division process, cell death mechanism, and major types of drug products synthesised by mammalian cells are discussed.

2.1.1 Structure of the Mammalian Cell

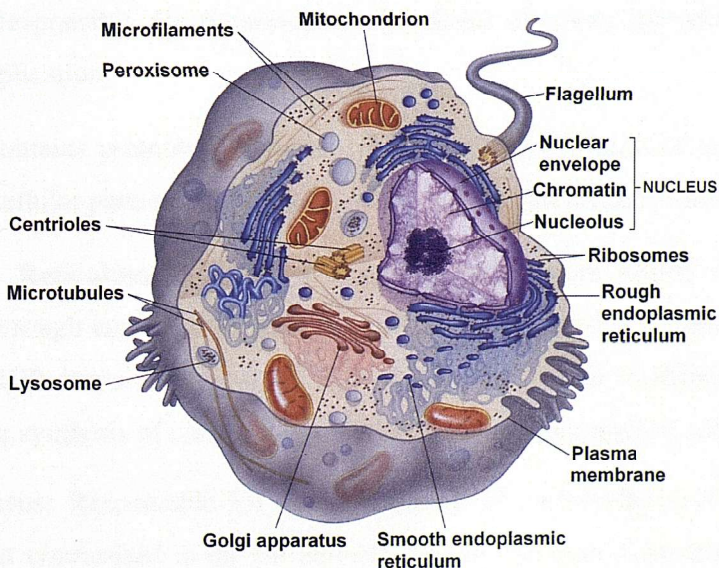


Figure 2.1: A eukaryotic cell showing major typical structures. (Source: Bergin 2008)

Mammalian cells are a type of eukaryotic cells. Eukaryotic cells possess a membrane enclosed nucleus (Bailey and Ollis, 1986). Mammalian cells are one of the most complex forms of eukaryotic cells with highly specialised internal compartments. A general diagram of eukaryotic cell is shown in Figure 2.1. The only main difference between mammalian cells and Figure 2.1 is the absence of flagellum in the former which enables movement of single-cell organisms. The major internal elements in a mammalian cell include the nucleus, mitochondria, peroxisomes, centrioles, lysosomes, endoplasmic reticulum (ER), Golgi apparatus, ribosomes, microfilaments and microtubules, and the plasma membrane. Below is a brief description of each element according to Campbell and Smith (2000) and Alberts et al. (2002):

Nucleus: Contains DNA organized into separate chromosomes which consist of chromatin (DNA-protein complex). The nuclear envelope has nuclear pores for transfer of substances into and out of the nucleus. The nucleolus is the site for processing ribosomal ribonucleic acids (RNAs) and their assembly into ribosomes.

Mitochondrion: Contains a small amount of mitochondrial DNA. The mitochondrion is responsible for production of adenosine triphosphate (ATP). It consists of an outer and inner membrane. The inner membrane is highly folded to increase surface area for exchange of substances. The mitochondrion is also involved in catabolism of fatty acids and controlling calcium level in the cell.

Peroxisome: Contains oxidative enzymes to eliminate hydrogen peroxide produced by fatty acid oxidation and free radicals or to oxidise other toxic molecules.

Centrioles: Responsible for organisation of cellular elements including the nucleus during cell duplication.

Lysosome: Contains proteolytic enzymes for controlled digestion of macromolecules, e.g. obsolete cellular parts and macromolecules taken up from extracellular fluid.

Endoplasmic Reticulum (ER): A network of membranes which can be further classified into rough endoplasmic reticulum (RER) and smooth endoplasmic reticulum (SER). The RER bears ribosomes on the surface for protein synthesis. The SER is responsible for synthesis of complex lipids and control of calcium ion concentration.

Golgi apparatus: Responsible for further addition of carbohydrates to proteins after they have been synthesised in the ER and subsequent transport of proteins to their final destinations.

Ribosome: A large and complex structure containing proteins, RNA, and magnesium ions. It is responsible for synthesis of polypeptides.

Microfilaments and Microtubules: Part of a lattice structure providing structural support to the cell.

Plasma Membrane: Made up of double-layer lipids. It contains various surface receptors and is responsible for selective transport of substances across the cell.

Within the complex cellular structure, a large number of reactions take place to convert nutrients into energy, proteins, enzymes, cell mass etc. and break down or excrete unwanted molecules in order to maintain survival of the cells. In mathematical modelling of mammalian cells, simplification is often necessary to overcome the bottleneck of incomplete biological knowledge and the impossibility to measure all molecules within the system unless only a small part of the cell is considered.

2.1.2 Nutritional Requirement of Mammalian Cells

A typical medium for cultivation of mammalian cells mainly contains glucose, glutamine, other amino acids, salts, and vitamins (Alberts et al., 2002). Penicillin-streptomycin and phenol red are also added to prevent bacterial contamination and indicate pH respectively. Serum is often used to stimulate cell growth but there is a gradual preference to exclude it from the medium because it is chemically undefined, its quality varies depending on its source, and it could be a source of virus contamination (Keay, 1978; Spier 1997; Jayme and Smith, 2000; Birch and Racher, 2006). Mammalian cells have a narrow pH tolerance around about pH7 beyond which the cell viability would be significantly affected. For example, a hybridoma cell-line studied by Miller et al. (1988) had an optimum pH of 7.1 – 7.4. The standard cultivation temperature and air composition is 37°C and 5% CO₂ (Alberts et al., 2002). Many modelling studies have focused on glucose, glutamine, and sometimes other amino acids because they are the major sources of energy and cell mass (Bree and Dhurjati, 1988; Batt and Kompala, 1989; Dalili et al., 1990; Duval et al., 1991; Lourenco da Silva et al., 1996; Jang and Barford, 2000a,b; Simon and Karim, 2002; Provost and Bastin, 2004). Other cell culture variables have also been studied: temperature (Laszlo and Li, 1985; Hahn and Shiu, 1985; Abravaya et al., 1991; Fox et al., 2004), pH (Osman et al.,

2001), osmotic stress (Oh et al., 1993; Wu et al., 2004), and shear stress (Frangos et al., 1988; Kretzmer and Schugerl, 1991).

2.1.3 Cell-Cycle

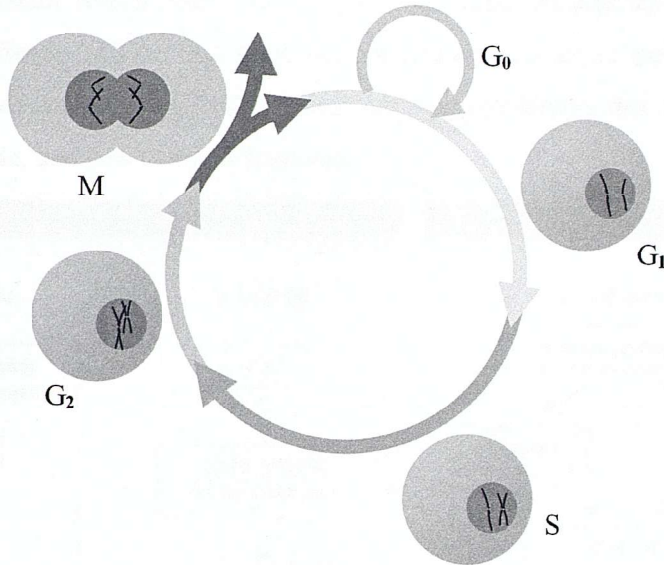


Figure 2.2: Illustration of the major phases in mammalian cell-cycle.

The growth of mammalian cells can be divided into several stages: G_1 , S, G_2 , and M (Alberts et al., 2002). In the G_1 phase, enzymes for DNA replication are being synthesised. When the cell is ready to initiate DNA replication, it enters the S phase where the chromosomes are duplicated. In the G_2 phase, the cell is preparing for cell division and necessary proteins including microtubules are being synthesised. The cell is separated into two daughter cells in the M (mitosis) phase, after which they either enter G_1 phase or a specialised resting state known as G_0 . Cells in the G_0 phase do not participate in cell growth. The cycle contains two restriction points: one at the end of the G_1 phase which decides whether to replicate its DNA, and another one at the end of the G_2 phase which decides whether to initiate mitosis (Pardee, 1974; Campbell and Smith, 2000). An illustration of cell-cycle for mammalian cells is shown in Figure 2.2. Further details about the relationship between cell-cycle and productivity can be found in Chapter 3.

2.1.4 Apoptosis

Cell death in mammalian cell cultures is caused predominantly by a mechanism known as apoptosis or programmed cell death (Moore et al., 1995; Goswami et al., 1999). The definition of apoptosis aims to exclude cell death that results from external agents such as toxins which cause cells to swell and burst by a process called necrosis (Campbell and Smith, 2000). Apoptosis is controlled by a set of pathways shown in Figure 2.3 (Rowe and Chuang, 2004). There are three pathways that regulate cell fate: extrinsic, intrinsic, and cell survival pathways.

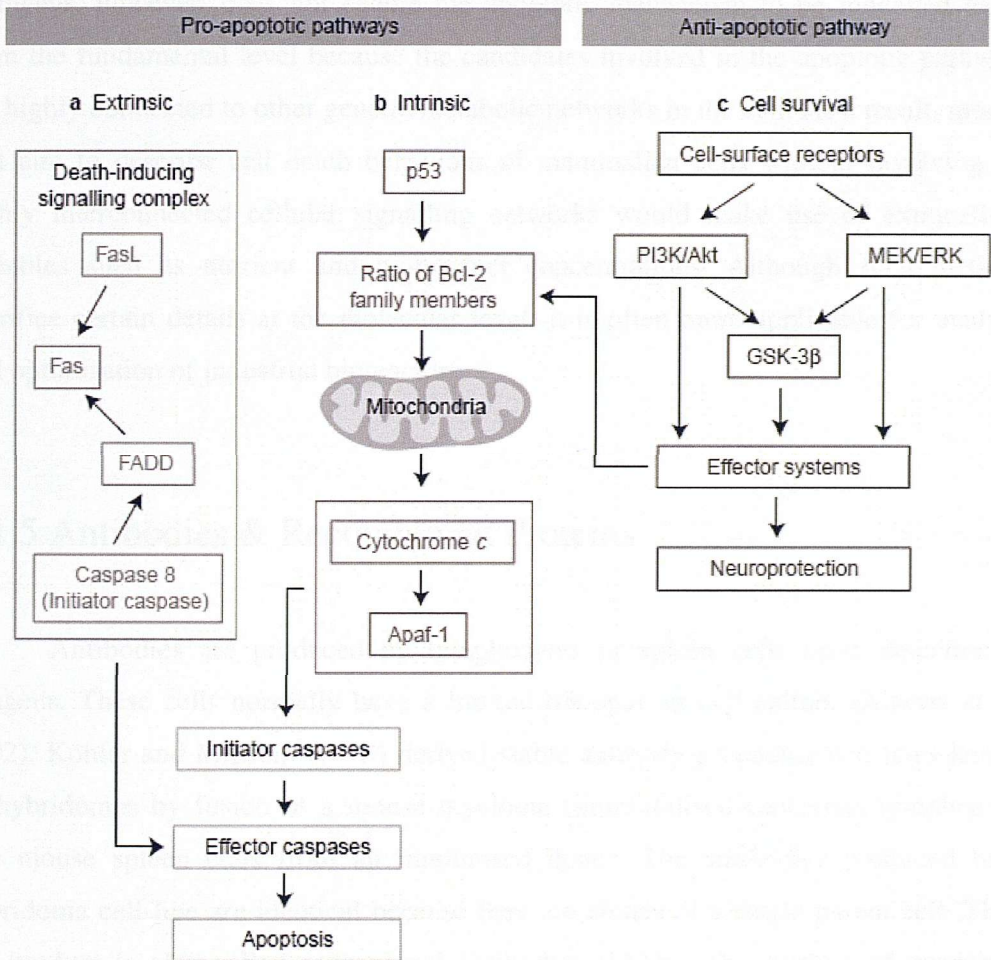


Figure 2.3: An overview of cellular pathways regulating apoptosis (Rowe and Chuang, 2004).

The extrinsic pathway is induced when death receptors on the cell surface, e.g. Fas, are triggered. Binding of a ligand (*FasL*) to Fas results in binding of the cytosolic death domain of the receptor to an adaptor protein (*FADD*) containing a death domain which subsequently activates the effector caspases for apoptosis. The intrinsic pathway

senses the integrity of the mitochondria, which is maintained by the *Bcl-2* family containing pro-apoptotic and anti-apoptotic members. The ratio of the pro- and anti-apoptotic *Bcl-2* family members is regulated by molecules including *p53*. If the ratio of the *Bcl-2* family members tips towards the pro-apoptotic side, the mitochondria's membrane integrity decreases and the pro-apoptotic factors, such as cytochrome *c*, are released which eventually initiate apoptosis. The cell-survival pathway starts with the activation of cell-surface receptors such as *TrkB* by growth factors. The anti-apoptotic pathways including *PI3K/Akt* and *MEK/ERK* are then activated to suppress the intrinsic pathway (Rowe and Chuang, 2004). Such detailed understanding of the apoptotic pathways, however, does not enable the apoptotic mechanism to be modelled easily from the fundamental level because the candidates involved in the apoptotic pathways are highly connected to other genetic/metabolic networks in the cell. As a result, models that aim to describe cell death behaviour of mammalian cells without involving the highly interconnected cellular signalling networks would make use of extracellular variables such as nutrient and by-product concentrations. Although such methods sacrifice certain details at the molecular level, it is often more applicable for analysis and optimisation of industrial bioreactors.

2.1.5 Antibodies & Recombinant Proteins

Antibodies are produced by lymphocytes or spleen cells upon detection of antigens. These cells normally have a limited life-span in cell culture (Alberts et al., 2002). Köhler and Milstein (1975) derived stable antibody-producing cell-lines known as hybridomas by fusion of a mouse myeloma (immortalised cancerous lymphocyte) and mouse spleen cells from an immunised donor. The antibodies produced by a hybridoma cell-line are identical because they are clones of a single parent cell. Thus, the product is also called monoclonal antibodies (MAb). The method of producing hybridoma cell-lines has been widely used for synthesis of antibodies (James and Bell, 1987). Alternatively, antibodies can also be produced using recombinant technology described below (Birch and Racher, 2006).

Proteins with therapeutic applications can be expressed in mammalian cells by transfecting the cells with vectors, such as non-pathogenic viruses and lipid reagents (Makrides, 2003; Masson et al., 2003), that contain the DNA sequence of the

therapeutic proteins (Andersen and Krummen, 2002; Wurm, 2004). An example from this study is interferon- γ (IFN γ) which is normally produced by T-cells or lymphocytes in humans. Its gene sequence is inserted (or 'recombined') into the genes of Chinese Hamster Ovary (CHO) cells, one of the most widely used mammalian cell-lines for therapeutic protein production (Werner et al., 1992; Chu and Robinson, 2001; Kaufmann, H. and Fussenegger, 2003), and this gives rise to the name 'recombinant protein'. Recombinant proteins are produced in mammalian cells in the same way as other cellular proteins except that they are not needed for normal functions of the cells and would be secreted to the extra-cellular medium (Campbell and Smith, 2000).

Both monoclonal antibodies and recombinant therapeutic proteins are valuable drug products. Monoclonal antibodies have a global market that is predicted to increase from US\$5.4 billion in 2002 to US\$16.7 billion in 2008 (Reichert and Pavlou, 2004; Pavlou and Belsey, 2005). Similarly, recombinant DNA therapeutics has a projected increase in market value from US\$41.7 billion in 2006 to US\$52.2 billion in 2010 (Pavlou and Reichert, 2004). Thus, there is a high incentive among the bioindustry and academic research groups to improve production efficiency and reduce costs. In this research, it was intended to enhance the understanding of cell culture dynamics and efficiency of selection of nutrient supplementation time-profiles and/or cell-cycle arrest time using mathematical modelling. A review of cell culture processes and modelling approaches is presented in next chapter followed by discussion of model developments for a hybridoma cell-line producing monoclonal antibodies and a Chinese Hamster Ovary (CHO) cell-line producing IFN γ .

2.2 Literature Review

2.2.1 Cell Hosts & Bioreactors for Synthesis of Biopharmaceuticals

Possible Hosts for Biopharmaceuticals

Biological drugs can be produced by mammalian cell cultures as well as bacteria, filamentous fungi, yeast, insect cells, transgenic plants, and transgenic animals (Verma et al., 1998; Makrides and Prentice, 2003). The major advantages of mammalian cell cultures over most other hosts are proper folding of proteins, high quality glycosylation (an enzymatic process linking saccharides to proteins/lipids to give characteristic biochemical and biophysical properties/functions), and extensive post-translational modifications (Electricwala, 1992; Verma et al., 1998; Makrides and Prentice, 2003; Stoger et al., 2003; Wurm, 2004).

Bacteria and filamentous fungi grow much faster with lower costs than mammalian cells but they lack certain glycosylation or post-translational machinery and the protein folding are often incorrect (Marino, 1989; Verma et al., 1998; Joosten et al., 2003; Ma et al., 2003). Yeast has a more advanced protein folding mechanism than bacteria and, apart from sharing the low cost attractiveness as bacteria, is capable of glycosylation of proteins. But its glycosylation is not the same as those found in mammalian cells (Kukuruzinska et al., 1987). Insect cells are able to produce functionally active drug products (zu Putlitz et al., 1990; Maeda, 1989). However, insect cells are incapable of carrying out complex forms of glycosylation as in mammalian cells (Kuroda et al., 1986; Marino, 1989; Verma et al., 1998; Ma et al., 2003). Transgenic plants have advantages in terms of low production costs, high scale-up capacity, good product quality, and low risk of virus contamination (Ma et al., 2003; Stoger et al., 2003). But the glycosylation structures provided by transgenic plants have minor differences when compared with mammalian cells and this could potentially change the activity of the product (Ma et al., 2003). Transgenic animals are the most similar hosts to mammalian cell cultures. The animals involved are mainly mouse/livestock and there is a longer production timescale than mammalian cell cultures due to the slow animal growth (Echelard and Meade, 2003; Ma et al., 2003). But the use of transgenic animals is still a relatively new technology. Until now,

mammalian cell cultures remain a popular and well established method in the bioindustry (Chu and Robinson, 2001; Joosten et al., 2003; Wurm, 2004).

Fed-batch Processes versus Batch & Perfusion

There are many possible methods to run suspension cell cultures. Some basic modes include batch, fed-batch, continuous, and perfusion stirred tank bioreactors. Other more complex bioreactors such as dialysis membrane, hollow fibre, electrophoretic bioreactor etc. had also been used for cell culture studies (Portner et al., 1994; Chang et al., 1995; Mancuso et al., 1998; Schwabe et al., 1999; Frahm et al., 2003). Perfusion and hollow fibre bioreactors are able to achieve higher cell yield and product concentration than batch/ fed-batch cultures (Stoll et al., 1995; Yang et al., 2000; Kretzmer, 2002). Continuous culture is similar to perfusion except the cells in the outlet stream are not retained in the continuous mode. Thus, continuous culture is not popular for mass production of therapeutic proteins/ antibodies due to significant cell loss. Perfusion is sometimes referred to as a continuous process based on the continuous inlet and outlet streams which should not be confused with the continuous operation mode discussed above. Dialysis membrane and electrophoretic bioreactor allow selective removal of metabolic byproducts which are toxic to cell cultures so the productive time can be extended (Chang et al., 1995; Frahm et al., 2003).

Despite the fact that batch and fed-batch cell cultures yield a relatively lower cell density and product concentration, there are several reasons making them more favourable in therapeutics production. Contamination, process consistency, length of process validation, and reactor down time are key factors affecting the quality of product, production costs, and time to market (Werner et al., 1992; Xie and Wang, 1997). The most frequent sources of contamination are the media supply and sampling system (Werner et al., 1992). Thus, the contamination risk is relatively lowest in batch cultures and, due to simplicity in the process control, there is high consistency in the process output and flexibility for implementation in multipurpose facilities (Xie and Wang, 1997; Kretzmer, 2002). Fed-batch cultures share most of the advantages of batch cultures plus higher cell and product yields because of nutrient supplementation so they are more attractive when compared to batch cultures (Bibila and Robinson 1995). As all bioprocesses must have their identity, purity, safety, genetic stability, and productivity

characterized and validated within and beyond the fixed production time scale, perfusion bioreactors are more expensive and time consuming to be licensed for production (Werner et al., 1992; Kretzmer, 2002). In terms of reactor down time for maintenance and decontamination, perfusion system and other more complex bioreactors require much longer period than batch/ fed-batch bioreactors. Together with the concern that transformed cell-lines might show genetic instability in long-term cultures due to possible variations in their chromosomes (Werner et al., 1992), batch and fed-batch processes are the most widely used modes in the bioindustry (Bibila and Robinson 1995; Xie and Wang, 1997; Birch and Racher, 2006; Whitford 2006). As fed-batch cultures enjoy higher yields than batch cultures, the former is an important and interesting area for process optimisation studies.

2.2.2 Modelling Mammalian, Yeast, and Microbial Cell Cultures

2.2.2.1 Modelling Bacterial and Yeast Cells

Due to the relative simplicity of the structure of bacterial cells among all other living organisms, bacteria were those early candidates to be modelled mathematically. Models that focused on the genetic regulations of bacteria commonly assumed the rate-limiting step was at the transcriptional level where activated genes were copied into mRNAs (McAdams and Arkin, 1998) although there were suggestions that the translational level, where the mRNA ‘templates’ were used to synthesize proteins, or mRNA/ protein degradation had a stronger regulation over the activity of the gene products (Neidhardt et al., 1990; Moat et al., 2002). In order to build a genetic model, it is necessary to know much detail about the connectivity in the gene network. The activities of gene had been modelled using Boolean (on/off) algebra. For example, Kauffman (1974) studied the lactose (*lac*) operator of *Escherichia coli* (*E. coli*) and examined the response of the operator to saturating/minimum concentrations of its controlling molecular variables. Since a repressor is bound to the operator only when another substance, allolactose, is absent, ‘0’ was used for the unbounded state and ‘1’ for the bounded state of the operator.

Lee and Bailey (1984a, 1984b) described quantitatively the regulation of expression of the *lac* operon and *lac* promoter-operator function in *E. coli*. The model

was genetically structured such that a nucleotide sequence change affecting transcription initiation at the *lac* promoter-operator would influence one or few corresponding model parameters. Such model incorporated a translational efficiency factor to account for translational control. A different way of genetic modelling was described by Collado-Vides (1989) that a ‘language’ known as transformational-grammar approach was used to describe the genome organization and regulation of gene expression. But this approach did not gain as much popularity as other mathematical methods because it was not directly usable for prediction purposes.

Genetic regulation had also been modelled as a circuit. The most typical example is bacterial phage- λ which is a virus that infects bacteria which was modelled using a combination of differential algebraic equations and on/off logic gates (Reinitz and Vaisnys, 1990; Chung and Stephanopoulos, 1996; McAdams and Shapiro, 1995). Genetic circuit can be combined with Boolean logic to form a Boolean threshold logic paradigm (Thieffry and Thomas, 1995; Thomas, 1973; Thomas, 1991; Thomas et al., 1995; Prokudina et al., 1991; Tchuraev, 1991). The modelling equation has a general form as:

$$\dot{x}_i = k_i F_i(x_1, x_2, \dots, x_n) - k_{di} x_i \quad (2.1)$$

where x_i is the concentration of the i -th protein species, k_i is the rate of protein production when the gene type i is ‘on’, and k_{di} is the degradation rate constant for protein type i . F_i represent step-functions, assumed to equal ‘0’ or ‘1’ depending on the concentration of x_i relative to threshold values determined by the kinetics of the promoter sites. More details were discussed by McAdams and Arkin (1998).

With the accumulation of knowledge about the interactions between nutrient concentrations and genetic expressions for bacteria, genetic models of bacterial metabolisms could be formulated with greater details. Kremling and coworkers (Kremling et al., 2000; Kremling and Gilles, 2001a; Kremling et al., 2001b) proposed a decomposition of complex metabolic networks into manageable smaller functional units based on three criteria: (1) common physiological task; (2) common genetic units; (3) and common signal transduction network. In each functional unit, metabolic pathways were divided into a metabolic and a genetic regulatory sub-network. The regulatory network described the local signal transduction in the unit and the biosynthesis of the specific enzymes, while the metabolic network described the metabolic flux affected by

enzyme-catalyzed reactions. Such approach has been applied to *E. coli*'s glucose and lactose metabolism (Kremling et al., 2001b), sucrose and glycerol metabolism (Wang et al., 2001), and tryptophan biosynthesis (Schmid et al., 2004). Modelling of transcriptional and translational regulations often make use of algebraic and ordinary differential equations (Axe and Bailey, 1994; Laffend and Shuler, 1994a) although it is also possible to use stochastic simulation to capture the randomness in gene networks. Common computational methods for modelling genetic regulatory systems have been reviewed in details from the use of binary logic to differential algebraic equations and stochastic kinetics (McAdams 1998; Hasty et al., 2001). The choice of method is dependent on the level of knowledge of the gene network and the type of prediction required from the model.

2.2.2.1.1 Genetic Network Inference

As bacterial systems are studied experimentally at the genetic level, it is important to understand how the genes are related to each other. There are various ways to infer the genetic network connectivity from gene expression data. Some common methods are discussed in the following paragraphs. The interconnections among genes are commonly estimated from changes in gene expression level upon introduction of disturbances, e.g. gene over-expression, gene deletion, change in cell culture conditions etc. Depending on the number of genes involved in the system, the scale of gene network inference can range from an order of 10 to 10,000. It is important to be aware that genes are not only regulated by other genes, but also proteins and other factors in many cases. Thus, the gene network alone is insufficient though valuable for understanding the entire mechanism of the genetic regulation. Below is a summary of common methods for inference of gene connectivity with a couple of literature examples for each method.

Steady-State vs. Transient-State Gene Expression after Perturbation:

When a perturbation is introduced into a gene network, the change in gene expression can be measured at transient-state or steady-state. Tegner et al. (2003) identified a simple network topology by analyzing the steady-state changes in gene expression resulting from the systematic perturbation of a particular node in the

network. The perturbations were delivered around a steady-state so that the network dynamics could be projected onto a general linear mapping model. The linearised mapping model for gene x_i around a steady-state a_i was:

$$\tau_i \frac{dx_i}{dt} = -\gamma_i(x_i - a_i) + [w_{i1}(x_1 - a_1) + w_{i2}(x_2 - a_2) + \dots + w_{iN}(x_N - a_N)] + P_i, \quad i = 1 \dots N \quad (2.2)$$

where τ_i was the time-scale; N was the total number of genes; γ_i was the degradation rate of the i -th mRNA; w_{ij} was the effective gene-to-gene coupling coefficient between the i -th and j -th genes; P_i was a ramp function representing the perturbation. At steady-state, the above equation became:

$$0 = w'_{i1}(x_1 - a_1) + w'_{i2}(x_2 - a_2) + \dots + w'_{iN}(x_N - a_N) \quad (2.3)$$

where γ_i and w_{ij} were combined into w'_{ij} , leaving only N^2 unknown parameters. It was further assumed that cellular networks had a sparse topology which would make some w'_{ij} to be zero. This constraint reduced the search space and the number of computations since N was replaced by k_{max} where $k_{max} \ll N$.

A similar method for construction of a first-order gene and protein regulatory network using only steady-state expression measurements was discussed by Gardner et al. (2003). The use of steady-state gene expression avoids/minimizes the complication of noise which would be maximal at transient-state. But for very large networks, the required number of perturbation can still be unfeasibly huge.

Hoon et al. (2002) suggested fitting a linear system of differential equations to the transient-state gene expression data to infer the gene network. The approach was similar to that above, except the differential terms were non-zero and were estimated from transient-state data. They also proposed a formal way of estimating the non-zero coefficients by using Akaike's Information Criterion which took into account the number of estimated parameters and the likelihood of the estimated model. Transient-state gene expression data potentially contains rich information of gene interactions, though it shares a similar disadvantage as above for large networks. The decision between steady-state and transient-state data is likely to be based on the nature of specific experiments.

MacCarthy et al. (2005) used a simple enumerative reconstruction method based on a discrete dynamic system model to study how microarray experiments

involving global perturbations could be designed to obtain reasonably accurate gene network reconstructions. The method was tested on artificial gene networks with biologically realistic in/out characteristics. For a system of N genes, the state of each gene s_i ($i = 1, \dots, N$) was represented by binary values 0(OFF) and 1(ON). Each gene state was assigned a default ON/OFF state $\theta_i \in [0,1]$. The gene interactions were described by an $N \times N$ matrix C , where $C_{ij} \in [-1, 0, +1]$, representing positive[+1], zero[0] or negative[-1] influence of gene j on gene i . The state of the i -th gene at the next time-step was determined by a balance of positive versus negative inputs which were ON at the previous time-step. Discrete model has an advantage over continuous model that integer computation is faster than floating point computation. However, the description of gene states being discrete may not well represent the continuous nature of gene expression in many cases.

Singular Value Decomposition:

Singular value decomposition (SVD) aims at reverse-engineering the gene network connectivity based on gene transcription data via matrix transformation (Alter et al., 2000; Holter et al., 2001). Yeung et al. (2002) discussed in details a scheme to reverse-engineer gene networks on a genome-wide scale using a relatively small amount of gene expression data from microarray experiments. They used SVD supplemented by extra conditions based on biological knowledge to construct a family of candidate solutions and then used robust regression to identify the solution with the smallest number of connections as the most likely solution. Such algorithm had an order of $\log(N)$ sampling complexity but an order of N^4 computational complexity, where N is the number of genes.

Firstly, SVD was used to construct a set of feasible solutions that are consistent with the measured data and then use robust regression to select the sparsest one as the solution. E.g. for a system operating near steady-state where the dynamics could be approximated by a linear system of ordinary differential equations:

$$\dot{x}_i(t) = -\lambda_i x_i(t) + \sum_{j=1}^N W_{ij} x_j(t) + b_i(t) + \xi_i(t) \quad , \text{ for } i = 1, 2, \dots, N. \quad (2.4)$$

where x_i was the concentration of the i -th mRNA, λ_i was the self-degradation rates, b_i was the external stimuli, and ξ_i represented noise. The matrix element, W_{ij} , consisted of real numbers that described the type and strength of the influence of

the j th gene on the i -th gene, with a positive sign for activation and negative sign for repression. Then in experiment, a prescribed stimulus $(b_1, b_2, \dots, b_N)^T$ was applied and the concentrations of all N different mRNAs were measured. After repeating the procedure for M times, the results could be tabulated as:

$$X_{N \times M} = \begin{pmatrix} x_1^1 & x_1^2 & \dots & x_1^M \\ x_2^1 & x_2^2 & \dots & x_2^M \\ \vdots & \vdots & \ddots & \vdots \\ x_N^1 & x_N^2 & \dots & x_N^M \end{pmatrix} \quad (2.5)$$

The original equation could be rewritten as: $\dot{X}_{N \times M} = A_{N \times M} X_{N \times M} + B_{N \times M}$, where the noise was neglected and the self-degradation rate was absorbed into W_{ij} , i.e. $A_{ij} = W_{ij} - \delta_{ij} \lambda_{ij}$. The goal of the reverse engineering was to use the measured data B , X , and \dot{X} to deduce A and hence W . Because SVD leads to non-unique solutions, additional constraints were needed to isolate the true solution from the entire family of solutions. These constraints may come from knowledge of the biological system.

Singular value decomposition offers a way to infer complex gene networks from a reasonably small number of samples. But the order of computational complexity increases exponentially as networks become large.

Clustering:

Clustering is a method that groups together genes with similar expression patterns over time. This approach is likely (though not always) to group genes that specialize on certain cellular functions of interest. It is useful in uncovering the function of novel genes when they are co-expressed with genes functionally known (Eisen et al., 1998; Tamayo et al., 1999; Tavazoie et al., 1999). Many different clustering methods has been suggested and the choice depends on how the results are to be used (D'haeseleer et al., 2000; Herrero et al., 2003). For data that naturally falls into distinct groups and is well separated, all clustering methods produce the same gene clusters. But if the data is more uniformly distributed, each algorithm places the cluster boundaries differently (Bittner et al., 1999).

Genetic Algorithm and Genetic Programming:

Genetic algorithm optimises model parameters of a pre-defined set of equations that generate an expression pattern that is most similar to the given experimental results (Iba and Mimura, 2002; Pan et al., 2002). It can be used, for instance, to optimise parameters of enzymatic regulation in a model of metabolic network based on an objective (Gilman and Ross, 1995) or to select the optimal parameter values to describe experiment data of a genetic model. For example, if a system could be described by a set of differential equations of the following form (Ando et al., 2002):

$$\frac{dX_i}{dt} = \alpha_i \prod_{j=1}^n X_j^{g_{ij}} - \beta_i \prod_{j=1}^n X_j^{h_{ij}}, \quad i = 1, 2, \dots, n \quad (2.6)$$

which is an S-system (a type of power-law formalism) where X_i was a state variable. The first term on the right represented all influences that increased X_i ; the second term represented all the influences that decreased X_i . Then genetic algorithm could be used to optimise the unknown parameters α_i , β_i , g_{ij} , and h_{ij} .

Genetic programming is an extension of genetic algorithm. The improvement in genetic programming is that no pre-defined set of system equations is needed to start with (Sugimoto et al., 2005; Koza, 1994). Instead, state variables are selected randomly to fit experimentally observed results. As an example, let's consider the following general form (Ando et al., 2002):

$$\frac{dX_i}{dt} = f_i(X_1, X_2, \dots, X_n), \quad i = 1, 2, \dots, n \quad (2.7)$$

where X_i was the state variable and n was the number of observable components.

Genetic programming could then evolve the differential equations from the observed time series of the state variables. Although genetic programming is effective in finding the suitable structure, it is sometimes difficult to optimise the parameters, such as constants or coefficients of the polynomials. This is because the ordinary genetic programming simply uses randomly generated constants. To overcome such difficulty, Ando et al. (2002) introduced a least mean square

method to improve selection of model candidates based on the least mean square fitness of each model to the experimental data.

Styczynski and Stephanopoulos (2005) commented on genetic algorithm as being initialization-dependent and thus potentially unreliable for determining a final network structure, but served as an excellent purpose for algorithms that need a few strong candidates. Genetic programming, being an improved version of genetic algorithm, requires all relevant state variables of a system to be known in order to generate a true model of the system. For large networks, the presence of unknown state variables is unavoidable; and the large number of state variables involved is like to affect the computational efficiency.

There are also other gene network identification methods such as the ensemble method used by Battogtokh et al. (2002) which identified an ensemble of models consistent with, and constrained by, the available RNA and protein profiling data based on Monte Carlo simulation techniques. The idea behind such method was the fact that biologically realistic models are often parameter rich and data poor even with the advent of RNA and protein profiling. It was applied in a chemical reaction network responsible for regulation of a gene cluster in bread mould and successfully identified an ensemble of models fitting available RNA profiling data of the gene cluster. The applicability of this method for other organisms would depend on the simulation complexity involved if all possible models that would fit the data have to be explored. Hoon et al., (2002) used differential equations and the Akaike's Information Criterion (a method for determination of network sparseness) to infer gene regulatory networks from gene expression data.

With the availability of DNA arrays and computational analysis, much progress have been made towards understanding the genetic networks of simple organisms, especially for yeast (Cho et al., 1998; Spellman et al., 1998; Ogawa et al., 2000; Kel et al., 2001; Guelzim et al., 2002; Lee et al., 2002; Wang et al., 2002). For example, Wang et al. (2002) analyzed yeast cell gene expression profiling under various environmental and genetic perturbations and were able to construct transcription modules with good predictions. Cho et al. (1998) found in budding yeast that 416 out of 6220 monitored mRNA had cell cycle-dependent periodicity. Spellman et al. (1998) identified 800 yeast genes that were related to cell-cycle regulation and found that more than half of them

responded to G1 cyclin *Cln3p* or B-type cyclin *Clb2p*. Guelzim et al. (2002) summarized 909 genetic or biochemical interactions among 491 yeast genes based on available databases and an earlier work by Svetlov and Cooper (1995). Kel et al. (2001) created a program to locate binding sites of transcription factors of the *E2F* family which are key regulators of cell cycle (for eukaryotic organisms) and some new *E2F* target genes were successfully identified. The fact that many studies has focused on yeast cells is related to the availability of microarray chips for gene expression analysis of yeast. Developments in DNA microarray technology will enable similar studies to be carried out on more complex organisms.

A general feature of all the genetic modelling methods mentioned so far is that all of them described a small part of the virus/bacteria. Application for an entire cell would only be possible when all the connectivity details in the whole genome are well understood. Insufficient current biological knowledge at the genetic control of an entire cell is a bottleneck for immediate application of such approach to a whole-cell level.

2.2.2.1.2 Metabolic Modelling of Bacterial/Yeast Cells

Monod-Type Models

Not all bacterial cell culture models were directed towards the genetic level. The overall growth and metabolic activities of bacterial cells are more suitably modelled using variables that can be easily measured in the cell cultures. A common structure of bacterial growth kinetics is named after Monod (1949) who proposed a first order saturation relationship between the growth rate and concentration of a single nutrient:

$$R = R_K \cdot \frac{C}{C_1 + C} \quad (2.8)$$

where R is the growth rate, C is the concentration of nutrient, R_K is the rate limit for increasing concentrations of C , C_1 is the concentration of nutrient at which the rate is half of the maximum.

Inhibition Models

Inhibition relationship between specific growth rate and concentration of nutrient has been applied in bacterial suspension cell cultures with a single nutrient source (Aiba et al., 1968; Jackson and Edwards, 1975; Tan et al., 1996; Canovas et al., 2002). In bacterial cell cultures, inhibitions of growth by the biomass concentration and sometimes product concentration have been observed (Aiba et al., 1968; O'Neil and Lyberatos, 1990). For example, O'Neil and Lyberatos (1990) used three types of biomass inhibition model for a continuous yeast culture:

$$\text{Contois model: } \mu = \frac{\mu_m \cdot s}{B \cdot x + s} \quad (2.9)$$

$$\text{Competitive inhibition model: } \mu = \frac{A \cdot s}{B \cdot x + C + s} \quad (2.10)$$

$$\text{Non-competitive inhibition type model: } \mu = \frac{A \cdot s}{(B + s) \cdot (C + x)} \quad (2.11)$$

where μ_m : maximum specific growth rate

μ : specific growth rate

s : residual substrate concentration

x : biomass concentration

A, B, C : model parameters

An example of product inhibition is shown below for a yeast culture producing ethanol from glucose (Aiba et al., 1968):

$$\mu = \mu_0 \cdot \exp^{-k_1 \cdot p} \cdot \frac{S}{K_s + S} \quad (2.12)$$

where p : ethanol (product) concentration

S : glucose concentration

μ_0 : specific growth rate when $p = 0$

μ : specific growth rate

k_1 : empirical exponent

K_s : saturation constant

Some growth kinetics of bacterial cultures involves a nutrient inhibition term at high concentrations. A commonly used substrate inhibition kinetics takes the following form (Andrews et al., 1968):

$$\mu = \frac{\hat{\mu}}{1 + \frac{K_s}{S} + \frac{S}{K_i}} \quad (2.13)$$

where $\hat{\mu}$: maximum specific growth rate

μ : specific growth rate

S : limiting substrate

K_s : saturation constant

K_i : inhibition constant

The specific growth rate in bacterial cultures has also been modelled as proportional to the nutrient transport rate (Kremling et al., 2001b). Bailey and Ollis (1986) have provided a detailed introduction of various equations for biomass production in bacterial and yeast cell cultures.

Metabolic Flux Analysis

As cell metabolism is controlled by gene expression, small metabolic networks such as the central carbohydrate metabolism and amino acid synthesis have been modelled dynamically with connection to the genetic regulation (Kremling and Gilles, 2001; Schmid et al., 2004). But dynamic simulations (involving the time-differential of variables) are limited to small networks where the kinetic relationship among the variables has been characterised. For genome-scale metabolic networks, most of the existing models make use of steady-state assumption to avoid the use of uncharacterised kinetic equations. The metabolites are connected in the model using linear stoichiometric relations or Michalis-Menten-type equations and their concentrations (which are not measured) are assumed to be independent of time. The main focus of those models is the flux of metabolites in all of the metabolic reactions. Thus they are known as flux balance analysis (FBA) or metabolic flux analysis (MFA) (Christensen and Nielsen, 1999). MFA has been used to interpret the reconstructed metabolic network of numerous bacteria including *E. coli*, yeast, and *Haemophilus influenzae* (Pramanik and Keasling, 1997; Schilling et al., 1999; Edwards and Palsson, 2000;

Schilling and Palsson, 2000; Covert et al., 2001; Edwards et al., 2001; Papin et al., 2002; Schuster et al., 2002; Allen and Palsson, 2003; Famili and Palsson, 2003; Fong et al., 2003; Forster et al., 2003; Price et al., 2003; Duarte et al., 2004; Herrgard et al., 2004; Papin et al., 2004a; Papin et al., 2004b; Shimizu 2004; Riascos et al., 2005; Puchalka et al., 2008). It can qualitatively estimate the metabolic network properties, such as the growth potential of mutant bacterial strains (Edwards and Palsson, 2000) and potential gene knock-out targets for metabolic flux improvement (Puchalka et al., 2008). MFA can also be applied on signal transduction networks (Papin and Palsson, 2004).

Single-Cell Models

Models describing the detailed metabolic kinetics of an entire bacterial cell have been studied (Shuler et al., 1979; Domach et al., 1983; Peretti and Bailey, 1986; Jeong and Ataa, 1990; Jeong et al., 1990). For instance, Shuler et al. (1979) modelled the dynamic details of protein synthesis, degradation, transportation, and metabolite conversion and transport in *Escherichia coli* cells. The cell content was grouped into five main categories (protein, RNA, DNA, cell envelope, and glycogen) each having its precursors (amino acids, ribonucleotides, deoxyribonucleotides, cell envelope precursors, and glucose). Most of the rate kinetics were assumed to be Monod-type. The model was able to describe known phenomenon of the cell culture but the values of many kinetic parameters could not be estimated with high confidence. There appears to be a trade-off between the complexity of cell culture models and the confidence level of parameter values. Thus, many cell culture models tend to simplify the cell system using various assumptions in order to reduce the difficulty in parameter estimation.

S-system Models

When the cell culture is operated at steady-states, it is often possible to simplify the kinetic equations of growth and metabolism. A popular choice of equation is the S-system which makes use of power-law model structure (Kitayama et al., 2006). As discussed earlier in Genetic Algorithm (Equation 2.6), S-system represents the rate of change of a variable (X_i) in terms of the multiple of factors causing an increase in X_i less the multiple of factors causing a decrease in X_i . In the equation below, α_i and β_i are positive real coefficients; g_{ij} , and h_{ij} are the exponentials of the factors affecting X_i .

$$\frac{dX_i}{dt} = \alpha_i \prod_{j=1}^n X_j^{g_{ij}} - \beta_i \prod_{j=1}^n X_j^{h_{ij}}, \quad i = 1, 2, \dots, n \quad (2.14)$$

Below is an example of growth kinetics for *Escherichia coli* perfusion cell culture using S-system equation (Alvarez-Vasquez et al., 2002):

$$\mu = \alpha_4 \cdot G^{g_{X,G}} \cdot \mu_{maxg}^{g_{X,\mu}} \quad (2.15)$$

where μ : specific growth rate

G : glycerol concentration

X : biomass concentration

μ_{maxg} : maximum anaerobic specific growth rate

But for cell cultures that do not reach steady-state, e.g. batch and fed-batch cultures, S-system is a less appropriate choice as its approximation is likely to miss out certain cell culture dynamics.

Cybernetic Modelling

A new approach of modelling genetic regulation via replacing genetic expression terms by ‘cybernetic’ variables has been described by Varner and Ramkrishna (1999a; 1999b). It was postulated that metabolic network had physiological objectives; and genetic alteration did not alter the presumed goals of the genetic network which are in place because of millions of years of evolutionary pressure. This approach was originally used to model genetic regulation of nutrients uptake (substitutable/complementary) of bacteria assuming such organisms had a goal to maximize growth. For example:

(i) The elementary cybernetic variable that governs the allocation of critical resources for enzyme synthesis for a *substitutable* process follows from the matching law and is given functionally by:

$$u_j = \frac{r_j}{\sum_{i=1}^k r_i}, \quad j = 1, 2, \dots, k \quad (2.16)$$

where r_j denotes the j th specific reaction rate and the index k denotes the number of enzymes competing for resources from the same pool. The elementary cybernetic

variable that governs enzyme activity for a substitutable process follows from the proportional law and is given by:

$$v_j = \frac{r_j}{\max_i(r_i)} \quad , i = 1, 2, \dots, k ; j = 1, 2, \dots, k \quad (2.17)$$

(ii) The functional form of the elementary cybernetic variable that governs the allocation of critical resources for a *complementary* process follows from the matching law and takes the following form:

$$u_j = \frac{r_j / p_{j+1}}{\sum_{i=1}^z r_i / p_{i+1}} \quad , j = 1, 2, \dots, z \quad (2.18)$$

where p_{k+1} denotes the specific level of product being produced by r_k and the index z denotes the number of enzymes competing from the same elementary resource pool. The elementary cybernetic variable that governs the activity of the j th key enzyme belonging to a complementary elementary pathway follows from the proportional law which is as follows:

$$v_j = \frac{r_j / p_{j+1}}{\max_i(r_i / p_{i+1})} \quad , i = 1, 2, \dots, z ; j = 1, 2, \dots, z \quad (2.19)$$

For bacteria, it has been shown that the assumption of growth maximization was useful in predicting genetic regulation (Venkatesh et al., 1997; Edwards et al., 2001). The Cybernetic approach has been applied to bacterial cell models (Kompala et al., 1986; Straight and Ramkrishna, 1991; Ramakrishna et al. 1996; Varner and Ramkrishna, 1998) but there is no solid evidence that other higher organisms, e.g. mammalian cells, would have the same objective. Below is an example of microbial multiple substrate growth kinetics being modelled using the cybernetic approach (Kompala et al., 1984):

$$\mu = \sum_i \left(\frac{\mu_i \cdot e_i \cdot s_i}{K_i + s_i} \cdot v_i \right) \quad (2.20)$$

where μ : specific growth rate

μ_i : growth coefficient

e_i : specific level of key enzyme i

s_i : substrate i concentration

K_i : Michaelis constant for substrate i

v_i : Cybernetic variable for substrate i

Other Types of Bacteria/Yeast Cell Culture Models

The mathematical model structures discussed in previous sections are systematic modelling methods commonly used in the literature for microbial and yeast cell cultures when there is a single carbon source (or multiple substrates in Equation 2.20). Other types of equations have also been used, such as a discrete model to describe an asymmetric metabolic response to a shift-up versus shift-down of the specific growth rate (Lievens et al., 1989), experimental interpolation (Oh *et al.*, 1993), powered Monod equations, multi-substrate growth kinetics using summation of the consumption of each carbon source, and logarithmic kinetics etc. Kovarova-Kovar and Egli (1998). The effects of pH and temperature which are usually fixed in cell cultures have also been included in the growth kinetics by Leroy and Vuyst (2003). They are outside the main focus of this study and so will not be discussed in detail.

2.2.2.1.3 Mathematical Classification of Cell Culture Models

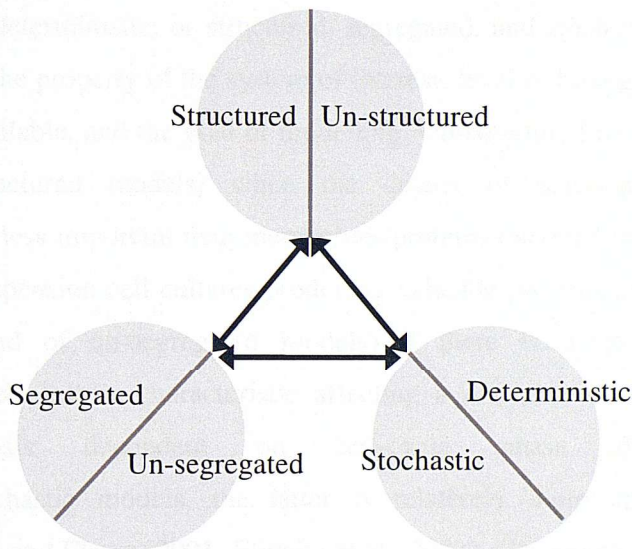


Figure 2.4: Schematic diagram for different types of models of cell cultures.

Cell culture models can be classified as structured versus un-structured, segregated versus un-segregated, and deterministic versus stochastic (Figure 2.4). Structured models take into account the realistic multi-components inside a cell (e.g. mitochondria, lysosome, nucleus etc.) and include transportation of metabolites and molecules to and from these components (Barford, 1990a; Barford, 1990b; Rizzi et al.,

1997); but un-structured models assume a simplified homogeneous cellular unit (Tziampazis and Sambanis, 1994; Bailey 1998; Sidoli et al., 2004). Segregated models treat the cell population as heterogeneous, i.e. each cell may operate at a different state relative to other cells; but un-segregated (also called distributed) models assume a homogeneous population so the actual heterogeneity is averaged into a single state (Tsuchiya et al., 1966; Tziampazis and Sambanis, 1994; Bailey 1998). Deterministic models predict an exact value of model variables at any specific time; but stochastic models use probability functions to predict the likelihood of different values for each model variable (Tsuchiya et al., 1966). Stochastic models are particularly useful for events that the inducing molecules have low copy number (N) (Elowitz et al., 2002; Kierzek et al., 2001; Blake et al., 2003), causing the occurrence of a reaction or signal transduction to be uncertain even when those molecules are present. But when N is large, the average of the predictions from a stochastic model will tend towards the output from a deterministic model.

A cell culture model can take any combinations of the three categories discussed above (also illustrated in Figure 2.4). For example, a model can be un-structured, un-segregated, and deterministic; or structured, segregated, and stochastic etc. The choice is dependent on the property of the system of interest, level of biological understanding, types of data available, and the goal of modelling. Un-structured models are often used (instead of structured models) when the details of reactions in intracellular compartments is less important than metabolites/proteins excreted into the extracellular medium (e.g. suspension cell cultures producing valuable proteins). Segregated models are used (instead of un-segregated models) if there is at least one important heterogeneous cell culture characteristic affecting a desirable cellular property (e.g. protein synthesis dependent on cell-cycle phase distribution). For deterministic/stochastic models, the latter is relatively more applied for genetic networks (Kepler and Elston, 2001; Elowitz et al., 2002). Gene expression is not always a continuous process which can be deterministically described by differential equations (Kaern et al., 2005; Salis and Kaznessis, 2005). Arkin et al. (1998) noted that fluctuations in the rate of gene expression could produce highly erratic time patterns of protein production in individual cells and wide diversity in instantaneous protein concentrations across cell populations. McAdams and Arkin (1997) simulated the processes of gene expression which showed that random pattern of expression of competitive effectors can produce probabilistic outcomes in switching mechanisms that

select between alternative genetic regulatory paths. The result could be a partitioning of the cell population into different phenotypes as the cells follow different paths. But metabolic networks and cell growth are generally modelled deterministically as the cost of computational time is often very high. Although there has been study of stochastic simulations of bacterial metabolic networks indicating the possibility that the randomness of gene expression can propagate to the metabolic level (Puchalka, J. and Kierzek, 2004), experimentally such randomness is not explicitly observed in metabolic data.

2.2.2.1.4 In Silico Cells

In order to model an entire cell without the limitation that some genes are still not well understood, hypothetical cells with ‘minimum’ number of genes to sustain normal cell functions have been proposed. One of those minimum gene sets has been developed into a ‘whole-cell’ modelling software known as E-CELL (Ishii et al., 2004; Kikuchi et al., 2003; Tomita et al., 1999; Takahashi et al., 2004). The genes in E-CELL are mostly based on the smallest bacterial genome *Mycoplasma genitalium* (Fraser et al., 1995). Many major cellular activities are modelled in E-CELL though some of the reaction kinetics are simplified. Enzymes and proteins are modelled to degrade spontaneously over time. The protein synthesis is implemented by modelling the molecules necessary for transcription and translation, namely RNA polymerase, ribosomal subunits, rRNAs, tRNAs, and tRNA ligases. The model cell does not need to switch the genes on and off so it does not have any regulatory factors. The E-CELL software is a valuable tool for the study of cell behaviours (Tomita, 2001a; Tomita, 2001b; Takahashi et al., 2003; Takahashi et al., 2004; Kikuchi et al., 2003; Sugimoto et al., 2005).

Similarly, Castellanos *et al* (2004) proposed a genetically and chemically detailed model of a ‘minimal cell’ based on a ‘coarse-grain’ parameter computer model of *E. coli*. The equations for metabolisms were formulated by writing pseudo-chemical reactions that included the relationship between the nucleotides inside the cell; developing kinetic relationships that reflect the metabolic pathways; and including metabolic control using the concentration of the chemical components as signals. Those kinetic relationships were typically semi-empirical in form and reflected the known factors modulating activity. But there were no direct experimental data to test the model,

so available data from several bacterial organisms were used only for determining whether the overall model response was physiologic in nature or not. There are many software tools for cell system simulations, e.g. VCell (Schaff et al., 1997; Slepchenko et al., 2003), SmartCell (Dublanche 2006), CellDesigner (Funahashi et al., 2003) etc. Computational studies of gene and metabolic networks enable testing of hypotheses and screening of possible network alternatives before doing further wet-lab experiments. *In silico* simulation of hypothetical cells is a valuable tool for investigation of cellular dynamics without the presence of unknown interactions or noise.

2.2.2.2 Mammalian Cell Culture Modelling

There are many similarities between mammalian and bacterial/yeast cells. Some of the growth and nutrient consumption kinetics for mammalian cell cultures are adapted from bacterial and yeast models. All of the modelling methods discussed in Section 2.2.2.1 for bacterial and yeast cell cultures can theoretically be applied on mammalian cell cultures either directly or with modifications. However, some of those methods tend to be more favoured than others for mammalian cell cultures.

2.2.2.2.1 Monod-Type Kinetics

The Monod-type kinetics is the most popular relationship between the nutrients concentration and specific growth rate of mammalian cell cultures and it has been modified in various ways to suit the mammalian cells' requirement of more than one nutrient (Portner and Schafer, 1996). Models that describe mammalian cell proliferation, nutrients metabolism, and antibody production etc. has mainly focused on the influence of a few major nutrients and by-products upon those cellular activities (Bree and Dhurjati, 1988; Batt and Kompala, 1989; Dalili et al., 1990; Bakker et al., 1996; da Silva et al., 1996; Zeng and Deckwer, 1999; Jang and Barford, 2000b; Fox et al., 2004; Provost and Bastin, 2004; Teixeira et al., 2005). Some of these models provide insights into the mechanisms of how relevant enzymes, proteins, and substrates (nutrients/wastes) are involved in various cellular activities. An example of such kind of growth kinetics is shown below:

$$\mu = \mu_{\max} \left(\frac{[GLC]}{K_{glc} + [GLC]} \right) \left(\frac{[GLN]}{K_{gln} + [GLN]} \right) \left(\frac{KI_{amm}}{KI_{amm} + [AMM]} \right) \left(\frac{KI_{lac}}{KI_{lac} + [LAC]} \right) \quad (2.21)$$

where Jang and Barford (2000b) related the specific growth rate, μ (h^{-1}), of batch/fed-batch cultures of murine hybridoma AFP-27 cell-line to the concentration of glucose ($[GLC]$), glutamine ($[GLN]$), ammonium ($[GLC]$), and lactate ($[GLC]$). In the equation above, μ_{\max} (h^{-1}) is the maximum specific growth rate; K_{glc} (mM) and K_{gln} (mM) are the half-saturation constants of glucose and glutamine respectively; KI_{amm} (mM) and KI_{lac} (mM) are the growth-inhibition constants of the byproducts ammonium and lactate respectively. This type of growth kinetics is commonly used in batch/fed-batch mammalian cell culture models (Zeng et al., 1998a) but sometimes the concentration of the byproducts are not linked to the specific growth rate (Heidemann et al., 1998; Frahm et al., 2003). But the growth rate in continuous cultures is typically directly related to the dilution rate (Suzuki and Ollis, 1989; Zeng, 1996) because both the specific growth rate and dilution rate are equal at steady-states.

Modifications of the Monod-type kinetics also appear in mammalian cell culture models. Below is an example for mouse hybridoma CRL-1606 batch cultures taking into account the effect of serum and cell concentration on growth rate (Glacken et al., 1988):

$$\mu = \frac{\mu_{\max} \cdot S \cdot G}{[S + (K_s)_0 \cdot X^{-\beta}] \cdot [G + K_G]} \cdot \frac{1}{\left[1 + \frac{A^2}{K_A}\right] \cdot \left[1 + \frac{L^2}{K_L}\right]} \quad (2.22)$$

where μ : specific growth rate

μ_{\max} : maximum specific growth rate

S : serum level

G : glutamine concentration

X : cell concentration

A : ammonium concentration

L : lactate concentration

$(K_s)_0$: initial value of Monod constant in serum

K_G : Monod constant for glutamine

K_A : inhibition constant for ammonium

K_L : inhibition constant for lactate

Some models include amino acids in the growth kinetics. For instance, Duval et al. (1991) related a general ‘amino acids’ term (a lumped variable for several amino acids) to the growth of hybridoma cells VO 208 & 6H₂ batch and semi-continuous

cultures supplemented with extra amino acids; (Simon and Karim, 2002) measured amino acid concentrations in Chinese hamster ovary batch cultures and identified asparagine and glutamine as important for the growth model. But it is not common to include amino acids in the growth kinetics due to the difficulty in measuring all of the amino acids in the cell cultures.

Cell growth is not always the main interest in mammalian cell modelling. Bibila and Flickinger, (1991a) detailed the heavy and light chain synthesis steps for monoclonal antibody (MAb) production in a mouse hybridoma cell-line. They also modelled the transient steps of MAb synthesis from the endoplasmic reticulum to Golgi apparatus and their excretion into the medium (Bibila and Flickinger, 1991b). The main purpose of those models was to study the secretion of MAb in order to optimise the production rate (Bibila and Flickinger, 1992a; Bibila and Flickinger, 1992b).

2.2.2.2.2 Single-Cell Models

The dynamics of metabolic reactions at a whole-cell level is important for understanding the overall response of mammalian cells to different physiological conditions. Thus, some mammalian cell models have focused upon the details of the dynamics of all known metabolic reactions (Wiechert, 2002; Haag et al., 2003; Sidoli et al., 2004). Wu et al. (1992) had described a detailed single-cell model for CHO-K1 cells by lumping cell components into several major groups and modelled their interactions (similar to Shuler et al. (1979) for a single bacterial cell model in Section 2.2.2.1.2). The equations involved material transport across cell membrane, nutrient metabolism, formation of macromolecules, ATP, DNA, RNA, and byproducts etc. But many parameter values were taken from other cell types which may not reflect the actual property of CHO cells. Sanderson (1997) and co-workers (Sanderson et al., 1995; 1997; 1999) had simulated the major metabolic pathways of hybridoma cells detailing the glycolysis pathway, pentose phosphate pathway, mitochondrial citric acid cycle, glutaminolysis pathway, and amino acid interconversions etc. for optimisation of antibody synthesis. It is a challenge to apply highly detailed intracellular models to industrial cell culture processes due to the difficulty to monitor intracellular variables. Cell-cycle signalling mechanism which affects cell growth is another aspect of mammalian cell (as well as yeast) which has been modelled in detail (Novak et al., 1998;

Novak and Tyson, 2004) but these models are often too complex for the purpose of cell culture process optimisation.

2.2.2.2.3 Population Balance Models

Population balance is used in segregated models (Section 2.2.2.1.3) that the heterogeneity in the cell population with respect to certain characteristic is taken into account (Uchiyama and Shioya, 1999; Sidoli et al., 2004; Henson 2005; Mantzaris, 2005). It is mainly applied in mammalian cell cultures instead of bacterial cultures due to the slower growth rate and higher experimentation cost of the former which make optimisation of the segregation behaviour more beneficial. A general equation for cell population balance was discussed by Mantzaris et al. (1999; 2001a; 2001b; 2001c) based on Fredrickson et al. (1967) and Ramkrishna (1979) for continuous cell cultures:

$$\begin{aligned} \frac{\partial N(\mathbf{x},t)}{\partial t} + \nabla_{\mathbf{x}}[r(\mathbf{x},\mathbf{S}) \cdot N(\mathbf{x},t)] + \Gamma(\mathbf{x},\mathbf{S}) \cdot N(\mathbf{x},t) + D \cdot N(\mathbf{x},t) \\ = 2 \int_{\mathbf{x}}^{\mathbf{x}^{\max}} \Gamma(\mathbf{y},\mathbf{S}) \cdot p(\mathbf{x},\mathbf{y},\mathbf{S}) \cdot N(\mathbf{y},t) \, d\mathbf{y} \end{aligned} \quad (2.23)$$

where $N(\mathbf{x},t)$: time-dependent state of cell population
 \mathbf{x} : physiological state vector of a cell
 \mathbf{S} : state vector of nutrient environment
 \mathbf{y} : physiological state vector of a dividing cell
 r : single-cell growth rate
 D : dilution rate
 Γ : cell division rate
 p : probability density function

The above equation can be simplified with assumptions to simple ordinary differential equations. A simple population balance model of the cell-cycle was used by Nielsen et al. (1997) to explain the phenomenon in animal cell culture (and microbial systems) that cell number dynamics lag behind biomass dynamics. Population balance model is a more accurate representation of the actual heterogeneity among cells in cell cultures. But the additional complexity of the model structure may hamper the predictive capability of the cell culture models.

2.2.2.2.4 Multiple Steady-State Models

'Multiple steady-states' was defined by Qu et al. (2003) as multiple solutions of mathematical representation of the biological system at steady state. In many mammalian continuous cell culture experiments, it has been observed that the cell culture history can occasionally switch the cells to a different steady-state for the same final cell culture input conditions. Europa et al. (2000) studied hybridoma MAK cells in continuous culture. Those cells pre-grown in fed-batch culture versus cells from batch culture gave different steady-state cell density and metabolite concentration after both cultures were switched to continuous culture. A similar phenomenon was reported by Follstad et al. (1999) in hybridoma CRL-1606 chemostat cultures. Smolen et al. (1998) attempted to develop a conceptual framework for investigating the function of genetic regulatory systems. Simple kinetic models that incorporate known feature of genetic regulatory systems, e.g. phosphorylation of transcription factors, crosstalk, feedback etc., were used and multiple stable steady-states were manifested that brief perturbations could switch the model between these states.

There has been attempts to model the multiple steady-states (under identical input conditions) exhibited by mammalian cells using the *cybernetic* approach discussed in Section 2.2.2.1.2 (Namjoshi et al., 2003; Namjoshi et al., 2005; Guardia et al., 2000). The Cybernetic approach has been modified to model the partially substitutable, partially complementary nature of glucose and glutamine metabolism in mammalian cells (Namjoshi et al., 2003; Guardia et al., 2000). The model by Guardia *et al* was able to predict two steady-states (though more than two steady-states were expected in real cases); and the model by Namjoshi *et al* captured three experimentally observed steady-states. The model by Namjoshi *et al* has been repeated and the simulation results are shown in Figure 3.3 and 3.4. It involves roughly 30 parameters and 26 variables (of which 12 are cybernetic variables) describing a simplified network of mammalian cell growth and glucose/glutamine metabolism. The cybernetic approach is able to capture the multiple steady-states behaviour of mammalian cells but it requires a large quantity of model parameters to describe a small number of cell culture behaviour (about 30 parameters for the lactate production and total cell concentration in the model of Namjoshi et al. (2003)). When the ratio of parameters to measured variables is large, the parameter estimation from experimental data will result in numerous sets of possible solution which are difficult to discriminate.

2.2.2.2.5 Other Types of Mammalian Cell Models

Mammalian cells have been modelled with diverse types of equation structure. Some are based on empirical correlations such as the power-law equation for serum degradation in hybridoma CRL-1606 fed-batch cultures used by Glacken et al. (1989). The level of ATP in mammalian cells has also been incorporated into the growth kinetics using exponential equation (DiMasi and Swartz, 1995). Signalling pathway models consisting of first-order, second-order, Monod-type, Michaelis-Menten, and stochastic kinetics are used to describe the details of various sensing mechanisms in part of a mammalian cell (Schroder et al., 1999; Fussenegger et al., 2000; Takahashi et al., 2002; Hatakeyama et al., 2003) and also similarly for insect cells (Rensing et al., 1982). Genome-scale linear metabolic models have also been made for mammalian cells (Sheikh et al., 2005) but they are less common than bacterial/yeast cells (Section 2.2.2.1.2) due to the complexity of mammalian genomes. Metabolic flux analyses for the central mammalian metabolic pathways have provided much valuable information towards the flux distribution of important metabolites at steady-states (Zupke and Stephanopoulos, 1995; Xie and Wang, 1996; Altamirano et al., 2001) though the dynamic details, such as variation of nutrient consumption ratio and byproduct yield (Zeng et al., 1998b), are missing. Metabolic network modelling for red blood cells (RBC) has exceptionally assumed simple kinetic relationship (due to a lack of nucleus and thus metabolic regulation at the genetic level in RBC) to model the metabolic characteristics dynamically (Lee and Palsson, 1992; Jamshidi et al., 2001; Kuchel 2004) as well as the oxygen transport kinetics to and from RBC (Beyer et al., 2002). There is no universal standard of model structure for each specific mammalian cell system. The choice of model for mammalian cultures is generally based on the purpose of modelling and the amount of data available.

2.2.3 Applications of Model-Based Optimisation in Cell Cultures & Bioindustrial Processes

There are not many cases in the bioindustry that mathematical models are used to predict cell culture productivity of proteins and drugs. Although computational measurement tools are extensively used to monitor the states of cell cultures, the use of those data for prediction of cell culture dynamics is generally missing. Some of the adopted control methods are simple unstructured models, engineering judgement, artificial neural networks, fuzzy logic, expert systems, and adaptive control (Luttmann et al., 1985; Semones and Lim, 1989; Lenas et al., 1997; Guan and Kemp, 1999; Hammond and Hammond, 2001; Portner et al., 2004; Julien and Whitford, 2007). The latter three methods require a considerable size of experiment data to test or train the control systems which would be expensive when the experimentation cost is high. A common practice for mammalian cell cultures is experimental optimisation with limited variations in the adjustable variables (Clark and Hirtenstein, 1981; Suzuki and Ollis, 1990; McKinney et al., 1995; Cheng et al., 1997; Chuppa et al., 1997; Gorfien et al., 2003). The use of mathematical models to improve or optimise cell cultures is still mainly at the research stage (Parulekar and Lim, 1985; de Tremblay et al., 1993; Fu and Barford, 1994; Portner et al., 1996; Roubos et al., 1997; Dhir et al., 2000; Lavric et al., 2006). For example, Gadkar et al. (2003) developed a cybernetic model for poly- β -hydroxybutyrate (PHB) production in perfusion cultures of *Alcaligenes eutrophus*. The model was interfaced to a model predictive control algorithm to optimise PHB productivity by adjusting the dilution rate and recycle ratio. Cheema et al. (2002) applied genetic programming to develop a model for gluconic acid production from glucose in bacterial batch culture using historic process input-output data. The model was then used to optimise cell culture productivity. Frahm et al. (2002, 2003) used a model-based adaptive control strategy to optimise the nutrient feeding time-profiles at the same time that the fed-batch mouse hybridoma cell cultures were operating. It is a common practice to use simple cell culture models to estimate the amount of nutrient required to achieve a particular growth rate or to maximise product yield (Xie and Wang, 1994; Zhou et al., 1995; Zhou et al., 1997b; Jang and Barford, 2000a; Kontoravdi et al., 2007). Other degrees of freedom for model-based optimisation include temperature (Fox et al., 2004) and osmolarity (Ho, 2007). When the cell culture models are linear, e.g. metabolic network models, the system is optimised via linear optimisation (Hatzimanikatis et al., 1996a,b; Riascos et al., 2005). Non-linear cell culture models are

either linearised before model-based optimisation or are optimised via non-linear methods (Torres et al., 1997; Rodriguez-Acosta, et al., 1999; Alvarez-Vasquez et al., 2000; Marin-Sanguino and Torres, 2000). Non-linear optimisation methods will be discussed in greater detail in Chapter 6.

Concerns about Hydrolysis/Proteolysis of Products

The loss of antibodies or recombinant proteins in cell cultures due to hydrolysis or proteolysis (due to proteolytic enzymes released from dead cells) is seldom studied. Goldman et al. (1997) analysed the proteolytic cleavage of recombinant human interferon- γ produced by Chinese hamster ovary cells during batch culture. It was found that the proteolysis of interferon- γ increased towards the end of the cell culture especially during the death phase, resulting in higher heterogeneity of the peptide change and a reduction in biological activity. When the time length of cell culture is increased to achieve higher product concentration, there is also a possibility that protein hydrolysis/proteolysis will become more significant. In practice, the viability of cells is monitored and the cell culture would be terminated once the viability drops below certain level. A high viability threshold should be able to minimize the side effect of longer cell culture time on product quality.

2.2.4 The Dynamic Nature of Biological Cell Cultures

Many dynamic properties in bacterial, yeast, and mammalian cell cultures have been observed in experiments. In bacterial cultures, the transcription time-profiles of the same promoters have been observed to have significantly different time-lag and maximum fold increase when the cells were cultured in nutrient-rich versus minimal medium (Marques et al., 1994). Yeast is one of the most studied cell-type at the gene level. The global-scale gene response in yeast has been studied at different concentrations of glucose (Yin et al., 2003) and it was found that more genes responsible for amino acids metabolism, carbon metabolism, energy, protein synthesis, cellular transport were up regulated at low glucose concentration (0.01%) relative to medium (0.1%) and high (1%) levels (Figure 2.5).

Table 1. Proportion of ORFs in each functional category that showed \geq twofold regulation in response to different glucose signals.^{ab}

Functional categories	All ORFs	0.01% Glucose		0.1% Glucose		1.0% Glucose	
		Up	Down	Up	Down	Up	Down
1. Metabolism	17%	44%	18%	30%	14%	27%	14%
1.1 Amino acids	3%	3%	2%	7%	2%	9%	2%
1.2 Nitrogen and sulphur	1%	0%	1%	1%	0%	1%	1%
1.3 Nucleotides	2%	3%	2%	4%	2%	4%	1%
1.4 Phosphate	1%	0%	0%	0%	0%	1%	0%
1.5 Carbon	6%	38%	7%	16%	8%	9%	9%
1.6 Lipids and fatty-acids	3%	0%	4%	3%	2%	4%	2%
1.7 Vitamins and cofactors	1%	0%	1%	1%	0%	1%	0%
1.8 Secondary metabolism	0%	0%	0%	0%	0%	0%	0%
2. Energy	4%	16%	8%	11%	7%	5%	10%
3. Cell cycle and DNA processing	10%	0%	8%	5%	5%	5%	4%
4. Transcription	12%	6%	11%	6%	9%	9%	7%
5. Protein synthesis	6%	38%	5%	35%	2%	28%	2%
6. Protein fate	9%	6%	10%	4%	5%	4%	7%
7. Cellular transport	8%	19%	7%	3%	5%	5%	5%
8. Cellular communication/signal transduction	1%	0%	0%	1%	1%	1%	1%
9. Cell rescue	4%	3%	5%	4%	3%	4%	2%
10. Interaction with cellular environment	3%	3%	4%	2%	2%	2%	2%
11. Cell fate	7%	0%	8%	2%	5%	3%	4%
12. Transposable elements	2%	0%	0%	1%	0%	1%	0%
13. Cellular organization	3%	0%	4%	2%	2%	3%	2%
14. Subcellular localization	35%	78%	39%	65%	29%	57%	29%
15. Protein activity regulation	0%	0%	0%	0%	0%	0%	0%
16. Proteins with binding functions	0%	0%	0%	0%	0%	0%	0%
17. Transport facilitation	5%	19%	5%	3%	4%	5%	4%
18. Classification not yet clear cut	2%	0%	1%	2%	5%	1%	1%
19. Unclassified proteins	37%	6%	36%	15%	22%	14%	18%
Number of ORFs ^c	6450	32	238	191	294	352	368

a. ORFs can belong to more than one functional category in the MIPS database (<http://mips.gsf.de/proj/yeast/CYGD/db/index.html>; January 2003).

b. Expressed as percentage of number of ORFs belonging to each functional category.

c. Total number of ORFs regulated by each glucose signal are given.

Figure 2.5: Data of global-scale gene response of a yeast cell culture exposed to low, medium, and high concentration of glucose (Yin et al., 2003).

The glucose sensing pathway in yeast is one of the most studied cellular signalling mechanism. Geladé et al. (2003) summarised three different pathways in yeast related to glucose availability:

- Figure 2.6(a) shows the repression of genes related to respiration, gluconeogenesis, and metabolism of alternative carbon sources by high glucose concentrations;
- Figure 2.6(b) illustrates the *Snf3/Rgt2* glucose-sensing pathway
 - (i) When there is no glucose, the transcription factor *Rgt1* forms a complex with *Mth1* and *Std1* causing the transcription of the hexose transporters for glucose to be inactivated the presence of glucose inactivates *Rgt1* and initiates transcription of *HXT1-HXT4* transporters;
 - (ii) High concentration of glucose would further enhance the expression of *HXT1*.
- Figure 2.6(c) shows the *Gpr1/Gpa2* glucose-sensing pathway. High glucose concentration activate cAMP production in a glucose-phosphorylation-dependent manner resulting in activation of protein kinase A (*PKA*) which affects many cellular functions including carbon metabolism, stress resistance etc.

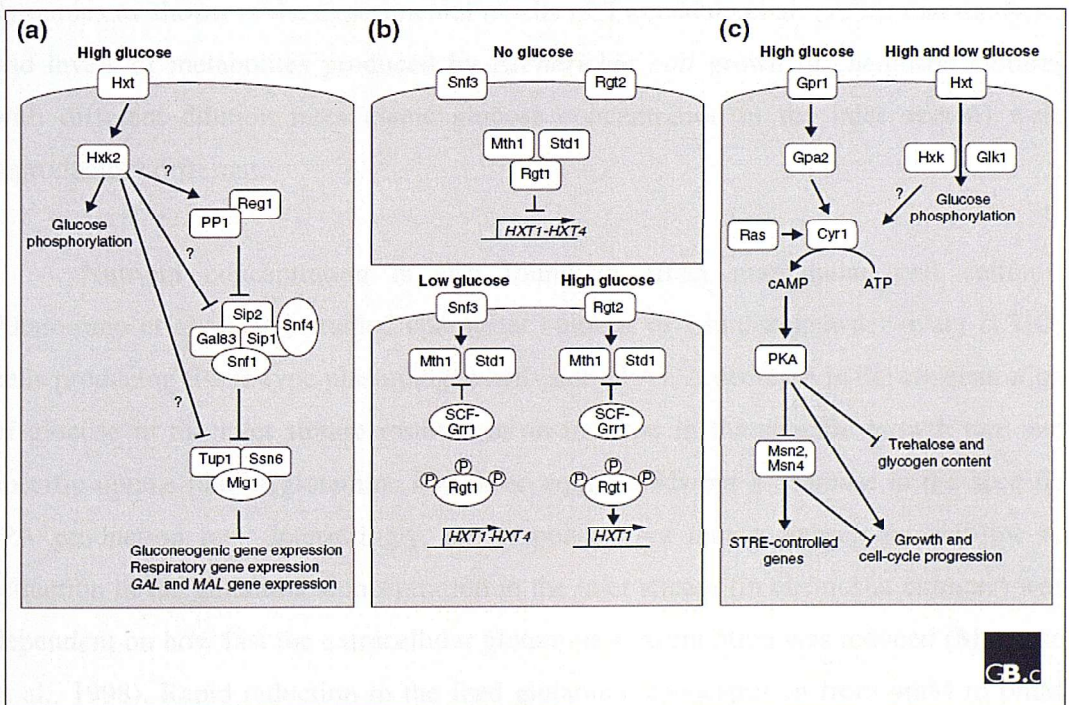


Figure 2.6: Simplified glucose-response pathways in yeast (Geladé et al., 2003).

The glucose-dependent expression of hexose transporters in yeast is clearly demonstrated by the study of Ozcan and Johnston (1995) who showed experimentally

that some hexose transporters are more strongly expressed at low glucose concentrations and vice versa (Figure 2.7).

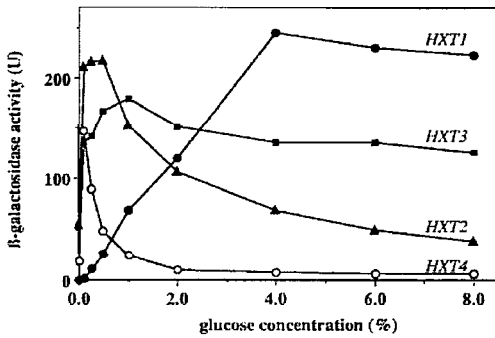


Figure 2.7: Level of *HXT* gene expression for different hexose transporters in yeast at different glucose concentrations (Ozcan and Johnston 1995).

The responses in the glucose-signalling pathways in yeast can be caused by either the extracellular glucose concentration or glucose flux. A dependency of the signalling pathways on the extracellular glucose concentration but not glucose flux has been observed in yeast (Meijer et al., 1998; Ozcan et al., 1998) and *Escherichia coli* (Phue et al., 2005). The overall availability of glucose is also likely to affect cell culture dynamics as shown in the experimental results of Tweeddale et al. (1998) that the types and levels of metabolites produced by *Escherichia coli* grown in chemostat cultures with different dilution rates (same glucose concentration in the inlet stream) were reproducibly different.

Nutrient concentration is also found to affect mammalian cell cultures. Altamirano et al. (2001) studied chemostat cultures of Chinese hamster ovary (CHO) cells producing tissue-type plasminogen activator (tPA). A decrease in the concentration of glucose in the inlet stream resulted in an increase in the specific growth rate and specific uptake rate of glutamine and some amino acids but a decrease in the specific tPA production rate. Interestingly, the response of a mouse hybridoma cell-line to reduction in the glutamine concentration in the inlet stream (in chemostat cultures) was dependent on how fast the extracellular glutamine concentration was reduced (Mancuso et al., 1998). Rapid reduction in the feed glutamine concentration from 4mM to 0mM for a short time which caused a rapid drop in residual glutamine from 0.67mM to 0mM had a strong stimulation for the specific antibody production rate. But a slow reduction in the feed glutamine concentration from 2.4mM to 1.2mM which caused a gradual decrease in residual glutamine from 0.30mM to 0.08mM has no significant effect on the

antibody synthesis rate. Similar observation was also reported for *Escherichia coli* that an abrupt reduction of the dilution rate in continuous or fed-batch culture triggered accumulation of the sigma factor σ^S (Teich et al., 1999) or degradation of ribosomal RNA (Rinas et al., 1995) but gradual changes fail to induce these responses (Teich et al., 1999; Rinas et al., 1995).

Jang and Barford observed an increase in specific antibody production rate and a decrease in the lactate yield from glucose in fed-batch cultures of a mouse hybridoma cell-line operating at very low specific growth rates (2000a). The study by Teich et al. (1999) about the stringent response and general stress response (which are related to nutrient limitation) in *Escherichia coli* may provide an explanation: the regulators *ppGpp* and σ^S of both responses were monitored in glucose-limited fed-batch and continuous cultures; both regulators responded significantly to a fast shift in glucose level but less when the change was gradual. It has been shown in the case of myeloma cells that the regulation of fluxes in the central metabolism can be regulated by activation/deactivation of the enzymes instead of at transcription or translation levels (Vriezen and van Dijken, 1998). The detailed mechanism of cellular response of both bacterial/yeast and mammalian cells to nutrient concentrations is still not well understood although the phenomenon has been observed for decades. Such cellular response would be useful for antibody/recombinant protein synthesis if the resulting effect is an increase in the specific product synthesis rate and at the same time the specific growth rate is not compromised.

Other Types of Stress for Cell Cultures

Nutrient limitation can be regarded as a 'stress' for cell cultures. There are many other types of stress that can be imposed on bacterial, yeast, and mammalian cells but they are outside the scope of this study. Below are several physical and chemical stresses that have been studied in cell cultures:

(i) Temperature change:

Mammalian cells including Chinese hamster fibroblasts, HeLa cells, and Chinese hamster ovary (CHO) cells have been reported to develop thermo-tolerance after being heated up to 41 – 45 °C and *hsp70* transcription was reported to increase in the case of HeLa cells (Hahn and Shiu, 1985; Laszlo and Li, 1985; Abravaya *et al.*, 1991). A reduction in cell culture temperature has caused an increase in the productivity of CHO cells due to elevated mRNA levels responsible for recombinant protein synthesis (Fox *et al.*, 2004; Bollati *et al.*, 2005) (Fox *et al.*, 2005). A detailed review of the physiological responses is made by Wick and Egli (2004) regarding the heat-shock and cold-shock phenomena in *Escherichia coli* which should have certain similarity with mammalian cells.

(ii) pH change:

The operating pH of cell cultures is typically around pH 7. Osman *et al.*, (2001) studied pH shifts in a range of pH 6.5 – 9.0 in GS-NS0 myeloma cell cultures. Maximum specific growth rate was observed after the pH was shifted to pH 7.3 – 7.5 and glucose consumption was found to increase with increasing pH. The cell cultures were able to return to original growth and metabolic behaviour after pH recovery.

(iii) Osmotic stress change:

A shift-up in cell culture osmolarity was found to increase the specific productivity (Wu *et al.*, 2004), culture longevity (Oh *et al.*, 1993), or amino acid metabolism (Cherlet and Marc, 1999) in mammalian cells and activation of myelin basic protein phosphorylation kinases in tobacco cells (Mikolajczyk *et al.*, 2000). The effects appear to be cell-type dependent and may not always be associated with an

increase in cell culture productivity. In certain case the effect of osmolarity on productivity did not indicate a clear upward or downward trend (Kimura and Miller, 1996).

(iv) *Shear stress change:*

Shear stress on cells is caused by interaction with the reactor and agitator and it varies with the reactor designs, e.g. stirred tanks, shake flasks, roller bottles, bubble columns etc. (Henzler 2000). An increase in shear stress caused higher metabolite production by human umbilical vein endothelial cells (Frangos *et al.*, 1988) but a negative effect on cell viability for baby hamster kidney (BHK) cells has been reported (Kretzmer and Schugerl, 1991). The shear stress in cell cultures is typically maintained low because cell viability has a significant impact on product quality.

(v) *Stress due to recombinant protein production:*

The production of recombinant proteins in *Escherichia coli* has been shown to compete for protein resources with cell growth (Hoffmann and Rinas, 2004). The additional energy required to synthesize recombinant protein was also reflected by higher maintenance substrate consumption in recombinant protein producing cells (Hoffmann and Rinas, 2004). Such stress is unavoidable in cell cultures producing foreign proteins.

(iv) *Chemical stress:*

The presence of highly oxidative compounds, e.g. superoxide anions, hydrogen peroxide etc., cause oxidative stress to cell cultures and can damage DNA and proteins (Moat *et al.*, 2002; Arrigo *et al.*, 2005). But these compounds are normally absent from cell cultures that are used to produce antibodies and recombinant proteins.

Summary

Biological cell cultures are full of diversity in terms of growth characteristics, applications for synthesis of various products, and responses to different types of stress in the surrounding environment. There is an equally wide range of mathematical models in the literature describing cell culture properties from the genetic level to the whole cell level with different extent of complexity. Modelling is becoming more popular in the biological world but there are still many challenges to be overcome when applying traditional mathematical and engineering approaches on cell cultures of which the full properties are yet to be explored.

Chapter 3

— Hybridoma Culture Cell-Cycle Modelling & Optimisation

Mammalian cell culture modelling often focus upon choosing the best nutrient supplementation strategy for a fixed type of culturing mode (batch/fed-batch/continuous/perfusion). However, there are other degrees of freedom involving discrete selections, e.g. arresting cell growth, triggering a change in metabolism, stepping-up osmolarity, switching cell culture temperature etc., that are encountered in cell culture processes. It is important to develop a modelling and optimisation framework to handle both continuous and discrete degrees of freedom of dynamic cell cultures simultaneously to enable efficient analysis and improvement of the productivity. Two types of discrete degrees of freedom are studied in this work: cell-cycle arrest and metabolism alteration in hybridoma and CHO-IFN γ cell cultures respectively. The cell-cycle modelling for hybridoma cells is presented in this chapter followed by the CHO-IFN γ cell culture model in Chapter 4.

3.1 Cell-Cycle & Productivity Modelling

3.1.1 Relationship between Cell-Cycle and Productivity

Mammalian cells reproduce by self-duplication which involves four cell-cycle phases: G_1 , S, G_2 , and M (Figure 3.1). Cells in the G_1 phase enter the S phase where DNA replication takes place when the cell culture environment is favourable and the required cellular signals are present. Then in the G_2 phase the cells prepare themselves for division and finally in the M phase each cell is separated into two. There is a dormant phase called G_0 that the cells do not participate in the cell-cycle. The cell-cycle is regulated by various cyclins, cyclin-dependent protein kinases, and protein complexes (Pines and Hunter, 1989; Norbury and Nurse, 1992; Gu et al., 1992; Lew and Reed, 1993; Fussenegger and Bailey 1998; Kohn, 1999; Ekholm and Reed, 2000; Simon et al., 2001; Barre and Perkins, 2007) which govern the initiation and progression of each cell-cycle phase. Many studies had been done to identify which of the cell-cycle phases is the most productive in terms of antibody and recombinant protein synthesis. Cherlet et al. measured cell DNA content and antibody content on the surface of hybridoma AFP-27 cells using flow cytometry analysis and found that the G_1 cells showed a lower specific antibody secretion rate than the G_2/M cells (Cherlet et al., 1995). Al-Rubeai and Emery studied TB/C3 murine hybridoma cells synchronised by thymidine block and measured antibody synthesis using pulse-labelling (Al-Rubeai and Emery, 1990). The rate of synthesis was at maximum during the G_1/S phases and the specific antibody production rate was increased when cells were arrested and maintained in the late G_1/S phases (Al-Rubeai and Emery, 1990). Kromenaker and Srienc studied various AFP-27 cell-lines and found that the accumulation of antibody in the cells was highest in the G_1 phase and lowest in the G_2/M phase; and the specific antibody secretion rate increased when specific growth rate decreased (Kromenaker and Srienc, 1991; Kromenaker and Srienc, 1994a,b). Al-Rubeai et al. compared specific antibody productivity of 3 different hybridoma cell-lines (TB/C3, PQXB1/1, I.13.17) at the growth phase and death phase of the cell cultures but there was no consistent trend in the specific productivity between the two phases among those cell-lines (Al-Rubeai et al., 1992).

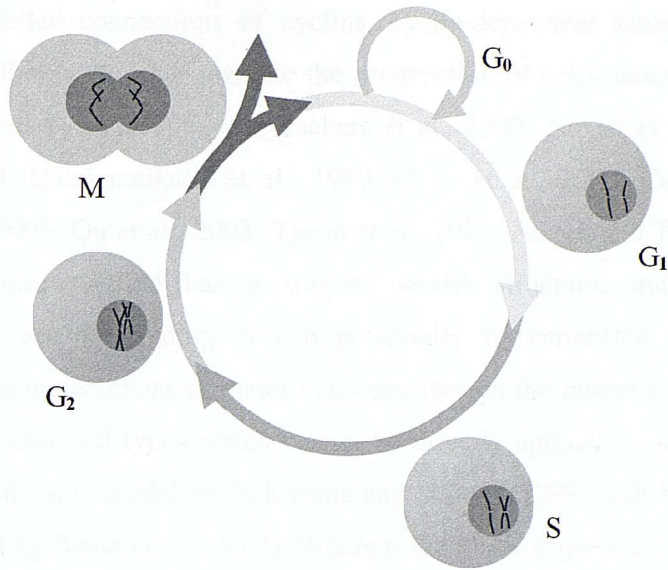


Figure 3.1: Illustration of the major phases in mammalian cell-cycle (same as Figure 2.2).

Comparisons done by Lloyd et al. for the productivity of a wide range of mammalian cells including hybridoma and CHO cells showed variations in the phase(s) of maximal expression, e.g. G₀/G₁, G₁, G₁/S, or G₂/M, for different cell-lines and promoters (Lloyd et al., 1999; Lloyd et al., 2000). Thus, the most productive cell-cycle phase appeared to be dependent on the cell type and each cell-line and product of interest should be studied independently to determine the cell-cycle phase of maximal product expression. The growth arrest had also been reported to increase specific productivity in other mammalian cell-lines (Mazur et al., 1998; Seifert and Phillips 1999; Watanabe et al., 2002; Ho, 2007) apart from the hybridoma cell-lines discussed above. It is important to understand and model such cell-cycle and growth dependency of productivity systematically in order to fully utilize this potential to improve product yield.

3.1.2 Cell-Cycle Modelling

Cell-cycle modelling can be grouped into two main categories: population balance of each cell-cycle phase versus modelling the detailed phase transition regulation by growth factors. Population balance approach models the number or fraction of cells in G₁, S, G₂, and M phases as a function of growth rate (Suzuki and Ollis, 1989; Nielsen et al., 1997; Cain and Chau, 1998; Uchiyama and Shioya, 1999; Faraday et al., 2001; Basse et al., 2003). Phase transition regulation approach takes into

account the detailed connections of cyclins, cyclin-dependent kinases, transcription factors, and inhibitors etc. that regulate the progression of cells across each cell-cycle phase (Novak and Tyson, 1997; Obeyesekere et al., 1997; Novak et al., 1998; Aguda and Tang, 1999; Hatzimanikatis et al., 1999; Chen et al., 2000; Cross et al., 2002; Deineko et al., 2003; Qu et al., 2003; Tyson et al., 2003; Novak and Tyson, 2004). The population balance method has a simpler model structure, making the model computationally less demanding. It can potentially be connected to other cellular functions such as metabolisms of major nutrients, though the model equations are often specific to particular cell types which cannot be directly applied to other cell cultures, e.g. the yeast cell-cycle model by Uchiyama and Shioya (1999) and the human tumour cell-cycle model by Basse et al. (2003). Whereas the phase transition regulation method provides deep insight into the detailed biological mechanisms governing the cell-cycle process but there would be difficulties in expanding the model due to its complexity.

Optimisation of biological cell cultures using mathematical models has mainly been performed in bacterial or yeast cultures (Modak et al., 1986; Lim et al., 1986; Chen and Hwang, 1990) due to their simple nutrient requirement. Most of the objectives in model-based bacterial/yeast culture optimisation are feed rate profiles of nutrients (Modak et al., 1986; Lim et al., 1986; Park and Ramirez, 1988; San and Stephanopoulos, 1989; Chen and Hwang, 1990; Lee and Ramirez, 1994) which are variables that can take any continuous values. Mammalian cell cultures are by nature more complex than bacteria and yeast so their optimisation is often highly dependent on experiments. In the context of cell-cycle distribution which can be manipulated by addition of chemicals in a one-off manner, the incorporation of logic-type binary variable is an interesting and useful application to be explored. In the next sections, the development of a mathematical cell-cycle model for a hybridoma cell cultures and application on optimisation of both continuous and logic-type degrees of freedom is discussed and the model prediction is compared with experiment results.

3.2 Development of Cell-Cycle Model for Hybridoma CRL-1606

In this section, modelling and optimisation of a mammalian suspension cell culture based on first-principles and population balance for off-line optimisation of time-varying and logic-type degrees of freedom was carried out. The population in various phases of the cell-cycle (G_0/G_1 , S, G_2/M) was tracked in the model and the specific productivity of each sub-population was taken into account. Control of fed-batch biological cultures sometimes involve not only continuous variables such as nutrient supplementation rate but also logic-type variables such as, in cell-cycle, the growth-arrest time which has a binary irreversible property. The aim of this work is to develop a comprehensive cell-cycle model for a hybridoma culture producing monoclonal antibody and design a mathematical strategy to incorporate binary irreversible variables into the dynamic optimisation strategy. The ability to computationally optimise such system would save experimentation time since fewer combinations of the two types of degree of freedom are required to be tested in wet lab.

3.2.1 Model Structure

3.2.1.1 Development of Model Equations

The equations for cell growth, death, nutrient uptake, and major metabolism were modified from Kontoravdi et al. (2005), Jang and Barford (2000b), and Tatiraju et al. (1999). The model was further developed in this study to include description of cell-cycle sub-populations and the changes are detailed below. The cell-cycle representation was based on the yeast model of Uchiyama & Shioya (1999) and the tumour cell model of Basse *et al.* (2003) but adapted using first-principles to suit the replication rate of hybridoma cells which is dependent on more factors than yeast cells and slower than the tumour cells. Equations 3.2 – 3.5 express viable cell concentration (X_v) in terms of cells in G_0/G_1 , S, and G_2/M phases. The G_2 phase and M phase were treated as one group because they both have twice the DNA content of a non-growing cell making them undistinguishable from each other under common cell-cycle analysis methods with flow cytometry. As a simplification in notation, G_0/G_1 cells will be indicated as G_1 unless

otherwise stated. Detailed definition of all variables and parameters can be found in Section 3.2.6.

Cell culture volume:

$$\frac{dV}{dt} = F_{in} - F_{out} - F_{sam} \quad (3.1)$$

The effect of volume increase by addition of concentrated nutrients on the residual concentration of cells, nutrients, product, and byproducts was negligible in this hybridoma cell culture experiment. Thus, an approximation of volume independency was made in the mass balance equations of the concentration of cells, nutrients, product, and byproducts. But this assumption could not be made in Chapter 4 for the CHO-IFN γ fed-batch cell cultures as the feedback controller in those experiments could add significant volume of nutrients to the cell cultures. Sampling caused a negligible reduction in volume and did not disturb the concentration of substances.

Cell-Cycle & Cell Concentrations:

$$X_v = X_{G1} + X_s + X_{G2/M} \quad (3.2)$$

$$\frac{dX_{G1}}{dt} = 2b \cdot X_{G2/M} - k_1 \cdot X_{G1} - \mu_d \cdot X_{G1} - \left(\frac{F_{out}}{V}\right) \cdot X_{G1} \quad (3.3)$$

$$\frac{dX_s}{dt} = k_1 \cdot X_{G1} - k_2 \cdot X_s - \mu_d \cdot X_s - \left(\frac{F_{out}}{V}\right) \cdot X_s \quad (3.4)$$

$$\frac{dX_{G2/M}}{dt} = k_2 \cdot X_s - b \cdot X_{G2/M} - \mu_d \cdot X_{G2/M} - \left(\frac{F_{out}}{V}\right) \cdot X_{G2/M} \quad (3.5)$$

Assuming any possible cell lysis is negligible:

$$\frac{dX_d}{dt} = \mu_d \cdot X_v \quad (3.6)$$

$$X_l = X_v + X_d \quad (3.7)$$

Since $\frac{dX_v}{dt} = (\mu - \mu_d) \cdot X_v$, k_1 , k_2 , b can be expressed in terms of μ :

$$k_1 = \frac{2 - x_{G1}}{x_{G1}} \cdot \left(\mu + \frac{F_{out}}{V} \right) \quad (3.8)$$

$$k_2 = \frac{1 + x_{G2/M}}{x_s} \cdot \left(\mu + \frac{F_{out}}{V} \right) \quad (3.9)$$

$$b = \frac{1}{x_{G2/M}} \cdot \left(\mu + \frac{F_{out}}{V} \right) \quad (3.10)$$

where x_i is fraction of cells in cell-cycle phase i . x_i is related to the specific growth rate (Uchiyama & Shioya, 1999; Slater *et al.*, 1977) and are expressed as follow:

$$x_{G1} = 1 - \frac{(t_S + t_{G2/M}) \cdot \mu}{\log 2} - \theta_S - \theta_{G2/M} \quad (3.11)$$

$$x_S = \frac{t_S \cdot \mu}{\log 2} + \theta_S \quad (3.12)$$

$$x_{G2/M} = 1 - x_{G1} - x_S \quad (3.13)$$

where θ_i represents the fraction of cells in cell-cycle phase i when specific growth rate is zero; and t_S and $t_{G2/M}$ represent the time-length of the S phase and G₂+M phase respectively.

Antibody synthesis:

$$\frac{d[MAB]}{dt} = f(v) \cdot (Q_{MAB,G1} \cdot X_{G1} + Q_{MAB,S} \cdot X_S + Q_{MAB,G2/M} \cdot X_{G2/M}) - \left(\frac{F_{out}}{V}\right) \cdot [MAB] \quad (3.14)$$

$$\text{where } f(v) = \begin{cases} 0 & , v \geq v_{cr} \\ \frac{1}{1 + \frac{K_{MAB}}{v}} & , v < v_{cr} \end{cases} \quad (3.15)$$

$$\begin{aligned} Q_{MAB,G1} &= (y_1 \cdot Q_{MAB,G1,1} + y_2 \cdot Q_{MAB,G1,2}) \\ Q_{MAB,S} &= (y_1 \cdot Q_{MAB,S,1} + y_2 \cdot Q_{MAB,S,2}) \\ Q_{MAB,G2/M} &= (y_1 \cdot Q_{MAB,G2/M,1} + y_2 \cdot Q_{MAB,G2/M,2}) \end{aligned} \quad (3.16)$$

Equations 3.14 – 3.15 take into account the production of MAb by each cell-cycle phase. The introduction of viability, v , in the specific MAb productivity, Q_{MAB} , was based on the results of Glacken *et al.* (1988a) which demonstrated that cell culture productivity of hybridoma CRL-1606 was affected by low viability. It was also observed in our experiments that specific productivity decreased for this cell-line during death phase. The model has used binary variables, y_1 and y_2 , when parameter values are affected under cell-cycle arrest condition (Equation 3.16). This is further discussed in the cell-cycle arrest session below.

Glucose/lactate consumption/production:

$$Q_{glc} = \frac{\mu}{(y_1 \cdot Y_{x,glc,1} + y_2 \cdot Y_{x,glc,2})} \cdot \frac{[Glc]^2}{K_{Q_{glc}} + [Glc]^2} \quad (3.17)$$

$$Q_{lac} = Y_{maxlac,glc} \cdot Q_{glc} \frac{[Glc]}{K_{lac,glc} + [Glc]} \quad (3.18)$$

The specific glucose uptake rate, Q_{glc} , and specific lactate production rate, Q_{lac} , were modified from Kontoravdi *et al.* (2005) based on results of the test fed-batch culture showing both specific glucose consumption rate and lactate yield decreased when glucose reached a level much lower than that in batch cultures. Thus in Equation 3.17 – 3.18, Q_{glc} and Q_{lac} are proportional to glucose concentration.

Ammonium production:

$$Q_{amm} = Y_{amm,gln} \cdot Q_{gln} \quad (3.19)$$

The specific ammonium production rate, Q_{amm} , was proportional to the specific glutamine consumption rate, Q_{gln} .

Cell growth/death:

$$\mu = (y_1 \mu_{max1} + y_2 \mu_{max2}) \cdot \frac{[Glc]}{K_{glc} + [Glc]} \cdot \frac{[Gln]}{K_{gln} + [Gln]} \cdot \frac{K_{I,lac}}{K_{I,lac} + [Lac]} \cdot \frac{K_{I,amm}}{K_{I,amm} + [Amm]} \quad (3.20)$$

$$\mu_d = \frac{\mu_{d,max}}{1 + \left(\frac{(y_1 K_{d,amm1} + y_2 K_{d,amm2})}{[Amm]} \right)^n}, n > 1 \quad (3.21)$$

The model has used binary variables, y_1 and y_2 , when the parameter values are affected under cell-cycle arrest condition which is discussed in Equation 3.28 – 3.29.

Equation 20 uses multiplicative terms to represent the dependence of the specific growth rate on various substrates and by-products. This equation structure is commonly used to describe cell growth although growth itself is not a multi-order ‘reaction’ and the effects of by-product inhibition (from *Amm* and *Lac*) may not be fully independent from other variables in the growth kinetics. The biological details of growth inhibition by toxic by-products require further experimental investigation to identify, for example,

whether the inhibition mechanism is competitive or non-competitive and the possibility of a more mechanistic structure for the growth kinetics.

The equations for the specific glutamine consumption rate, Q_{gln} , and the mass balance equations for glucose, glutamine, lactate, and ammonium are the same as Kontoravdi et al. (2005):

$$\frac{d[Glc]}{dt} = -Q_{glc} \cdot X_v + \frac{F_{in}}{V} \cdot [Glc]_{in} - \frac{F_{out}}{V} \cdot [Glc] \quad (3.22)$$

$$\frac{d[Gln]}{dt} = -Q_{gln} \cdot X_v - K_{d,gln} \cdot [Gln] + \frac{F_{in}}{V} \cdot [Gln]_{in} - \frac{F_{out}}{V} \cdot [Gln] \quad (3.23)$$

$$\frac{d[Lac]}{dt} = Q_{lac} \cdot X_v - \frac{F_{out}}{V} \cdot [Lac] \quad (3.24)$$

$$\frac{d[Amm]}{dt} = Q_{amm} \cdot X_v + K_{d,gln} \cdot [Gln] - \frac{F_{out}}{V} \cdot [Amm] \quad (3.25)$$

$$Q_{gln} = \frac{\mu}{Y_{x,gln}} + m_{gln} \quad (3.26)$$

$$m_{gln} = \frac{a_1 \cdot [Gln]}{a_2 + [Gln]} \quad (3.27)$$

3.2.1.2 Cell-Cycle Arrest Simulation

Two binary variables were used to activate/inactivate parameters of which the values were affected by the cell-cycle arrest. In Equation 3.28 – 3.29, y_1 represents activation of parameters during normal condition and y_2 represents activation of parameters during arrested condition.

$$y_2 = \begin{cases} 0 & , t < t_a \\ 1 & , t \geq t_a \end{cases} \quad (3.28)$$

$$y_1 = 1 - y_2 \quad (3.29)$$

where t_a is the cell-cycle arrest time which can be any positive real value.

3.2.2 Materials and Methods

3.2.2.1 Batch and Fed-batch Cultures

The hybridoma CRL-1606 cell-line (ATCC) producing IgG1 monoclonal antibody (MAb) against human fibronectin was used. Batch cultures were inoculated with mid-exponential phase cells at $1.5\text{-}2.0 \times 10^5$ cell ml⁻¹ in 100 ml medium containing DMEM (GIBCO) supplemented with 25 mM glucose and 4 mM glutamine (GIBCO), 2.5% v/v Calf Bovine Serum (ATCC) and 1% v/v Penicillin-Streptomycin (10,000 units of penicillin and 10,000 µg of streptomycin per ml stock (GIBCO)). The shake-flask cultures were incubated at 37°C, 5% CO₂, 100% humidity, and 120 rpm. Samples were taken every 8 hrs. The batch culture started with 6 replicates and half of them were arrested with 0.5% v/v Dimethyl Sulfoxide (DMSO) (Wang *et al.*, 2004) of ≥99.7% pure sterile stock (Sigma) at 44 hrs. Fed-batch cultures were performed in triplicates with the same initial conditions as the batch cultures. In the test fed-batch culture, concentrated glutamine (Sigma) at 200 mM was added twice a day after the glutamine in the original culture was depleted. Fed-batch cultures for model validation were carried out following a computationally optimised feeding strategy and were arrested with 0.5% DMSO at certain time. Three different cell-cycle arrest times at 78 hrs, 96 hrs, and 126 hrs which gave similarly high yield in the simulations were tested in separate fed-batch cultures. The feed contained DMEM (GIBCO) with 200 mM glutamine (Sigma) and 500mM glucose (Sigma). All of the arrested fed-batch cultures were carried out in triplicates.

3.2.2.2 Cell Culture Analyses

Cell concentration and viability were determined with a Neubauer haemocytometer (Assistant) by employing the dye exclusion method with trypan-blue (Sigma, 0.4% w/v stock). The trypan-blue stock solution was diluted ten times in PBS (GIBCO) solution before use. Each suspension cell sample from cell culture flask was diluted 2 – 8 times with working solution of trypan blue and then one drop was put onto the haemocytometer with a glass slide. The number of cells was counted in five out of nine 1mm squares (four corners and centre) on the haemocytometer under a microscope

(Lica). The average number of cells per 1mm square corresponds to the amount of cells in every 10^{-4} ml.

Glucose, glutamine, lactate, and ammonium were detected using a BioProfile 200 analyser (Nova Biomedical) pre-calibrated with internal standards of different range of substrate/metabolite concentration. Cells were fixed with 50% v/v ethanol and stained with PBS (Gibco) solution containing 50 μ g/ml propidium-iodide of 1mg/ml stock (Sigma), 25 μ g/ml RNase Type I-A (Sigma) for cell-cycle analysis using an Epics Altra flow cytometer (Beckman Coulter). The flow cytometer was calibrated using Flow-Check fluorospheres (Beckman Coulter) and then the cell samples were measured at 605-615nm wavelength. The data were analyzed for cell-cycle distribution using Cylchred software (Cytonet UK). Antibody concentration was measured using an enzyme-linked immunosorbent assay (ELISA) modified from Kontoravdi (2007). Microplates (Corning) were coated with 100 μ l of 1 μ g/ml anti-human fibronectin antibody from rabbit (Sigma) in each well overnight at 4°C. After blocking non-specific binding with 250-300 μ l per well of 0.5% w/v casein (BDH), each well was incubated with 100 μ l of 0.2 μ g/ml human fibronectin (Chemicon) for 1 hour. The plates were then incubated with 100 μ l of diluted samples per well in triplicates and separately with 100 μ l per well of serial dilutions of the standard antibody anti-human fibronectin antibody from mouse (Sigma) in duplicates for 2 hours. This was followed by incubation with 100 μ l per well of 0.64 μ g/ml of anti-mouse Fc antibody from goat (Sigma) for 1 hour. Afterwards, 100 μ l per well of TMB (Sigma) solution with 0.2 μ l/ml of fresh 30% H₂O₂ (Sigma) was added and the reaction was stopped with 50 μ l of 2.5 M sulphuric acid (BDH) after 10-45 minutes. Absorbance was measured at 450 nm with an ELX 808 Ultra Microplate Reader (Bio-Tek Instruments Inc.). A detailed ELISA protocol is available in Appendix 1.

3.2.2.3 Parameter Estimation

The model was implemented in gPROMS ModelBuilder 3.0.3 (Process Systems Enterprise Ltd.). Model parameters were estimated using a general maximum likelihood approach in gPROMS mainly based on the normal and arrested batch culture data. Data from the test fed-batch culture were used to estimate the parameters for glucose consumption and lactate production as glucose dropped to a lower level in fed-batch cultures than batch cultures. The maintenance consumption of glucose was estimated using glucose consumption data in the death phase of fed-batch cultures.

The specific antibody productivities in the G_1 , S , and G_2/M phases were estimated based on the cell-cycle distribution analysis, the average specific antibody productivity, Q_{MAb} , measured from ELISA, and the viable cell concentration in the batch and test fed-batch cultures. The Q_{MAb} in the early exponential phase was found to be relatively lower than in the mid-exponential phase; and there was no significant change in Q_{MAb} in the early death phase but a reduction at low viability in mid- and late death phase. Since G_1 cells are more abundant than S and G_2/M cells in the early exponential phase — the opposite is true in the mid-exponential phase — G_1 cells are assumed to be less productive than S and G_2/M cells. This assumption is only applicable for the CRL-1606 cell culture tested in this work as the relationship between cell-cycle and productivity had been reported to be cell-line and promoter dependent (Al-Rubeai and Emery, 1990; Al-Rubeai et al., 1992; Lloyd et al., 1999). There were multiple solutions for the specific productivities of each cell-cycle phase as a result of the number of measured variables for antibody production being less than the number of the corresponding model parameters. Thus, the system was simplified by a further assumption based on the trend of cell-cycle related specific productivity reported in the literature that the specific product secretion rate is highest in G_2/M phase followed by S phase and G_1 phase (Lloyd et al., 1999; Lloyd et al., 2000). It is assumed that $Q_{MAb,G1}$ is twice smaller than $Q_{MAb,S}$; and $Q_{MAb,S}$ is the same as $Q_{MAb,G2/M}$.

The time-length of each cell-cycle phase was estimated based on the study of Volpe and Eremenko that most mammalian cells grown at 37°C have cell-cycle phases ranging in 6 – 9 h for S , 2 – 5 h for G_2 , 1 – 2 h for M , and 0 – 30⁺ h for G_1 (Volpe and Eremenko, 1973).

There are 13 differential equations ($V, G_I, S, G_2/M, X_V, X_d, MAb_{G_I}, MAb_S, MAb_{G_2M}, Glc, Gln, Lac, Amm$) and 26 parameters in the model, of which 7 parameters ($K_{d,amm}, \mu_{max}, Y_{x,glc}, Y_{x,gln}, Q_{MAb,G_I}, Q_{MAb,S}, Q_{MAb,G_2M}$) were affected by cell-cycle arrest. The values of those affected parameters were programmed to switch automatically in the model when the cell-cycle arresting chemical was introduced.

3.2.3 Productivity Optimisation

As a case study for product yield optimisation, the amount of feed, $F_{in}(t)$, and the cell-cycle arrest time, t_a , were varied while all other conditions, e.g. initial conditions, feed compositions, time intervals etc., were fixed. For practical purpose, the time interval was fixed to be a repeating cycle of 6 h \rightarrow 6 h \rightarrow 12 h. The objective was to maximize MAb yield by increasing the longevity and productivity of the cell culture. The model-based optimisation was done using a mixed-integer dynamic optimisation (MIDO) algorithm (Bansal *et al.*, 2003) implemented in gPROMS with a grid of different initial values for the two degrees of freedom concerned ($F_{in}(t)$ and t_a). Further discussion of the literature background of MIDO is available in Chapter 6. A total of 100 different combinations of initial conditions of $F_{in}(t)$ and t_a were analysed. The optimised profile of $F_{in}(t)$ and t_a with the highest antibody yield was selected for experimental validation. Two more fed-batch cultures were performed with the same optimised $F_{in}(t)$ but two different values of t_a to investigate if the model was able to predict the cell culture variations.

3.2.3.1 Model Transformation for Optimisation

In order to carry out simultaneous optimisation of t_a and $F_{in}(t)$, Equation 3.28 and t_a were transformed into Equation 3.30 – 3.33. The cell culture time was divided into sub-intervals and ω_i was a degree of freedom that can be either 0 (normal condition) or 1 (arrested condition) in each short time interval. Equation 3.31 – 3.33 translated the ‘decision’ of ω_i into a binary value for y_2 and this decision is irreversible from 0 to 1 when ω_i is set at 1 at anytime in the history of the cell culture.

$$\omega_1 = 0 \text{ or } 1 \quad (3.30)$$

$$\frac{d\omega_2}{dt} = M_\omega \omega_1 \quad (3.31)$$

$$\omega_3 = \frac{\omega_2}{(\delta + \omega_2)} \quad (3.32)$$

$$y_2 = \omega_3 \quad (3.33)$$

where $M_\omega \gg 1$, $\delta \ll 1$ such that Equation 3.32 would saturate rapidly once ω_1 was first set to 1. In the above optimisation, $\delta = 10^{-4}$, $M_\omega = 10^4$. A schematic diagram showing the role of the binary variable in the model simulation and optimisation is shown in Figure 3.2.

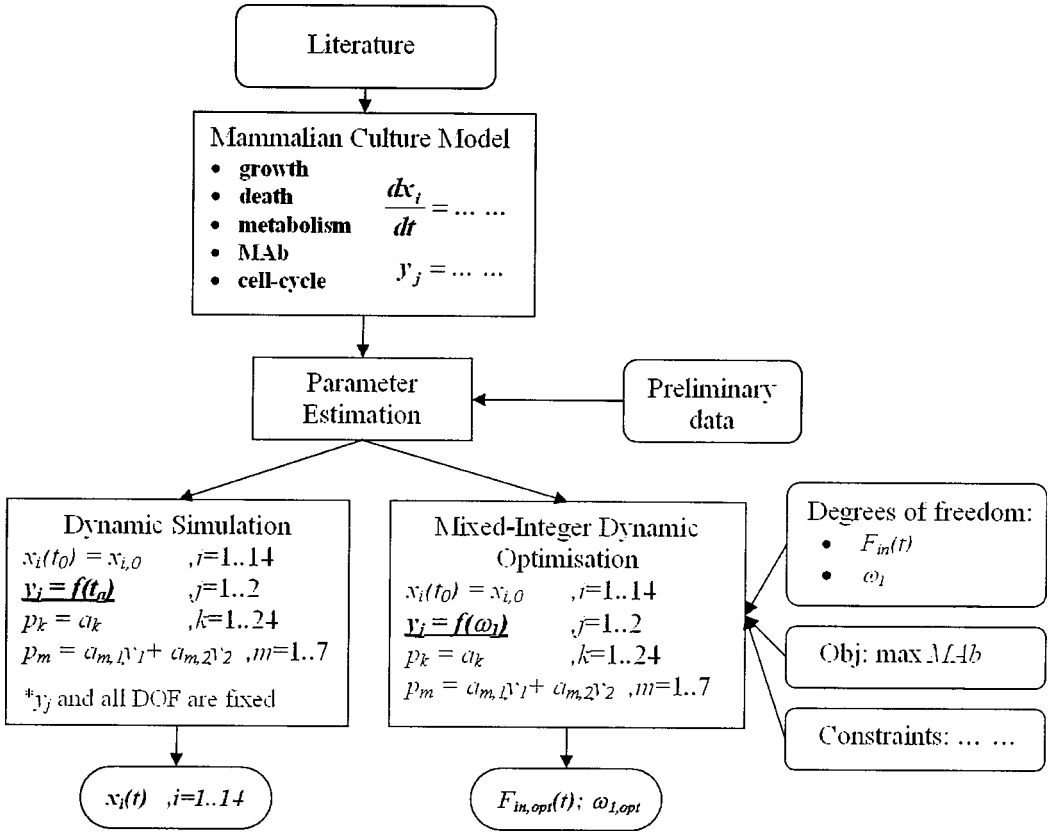


Figure 3.2: Schematic diagram of the proposed mixed-integer dynamic simulation and optimisation framework. The parameter values of the cell-cycle model with continuous and binary variables are estimated using experiment data. During dynamic simulation, the binary variables are dependent on the cell-cycle arrest time (t_a) which is fixed. In the mixed-integer dynamic optimisation (MIDO), the dependency of the binary variables is changed to a binary number ω_j which can be either 0 or 1 in any time interval. The first instance that ω_j becomes 1 will cause y_2 to switch from 0 to 1 and vice versa for y_1 permanently regardless of the subsequent values of ω_j in later time intervals. The optimised profile of $F_{in}(t)$ and cell-cycle arrest time with the highest MAb yield was tested by experiment.

3.2.4 Results & Discussion

3.2.4.1 Deviations in the Original Model

The main trends of the concentration of viable cell, monoclonal antibody, glucose, lactate, glutamine, ammonium and the distribution of cell-cycle in the batch and test fed-batch cultures were able to be simulated accurately by the model (Figure 3.3 – 3.10). However, there are significant deviations in the prediction for the optimised arrested fed-batch cultures which make it necessary to re-evaluate the original model structure. In the optimised arrested fed-batch cultures, the viable cell concentrations appeared to be significantly overpredicted (Figure 3.11) though the predicted antibody concentrations were close to the experiment data (Figure 3.12). For example, the viable cell concentration of the optimised fed-batch culture arrested at 96 h was over-predicted by up to about $1.2 \times 10^6 \text{ cell L}^{-1}$ in the death phase and the peak viable cell concentration was higher than the experimental result by $0.3 \times 10^6 \text{ cell L}^{-1}$. The over-prediction for the optimised fed-batch cultures arrested at 78 h and 126 h followed similar trends.

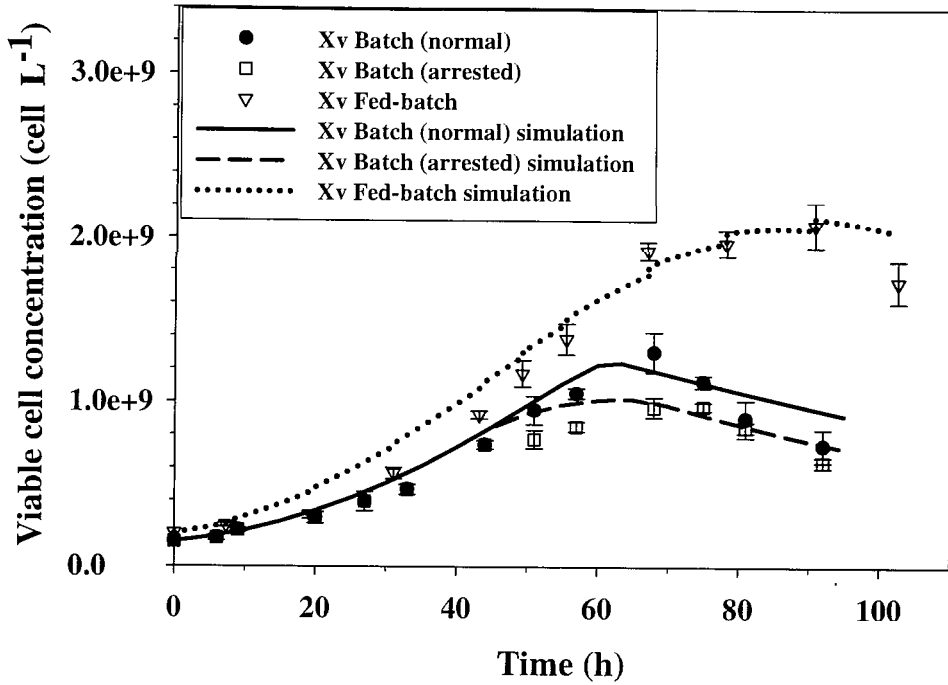


Figure 3.3: Viable cell concentration in **batch** and **test fed-batch** hybridoma cell cultures. Symbols represent experiment data and lines represent model simulation.

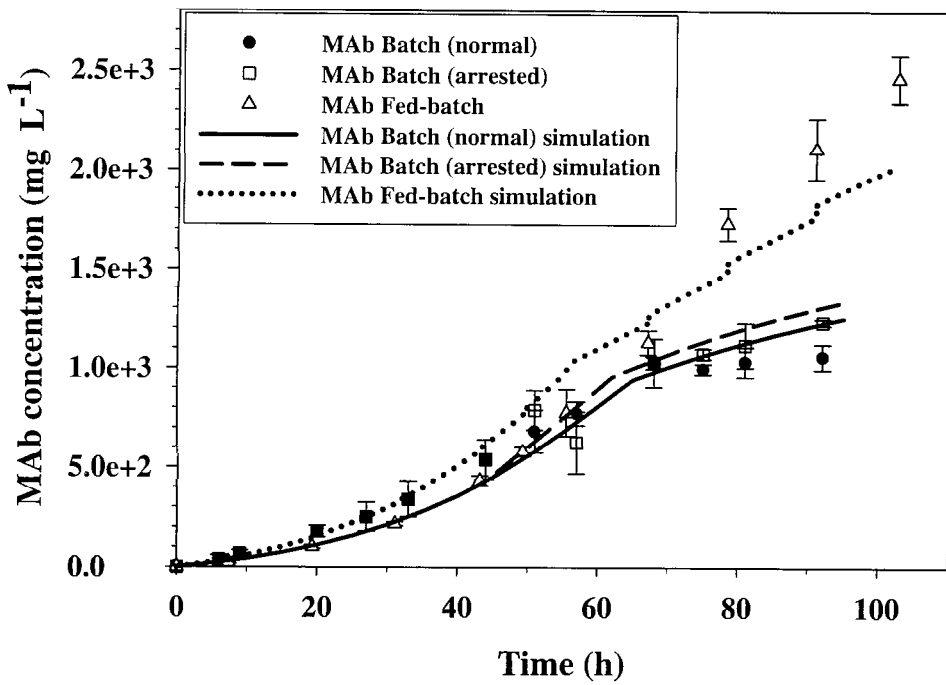


Figure 3.4: Monoclonal antibody (MAb) concentration in **batch** and **test fed-batch** hybridoma cell culture. Symbols represent experiment data and lines represent model simulation.

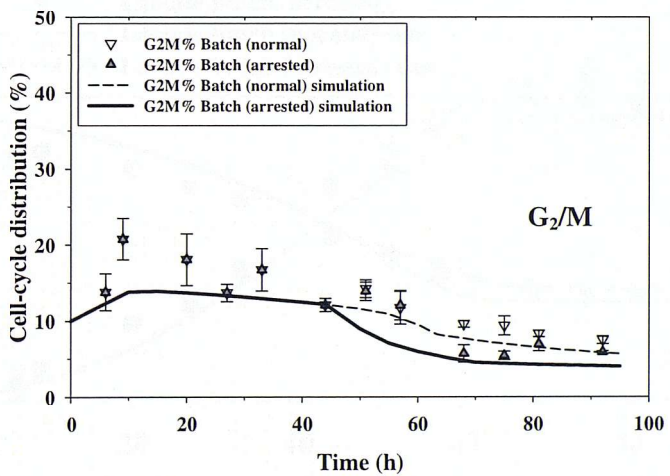
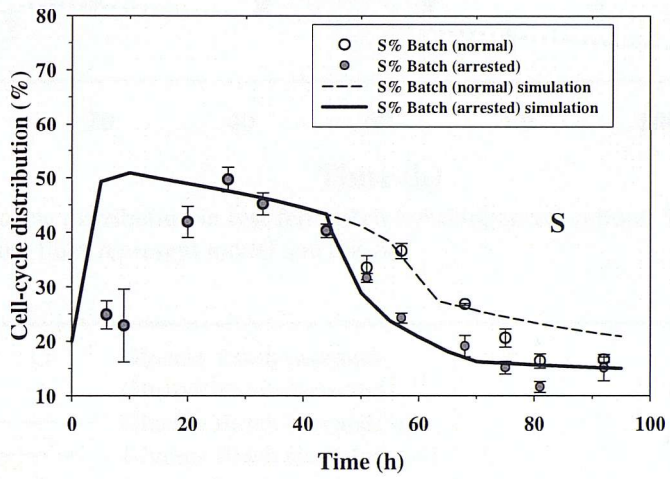
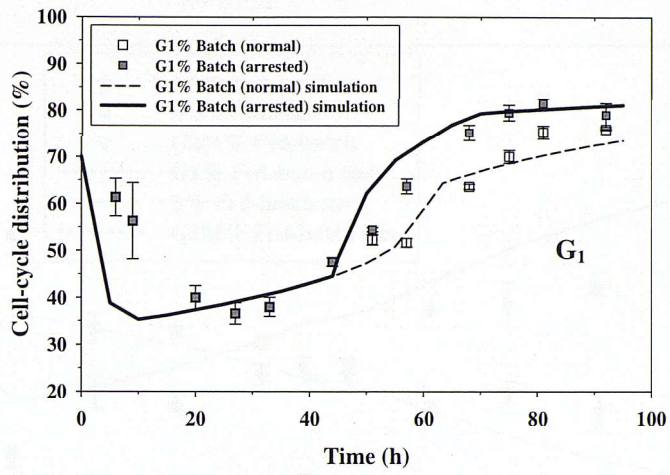


Figure 3.5: Cell-cycle distribution in **batch** hybridoma cell cultures. Symbols represent experiment data and lines represent model simulation.

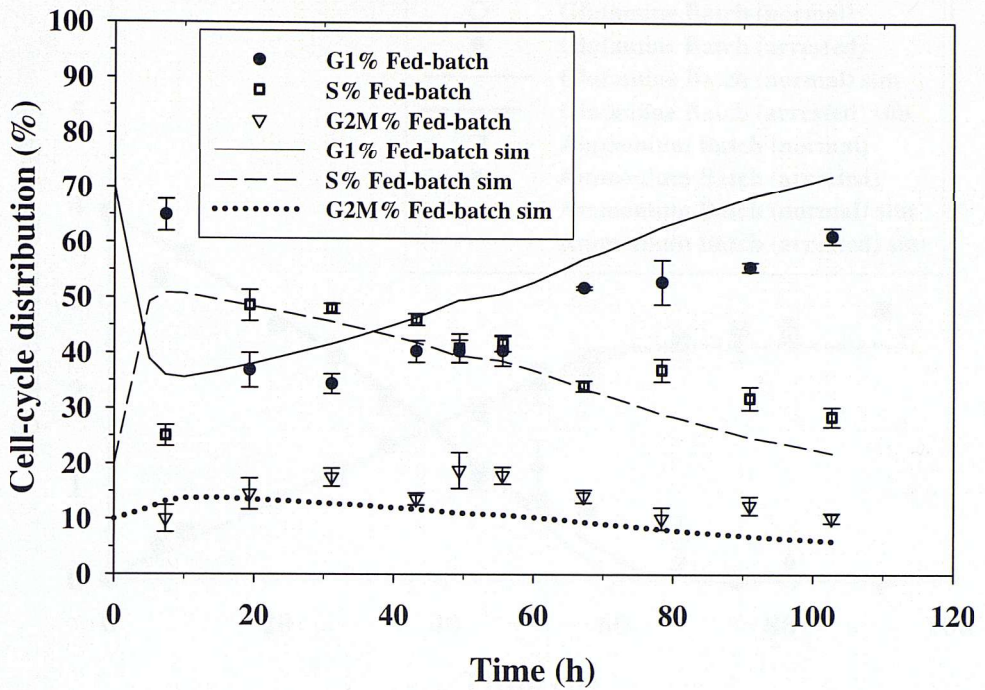


Figure 3.6: Cell-cycle distribution in **test fed-batch** hybridoma cell culture. Symbols represent experiment data and lines represent model simulation.

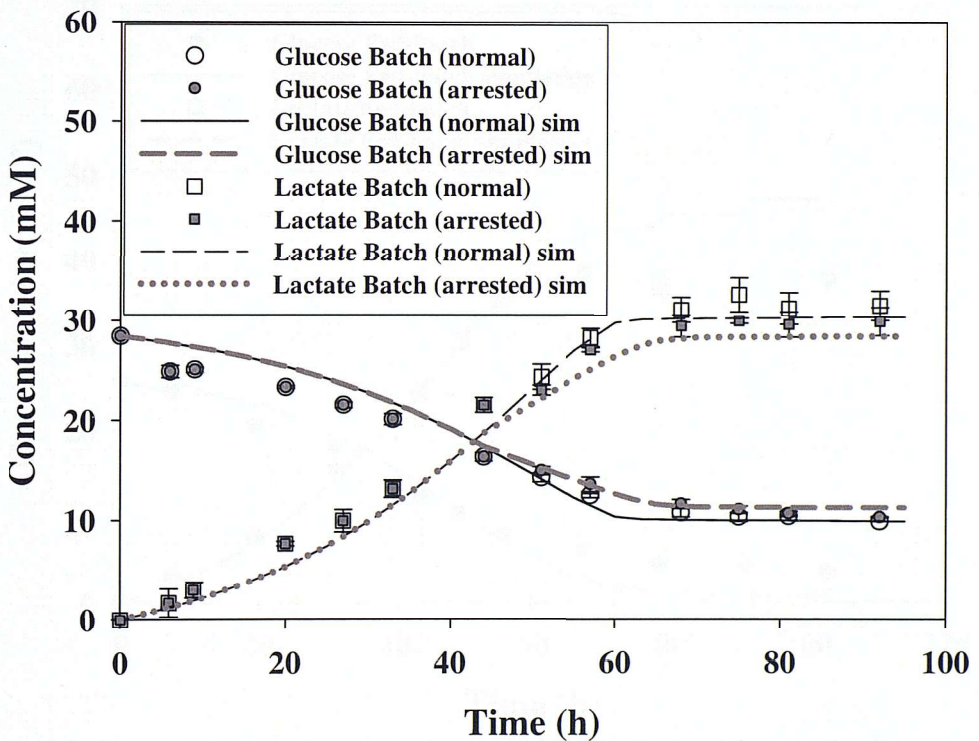


Figure 3.7: Glucose and lactate concentration in **batch** hybridoma cell cultures. Symbols represent experiment data and lines represent model simulation.

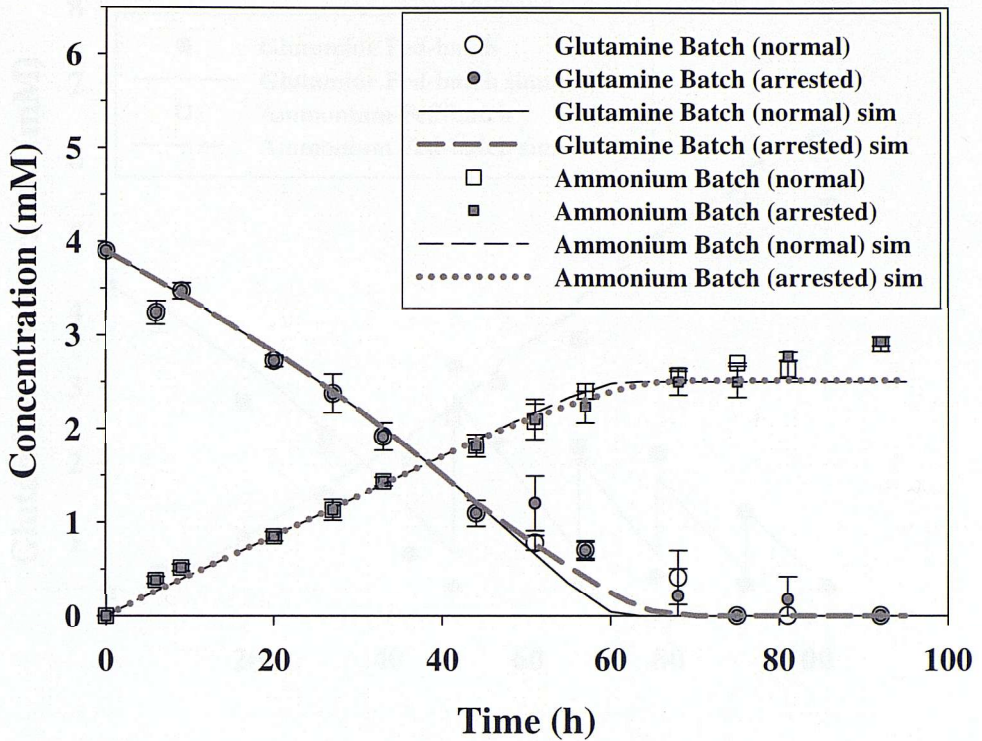


Figure 3.8: Glutamine and ammonium concentration in **batch** hybridoma cell cultures. Symbols represent experiment data and lines represent model simulation.

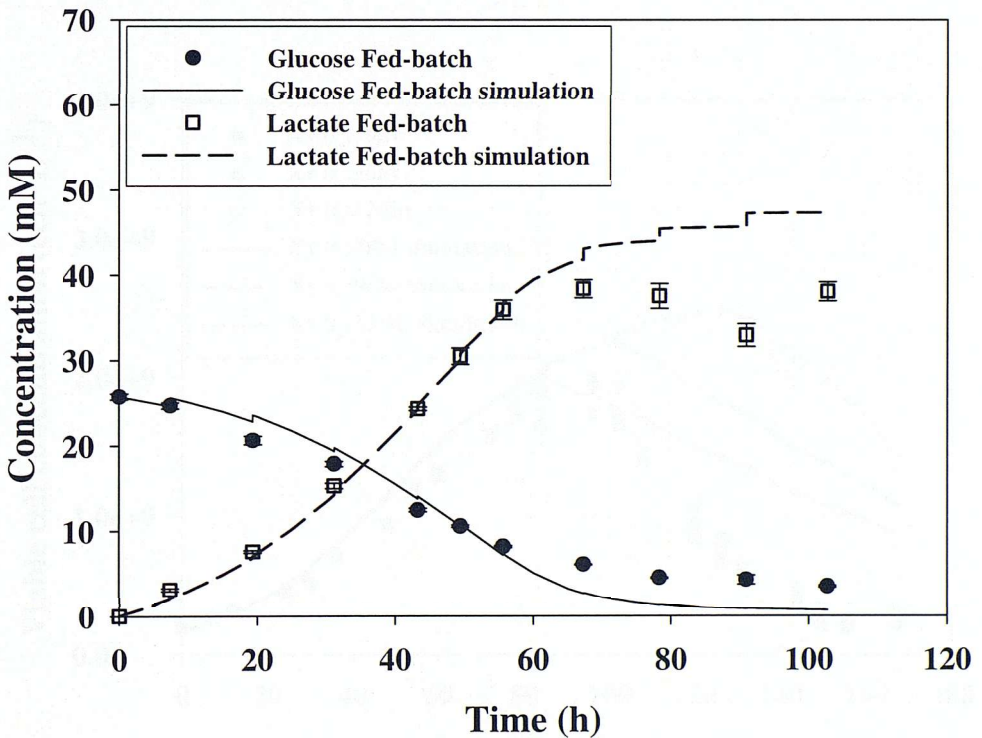


Figure 3.9: Glucose and lactate concentration in **test fed-batch** hybridoma cell culture. Symbols represent experiment data and lines represent model simulation.

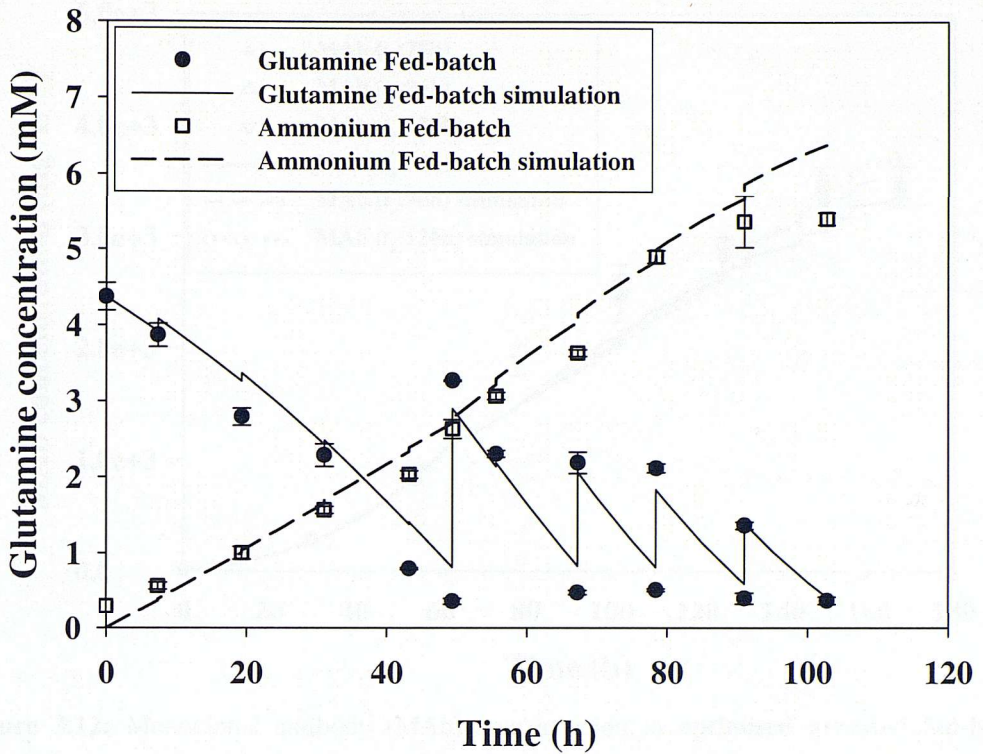


Figure 3.10: Glutamine and ammonium concentration in **test fed-batch** hybridoma cell culture. Symbols represent experiment data and lines represent model simulation.

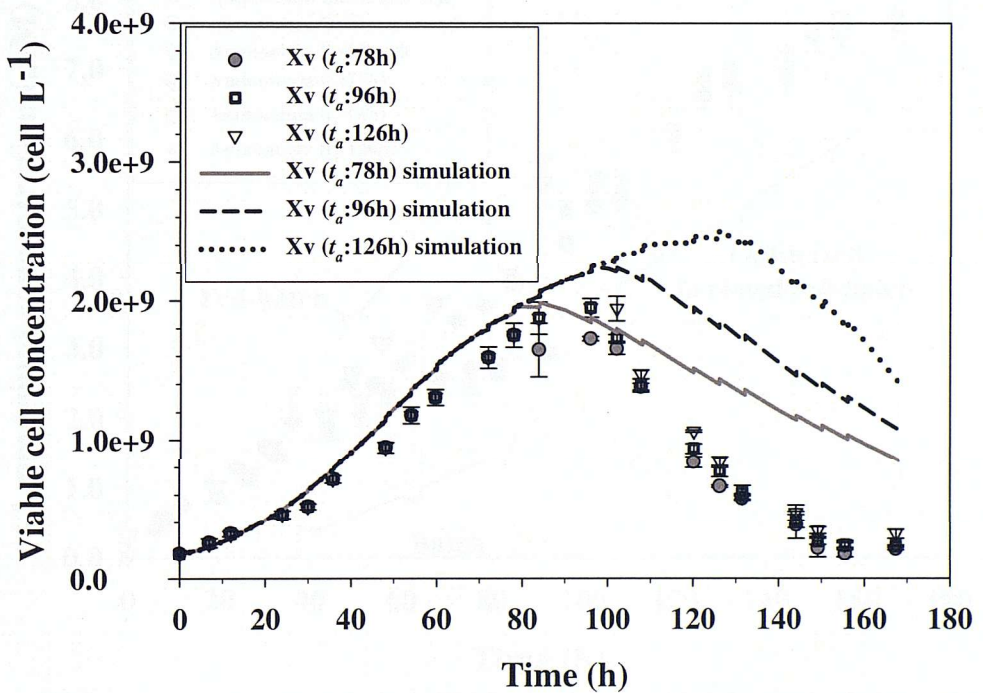


Figure 3.11: Viable cell concentration in **optimised arrested fed-batch** hybridoma cell culture showing 3 different cell-cycle-arrest time (t_a). Symbols represent experiment data and lines represent model simulation.

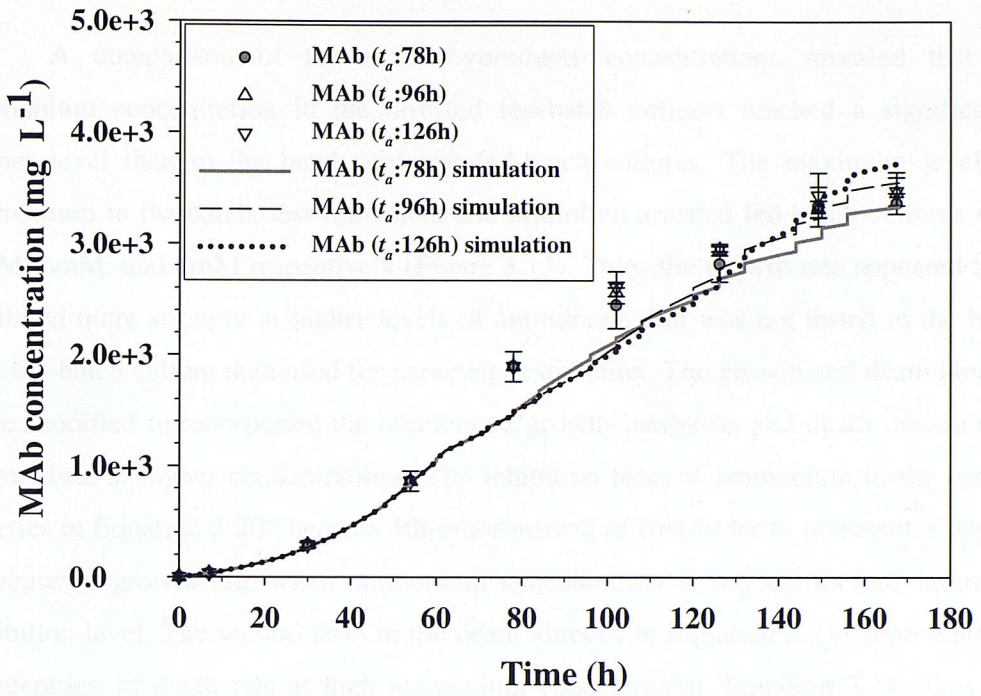


Figure 3.12: Monoclonal antibody (MAb) concentration in **optimised arrested fed-batch** hybridoma cell culture showing three different cell-cycle-arrest time (t_a). Symbols represent experiment data and lines represent model simulation.

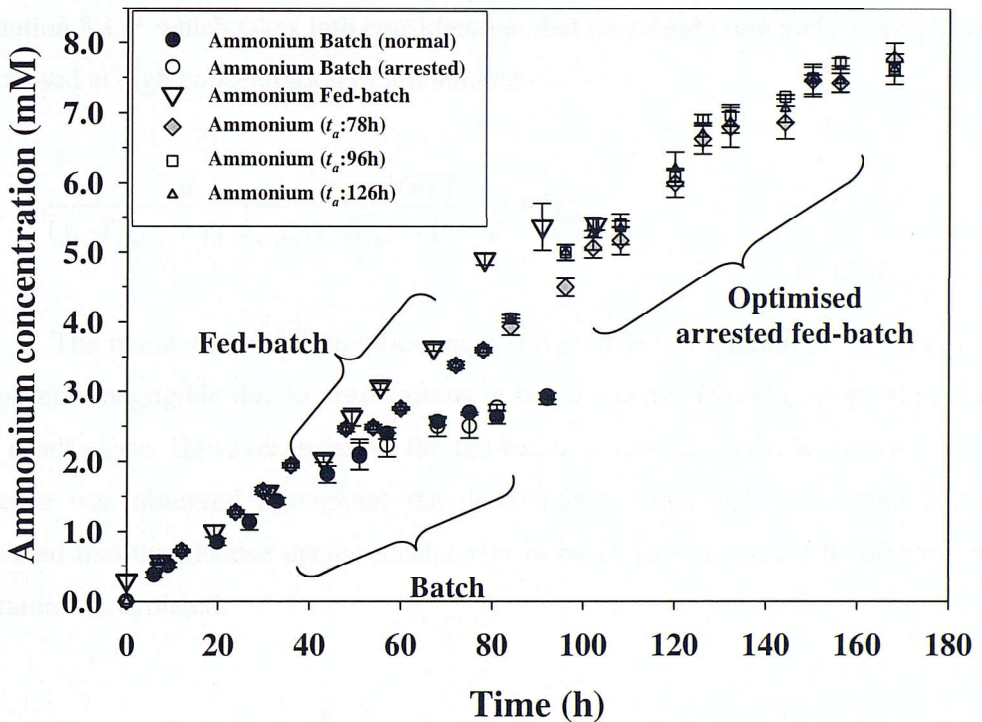


Figure 3.13: Ammonium concentration in **batch**, **test fed-batch**, and **optimised arrested fed-batch** hybridoma cell cultures.

A comparison of the toxic byproducts concentrations revealed that the ammonium concentration in the arrested fed-batch cultures reached a significantly higher level than in the batch and test fed-batch cultures. The maximum levels of ammonium in the batch, test fed-batch, and optimised arrested fed-batch cultures were 3mM, 6mM, and 8mM respectively (Figure 3.13). Thus, the growth rate appeared to be inhibited more strongly at higher levels of ammonium that was not tested in the batch and fed-batch culture data used for parameter estimation. The growth and death kinetics were modified to incorporate the accelerated growth inhibition and death initiation by ammonium at higher concentrations. The inhibition term of ammonium in the growth kinetics in Equation 3.20* became 4th-order instead of first-order to represent a sharper decrease in growth rate when ammonium concentration is beyond its half-saturation inhibition level. The second term in the death kinetics in Equation 3.21* represents the acceleration of death rate at high ammonium concentration. Equation 3.34 takes into account that the presence of glutamine could increase the cells' tolerance of ammonium, thus reducing death rate. The ammonium yield from glutamine was also found to be non-linear at high ammonium concentration and it is represented by the third term in Equation 3.19* which takes into consideration that the ammonium yield from glutamine decreased at high concentration of ammonium.

$$Q_{glc} = \frac{\mu}{(y_1 \cdot Y_{x,glc,1} + y_2 \cdot Y_{x,glc,2})} \cdot \frac{[Glc]^2}{K_{Q_{glc}}^2 + [Glc]^2} + m_{glc} \quad (3.17^*)$$

The maintenance consumption, m_{glc} , for glucose in Equation 3.17* was initially considered negligible due to observations in batch cultures that Q_{glc} dropped to zero in the death phase. However, in all of the fed-batch cultures a significant consumption of glucose was observed throughout the death phase. Thus m_{glc} is restored and it is assumed that the glucose uptake mechanism in batch cultures might be affected when glutamine is depleted.

$$Q_{amm} = Y_{amm,gln} \cdot Q_{gln} \cdot \frac{1}{1 + \left(\frac{[Amm]}{K_{rev,amm}} \right)^2} \quad (3.19^*)$$

$$\mu = (y_1 \mu_{max1} + y_2 \mu_{max2}) \cdot \frac{[Glc]}{K_{glc} + [Glc]} \cdot \frac{[Gln]}{K_{gln} + [Gln]} \cdot \frac{K_{l,lac}}{K_{l,lac} + [Lac]} \cdot \frac{K_{l,amm}^4}{K_{l,amm}^4 + [Amm]^4} \quad (3.20^*)$$

$$\mu_d = \frac{\mu_{d \max}}{1 + \left(\frac{(y_1 K_{d,amm1} + y_2 K_{d,amm2}) \cdot f(Gln)}{[Amm]} \right)^n} \cdot \left(1 + \frac{1}{1 + \left(\frac{K'_{d,amm}}{[Amm]} \right)^m} \right) \quad , n, m > 1 \quad (3.21^*)$$

$$\text{where } f(Gln) = 1 + \frac{1}{1 + \left(\frac{K_{inh,gln}}{[Gln]} \right)^2} \quad (3.34)$$

The new model has 31 parameters due to 5 new parameters being introduced: m_{glc} (Equation 3.17*), $K_{rev,amm}$ (Equation 3.19*), $K'_{d,amm}$ (Equation 3.21*), m (Equation 3.21*), and $K_{inh,gln}$ (Equation 3.34).

Because of changes in part of the equations in the model, the values of 8 parameters from the old model were affected: $K_{l,amm}$ (Equation 3.20*), $Y_{x,gln}$ in normal and arrested culture (Equation 3.26), α_1 (Equation 3.27), α_2 (Equation 3.27), n (Equation 3.21*), $K_{d,amm}$ (Equation 3.21*), and K_{glc} (Equation 3.20*). All the parameter values can be found in Table 3.2 at the end of Section 3.2.4.

3.2.4.2 Results of the Adjusted Model

3.2.4.2.1 Growth and Cell-Cycle Distribution

The new simulation results for cell concentrations in batch and test fed-batch cultures are shown in Figure 3.14. The simulated viable cell concentrations in the batch cultures were well predicted as the original model (Figure 3.3) though there was a mild under-prediction of the peak viable cell concentration of the test fed-batch culture by 0.2×10^6 cell L⁻¹ (Figure 3.14). The monoclonal antibody (MAB) concentrations of the batch and test fed-batch cultures in Figure 3.15 also followed the experiment data. The higher simulated MAB concentration in the batch cultures in Figure 3.15 than in Figure 3.4 was resulted from a slightly higher simulated viable cell concentration using the new model. The new cell-cycle distribution for batch cultures in Figure 3.17 was very similar to Figure 3.5. But in Figure 3.18, the predicted cell-cycle distribution of the G_1 and S phase in the test fed-batch culture was significantly different from the experiment data. Investigation into the original model predictions revealed that the old total cell concentration for test fed-batch culture was significantly overpredicted (Figure 3.19). Thus, the original apparent simulation success in the cell-cycle distribution of the test-

fed-batch culture in Figure 3.6 was caused by an over-prediction in the growth rate. Traditionally, the dead cell concentration was considered to be less important than the viable cell concentration because most cell culture models assume dead cells to be non-productive which means their concentration would not affect the predicted productivity. With the correct prediction of total cell concentrations using the new model, the simulated G_1 phase relative population was over-predicted and the S phase relative population was under-predicted in the test fed-batch culture between 50 – 100 h with a deviation of 10 – 20% (Figure 3.18); and in the optimised arrested fed-batch cultures such deviation was between 70 – 170 h (Figure 3.20). The G_2/M phase relative population remained at 10 – 20% throughout all fed-batch cultures. The cell-cycle distribution data of the optimised arrested fed-batch cultures did not show significant differences among various cell-cycle arrest time (t_a) which was also reflected in the simulation (Figure 3.20).

The cell-cycle distribution in the batch cultures showed a dynamic variation in the G_1 and S phase relative population throughout the whole cell culture time (Figure 3.17). The G_2/M phase relative population was more stable in between 10 – 20% before and during exponential phase and then dropped to 5 – 10% during death phase. The introduction of 0.5% DMSO at 44 h to arrest the batch culture resulted in an increase in G_1 phase relative population by roughly 10% and a corresponding decrease in S phase by a similar extent. The G_2/M phase data did not show significant difference between the normal and arrested culture though the simulation results showed a slight reduction of the G_2/M phase relative population in the arrested culture by about 2%. There appeared to be a lag of about 10 h between the data and model prediction at the early culture time particularly for G_1 and S phases.

As mentioned above, the cell-cycle equations in the adjusted model with correct total cell concentration predictions were not able to predict the higher percentage of cells in the S phase and lower percentage in the G_1 phase after mid-exponential phase of all the fed-batch cultures (Figure 3.18 & 3.20). About 10 – 20% more cells appeared to remain in the S phase in the fed-batch cultures during death phase than in the batch cultures (Figure 3.17, 3.18, 3.20). Current knowledge about the dynamic variation of mammalian cell-cycles in the literature is very limited. There might be a change in the time-length of the cell-cycle in the late-exponential and death phase of the fed-batch cultures due to growth inhibition by lactate/ammonium. The time lag between the cell-

cycle data and simulation results in the first 10 h of the cell culture time indicated the presence of an adaptation period right after inoculation. This can be addressed in the model by introducing a time delay in the cell-cycle equations.

3.2.4.2.2 Metabolism

The adjusted model followed the changes in glutamine and ammonium concentrations in all of the batch and fed-batch cultures (Figure 3.27 – 3.30). The glucose concentration is also well simulated (Figure 3.23 – 3.25) but the measured lactate concentration in the optimised arrested fed-batch cultures was unexpectedly low (Figure 3.26). It was surprising that the lactate concentration in the optimised arrested fed-batch cultures did not increase beyond 35 mM despite ongoing consumption of glucose in all of the 9 shake-flask cultures performed. Lactate production in mammalian fed-batch cultures had been reported to level-off despite continuous glucose consumption (Zhou et al., 1997a) or in some cases a transient net consumption was observed (Zhou et al., 1997b). The metabolic pattern of lactate production may have changed at the later stage of the fed-batch cultures. The deviation in the prediction of lactate concentration did not have a significant effect on the prediction of viable cell concentration and productivity because lactate has a much lower impact on the growth kinetics than ammonium. As the viable cell concentration is dependent on the levels of nutrients and byproducts, it is encouraging that most of them were properly simulated by the model.

3.2.4.2.3 Antibody Productivity

The average specific antibody productivities, Q_{MAb} , of the batch and test fed-batch cultures are shown in Figure 3.16. The mean Q_{MAb} data of the arrested batch culture after cell-cycle arrest at 44 h was higher than that of the normal batch culture in 4 out of 6 analyzed time points, so the arrested culture had higher productivity than the normal culture. The Q_{MAb} of the test fed-batch culture at 7 h was significantly lower than that between 20 – 40 h (Figure 3.16). As the G_1 phase was more dominant in the early few hours of cell culture time than in 20 – 40 h (Figure 3.18), the experiment data indicated a relatively higher specific productivity in the S or G_2/M phase than the G_1 phase. The corresponding Q_{MAb} of the batch cultures were inconclusive about the relative specific productivity between the early exponential phase and mid-exponential phase due to a higher measurement uncertainty. The batch and fed-batch cultures in this study had identical initial medium compositions and similar inoculum density. Thus, their specific antibody productivity, Q_{MAb} , should be the same in the early hours of the cell culture before any disruption by DMSO at 44 h or later on the addition of nutrients. During the death phase, the mean Q_{MAb} of the batch cultures appeared to drop though that of the test fed-batch culture did not decrease significantly (Figure 3.16). The simulation captured the relative trend of Q_{MAb} with a two-fold reduction in the death phase when viability was low and a higher specific productivity when the cells were arrested.

Various cell-cycle phases had been reported to have the highest antibody production rate, depending on the cell-lines studied (Ho, 2007; Cherlet et al., 1995; Al-Rubeai and Emery, 1990; Lloyd et al., 1999; Lloyd et al., 2000). Kromenaker and Srienc studied several AFP hybridoma cell-lines and suggested there was a net accumulation of antibodies in G_1 phase but a net secretion in G_2+M phase (1991; 1994a; 1994b). Lloyd et al. (2000) showed the specific productivity of four different mammalian cell-lines had the same trend that specific productivity increased from G_1 to S and to G_2/M . The simulation results of antibody concentration, MAb , with an assumption of the relative values of $Q_{MAb,G1}$, $Q_{MAb,S}$, and $Q_{MAb,G2/M}$ discussed in the Modelling section was able to follow the different MAb yields in the batch and fed-batch cultures. In terms of growth phase dependency of specific productivity, i.e. whether Q_{MAb} is higher in the growth phase or death phase, it had been shown to be cell-

line dependent (Al-Rubeai et al., 1992). The hybridoma cell-line used in this study appeared to be less productive in the death phase.

The MAb yield in the optimised arrested fed-batch cultures reached about 3.5 g L^{-1} as compared to about 2.5 g L^{-1} in the initial fed-batch culture and approximately 1.3 g L^{-1} in the arrested batch cultures (Figure 3.15 & 3.22). The arrested batch culture achieved a higher MAb concentration than batch culture and this is reflected in the simulation with the adjusted model although the simulated values are slightly higher than the data by $0.2\text{-}0.3 \text{ g L}^{-1}$ towards the end of culture time (Figure 3.15). The MAb yield from the test fed-batch culture was approximately twice the amount in the batch cultures. The MAb concentration in the optimised arrested fed-batch cultures reached 3.4 g L^{-1} ($\pm 0.2 \text{ g L}^{-1}$) with no significant differences among the cultures arrested at different times (Figure 3.22). The simulation result was able to capture this trend with a negligible decrease in the predicted MAb yield when the cell-cycle arrest time (t_a) increased from 78 h to 126 h.

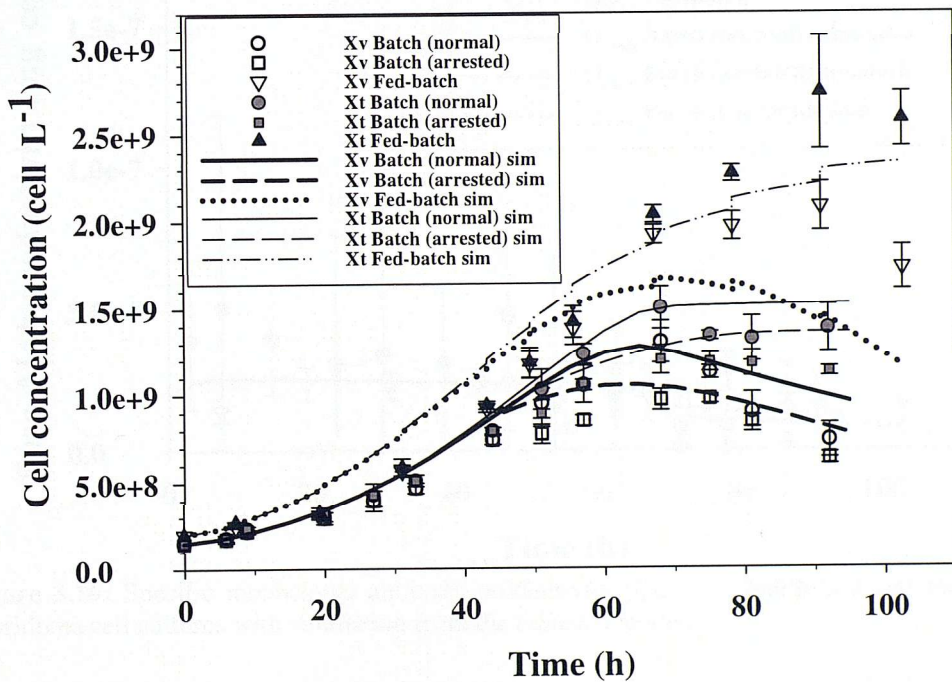


Figure 3.14: Viable and total cell concentration in **batch** and **test fed-batch** hybridoma cell cultures with simulation from the *adjusted model*.

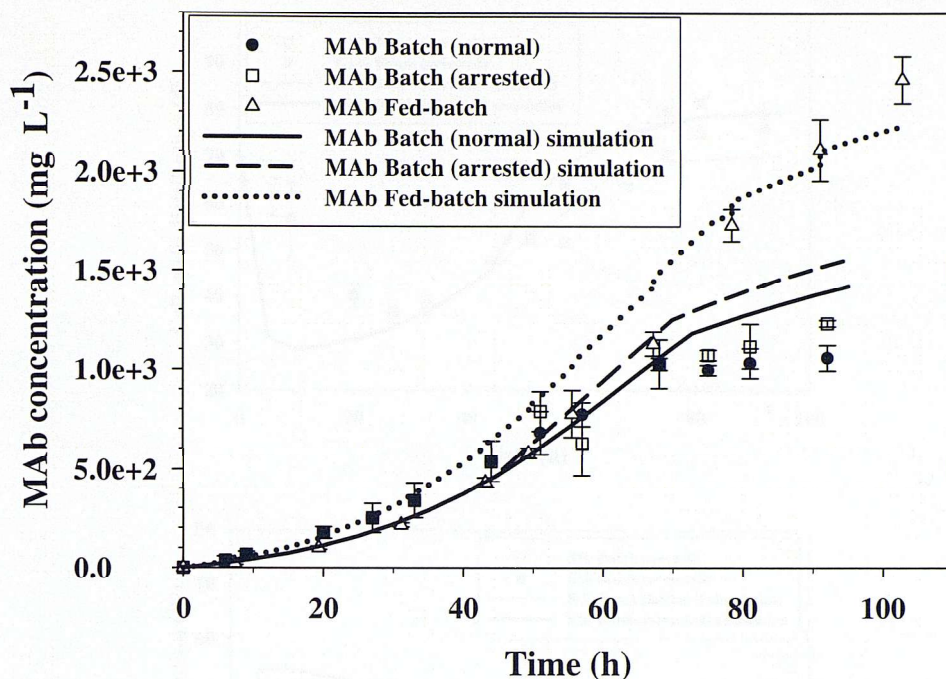


Figure 3.15: Monoclonal antibody (MAB) concentration in **batch** and **test fed-batch** hybridoma cell cultures with simulation from the *adjusted model*.

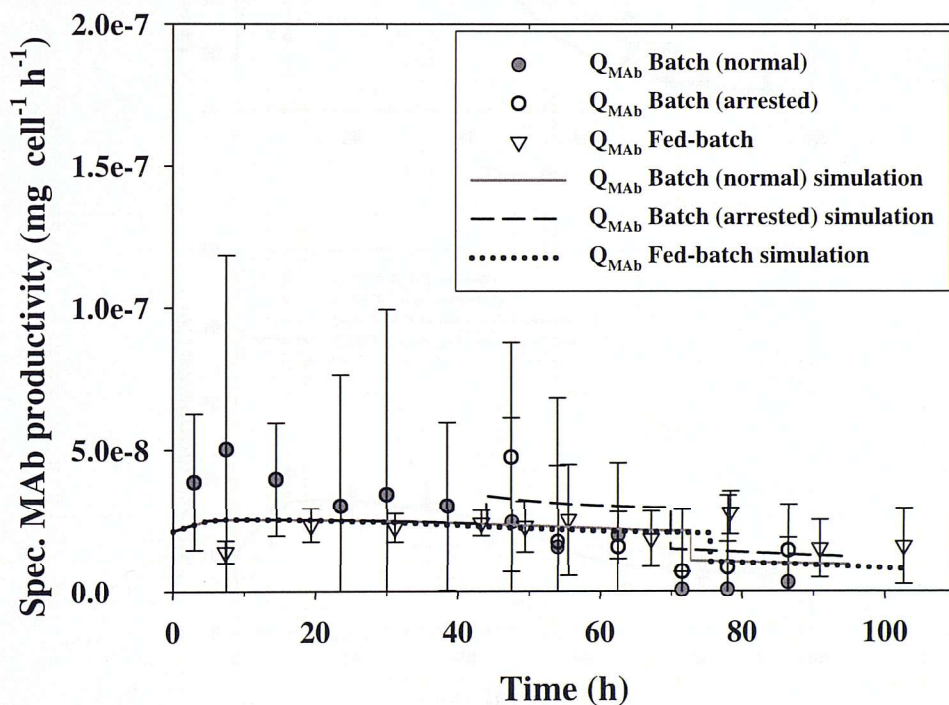


Figure 3.16: Specific monoclonal antibody productivity (Q_{MAB}) in **batch** and **test fed-batch** hybridoma cell cultures with simulation from the *adjusted model*.

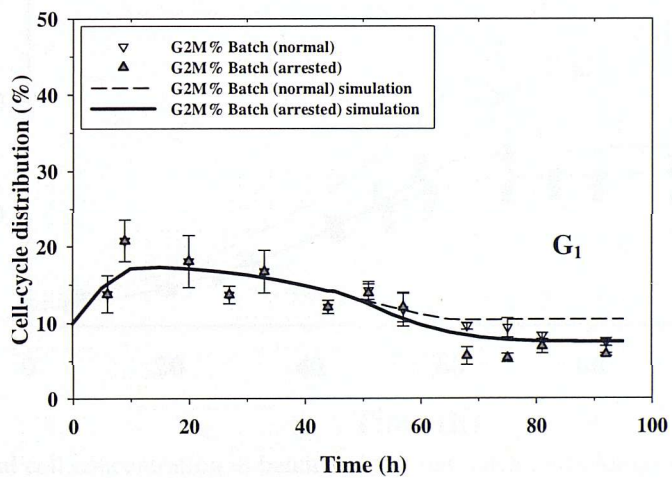
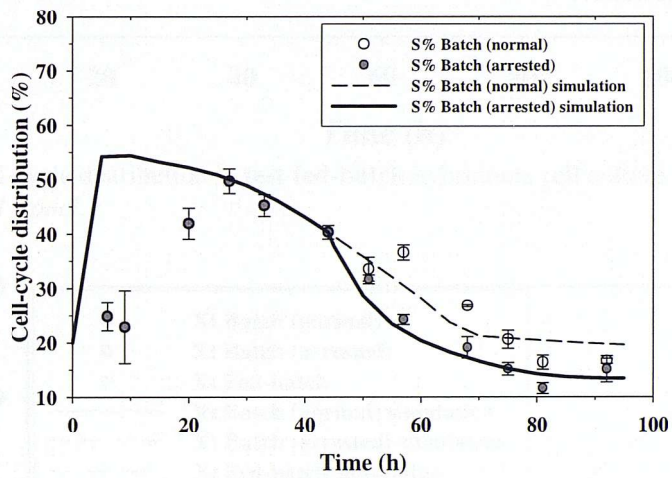
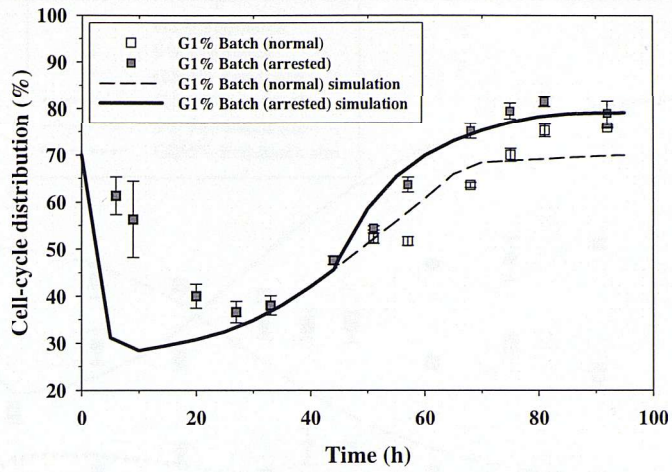


Figure 3.17: Cell-cycle distribution in **batch** hybridoma cell cultures with simulation from the *adjusted model*.

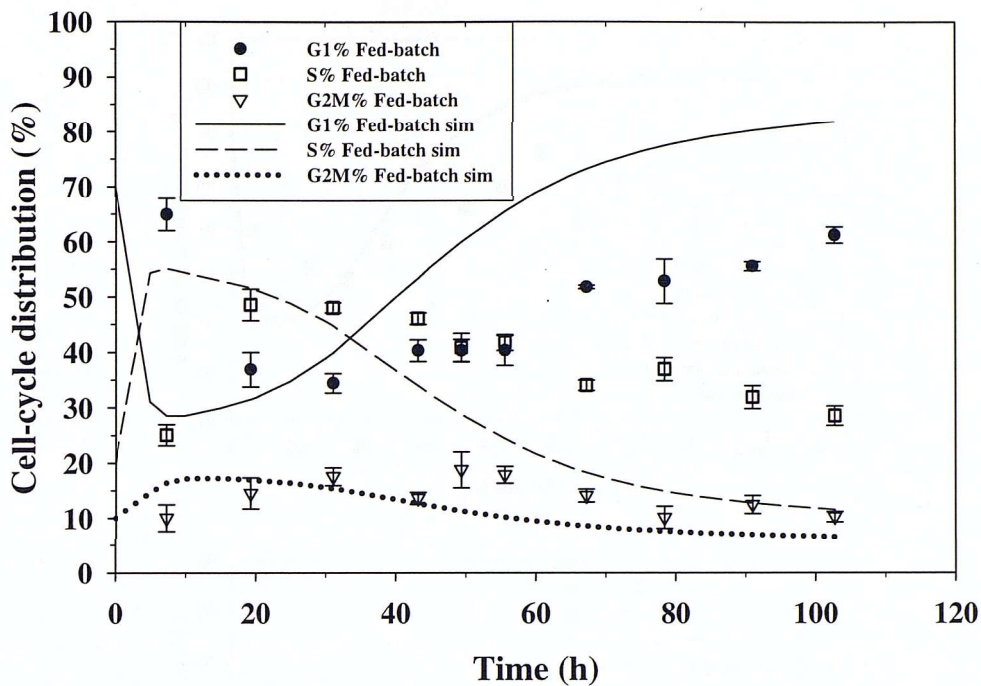


Figure 3.18: Cell-cycle distribution in test fed-batch hybridoma cell culture with simulation from the *adjusted model*.

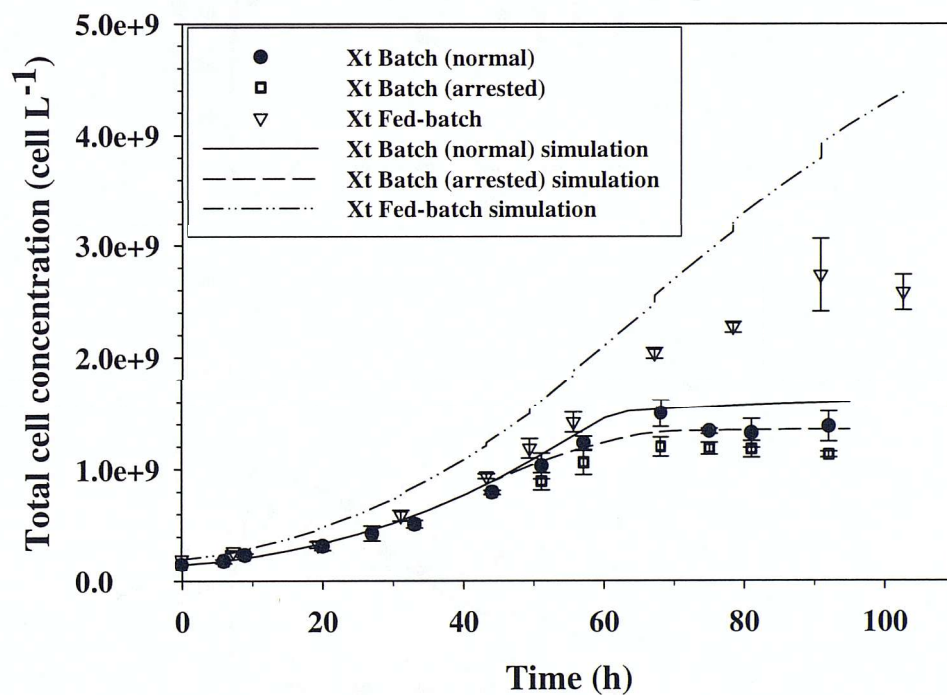


Figure 3.19: Total cell concentration in batch and test fed-batch hybridoma cell cultures using simulation from the *old model*. There was overprediction in the test fed-batch culture although the cell-cycle simulation in Figure 3.4.

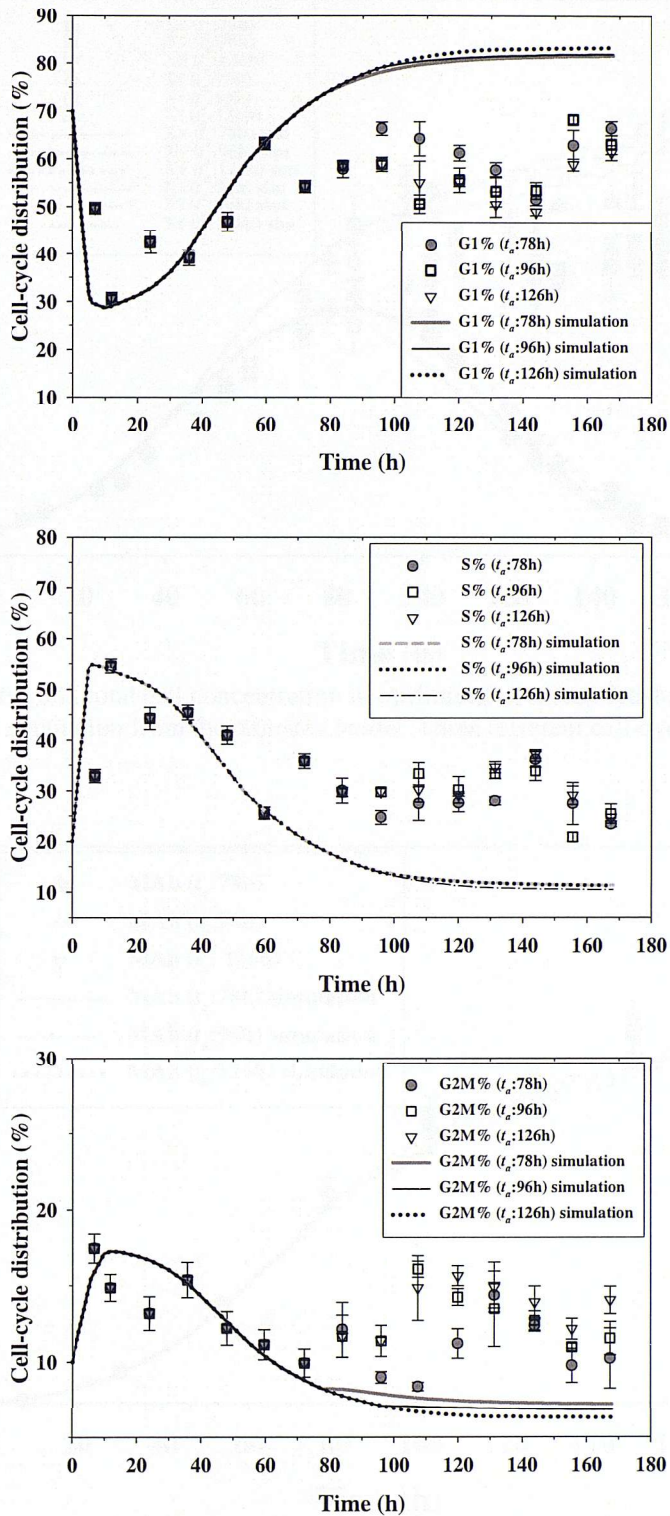


Figure 3.20: Cell-cycle distribution in **optimised arrested fed-batch** hybridoma cell with simulation from the *adjusted model*. Three different cell-cycle-arrest time (t_a) are illustrated.

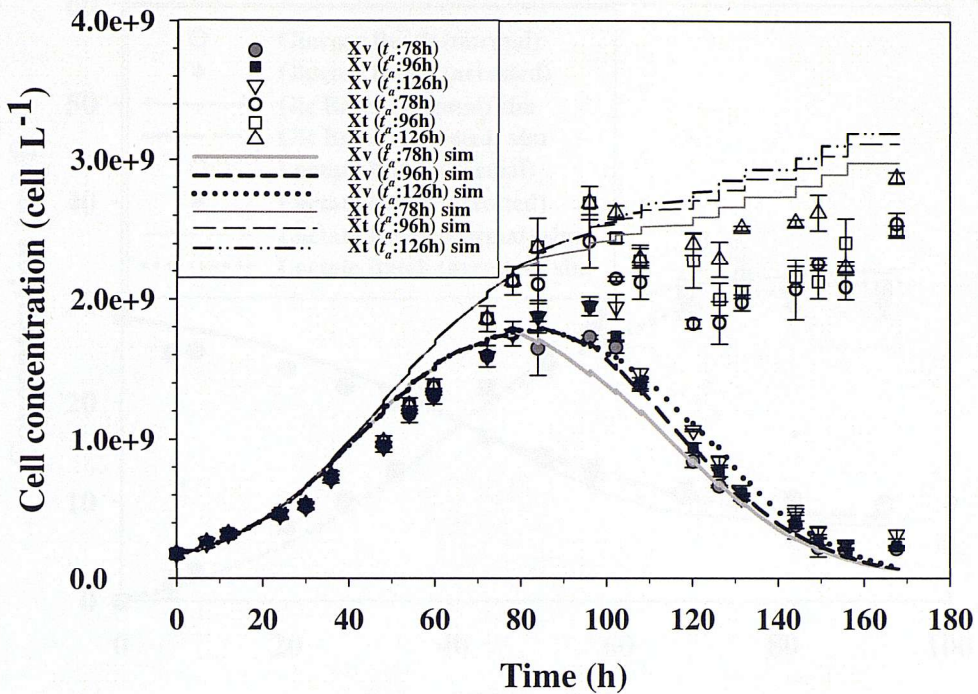


Figure 3.21: Viable and total cell concentration in **optimised arrested fed-batch** hybridoma cell cultures with simulation from the *adjusted model*. Three different cell-cycle-arrest time (t_a) are illustrated.

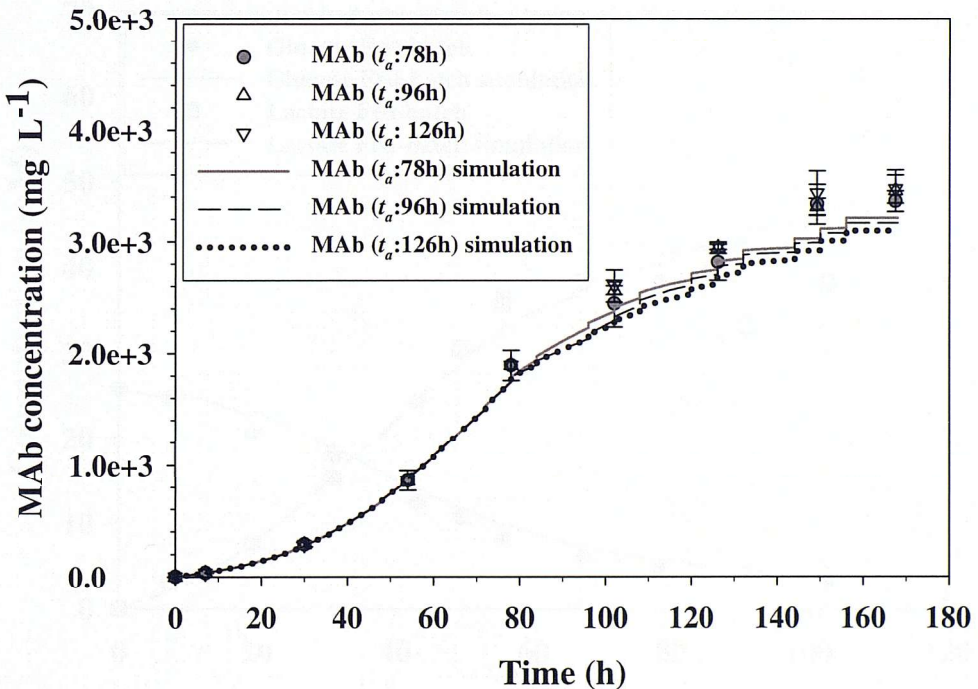


Figure 3.22: Monoclonal antibody (MAb) concentration in **optimised arrested fed-batch** hybridoma cell cultures with simulation from the *adjusted model*. Three different cell-cycle-arrest time (t_a) are illustrated.

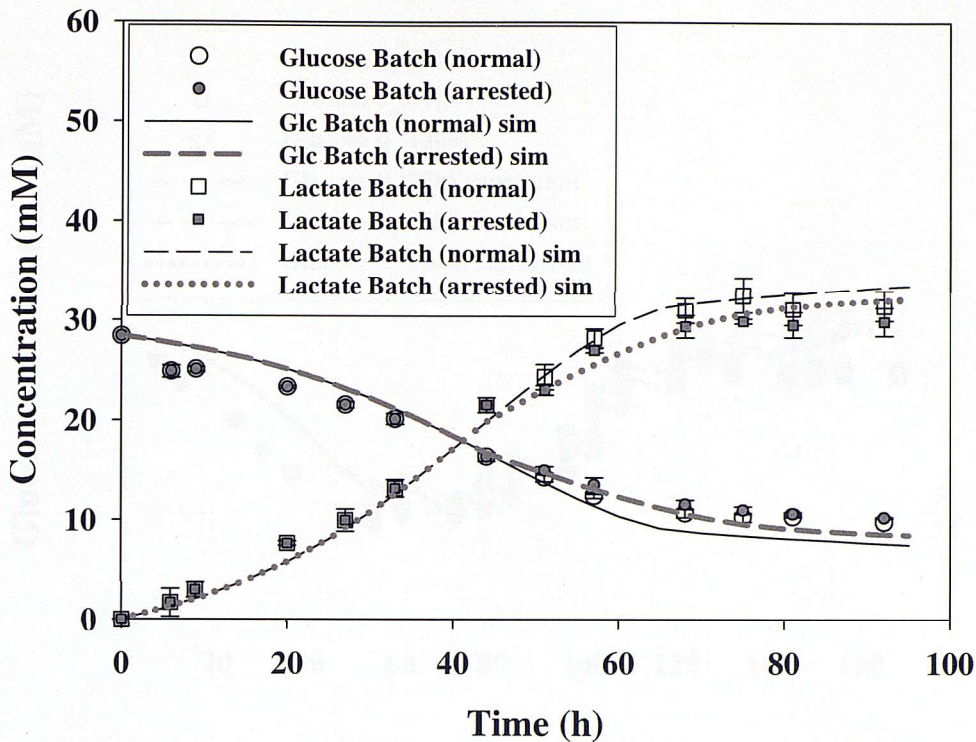


Figure 3.23: Glucose and lactate concentration in **batch** hybridoma cell cultures with simulation from the *adjusted model*.

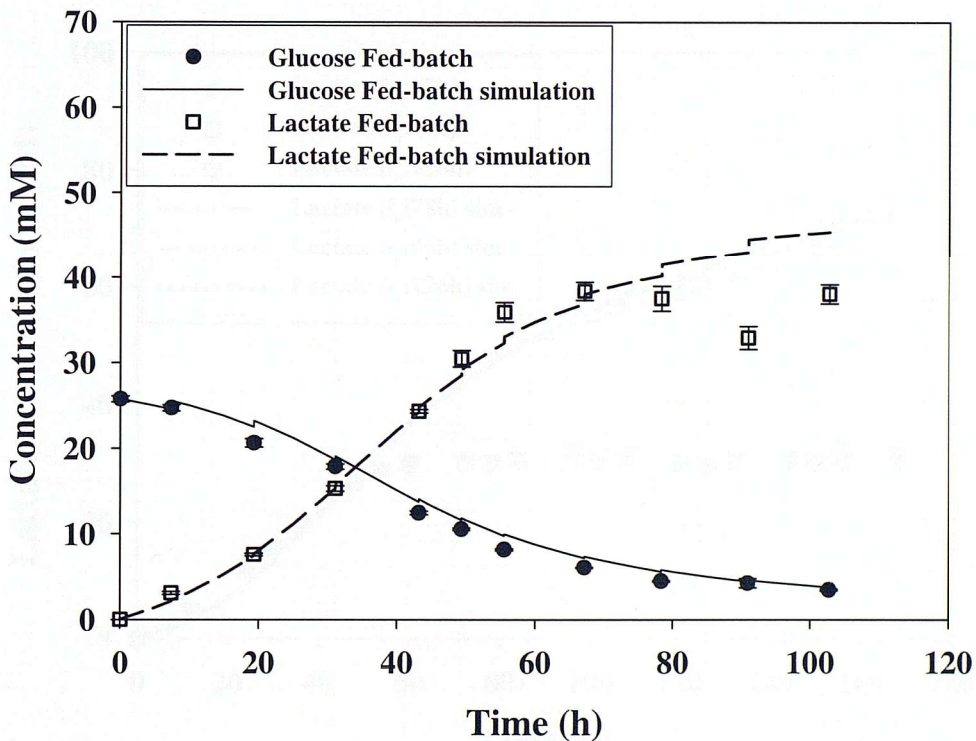


Figure 3.24: Glucose and lactate concentration in **test fed-batch** hybridoma cell culture with simulation from the *adjusted model*.

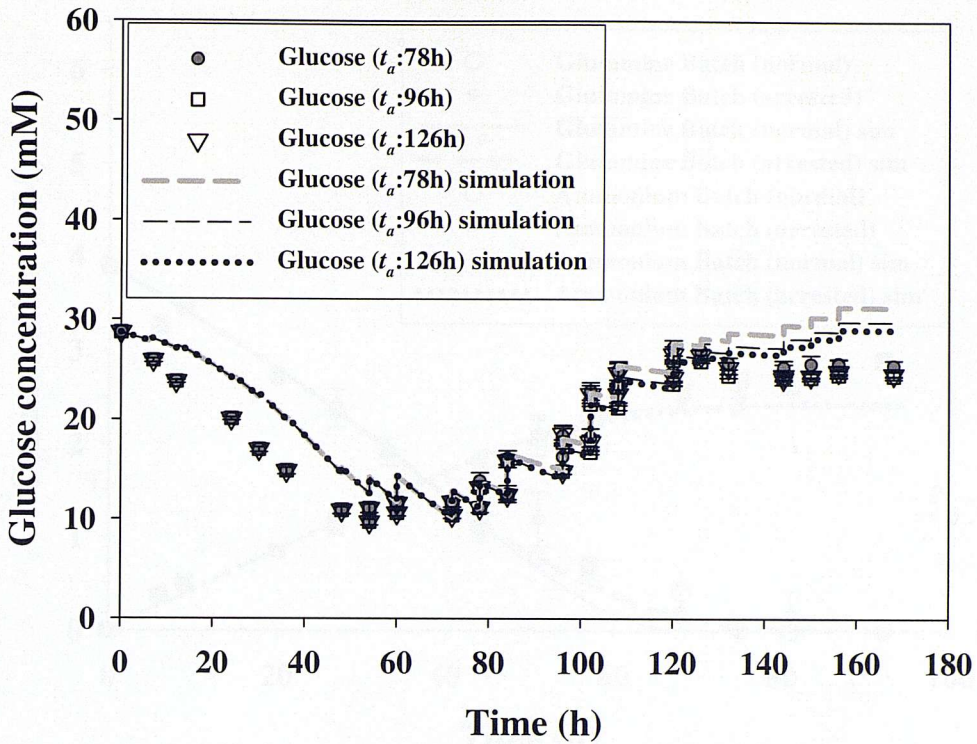


Figure 3.25: Glucose concentration in **optimised arrested fed-batch** hybridoma cell cultures with simulation from the *adjusted model*. Three different cell-cycle-arrest time (t_a) are illustrated.

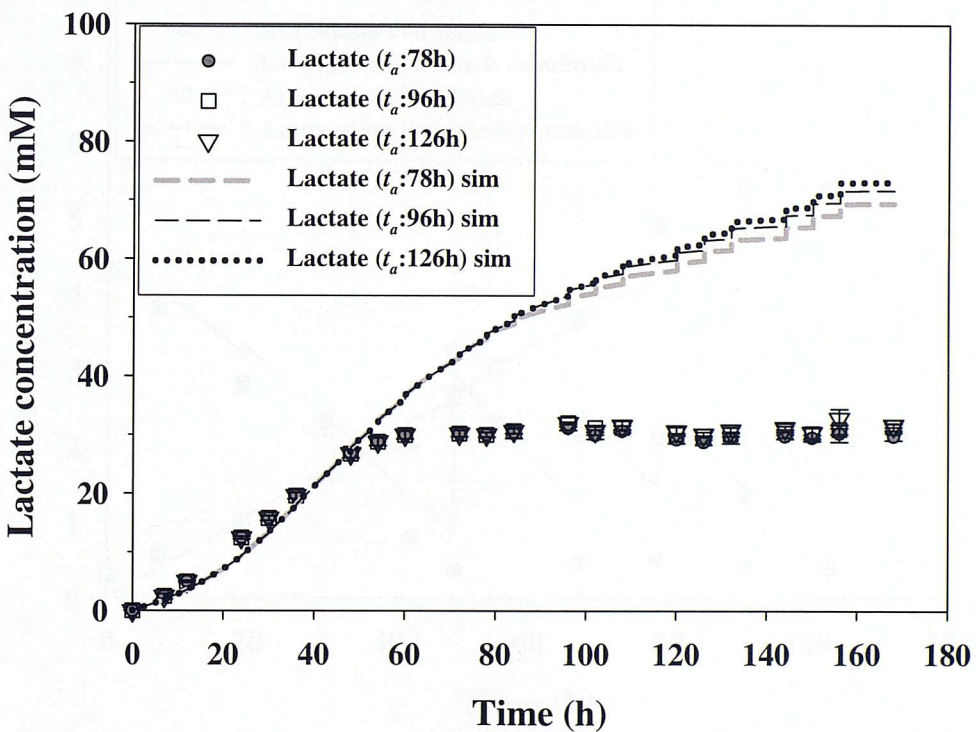


Figure 3.26: Lactate concentration in **optimised arrested fed-batch** hybridoma cell cultures with simulation from the *adjusted model*. Three different cell-cycle-arrest time (t_a) are illustrated.

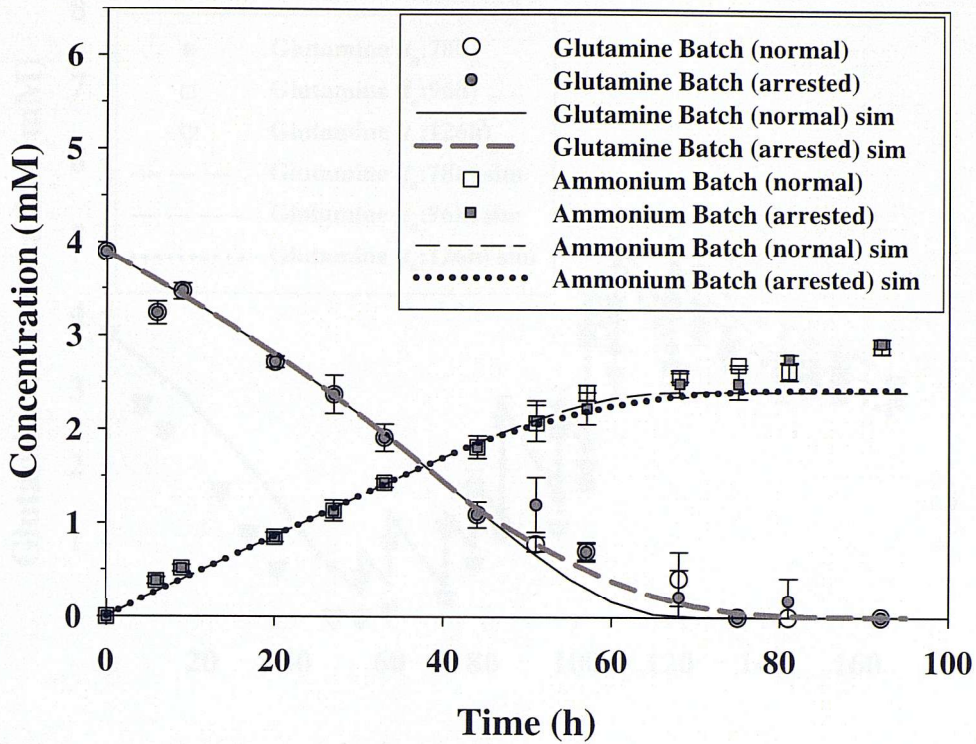


Figure 3.27: Glutamine and ammonium concentration in **batch** hybridoma cell cultures with simulation from the *adjusted model*.

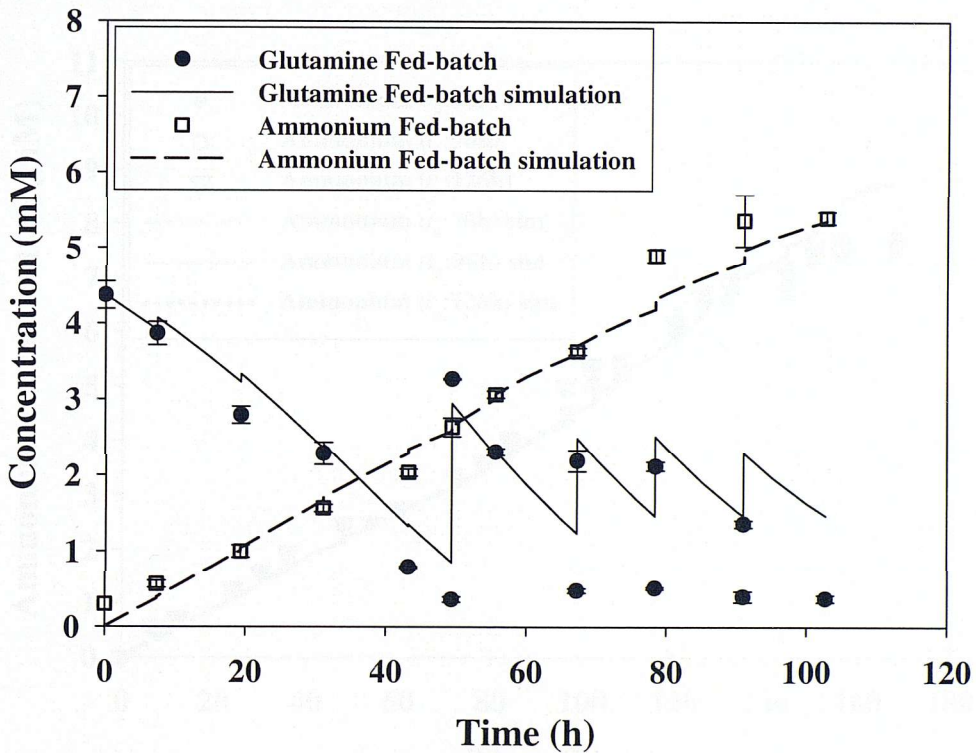


Figure 3.28: Glutamine and ammonium concentration in **test fed-batch** hybridoma cell cultures with simulation from the *adjusted model*.

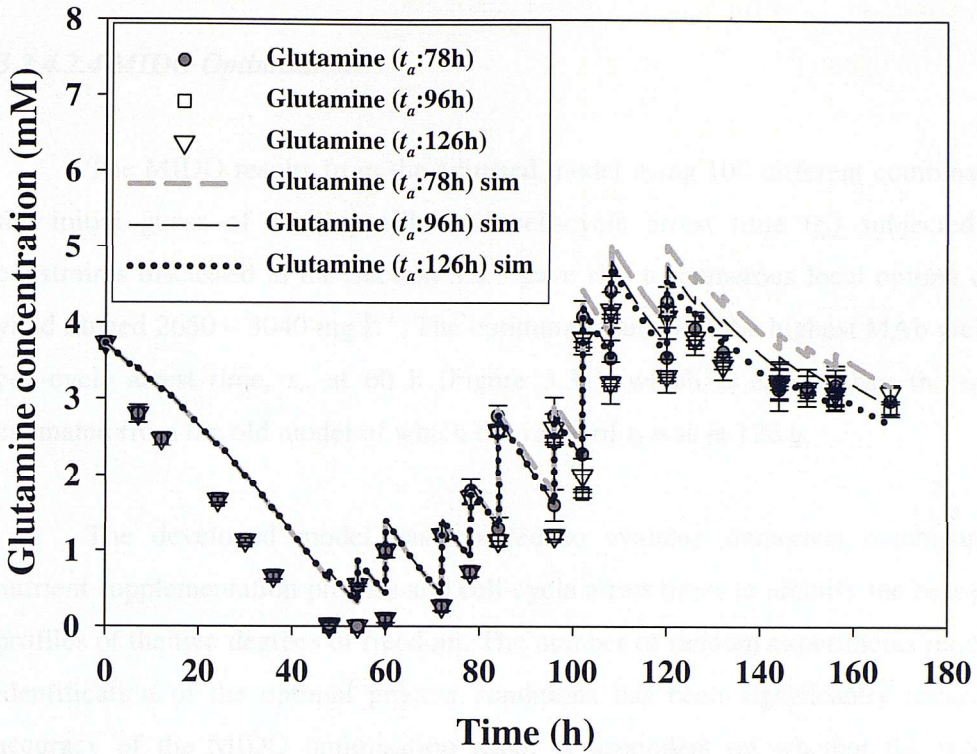


Figure 3.29: Glutamine concentration in **optimised arrested fed-batch** hybridoma cell cultures with simulation from the *adjusted model*. Three different cell-cycle-arrest time (t_a) are illustrated.

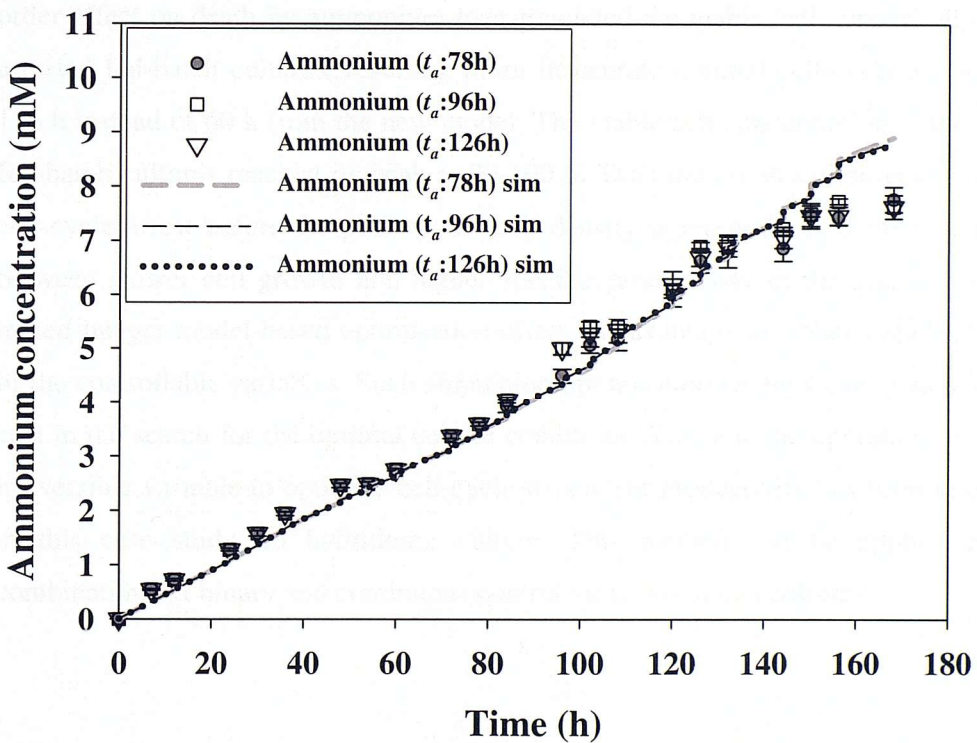


Figure 3.30: Ammonium concentration in **optimised arrested fed-batch** hybridoma cell cultures with simulation from the *adjusted model*. Three different cell-cycle-arrest time (t_a) are illustrated.

3.2.4.2.4 MIDO Optimisation

The MIDO results from the adjusted model using 100 different combinations of the initial guess of $F_{in}(t)$ profile and cell-cycle arrest time (t_a) subjected to the constraints discussed in the Section 3.2.3 gave rise to numerous local optima of MAb yield ranged 2650 – 3040 mg L⁻¹. The optimum result with the highest MAb yield had a cell-cycle arrest time, t_a , at 60 h (Figure 3.31), which is earlier than the optimum estimated from the old model of which the value of t_a was at 126 h.

The developed model has assisted to evaluate numerous combinations of nutrient supplementation profiles and cell-cycle arrest times to identify the best possible profiles of the two degrees of freedom. The number of random experiments required for identification of the optimal process conditions has been significantly reduced. The accuracy of the MIDO optimisation result is dependent on whether the model can sufficiently represent the system for the whole range of variable values encountered. The old model which assumed a first-order inhibition of growth and a simple second-order effect on death by ammonium over-predicted the viable cell concentration in the arrested fed-batch cultures, resulting in an inaccurate optimal cell-cycle arrest time at 126 h instead of 60 h from the new model. The viable cell concentration in the arrested fed-batch cultures reached its peak at 90-100 h. Thus the optimisation result suggested cell-cycle arrest before the peak viable cell density is reached. As there is a trade-off between slower cell growth and higher specific productivity in the arrested cells, the mixed-integer model-based optimisation offers an advantage to isolate important ranges of the controllable variables. Such simulation/optimisation strategy can reduce time and cost in the search for the optimal culture conditions. The new incorporation of a binary irreversible variable to optimise cell-cycle-dependent productivity has been very useful in this case study on hybridoma culture. This method can be applied to other combinations of binary and continuous control variables in cell cultures.

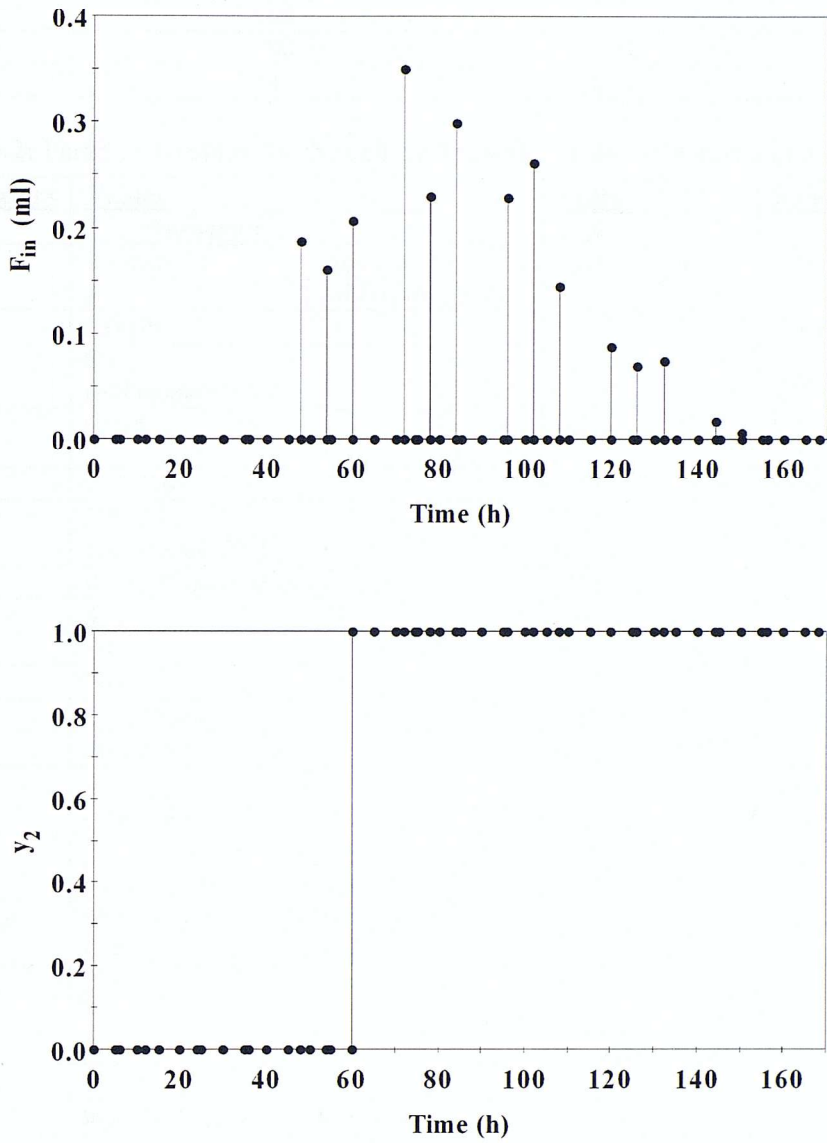


Figure 3.31: Optimisation results for nutrient supplementation profile (top), $F_{in}(t)$, and cell-cycle arrest time indicated by y_2 (bottom) switching from 0 to 1.

Table 3.1: Degrees of freedom in the simulation of the hybridoma cell culture.

Degrees of Freedom	Values	Units
F_{in}	0 (initial value)	L h ⁻¹
F_{out}	0	L h ⁻¹
F_{sam}	0 (initial value)	L h ⁻¹
$[Glc]_{in}$	500	mM
$[Gln]_{in}$	200	mM
t_a	44	h

Table 3.2: Parameter values for the cell-cycle model of the hybridoma cell culture.

Parameters	Values	Units	Reference
$K'_{d,amm}$	7 (**newpara)	mM	-
$K_{d,amm}$	normal: 2.6; arrested: 2.0 (old model: 2.4)	mM	-
$K_{d,gln}$	0.0096	h ⁻¹	Kontoravdi 2007
K_{glc}	0.1 (old model: 0.5)	mM	-
K_{gln}	0.075	mM	Kontoravdi 2007, Jang & Barford 2000b
$K_{l,lac}$	171.756	mM	Kontoravdi 2007
$K_{l,amm}$	2.5 (old model: 28.5)	mM	-
$K_{inh,gln}$	0.5 (**newpara)	mM	-
$K_{lac,glc}$	4	mM	-
K_{MAb}	80	%	-
K^*_{Qglc}	16	mM ²	-
$K_{rev,amm}$	6 (**newpara)	mM	-
m_{glc}	4e-11 (**newpara)	mmol _{glc} cell ⁻¹ h ⁻¹	-
n	2 (old model: 2.5)	-	Kontoravdi 2007, Jang & Barford 2000b
m	2 (**newpara)	-	-
$Q_{MAb,G1}$	normal: 1.8e-8; arrested: 2.58e-8	mg cell ⁻¹ h ⁻¹	-
$Q_{MAb,G2/M}$	normal: 2.8e-8; arrested: 4.0e-8	mg cell ⁻¹ h ⁻¹	-
$Q_{MAb,S}$	normal: 2.8e-8; arrested: 4.0e-8	mg cell ⁻¹ h ⁻¹	-
$t_{G2/M}$	2	h	-
t_S	7	h	-
$Y_{amm,gln}$	0.48	mol _{amm} mol ⁻¹ _{gln}	-
$Y_{max,lac,glc}$	2	mol _{lac} mol ⁻¹ _{glc}	-
$Y_{x,glc}$	normal: 6.5e7; arrested: 4.1e7	cell mmol _{glc} ⁻¹	-
$Y_{x,gln}$	normal: 8e8; arrested: 7e8 (old model: 4.7e8) (old model: 2.5e8)	cell mmol _{gln} ⁻¹	-
α_1	5e-11 (old model: 1e-15)	mmol _{gln} cell ⁻¹ h ⁻¹	-
α_2	0.6 (old model: 4)	mM	-
$\mu_{d,max}$	0.023	h ⁻¹	-
μ_{max}	normal: 0.048; arrested: 0.02	h ⁻¹	-
v_{cr}	80	%	-
$\theta_{G2/M}$	0.04	-	-
θ_S	0.07	-	-

3.2.5 Conclusions of the Cell-Cycle Model

The developed model was able to predict the cell culture dynamics for most of the major variables in all the batch and fed-batch cultures studied. The two selected degrees of freedom in the hybridoma cell culture: nutrient addition profile and cell-cycle arrest time, were computationally optimised simultaneously based on the model and initial experiment data. Among all the cell cultures performed, the monoclonal antibody yield in the arrested fed-batch cultures was about 3.5 g L^{-1} which was roughly 40% higher than in the test fed-batch culture. With the optimisation results, only three sets of arrested fed-batch cultures were performed for validation instead of carrying out a lot more experiments to select the best control strategy from. Further work is necessary to understand the change in metabolic pattern for lactate production and cell-cycle distribution in fed-batch cultures which appeared to be significantly different from that in batch cultures. It would also be interesting to investigate different cell culture initial conditions and higher degrees of freedom in this model-based optimisation.

Overall, with the aid of model predictions, fewer experiments were needed in order to explore the possible limits of the cell culture production capacity. In the optimised fed-batch culture, the culture life-time was extended as indicated by the X_v peaking at about 100 h while the corresponding peaking time for the initial fed-batch and batch cultures were about 90 h and 65 h respectively; and the MAb yield reached $\sim 3.5 \times 10^3 \text{ mg L}^{-1}$ as compared to $\sim 2.5 \times 10^3 \text{ mg L}^{-1}$ in the initial fed-batch culture and $\sim 1.3 \times 10^3 \text{ mg L}^{-1}$ in the batch cultures. The fact that the original model over-predicted certain cell concentrations in fed-batch cultures and the adjusted model slightly under-predicted viable cell concentration in a test fed-batch culture indicated a deficiency in the growth kinetics. In this cell-cycle model, only two major nutrients, glucose and glutamine, is related to the specific growth rate although there are other amino acids that are essential for growth being supplemented to the cell culture. This will be addressed in Chapter 4 where amino acids are modelled explicitly for a CHO-IFN γ cell-line.

3.2.6 Notations for the Cell-Cycle Model of Hybridoma Culture

Table 3.3: Notations for the cell-cycle model of the hybridoma culture.

Symbol	Definition	Units
$[Amm]$	ammonium concentration	mM
b	transition rate of cells from G_1 to S	h^{-1}
F_{in}	inlet flowrate	$L h^{-1}$
F_{out}	outlet flowrate	$L h^{-1}$
F_{sam}	sampling rate	$L h^{-1}$
$[Glc]$	glucose concentration	mM
$[Glc]_{in}$	feed glucose concentration	mM
$[Gln]$	glutamine concentration	mM
$[Gln]_{in}$	feed glutamine concentration	mM
$K'_{d,amm}$	half-saturation constant for high ammonium inhibition on death rate	mM
k_1	transition rate of cells from S to G_2/M	h^{-1}
k_2	transition rate of cells from G_2/M to G_1	h^{-1}
$K_{d,amm1}$	half-saturation constant for ammonium inhibition on death rate	mM
$K_{d,amm2}$	half-saturation constant for ammonium inhibition on death rate in arrested culture	mM
$K_{d,gln}$	degradation rate of glutamine	h^{-1}
K_{glc}	half-saturation constant of glucose on growth rate	mM
K_{gln}	half-saturation constant of glutamine on growth rate	mM
$K_{I,amm}$	inhibition constant of ammonium on growth rate	mM
$K_{I,lac}$	inhibition constant of lactate on growth rate	mM
$K_{inh,gln}$	inhibition constant of glutamine on death rate via increasing $[Amm]$ tolerance	mM
$K_{lac,glc}$	half-saturation constant for lactate production with respect to $[Glc]$	mM
K_{MAb}	inhibition constant for MAb production with respect to cell viability	%
$K_{Q_{glc}}$	half-saturation constant for glucose uptake	mM^2
$K_{rev,amm}$	inhibition constant of ammonium on ammonium yield from glutamine	mM
$[Lac]$	lactate concentration	mM
m	exponential order in death kinetics	-
$[MAb]$	monoclonal-antibody concentration	$mg L^{-1}$
m_{glc}	maintenance consumption of glucose	$mmol cell^{-1} h^{-1}$
m_{gln}	maintenance consumption of glutamine	$mmol cell^{-1} h^{-1}$
n	exponential order in death kinetics	-
Q_{Amm}	specific ammonium production rate	$mmol cell^{-1} h^{-1}$
Q_{glc}	specific glucose uptake rate	$mmol cell^{-1} h^{-1}$
Q_{lac}	specific lactate production rate	$mmol cell^{-1} h^{-1}$
Q_{MAb}	average specific MAb production rate	$mg cell^{-1} h^{-1}$
$Q_{MAb,i}$	specific MAb production rate of cell-cycle phase i	$mg cell^{-1} h^{-1}$
t	time	h
t_a	cell-cycle arrest time	h
$t_S, t_{G2/M}$	Time-length of the S phase and G_2+M phase respectively	h
v	viability	%
V	Cell culture volume	L
v_{cr}	critical viability	%
$X_{G1}, X_S, X_{G2/M}$	concentrations of viable cells in G_0/G_1 , S, and G_2/M phase respectively	$cell L^{-1}$
x_i	fraction of cells in cell-cycle phase i	-

X_v	viable cell concentration	cell L ⁻¹
y_1	binary variable for normal culture condition	-
y_2	binary variable for arrested culture condition	-
$Y_{amm,gln}$	ammonium yield from glutamine	mmol mmol ⁻¹
$Y_{max lac,glc}$	maximum lactate yield from glucose	mmol mmol ⁻¹
$Y_{x,glc}$	cell yield from glucose	cell mmol ⁻¹
$Y_{x,gln}$	cell yield from glutamine	cell mmol ⁻¹
α_1	maximum maintenance consumption of glutamine	mmol cell ⁻¹ h ⁻¹
α_2	half-saturation constant for maintenance consumption of glutamine	mM
μ	specific growth rate	h ⁻¹
μ_d	specific death rate	h ⁻¹
$\mu_{d max}$	maximum specific death rate	h ⁻¹
μ_{max1}	maximum specific growth rate	h ⁻¹
μ_{max2}	maximum specific growth rate in arrested culture	h ⁻¹
θ_i	fraction of cells in cell-cycle phase i when growth rate is zero	-
ω_1	binary degree of freedom for optimisation of t_a	-
ω_2, ω_3	continuous variables for optimisation of t_a	-

Chapter 4

— Model Development for CHO- IFN γ Cell Culture Including Amino Acids & Cellular Regulations

As concluded in the previous chapter, amino acids except glutamine are often not considered in mammalian cell culture models though certain amino acids are known to be essential for growth. This is partly due to the difficulty in measuring the concentration of all amino acids in the cell culture; and partly because of the complexity of models that attempt to track the relationship between growth and amino acids concentration as well as interconversions of amino acids. In Section 4.1 of this chapter, a simple amino acid model is created for a mammalian cell-line (Chinese hamster ovary cells) commonly used in the bioindustry. The model was able to simulate cell growth, product synthesis, and consumption/production of most amino acids but certain insufficiency was noticed when applying such model to fed-batch cell cultures. As a result, a more detailed model is developed in Section 4.2 taking into account certain changes in the cell culture dynamics when the cells are subjected to a different condition in the cell culture medium. The model in Section 4.2 is further analysed in Chapter 5 and subsequently used for model-based optimisation in Chapter 6.

4.1 A Simple Amino Acid Model for CHO-IFN γ Culture

4.1.1 Cell-Line & Experiment Setup

Data of Chinese hamster ovary (CHO) cell-line producing recombinant human interferon gamma (IFN γ) adapted to serum-free suspension culture were kindly provided by Dr. Danny Wong (Bioprocessing Technology Institute, BTI-A*Star, Singapore). The cell culture experiment was performed in serum-free and protein-free media (Wong et al., 2005). Detailed methodology has been described in Wong et al. (2005). The CHO-IFN γ cells were cultivated in 4 L stirred-tank bioreactors at 37°C and pH 7 in batch and fed-batch conditions. The fed-batch cultures were controlled at low-glutamine or low-glutamine plus low glucose conditions using on-line feed-back controllers with different set-points of glutamine and glucose concentrations. The dynamic feed profile records were only available for at least one of each fed-batch conditions tested: (i) 0.1mM glutamine set-point, (ii) 0.3mM glutamine set-point, (iii) 0.5mM glutamine set-point, (iv) 0.3mM glutamine set-point plus 0.35mM glucose set-point, and (v) 0.3mM glutamine set-point plus 0.7mM glucose set-point. Concentrated nutrient stream containing glutamine, glucose, and other amino acids were used to supplement the fed-batch cultures. Analyses of glucose, glutamine, and lactate were carried out using a biochemical analyser; ammonium was detected using UV spectrophotometry; IFN γ concentration was analysed using enzyme-linked immunosorbent assay (ELISA), and amino acid concentrations were measured using reverse-phase HPLC (Wong et al., 2005). A total of 19 amino acids were measured: alanine, arginine, asparagine, aspartate, cysteine, glutamine, glutamate, glycine, histidine, isoleucine, leucine, lysine, methionine, phenylalanine, proline, serine, threonine, tyrosine, and valine. Tryptophan was not able to be measured due to technical problems in resolving its peak in the HPLC analysis (personal conversation with Dr. Danny Wong).

4.1.2 Model Development

4.1.2.1 Essential Amino Acids for Mammalian Cell Cultures

Mammalian cells are known to be unable to synthesise certain amino acids which must be supplemented in the cell culture to sustain cell growth. A comparison of the essential amino acids of several mammalian cell types is shown in Table 4.1.

The lists of amino acids that cannot be produced by mammalian cells appear to be cell-line dependent (Table 4.1). It should be noted that the data for murine hybridoma TB/C3 by Simpson et al. (1998) did not distinguish between amino acids that the cells cannot produce versus growth-stimulating amino acids that can be synthesised from other amino acids. To avoid confusion, 'essential amino acids' will be used to refer to amino acids that *cannot* be synthesised by mammalian cells for the rest of this chapter. There are several common essential amino acids for all the cell-lines in Table 4.1: lysine, tryptophan, methionine, threonine, and leucine. Chinese Hamster Ovary (CHO) cells are genetically closer to mouse (murine) and human than other organisms (refer to Appendix 3 for lineage relationship). Thus, those amino acids that are essential or growth-stimulating for human and murine hybridoma TB/C3 have been assumed to be important for the growth of CHO cells. Several literature studies have reported partial lists of essential or non-essential amino acids for various CHO cell-lines: CHO-IFN γ chemostat cell cultures studied by Hayter et al. (1992) showed net productions of glutamic acid, aspartic acid, serine, and alanine at various steady-states, indicating they are non-essential amino acids; Heal and McGivan (1997) reported tryptophan, histidine, and phenylalanine to be essential for CHO-K1 cells; Altamirano et al. (2001) studied a CHO cell-line producing tissue-type plasminogen activator (tPA) in chemostat and alanine, glycine, and aspartic acids were produced by the cells; the CHO-IFN γ cell culture modelled in this chapter showed net productions of alanine, glycine, and proline. All these examples are in agreement with the lists of essential/growth-stimulating versus non-essential amino acids of human and murine hybridoma TB/C3. The amino acids considered in the growth kinetics of CHO-IFN γ are indicated in Table 4.1.

Table 4.1: Comparison of essential versus non-essential amino acids for different mammalian cells reported by Morgan (1958) and Simpson et al. (1998).

	Mammalian Organisms								Model
	Chick fibroblasts ⁽¹⁾	L. strain ⁽¹⁾	HeLa cell ⁽¹⁾	Walker ⁽¹⁾	Rabbit fibroblasts ⁽¹⁾	<i>Tetrahymena gelei</i> ⁽¹⁾	Adult human ⁽¹⁾	Murine hybridoma TB/C3 ⁽²⁾	Amino acids assumed essential/ growth-stimulating in the CHO model
Arginine	E	E	E	E	E	nE,S	nE,S	E*	√
Histidine	E	E	E	E	E	E	nE	E	√
Lysine	E	E	E	E	E	E	E	E	√
Tryptophan	E	E	E	E	E	E	E	E	√
Phenylalanine	E	E	E	E	E	E	E	n/a	√
Tyrosine	E	E	E	E	E	nE	nE,S	E*	√
Cysteine	E	E	E	E	E	nE	nE,S	E*	√
Methionine	E	E	E	E	E	E	E	E	√
Serine	nE	nE	nE	nE	E	nE,S	nE	nE	-
Threonine	E	E	E	E	E	E	E	E	√
Leucine	E	E	E	E	E	E	E	E	√
Isoleucine	nE	E	E	E	E	E	E	E	√
Valine	E	E	E	E	E	nE,S	E	E	√
Glutamic acid	inh	nE	nE	nE	nE	nE	nE	nE	-
Aspartic acid	inh	nE	nE	nE	nE	nE	nE	nE	-
Alanine	inh	nE	nE	nE	nE	nE	nE	n/a	-
Proline	inh	nE	nE	nE	nE	nE	nE	nE	-
Hydroxyproline	inh	nE	nE	nE	nE	nE	nE	n/a	-
Glycine	nE	nE	nE	nE	nE	nE	nE	nE	-
Glutamine	nE	E	E	E	E	n/a	n/a	E	energy source
Asparagine	n/a	n/a	n/a	E	n/a	n/a	n/a	nE	-

Remarks:

E: Essential amino acid (cannot be produced by cells)

nE: Non-essential amino acid

S: Stimulating (enhance growth rate because of a slow rate of synthesis by the organism)

inh: Inhibitory

n/a: Not available

*: Simpson et al. (1998) did not classify between essential amino acids that the cells cannot produce versus growth-stimulating amino acids that can be produced from other amino acids.

⁽¹⁾ Summarised by Morgan (1958) from experiments of Eagle (1955a; 1955b), Eagle et al. (1956), Haff et al. (1956), Kidder and Dewey (1945), McCoy et al. (1956), and Rose et al. (1954).

⁽²⁾ Data from Simpson et al. (1998) depleting amino acids one at a time in chemostat cultures of hybridoma TB/C3 and studied cell viability after 48h of removal of each amino acid.

4.1.2.2 Structure of Model Equations

In this section, all the variables and parameters are summarised in Section 4.1.6 with detailed definition.

Specific Growth Rate

The specific growth rate of CHO-IFN γ cell culture is related to the concentrations of glucose, glutamine, and essential/growth-stimulating amino acids discussed in Section 4.1.2.1 except tryptophan which was not able to be measured in the experiment. It is assumed that the concentration of tryptophan never dropped to zero in the cell cultures and the effect of tryptophan on specific growth rate (μ) is less significant than other essential amino acids.

$$\begin{aligned} \mu = \mu_{\min} + (\mu_{\max} - \mu_{\min}) \cdot & \left[\frac{[GLC] \cdot [GLN]}{(K_{glc} + [GLC]) \cdot (K_{gln} + [GLN])} \right. \\ & + \frac{[VAL] \cdot [LYS] \cdot [THR] \cdot [HIS] \cdot [ILE] \cdot [PHE]}{(K_{val} + [VAL]) \cdot (K_{lys} + [LYS]) \cdot (K_{thr} + [THR]) \cdot (K_{his} + [HIS]) \cdot (K_{ile} + [ILE]) \cdot (K_{phe} + [PHE])} \\ & \left. \cdot \frac{[LEU] \cdot [MET] \cdot [ARG] \cdot [TYR] \cdot [CYS]}{(K_{leu} + [LEU]) \cdot (K_{met} + [MET]) \cdot (K_{arg} + [ARG]) \cdot (K_{tyr} + [TYR]) \cdot (K_{cys} + [CYS])} \right] \end{aligned} \quad (4.1.1)$$

where μ_{\min} (h^{-1}) is the minimum specific growth rate, μ_{\max} (h^{-1}) is the maximum specific growth rate, K_i represents the Monod-type constant of nutrient i which is the concentration of i to have half of the maximum stimulation on specific growth rate.

In the above equation, glucose and glutamine are separated from other amino acids because the CHO-IFN γ batch culture appeared to exhaust glucose and glutamine earlier than the amino acids and cell growth did not stop when there was no glucose/glutamine in the cell culture medium (Figure 4.1). The role of the minimum growth rate (μ_{\min}) is to compensate for possible under-estimation of μ due to any under-prediction of amino acid concentrations.

Volume

Assuming the sampling volume is negligible relative to the flowrates of the inlet stream(s):

$$\frac{dV}{dt} = F_{in} + F_{glc} - F_{out} \quad (4.1.2)$$

The effect of volume increase by addition of concentrated nutrients on residual concentration of cells, nutrients, product, and byproducts is taken into account by modelling the total amount of each substance in the mass balance.

Specific Death Rate

The relationship between specific death rate (μ_d) and ammonium concentration ($[AMM]$) proposed by Ludemann et al. (1994) was adopted for CHO-IFN γ cells with the inclusion of another toxic by-product lactate ($[LAC]$). Detailed explanation of the death rate equation can be found in Section 4.2.1.2 (Equation M10). The values of critical concentration of ammonium and lactate ($[AMM]_{cr}$ and $[LAC]_{cr}$) were estimated based on findings by Hayter et al. (1991) that CHO cell-line could tolerate ammonia concentration up to about 5mM and was not affected by lactate concentration as high as 17.5mM.

$$\mu_d = \mu_{d,\min} \cdot \left(\frac{K_{d,amm} + ([AMM] - [AMM]_{cr})}{K_{d,amm}} \right) \cdot \left(\frac{K_{d,lac} + ([LAC] - [LAC]_{cr})}{K_{d,lac}} \right) \quad (4.1.3)$$

where $([AMM] - [AMM]_{cr}) = 0$ and $([LAC] - [LAC]_{cr}) = 0$ if $[AMM] < [AMM]_{cr}$ and $[LAC] < [LAC]_{cr}$ respectively.

Cell Concentrations

$$\frac{d(X_v \cdot V)}{dt} = \mu \cdot X_v \cdot V - \mu_d \cdot X_v \cdot V - F_{out} \cdot X_v \quad (4.1.4)$$

$$\frac{d(X_d \cdot V)}{dt} = \mu_d \cdot X_v \cdot V - r_{frag} \cdot X_d \cdot V - F_{out} \cdot X_d \quad (4.1.5)$$

$$X_t = X_v + X_d \quad (4.1.6)$$

where X_v , X_d , and X_t (cell L⁻¹) are the viable, dead, and total cell concentrations respectively. Possible loss of dead cells is represented by r_{frag} (h⁻¹) in Equation 4.1.4. A more detailed discussion of cell lysis can be found in Section 4.2.1.2.

Glucose ([GLC])

$$\frac{d([GLC] \cdot V)}{dt} = Q_{glc} \cdot X_v \cdot V + F_{glc} \cdot [GLC]_{in} - F_{out} \cdot [GLC] \quad (4.1.7)$$

$$Q_{glc} = -\frac{\mu}{Y_{x,glc}} - M_{glc} \quad (4.1.8)$$

where Q_{glc} (mmol cell⁻¹ h⁻¹) is the specific consumption rate of glucose, F_{glc} (L h⁻¹) is the flowrate of glucose-containing stream, $Y_{x,glc}$ (cell mmole⁻¹) is the cell yield from glucose, M_{glc} (mmol cell⁻¹ h⁻¹) is the maintenance glucose consumption.

Amino Acids

The interconversions of amino acids is based on discussions with Dr. Yih Yean Lee (BTI-A*Star, Singapore) based on their experimental results and the list of essential amino acids discussed in Section 4.1.2.1 that cannot be synthesised by mammalian cells. Below is a list of interconversions of amino acids included in this simple amino acid model:

Arginine \leftrightarrow Glutamic acid

Arginine \leftarrow Proline

Arginine \leftrightarrow Aspartic acid

Asparagine \leftarrow Aspartic acid

Asparagine \leftarrow Arginine

Cysteine \leftarrow Serine

Glutamic acid \leftrightarrow Proline

Glutamic acid \leftarrow Histidine

Glutamic acid \leftarrow Glutamine

Glycine \leftrightarrow Serine

Proline \leftarrow Arginine

Tyrosine \leftarrow Phenylalanine

Glutamine ([GLN]):

$$\frac{d([GLN] \cdot V)}{dt} = Q_{gln} \cdot X_v \cdot V - r_{d,gln} \cdot [GLN] \cdot V + F_{in} \cdot [GLN]_{in} - F_{out} \cdot [GLN] \quad (4.1.9)$$

$$Q_{gln} = -\frac{\mu}{Y_{x,gln}} - M_{gln} + Y_{gln,glu} \cdot Q_{glu} \quad (4.1.10)$$

$$M_{gln} = \frac{\alpha_1 \cdot [GLN]}{\alpha_2 + [GLN]} \quad (4.1.11)$$

where Q_{gln} (mmole cell⁻¹ h⁻¹) is the specific consumption rate of glutamine, $r_{d,gln}$ (h⁻¹) is the spontaneous glutamine degradation rate, $Y_{x,gln}$ (cell mmole⁻¹) is the cell yield from glutamine, $Y_{gln,glu}$ (mmole mmole⁻¹) is the yield of glutamine from glutamic acid, Q_{glu} (mmole cell⁻¹ h⁻¹) is the specific consumption rate of glutamic acid, M_{gln} (mmole cell⁻¹ h⁻¹) is the maintenance glutamine consumption, α_1 (mmole cell⁻¹ h⁻¹) is the maximum maintenance consumption of glutamine and α_2 (mM) is the corresponding half-saturation constant.

The specific consumption/production rate, Q_i , is negative for consumption and positive for production of species i . The sign of $Y_{j,i} \cdot Q_i$, where $Y_{j,i}$ is the yield of amino acid j from i , is dependent on the sign of Q_i of the specific cell culture studied. Two exceptions occur for glutamate and arginine as their specific consumption/production rates altered between net consumption and net production in batch CHO-IFN γ culture. As a simplification, it is assumed that the sign of $Y_{j,glu}$ is positive and the sign of $Y_{j,arg}$ is negative.

Below are the mass balance and specific consumption equations for other amino acids starting from the essential/growth-stimulating amino acids.

Valine ([VAL]):

$$\frac{d([VAL] \cdot V)}{dt} = Q_{val} \cdot X_v \cdot V + F_{in} \cdot [VAL]_{in} - F_{out} \cdot [VAL] \quad (4.1.12)$$

$$Q_{val} = -\frac{\mu}{Y_{x,val}} \quad (4.1.13)$$

Lysine ([LYS]):

$$\frac{d([LYS] \cdot V)}{dt} = Q_{lys} \cdot X_v \cdot V + F_{in} \cdot [LYS]_{in} - F_{out} \cdot [LYS] \quad (4.1.14)$$

$$Q_{lys} = -\frac{\mu}{Y_{x,lys}} \quad (4.1.15)$$

Threonine ([THR]):

$$\frac{d([THR] \cdot V)}{dt} = Q_{thr} \cdot X_v \cdot V + F_{in} \cdot [THR]_{in} - F_{out} \cdot [THR] \quad (4.1.16)$$

$$Q_{thr} = -\frac{\mu}{Y_{x,thr}} \quad (4.1.17)$$

Histidine ([HIS]):

$$\frac{d([HIS] \cdot V)}{dt} = Q_{his} \cdot X_v \cdot V + F_{in} \cdot [HIS]_{in} - F_{out} \cdot [HIS] \quad (4.1.18)$$

$$Q_{his} = -\frac{\mu}{Y_{x,his}} \quad (4.1.19)$$

Isoleucine ([LEU]):

$$\frac{d([ILE] \cdot V)}{dt} = Q_{ile} \cdot X_v \cdot V + F_{in} \cdot [ILE]_{in} - F_{out} \cdot [ILE] \quad (4.1.20)$$

$$Q_{ile} = -\frac{\mu}{Y_{x,ile}} \quad (4.1.21)$$

Phenylalanine ([PHE]):

$$\frac{d([PHE] \cdot V)}{dt} = Q_{phe} \cdot X_v \cdot V + F_{in} \cdot [PHE]_{in} - F_{out} \cdot [PHE] \quad (4.1.22)$$

$$Q_{phe} = -\frac{\mu}{Y_{x,phe}} \quad (4.1.23)$$

Leucine ([LEU]):

$$\frac{d([LEU] \cdot V)}{dt} = Q_{leu} \cdot X_v \cdot V + F_{in} \cdot [LEU]_{in} - F_{out} \cdot [LEU] \quad (4.1.24)$$

$$Q_{leu} = -\frac{\mu}{Y_{x,leu}} \quad (4.1.25)$$

Methionine ([MET]):

$$\frac{d([MET] \cdot V)}{dt} = Q_{met} \cdot X_v \cdot V + F_{in} \cdot [MET]_{in} - F_{out} \cdot [MET] \quad (4.1.26)$$

$$Q_{met} = -\frac{\mu}{Y_{x,met}} \quad (4.1.27)$$

Arginine ([ARG]):

$$\frac{d([ARG] \cdot V)}{dt} = Q_{arg} \cdot X_v \cdot V + F_{in} \cdot [ARG]_{in} - F_{out} \cdot [ARG] \quad (4.1.28)$$

$$Q_{arg} = -\frac{\mu}{Y_{x,arg}} + Y_{arg,glu} \cdot Q_{glu} + Y_{arg,pro} \cdot Q_{pro} - Y_{arg,asp} \cdot Q_{asp} \quad (4.1.29)$$

Tyrosine ([TYR]):

$$\frac{d([TYR] \cdot V)}{dt} = Q_{tyr} \cdot X_v \cdot V + F_{in} \cdot [TYR]_{in} - F_{out} \cdot [TYR] \quad (4.1.30)$$

$$Q_{tyr} = -\frac{\mu}{Y_{x,tyr}} - Y_{tyr,phe} \cdot Q_{phe} \quad (4.1.31)$$

Cysteine ([CYS]):

$$\frac{d([CYS] \cdot V)}{dt} = Q_{cys} \cdot X_v \cdot V + F_{in} \cdot [CYS]_{in} - F_{out} \cdot [CYS] \quad (4.1.32)$$

$$Q_{cys} = -\frac{\mu}{Y_{x,cys}} - Y_{cys,ser} \cdot Q_{ser} \quad (4.1.33)$$

Alanine ([ALA]):

$$\frac{d([ALA] \cdot V)}{dt} = Q_{ala} \cdot X_v \cdot V + F_{in} \cdot [ALA]_{in} - F_{out} \cdot [ALA] \quad (4.1.34)$$

$$Q_{ala} = -\frac{\mu}{Y_{x,ala}} + r_{ala,x} \quad (4.1.35)$$

where $r_{ala,x}$ (mmole cell⁻¹ h⁻¹) represents a specific production rate of alanine from cells as there are many possible amino acid sources for alanine, making it difficult to track all the sources. This is also the case for aspartic acid and glutamic acid below.

Asparagine ([ASN]):

$$\frac{d([ASN] \cdot V)}{dt} = Q_{asn} \cdot X_v \cdot V + F_{in} \cdot [ASN]_{in} - F_{out} \cdot [ASN] \quad (4.1.36)$$

$$Q_{asn} = -\frac{\mu}{Y_{x,asn}} - Y_{asn,asp} \cdot Q_{asp} \quad (4.1.37)$$

Aspartic acid ([ASP]):

$$\frac{d([ASP] \cdot V)}{dt} = Q_{asp} \cdot X_v \cdot V + F_{in} \cdot [ASP]_{in} - F_{out} \cdot [ASP] \quad (4.1.38)$$

$$Q_{asp} = -\frac{\mu}{Y_{x,asp}} - Y_{asp,arg} \cdot Q_{arg} + r_{asp,x} \quad (4.1.39)$$

Glutamic acid ([GLU]):

$$\frac{d([GLU] \cdot V)}{dt} = Q_{glu} \cdot X_v \cdot V + F_{in} \cdot [GLU]_{in} - F_{out} \cdot [GLU] \quad (4.1.40)$$

$$Q_{glu} = -\frac{\mu}{Y_{x,glu}} + Y_{glu,pro} \cdot Q_{pro} - Y_{glu,his} \cdot Q_{his} - Y_{glu,gln} \cdot Q_{gln} - Y_{glu,arg} \cdot Q_{arg} + r_{glu,x} \quad (4.1.41)$$

Glycine ([GLY]):

$$\frac{d([GLY] \cdot V)}{dt} = Q_{gly} \cdot X_v \cdot V + F_{in} \cdot [GLY]_{in} - F_{out} \cdot [GLY] \quad (4.1.42)$$

$$Q_{gly} = -\frac{\mu}{Y_{x,gly}} - Y_{gly,ser} \cdot Q_{ser} \quad (4.1.43)$$

Proline ([PRO]):

$$\frac{d([PRO] \cdot V)}{dt} = Q_{pro} \cdot X_v \cdot V + F_{in} \cdot [PRO]_{in} - F_{out} \cdot [PRO] \quad (4.1.44)$$

$$Q_{pro} = -\frac{\mu}{Y_{x,pro}} + Y_{pro,glu} \cdot Q_{glu} - Y_{pro,arg} \cdot Q_{arg} \quad (4.1.45)$$

Serine ([SER]):

$$\frac{d([SER] \cdot V)}{dt} = Q_{ser} \cdot X_v \cdot V + F_{in} \cdot [SER]_{in} - F_{out} \cdot [SER] \quad (4.1.46)$$

$$Q_{ser} = -\frac{\mu}{Y_{x,ser}} + Y_{ser,gly} \cdot Q_{gly} \quad (4.1.47)$$

Byproducts

Lactate ([LAC]) is produced mainly during metabolism of glucose. Thus, the specific production rate of lactate, Q_{lac} (mmole cell⁻¹ h⁻¹), is linked to specific glucose consumption rate (Q_{glc}) via a term representing lactate yield from glucose, $Y_{lac,glc}$ (mmole mmole⁻¹).

$$\frac{d([LAC] \cdot V)}{dt} = Q_{lac} \cdot X_v \cdot V - F_{out} \cdot [LAC] \quad (4.1.48)$$

$$Q_{lac} = -Y_{lac,glc} \cdot Q_{glc} \quad (4.1.49)$$

Ammonium ([AMM]) is mainly produced from metabolism of glutamine and spontaneous glutamine degradation ($r_{d,gln}$). The specific production rate of ammonium, Q_{amm} (mmole cell⁻¹ h⁻¹), is related to specific glutamine consumption rate (Q_{gln}) via a term representing ammonium yield from glutamine, $Y_{amm,gln}$ (mmole mmole⁻¹).

$$\frac{d([AMM] \cdot V)}{dt} = Q_{amm} \cdot X_v \cdot V + r_{d,gln} \cdot [GLN] \cdot V + F_{in} \cdot [AMM]_{in} - F_{out} \cdot [AMM] \quad (4.1.50)$$

$$Q_{amm} = -Y_{amm,gln} \cdot Q_{gln} \quad (4.1.51)$$

IFN γ

A simple equation is used to relate the production of IFN γ to viable cell concentration:

$$\frac{d([IFN] \cdot V)}{dt} = r_{IFN} \cdot X_v \cdot V - F_{out} \cdot [IFN] \quad (4.1.52)$$

where r_{IFN} (mg cell $^{-1}$ h $^{-1}$) is the average specific production rate of IFN γ .

4.1.3 Model Parameter Estimation

The model contains 67 parameters with 26 measured variables. The parameter values were estimated in gPROMS (Process Systems Enterprise Ltd.) using a general maximum likelihood approach similar to in Chapter 3. Below are the parameter values for the CHO-IFN γ batch culture.

Table 4.2: Parameter values of the simple amino acid model for batch culture of CHO-IFN γ cells.

Parameter	Value	Units
$[AMM]_{cr}$	5	mM
K_{arg}	6×10^{-2}	mM
K_{cys}	1.2×10^{-2}	mM
$K_{d,amm}$	5×10^{-2}	mM
$K_{d,lac}$	4.5	mM
K_{glc}	1.5×10^{-1}	mM
K_{gln}	2.2×10^{-1}	mM
K_{his}	5×10^{-3}	mM
K_{ile}	2.5×10^{-2}	mM
K_{leu}	2×10^{-2}	mM
K_{lys}	1×10^{-2}	mM
K_{met}	8×10^{-3}	mM
K_{phe}	4×10^{-2}	mM
K_{thr}	5×10^{-2}	mM
K_{tyr}	1×10^{-2}	mM
K_{val}	1.5×10^{-2}	mM
$[LAC]_{cr}$	20	mM
M_{glc}	1×10^{-14}	mmole cell $^{-1}$ h $^{-1}$
$r_{ala,x}$	5.5×10^{-11}	mmole cell $^{-1}$ h $^{-1}$
$r_{asp,x}$	2×10^{-16}	mmole cell $^{-1}$ h $^{-1}$
$r_{glu,x}$	4×10^{-13}	mmole cell $^{-1}$ h $^{-1}$
$r_{d,gln}$	9×10^{-3}	h $^{-1}$
r_{frag}	1×10^{-4}	h $^{-1}$
$Y_{amm,gln}$	1.2	mmole mmole $^{-1}$
$Y_{arg,asp}$	1×10^{-3}	mmole mmole $^{-1}$

$Y_{arg,glu}$	1×10^{-2}	mmole mmole ⁻¹
$Y_{arg,pro}$	1×10^{-3}	mmole mmole ⁻¹
$Y_{asn,asp}$	1×10^{-2}	mmole mmole ⁻¹
$Y_{asp,arg}$	1×10^{-4}	mmole mmole ⁻¹
$Y_{cys,ser}$	1×10^{-1}	mmole mmole ⁻¹
$Y_{gln,glu}$	1×10^{-1}	mmole mmole ⁻¹
$Y_{glu,arg}$	1×10^{-3}	mmole mmole ⁻¹
$Y_{glu,gln}$	7×10^{-1}	mmole mmole ⁻¹
$Y_{glu,his}$	5×10^{-1}	mmole mmole ⁻¹
$Y_{glu,pro}$	1×10^{-2}	mmole mmole ⁻¹
$Y_{gly,ser}$	6.5×10^{-1}	mmole mmole ⁻¹
$Y_{lac,glc}$	1.5	mmole mmole ⁻¹
$Y_{pro,arg}$	6×10^{-1}	mmole mmole ⁻¹
$Y_{pro,glu}$	5×10^{-1}	mmole mmole ⁻¹
$Y_{ser,gly}$	1×10^{-3}	mmole mmole ⁻¹
$Y_{tyr,phe}$	5×10^{-1}	mmole mmole ⁻¹
$Y_{x,ala}$	1×10^9	cell mmole ⁻¹
$Y_{x,arg}$	2×10^9	cell mmole ⁻¹
$Y_{x,asn}$	1.5×10^9	cell mmole ⁻¹
$Y_{x,asp}$	1.1×10^9	cell mmole ⁻¹
$Y_{x,cys}$	6×10^8	cell mmole ⁻¹
$Y_{x,glc}$	7.7×10^7	cell mmole ⁻¹
$Y_{x,gln}$	8×10^8	cell mmole ⁻¹
$Y_{x,glu}$	9.6×10^8	cell mmole ⁻¹
$Y_{x,gly}$	1.6×10^9	cell mmole ⁻¹
$Y_{x,his}$	4.6×10^9	cell mmole ⁻¹
$Y_{x,ile}$	2×10^9	cell mmole ⁻¹
$Y_{x,leu}$	1.5×10^9	cell mmole ⁻¹
$Y_{x,lys}$	1.3×10^9	cell mmole ⁻¹
$Y_{x,met}$	5.2×10^9	cell mmole ⁻¹
$Y_{x,phe}$	4.1×10^9	cell mmole ⁻¹
$Y_{x,pro}$	2.1×10^9	cell mmole ⁻¹
$Y_{x,ser}$	2.5×10^9	cell mmole ⁻¹
$Y_{x,thr}$	1.8×10^9	cell mmole ⁻¹
$Y_{x,tyr}$	2.6×10^9	cell mmole ⁻¹
$Y_{x,val}$	3×10^9	cell mmole ⁻¹
α_1	2×10^{-14}	mmole cell ⁻¹ h ⁻¹
α_2	2	mM
$\mu_{d,min}$	5×10^{-4}	h ⁻¹
μ_{min}	2×10^{-3}	h ⁻¹
μ_{max}	1.9×10^{-2}	h ⁻¹
r_{IFN}	1.8×10^{-11}	mg cell ⁻¹ h ⁻¹

The simulation results of the CHO-IFN γ batch culture using the parameter values in Table 4.2 are shown in Figure 4.1 for the concentrations of IFN γ , viable and total cell, glutamine, glucose, isoleucine (example for essential amino acid), alanine (example for non-essential amino acid), ammonium, and lactate. The model is able to follow the trends of all major variables. However, there are significant deviations in all

fed-batch cultures unless certain parameter values were changed for each individual fed-batch culture. A comparison of fed-batch culture simulation results using parameter values from Table 4.2 versus parameters individually adjusted by trial and error is made in Figure 4.2 – 4.7. The affected parameters are listed in Table 4.4 in Section 4.1.4.2. The discrepancy in the predictions of IFN γ and cell concentrations of fed-batch cultures when batch parameter values were used indicated certain changes had occurred in the cell culture when the cultivation method was changed from batch to low-glutamine/low-glucose fed-batch.

In order to systematically identify the model parameters that affect the prediction of productivity, Global Sensitivity Analysis (GSA) was performed to quantify the relative influence of each parameter upon the model prediction of cell growth. In next section, an overview of existing sensitivity analysis methods is presented followed by an application of GSA on the simple amino acid model of the CHO-IFN γ cell culture.

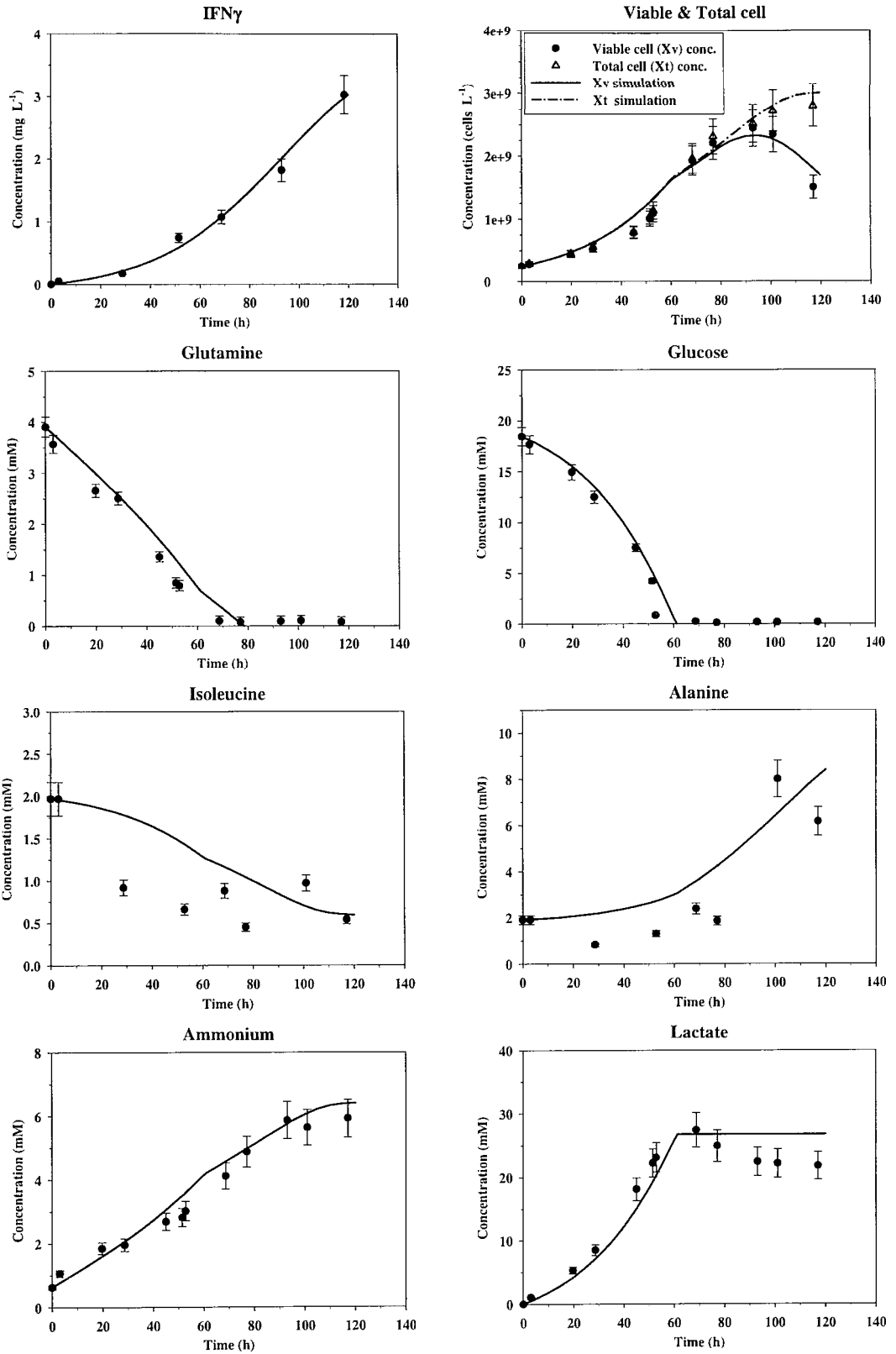


Figure 4.1: Simulations of the simple amino acid CHO-IFN γ model for **batch** culture and comparison with the corresponding experiment data.

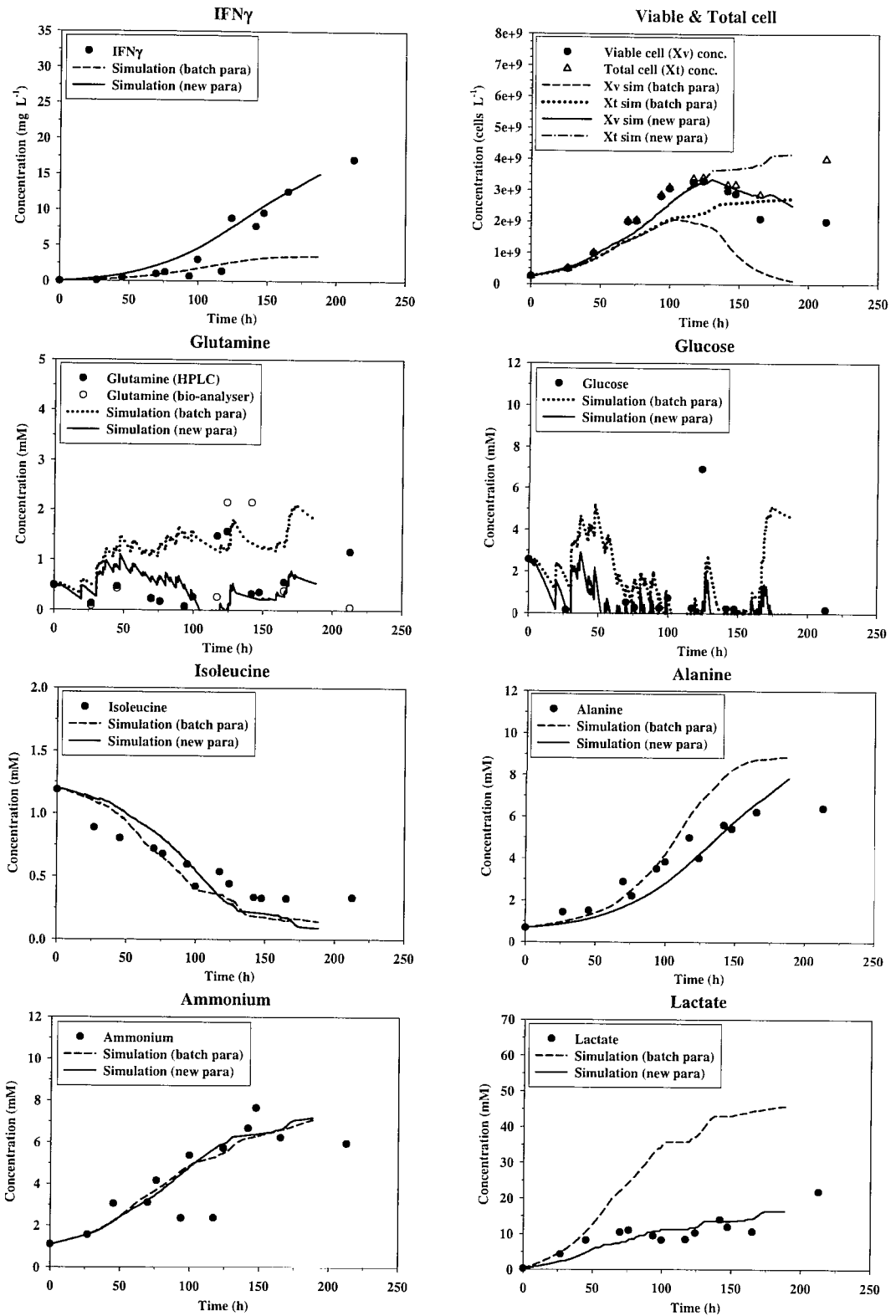


Figure 4.2: Simulations of the simple amino acid CHO-IFN γ model for fed-batch culture with glutamine set-point at 0.1mM using parameter values from batch culture versus adjusted new parameter values. Circles represent experiment data.

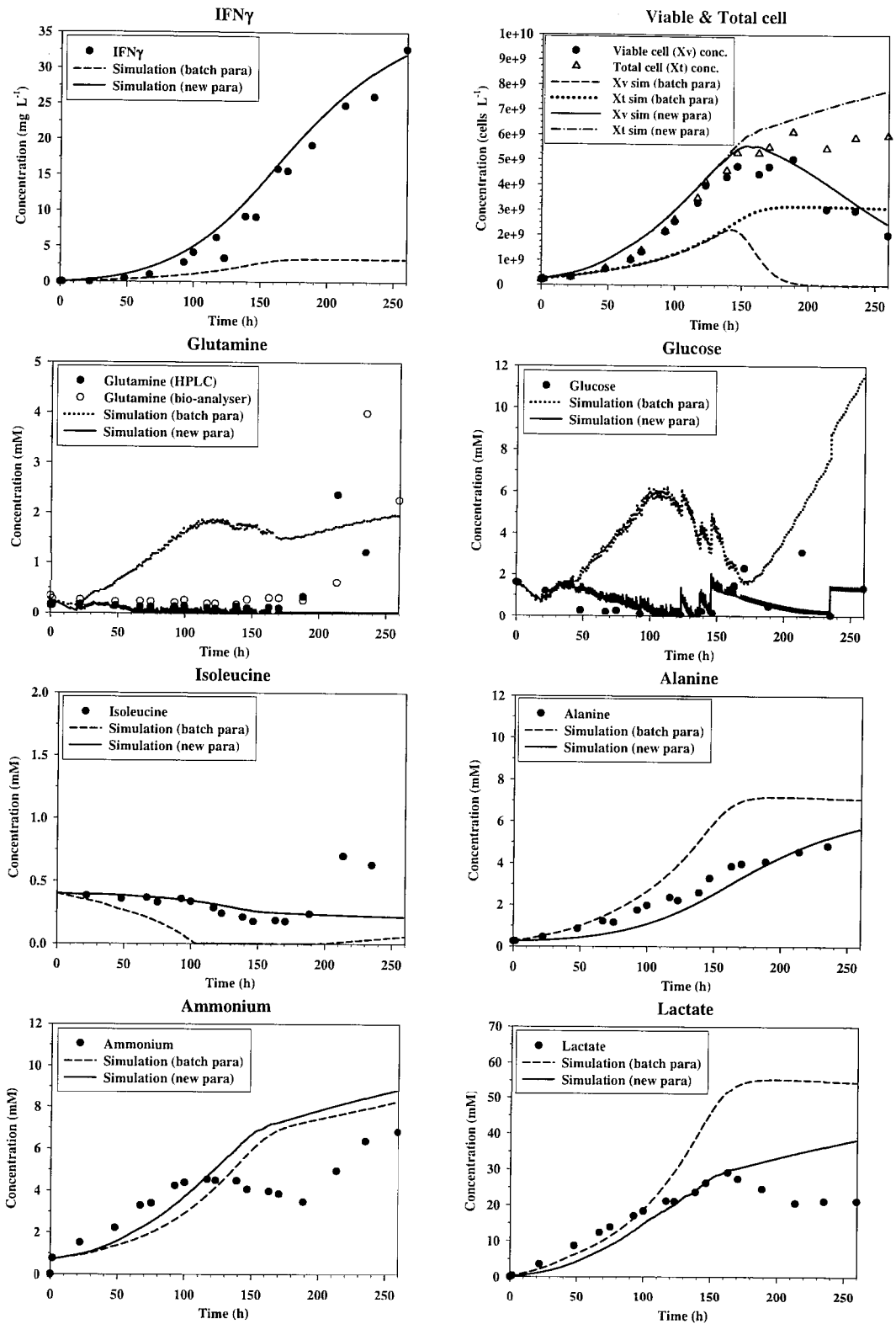


Figure 4.3: Simulations of the simple amino acid CHO-IFN γ model for fed-batch culture with glutamine set-point at 0.3mM (1st experiment) using parameter values from batch culture versus adjusted new parameter values. Circles represent experiment data.

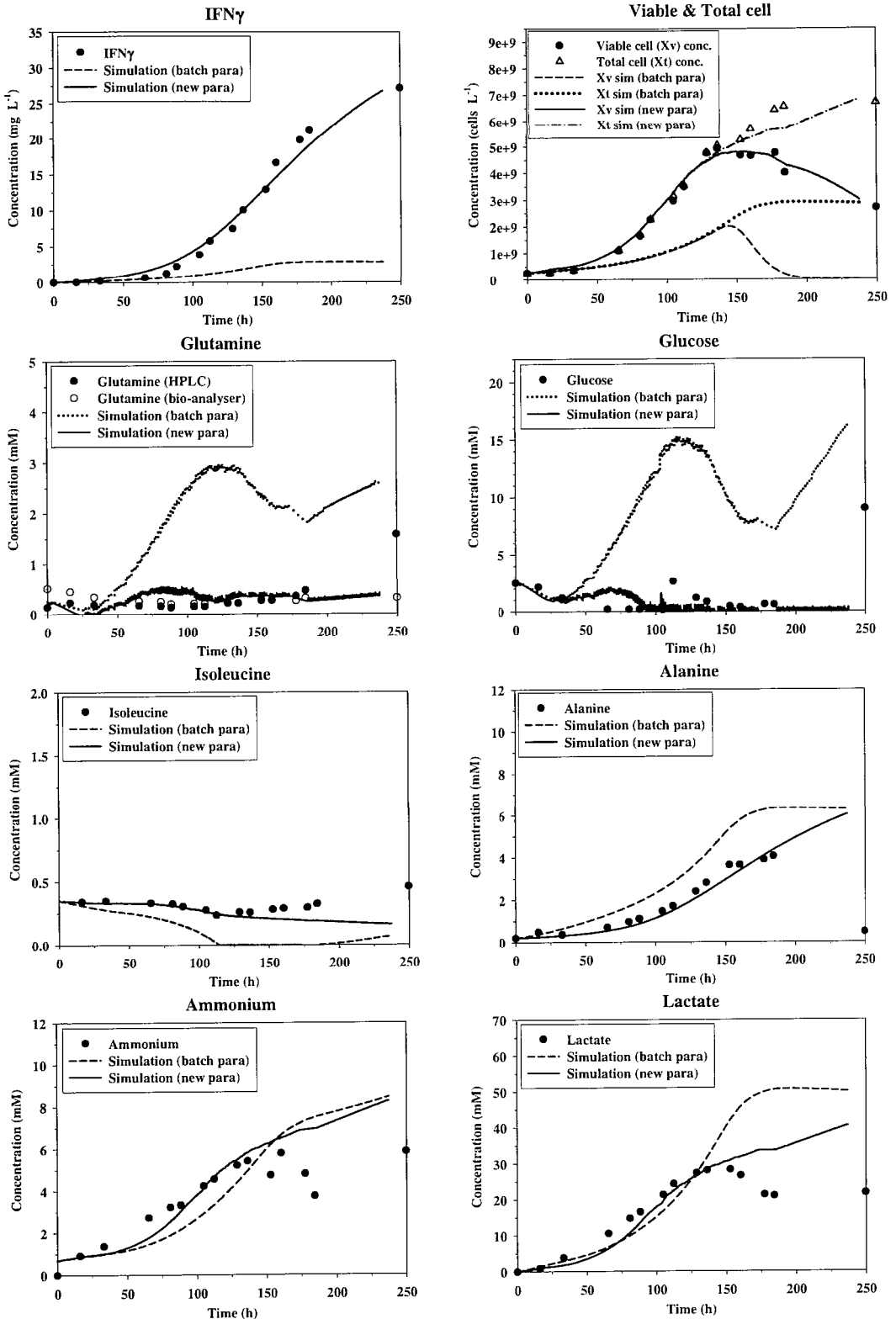


Figure 4.4: Simulations of the simple amino acid CHO-IFN γ model for fed-batch culture with glutamine set-point at 0.3mM (2nd experiment) using parameter values from batch culture versus adjusted new parameter values. Circles represent experiment data.

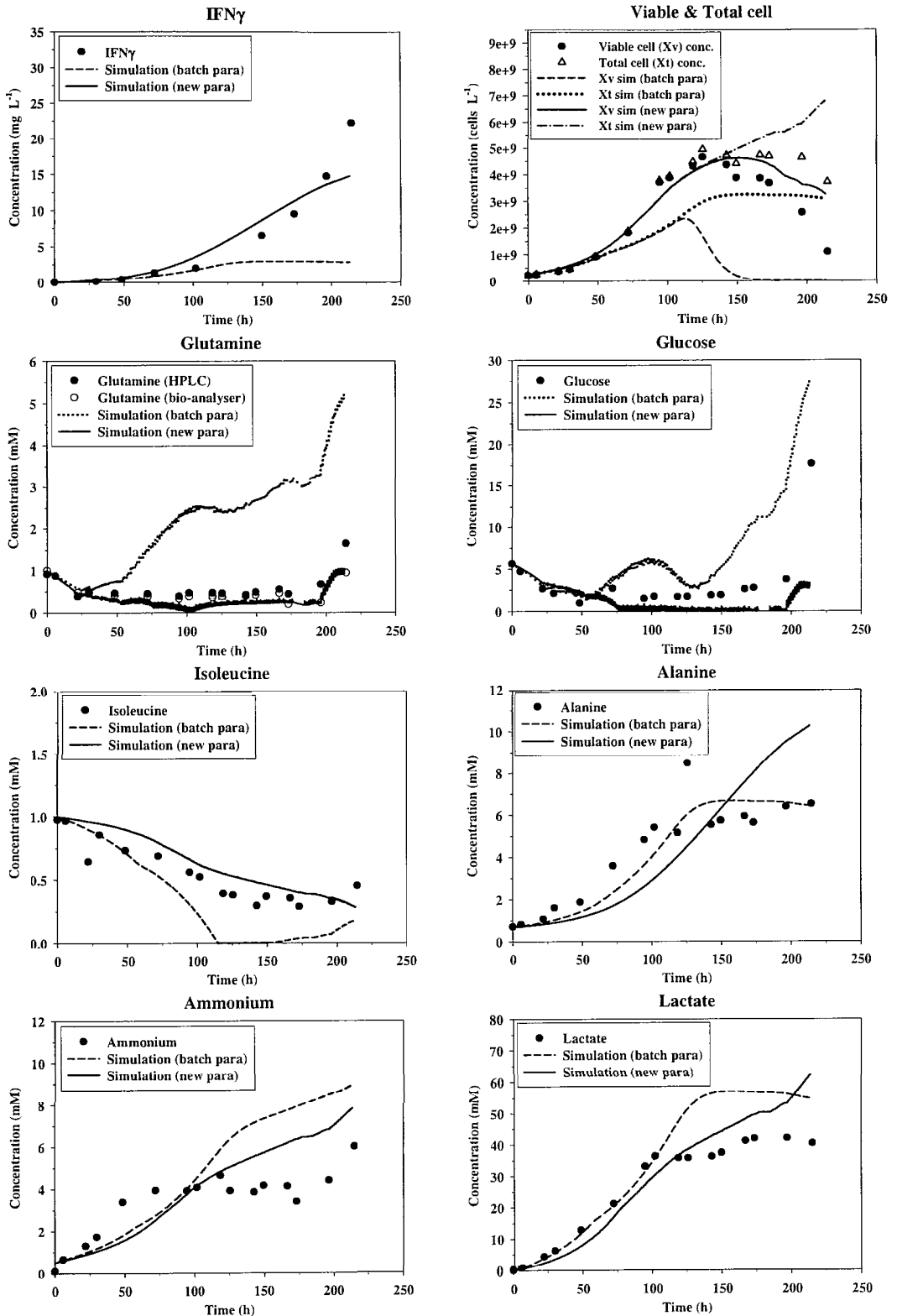


Figure 4.5: Simulations of the simple amino acid CHO-IFN γ model for fed-batch culture with glutamine set-point at 0.5mM using parameter values from batch culture versus adjusted new parameter values. Circles represent experiment data.

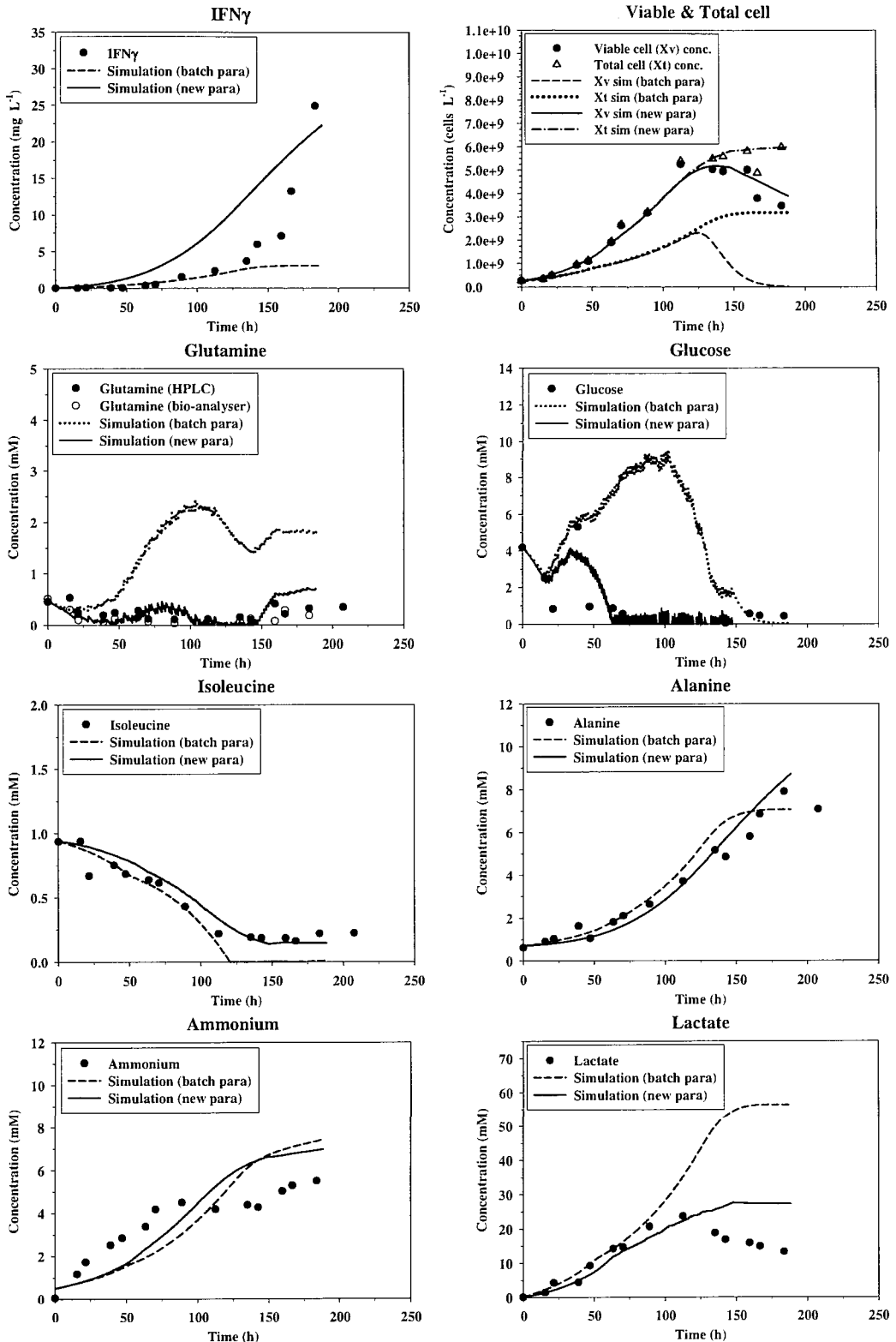


Figure 4.6: Simulations of the simple amino acid CHO-IFN γ model for fed-batch culture with **glutamine set-point at 0.3mM** and **glucose set-point at 0.7mM** using parameter values from batch culture vs. adjusted new parameter values. Circles represent experiment data.

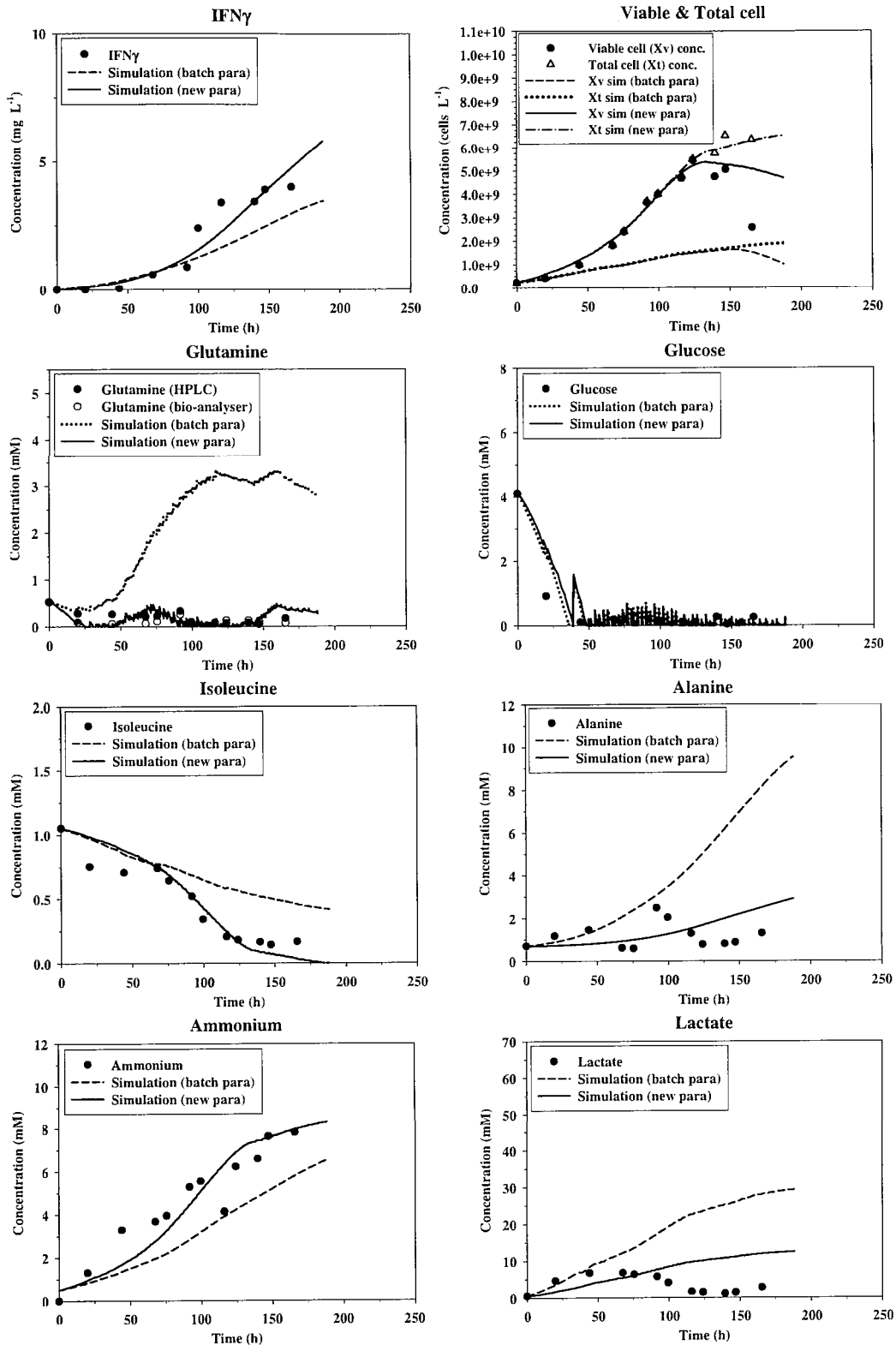


Figure 4.7: Simulations of the simple amino acid CHO-IFN γ model for fed-batch culture with glutamine set-point at 0.3mM and glucose set-point at 0.35mM using parameter values from batch culture versus adjusted new parameter values. Circles represent experiment data.

4.1.4 Parameter Sensitivity Analysis

4.1.4.1 Sensitivity Analysis Methods & the Method of Sobol'

The relative importance of model parameters with respect to model outputs can be analysed by varying the parameter values to see how the outputs are affected. The methods for sensitivity analysis can be classified into screening, local sensitivity, and global sensitivity (Saltelli et al., 2000). Screening methods rank the input factors in the order of importance but do not quantify the exact percentage of influence that each input factor has on the total output (Campolongo et al., 2000). Local sensitivity analysis methods either numerically vary the input factors within a small interval around a nominal value or directly solve the differentiation of output variables with respect to input factors (Turanyi and Rabitz, 2000). As the local sensitivity analysis methods do not explore the whole range of possible values of the input factors, it is not suitable for non-linear models which are common in dynamic biological systems.

Global sensitivity analysis (GSA) methods vary the input factors over their ranges of existence and relate their importance to the output uncertainty. It evaluates the effect of each input factor while all other factors are varied as well (Saltelli et al., 2000). Both sampling-based methods and variance-based methods can be used for GSA. Sampling-based methods sample the whole domain of the input factors. But certain *a priori* knowledge of the model is required to select an appropriate distribution of the input factors within their ranges (Helton and Davis, 2000). This knowledge may be the fact that the model is linear or at least monotonic, or the information about the relative importance of the variables. Variance-based methods use variance to indicate the significance of input factors. There are several approaches to evaluate the variance, all of which include calculating the following quantity with or without higher order interactions of input factors (Saltelli et al., 1999; Chan et al, 2000):

$$\text{var}_X [E(Y|X)] \tag{4S.1}$$

or

$$\frac{\text{var}_X [E(Y|X)]}{\text{var}(Y)} \tag{4S.2}$$

or other combinations of the numerator and denominator in Equation 4S.2. In Equation 4S.1 & 4S.2, Y is the output variable, X is the input factor, $E(Y|X)$ is the expectation of Y conditional on a fixed value of X , and var_X is the variance taken over all possible values of X .

Correlation ratio method, Fourier amplitude sensitivity test (FAST) and Sobol' method are often used in GSA to measure the variance. Correlation ratio is a simple way to evaluate the importance of an input factor. It is equivalent to the first-order sensitivity indices in FAST and Sobol' method (Chan et al, 2000). FAST was first proposed by Cukier et al. (1978) involving the use of transformation functions to translate the probability density of the variation of input factors into an s -space in order to convert the n -dimensional integral in the input factor space into a one-dimensional integral in s -space. The FAST method is model independent and it calculates the higher order terms of interactions of input factors though the number of model evaluations required is often large (Saltelli et al., 1999; Haaker, 2004). But it is important to use an appropriate set of transformation function for FAST and the best choice is up to the user (McRae et al., 1982). The Sobol' method is an alternative to FAST but does not involve any user-selected transformation (Sobol', 2001). The method of Sobol' was used in the sensitivity analysis of the simple amino acid CHO-IFN γ model in Section 4.1 and the more complex CHO-IFN γ model in Chapter 5. Below is a detailed description of the Sobol' method (Sobol', 2001).

Sobol' Method for Global Sensitivity Analysis (GSA)

If a function $f(\mathbf{x})$ can be integrated and $\mathbf{x} = (x_1, \dots, x_n)$ is a point in an n -dimensional unit hypercube with a range of 0 – 1, the function $f(\mathbf{x})$ can be decomposed into summands of increasing dimensionality as the following:

$$\begin{aligned}
f(x_1, \dots, x_n) &= f_0 + \sum_{s=1}^n \sum_{i_1 < \dots < i_s} f_{i_1 \dots i_s}(x_{i_1}, \dots, x_{i_s}) \\
&= f_0 + \sum_{i=1}^n f_i(x_i) + \sum_{i < j} f_{ij}(x_i, x_j) + \dots + f_{1,2,\dots,n}(x_1, \dots, x_n)
\end{aligned} \tag{4.S3}$$

Equation 4.S3 is valid if:

$$\int f_{i_1 \dots i_s}(x_{i_1}, \dots, x_{i_s}) dx_{i_k} = 0 \quad k = i_1, \dots, i_s \tag{4.S4}$$

A consequence of Equation 4.S4 is that the right-hand-side terms in Equation 4.S3 can be expressed as integrals of $f(\mathbf{x})$. For example:

$$\int f(\mathbf{x}) d\mathbf{x} = f_0 \tag{4.S5}$$

$$\int f(\mathbf{x}) \prod_{k \neq i} dx_k = f_0 + f_i(x_i) \tag{4.S6}$$

$$\int f(\mathbf{x}) \prod_{k \neq i, j} dx_k = f_0 + f_i(x_i) + f_j(x_j) + f_{ij}(x_i, x_j) \tag{4.S7}$$

and so on.

Assuming that $f(\mathbf{x})$ can be square integrated (i.e. the integral of the square of the function over the whole interval of the unit hypercube is finite), the total variance, D , of the function $f(\mathbf{x})$ can then be calculated from:

$$D = \int f^2(\mathbf{x}) d\mathbf{x} - f_0^2 = \sum_{s=1}^n \sum_{i_1 < \dots < i_s} \int f_{i_1 \dots i_s}^2 dx_{i_1} \dots dx_{i_s} = \sum_{s=1}^n \sum_{i_1 < \dots < i_s} D_{i_1 \dots i_s} \tag{4.S8}$$

The global sensitivity indices can be defined as:

$$S_{i_1 \dots i_s} = \frac{D_{i_1 \dots i_s}}{D} \tag{4.S9}$$

Because $D = \sum_{s=1}^n \sum_{i_1 < \dots < i_s} D_{i_1 \dots i_s}$,

$$\sum_{s=1}^n \sum_{i_1 < \dots < i_s} S_{i_1 \dots i_s} = 1 \tag{4.S10}$$

where $0 \leq S_{i_1 \dots i_s} \leq 1$. If the sensitivity index of an input factor is close to zero, the factor has no significant impact on the output variable of interest within its possible range of variation. The opposite is true if the sensitivity index is close to one.

Sobol' Sensitivity Indices for a Subset of Input Factors

If \mathbf{x} is consisted of two subsets of variables \mathbf{y} and \mathbf{z} , such that:

$$\mathbf{y} = (x_{k_1}, \dots, x_{k_m}), \quad 1 \leq k_1 < \dots < k_m \leq n \quad (4.S11)$$

and \mathbf{z} is the set of $n - m$ complementary variables. Then, the variance corresponding to \mathbf{y} is:

$$D_{\mathbf{y}} = \sum_{s=1}^m \sum_{(i_1 < \dots < i_s) \in K} D_{i_1 \dots i_s} \quad (4.S12)$$

The total variance corresponding to \mathbf{y} also involves the interactions between \mathbf{y} and \mathbf{z} except the variance of \mathbf{z} :

$$D_{\mathbf{y}}^{tot} = D - D_{\mathbf{z}} \quad (4.S13)$$

$$S_{\mathbf{y}}^{tot} = \frac{D_{\mathbf{y}}^{tot}}{D} \quad (4.S14)$$

Thus, $0 \leq S_{\mathbf{y}} \leq S_{\mathbf{y}}^{tot} \leq 1$.

An implementation of the Sobol' GSA method coded in C++ and linked to gPROMS for model solving was kindly provided by Dr. Sergei Kucherenco (Centre for Process Systems Engineering, Chem Eng Dept., Imperial College London). The C++ codes employed a Sobol' sequence (Sobol', 1967; Sobol', 1976) for sampling the parameter space. The Sobol' sequence has a uniformity property for small number of samples and optimal uniformity of sample distribution when the length of the sequence tends to infinity which makes it more superior than random numbers (Chan et al., 2000). The GSA analysis results of the simple amino acid model for CHO-IFN γ cell culture is discussed in the next section.

4.1.4.2 GSA for the Simple Amino Acid CHO-IFN γ Model

In this section, the Sobol' method of Global Sensitivity Analysis (GSA) is used to analyse the relative importance of the parameters of the simple amino acid CHO-IFN γ model with respect to the viable cell concentration which directly affects the total production rate. The specific IFN γ production rate (r_{IFN}) was excluded from the GSA analysis because by definition it is a very significant parameter for the specific productivity of the cell culture.

Due to the large number of parameters involved, they were grouped according to parameter types as shown in Table 4.3.

Table 4.3: Parameter groups for Global Sensitivity Analysis (GSA) of the simple amino acid model for the CHO-IFN γ culture.

<u>Group</u>	<u>Parameter Type</u>
1	Minimum and maximum specific growth rates.
2	Half-saturation constants relating amino acid concentration to specific growth rate. E.g. K_{thr} (overall insensitive w.r.t. X_v)
3	Parameters for specific death rate. E.g. AMM_{cr}
4	Parameters for specific consumption of glutamine. E.g. $Y_{x,gln}$
5	Parameters for specific consumption of glucose. E.g. $Y_{x,glc}$
6	Cell yields from amino acids. E.g. $Y_{x,glu}$
7	Specific production rates of non-essential amino acids. E.g. $r_{glu,x}$ (overall insensitive w.r.t. X_v)
8	Yield of non-essential amino acids from other amino acids. E.g. $Y_{ser,gly}$ (overall insensitive w.r.t. X_v)
9	Yield of byproducts from energy sources. E.g. $Y_{amm,gln}$

The parameters were varied by $\pm 100\%$ of their nominal values in Table 4.2. The sensitivity indices were normalised to a range of 0 – 1. A cut-off threshold of 0.05 was used to separate the sensitive parameter groups (> 0.05) from the insensitive parameter groups (< 0.05). The individual parameters in each sensitive parameter group were then further analysed using GSA to identify those parameters that have significant effects on the viable cell concentration. The cut-off threshold of the sensitivity indices for the individual parameters was also 0.05. A total of 21 parameters out of 66 analysed parameters were identified as sensitive with respect to viable cell concentration. Thus, overall there are 22 sensitive parameters including r_{IFN} that are significantly affecting $IFN\gamma$ productivity within $\pm 100\%$ of their nominal values. Among the 22 sensitive parameters, 17 of them require a change in values in order to be able to correctly simulate the fed-batch CHO- $IFN\gamma$ cell cultures. The remaining 5 unchanged sensitive parameters are: $K_{d,amm}$, $K_{d,lac}$, $[AMM]_{cr}$, $[LAC]_{cr}$, and $r_{d,glc}$. A list of parameters of which the values are different between batch and fed-batch cultures is shown in Table 4.4.

Table 4.4: List of sensitive parameters of the simple amino acid CHO-IFN γ model identified by GSA.

Parameters of which the values changed in FB	Sensitive parameters	Normalised parameter fluctuation*
$\mu_{d,min}$	•	0.2 – 1
$Y_{x,glc}$	•	0.8 – 2.3
K_{gln}	-	0.05 – 1
μ_{max}	•	0.9 – 1.4
$Y_{x,glu}$	•	0.6 – 1
$Y_{x,tyr}$	-	1 – 7.7
$Y_{x,cys}$	-	1 – 67
$Y_{x,met}$	-	1 – 3.8
$Y_{x,arg}$	•	1 – 10
$Y_{x,thr}$	•	1 – 11
$Y_{x,gln}$	•	0.8 – 1.1
$Y_{x,lys}$	•	1 – 6.2
$Y_{x,ser}$	•	1 – 12
$Y_{x,val}$	•	1 – 6.7
$Y_{x,his}$	•	1 – 6.5
$Y_{x,phe}$	•	1 – 7.3
$Y_{x,leu}$	•	1 – 6
$Y_{x,ile}$	•	1 – 7.5
$Y_{x,pro}$	-	1 – 48
$Y_{x,ala}$	-	1 – 100
$Y_{x,asn}$	-	1 – 3.3
$Y_{x,gly}$	-	1 – 63
$Y_{glu,x}$	-	0.5 – 1
$Y_{ala,x}$	-	0.07 – 1
$Y_{lac,glc}$	•	0.3 – 1.1
$Y_{amm,gln}$	•	0.5 – 1
μ_{min}	-	0.5 – 1
K_{glc}	-	0.3 – 1
r_{IFN}	•**	0.6 – 2.3

* Parameter fluctuation expressed as multiple of the corresponding nominal value in the batch culture. The range represented the lower and upper bounds of the parameter values in fed-batch cultures after normalisation.

** Parameter sensitive for product synthesis instead of viable cell concentration.

Apart from 17 sensitive parameters having different values in fed-batch cultures, the values of 12 other insensitive parameters are also changed (Table 4.4) but the influence of the latter on productivity prediction is relatively negligible. The varied sensitive parameters are mainly related to specific growth rate, cell yield from most of the essential/growth-stimulating amino acids, and byproduct yields. The varied insensitive parameters are mainly related to non-essential amino acids. The variation of certain parameters is much larger than the 2-fold range analysed in the GSA, e.g. one of the sensitive parameters, $Y_{x,ser}$, is changed up to 12-fold; and one of the insensitive parameters, $Y_{x,ala}$, is changed up to 100-fold. This revealed a highly dynamic nature of the mammalian cell culture system. It would be necessary to model the cell culture in

greater details particularly regarding any possible changes in cellular regulations that might be encountered in batch and fed-batch cultures.

4.1.5 Conclusions of the Simple Amino Acid Model

In Section 4.1 it has been attempted to build a simple cell culture model including amino acids to describe the growth kinetics and productivity of a CHO-IFN γ cell-line. The model started with simulation of the batch culture and was able to capture the patterns of all major variables. But subsequent simulations for fed-batch cultures revealed significant prediction discrepancy unless the values of certain model parameters were changed for each individual fed-batch culture. It is necessary to model the cell culture in greater details and include variations of the cell culture dynamics in batch/fed-batch cultures that have been reported in the literature.

4.1.6 Notations for the Simple CHO-IFN γ Amino Acid Model

Table 4.5: Notations for the simple amino acid model of the CHO-IFN γ culture.

Symbol	Definition	Units
Variables:		
$[a.a.]_{in}$	Feed concentration of amino acid (a.a.)	mM
$[ALA]$	Extracellular concentration of alanine	mM
$[AMM]$	Extracellular concentration of ammonium	mM
$[AMM]$	Ammonium concentration in inlet stream	mM
$[ARG]$	Extracellular concentration of arginine	mM
$[ASN]$	Extracellular concentration of asparagine	mM
$[ASP]$	Extracellular concentration of aspartate (aspartic acid)	mM
$[CYS]$	Extracellular concentration of cysteine	mM
$[GLC]$	Extracellular concentration of glucose	mM
$[GLC]_{in}$	Glucose concentration in inlet stream	mM
$[GLN]$	Extracellular concentration of glutamine	mM
$[GLU]$	Extracellular concentration of glutamate (glutamic acid)	mM
$[GLY]$	Extracellular concentration of Glycine	mM
$[HIS]$	Extracellular concentration of histidine	mM
$[ILE]$	Extracellular concentration of isoleucine	mM
$[LAC]$	Extracellular concentration of lactate	mM
$[LEU]$	Extracellular concentration of leucine	mM
$[LYS]$	Extracellular concentration of lysine	mM
$[MET]$	Extracellular concentration of methionine	mM
$[PHE]$	Extracellular concentration of phenylalanine	mM
$[PRO]$	Extracellular concentration of proline	mM
$[SER]$	Extracellular concentration of serine	mM
$[THR]$	Extracellular concentration of threonine	mM
$[TYR]$	Extracellular concentration of tyrosine	mM
$[VAL]$	Extracellular concentration of valine	mM
F_{glc}	Flowrate of glucose-containing stream	L h ⁻¹
F_{in}	Flowrate of concentrated amino acids stream	L h ⁻¹
F_{out}	Outlet flowrate	L h ⁻¹
M_{gln}	Maintenance consumption of glutamine	mmole cell ⁻¹ h ⁻¹
Q_{amm}	Specific ammonium production rate	mmole cell ⁻¹ h ⁻¹
Q_{glc}	Specific glucose consumption rate	mmole cell ⁻¹ h ⁻¹
Q_{gln}	Specific glutamine consumption rate	mmole cell ⁻¹ h ⁻¹
Q_i	Specific consumption/production rate of amino acid i	mmole cell ⁻¹ h ⁻¹
Q_{lac}	Specific lactate production rate	mmole cell ⁻¹ h ⁻¹
V	Cell culture volume	L
X_d	Dead cell concentration	cell L ⁻¹
X_t	Total cell concentration	cell L ⁻¹
X_v	Viable cell concentration	cell L ⁻¹
μ	Specific growth rate	h ⁻¹
μ_d	Specific death rate	h ⁻¹
Parameters:		
$[AMM]_{cr}$	critical ammonium concentration for specific death rate	mM
K_{arg}	Monod-type constant of arginine for specific growth rate	mM
K_{cys}	Monod-type constant of cysteine for specific growth rate	mM
$K_{d,amm}$	Effective concentration of ammonium to double the specific death rate	mM

$K_{d,lac}$	Effective concentration of lactate to double the specific death rate	mM
K_{glc}	Monod-type constant of glucose for specific growth rate	mM
K_{gln}	Monod-type constant of glutamine for specific growth rate	mM
K_{his}	Monod-type constant of histidine for specific growth rate	mM
K_{ile}	Monod-type constant of isoleucine for specific growth rate	mM
K_{leu}	Monod-type constant of leucine for specific growth rate	mM
K_{lys}	Monod-type constant of lysine for specific growth rate	mM
K_{met}	Monod-type constant of methionine for specific growth rate	mM
K_{phe}	Monod-type constant of phenylalanine for specific growth rate	mM
K_{thr}	Monod-type constant of threonine for specific growth rate	mM
K_{tyr}	Monod-type constant of tyrosine for specific growth rate	mM
K_{val}	Monod-type constant of valine for specific growth rate	mM
$[LAC]_{cr}$	critical lactate concentration for specific death rate	mM
M_{glc}	Maintenance consumption rate for glucose	mmole cell ⁻¹ h ⁻¹
$r_{ala,x}$	Specific production rate of alanine from cell	mmole cell ⁻¹ h ⁻¹
$r_{asp,x}$	Specific production rate of aspartate from cell	mmole cell ⁻¹ h ⁻¹
$r_{glu,x}$	Specific production rate of glutamate from cell	mmole cell ⁻¹ h ⁻¹
$r_{d,gln}$	Degradation rate of glutamine	h ⁻¹
r_{frag}	Rate of loss of dead cells	h ⁻¹
$Y_{amm,gln}$	Yield of ammonium from glutamine	mmole mmole ⁻¹
$Y_{arg,asp}$	Yield of arginine from aspartate	mmole mmole ⁻¹
$Y_{arg,glu}$	Yield of arginine from glutamate	mmole mmole ⁻¹
$Y_{arg,pro}$	Yield of arginine from proline	mmole mmole ⁻¹
$Y_{asn,asp}$	Yield of asparagine from aspartate	mmole mmole ⁻¹
$Y_{asp,arg}$	Yield of aspartate from arginine	mmole mmole ⁻¹
$Y_{cys,ser}$	Yield of cysteine from serine	mmole mmole ⁻¹
$Y_{gln,glu}$	Yield of glutamine from glutamate	mmole mmole ⁻¹
$Y_{glu,arg}$	Yield of glutamate from arginine	mmole mmole ⁻¹
$Y_{glu,gln}$	Yield of glutamate from glutamine	mmole mmole ⁻¹
$Y_{glu,his}$	Yield of glutamate from histidine	mmole mmole ⁻¹
$Y_{glu,pro}$	Yield of glutamate from proline	mmole mmole ⁻¹
$Y_{gly,ser}$	Yield of glycine from serine	mmole mmole ⁻¹
$Y_{lac,glc}$	Yield of lactate from glucose	mmole mmole ⁻¹
$Y_{pro,arg}$	Yield of proline from arginine	mmole mmole ⁻¹
$Y_{pro,glu}$	Yield of proline from glutamate	mmole mmole ⁻¹
$Y_{ser,gly}$	Yield of serine from glycine	mmole mmole ⁻¹
$Y_{tyr,phe}$	Yield of tyrosine from phenylalanine	mmole mmole ⁻¹
$Y_{x,ala}$	Cell yield from alanine	cell mmole ⁻¹
$Y_{x,arg}$	Cell yield from arginine	cell mmole ⁻¹
$Y_{x,asn}$	Cell yield from asparagine	cell mmole ⁻¹
$Y_{x,asp}$	Cell yield from aspartate	cell mmole ⁻¹
$Y_{x,cys}$	Cell yield from cysteine	cell mmole ⁻¹
$Y_{x,glc}$	Cell yield from glucose	cell mmole ⁻¹
$Y_{x,gln}$	Cell yield from glutamine	cell mmole ⁻¹
$Y_{x,glu}$	Cell yield from glutamate	cell mmole ⁻¹
$Y_{x,gly}$	Cell yield from glycine	cell mmole ⁻¹
$Y_{x,his}$	Cell yield from histidine	cell mmole ⁻¹
$Y_{x,ile}$	Cell yield from isoleucine	cell mmole ⁻¹

$Y_{x,leu}$	Cell yield from leucine	cell mmole ⁻¹
$Y_{x,lys}$	Cell yield from lysine	cell mmole ⁻¹
$Y_{x,met}$	Cell yield from methionine	cell mmole ⁻¹
$Y_{x,phe}$	Cell yield from phenylalanine	cell mmole ⁻¹
$Y_{x,pro}$	Cell yield from proline	cell mmole ⁻¹
$Y_{x,ser}$	Cell yield from serine	cell mmole ⁻¹
$Y_{x,thr}$	Cell yield from threonine	cell mmole ⁻¹
$Y_{x,tyr}$	Cell yield from tyrosine	cell mmole ⁻¹
$Y_{x,val}$	Cell yield from valine	cell mmole ⁻¹
α_1	Maximum maintenance consumption rate for glutamine	mmole cell ⁻¹ h ⁻¹
α_2	Half-saturation concentration for glutamine maintenance consumption	mM
$\mu_{d,min}$	Minimum specific death rate	h ⁻¹
μ_{min}	Minimum specific growth rate	h ⁻¹
μ_{max}	Maximum specific growth rate	h ⁻¹
r_{IFN}	Specific production rate of IFN γ	mg cell ⁻¹ h ⁻¹

4.2 A CHO-IFN γ Model including Amino Acids & Cellular Regulations

The main motivation of developing a more detailed growth and amino acid model for CHO-IFN γ cell culture was the inability of the simple cell culture model developed in Section 4.1 to predict both batch and fed-batch cell culture behaviours using the same set of parameter values. In this section, the evidence in the literature regarding mammalian cell cultures exhibiting a change in cell culture dynamics is discussed. An approximation has been introduced to incorporate the variation between the batch and fed-batch CHO-IFN γ cultures into the mathematical model. Certain simplifications have also been made to the modelling of non-essential amino acid consumptions and interconversions in order to reduce the number of under-specified parameters that have no significant influence upon cell density and productivity predictions.

4.2.1 Development of Model Equations

4.2.1.1 Alterations in Cell Culture Dynamics

A 'Shift' in Cell Culture Responses

The response of cells to changes in nutrient concentration is better understood for yeast cells than other cell cultures. In yeast cells, there are distinct glucose-sensing pathways providing 3 different responses at different glucose concentrations (Geladé et al., 2003). As shown in figure 4.8, the *Snf3/Rgt2* glucose sensing pathway is inactive in the absence of glucose and the *Rgt1-Std1-Mth1* complex represses transcription of the *HXT1-HXT4* genes responsible for glucose transport. The presence of glucose inactivates *Rgt1* via *SCF-Grr1*-mediated inactivation and degradation of *Mth1/Std1* and hyperphosphorylation of *Rgt1*, thus activating the *HXT* promoters. Low glucose concentrations cause *Snf3* to trigger the expression of *HXT1-HXT4*; whereas high glucose concentrations cause *Rgt2* to further enhance *HXT1* expression (Geladé et al.,

2003). A similar glucose-sensing mechanism is also discussed by Ozcan and Johnston (1995), Diderich et al. (1999), and Rolland et al. (2001) for yeast cells.

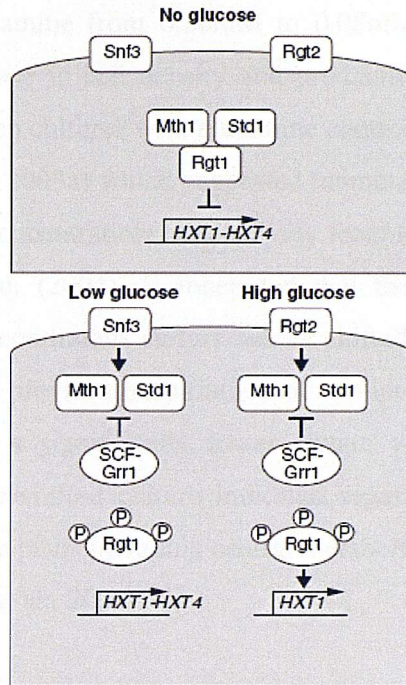


Figure 4.8: The *Snf3/Rgt2* glucose sensing pathway in yeast by Geladé et al. (2003).

At the genetic level of yeast cells, high glucose concentrations were found to suppress genes responsible for the citric acid cycle which fully oxidises glucose into CO₂ while producing ATP; and more genes responsible for amino acids metabolism, carbon metabolism, energy, protein synthesis, and cellular transport were up regulated at low glucose levels than high glucose levels (Yin et al., 2003). The effect of glucose signalling in yeasts was also found to be only dependent on extracellular glucose concentration but *not* glucose flux (Meijer et al., 1998; Ozcan et al., 1998).

Mammalian cell cultures also showed different responses to various levels of extracellular nutrient concentrations. For example, low glucose concentration in a CHO chemostat culture producing tissue-type plasminogen activator (tPA) caused an increase in viable cell concentration (Altamirano et al., 2001); low glucose/glutamine fed-batch cultures of a murine hybridoma cell-line showed a lower lactate yield from glucose and lower ammonium yield from glutamine (Zhou et al., 1997a); glutamine-limited fed-batch cultures of a murine myeloma cell-line had higher cell yield from glucose, glutamine, and essential amino acids (Ljunggren and Häggström, 1994). Mancuso et al. (1998) had carried out a detailed study of the effect of glutamine concentration on perfusion cultures of murine hybridoma 4A2 cell-line producing IgG type antibody. It was found that a rapid removal of

feed glutamine for a short time produced a rapid change in residual glutamine from 0.67mM to below 0.3mM plus a strong stimulation of the specific and total antibody synthesis; but a slow reduction in feed glutamine concentration which caused a similar reduction in residual glutamine from 0.30mM to 0.08mM did not increase antibody production rate. An increase in cell density and productivity for a human embryonic kidney cell-line in fed-batch cultures with glutamine controlled at 0.1 – 0.3mM had also been observed (Lee et al., 2003a) which suggested mammalian cells tend to respond to such range of glutamine concentrations distinctively from higher concentrations. At the genetic level, Korke et al. (2004) demonstrated that the metabolic state of mouse hybridoma MAK cells in continuous culture can be shifted by culture the cells in low-glucose fed-batch cultures previous to initiation of continuous culture; and the cells in the shifted state showed a significantly lower lactate yield from glucose. Genetic expression analysis of the shifted culture indicated regulations of a large variety of genetic functions had taken place including central metabolism, mitochondrial transport, RNA binding etc. (Korke et al., 2004).

Approximation Factor for Changes in Cell Culture Behaviour

When only high versus low range of concentration of major nutrients are the main interests of process design, i.e. the intermediate range of nutrient concentration provides no particular advantage for enhancing product yield or quality, a system that behaves differently in the high versus low range of concentration of major nutrients may be described by the following approximation:

$$\mathcal{R}_i = f(x_i, \tau_i, y_i)$$

where \mathcal{R}_i is a dimensionless quantity representing cell culture response, x_i is cell culture variable, τ_i is a hypothetical threshold separating x_i into two regions, y_i is a binary variable responsible for activation/deactivation of \mathcal{R}_i depending on the value of x_i such that:

$$y_i = \begin{cases} 1 & , x_i \leq \tau_i \\ 0 & , x_i > \tau_i \end{cases} \quad (\text{R0})$$

A graphical illustration of the relationship between the hypothetical response and cell culture variable x_i is shown below:

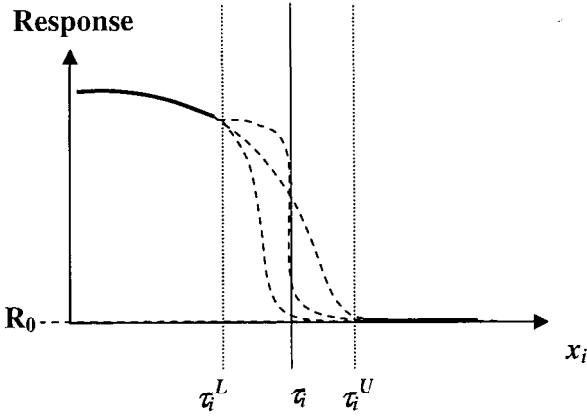


Figure 4.9: Conceptual representation of the response factor.

Since such ‘step-change’ is an approximation of the system’s behaviour, τ_i has an uncertainty range of $[\tau_i^L, \tau_i^U]$ unless the change is known to be sharp around τ_i .

Such response factor is applied on glucose- and glutamine-controlled fed-batch cultures of CHO-IFN γ versus batch culture. According to the glucose-sensing pathways of yeast cells reported by Geladé et al. (2003), there is a third signalling response at zero glucose concentration that all glucose sensors and transporters became inactive. There are many similarities in the signalling network between yeast and mammalian cells. Examples include the Snf1 gene in yeast responsible for activating glucose-repressed gene and regulating fatty acid synthesis is structurally very similar to a mammalian protein kinase AMPK responsible for glucose and lipid metabolism (Carling et al., 1994; Mitchelhill et al., 1994; Woods et al., 1994); and one out of three identified activating molecules of the SNF1 kinase in yeast was able to activate mammalian AMPK (Hong et al., 2003) which suggested functional conservation of signalling pathway between yeast and mammalian cells. Thus, the binary variable in Equation R0 is extended to include a third region for $Glc = 0$:

$$y_1 = \begin{cases} 0, & Glc = 0 \\ 1, & 0 < Glc < \tau_{Glc} \\ 0, & Glc \geq \tau_{Glc} \end{cases} \quad (M1)$$

where y_1 is the binary variable for glucose, Glc (mM) is glucose concentration in the cell culture, τ_{Glc} is the threshold level of glucose below which certain cellular activities might appear to be shifted to a different trend.

It is assumed that the cellular responses to different levels of glutamine have a similar structure as glucose:

$$y_2 = \begin{cases} 0, & Gln = 0 \\ 1, & 0 < Gln < \tau_{Gln} \\ 0, & Gln \geq \tau_{Gln} \end{cases} \quad (M2)$$

where y_2 is the binary variable for glucose, Gln (mM) is glutamine concentration in the cell culture, τ_{Gln} is the threshold level of glutamine below which certain cellular activities might appear to be shifted to a different trend.

The response functions for glucose and glutamine take the following form:

$$\frac{d(x_{res,Glc})}{dt} = rmax_{res,Glc} \cdot \log[1 + y_1 \cdot (\tau_{Glc} - Glc)] - d_{res,Glc} \cdot x_{res,Glc} \quad (M3)$$

$$\frac{d(x_{res,Gln})}{dt} = rmax_{res,Gln} \cdot \log[1 + y_2 \cdot (\tau_{Gln} - Gln)] - d_{res,Gln} \cdot x_{res,Gln} \quad (M4)$$

where $x_{res,i}$ is the hypothetical dimensionless response variable, $rmax_{res,i}$ is an activation coefficient, and $d_{res,i}$ (h^{-1}) is a degradation rate of the response. The logarithmic function serves to restrict the upper limit of $y_1 \cdot (\tau_{Glc} - Glc)$ and $y_2 \cdot (\tau_{Gln} - Gln)$ for large values of τ_{Glc} and τ_{Gln} but in this study the values of the two parameters are relatively small that the function remains unsaturated.

Because the response functions cannot be validated by cell culture data, the response variables $x_{res,Glc}$ and $x_{res,Gln}$ are linked to parameters that quantify the changes between batch and glucose-/glutamine-controlled fed-batch cultures. The usefulness of such response functions would then be judged by whether the overall model predictions are able to capture the trends of the cell culture dynamics under both batch and fed-batch conditions or not and this is discussed in Chapter 5.

4.2.1.2 Growth/Death Rate & Cell Lysis

Specific Growth Rate

Ammonium is one of the byproducts that would inhibit cell growth and trigger cell death (Ryll et al., 1994). Hayter et al. (1991) reported that an initial level of 4.5mM ammonium inhibited the growth of CHO cells in batch culture but a level of 2mM had no significant effect; the cell growth was also unaffected by an initial lactate concentration of 17.5mM. Schlaeger and Schumpp (as cited in Hayter et al., 1991) found in their study that 8 – 10 mM ammonium and 90 – 110 mM lactate were required to give 50% inhibition of CHO cell growth.

Ludemann et al. (1994) studied a hybridoma cell-line and proposed an equation structure for the toxic effect of ammonium based on a threshold level of ammonium below which the toxicity would be negligible. The specific growth rate was modelled to be proportional to the following equation:

$$\frac{k_i}{(NH_3 - NH_{3cr}) + k_i} \quad (R1)$$

where k_i is an inhibition constant, NH_3 is the ammonia concentration in the medium, NH_{3cr} is the critical level of ammonia below which $(NH_3 - NH_{3cr}) = 0$. In this section, the symbol 'R' is used to represent terms and equations referenced from other literature as opposed to equations for the CHO-IFN γ model ('M'). In the above equation, the concentration of ammonia was used instead of ammonium (NH_4^+) because a significant relationship between the specific growth rate and NH_3 was detected but not the total ammonium concentration (Ludemann et al., 1994). As the amount of dissociated NH_3 in an ammonium solution is pH dependent, the Henderson-Hasselbach equation was used to calculate NH_3 concentration from measured values of NH_4^+ concentration:

$$pH = pK_a + \log\left(\frac{NH_3}{NH_4^+}\right) \quad (M5)$$

The pK_a value at 37°C is 9.27 based on the equation of Edwards et al. (1975). The pH in the CHO-IFN γ cell culture studied in this work was controlled at pH 7 (Wong et al., 2005) so the concentration of NH_3 and NH_4^+ became linearly related. If there were fluctuations in the cell culture pH, Equation M5 would have a more significant role in every time step of the model simulations.

The inhibitive level of ammonium appeared to be cell-line dependent as different values had been reported for various types of cells and ranges from less than 1mM to about 5mM had been reported (Glacken et al., 1986; Reuveny et al., 1986; Visek et al., 1972; Hassell et al., 1991).

Lactate is another major metabolic byproduct that would inhibit growth rate and accelerate death rate in the cell culture. Omasa et al. (1992) performed a detailed study towards the effect of lactate on growth rate in a fed-batch hybridoma cell culture. It was tested whether replacing sodium lactate by sodium chloride would produce the same growth inhibition. When the osmotic pressure was adjusted to the same condition as that of lactate using sodium chloride, the specific growth rate showed the same degree of growth inhibition (Omasa et al., 1992). Thus, it was the increase in osmotic pressure caused by high lactate concentration that induced an inhibition of specific growth rate (Kurano et al., 1990a; Kurano et al., 1990b; Omasa et al., 1992); whereas ammonium started to inhibit cell growth at low concentrations before osmolarity can be affected (Kurano et al., 1990b). As lactate is one of the major byproducts contributing to increasing the osmotic pressure, its concentration is assumed to be proportional to osmotic pressure and the inhibition equation (R1) has been extended to include lactate concentration:

$$f_{inh}(NH_3, Lac) = \left(\frac{k_{inh,NH3}}{(NH_3 - NH_{3cr}) + k_{inh,NH3}} \right) \cdot \left(\frac{k_{inh,Lac}}{(Lac - Lac_{cr}) + k_{inh,Lac}} \right) \quad (M6)$$

where where $k_{inh,NH3}$ and $k_{inh,Lac}$ (mM) are inhibition constants of ammonium and lactate respectively, Lac (mM) is the concentration of lactate, Lac_{cr} is the critical level of lactate below which $(Lac - Lac_{cr}) = 0$.

The growth inhibition of ammonium and lactate had been linked to specific nutrient consumption indirectly by Jang and Barford (2000b) using the following function:

$$q_s \propto \frac{\mu}{Y_{x,s}} + m_s \quad (R2)$$

where q_s was the specific uptake rate of nutrient S, $Y_{x,s}$ was the cell yield from S, m_s was the growth-independent consumption, and μ was a function of glucose, glutamine, ammonium and lactate. The same phenomenon of ammonium inhibition upon q_s can

also be modelled directly by adding the inhibition function to the nutrient uptake equation:

$$q_s \propto \frac{S}{K_s + S} \cdot f_{inh}(NH_3, Lac) \quad (R3)$$

where S is the concentration of nutrient S , K_s is a half-saturation constant for nutrient consumption, and $f_{inh}(NH_3, Lac)$ is defined in Equation M6. The difference between Equation R2 and R3 is that the latter is not linked to other growth limiting nutrients. Equation R2 separated the specific nutrient consumption into growth related ($\mu/Y_{x,s}$) and non-growth related (m_s) terms. Equation R3 combines both growth and non-growth related consumptions into one overall term which tends to $\mu/Y_{x,s} + m_s$ at low concentration of NH_3 and/or lactate; but tends to a non-zero value of m_s at high NH_3 and/or lactate concentrations. By using Equation R3, the $f_{inh}(NH_3, Lac)$ function would not appear directly in the specific growth rate equation. The growth inhibition effects of NH_3 and lactate would be executed in the model via a reduction in q_s at high levels of byproducts. Equation R3 is an approximation of Equation R2 both relating the high byproduct levels to a decrease in μ and q_s . Such approximation is appropriate for (i) batch and fed-batch cultures up to exponential growth phase when all growth-limiting nutrients are still abundant; and (ii) continuous and perfusion cultures when all growth limiting nutrients are supplied in the feed stream. This has an advantage of fewer model parameters being directly associated with the measurable quantity q_s , especially when the specific growth rate is linked to all essential amino acids on top of glucose and glutamine. A lower number of parameters directly connected to a measurable quantity (without changing the biological relation) can reduce the number of multiple solutions in the parameter estimation stage.

For the relationship between specific growth rate (μ) and essential nutrients, many batch/fed-batch culture models in the literature related μ to the extracellular nutrient concentrations using the following equation structure:

$$\mu \propto \frac{S}{K_{g,s} + S} \quad (R4)$$

where S is the concentration of a growth-limiting nutrient and $K_{g,s}$ is a half-saturation constant. In the equation above, μ is modelled using Monod-type kinetics (Monod, 1949) in terms of the nutrient concentration. However, in continuous cell culture it had been reported that the specific growth rate remained high when the extracellular

concentration of a rate-limiting nutrient was close to zero (Altamirano et al., 2001). In continuous cell culture models, μ is often linked to the nutrient supplementation rate (dilution rate) instead of using Equation R4. At steady state, μ is equal to the dilution rate and the cell concentration is related to the dilution rate (Heidemann et al., 1998). The dilution rate in a batch culture is zero so a different equation structure for μ is required when changing from batch to continuous culture and vice versa.

In this study, it is proposed that μ of a batch/ fed-batch/ continuous culture can be related to the availability of the limiting nutrient in the following form:

$$\mu \propto \frac{q_s}{K_{g,q_s} + q_s} \quad (M7)$$

where q_s (mmole 10^{-6} cell $^{-1}$ h $^{-1}$) is the specific uptake rate of the limiting nutrient per unit cell, and K_{g,q_s} (mmole 10^{-6} cell $^{-1}$ h $^{-1}$) is a half-saturation constant. In a batch culture, the specific uptake rate of a limiting nutrient is related to its extracellular concentration. But in a continuous culture, the dilution rate and composition of the inlet stream also play a role in affecting the specific uptake rate of the nutrient. For example, if the supply and consumption of the limiting nutrient in a continuous culture are equal such that at steady state the residual nutrient concentration in the medium is close to zero, the specific nutrient uptake rate would remain positive. Thus, Equation M7 would predict a positive specific growth rate when Equation R4 would predict a near-zero growth rate in fed-batch or continuous cultures.

Equation M7 can be reduced to Equation R4 when $q_s = \frac{rmax_s \cdot S}{K_s + S}$. However, if

q_s is also affected by other substrate and by-products, e.g.

$$q_s = \frac{rmax_s \cdot S}{K_s + S} \cdot f_{inh}(NH_3, Lac) \cdot f(x_{res}) \quad (\text{Equation M17}), \text{ the R.H.S. of Equation M7}$$

becomes:

$$\frac{\frac{rmax_s \cdot S}{K_s + S} \cdot f_{inh}(NH_3, Lac) \cdot f(x_{res})}{K_{g,q_s} + \frac{rmax_s \cdot S}{K_s + S} \cdot f_{inh}(NH_3, Lac) \cdot f(x_{res})} \quad (D1)$$

$$= \frac{rmax_s \cdot S}{K_{g,q_s} \cdot \left(\frac{K_s + S}{f_{inh}(NH_3, Lac) \cdot f(x_{res})} \right) + rmax_s \cdot S} \quad (D2)$$

$$= \frac{rmax_s \cdot S}{\frac{K_{g,q_s} \cdot K_s}{f_{inh}(NH_3, Lac) \cdot f(x_{res})} + \left(\frac{K_{g,q_s}}{f_{inh}(NH_3, Lac) \cdot f(x_{res})} + rmax_s \right) \cdot S} \quad (D3)$$

$$= \frac{\left(\frac{rmax_s}{\frac{K_{g,q_s}}{f_{inh}(NH_3, Lac) \cdot f(x_{res})} + rmax_s} \right) \cdot S}{\left(\frac{K_{g,q_s} \cdot K_s}{K_{g,q_s} + rmax_s \cdot f_{inh}(NH_3, Lac) \cdot f(x_{res})} \right) + S} \quad (D4)$$

which would reduce to a simple Monod-type kinetics of S only when the effects of NH_3 , Lac , and x_{res} are negligible. Otherwise q_s is dependent on more than one variable. The upper limit of the dependent variable q_s is bounded by the availability of S , the substrate uptake capacity, and the effect of the virtual response variable x_{res} .

Using Equation M7 and assuming essential/growth-stimulating amino acids (Table 4.1) and glucose + glutamine are the only growth-limiting substrates, the specific growth rate equation is proposed to be the following:

$$\mu = \mu_{max1} \cdot \left[\left(\prod_k \frac{q_{AA,k}}{K_{g,k}^* + q_{AA,k}} \right) \cdot \left(1 + \frac{\mu_{max2}}{\mu_{max1}} \cdot \frac{q_{Glc}}{K_{g,Glc}^* + q_{Glc}} \cdot \frac{q_{Gln}}{K_{g,Gln}^* + q_{Gln}} \right) \right] \quad (M8)$$

$$= \left(\overbrace{\mu_{max1} \cdot \left(\prod_k \frac{q_{AA,k}}{(K_{g,k}^* + q_{AA,k})} \right)}^{\mu_{min}} + \overbrace{\mu_{max2} \cdot \left(\prod_k \frac{q_{AA,k}}{(K_{g,k}^* + q_{AA,k})} \right) \cdot \left(\frac{q_{Glc}}{(K_{g,Glc}^* + q_{Glc})} \cdot \frac{q_{Gln}}{(K_{g,Gln}^* + q_{Gln})} \right)}^{\mu_{max}} \right) \quad (M8')$$

where $k = Val, Leu, Ile, Met, Phe, Trp, Thr, Lys, His, Arg, Tyr,$ or Cys (common essential and growth-stimulating amino acids for mammalian cells from Table 4.1). μ_{max1} (h^{-1}) is the maximum specific growth rate associated with essential/growth-stimulating amino acids, μ_{max2} (h^{-1}) is the maximum specific growth rate associated with glucose and glutamine, $K_{g,k}^*$ and $K_{g,Glc/Gln}^*$ ($mmole \cdot 10^{-6} cell^{-1} h^{-1}$) are the apparent half-saturation constants of growth for amino acids and glucose/glutamine respectively and are expressed in terms of the glutamine response variable ($x_{res,Gln}$):

$$K_{g,l}^* = K_{g,l} \cdot \left(1 - \frac{x_{res,Gln}}{\rho_g + x_{res,Gln}} \right) \quad (M9)$$

where $l = Val, Leu, Ile, Met, Phe, Trp, Thr, Lys, His, Arg, Tyr, Cys, Glc,$ or Gln .

$K_{g,l}$ (mmole 10^{-6} cell $^{-1}$ h $^{-1}$) is the corresponding intrinsic half-saturation constant of growth for nutrient l , ρ_g is a half-saturation constant relating the cell culture response at low-glutamine concentration to any possible reduction in $K_{g,l}^*$. The glucose response variable is not included in Equation M9 because no further change in the growth pattern was observed in low-glucose-glutamine cultures relative to low-glutamine cultures.

When the essential and growth-stimulating amino acids are abundant in the cell culture, Equation M8 may be interpreted as Equation M8' which resembles common growth kinetics that only model glucose and glutamine but not other amino acids.

Glutamine is not an irreplaceable energy source in mammalian cell cultures (Kurano et al., 1990b). Hansen and Emborg cultured CHO cells producing tissue-type plasminogen activator (tPA) in chemostat with higher concentration of asparagine than glutamine in the medium, leading to a higher consumption rate of asparagine than other amino acids (Hansen and Emborg, 1994a). Altamirano et al. (2001) replaced glutamine by glutamate in CHO chemostat culture producing tPA with no significant difference in cell growth and tPA production. Thus, the role of glutamine in the equation above represents a dominating amino acid energy source in the medium that might be a different candidate when the medium composition is changed.

Specific Death Rate

The specific death rate equation from Ludemann et al. (1994) with an addition of a lactate term similar to equation M6 is used in this model:

$$\mu_d = \mu_{d,min} \cdot \left(\frac{k_{d,NH_3} + (NH_3 - NH_{3cr})}{k_{d,NH_3}} \right) \cdot \left(\frac{k_{d,Lac} + (Lac - Lac_{cr})}{k_{d,Lac}} \right) \cdot \left(1 - \frac{x_{resGln}}{\rho_{d,Gln} + x_{resGln}} \right) \cdot \left(1 - \frac{x_{resGlc}}{\rho_{d,Glc} + x_{resGlc}} \right) \quad (M10)$$

where μ_d (h^{-1}) is the specific death rate, $\mu_{d,min}$ (h^{-1}) is the minimum death rate, k_{d,NH_3} and $k_{d,Lac}$ (mM) are constants relating ammonium and lactate respectively to specific death rate. The last two terms on the right hand side relate cell culture responses ($x_{res,Gln}$ and $x_{res,Glc}$) at low-glutamine or low-glucose conditions to changes in μ_d with $\rho_{d,Gln}$ and $\rho_{d,Glc}$ being the corresponding half-saturation constants.

Another type of equation using Hill function to relate NH_4^+ concentration to death rate was proposed by Jang and Barford (2000). But Ludemann et al. (1994) had done a more in depth study into the death kinetics of mammalian cells, so their equation structured was applied to the CHO-IFN γ cell culture model.

Cell Lysis

Cell breakage can occur to dead cells (Jang and Barford, 2000b) or living cells (Georgen et al. 1993; Bakker et al., 1996) in mammalian cell cultures and both had been called cell lysis in the literature. A study of the pH dependence of lysis of living cells in a continuous mammalian culture by Georgen et al. (1993) reported that cell lysis was negligible at pH 7 but increased at pH 6.8. From our experience with the hybridoma cell cultures studied in Chapter 3 that only a negligible amount of dead cells fragmentation was observed, it is believed that the lysis of living cells is dependent on cell-lines and culture conditions. The CHO-IFN γ cell cultures were controlled at pH 7 (Wong et al., 2005) and no significant decrease in total cell concentration was observed in the batch and fed-batch cultures. Thus, only fragmentation of dead cells is considered in this model:

$$\frac{d(X_d \cdot V)}{dt} = \mu_d \cdot X_v \cdot V - r_{frag} \cdot X_d \cdot V - F_{out} \cdot X_d \quad (M11)$$

where X_d (10^6 cells L^{-1}) is the dead cell concentration and r_{frag} (h^{-1}) is the fragmentation rate of dead cells.

4.2.1.3 *IFN*γ Production

The production of *IFN*γ in the cell culture is modelled using a simple relationship with the viable cell concentration. Hayter et al. (1991) reported that in CHO-*IFN*γ stirred batch cultures *IFN*γ production would continue in the absence of cell proliferation, suggesting that the specific production rate in different cell-cycle phase might be similar. The mass balance of *IFN*γ below is linked to glutamine and glucose response variables ($x_{res,Gln}$ and $x_{res,Glc}$):

$$\frac{d(IFN\gamma \cdot V)}{dt} = r_{max_{IFN\gamma}} \cdot X_v \cdot V \cdot \left(1 + \frac{r_{max_{res,IFN_Gln}} \cdot x_{res,Gln}}{\rho_{IFN_Gln} + x_{res,Gln}} \right) \cdot \left(1 + \frac{r_{max_{res,IFN_Glc}} \cdot x_{res,Glc}}{\rho_{IFN_Glc} + x_{res,Glc}} \right) - IFN\gamma \cdot F_{out} \quad (M12)$$

where $IFN\gamma$ (mg L⁻¹) is the concentration of *IFN*γ, $r_{max_{IFN\gamma}}$ (mg 10⁻⁶cell⁻¹ h⁻¹) is the maximum *IFN*γ specific production rate in batch culture, $r_{max_{res,IFN_Gln}}$ and $r_{max_{res,IFN_Glc}}$ are the maximum coefficient of productivity response to low-glutamine and low-glucose conditions respectively, ρ_{IFN_Gln} & ρ_{IFN_Glc} are the half-saturation constants of $x_{res,Gln}$ and $x_{res,Glc}$ on productivity.

4.2.1.4 Consumption of Nutrients

Glucose

An ‘effective concentration’ term is used to represent the amount of glucose available in the extracellular medium in both batch and fed-batch cell cultures. From the mass balance of glucose in a bioreactor,

$$\frac{d(Glc \cdot V)}{dt} = F_{in} \cdot Glc_{in} + F_{in,glc} \cdot Glc_{in} - F_{out} \cdot Glc - q_{Glc} \cdot X_v \cdot V \quad (D5)$$

$$V \cdot \frac{dGlc}{dt} + Glc \cdot \frac{dV}{dt} = F_{in} \cdot Glc_{in} + F_{in,glc} \cdot Glc_{in} - F_{out} \cdot Glc - q_{Glc} \cdot X_v \cdot V \quad (D6)$$

$$\frac{dGlc}{dt} = -\frac{Glc}{V} \cdot \frac{dV}{dt} + \frac{F_{in}}{V} \cdot Glc_{in} + \frac{F_{in,glc}}{V} \cdot Glc_{in} - \frac{F_{out}}{V} \cdot Glc - q_{Glc} \cdot X_v \quad (D7)$$

Assuming $\frac{dV}{dt} \sim 0$ when $(F_{in} + F_{in,glc} - F_{out}) \sim 0$ for a short time interval and $Glc \sim Glc_i$:

$$\frac{dGlc}{dt} \sim \frac{F_{in}}{V} \cdot Glc_{in} + \frac{F_{in,glc}}{V} \cdot Glc_{in} - \frac{F_{out}}{V} \cdot Glc - q_{Glc} \cdot X_v \quad (D8)$$

$$\frac{\Delta Glc}{\Delta t} \sim \frac{F_{in}}{V} \cdot Glc_{in} + \frac{F_{in,glc}}{V} \cdot Glc_{in} - \frac{F_{out}}{V} \cdot Glc_i - q_{Glc} \cdot X_v \quad (D9)$$

$$Glc_f - Glc_i \sim \left(\frac{F_{in}}{V} \cdot Glc_{in} + \frac{F_{in,glc}}{V} \cdot Glc_{in} - \frac{F_{out}}{V} \cdot Glc_i - q_{Glc} \cdot X_v \right) \cdot \Delta t \quad (D10)$$

$$Glc_f \sim \left(\frac{F_{in}}{V} \cdot Glc_{in} + \frac{F_{in,glc}}{V} \cdot Glc_{in} - \frac{F_{out}}{V} \cdot Glc_i - q_{Glc} \cdot X_v \right) \cdot \Delta t + Glc_i \quad (D11)$$

where Glc_i (mM) and Glc_f (mM) are the initial and final glucose concentration of the time interval respectively.

In a batch culture, Equation D11 becomes:

$$Glc_f \sim -q_{Glc} \cdot X_v \cdot \Delta t + Glc_i \quad (D12)$$

For continuous culture under glucose limitation, $\frac{dGlc}{dt} = 0$, $\frac{dV}{dt} = 0$, and $Glc_i = 0$,

$$Glc_f = \left(\frac{F_{in}}{V} \cdot Glc_{in} + \frac{F_{in,glc}}{V} \cdot Glc_{in} - q_{Glc} \cdot X_v \right) \cdot \Delta t = 0 \quad (D13)$$

Thus glucose availability cannot be associated with residual glucose concentration in glucose-limited continuous culture. Instead, it has always been associated with the dilution rate (D ; $D = \frac{(F_{in} + F_{in,glc})}{V}$) and inlet glucose concentration.

In a fed-batch culture with nutrient (e.g. glucose) controlled at very low concentration by a feed-back controller (e.g. 0.35mM residual glucose in one of the

CHO fed-batch experiments in this study), the residual nutrient concentration is close to zero and thus cannot reflect the actual availability of the nutrient. The specific glucose consumption rate, q_{Glc} , is often linked to residual glucose concentration in batch culture (e.g. using Monod kinetics) since $Glc > 0$ until glucose exhaustion (Equation D12); but is linked to dilution rate in continuous culture since Glc_i and $Glc_f = 0$ under glucose limitation (Equation D13). For example, $q_{Glc} = \frac{D \cdot (C_{Glc}^E - C_{Glc}^S)}{X_v} \cdot 10^3$ in a CHO chemostat model by Altamirano et al. (2001) where C^E and C^S (mM) are the concentration at reactor inlet and outlet respectively. The two different approaches of estimating q_{Glc} cannot be cross-applied because $D = 0$ in batch culture and Glc can be zero in continuous culture. The common practice of relating q_{Glc} to D , X_v , and glucose inlet/outlet concentration in continuous culture is a backward-calculation approach instead of a forward-prediction approach based on a mechanistic relation between q_{Glc} and glucose availability. In order to search for a general predictive equation structure for q_{Glc} under batch/fed-batch/continuous conditions, it is proposed in this study to relate q_{Glc} to the amount of glucose in a cell-free reactor (i.e. $X_v=0$) during time interval Δt . An effective concentration term representing the amount of glucose available in the cell culture within a unit time interval is thus expressed as follow:

$$Glc_{eff} = \beta \cdot (Glc_{in} \cdot \frac{F_{in}}{V} + Glc'_{in} \cdot \frac{F_{in,glc}}{V} - Glc \cdot \frac{F_{out}}{V}) + Glc \quad (M13)$$

where Glc_{eff} (mM) is the effective glucose concentration, β (h) is one unit time interval, Glc_{in} is the glucose concentration in the inlet stream F_{in} ($L h^{-1}$) that also contains other amino acids (mM), Glc'_{in} (mM) is the glucose concentration in the pure glucose stream $F_{in,glc}$ ($L h^{-1}$). Glc (mM) is the glucose concentration in the cell culture.

In the above equation, $\beta = 1$ h by default but this does not affect the actual time interval of recalculating Glc_{eff} . The simulation would re-evaluate the effective concentration everytime when a pulse of F_{in} or $F_{in,glc}$ occurs. Alternatively, the simulation time-step can be set equal to the time-width of a pulse of nutrient supplementation. In the absence of any inlet/outlet stream, the effective glucose concentration becomes the same as the residual glucose concentration in a batch situation.

The same concept of effective concentration is applied to all other simulated nutrients: glutamine (*Gln*), valine (*Val*), leucine (*Leu*), isoleucine (*Ile*), methionine (*Met*), phenylalanine (*Phe*), tryptophan (*Trp*), threonine (*Thr*), lysine (*Lys*), histidine

(*His*), alanine (*Ala*), glycine (*Gly*), proline (*Pro*), aspartic acid (*Asp*), glutamic acid (*Glu*), asparagine (*Asn*), serine (*Ser*), tyrosine (*Tyr*), cysteine (*Cys*), and arginine (*Arg*). Below are the effective concentration equations for glutamine and other amino acids:

$$Gln_{eff} = \beta \cdot (Gln_{in} \cdot \frac{F_{in}}{V} - Gln \cdot \frac{F_{out}}{V}) + Gln \quad (M14)$$

$$AA_{eff,i} = \beta \cdot (AA_{in,i} \cdot \frac{F_{in}}{V} - AA_i \cdot \frac{F_{out}}{V}) + AA_i \quad (M15)$$

where i : *Val, Leu, Ile, Met, Phe, Trp, Thr, Lys, His, Ala, Gly, Pro, Asp, Glu, Asn, Ser, Tyr, Cys, or Arg.*

Coming back to glucose, the mass balance is as follow:

$$\frac{d(Glc \cdot V)}{dt} = Glc_{in} \cdot F_{in} + Glc_{in} \cdot F_{in,glc} - Glc \cdot F_{out} - q_{Glc} \cdot X_v \cdot V \quad (M16)$$

where q_{Glc} (mmole 10^{-6} cell $^{-1}$ h $^{-1}$) is the specific consumption rate of glucose.

The specific glucose consumption rate is modelled as follow:

$$q_{Glc} = \frac{rmax_{Glc} \cdot Glc_{eff}}{K_{Glc} + Glc_{eff}} \cdot f_{inh}(NH_3, Lac) \cdot \left(1 + \frac{rmax_{res,Glc_Gln} \cdot x_{res,Gln}}{\rho_{Glc_Gln} + x_{res,Gln}} \right) \quad (M17)$$

where $rmax_{Glc}$ (mmole 10^{-6} cell $^{-1}$ h $^{-1}$) is the maximum specific glucose consumption rate in batch culture, Glc_{eff} (mM) is the effective glucose concentration defined in Equation M13, K_{Glc} (mM) is the half-saturation constant for glucose consumption, $f_{inh}(NH_3, Lac)$ is an inhibition function defined in Equation M6, $rmax_{res,Glc_Gln}$ represents any possible effect on glucose consumption in low-glutamine condition and ρ_{Glc_Gln} is the corresponding half-saturation constant.

Glutamine & Glutamine Decomposition

Glutamine would spontaneously decompose to pyrrolidone carboxylic acid during cell culture incubation at 37°C (Bray et al., 1949; Tritsch and Moore, 1962; Glacken et al., 1986; Ozturk and Palsson, 1990). For example, Glacken et al. (1986) reported a first-order glutamine decomposition rate constant of 0.0048 h $^{-1}$ in fructose medium with/without 5% foetal calf serum without cells at 37°C and 10% CO $_2$. Ozturk and Palsson (1990) studied the glutamine decomposition with different media composition and represented the relation between the decomposition rate constant, k , and pH with the following equation:

$$\ln(k) = a + b \cdot pH \quad (R5)$$

Using the parameter values from Ozturk and Palsson (1990), the decomposition rate constant for several media at pH 7 was calculated and shown in Table 4.6 below.

Table 4.6: Chemical decomposition of glutamine to ammonia and pyrrolidone carboxylic acid studied at 37°C and pH 6.8 – 7.8 with different media containing foetal bovine serum (Ozturk and Palsson, 1990).

<u>Media</u>	<u>a</u>	<u>b</u>	<u>k (at pH 7) [h⁻¹]</u>
IMDM	-18.31 (±1.21)	1.685 (±0.095)	0.0015
OPTI-MEM	-16.76 (±1.11)	1.458 (±0.065)	0.0014
DMEM	-17.07 (±1.12)	1.478 (±0.073)	0.0012
RPMI-1640	-13.85 (±1.19)	1.133 (±0.055)	0.0027

Higher ranges of glutamine degradation rate had also been reported. For example, Schmid and Keller (1992) determined that the glutamine in a continuous hybridoma culture at 37°C and pH ~7 in serum-free low protein lipid-free medium degraded at ~7.5% day⁻¹ (~0.03 h⁻¹). A summary made by Schneider et al. (1996) of glutamine half-lives reported in various literature showed variations up to 10-fold. The glutamine degradation rate in the CHO-IFN γ cell cultures is assumed to be constant in the model since the stirred-tank reactor was controlled at 37°C and pH 7 (Wong et al., 2005). Below is the mass balance and specific consumption rate of glutamine:

$$\frac{d(Gln \cdot V)}{dt} = Gln_{in} \cdot F_{in} - Gln \cdot F_{out} - q_{Gln} \cdot X_v \cdot V - r_{d,Gln} \cdot Gln \cdot V \quad (M18)$$

$$q_{Gln} = \frac{rmax_{Gln} \cdot Gln_{eff}}{K_{Gln} + Gln_{eff}} \cdot \left(\frac{K_{inh,Glc}}{K_{inh,Glc} + Glc_{eff}} \right) \cdot f_{inh}(NH_3, Lac) \cdot \left(1 + \frac{rmax_{res,Gln_Glc} \cdot x_{res,Glc}}{\rho_{Gln_Glc} + x_{res,Glc}} \right) \quad (M19)$$

where $r_{d,Gln}$ (h⁻¹) is the glutamine degradation rate, $rmax_{Gln}$ (mmole 10⁻⁶cell⁻¹ h⁻¹) is the maximum specific glutamine consumption rate in batch culture, Gln_{eff} and Glc_{eff} (mM) are the effective glutamine and glucose concentration defined in Equation M14 and M13 respectively, $K_{inh,Glc}$ (mM) is a glucose inhibition constant for glutamine consumption, $f_{inh}(NH_3, Lac)$ is an inhibition function defined in Equation M6, $rmax_{res,Gln_Glc}$ represents any possible effect on glutamine consumption in low-glucose condition and ρ_{Gln_Glc} is the corresponding half-saturation constant.

Other Amino Acids

The amino acid network considered in this model is based on that of a CHO cell culture from Altamirano et al. (2001) and a mouse hybridoma cell culture from Europa et al. (2000) together with discussions with Dr. Yih Yean Lee (BTI-A*Star, Singapore). The modelled interconversions of amino acids are similar to Section 4.1 except the excretion of aspartic acid and glutamic acid are assumed to be insignificant because their extracellular concentrations dropped to zero rapidly in all batch and fed-batch cultures; and reversible conversions are simplified into net conversions based on the amino acid time-profiles of the CHO-IFN γ cultures.

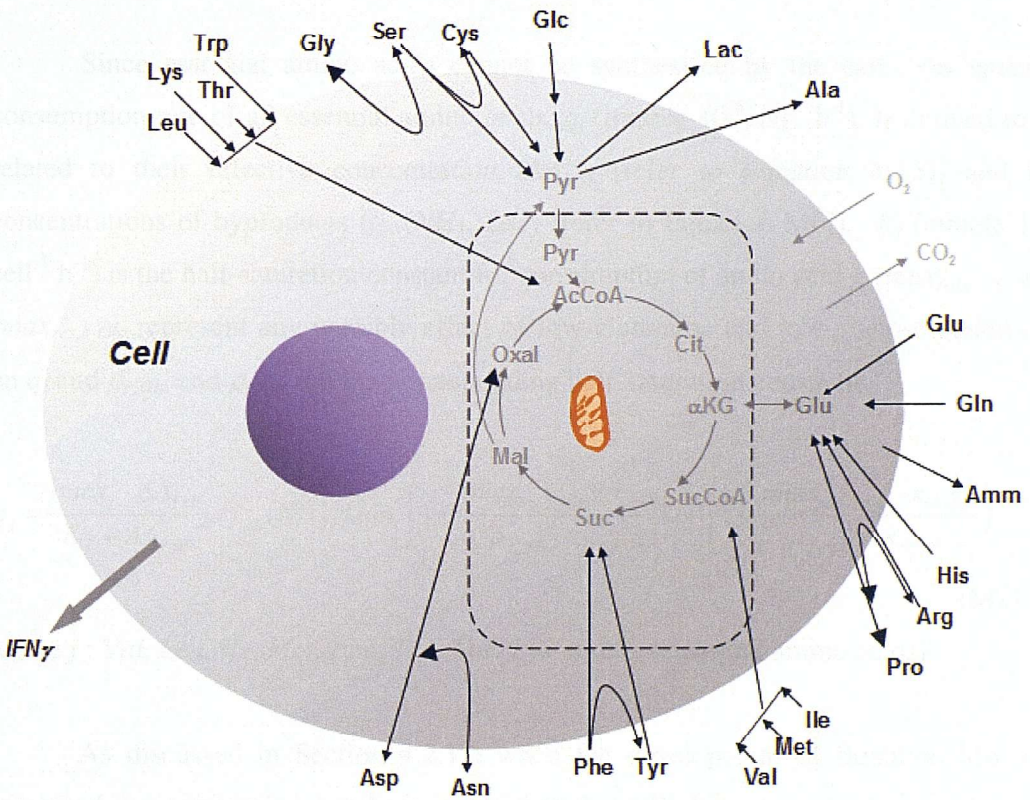


Figure 4.10: Amino acid network for the general model of CHO-IFN γ cell culture.

Overall Mass Balance:

The mass balance of all amino acids is as follow:

$$\frac{d(AA_i \cdot V)}{dt} = AA_{in,i} \cdot F_{in} - AA_i \cdot F_{out} - q_{AA,i} \cdot X_v \cdot V \quad (M20)$$

where $q_{AA,i}$ (mmole 10^{-6} cell $^{-1}$ h $^{-1}$) is the specific consumption rate of amino acid i , $i = Val, Leu, Ile, Met, Phe, Trp, Thr, Lys, His, Ala, Gly, Pro, Asp, Glu, Asn, Ser, Tyr, Cys, or Arg$.

Essential Amino Acids:

Since essential amino acids cannot be synthesised by the cells, the specific consumption rate of all essential amino acids, q_j (mmole 10^{-6} cell $^{-1}$ h $^{-1}$), is defined to be related to their effective concentration ($AA_{j,eff}$ [refer to Equation M15]) and the concentrations of byproducts ($f_{inh}(NH_3, Lac)$ [refer to Equation M6]). K_j (mmole 10^{-6} cell $^{-1}$ h $^{-1}$) is the half-saturation constant for consumption of amno acid j . $rmax_{res,j_Gln}$ and $rmax_{res,j_Glc}$ represent any possible effect of low-glutamine and low-glucose conditions on q_j and ρ_{j_Gln} and ρ_{j_Glc} are the corresponding half-saturation constants.

$$q_j = \frac{rmax_j \cdot AA_{j,eff}}{K_j + AA_{j,eff}} \cdot f_{inh}(NH_3, Lac) \cdot \left(1 + \frac{rmax_{res,j_Gln} \cdot x_{res,Gln}}{\rho_{j_Gln} + x_{res,Gln}}\right) \cdot \left(1 + \frac{rmax_{res,j_Glc} \cdot x_{res,Glc}}{\rho_{j_Glc} + x_{res,Glc}}\right) \quad (M21)$$

where $j : Val, Leu, Ile, Met, Phe, Trp, Thr, Lys, or His$ (essential amino acids).

As discussed in Section 4.2.1.2 when the development of Equation M6 was presented, an assumption has been made that the cells have a non-zero maintenance consumption of all nutrients. The knowledge of maintenance consumption of amino acids in mammalian cell cultures in the literature is insufficient to judge which of the 19 amino acids might not be consumed when the specific growth rate is zero. The model performance will be discussed in Chapter 5 and any deviations caused by this assumption will be highlighted.

Non-essential Amino Acids:

Alanine —

Alanine is produced from pyruvate which comes from nearly all amino acids (figure 4.10). The intracellular sources of alanine are assumed to be from specific consumption of the two dominating nutrients glucose (q_{Glc}) and glutamine (q_{Gln}), and a non-negligible background production rate, $q_{Ala,min}$ (mmole 10^{-6} cell $^{-1}$ h $^{-1}$). Below is the proposed equation for specific alanine consumption:

$$q_{Ala} = \left(\frac{rmax_{Ala} \cdot Ala_{eff}}{K_{Ala} + Ala_{eff}} - q_{Ala,min} \right) \cdot \left(1 + \frac{rmax_{res,Ala_Gln} \cdot x_{res,Gln}}{\rho_{Ala_Gln} + x_{res,Gln}} \right) \cdot \left(1 + \frac{rmax_{res,Ala_Glc} \cdot x_{res,Glc}}{\rho_{Ala_Glc} + x_{res,Glc}} \right) - rmax_{Ala_Glc} \cdot q_{Glc} - rmax_{Ala_Gln} \cdot q_{Gln} \quad (M22)$$

where $rmax_{Ala}$ (mmole 10^{-6} cell $^{-1}$ h $^{-1}$) is the maximum specific consumption rate of alanine in batch culture, K_{Ala} (mM) is the half-saturation constant for alanine consumption. Ala_{eff} (mM), $rmax_{res,Ala_Gln}$, $rmax_{res,Ala_Glc}$, ρ_{Ala_Gln} , and ρ_{Ala_Glc} are the effective concentration and response coefficients/constants for alanine similar to Equation M21. $rmax_{Ala_Glc}$ (mmole mmole $^{-1}$) and $rmax_{Ala_Gln}$ (mmole mmole $^{-1}$) are the linear yield coefficients of alanine from glucose and glutamine respectively.

In Equation M22, $q_{Ala,min}$ is linked to the response variables $x_{res,Gln}$ and $x_{res,Glc}$ based on observation of variations of $q_{Ala,min}$ in the fed-batch CHO-IFN γ cultures. Such phenomenon was not found in the case of glycine or proline which are the other two amino acids being significantly produced by the CHO-IFN γ cells. The sign of q_{Ala} would be positive if specific consumption > specific production and negative in the opposite case.

Glycine —

Glycine is assumed to be mainly produced from serine plus a non-negligible background production rate, $q_{Gly,min}$ (mmole 10^{-6} cell $^{-1}$ h $^{-1}$):

$$q_{Gly} = \frac{rmax_{Gly} \cdot Gly_{eff}}{K_{Gly} + Gly_{eff}} \cdot \left(1 + \frac{rmax_{res,Gly_Gln} \cdot x_{res,Gln}}{\rho_{Gly_Gln} + x_{res,Gln}} \right) \cdot \left(1 + \frac{rmax_{res,Gly_Glc} \cdot x_{res,Glc}}{\rho_{Gly_Glc} + x_{res,Glc}} \right) - q_{Gly,min} - rmax_{Gly_Ser} \cdot q_{Ser} \quad (M23)$$

where $rmax_{Gly}$ (mmole 10^{-6} cell $^{-1}$ h $^{-1}$) is the maximum specific consumption rate of glycine in batch culture, K_{Gly} (mM) is the half-saturation constant for glycine consumption. Gly_{eff} (mM), $rmax_{res,Gly_Gln}$, $rmax_{res,Gly_Glc}$, ρ_{Gly_Gln} , and ρ_{Gly_Glc} are the effective concentration and response coefficients/constants for glycine similar to Equation M21. $rmax_{Gly_Ser}$ (mmole mmole $^{-1}$) is the linear yield coefficient of glycine from specific serine consumption (q_{Ser}).

Proline —

Proline is assumed to be mainly produced from glutamic acid and arginine plus a non-negligible background production rate, $q_{Pro,min}$ (mmole 10^{-6} cell $^{-1}$ h $^{-1}$):

$$q_{Pro} = \frac{rmax_{Pro} \cdot Pro_{eff}}{K_{Pro} + Pro_{eff}} \cdot \left(1 + \frac{rmax_{res,Pro_Gln} \cdot x_{res,Gln}}{\rho_{Pro_Gln} + x_{res,Gln}} \right) \cdot \left(1 + \frac{rmax_{res,Pro_Glc} \cdot x_{res,Glc}}{\rho_{Pro_Glc} + x_{res,Glc}} \right) - q_{Pro,min} - rmax_{Pro_Glu} \cdot q_{Glu} - rmax_{Pro_Arg} \cdot q_{Arg} \quad (M24)$$

where $rmax_{Pro}$ (mmole 10^{-6} cell $^{-1}$ h $^{-1}$) is the maximum specific consumption rate of proline in batch culture, K_{Pro} (mM) is the half-saturation constant for proline consumption. Pro_{eff} (mM), $rmax_{res,Pro_Gln}$, $rmax_{res,Pro_Glc}$, ρ_{Pro_Gln} , and ρ_{Pro_Glc} are the effective concentration and response coefficients/constants for proline similar to Equation M21. $rmax_{Pro_Glu}$ (mmole mmole $^{-1}$) and $rmax_{Pro_Arg}$ (mmole mmole $^{-1}$) are the linear yield coefficients of proline from specific consumption of glutamic acid (q_{Glu}) and arginine (q_{Arg}) respectively.

Aspartic acid—

The excretion rate of aspartic acid into the extracellular medium is assumed to be negligible because the residual aspartic acid concentration decreased rapidly to zero in all batch and fed-batch cultures. Although aspartic acid can be produced from asparagine (figure 4.10), this is assumed to take place at the intracellular level which would not be included in the model equation.

$$q_{Asp} = \frac{rmax_{Asp} \cdot Asp_{eff}}{K_{Asp} + Asp_{eff}} \cdot \left(1 + \frac{rmax_{res,Asp_Gln} \cdot x_{res,Gln}}{\rho_{Asp_Gln} + x_{res,Gln}} \right) \cdot \left(1 + \frac{rmax_{res,Asp_Glc} \cdot x_{res,Glc}}{\rho_{Asp_Glc} + x_{res,Glc}} \right) \quad (M25)$$

where $rmax_{Asp}$ (mmole 10^{-6} cell $^{-1}$ h $^{-1}$) is the maximum specific consumption rate of aspartic acid in batch culture, K_{Asp} (mM) is the half-saturation constant for aspartic acid consumption. Asp_{eff} (mM), $rmax_{res,Asp_Gln}$, $rmax_{res,Asp_Glc}$, ρ_{Asp_Gln} , and ρ_{Asp_Gln} are the effective concentration and response coefficients/constants for aspartic acid similar to Equation M21.

Glutamic acid—

Similar to aspartic acid, the excretion rate of glutamic acid is assumed to be negligible as the cellular consumption rate of glutamic acid was dominating in the CHO-IFN γ cultures.

$$q_{Glu} = \frac{rmax_{Glu} \cdot Glu_{eff}}{K_{Glu} + Glu_{eff}} \cdot \left(1 + \frac{rmax_{res,Glu_Gln} \cdot x_{res,Gln}}{\rho_{Glu_Gln} + x_{res,Gln}} \right) \cdot \left(1 + \frac{rmax_{res,Glu_Glc} \cdot x_{res,Glc}}{\rho_{Glu_Glc} + x_{res,Glc}} \right) \quad (M26)$$

where $rmax_{Glu}$ (mmole 10^{-6} cell $^{-1}$ h $^{-1}$) is the maximum specific consumption rate of glutamic acid in batch culture, K_{Glu} (mM) is the half-saturation constant for glutamic acid consumption. Glu_{eff} (mM), $rmax_{res,Glu_Gln}$, $rmax_{res,Glu_Glc}$, ρ_{Glu_Gln} , and ρ_{Glu_Gln} are the effective concentration and response coefficients/constants for glutamic acid similar to Equation M21.

Asparagine —

The production of asparagine from aspartic acid is assumed to be less significant than the reverse conversion (figure 4.10). Thus, this is not included in the equation below:

$$q_{Asn} = \frac{rmax_{Asn} \cdot Asn_{eff}}{K_{Asn} + Asn_{eff}} \cdot \left(1 + \frac{rmax_{res,Asn_Gln} \cdot x_{res,Gln}}{\rho_{Asn_Gln} + x_{res,Gln}} \right) \cdot \left(1 + \frac{rmax_{res,Asn_Glc} \cdot x_{res,Glc}}{\rho_{Asn_Glc} + x_{res,Glc}} \right) \quad (M27)$$

where $rmax_{Asn}$ (mmole 10^{-6} cell $^{-1}$ h $^{-1}$) is the maximum specific consumption rate of asparagine in batch culture, K_{Asn} (mM) is the half-saturation constant for asparagine consumption. Asn_{eff} (mM), $rmax_{res,Asn_Gln}$, $rmax_{res,Asn_Glc}$, ρ_{Asn_Gln} , and ρ_{Asn_Gln} are the effective concentration and response coefficients/constants for asparagine similar to Equation M21.

Serine —

It is assumed that the conversion of serine to glycine is more dominating than the opposite conversion (figure 4.10). Thus, the specific consumption of serine takes the following form:

$$q_{Ser} = \frac{rmax_{Ser} \cdot Ser_{eff}}{K_{Ser} + Ser_{eff}} \cdot \left(1 + \frac{rmax_{res,Ser_Gln} \cdot x_{res,Gln}}{\rho_{Ser_Gln} + x_{res,Gln}} \right) \cdot \left(1 + \frac{rmax_{res,Ser_Glc} \cdot x_{res,Glc}}{\rho_{Ser_Glc} + x_{res,Glc}} \right) \quad (M28)$$

where $rmax_{Ser}$ (mmole 10^{-6} cell $^{-1}$ h $^{-1}$) is the maximum specific consumption rate of serine in batch culture, K_{Ser} (mM) is the half-saturation constant for serine consumption. Ser_{eff} (mM), $rmax_{res,Ser_Gln}$, $rmax_{res,Ser_Glc}$, ρ_{Ser_Gln} , and ρ_{Ser_Gln} are the effective concentration and response coefficients/constants for serine similar to Equation M21.

Tyrosine —

Tyrosine can be produced from phenylalanine (figure 4.10). Below is the specific consumption rate of tyrosine:

$$q_{Tyr} = \frac{rmax_{Tyr} \cdot Tyr_{eff}}{K_{Tyr} + Tyr_{eff}} \cdot \left(1 + \frac{rmax_{res,Tyr_Gln} \cdot x_{res,Gln}}{\rho_{Tyr_Gln} + x_{res,Gln}} \right) \cdot \left(1 + \frac{rmax_{res,Tyr_Glc} \cdot x_{res,Glc}}{\rho_{Tyr_Glc} + x_{res,Glc}} \right) - rmax_{Tyr_Phe} \cdot q_{Phe} \quad (M29)$$

where $rmax_{Tyr}$ (mmole 10^{-6} cell $^{-1}$ h $^{-1}$) is the maximum specific consumption rate of tyrosine in batch culture, K_{Tyr} (mM) is the half-saturation constant for tyrosine consumption. Tyr_{eff} (mM), $rmax_{res,Tyr_Gln}$, $rmax_{res,Tyr_Glc}$, ρ_{Tyr_Gln} , and ρ_{Tyr_Glc} are the effective concentration and response coefficients/constants for tyrosine similar to Equation M21. $rmax_{Tyr_Phe}$ (mmole mmole $^{-1}$) is the linear yield coefficient of tyrosine from specific phenylalanine consumption (q_{Phe}).

Cysteine —

Cysteine can be produced from serine (figure 4.10). The specific consumption rate of cysteine is as follow:

$$q_{Cys} = \frac{rmax_{Cys} \cdot Cys_{eff}}{K_{Cys} + Cys_{eff}} \cdot \left(1 + \frac{rmax_{res,Cys_Gln} \cdot x_{res,Gln}}{\rho_{Cys_Gln} + x_{res,Gln}} \right) \cdot \left(1 + \frac{rmax_{res,Cys_Glc} \cdot x_{res,Glc}}{\rho_{Cys_Glc} + x_{res,Glc}} \right) - rmax_{Cys_Ser} \cdot q_{Ser} \quad (M30)$$

where $rmax_{Cys}$ (mmole 10^{-6} cell $^{-1}$ h $^{-1}$) is the maximum specific consumption rate of cysteine in batch culture, K_{Cys} (mM) is the half-saturation constant for cysteine consumption. Cys_{eff} (mM), $rmax_{res,Cys_Gln}$, $rmax_{res,Cys_Glc}$, ρ_{Cys_Gln} , and ρ_{Cys_Glc} are the effective concentration and response coefficients/constants for cysteine similar to Equation M21. $rmax_{Cys_Ser}$ (mmole mmole $^{-1}$) is the linear yield coefficients of cysteine from specific serine consumption (q_{Ser}).

The production of arginine from proline is assumed to be less significant than the reverse conversion (figure 4.10). Thus, the specific arginine consumption rate is modelled as follow:

$$q_{Arg} = \frac{rmax_{Arg} \cdot Arg_{eff}}{K_{Arg} + Arg_{eff}} \cdot \left(1 + \frac{rmax_{res,Arg_Gln} \cdot x_{res,Gln}}{\rho_{Arg_Gln} + x_{res,Gln}} \right) \cdot \left(1 + \frac{rmax_{res,Arg_Glc} \cdot x_{res,Glc}}{\rho_{Arg_Glc} + x_{res,Glc}} \right) \quad (M31)$$

where $rmax_{Arg}$ (mmole 10^{-6} cell $^{-1}$ h $^{-1}$) is the maximum specific consumption rate of arginine in batch culture, K_{Arg} (mM) is the half-saturation constant for arginine consumption. Arg_{eff} (mM), $rmax_{res,Arg_Gln}$, $rmax_{res,Arg_Glc}$, ρ_{Arg_Gln} , and ρ_{Arg_Glc} are the effective concentration and response coefficients/constants for arginine similar to Equation M21.

4.2.1.5 Metabolic Byproducts

Ammonium

Ammonium is one of the major metabolic byproducts in the cell culture. Apart from glutamine and glutamic acid, ammonium is also produced from metabolism of histidine (His), serine (Ser), asparagine (Asn), lysine (Lys), methionine (Met), and tryptophan (Trp) (Altamirano et al., 2001). In a detailed study of CHO chemostat culture metabolism by Altamirano et al. (2001), the metabolic flux of His, Ser, and Asn was higher than Lys, Met, and Trp at different steady-states. Thus, His, Ser, and Asn were approximated to be the alternative sources of ammonium production in the absence of glutamine in the CHO-IFN γ cell cultures. Glutamic acid was rapidly consumed by the CHO-IFN γ cells such that there was negligible concentration in the extracellular medium. Because glutamine was supplemented more than glutamic acid by 80 times in batch culture and by 100 times in fed-batch cultures, the contribution of ammonium production from glutamic acid is assumed to be negligible.

The specific ammonium yield from amino acids is assumed to be proportional to the specific consumption of amino acids. The specific ammonium production rate also contains a non-negligible background production term, $rmin_{Amm}$ (mmole 10^{-6} cell $^{-1}$ h $^{-1}$),

which is based on observation that the ammonium production rate in CHO-IFN γ batch culture remained positive when most major sources of ammonium had been exhausted.

A limited number of studies in the literature suggested that the nitrogen in amino acids could end up in other non-essential amino acids instead of ammonium. It had been reported that the NH $_3$ group in glutamate (glutamic acid), a major metabolite from glutamine, can be channelled into alanine and aspartic acid via aminotransferase in rat lymphocytes and mouse tumour cells (Ardawi and Newsholme, 1982; Moreadith and Lehninger, 1984). In the CHO-IFN γ cell culture studied in this chapter, there was a significant accumulation of alanine in all batch and fed-batch cultures; the ammonium accumulation also became less positive at high concentration of ammonium despite ongoing consumption of glutamine. Thus, a ‘reverse’ reaction term, $q_{Amm,rev}$ (mmole 10 $^{-6}$ cell $^{-1}$ h $^{-1}$), representing the possible channelling of metabolites away from ammonium production is proposed for the mass balance of ammonium:

$$\frac{d(Amm \cdot V)}{dt} = r_{d,Gln} \cdot Gln \cdot V + (q_{Amm} - q_{Amm,rev}) \cdot X_v \cdot V - Amm \cdot F_{out} \quad (M32)$$

where Amm (mM) is the ammonium concentration, $r_{d,Gln}$ (h $^{-1}$) is the spontaneous glutamine degradation rate, Gln (mM) is the glutamine concentration, and q_{Amm} (mmole 10 $^{-6}$ cell $^{-1}$ h $^{-1}$) is the specific ammonium production rate.

The equation for $q_{Amm,rev}$ is defined as follow:

$$q_{Amm,rev} = rmin_{Amm,rev} \cdot Amm^m, m > 1 \quad (M33)$$

where $rmin_{Amm,rev}$ (mmole $^{(1-m)}$ L m 10 $^{-6}$ cell $^{-1}$ h $^{-1}$) represents the minimum specific rate of metabolite redirection away from ammonium production, and m is an exponential of ammonium concentration.

Below is the proposed equation for specific ammonium consumption:

$$q_{Amm} = \left\{ \begin{aligned} & rmin_{Amm} + \left[\frac{rmax_{Amm_Gln} \cdot q_{Gln}}{K_{Amm_Gln} + q_{Gln}} \right] \cdot q_{Gln} \\ & + \left[\frac{rmax_{Amm_His,Ser,Asn} \cdot (q_{His} + q_{Ser} + q_{Asn})}{\left(\varepsilon + \frac{q_{Gln}}{K_{scale} + q_{Gln}} \right) \cdot K_{Amm_His,Ser,Asn} + (q_{His} + q_{Ser} + q_{Asn})} \right] \cdot (q_{His} + q_{Ser} + q_{Asn}) \end{aligned} \right\} \cdot \left(1 - \frac{x_{resGln}}{\rho_{Amm_Gln} + x_{resGln}} \right) \quad (M34)$$

where $rmax_{Amm_Gln}$ (mmole mmole⁻¹) is the stoichiometric maximum ammonium yield from glutamine and K_{Amm_Gln} (mmole 10⁻⁶cell⁻¹ h⁻¹) is the corresponding half-saturation constant. Similarly, $rmax_{Amm_His,Ser,Asn}$ (mmole mmole⁻¹) is the stoichiometric maximum ammonium yield from histidine + serine + asparagine and $K_{Amm_His,Ser,Asn}$ (mmole 10⁻⁶cell⁻¹ h⁻¹) is the corresponding half-saturation constant. K_{scale} (mmole 10⁻⁶cell⁻¹ h⁻¹) represents a low level of glutamine consumption that would cause the cells to consume other amino acids, causing a change in the ammonium yield from those amino acids. ε is a constant $\ll 1$ that prevents the denominator from approaching zero when q_{Gln} , q_{His} , q_{Ser} , and q_{Asn} tend to zero. ρ_{Amm_Gln} is a response constant relating the cell culture low-glutamine response ($x_{res,Gln}$) to any possible further reduction of q_{Amm} .

Lactate

Wu et al. (1992) studied CHO-K1 cells chemostats and used ¹⁴C radioisotope glucose and glutamine to track the fates of glucose and glutamine carbons. It was found that 68-81% of glucose carbon ended up in lactate, 14-23% of glutamine carbon ended up in lactate, 22-64% of glutamine carbon became amino acid and other macromolecules of the cells, 5-8% of glutamine degraded in the medium, and the rest of glucose and glutamine carbons were fully oxidised and ended up as CO₂. Thus, glutamine is also contributing to the production of lactate in CHO cell cultures apart from glucose and this is taken into account in the model.

Unlike ammonium, lactate consumption by mammalian cell cultures is known to take place at low glucose concentrations (Gmunder et al., 1988; Kurano et al., 1990a). Syrian hamster kidney cells grown on microcarriers in 2ml cell culture tube is reported to use

lactate as an energy source when all glucose was depleted (Gmunder et al., 1988); CHO cell static cultures studied by Kurano et al. (1990a) continued to grow accompanied with a decrease in lactate concentration after glucose depletion. Thus, a lactate consumption term is included in the mass balance of lactate below:

$$\frac{d(Lac \cdot V)}{dt} = \left(q_{Lac,Glc} + q_{Lac,Gln} - \frac{y_l \cdot rmax_{Lac,rev} \cdot Lac}{K_{Lac,rev} + Lac} \right) \cdot X_v \cdot V - Lac \cdot F_{out} \quad (M35)$$

where $q_{Lac,Glc}$ (mmole 10^{-6} cell $^{-1}$ h $^{-1}$) is the specific lactate production rate from glucose, $q_{Lac,Gln}$ (mmole 10^{-6} cell $^{-1}$ h $^{-1}$) is the specific lactate production rate from glutamine, y_l is a binary variable associated with glucose concentration and is defined in Equation M1, $rmax_{Lac,rev}$ (mmole 10^{-6} cell $^{-1}$ h $^{-1}$) is the maximum lactate consumption rate at low concentration of glucose and $K_{Lac,rev}$ (mM) is the corresponding half-saturation constant.

In the equations of specific lactate production rate glucose and glutamine below, the lactate yield from glucose/glutamine is assumed to be proportional to the specific consumption rate of glucose(q_{Glc})/glutamine(q_{Gln}):

$$q_{Lac,Glc} = \left(\frac{rmax_{Lac_Glc} \cdot q_{Glc}}{K_{Lac_Glc} + q_{Glc}} \right) \cdot \left(1 - \frac{x_{res,Glc}}{(\rho_{Lac_Glc} + x_{res,Glc})} \right) \cdot q_{Glc} \quad (M36)$$

$$q_{Lac,Gln} = \left(\frac{rmax_{Lac_Gln} \cdot q_{Gln}}{K_{Lac_Gln} + q_{Gln}} \right) \cdot \left(1 - \frac{x_{res,Gln}}{(\rho_{Lac_Gln} + x_{res,Gln})} \right) \cdot q_{Gln} \quad (M37)$$

where $rmax_{Lac_Glc}$ (mmole mmole $^{-1}$) is the maximum stoichiometric yield of lactate from glucose, $rmax_{Lac_Gln}$ (mmole mmole $^{-1}$) is the maximum stoichiometric yield of lactate from glutamine. K_{Lac_Glc} (mmole 10^{-6} cell $^{-1}$ h $^{-1}$) is the half-saturation constant for lactate yield from glucose, and K_{Lac_Gln} (mmole 10^{-6} cell $^{-1}$ h $^{-1}$) is the half-saturation constant for lactate yield from glutamine. ρ_{Lac_Glc} and ρ_{Lac_Gln} are response constants relating the cell culture responses ($x_{res,Glc}$ and $x_{res,Gln}$) at low-glucose and low-glutamine levels to any possible further reduction of $q_{Lac,Glc}$ and $q_{Lac,Gln}$ respectively.

A summary of all the model equations that have been introduced is available in the next section. This model contains 192 parameters of which the values are more challenging to estimate than in Section 4.1. In Chapter 5, these 192 parameters are divided into different categories and a parameter estimation strategy is developed for this large model. This section (Section 4.2) is in conjunction with Chapter 5 where the model prediction performance is evaluated. Please refer to the next chapter for a detailed discussion of the parameter estimation method and model simulation results.

4.2.2 Model Equations Summary

Overall volume:

$$\frac{dV}{dt} = F_{in} + F_{in,glc} - F_{out} \quad (4.2.1)$$

(Note: It is assumed that the sampling volume is negligible relative to the flowrates of F_{in} and $F_{in,glc}$.)

Cell concentration:

$$\frac{d(X_v \cdot V)}{dt} = (\mu - \mu_d - \frac{F_{out}}{V}) \cdot X_v \cdot V \quad (4.2.2)$$

$$\frac{d(X_d \cdot V)}{dt} = \mu_d \cdot X_v \cdot V - r_{frag} \cdot X_d \cdot V - F_{out} \cdot X_d \quad (4.2.3)$$

$$X_t = X_v + X_d \quad (4.2.4)$$

Effective Nutrient concentrations for addition of small amount of concentrated nutrients:

$$Glc_{eff} = \beta \cdot (Glc_{in} \cdot \frac{F_{in}}{V} + Glc_{in} \cdot \frac{F_{in,glc}}{V} - Glc \cdot \frac{F_{out}}{V}) + Glc \quad (4.2.5)$$

$$Gln_{eff} = \beta \cdot (Gln_{in} \cdot \frac{F_{in}}{V} - Gln \cdot \frac{F_{out}}{V}) + Gln \quad (4.2.6)$$

$$AA_{eff,i} = \beta \cdot (AA_{in,i} \cdot \frac{F_{in}}{V} - AA_i \cdot \frac{F_{out}}{V}) + AA_i \quad (4.2.7 - 4.2.25)$$

where i : Val, Leu, Ile, Met, Phe, Trp, Thr, Lys, His, Ala, Gly, Pro, Asp, Glu, Asn, Ser, Tyr, Cys, or Arg.

Cellular regulation responses:

$$y_1 = \begin{cases} 0, & Glc = 0 \\ 1, & 0 < Glc < \tau_{Glc} \\ 0, & Glc \geq \tau_{Glc} \end{cases} \quad (4.2.26)$$

$$y_2 = \begin{cases} 0, & Gln = 0 \\ 1, & 0 < Gln < \tau_{Gln} \\ 0, & Gln \geq \tau_{Gln} \end{cases} \quad (4.2.27)$$

$$\frac{d(x_{res,Glc})}{dt} = rmax_{res,Glc} \cdot \log[1 + y_1 \cdot (\tau_{Glc} - Glc)] - d_{res,Glc} \cdot x_{res,Glc} \quad (4.2.28)$$

$$\frac{d(x_{res,Gln})}{dt} = rmax_{res,Gln} \cdot \log[1 + y_2 \cdot (\tau_{Gln} - Gln)] - d_{res,Gln} \cdot x_{res,Gln} \quad (4.2.29)$$

Nutrients uptake:

(i) Glucose —

$$\frac{d(\text{Glc} \cdot V)}{dt} = \text{Glc}_{in} \cdot F_{in} + \text{Glc}_{in,glc} \cdot F_{in,glc} - \text{Glc} \cdot F_{out} - q_{\text{Glc}} \cdot X_v \cdot V \quad (4.2.30)$$

$$q_{\text{Glc}} = \frac{rmax_{\text{Glc}} \cdot \text{Glc}_{eff}}{K_{\text{Glc}} + \text{Glc}_{eff}} \cdot f_{inh}(\text{NH}_3, \text{Lac}) \cdot \left(1 + \frac{rmax_{res.\text{Glc}_-\text{Gln}} \cdot X_{res.\text{Gln}}}{\rho_{\text{Glc}_-\text{Gln}} + X_{res.\text{Gln}}} \right) \quad (4.2.31)$$

$$f_{inh}(\text{NH}_3, \text{Lac}) = \left(\frac{k_{inh,\text{NH}_3}}{k_{inh,\text{NH}_3} + D_{\text{NH}_3}} \right) \cdot \left(\frac{k_{inh,\text{Lac}}}{k_{inh,\text{Lac}} + D_{\text{Lac}}} \right) \quad (4.2.32)$$

(ii) Glutamine —

$$\frac{d(\text{Gln} \cdot V)}{dt} = \text{Gln}_{in} \cdot F_{in} - \text{Gln} \cdot F_{out} - q_{\text{Gln}} \cdot X_v \cdot V - r_{d,\text{Gln}} \cdot \text{Gln} \cdot V \quad (4.2.33)$$

$$q_{\text{Gln}} = \frac{rmax_{\text{Gln}} \cdot \text{Gln}_{eff}}{K_{\text{Gln}} + \text{Gln}_{eff}} \cdot \left(\frac{K_{inh,\text{Glc}}}{K_{inh,\text{Glc}} + \text{Glc}_{eff}} \right) \cdot f_{inh}(\text{NH}_3, \text{Lac}) \cdot \left(1 + \frac{rmax_{res.\text{Gln}_-\text{Glc}} \cdot X_{res.\text{Glc}}}{\rho_{\text{Gln}_-\text{Glc}} + X_{res.\text{Glc}}} \right) \quad (4.2.34)$$

(iii) Amino acids —

$$\frac{d(\text{AA}_i \cdot V)}{dt} = \text{AA}_{in,i} \cdot F_{in} - \text{AA}_i \cdot F_{out} - q_{\text{AA},i} \cdot X_v \cdot V \quad (4.2.35 - 4.2.53)$$

where i : Val, Leu, Ile, Met, Phe, Trp, Thr, Lys, His, Ala, Gly, Pro, Asp, Glu, Asn, Ser, Tyr, Cys, or Arg.

$$q_j = \frac{rmax_j \cdot \text{AA}_{j,eff}}{K_j + \text{AA}_{j,eff}} \cdot f_{inh}(\text{NH}_3, \text{Lac}) \cdot \left(1 + \frac{rmax_{res,j_-\text{Gln}} \cdot X_{res,\text{Gln}}}{\rho_{j_-\text{Gln}} + X_{res,\text{Gln}}} \right) \cdot \left(1 + \frac{rmax_{res,j_-\text{Glc}} \cdot X_{res,\text{Glc}}}{\rho_{j_-\text{Glc}} + X_{res,\text{Glc}}} \right) \quad (4.2.54 - 4.2.62)$$

where j : Val, Leu, Ile, Met, Phe, Trp, Thr, Lys, or His (essential amino acids).

$$q_{\text{Ala}} = \left(\frac{rmax_{\text{Ala}} \cdot \text{Ala}_{eff}}{K_{\text{Ala}} + \text{Ala}_{eff}} - q_{\text{Ala},min} \right) \cdot \left(1 + \frac{rmax_{res,\text{Ala}_-\text{Gln}} \cdot X_{res,\text{Gln}}}{\rho_{\text{Ala}_-\text{Gln}} + X_{res,\text{Gln}}} \right) \cdot \left(1 + \frac{rmax_{res,\text{Ala}_-\text{Glc}} \cdot X_{res,\text{Glc}}}{\rho_{\text{Ala}_-\text{Glc}} + X_{res,\text{Glc}}} \right) - rmax_{\text{Ala}_-\text{Glc}} \cdot q_{\text{Glc}} - rmax_{\text{Ala}_-\text{Gln}} \cdot q_{\text{Gln}} \quad (4.2.63)$$

$$q_{\text{Gly}} = \frac{rmax_{\text{Gly}} \cdot \text{Gly}_{eff}}{K_{\text{Gly}} + \text{Gly}_{eff}} \cdot \left(1 + \frac{rmax_{res,\text{Gly}_-\text{Gln}} \cdot X_{res,\text{Gln}}}{\rho_{\text{Gly}_-\text{Gln}} + X_{res,\text{Gln}}} \right) \cdot \left(1 + \frac{rmax_{res,\text{Gly}_-\text{Glc}} \cdot X_{res,\text{Glc}}}{\rho_{\text{Gly}_-\text{Glc}} + X_{res,\text{Glc}}} \right) - q_{\text{Gly},min} - rmax_{\text{Gly}_-\text{Ser}} \cdot q_{\text{Ser}} \quad (4.2.64)$$

$$q_{\text{Pro}} = \frac{rmax_{\text{Pro}} \cdot \text{Pro}_{eff}}{K_{\text{Pro}} + \text{Pro}_{eff}} \cdot \left(1 + \frac{rmax_{res,\text{Pro}_-\text{Gln}} \cdot X_{res,\text{Gln}}}{\rho_{\text{Pro}_-\text{Gln}} + X_{res,\text{Gln}}} \right) \cdot \left(1 + \frac{rmax_{res,\text{Pro}_-\text{Glc}} \cdot X_{res,\text{Glc}}}{\rho_{\text{Pro}_-\text{Glc}} + X_{res,\text{Glc}}} \right) - q_{\text{Pro},min} - rmax_{\text{Pro}_-\text{Glu}} \cdot q_{\text{Glu}} - rmax_{\text{Pro}_-\text{Arg}} \cdot q_{\text{Arg}} \quad (4.2.65)$$

$$q_{Asp} = \frac{rmax_{Asp} \cdot Asp_{eff}}{K_{Asp} + Asp_{eff}} \cdot \left(1 + \frac{rmax_{res,Asp_Gln} \cdot x_{res,Gln}}{\rho_{Asp_Gln} + x_{res,Gln}} \right) \cdot \left(1 + \frac{rmax_{res,Asp_Glc} \cdot x_{res,Glc}}{\rho_{Asp_Glc} + x_{res,Glc}} \right) \quad (4.2.66)$$

$$q_{Glu} = \frac{rmax_{Glu} \cdot Glu_{eff}}{K_{Glu} + Glu_{eff}} \cdot \left(1 + \frac{rmax_{res,Glu_Gln} \cdot x_{res,Gln}}{\rho_{Glu_Gln} + x_{res,Gln}} \right) \cdot \left(1 + \frac{rmax_{res,Glu_Glc} \cdot x_{res,Glc}}{\rho_{Glu_Glc} + x_{res,Glc}} \right) \quad (4.2.67)$$

$$q_{Asn} = \frac{rmax_{Asn} \cdot Asn_{eff}}{K_{Asn} + Asn_{eff}} \cdot \left(1 + \frac{rmax_{res,Asn_Gln} \cdot x_{res,Gln}}{\rho_{Asn_Gln} + x_{res,Gln}} \right) \cdot \left(1 + \frac{rmax_{res,Asn_Glc} \cdot x_{res,Glc}}{\rho_{Asn_Glc} + x_{res,Glc}} \right) \quad (4.2.68)$$

$$q_{Ser} = \frac{rmax_{Ser} \cdot Ser_{eff}}{K_{Ser} + Ser_{eff}} \cdot \left(1 + \frac{rmax_{res,Ser_Gln} \cdot x_{res,Gln}}{\rho_{Ser_Gln} + x_{res,Gln}} \right) \cdot \left(1 + \frac{rmax_{res,Ser_Glc} \cdot x_{res,Glc}}{\rho_{Ser_Glc} + x_{res,Glc}} \right) \quad (4.2.69)$$

$$q_{Tyr} = \frac{rmax_{Tyr} \cdot Tyr_{eff}}{K_{Tyr} + Tyr_{eff}} \cdot \left(1 + \frac{rmax_{res,Tyr_Gln} \cdot x_{res,Gln}}{\rho_{Tyr_Gln} + x_{res,Gln}} \right) \cdot \left(1 + \frac{rmax_{res,Tyr_Glc} \cdot x_{res,Glc}}{\rho_{Tyr_Glc} + x_{res,Glc}} \right) - rmax_{Tyr_Phe} \cdot q_{Phe} \quad (4.2.70)$$

$$q_{Cys} = \frac{rmax_{Cys} \cdot Cys_{eff}}{K_{Cys} + Cys_{eff}} \cdot \left(1 + \frac{rmax_{res,Cys_Gln} \cdot x_{res,Gln}}{\rho_{Cys_Gln} + x_{res,Gln}} \right) \cdot \left(1 + \frac{rmax_{res,Cys_Glc} \cdot x_{res,Glc}}{\rho_{Cys_Glc} + x_{res,Glc}} \right) - rmax_{Cys_Ser} \cdot q_{Ser} \quad (4.2.71)$$

$$q_{Arg} = \frac{rmax_{Arg} \cdot Arg_{eff}}{K_{Arg} + Arg_{eff}} \cdot \left(1 + \frac{rmax_{res,Arg_Gln} \cdot x_{res,Gln}}{\rho_{Arg_Gln} + x_{res,Gln}} \right) \cdot \left(1 + \frac{rmax_{res,Arg_Glc} \cdot x_{res,Glc}}{\rho_{Arg_Glc} + x_{res,Glc}} \right) \quad (4.2.72)$$

Byproducts:

$$D_{NH_3} = \begin{cases} 0 & , NH_3 < NH_{3,cr} \\ NH_3 - NH_{3,cr} & , NH_3 \geq NH_{3,cr} \end{cases} \quad (4.2.73)$$

$$NH_3 = Amm \cdot 10^{(pH-9.3)} \quad , \text{assume } pH \sim 7.0 \quad (4.2.74)$$

$$NH_{3,cr} = Amm_{cr} \cdot 10^{(pH-9.3)} \quad (4.2.75)$$

$$\frac{d(Amm \cdot V)}{dt} = r_{d,Gln} \cdot Gln \cdot V + (q_{Amm} - q_{Amm,rev}) \cdot X_v \cdot V - Amm \cdot F_{out} \quad (4.2.76)$$

$$q_{Amm,rev} = rmin_{Amm,rev} \cdot Amm^m \quad , m > 1 \quad (4.2.77)$$

$$q_{Amm} = \left\{ \begin{aligned} & rmin_{Amm} + \left[\frac{rmax_{Amm_Gln} \cdot q_{Gln}}{K_{Amm_Gln} + q_{Gln}} \right] \cdot q_{Gln} \\ & + \left[\frac{rmax_{Amm_His,Ser,Asn} \cdot (q_{His} + q_{Ser} + q_{Asn})}{\left(\varepsilon + \frac{q_{Gln}}{K_{scale} + q_{Gln}} \right) \cdot K_{Amm_His,Ser,Asn} + (q_{His} + q_{Ser} + q_{Asn})} \right] \cdot (q_{His} + q_{Ser} + q_{Asn}) \end{aligned} \right\} \cdot \left(1 - \frac{x_{res,Gln}}{\rho_{Amm_Gln} + x_{res,Gln}} \right) \quad (4.2.78)$$

$$D_{Lac} = \begin{cases} 0 & , \quad Lac < Lac_{cr} \\ Lac - Lac_{cr} & , \quad Lac \geq Lac_{cr} \end{cases} \quad (4.2.79)$$

$$\frac{d(Lac \cdot V)}{dt} = \left(q_{Lac,Glc} + q_{Lac,Gln} - \frac{y_1 \cdot rmax_{Lac,rev} \cdot Lac}{K_{Lac,rev} + Lac} \right) \cdot X_v \cdot V - Lac \cdot F_{out} \quad (4.2.80)$$

$$q_{Lac,Glc} = \left(\frac{rmax_{Lac_Glc} \cdot q_{Glc}}{K_{Lac_Glc} + q_{Glc}} \right) \cdot \left(1 - \frac{x_{res,Glc}}{\rho_{Lac_Glc} + x_{res,Glc}} \right) \cdot q_{Glc} \quad (4.2.81)$$

$$q_{Lac,Gln} = \left(\frac{rmax_{Lac_Gln} \cdot q_{Gln}}{K_{Lac_Gln} + q_{Gln}} \right) \cdot \left(1 - \frac{x_{res,Gln}}{\rho_{Lac_Gln} + x_{res,Gln}} \right) \cdot q_{Gln} \quad (4.2.82)$$

Growth:

$$\mu = \mu_{max1} \cdot \left[\left(\prod_k \frac{q_{AA,k}}{K_{g,k}^* + q_{AA,k}} \right) \cdot \left(1 + \frac{\mu_{max2}}{\mu_{max1}} \cdot \frac{q_{Glc}}{K_{g,Glc}^* + q_{Glc}} \cdot \frac{q_{Gln}}{K_{g,Gln}^* + q_{Gln}} \right) \right] \quad (4.2.83)$$

where k : Val, Leu, Ile, Met, Phe, Trp, Thr, Lys, His, Arg, Tyr, or Cys (essential and growth-stimulating amino acids).

$$K_{g,l}^* = K_{g,l} \cdot \left(1 - \frac{x_{res,Gln}}{\rho_g + x_{res,Gln}} \right) \quad (4.2.84)$$

where l : Val, Leu, Ile, Met, Phe, Trp, Thr, Lys, His, Arg, Tyr, Cys, Glc, or Gln.

The second term on the right hand side of Equation 4.2.84 is to account for any possible change in the half-saturation constants in low glutamine fed-batch cultures.

Death:

$$\mu_d = \mu_{d,min} \cdot \left(\frac{k_{d,NH3} + D_{NH3}}{k_{d,NH3}} \right) \cdot \left(\frac{k_{d,Lac} + D_{Lac}}{k_{d,Lac}} \right) \cdot \left(1 - \frac{x_{res,Gln}}{\rho_{d,Gln} + x_{res,Gln}} \right) \cdot \left(1 - \frac{x_{res,Glc}}{\rho_{d,Glc} + x_{res,Glc}} \right) \quad (4.2.85)$$

Product synthesis:

$$\frac{d(IFNy \cdot V)}{dt} = rmax_{IFNy} \cdot X_v \cdot V \cdot \left(1 + \frac{rmax_{res,IFN_Gln} \cdot x_{res,Gln}}{\rho_{IFN_Gln} + x_{res,Gln}} \right) \cdot \left(1 + \frac{rmax_{res,IFN_Glc} \cdot x_{res,Glc}}{\rho_{IFN_Glc} + x_{res,Glc}} \right) - IFNy \cdot F_{out} \quad (4.2.86)$$

4.2.3 Notations for Complex CHO-IFN γ Model with Amino Acids

Table 4.7: Notation of parameters for the complex CHO-IFN γ model.

Parameters	Definition	Units
β	One unit-time	hr
ϵ	Engineering constant for <i>Amm</i> spec. production rate	-
τ_{Glc}	Response threshold for Glc	mmole L ⁻¹
τ_{Gln}	Response threshold for Gln	mmole L ⁻¹
$\mu_{d,min}$	Minimum specific death rate	h ⁻¹
μ_{max1}	Maximum specific growth rate dependent on essential/growth-stimulating amino acids	h ⁻¹
μ_{max2}	Mmaximum specific growth rate dependent on glucose & glutamine	h ⁻¹
Amm_{cr}	Critical ammonium concentration	mmole L ⁻¹ (= mM)
$d_{res,Glc}$	Degradation rate of of $x_{res,Glc}$	h ⁻¹
$d_{res,Gln}$	Degradation rate of of $x_{res,Gln}$	h ⁻¹
K_{Ala}	Half-saturation constant for alanine consumption	mmole L ⁻¹
K_{Amm_Gln}	Half-saturation constant for the <i>Amm</i> yield from glutamine	mmole 10 ⁻⁶ cell ⁻¹ h ⁻¹
$K_{Amm_His,Ser,Asn}$	Half-saturation constant for the <i>Amm</i> yield from histidine + serine + asparagine	mmole 10 ⁻⁶ cell ⁻¹ h ⁻¹
K_{Arg}	Half-saturation constant for arginine consumption	mmole L ⁻¹
K_{Asn}	Half-saturation constant for asparagine consumption	mmole L ⁻¹
K_{Asp}	Half-saturation constant for aspartic acid consumption	mmole L ⁻¹
K_{Cys}	Half-saturation constant for cysteine consumption	mmole L ⁻¹
$k_{d,Lac}$	Inhibition constant of lactate for cell death	mmole L ⁻¹
$k_{d,NH3}$	Inhibition constant of ammonium for cell death	mmole L ⁻¹
$K_{g,Arg}$	Half-saturation constant of arginine for cell growth in batch culture	mmole 10 ⁻⁶ cell ⁻¹ h ⁻¹
$K_{g,Cys}$	Half-saturation constant of cysteine for cell growth in batch culture	mmole 10 ⁻⁶ cell ⁻¹ h ⁻¹
$K_{g,Glc}$	Half-saturation constant of glucose for cell growth in batch culture	mmole 10 ⁻⁶ cell ⁻¹ h ⁻¹
$K_{g,Gln}$	Half-saturation constant of glutamine for cell growth in batch culture	mmole 10 ⁻⁶ cell ⁻¹ h ⁻¹
$K_{g,His}$	Half-saturation constant of histidine for cell growth in batch culture	mmole 10 ⁻⁶ cell ⁻¹ h ⁻¹
$K_{g,Ile}$	Half-saturation constant of isoleucine for cell growth in batch culture	mmole 10 ⁻⁶ cell ⁻¹ h ⁻¹
$K_{g,Leu}$	Half-saturation constant of leucine for cell growth in batch culture	mmole 10 ⁻⁶ cell ⁻¹ h ⁻¹
$K_{g,Lys}$	Half-saturation constant of lysine for cell growth in batch culture	mmole 10 ⁻⁶ cell ⁻¹ h ⁻¹
$K_{g,Met}$	Half-saturation constant of methionine for cell growth in batch culture	mmole 10 ⁻⁶ cell ⁻¹ h ⁻¹
$K_{g,Phe}$	Half-saturation constant of phenylalanine for cell growth in batch culture	mmole 10 ⁻⁶ cell ⁻¹ h ⁻¹
$K_{g,Thr}$	Half-saturation constant of threonine for cell growth in batch culture	mmole 10 ⁻⁶ cell ⁻¹ h ⁻¹
$K_{g,Trp}$	Half-saturation constant of tryptophan for cell growth in batch culture	mmole 10 ⁻⁶ cell ⁻¹ h ⁻¹

$K_{g,Tyr}$	Half-saturation constant of tyrosine for cell growth in batch culture	mmole 10^{-6} cell $^{-1}$ h $^{-1}$
$K_{g,Val}$	Half-saturation constant of valine for cell growth in batch culture	mmole 10^{-6} cell $^{-1}$ h $^{-1}$
K_{Glc}	Half-saturation constant for Glc uptake	mmole L $^{-1}$
K_{Gln}	Half-saturation constant for glutamine consumption	mmole L $^{-1}$
K_{Glu}	Half-saturation constant for glutamic acid consumption	mmole L $^{-1}$
K_{Gly}	Half-saturation constant for glycine consumption	mmole L $^{-1}$
K_{His}	Half-saturation constant for histidine consumption	mmole L $^{-1}$
K_{Ile}	Half-saturation constant for isoleucine consumption	mmole L $^{-1}$
$K_{inh,Glc}$	Glucose inhibition constant for glutamine consumption	mmole L $^{-1}$
$k_{inh,Lac}$	Inhibition constant of lactate for nutrient consumption	mmole L $^{-1}$
$k_{inh,NH3}$	Inhibition constant of ammonium for nutrient consumption	mmole L $^{-1}$
$K_{Lac,rev}$	Half-saturation constant of lactate for lactate consumption at low glucose level	mmole L $^{-1}$
K_{Lac_Glc}	Half-saturation constant for lactate yield from glucose	mmole 10^{-6} cell $^{-1}$ h $^{-1}$
K_{Lac_Gln}	Half-saturation constant for lactate yield from glutamine	mmole 10^{-6} cell $^{-1}$ h $^{-1}$
K_{Leu}	Half-saturation constant for leucine consumption	mmole L $^{-1}$
K_{Lys}	Half-saturation constant for lysine consumption	mmole L $^{-1}$
K_{Met}	Half-saturation constant for methionine consumption	mmole L $^{-1}$
K_{Phe}	Half-saturation constant for phenylalanine consumption	mmole L $^{-1}$
K_{Pro}	Half-saturation constant for proline consumption	mmole L $^{-1}$
K_{scale}	Half-saturation constant responsible for scaling down $K_{Amm, His, Ser, Asn}$ at low levels of q_{Gln}	mmole 10^{-6} cell $^{-1}$ h $^{-1}$
K_{Ser}	Half-saturation constant for serine consumption	mmole L $^{-1}$
K_{Thr}	Half-saturation constant for threonine consumption	mmole L $^{-1}$
K_{Trp}	Half-saturation constant for tryptophan consumption	mmole L $^{-1}$
K_{Tyr}	Half-saturation constant for tyrosine consumption	mmole L $^{-1}$
K_{Val}	Half-saturation constant for valine consumption	mmole L $^{-1}$
Lac_{cr}	Critical lactate concentration	mmole L $^{-1}$
m	Exponential of A_{mm} for $q_{Amm,rev}$ in the mass balance of ammonium	-
pH	pH of cell culture	-
$q_{Ala,min}$	Background specific production rate of alanine	mmole 10^{-6} cell $^{-1}$ h $^{-1}$
$q_{Gly,min}$	Background specific production rate of glycine	mmole 10^{-6} cell $^{-1}$ h $^{-1}$
$q_{Pro,min}$	Background specific production rate of proline	mmole 10^{-6} cell $^{-1}$ h $^{-1}$
$r_{d,Gln}$	Degradation rate of glutamine (hr $^{-1}$)	h $^{-1}$
r_{frag}	Rate of fragmentation of dead cells	h $^{-1}$
$rmax_{Ala}$	Maximum specific alanine consumption rate	mmole 10^{-6} cell $^{-1}$ h $^{-1}$
$rmax_{Ala_Glc}$	Linear yield coefficient of alanine from glucose	mmole mmole $^{-1}$
$rmax_{Ala_Gln}$	Linear yield coefficient of alanine from glutamine	mmole mmole $^{-1}$
$rmax_{Amm_Gln}$	Maximum stoichiometric ratio of ammonium from glutamine	mmole mmole $^{-1}$

$r_{max_{Amm_His,Ser,Asn}}$	Maximum stoichiometric ratio of ammonium from histidine + serine + asparagine	mmole mmole ⁻¹
$r_{max_{Arg}}$	Maximum specific arginine consumption rate	mmole 10 ⁻⁶ cell ⁻¹ h ⁻¹
$r_{max_{Asn}}$	Maximum specific asparagine consumption rate	mmole 10 ⁻⁶ cell ⁻¹ h ⁻¹
$r_{max_{Asp}}$	Maximum specific aspartic acid consumption rate	mmole 10 ⁻⁶ cell ⁻¹ h ⁻¹
$r_{max_{Cys}}$	Maximum specific cysteine consumption rate	mmole 10 ⁻⁶ cell ⁻¹ h ⁻¹
$r_{max_{Cys_Ser}}$	Linear yield coefficient of cysteine from serine	mmole mmole ⁻¹
$r_{max_{Glc}}$	maximum specific consumption rate for <i>Glc</i>	mmole 10 ⁻⁶ cell ⁻¹ h ⁻¹
$r_{max_{Gln}}$	Maximum specific consumption rate of glutamine	mmole 10 ⁻⁶ cell ⁻¹ h ⁻¹
$r_{max_{Glu}}$	Maximum spec. glutamic acid consumption rate	mmole 10 ⁻⁶ cell ⁻¹ h ⁻¹
$r_{max_{Gly}}$	Maximum specific glycine consumption rate	mmole 10 ⁻⁶ cell ⁻¹ h ⁻¹
$r_{max_{Gly_Ser}}$	Linear yield coefficient of glycine from serine	mmole mmole ⁻¹
$r_{max_{His}}$	Maximum specific histidine consumption rate	mmole 10 ⁻⁶ cell ⁻¹ h ⁻¹
$r_{max_{IFN\gamma}}$	Maximum specific production rate for <i>IFNγ</i>	mg 10 ⁻⁶ cell ⁻¹ h ⁻¹
$r_{max_{Ile}}$	Maximum specific isoleucine consumption rate	mmole 10 ⁻⁶ cell ⁻¹ h ⁻¹
$r_{max_{Lac,rev}}$	Maximum specific lactate consumption rate at low glucose level	mmole 10 ⁻⁶ cell ⁻¹ h ⁻¹
$r_{max_{Lac_Glc}}$	Maximum stoichiometric ratio of lactate from glucose	mmole mmole ⁻¹
$r_{max_{Lac_Gln}}$	Maximum stoichiometric ratio of lactate from glutamine	mmole mmole ⁻¹
$r_{max_{Leu}}$	Maximum specific leucine consumption rate	mmole 10 ⁻⁶ cell ⁻¹ h ⁻¹
$r_{max_{Lys}}$	Maximum specific lysine consumption rate	mmole 10 ⁻⁶ cell ⁻¹ h ⁻¹
$r_{max_{Met}}$	Maximum specific methionine consumption rate	mmole 10 ⁻⁶ cell ⁻¹ h ⁻¹
$r_{max_{Phe}}$	Maximum spec. phenylalanine consumption rate	mmole 10 ⁻⁶ cell ⁻¹ h ⁻¹
$r_{max_{Pro}}$	Maximum specific proline consumption rate	mmole 10 ⁻⁶ cell ⁻¹ h ⁻¹
$r_{max_{Pro_Arg}}$	Linear yield coefficient of proline from arginine	mmole mmole ⁻¹
$r_{max_{Pro_Glu}}$	Linear yield coefficient of proline from glutamic acid	mmole mmole ⁻¹
$r_{max_{res,Ala_Glc}}$	Maximum response coefficient for alanine consumption due to low glucose level	-
$r_{max_{res,Ala_Gln}}$	Maximum response coefficient for alanine consumption due to low glutamine level	-
$r_{max_{res,Arg_Glc}}$	Maximum response coefficient for arginine consumption due to low glucose level	-
$r_{max_{res,Arg_Gln}}$	Maximum response coefficient for arginine consumption due to low glutamine level	-
$r_{max_{res,Asn_Glc}}$	Maximum response coefficient for asparagine consumption due to low glucose level	-
$r_{max_{res,Asn_Gln}}$	Maximum response coefficient for asparagine consumption due to low glutamine level	-
$r_{max_{res,Asp_Glc}}$	Maximum response coefficient for aspartic acid consumption due to low glucose level	-
$r_{max_{res,Asp_Gln}}$	Maximum response coefficient for aspartic acid consumption due to low glutamine level	-
$r_{max_{res,Cys_Glc}}$	Maximum response coefficient for cysteine consumption due to low glucose level	-
$r_{max_{res,Cys_Gln}}$	Maximum response coefficient for cysteine consumption due to low glutamine level	-
$r_{max_{res,Glc}}$	Activation coefficient of $x_{res,Glc}$	h ⁻¹
$r_{max_{res,Glc_Gln}}$	Maximum response coefficient for glucose consumption due to low glutamine level	-
$r_{max_{res,Gln}}$	Activation coefficient of $x_{res,Gln}$	h ⁻¹
$r_{max_{res,Gln_Glc}}$	Maximum response coefficient for glutamine consumption due to low glucose level	-

$r_{max_{res,Glu_Glc}}$	Maximum response coefficient for glutamic acid consumption due to low glucose level	-
$r_{max_{res,Glu_Gln}}$	Maximum response coefficient for glutamic acid consumption due to low glutamine level	-
$r_{max_{res,Gly_Glc}}$	Maximum response coefficient for glycine consumption due to low glucose level	-
$r_{max_{res,Gly_Gln}}$	Maximum response coefficient for glycine consumption due to low glutamine level	-
$r_{max_{res,His_Glc}}$	Maximum response coefficient for histidine consumption due to low glucose level	-
$r_{max_{res,His_Gln}}$	Maximum response coefficient for histidine consumption due to low glutamine level	-
$r_{max_{res,IFN_Glc}}$	Maximum response coefficient for IFN γ production due to low glucose level	-
$r_{max_{res,IFN_Gln}}$	Maximum response coefficient for IFN γ production due to low glutamine level	-
$r_{max_{res,Ile_Glc}}$	Maximum response coefficient for isoleucine consumption due to low glucose level	-
$r_{max_{res,Ile_Gln}}$	Maximum response coefficient for isoleucine consumption due to low glutamine level	-
$r_{max_{res,Leu_Glc}}$	Maximum response coefficient for leucine consumption due to low glucose level	-
$r_{max_{res,Leu_Gln}}$	Maximum response coefficient for leucine consumption due to low glutamine level	-
$r_{max_{res,Lys_Glc}}$	Maximum response coefficient for lysine consumption due to low glucose level	-
$r_{max_{res,Lys_Gln}}$	Maximum response coefficient for lysine consumption due to low glutamine level	-
$r_{max_{res,Met_Glc}}$	Maximum response coefficient for methionine consumption due to low glucose level	-
$r_{max_{res,Met_Gln}}$	Maximum response coefficient for methionine consumption due to low glutamine level	-
$r_{max_{res,Phe_Glc}}$	Maximum response coefficient for phenylalanine consumption due to low glucose level	-
$r_{max_{res,Phe_Gln}}$	Maximum response coefficient for phenylalanine consumption due to low glutamine level	-
$r_{max_{res,Pro_Glc}}$	Maximum response coefficient for proline consumption due to low glucose level	-
$r_{max_{res,Pro_Gln}}$	Maximum response coefficient for proline consumption due to low glutamine level	-
$r_{max_{res,Ser_Glc}}$	Maximum response coefficient for serine consumption due to low glucose level	-
$r_{max_{res,Ser_Gln}}$	Maximum response coefficient for valine consumption due to low glutamine serine	-
$r_{max_{res,Thr_Glc}}$	Maximum response coefficient for threonine consumption due to low glucose level	-
$r_{max_{res,Thr_Gln}}$	Maximum response coefficient for threonine consumption due to low glutamine level	-
$r_{max_{res,Trp_Glc}}$	Maximum response coefficient for tryptophan consumption due to low glucose level	-
$r_{max_{res,Trp_Gln}}$	Maximum response coefficient for tryptophan consumption due to low glutamine level	-
$r_{max_{res,Tyr_Glc}}$	Maximum response coefficient for tyrosine consumption due to low glucose level	-
$r_{max_{res,Tyr_Gln}}$	Maximum response coefficient for tyrosine consumption due to low glutamine level	-

$r_{max_{res,Val_Glc}}$	Maximum response coefficient for valine consumption due to low glucose level	-
$r_{max_{res,Val_Gln}}$	Maximum response coefficient for valine consumption due to low glutamine level	-
$r_{max_{Ser}}$	Maximum specific serine consumption rate	mmole 10^{-6} cell $^{-1}$ h $^{-1}$
$r_{max_{Thr}}$	Maximum specific threonine consumption rate	mmole 10^{-6} cell $^{-1}$ h $^{-1}$
$r_{max_{Trp}}$	Maximum specific tryptophan consumption rate	mmole 10^{-6} cell $^{-1}$ h $^{-1}$
$r_{max_{Tyr}}$	Maximum specific tyrosine consumption rate	mmole 10^{-6} cell $^{-1}$ h $^{-1}$
$r_{max_{Tyr_Phe}}$	Linear yield coefficient of tyrosine from phenylalanine	mmole mmole $^{-1}$
$r_{max_{Val}}$	Maximum specific valine consumption rate	mmole 10^{-6} cell $^{-1}$ h $^{-1}$
$r_{min_{Amm}}$	Background specific production rate of <i>Amm</i>	mmole 10^{-6} cell $^{-1}$ h $^{-1}$
$r_{min_{Amm,rev}}$	Minimum specific rate of metabolite redirection away from <i>Amm</i> production	mmole $^{(1-m)}$ L m 10^{-6} cell $^{-1}$ h $^{-1}$
ρ_{Ala_Glc}	Response constant for alanine consumption due to low glucose level	-
ρ_{Ala_Gln}	Response constant for alanine production due to low glutamine level	-
ρ_{Amm_Gln}	Response constant for ammonium production due to low glutamine level	-
ρ_{Arg_Glc}	Response constant for arginine consumption due to low glucose level	-
ρ_{Arg_Gln}	Response constant for arginine production due to low glutamine level	-
ρ_{Asn_Glc}	Response constant for asparagine consumption due to low glucose level	-
ρ_{Asn_Gln}	Response constant for asparagine production due to low glutamine level	-
ρ_{Asp_Glc}	Response constant for aspartic acid consumption due to low glucose level	-
ρ_{Asp_Gln}	Response constant for aspartic acid production due to low glutamine level	-
ρ_{Cys_Glc}	Response constant for cysteine consumption due to low glucose level	-
ρ_{Cys_Gln}	Response constant for cysteine production due to low glutamine level	-
$\rho_{d,Glc}$	Response constant for cell death due to low glucose level	-
$\rho_{d,Gln}$	Response constant for cell death due to low glutamine level	-
ρ_g	Response constant of nutrients for cells growth due to low glutamine level	-
ρ_{Glc_Gln}	Response constant for glucose production due to low glutamine level	-
ρ_{Gln_Glc}	Response constant for glutamine consumption due to low glucose level	-
ρ_{Glu_Glc}	Response constant for glutamic acid consumption due to low glucose level	-
ρ_{Glu_Gln}	Response constant for glutamic acid production due to low glutamine level	-
ρ_{Gly_Glc}	Response constant for glycine consumption due to low glucose level	-
ρ_{Gly_Gln}	Response constant for glycine production due to low glutamine level	-
ρ_{His_Glc}	Response constant for histidine consumption due to low glucose level	-

ρ_{His_Gln}	Response constant for histidine production due to low glutamine level	-
ρ_{IFN_Glc}	Response constant for IFN γ production due to low glucose level	-
ρ_{IFN_Gln}	Response constant for IFN γ production due to low glutamine level	-
ρ_{Ile_Glc}	Response constant for isoleucine consumption due to low glucose level	-
ρ_{Ile_Gln}	Response constant for isoleucine production due to low glutamine level	-
ρ_{Lac_Glc}	Response constant for lactate production due to low glucose level	-
ρ_{Lac_Gln}	Response constant for lactate production due to low glutamine level	-
ρ_{Leu_Glc}	Response constant for leucine consumption due to low glucose level	-
ρ_{Leu_Gln}	Response constant for leucine production due to low glutamine level	-
ρ_{Lys_Glc}	Response constant for lysine consumption due to low glucose level	-
ρ_{Lys_Gln}	Response constant for lysine production due to low glutamine level	-
ρ_{Met_Glc}	Response constant for methionine consumption due to low glucose level	-
ρ_{Met_Gln}	Response constant for methionine production due to low glutamine level	-
ρ_{Phe_Glc}	Response constant for phenylalanine consumption due to low glucose level	-
ρ_{Phe_Gln}	Response constant for phenylalanine production due to low glutamine level	-
ρ_{Pro_Glc}	Response constant for proline consumption due to low glucose level	-
ρ_{Pro_Gln}	Response constant for proline production due to low glutamine level	-
ρ_{Ser_Glc}	Response constant for serine consumption due to low glucose level	-
ρ_{Ser_Gln}	Response constant for serine production due to low glutamine level	-
ρ_{Thr_Glc}	Response constant for threonine consumption due to low glucose level	-
ρ_{Thr_Gln}	Response constant for threonine production due to low glutamine level	-
ρ_{Trp_Glc}	Response constant for tryptophan consumption due to low glucose level	-
ρ_{Trp_Gln}	Response constant for tryptophan production due to low glutamine level	-
ρ_{Tyr_Glc}	Response constant for arginine consumption due to low glucose level	-
ρ_{Tyr_Gln}	Response constant for tyrosine production due to low glutamine level	-
ρ_{Val_Glc}	Response constant for valine consumption due to low glucose level	-
ρ_{Val_Gln}	Response constant for valine production due to low glutamine level	-

Table 4.8: Notations for major variables in the complex CHO-IFN γ model.

Variables	Definition	Units
AA^{**}	Amino acid concentration	mM
AA_{eff}^{**}	Effective amino acid concentration	mM
Amm	Ammonium (NH $_4^+$) concentration	mM
X_d	Dead cell concentration	10 6 cells L $^{-1}$
X_t	Total cell concentration	10 6 cells L $^{-1}$
X_v	Viable (living) cell concentration	10 6 cells L $^{-1}$
F_{in}	Flowrate of inlet stream containing glucose, glutamine, & amino acids	L h $^{-1}$
$F_{in,glc}$	Flowrate of pure glucose stream	L h $^{-1}$
F_{out}	Flowrate of outlet stream	L h $^{-1}$
Glc	Glucose concentration	mM
Glc_{eff}	Effective glucose concentration	mM
Gln	Glutamine concentration	mM
Gln_{eff}	Effective glutamine concentration	mM
$IFN\gamma$	Interferon- γ concentration	mg L $^{-1}$
Lac	Lactate concentration	mM
μ	Intrinsic specific growth rate	h $^{-1}$
μ_d	Specific death rate	h $^{-1}$
NH_3	Ammonia concentration	mM
q_{AA}^{**}	Specific consumption rate of amino acid	mmole 10 $^{-6}$ cell $^{-1}$ h $^{-1}$
q_{Amm}	Specific production rate of ammonia	mmole 10 $^{-6}$ cell $^{-1}$ h $^{-1}$
$q_{Amm,rev}$	Specific consumption rate of ammonia	mmole 10 $^{-6}$ cell $^{-1}$ h $^{-1}$
q_{Glc}	Specific consumption rate of glucose	mmole 10 $^{-6}$ cell $^{-1}$ h $^{-1}$
q_{Gln}	Specific consumption rate of glutamine	mmole 10 $^{-6}$ cell $^{-1}$ h $^{-1}$
$q_{Lac,Glc}$	Specific lactate production rate from glucose	mmole 10 $^{-6}$ cell $^{-1}$ h $^{-1}$
$q_{Lac,Gln}$	Specific lactate production rate from glutamine	mmole 10 $^{-6}$ cell $^{-1}$ h $^{-1}$
$r_{IFN\gamma}$	Specific production rate of IFN γ	mg 10 $^{-6}$ cell $^{-1}$ h $^{-1}$
t	time	h
V	bioreactor volume	L
$x_{res,Glc}$	Hypothetical response variable for low glucose concentrations	-
$x_{res,Gln}$	Hypothetical response variable for low glutamine concentrations	-

Remark:

- Amino acids other than glutamine: valine, leucine, isoleucine, methionine, phenylalanine, tryptophan, threonine, lysine, histidine, alanine, glycine, proline, aspartic acid, glutamic acid, asparagine, serine, tyrosine, cysteine, and arginine.
- **: amino acid concentration other than glutamine (mM)

Table 4.9: Concentration of glucose, glutamine and other amino acids in the inlet streams.

Parameters	Definition	Units
Glc _{in}	Feed glucose concentration in glutamine-controlled fed-batch cultures	mmole L ⁻¹
Glc' _{in}	Feed glucose concentration in glucose-controlled fed-batch cultures	mmole L ⁻¹
Gln _{in}	Feed glutamine concentration	mmole L ⁻¹
Val _{in} (valine)	Feed valine concentration	mmole L ⁻¹
Leu _{in} (leucine)	Feed leucine concentration	mmole L ⁻¹
Ile _{in} (isoleucine)	Feed isoleucine concentration	mmole L ⁻¹
Met _{in} (methionine)	Feed methionine concentration	mmole L ⁻¹
Phe _{in} (phenylalanine)	Feed phenylalanine concentration	mmole L ⁻¹
Trp _{in} (tryptophan)	Feed tryptophan concentration	mmole L ⁻¹
Thr _{in} (threonine)	Feed threonine concentration	mmole L ⁻¹
Lys _{in} (lysine)	Feed lysine concentration	mmole L ⁻¹
His _{in} (histidine)	Feed histidine concentration	mmole L ⁻¹
Ala _{in} (alanine)	Feed alanine concentration	mmole L ⁻¹
Gly _{in} (glycine)	Feed glycine concentration	mmole L ⁻¹
Pro _{in} (proline)	Feed proline concentration	mmole L ⁻¹
Asp _{in} (aspartic acid)	Feed aspartic acid concentration	mmole L ⁻¹
Glu _{in} (glutamic acid)	Feed glutamic acid concentration	mmole L ⁻¹
Asn _{in} (asparagine)	Feed asparagine concentration	mmole L ⁻¹
Ser _{in} (serine)	Feed serine concentration	mmole L ⁻¹
Tyr _{in} (tyrosine)	Feed tyrosine concentration	mmole L ⁻¹
Cys _{in} (cysteine)	Feed cysteins concentration	mmole L ⁻¹
Arg _{in} (arginine)	Feed arginine concentration	mmole L ⁻¹

Chapter 5

— Parameter Estimation for the Complex CHO-IFN γ Model

5.1 Parameter Estimation Strategy

With a set of model equations and experiment data, the model parameter values can be estimated such that the model predictions match experimental observation. Various parameter estimation approaches including trial and error, least square method, genetic algorithm, stochastic algorithm etc. had been used in the literature (Shuler et al., 1979; Park et al., 1997; Mendes and Kell, 1998; Pinchuk et al., 2000; Frahm et al., 2002b; Gadkar et al., 2003; Moles et al., 2003; Kotalik et al., 2004). Sometimes the parameter estimation complexity was reduced by model linearization or assuming certain relationships among parameters/variables (Shuler et al., 1979; Grosfils et al., 2007). But the number of model parameters often exceeds the number of measured variables in biological experiments that there exist multiple parameter solutions (Gadkar et al., 2003). In the case of the CHO-IFN γ model developed in Section 4.2, there are 192 parameters but only 26 measured cell culture variables. Thus, a strategy was developed for the estimation of all those parameters and it is presented in this chapter.

5.1.1 Framework of Parameter Estimation for Highly Underspecified Model

The complex CHO-IFN γ cell culture model developed in Section 4.2 consists of parameters that can be classified into the following categories:

- (1) Hypothesised parameters for cell culture responses at low levels of glutamine and glucose
- (2) Parameters based on engineering assumptions, stoichiometric ratios, or estimable from literature data
- (3) Directly measurable parameter
- (4) Parameters that can be isolated from the model structure
- (5) Parameters that are active in both batch and fed-batch conditions versus parameters that are only active in certain fed-batch conditions

The first two types of parameters were estimated using mammalian cell culture data reported in the literature plus certain engineering assumptions. For any parameter that could be directly measured, individual experiment was carried out to obtain the corresponding data. Some model equations only involve two variables which are both quantifiable from the measured data. Thus, assuming there is no unknown interaction with any third variable, the parameters can be ‘isolated’ from the rest of the model and estimated more accurately based on the values of the two corresponding variables. For the remaining parameters, those that are active in both batch and fed-batch conditions were initially estimated using batch culture data; some parameters are only active in fed-batch cultures were estimated using fed-batch culture data.

After an initial estimation of all parameter values, the relative importance of the parameters with respect to IFN γ production in batch cultures was quantified using Global Sensitivity Analysis (GSA). The sensitivity of those fed-batch parameters could not be easily quantified using GSA because different profiles of the inlet streams $F_m(t)$ and $F_{in,glc}(t)$ could result in different relative significance of the parameters but it is not feasible to scan all possible profile patterns. Thus, all those fed-batch parameters with non-zero influence on the model were considered ‘significant’ in the parameter estimation stage. The possible effect of parameter uncertainty is evaluated in Chapter 6.

The insensitive parameters were then fixed at their nominal values while the values of sensitive parameters were refined using regression and dynamic simulation in gPROMS. A schematic illustration of the parameter estimation process is shown in Figure 5.1. The resulting set of parameter values was used for model-based optimisation in the next chapter.

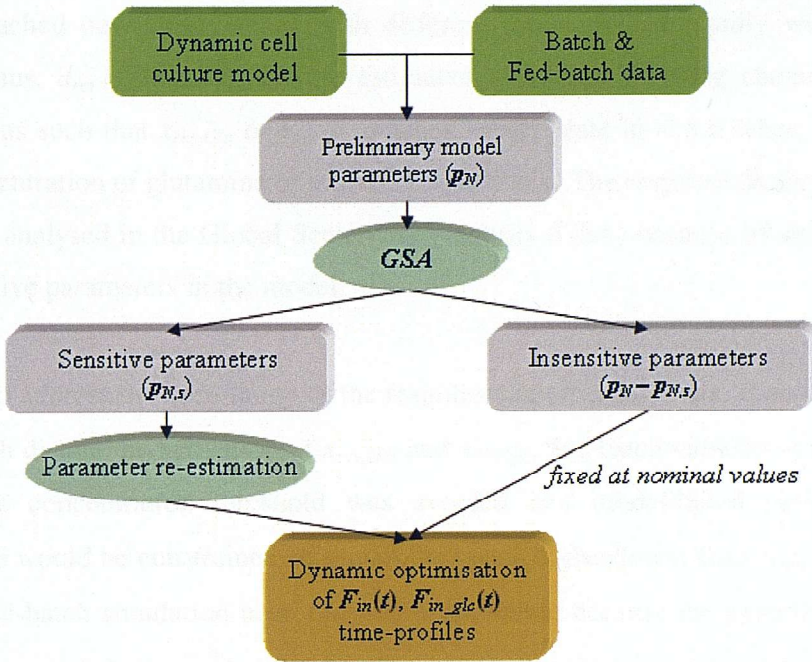


Figure 5.1: Schematic diagram showing the involvement of Global Sensitivity Analysis (GSA) in the estimation of model parameter values.

5.1.1.1. Response Factors Parameters

The parameters for the hypothetical dimensionless cell culture response variables $x_{res,Gln}$ and $x_{res,Glc}$ include a threshold value (τ_{Gln} , τ_{Glc}) based on glutamine and glucose concentration, an activation coefficient ($rmax_{res,Gln}$, $rmax_{res,Glc}$), and a degradation rate ($d_{res,Gln}$, $d_{res,Glc}$) of the response variables. Since such variables are not measurable, $rmax_{res,Gln}$ and $rmax_{res,Glc}$ were set at a default value of 1.

τ_{Gln} was estimated as 0.7mM based on literature findings of an increase in product synthesis in other mammalian cell-lines at glutamine concentration $< 0.3\text{mM}$ (Mancuso et al., 1998; Lee et al., 2003a) and the CHO-IFN γ fed-batch cultures performance which showed an increase in productivity at a tested level of glutamine concentration up to 0.5mM. τ_{Glc} was estimated as 0.5mM according to observation of

the CHO-IFN γ fed-batch cultures that productivity decreased and the production of lactate, a major byproduct of glucose, appeared to change from net secretion to net consumption at glucose concentrations $< \sim 0.5$ mM.

The values of $d_{res,Gln}$ and $d_{res,Glc}$ were assumed to be the same. It was reported by Altamirano et al. (2001) that CHO-tPA chemostat cultures subjected to low glucose levels reached new steady-states with different productivities rapidly within several hours. Thus, $d_{res,Gln}$ and $d_{res,Glc}$ were estimated to be 1.2 h^{-1} using chemostat culture simulations such that $x_{res,Gln}$ or $x_{res,Glc}$ reached steady state in < 5 h when activated by low concentration of glutamine or glucose respectively. The response factors parameters were not analysed in the Global Sensitivity Analysis (GSA) because by definition they are sensitive parameters in the model.

To address the uncertainty of the response factors parameters, especially τ_{Gln} and τ_{Glc} which dictate the activation of $x_{res,Gln}$ and $x_{res,Glc}$, fed-batch simulation near the τ_{Gln} glutamine concentration threshold was avoided and model-based optimisation in Chapter 6 would be constrained at glutamine levels higher/lower than τ_{Gln} . For glucose levels, fed-batch simulation near τ_{Glc} was unavoidable because the experimental range of glucose concentration in fed-batch cultures varied around the value of τ_{Glc} . In order to minimise any error due to such dilemma, the value of τ_{Glc} would be fine-tuned in the parameter re-estimation stage in Section 5.1.1.7 if necessary. There was no problem with τ_{Glc} in the model-based optimisation as the optimal glucose levels were found to be always above τ_{Glc} due to the fact that low glucose concentrations caused reduction in productivity.

5.1.1.2. Engineering, Stoichiometric, and Literature-Based Parameters

Three model parameters are constant by definition or engineering estimation: pH, β , and ε . The pH of the bioreactor is controlled at pH7, β is a unit-time coefficient of effective nutrient concentrations (Section 4.2.1.4: Equation M13) having a default value of 1 h, ε is an engineering parameter for specific ammonium production (Section 4.2.1.5: Equation M34) and is fixed at 0.01 such that $\varepsilon \ll 1$.

In the equations for specific production of byproducts (Section 4.2.1.5), $r_{max_{Amm_Gln}}$ (Equation M34), $r_{max_{Amm_His,Ser,Asn}}$ (Equation M34), $r_{max_{Lac_Glc}}$ (Equation M36), and $r_{max_{Lac_Gln}}$ (Equation M37) represent the stoichiometric relationships between the corresponding byproduct and nutrient source. Their values are 2, 4, 2, and 1 respectively (Altamirano et al., 2001).

The three engineering parameters and four stoichiometric factors discussed above are not analysed in the Global Sensitivity Analysis (GSA) due to the fact that their values are constant by default or engineering assumptions.

The critical concentrations of ammonia (NH_3) and lactate in Equation M6 and M10 of Section 4.2.1.2 represent the levels of byproducts beyond which there would be significant inhibition of growth rate and increase in death rate. The value of NH_{3cr} is related to the measurable ammonium (NH_4^+) concentration via Equation M5 (Section 4.2.1.2). It had been reported that CHO-IFN γ cell-line could tolerate ammonium concentration up to about 5mM and the culture was not affected by lactate concentration as high as 17.5mM (Hayter et al., 1991). Observations of the CHO-IFN γ cell culture modelled in this current study also indicated a significant decrease in growth rate when ammonium concentration reached ~5mM though no clear inhibitive level of lactate can be deduced. Therefore, the values of NH_{3cr} and Lac_{cr} are estimated to be 5mM and 20mM respectively.

5.1.1.3 Directly Measurable Parameter

The spontaneous glutamine degradation rate, $r_{d,Gln}$, in Equation M18 (Section 4.2.1.4) can be measured directly by culturing cell-free medium in 37°C and monitor the glutamine concentration. The value of $r_{d,Gln}$ is measured to be 0.005 h⁻¹. Detailed calculation can be found in Appendix 5.

5.1.1.4 Isolation of Parameters

The specific consumption rates of all essential amino acids (Section 4.2.2: Equation 4.2.54 – 4.2.62) and glucose (Equation 4.2.31) are only related to the effective concentration of each corresponding nutrient. Since both the specific consumption rate and effective concentration can be calculated from measured experimental data and it may be assumed that no third unknown variable is associated with each of the equations, the equations were ‘isolated’ from the model and the corresponding parameters were estimated individually based on relevant batch culture data up to the exponential growth phase where the byproducts were still below inhibitory levels. An example for essential amino acids is shown in Figure 5.2 where initial estimates of $r_{max_{Thr}}$ and K_{Thr} were obtained based on the data of specific threonine consumption rate versus average threonine concentration. Another example for glucose is shown in Figure 5.3. The data for tryptophan, one of the essential amino acids, were not able to be measured in the experiment. The values of $r_{max_{Trp}}$ and K_{Trp} were assumed to be the same as phenylalanine which has the most similar molecular structure (see Appendix 4 for amino acids structure). The estimates of parameters for specific consumption of essential amino acids and glucose can be found in Table 5.1.

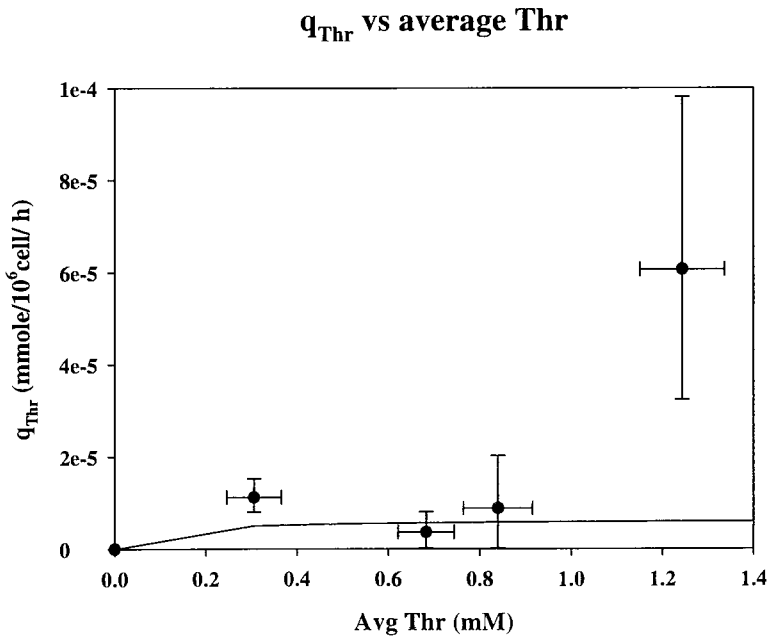


Figure 5.2: Specific threonine uptake rate versus threonine concentration in CHO-IFN γ batch culture. Solid line represents initial estimation of the relationship between the two variables.

q_{Glc} vs average Glc

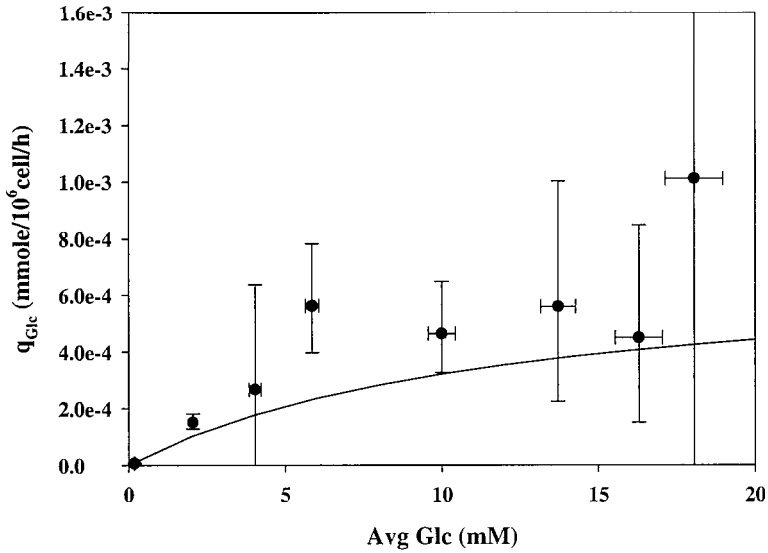


Figure 5.3: Specific glucose uptake rate versus glucose concentration in CHO-IFN γ batch culture. Solid line represents initial estimation of the relationship between the two variables.

The specific consumption rate equations of certain non-essential amino acids may be assumed independent of other amino acids if (i) their excretion rate from cells is negligible, (ii) any possible conversion from other amino acids may be assumed less significant than the reverse conversion or being refined to the intracellular medium, (iii) the time-profile of the amino acid in batch culture is monotonically decreasing. These requirements are satisfied in the case of aspartic acid (Equation 4.2.66), asparagine (Equation 4.2.68), and serine (Equation 4.2.69). An example is shown in Figure 5.4 for aspartic acid where initial estimates of $rmax_{Asp}$ and K_{Asp} were obtained. Glutamic acid and arginine cannot be handled this way because the extracellular concentration of glutamic acid in batch culture was as low as the measurement uncertainty (Figure 5.18d), making any estimation of $rmax_{Glu}$ and K_{Glu} inconclusive; the time-profile of arginine in batch culture had a wave-like pattern which may suggest a more complex interconversion pattern which is not well understood (Figure 5.18c). The estimates of parameters for specific consumption of aspartic acid, asparagine, and serine can be found in Table 5.1.

q_{Asp} vs average Asp

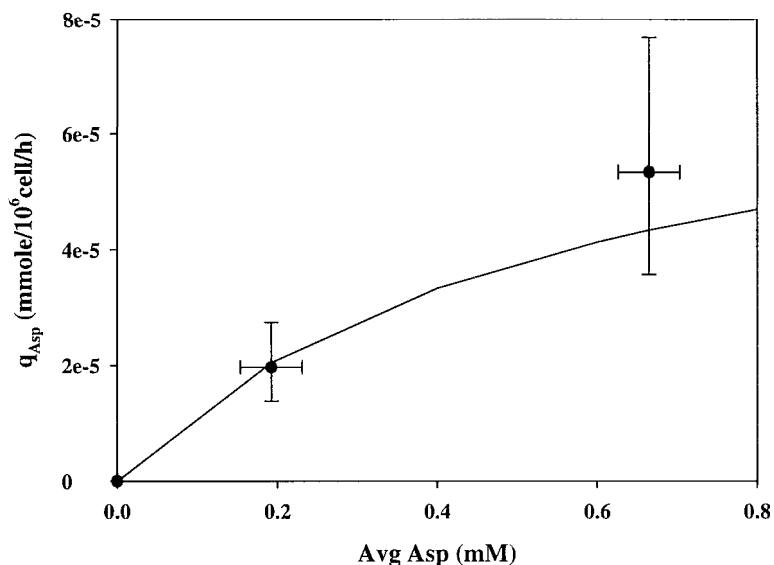


Figure 5.4: Specific aspartic acid uptake rate versus aspartic acid concentration in CHO-IFN γ batch culture. Solid line represents initial estimation of the relationship between the two variables.

The specific IFN γ production rate in the batch culture is shown in Figure 5.5. Apart from the earliest data point at roughly 1 h which had a high mean value but also very high uncertainty, the specific production rate appeared to be stable with time throughout the batch culture. The maximum specific IFN γ production rate, $r_{max_{IFN\gamma}}$, in Equation 4.2.86 was estimated within the shaded region in Figure 5.5 with an initial guess of $\sim 2 \times 10^{-5} \text{ mg } 10^{-6} \text{ cell}^{-1} \text{ h}^{-1}$.

For the maximum specific growth rates, μ_{max1} and μ_{max2} , (Section 4.2.1.2: Equation M8) and minimum specific death rate, $\mu_{d,min}$, (Section 4.2.1.2: Equation M10) in the batch culture, certain assumptions may be made in the growth and death equations in order to estimate their order of magnitude. Figure 5.6 shows the time-profile of the intrinsic specific growth rate of the batch culture. The word ‘intrinsic’ is to avoid confusion with the apparent specific growth rate which is the difference between specific growth rate and specific death rate. Glucose and glutamine in the batch culture were depleted around 68 h (Figure 5.18a). If the nutrients in the batch culture are assumed to be abundant in the early half of the cell culture time such that their corresponding terms in the specific growth rate equation tend to 1, an estimation can be made for $(\mu_{max1} + \mu_{max2})$. If the amino acids are assumed to be still sufficient shortly after glucose/glutamine depletion such that their corresponding terms remain close to 1, the value of μ_{max1} can be roughly estimated. Similarly, an initial estimate for $\mu_{d,min}$ was

made based on the time-profile of the specific death rate in batch culture (Figure 5.7) with an assumption that the byproduct concentration in the early cell culture time is insignificant to affect death rate. The estimated values for μ_{max1} , μ_{max2} , and $\mu_{d,min}$ are 0.01 h^{-1} , 0.025 h^{-1} , and 0.001 h^{-1} respectively. Detailed calculation is available in Appendix 5.

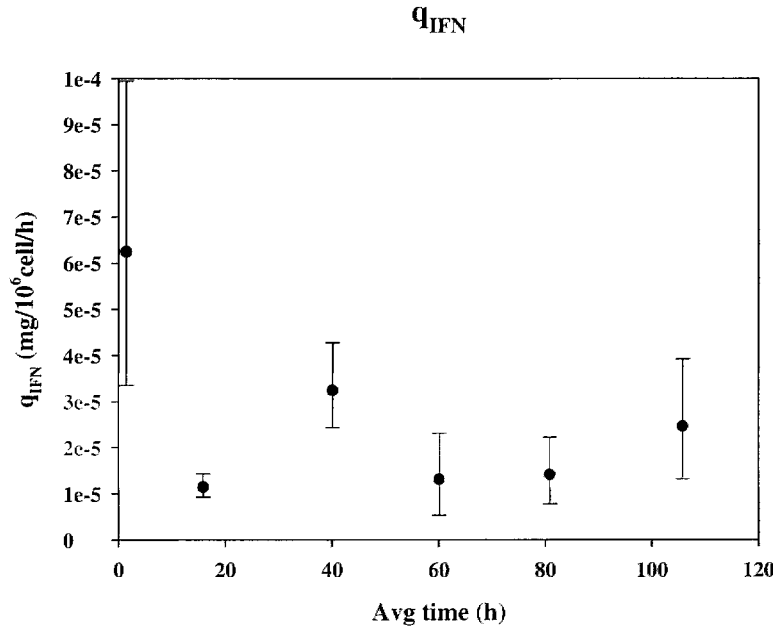


Figure 5.5: Specific production rate of IFN γ in CHO-IFN γ batch culture. The shaded region represents the possible range for maximum specific production rate in batch condition.

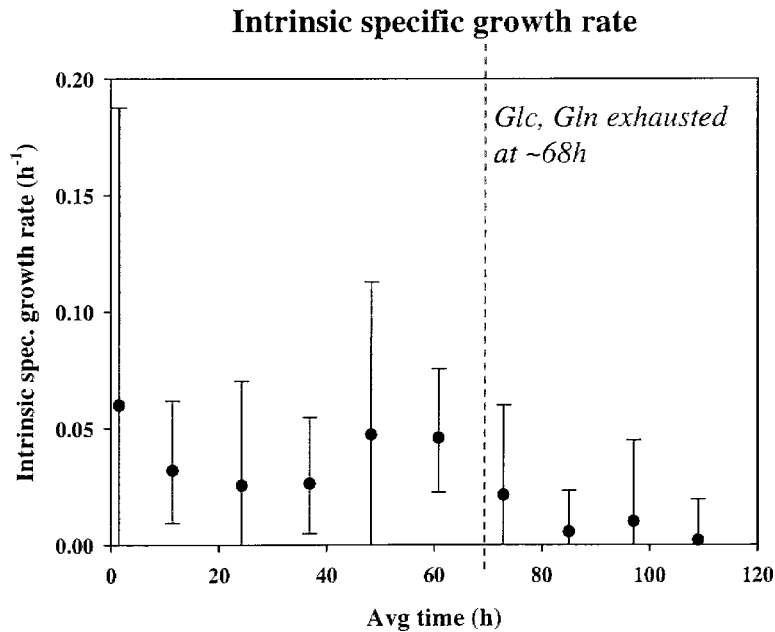


Figure 5.6: Intrinsic specific growth rate in CHO-IFN γ batch culture where glucose and glutamine were exhausted at ~68 h. The difference in specific growth rate before and after exhaustion of glucose and glutamine was used for estimation of the maximum specific growth rates.

Dead cells concentration

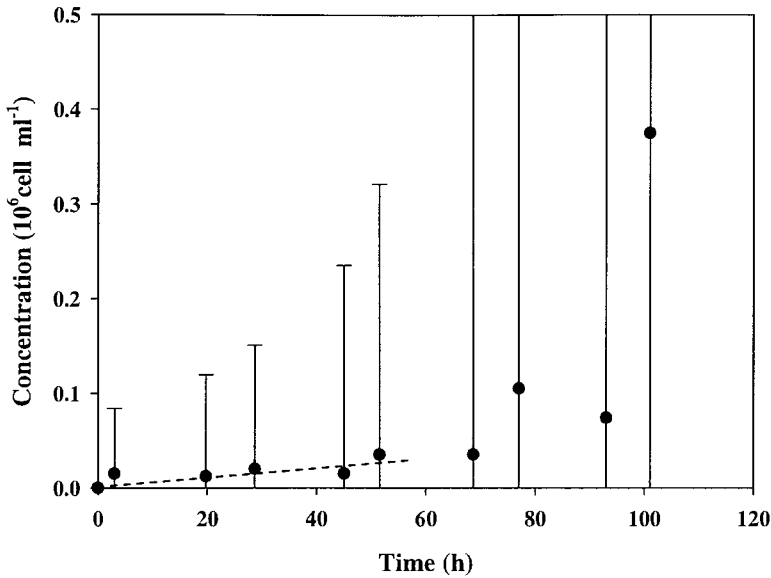


Figure 5.7: Concentration of dead cells in CHO-IFN γ batch culture. The dotted line represents linearization of dead cell concentration up to mid-exponential phase for estimation of minimum death rate.

5.1.1.5 Regression of the Remaining Parameters

The remaining parameters were separated into those that are based on batch cultures versus those that are related to low-glutamine/low-glucose responses in fed-batch cultures. The former were estimated with batch culture data in gPROMS (Process Systems Enterprise Ltd.) using a general maximum likelihood approach similar to in Chapter 3. The latter were then estimated with data of glutamine-controlled and glutamine-glucose-controlled fed-batch cultures using dynamic simulations. The estimated values of all batch and fed-batch parameters are listed in Table 5.1.

5.1.1.6 Identification of Sensitive Parameters via GSA

Global Sensitivity Analysis (GSA) was used to identify parameters in the CHO-IFN γ model that are sensitive with respect to IFN γ production. An introduction of sensitivity analysis methods is available in Section 4.1.4.1. A total of 179 parameters were analysed excluding 13 parameters discussed in Section 5.1.1.1 and 5.1.1.2. The lower and upper bounds of parameter range were selected as follow:

Upper bound ---

- 2 times standard deviation for those isolated parameters (Section 5.1.1.4) that were estimated via regression, e.g. $r_{max_{Thr}}$.
- A theoretical upper bound for the yield of certain non-essential amino acid from other amino acid, e.g. $r_{max_{Tyr_Phe}}$.
- 2 – 20 times of the initially estimated value depending on the uncertainty of each parameter.

Lower bound ---

- 10^{-6} for most positive parameters or a higher value in certain cases where more information is available to judge the feasible lower bounds such as $A_{mm_{cr}}$ and Lac_{cr} .
- A theoretical lower bound for the negative response coefficients, e.g. $r_{max_{res,Ala_Glc}}$.

A list of the lower and upper bounds for all the 179 parameters analysed in GSA can be found in Table 5.1. The parameters were grouped into thirteen categories according to their biological functions and parameter types:

1. IFN γ production
2. Specific growth rate
3. Specific uptake rate of essential amino acids
4. Glutamine concentration
5. Specific death rate
6. Glucose concentration
7. Specific uptake rate of non-essential amino acids
8. Interconversions of amino acids
9. Formation of byproducts
10. Response parameters related to essential amino acids
11. Half-saturation constants for response parameters related to essential amino acids
12. Response parameters related to non-essential amino acids
13. Half-saturation constants for response parameters related to non-essential amino acids

Table 5.1: List of grouped parameters of the complex CHO-IFN γ model for Global Sensitivity Analysis (GSA).

Group	Parameter	Initial Estimation (1-2 sig. fig.)	Lower Bound (1-2 sig. fig.)	Upper Bound (1-2 sig. fig.)	Units
IFN γ	$rmax_{IFN\gamma}$	1.5E-05	1E-6	4E-5	mg 10 ⁻⁶ cell ⁻¹ h ⁻¹
	$rmax_{res,IFN,Gln}$	7	1	10	-
	$\rho_{IFN,Gln}$	1	1E-6	10	-
	$rmax_{res,IFN,Glc}$	-1	-1	-1E-6	-
	$\rho_{IFN,Glc}$	1	1E-6	10	-
Growth	μ_{max1}	0.01	1E-6	0.1	h ⁻¹
	μ_{max2}	0.025	1E-6	0.1	h ⁻¹
	$K_{g,Glc}$	0.0004	1E-6	0.004	mmole 10 ⁻⁶ cell ⁻¹ h ⁻¹
	$K_{g,Gln}$	0.0004	1E-6	0.004	mmole 10 ⁻⁶ cell ⁻¹ h ⁻¹
	$k_{inh,NH3}$	0.0024	1E-6	0.024	mmole L ⁻¹
	$k_{inh,Lac}$	25	1E-6	50	mmole L ⁻¹
	$K_{g,Val}$	0.0002	1E-6	0.002	mmole 10 ⁻⁶ cell ⁻¹ h ⁻¹
	$K_{g,Leu}$	0.0002	1E-6	0.002	mmole 10 ⁻⁶ cell ⁻¹ h ⁻¹
	$K_{g,Ile}$	0.0002	1E-6	0.002	mmole 10 ⁻⁶ cell ⁻¹ h ⁻¹
	$K_{g,Met}$	0.0002	1E-6	0.002	mmole 10 ⁻⁶ cell ⁻¹ h ⁻¹
	$K_{g,Phe}$	0.0002	1E-6	0.002	mmole 10 ⁻⁶ cell ⁻¹ h ⁻¹
	$K_{g,Trp}$	0.0002	1E-6	0.002	mmole 10 ⁻⁶ cell ⁻¹ h ⁻¹
	$K_{g,Thr}$	0.0002	1E-6	0.002	mmole 10 ⁻⁶ cell ⁻¹ h ⁻¹
	$K_{g,Lys}$	0.0002	1E-6	0.002	mmole 10 ⁻⁶ cell ⁻¹ h ⁻¹
	$K_{g,His}$	0.0002	1E-6	0.002	mmole 10 ⁻⁶ cell ⁻¹ h ⁻¹
	$K_{g,Arg}$	0.0002	1E-6	0.002	mmole 10 ⁻⁶ cell ⁻¹ h ⁻¹
	$K_{g,Tyr}$	0.0002	1E-6	0.002	mmole 10 ⁻⁶ cell ⁻¹ h ⁻¹
	$K_{g,Cys}$	0.0002	1E-6	0.002	mmole 10 ⁻⁶ cell ⁻¹ h ⁻¹
	ρ_g	0.2	1E-6	2	-
Essential amino acids consumption	$rmax_{Val}$	0.02	1E-6	0.64	mmole 10 ⁻⁶ cell ⁻¹ h ⁻¹
	K_{Val}	1	1E-6	46.54	mmole L ⁻¹
	$rmax_{Met}$	0.02088	1E-6	0.53	mmole 10 ⁻⁶ cell ⁻¹ h ⁻¹
	K_{Met}	0.933	1E-6	28.47	mmole L ⁻¹
	$rmax_{Lys}$	0.02844	1E-6	0.82	mmole 10 ⁻⁶ cell ⁻¹ h ⁻¹
	K_{Lys}	1.373	1E-6	63.67	mmole L ⁻¹
	$rmax_{Ile}$	0.02528	1E-6	0.94	mmole 10 ⁻⁶ cell ⁻¹ h ⁻¹
	K_{Ile}	1.457	1E-6	74.94	mmole L ⁻¹
	$rmax_{Leu}$	0.02632	1E-6	7.93	mmole 10 ⁻⁶ cell ⁻¹ h ⁻¹
	K_{Leu}	1.365	1E-6	67.25	mmole L ⁻¹
	$rmax_{Phe}$	0.02115	1E-6	0.99	mmole 10 ⁻⁶ cell ⁻¹ h ⁻¹
	K_{Phe}	1.351	1E-6	77.65	mmole L ⁻¹
	$rmax_{Trp}$	0.02115	1E-6	0.99	mmole 10 ⁻⁶ cell ⁻¹ h ⁻¹
	K_{Trp}	1.351	1E-6	77.65	mmole L ⁻¹
	$rmax_{Thr}$	0.006279	1E-6	0.027479	mmole 10 ⁻⁶ cell ⁻¹ h ⁻¹
	K_{Thr}	0.07722	1E-6	2.55922	mmole L ⁻¹
$rmax_{His}$	0.01217	1E-6	1.30817	mmole 10 ⁻⁶ cell ⁻¹ h ⁻¹	
K_{His}	1.314	1E-6	171.314	mmole L ⁻¹	
Glutamine	$rmax_{Gln}$	0.7	1E-6	3	mmole 10 ⁻⁶ cell ⁻¹ h ⁻¹
	K_{Gln}	9	1E-6	44	mmole L ⁻¹
	$K_{inh,Glc}$	13	1E-6	63	mmole L ⁻¹
	$r_{d,Gln}$	0.005	1E-6	0.01	h ⁻¹
	$rmax_{res,Gln,Glc}$	0	1E-6	1	-
	$\rho_{Gln,Glc}$	1	1E-6	10	-
Death	Amm_{cr}	5	3	7	mM
	Lac_{cr}	20	15	40	mM
	$k_{d,NH3}$	0.0001	1E-6	0.001	mmole L ⁻¹
	$k_{d,Lac}$	42	1E-6	84	mmole L ⁻¹
	$\mu_{d,min}$	0.001	1E-6	0.002	h ⁻¹
	r_{frag}	0.008	1E-6	0.02	h ⁻¹

(Death [continue])	$\rho_{d,Gln}$	0.05	1E-6	1	-
	$\rho_{d,Glc}$	0.05	1E-6	1	-
Glucose	$rmax_{Glc}$	0.7	1E-6	2.31	mmole 10^{-6} cell $^{-1}$ h $^{-1}$
	K_{Glc}	12	1E-6	40	mmole L $^{-1}$
	$rmax_{res,Glc,Gln}$	0	1E-6	1	-
	$\rho_{Glc,Gln}$	1	1E-6	10	-
Non-essential amino acids consumption	$rmax_{Ala}$	0.294	1E-6	5.88	mmole 10^{-6} cell $^{-1}$ h $^{-1}$
	K_{Ala}	0.365	1E-6	7.3	mmole L $^{-1}$
	$rmax_{Gly}$	0.1087	1E-6	2.174	mmole 10^{-6} cell $^{-1}$ h $^{-1}$
	K_{Gly}	0.3126	1E-6	6.252	mmole L $^{-1}$
	$rmax_{Pro}$	1.6147	1E-6	32.3	mmole 10^{-6} cell $^{-1}$ h $^{-1}$
	K_{Pro}	3.788	1E-6	75.76	mmole L $^{-1}$
	$rmax_{Asp}$	0.0794	1E-6	0.3534	mmole 10^{-6} cell $^{-1}$ h $^{-1}$
	K_{Asp}	0.5536	1E-6	3.29	mmole L $^{-1}$
	$rmax_{Glu}$	0.212	1E-6	4.24	mmole 10^{-6} cell $^{-1}$ h $^{-1}$
	K_{Glu}	2.84	1E-6	56.8	mmole L $^{-1}$
	$rmax_{Asn}$	0.02853	1E-6	0.233	mmole 10^{-6} cell $^{-1}$ h $^{-1}$
	K_{Asn}	0.7116	1E-6	7.982	mmole L $^{-1}$
	$rmax_{Ser}$	0.003691	1E-6	0.32	mmole 10^{-6} cell $^{-1}$ h $^{-1}$
	K_{Ser}	0.3903	1E-6	97.95	mmole L $^{-1}$
	$rmax_{Tyr}$	0.0204	1E-6	0.408	mmole 10^{-6} cell $^{-1}$ h $^{-1}$
	K_{Tyr}	0.757	1E-6	15.14	mmole L $^{-1}$
$rmax_{Cys}$	0.253	1E-6	5.06	mmole 10^{-6} cell $^{-1}$ h $^{-1}$	
K_{Cys}	13.9	1E-6	278	mmole L $^{-1}$	
$rmax_{Arg}$	0.0438	1E-6	0.876	mmole 10^{-6} cell $^{-1}$ h $^{-1}$	
K_{Arg}	10.57	1E-6	211.4	mmole L $^{-1}$	
Non-essential amino acids interconversion	$q_{Ala,min}$	0.135	1E-6	1.35	mmole 10^{-6} cell $^{-1}$ h $^{-1}$
	$q_{Gly,min}$	0.0185	1E-6	0.185	mmole 10^{-6} cell $^{-1}$ h $^{-1}$
	$q_{Pro,min}$	0.0777	1E-6	0.777	mmole 10^{-6} cell $^{-1}$ h $^{-1}$
	$rmax_{Ala,Glc}$	0.2235	1E-6	0.5	mmole mmole $^{-1}$
	$rmax_{Ala,Gln}$	0.2205	1E-6	0.5	mmole mmole $^{-1}$
	$rmax_{Gly,Ser}$	0.1965	1E-6	0.8	mmole mmole $^{-1}$
	$rmax_{Pro,Glu}$	0.3996	1E-6	0.5	mmole mmole $^{-1}$
	$rmax_{Pro,Arg}$	0.3996	1E-6	0.8	mmole mmole $^{-1}$
$rmax_{Tyr,Phe}$	0.169	1E-6	1	mmole mmole $^{-1}$	
$rmax_{Cys,Ser}$	4.00E-05	1E-6	0.2	mmole mmole $^{-1}$	
Byproducts	$K_{Lac,Glc}$	0.4695	1E-6	4.695	mmole 10^{-6} cell $^{-1}$ h $^{-1}$
	$K_{Lac,Gln}$	1.5522	1E-6	15.52	mmole 10^{-6} cell $^{-1}$ h $^{-1}$
	$rmin_{Amm}$	0.01366	1E-6	0.02732	mmole 10^{-6} cell $^{-1}$ h $^{-1}$
	K_{scale}	0.04	1E-6	0.4	mmole 10^{-6} cell $^{-1}$ h $^{-1}$
	$K_{Amm,Gln}$	0.233	1E-6	0.466	mmole 10^{-6} cell $^{-1}$ h $^{-1}$
	$K_{Amm,His,Ser,Asn}$	1.78	1E-6	3.56	mmole 10^{-6} cell $^{-1}$ h $^{-1}$
	$rmin_{Amm,rev}$	6.00E-05	1E-6	3E-4	mmole $^{(1-m)}$ L m 10^{-6} cell $^{-1}$ h $^{-1}$
	$rmax_{Lac,rev}$	0.054	1E-6	0.54	mmole 10^{-6} cell $^{-1}$ h $^{-1}$
	$K_{Lac,rev}$	2.664	1E-6	26.64	mmole L $^{-1}$
	m	3	2	5	-
	$\rho_{Lac,Glc}$	50	1	100	-
	$\rho_{Lac,Gln}$	40	1	80	-
$\rho_{Amm,Gln}$	3	1E-6	10	-	
Essential amino acids fed-batch response coefficients	$rmax_{res,Val,Gln}$	0	1E-6	1	-
	$rmax_{res,Leu,Gln}$	0	1E-6	1	-
	$rmax_{res,Ile,Gln}$	0	1E-6	1	-
	$rmax_{res,Met,Gln}$	0	1E-6	1	-
	$rmax_{res,Phe,Gln}$	-1	-1	-1E-6	-
	$rmax_{res,Tyr,Gln}$	0	1E-6	1	-
	$rmax_{res,Thr,Gln}$	0	1E-6	1	-
	$rmax_{res,Lys,Gln}$	0	1E-6	1	-
$rmax_{res,His,Gln}$	0	1E-6	1	-	

(Essential amino acids fed-batch response coefficients [continue])	$r_{max_{res.Val_Glc}}$	0	1E-6	1	-
	$r_{max_{res.Leu_Glc}}$	0	1E-6	1	-
	$r_{max_{res.Ile_Glc}}$	0	1E-6	1	-
	$r_{max_{res.Met_Glc}}$	0	1E-6	1	-
	$r_{max_{res.Phe_Glc}}$	0	1E-6	1	-
	$r_{max_{res.Trp_Glc}}$	0	1E-6	1	-
	$r_{max_{res.Thr_Glc}}$	0	1E-6	1	-
	$r_{max_{res.Lys_Glc}}$	0	1E-6	1	-
	$r_{max_{res.His_Glc}}$	0	1E-6	1	-
Essential amino acids fed-batch response half-saturation constants	ρ_{Val_Gln}	1	1E-6	5	-
	ρ_{Leu_Gln}	1	1E-6	5	-
	ρ_{Ile_Gln}	1	1E-6	5	-
	ρ_{Met_Gln}	1	1E-6	5	-
	ρ_{Phe_Gln}	0.5	1E-6	2.5	-
	ρ_{Trp_Gln}	1	1E-6	5	-
	ρ_{Thr_Gln}	1	1E-6	5	-
	ρ_{Lys_Gln}	1	1E-6	5	-
	ρ_{His_Gln}	1	1E-6	5	-
	ρ_{Val_Glc}	1	1E-6	5	-
	ρ_{Leu_Glc}	1	1E-6	5	-
	ρ_{Ile_Glc}	1	1E-6	5	-
	ρ_{Met_Glc}	1	1E-6	5	-
	ρ_{Phe_Glc}	1	1E-6	5	-
	ρ_{Trp_Glc}	1	1E-6	5	-
	ρ_{Thr_Glc}	1	1E-6	5	-
	ρ_{Lys_Glc}	1	1E-6	5	-
ρ_{His_Glc}	1	1E-6	5	-	
Non-essential amino acids fed-batch response coefficients	$r_{max_{res.Ala_Gln}}$	-1	-1	-1E-6	-
	$r_{max_{res.Gly_Gln}}$	-1	-1	-1E-6	-
	$r_{max_{res.Pro_Gln}}$	-1	-1	-1E-6	-
	$r_{max_{res.Asp_Gln}}$	0	1E-6	1	-
	$r_{max_{res.Glu_Gln}}$	1	1E-6	2	-
	$r_{max_{res.Asn_Gln}}$	0	1E-6	1	-
	$r_{max_{res.Ser_Gln}}$	0	1E-6	1	-
	$r_{max_{res.Tyr_Gln}}$	0	1E-6	1	-
	$r_{max_{res.Cys_Gln}}$	0	1E-6	1	-
	$r_{max_{res.Arg_Gln}}$	0	1E-6	1	-
	$r_{max_{res.Ala_Glc}}$	-1	-1	-1E-6	-
	$r_{max_{res.Gly_Glc}}$	-1	-1	-1E-6	-
	$r_{max_{res.Pro_Glc}}$	-1	-1	-1E-6	-
	$r_{max_{res.Asp_Glc}}$	0	1E-6	1	-
	$r_{max_{res.Glu_Glc}}$	0	1E-6	1	-
	$r_{max_{res.Asn_Glc}}$	0	1E-6	1	-
	$r_{max_{res.Ser_Glc}}$	0	1E-6	1	-
	$r_{max_{res.Tyr_Glc}}$	0	1E-6	1	-
	$r_{max_{res.Cys_Glc}}$	0	1E-6	1	-
	$r_{max_{res.Arg_Glc}}$	0	1E-6	1	-
Non-essential amino acids fed-batch response half-saturation constants	ρ_{Ala_Gln}	1	1E-6	5	-
	ρ_{Gly_Gln}	1	1E-6	5	-
	ρ_{Pro_Gln}	1	1E-6	5	-
	ρ_{Asp_Gln}	1	1E-6	5	-
	ρ_{Glu_Gln}	1	1E-6	5	-
	ρ_{Asn_Gln}	1	1E-6	5	-
	ρ_{Ser_Gln}	1	1E-6	5	-
	ρ_{Tyr_Gln}	1	1E-6	5	-
	ρ_{Cys_Gln}	1	1E-6	5	-
	ρ_{Arg_Gln}	1	1E-6	5	-

(Non-essential amino acids fed-batch response half-saturation constants [continue])	ρ_{Ala_Glc}	1	1E-6	5	-
	ρ_{Gly_Glc}	1	1E-6	5	-
	ρ_{Pro_Glc}	1	1E-6	5	-
	ρ_{Asp_Glc}	1	1E-6	5	-
	ρ_{Glu_Glc}	1	1E-6	5	-
	ρ_{Asn_Glc}	1	1E-6	5	-
	ρ_{Ser_Glc}	1	1E-6	5	-
	ρ_{Tyr_Glc}	1	1E-6	5	-
	ρ_{Cys_Glc}	1	1E-6	5	-
	ρ_{Arg_Glc}	1	1E-6	5	-

The 13 parameter groups were subjected to GSA analysis with respect to IFN γ productivity. The normalised results are shown in Figure 5.8. A larger value of sensitivity index indicates a higher relative significance of the parameter group. A cut-off threshold of 0.01 was used to identify sensitive versus insensitive parameter groups.

The sensitivity indices in Figure 5.8 include higher-order interactions of each parameter group with all other groups (Section 4.1.4.1: Equation 4.S14). A comparison of the sensitivity indices with (S_{tot}) and without (S) higher-order interactions for the 8 sensitive parameter groups is shown in Figure 5.9. Apart from during the early cell culture time of ~10 h when both S and S_{tot} have similar magnitude, the values of S_{tot} in all the sensitive parameter groups are generally significantly higher than S , indicating quantitatively the highly non-linear nature of the mammalian cell culture model.

Those parameter groups with normalised sensitivity indices > 0.01 were further analysed using GSA to quantify the relative importance of each individual parameter within those groups. A cut-off threshold of 0.05 (similar to the threshold in Section 4.1.4.2) was used to identify the sensitive individual parameters. The GSA results of those 8 sensitive parameter groups are shown in Figure 5.10 – 5.17. The normalised sensitivity indices also include higher-order interactions.

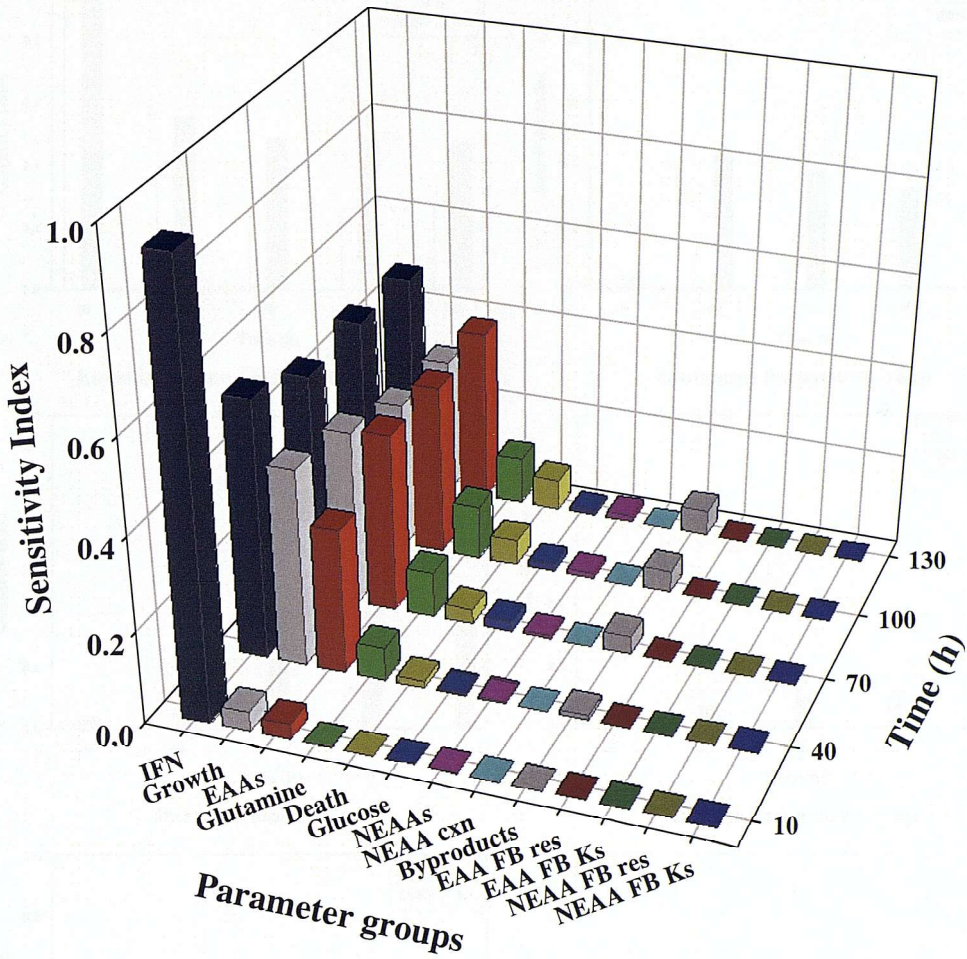


Figure 5.8: Normalised sensitivity index values for different parameter groups classified according to biological functions.

IFN — $IFN\gamma$ production

Growth — specific growth rate

EAAs — specific uptake rate of essential amino acids

Glutamine — glutamine concentration

Death — specific death rate

Glucose — glucose concentration

NEAAs — specific uptake rate of non-essential amino acids

NEAA cxn — non-essential amino acid conversion from other amino acids

Byproducts — formation of byproducts

EAA FB res — essential amino acid responses in fed-batch culture relative to batch culture

EAA FB Ks — half-saturation constants (K_p) for EAA responses in fed-batch cultures

NEAA FB res — non-essential amino acid responses in fed-batch culture relative to batch culture

NEAA FB Ks — half-saturation constants (K_p) for non-EAA responses in fed-batch cultures

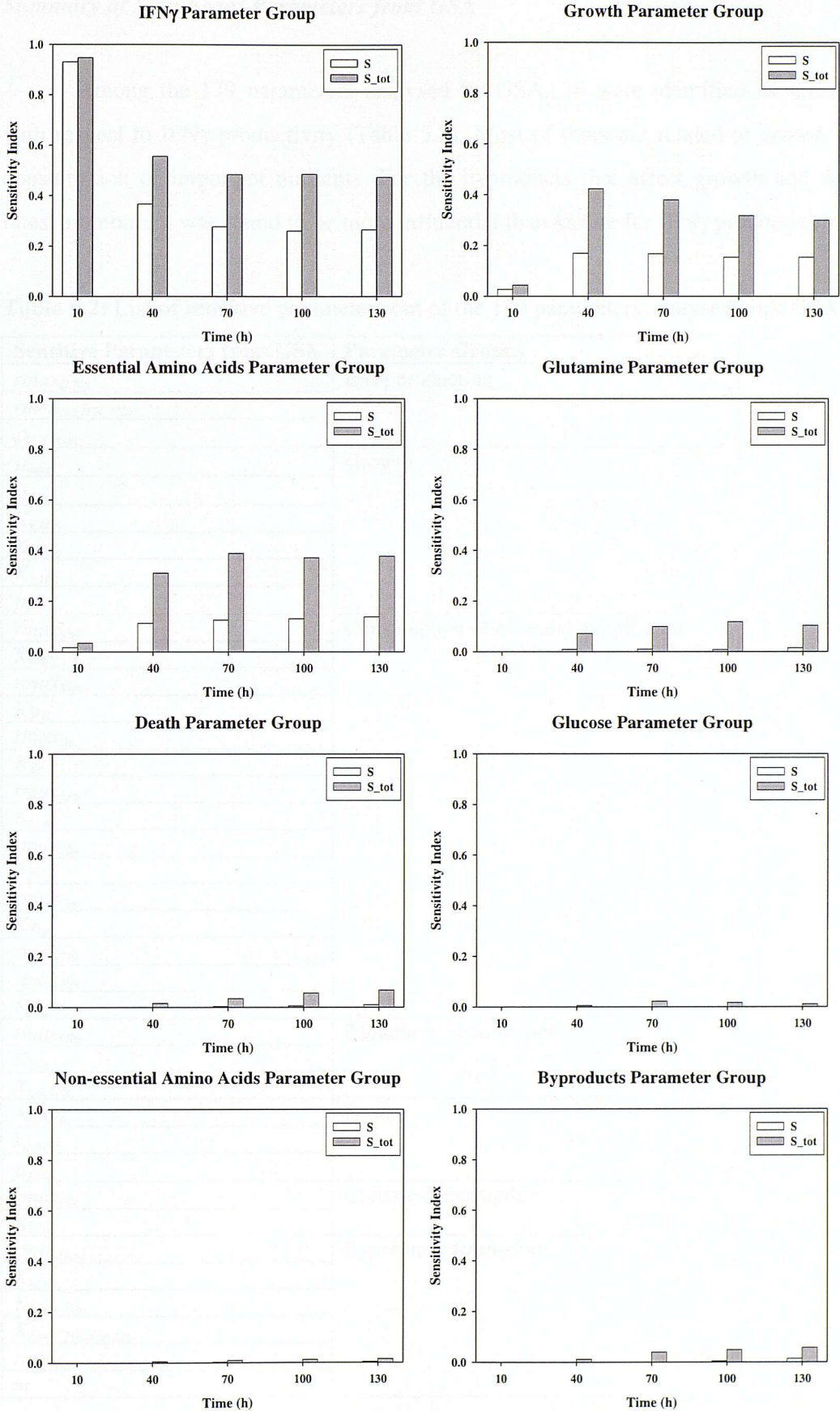


Figure 5.9: Comparison of S and S_{tot} for all sensitive parameter groups from GSA.

Summary of Significant Parameters from GSA

Among the 179 parameters analysed by GSA, 38 were identified as sensitive with respect to IFN γ productivity (Table 5.2). Most of them are related to growth and consumption of important nutrients. For the byproducts that affect growth and death rates, ammonium was found to be more influential than lactate for IFN γ production.

Table 5.2: List of sensitive parameters out of the 179 parameters analysed with GSA.

Sensitive Parameters from GSA	Parameter Groups
$rmax_{IFN\gamma}$	IFN γ production
$rmax_{res,IFN_Gln}$	
ρ_{IFN_Gln}	
μ_{max1}	Growth
μ_{max2}	
$K_{g,Met}$	
$K_{g,Phe}$	
$K_{g,His}$	
ρ_g	
$rmax_{Val}$	Consumption of essential amino acids
K_{Val}	
$rmax_{Met}$	
K_{Met}	
$rmax_{Ile}$	
K_{Ile}	
$rmax_{Leu}$	
K_{Leu}	
$rmax_{Phe}$	
K_{Phe}	
$rmax_{Trp}$	
K_{Trp}	
$rmax_{Thr}$	
$rmax_{His}$	
K_{His}	
$rmax_{Gln}$	
K_{Gln}	
$K_{inh,Glc}$	
Amm_{er}	Death
$k_{d,NH3}$	
$\mu_{d,min}$	
$rmax_{Glc}$	Glucose consumption
K_{Glc}	
$rmin_{Amm}$	Byproducts formation
K_{scale}	
K_{Amm_Gln}	
$K_{Amm_His,Ser,Asn}$	
$rmin_{Amm,rev}$	
m	

The sensitivity indices of the individual parameters are not always stable with cell culture time like the maximum specific IFN γ productivity ($r_{max_{IFN}}$) in Figure 5.10 and the maximum specific growth rates (μ_{max1} , μ_{max2}) in Figure 5.11. For example, the indices of parameters for specific consumption of leucine ($r_{max_{Leu}}$, K_{Leu}) increase significantly at later time of the batch culture (Figure 5.12) when the nutrient is less abundant; similar increase also happens to parameters for glutamine (Figure 5.13) and glucose (Figure 5.15) consumption. The parameters responsible for cell death (Figure 5.14) and byproducts formation (Figure 5.17) are significant in the later half of cell culture time when byproduct concentrations become sufficiently high to affect cell growth/death. The sensitivity indices of all the parameters for non-essential amino acid consumption are generally close to zero (Figure 5.16) which has been observed to happen due to rounding-up of small numerical values when the overall impact of the parameter group on the model output is very small.

The estimated values of the 38 sensitive parameters were then refined using either regression for batch parameters or dynamic simulations for fed-batch parameters with all other insensitive parameters fixed at their nominal values. Among the 179 parameters analysed by GSA, there are about 76 cell culture response parameters that are not active in batch condition and so could not be correctly identified as sensitive or insensitive by the GSA. Any of these parameters having non-zero values are regarded as significant during parameter estimation and their values were refined using dynamic simulations. The values of all 192 model parameters are shown in Table 5.3.

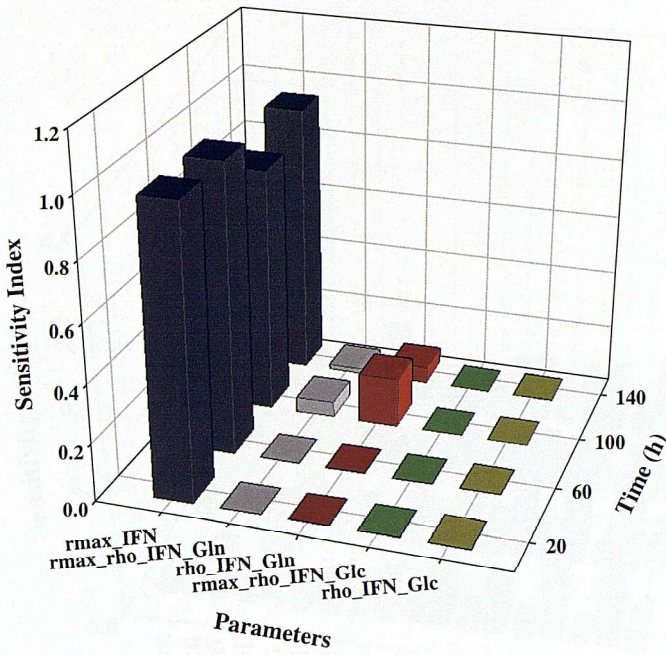


Figure 5.10: Normalised sensitivity index values for individual parameters that are related to the production of IFN γ .

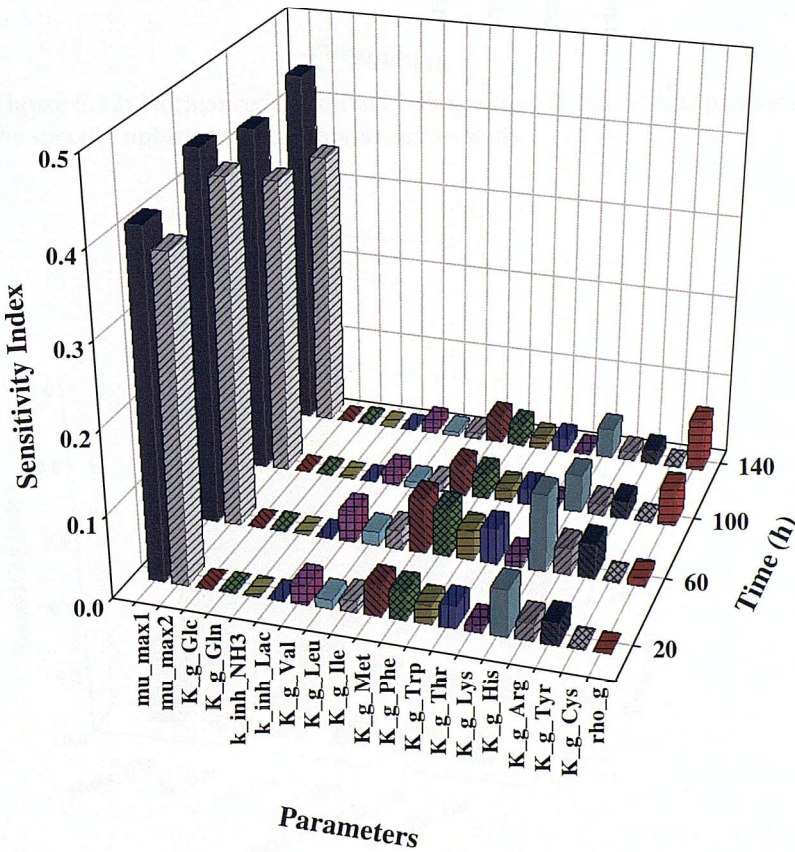


Figure 5.11: Normalised sensitivity index values for individual parameters that are related to the specific growth rate.

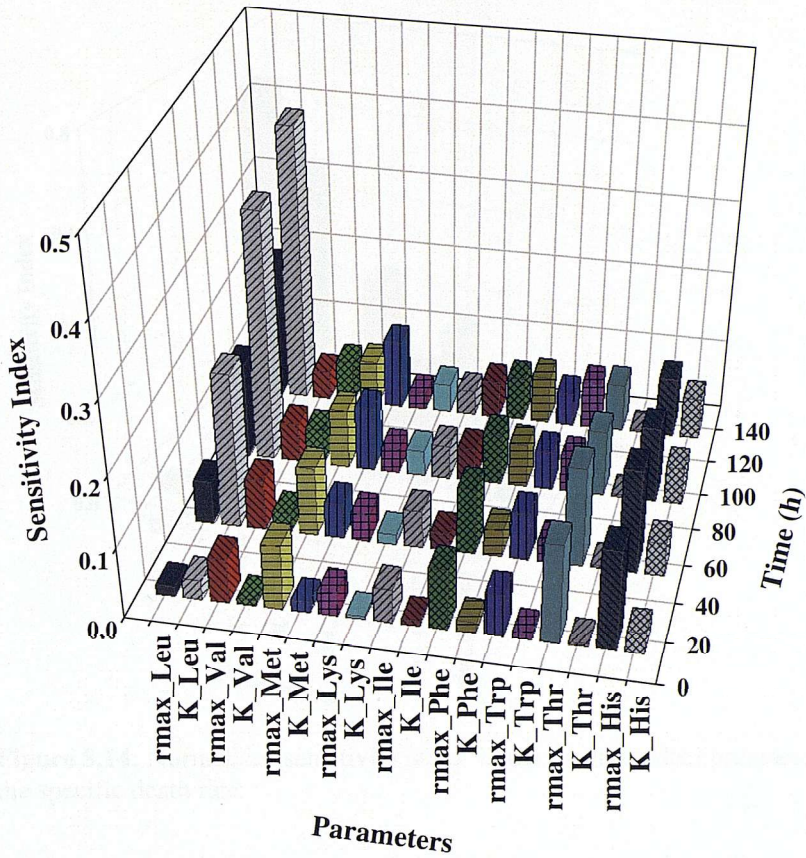


Figure 5.12: Normalised sensitivity index values for individual parameters that are related to the specific uptake rate of essential amino acids.

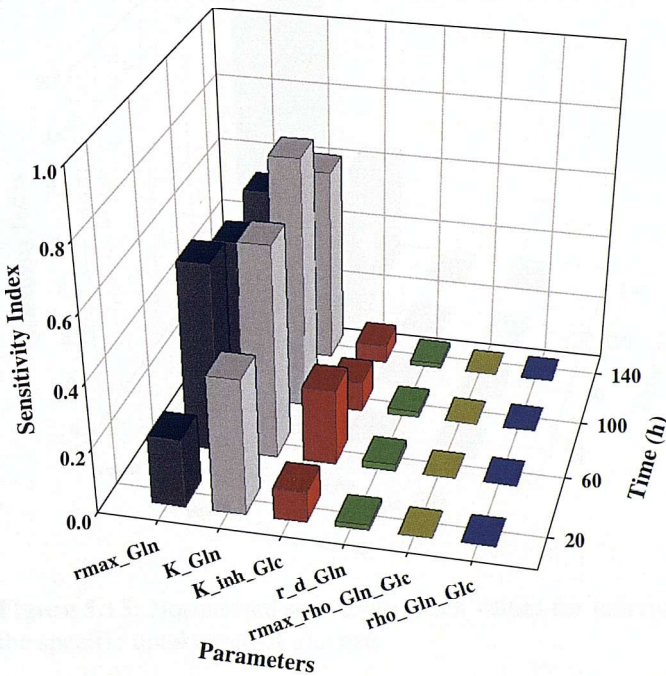


Figure 5.13: Normalised sensitivity index values for individual parameters that are related to the specific uptake rate of glutamine.

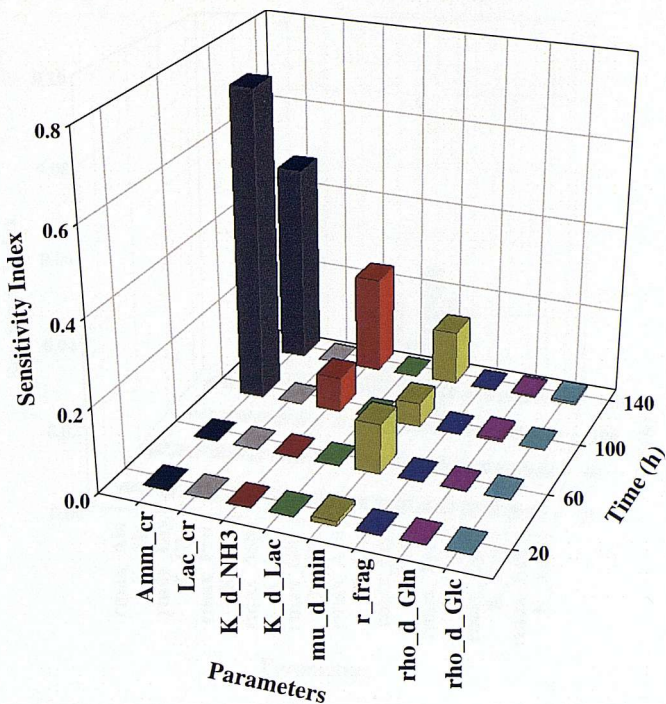


Figure 5.14: Normalised sensitivity index values for individual parameters that are related to the specific death rate.

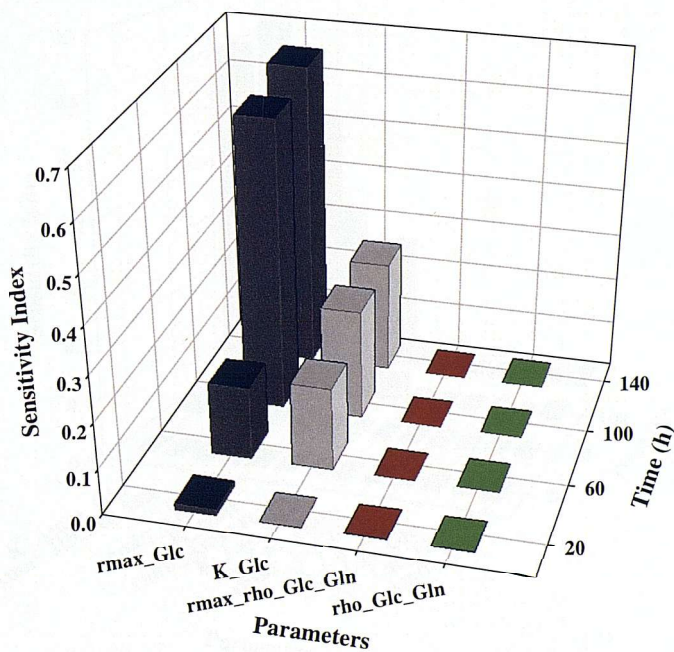


Figure 5.15: Normalised sensitivity index values for individual parameters that are related to the specific uptake rate of glucose.

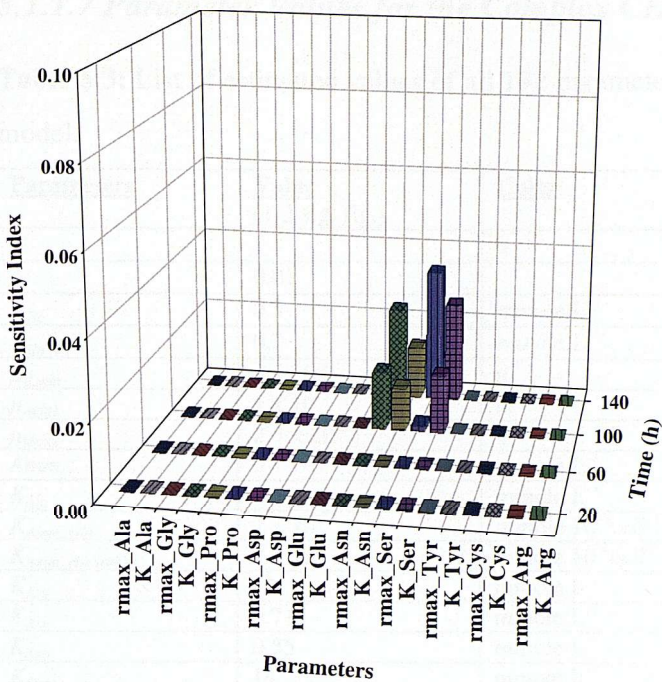


Figure 5.16: Normalised sensitivity index values for individual parameters that are related to the specific uptake rate of non-essential amino acids.

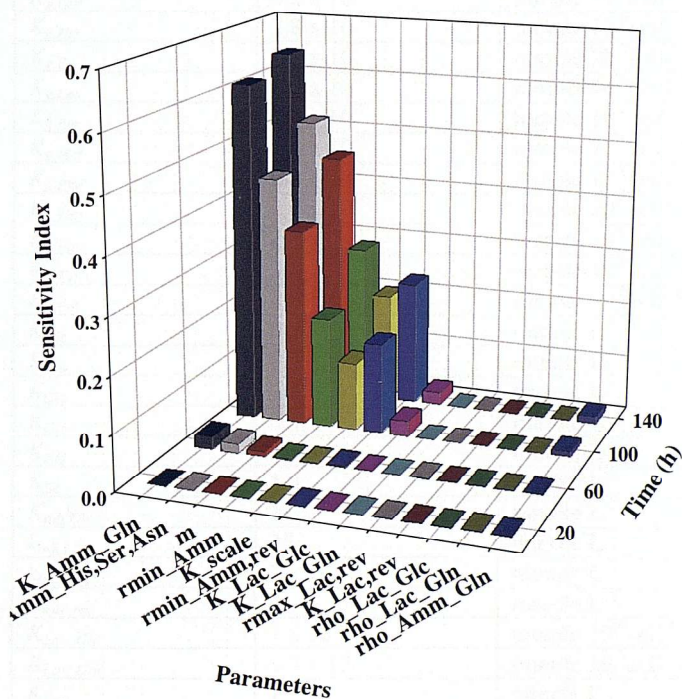


Figure 5.17: Normalised sensitivity index values for individual parameters that are related to the formation of byproducts.

5.1.1.7 Parameter Values for the Complex CHO-IFN γ Model

Table 5.3: List of estimated values of all 192 parameters in the complex CHO-IFN γ model.

<u>Parameters</u>	<u>Value</u> (1-2 sig. fig.)	<u>Units</u>
β	1	h
ε	0.01	-
τ_{Glc}	0.5	mmole L ⁻¹
τ_{Gln}	0.7	mmole L ⁻¹
$\mu_{d,min}$	1×10^{-3}	h ⁻¹
μ_{max1}	1×10^{-2}	h ⁻¹
μ_{max2}	2.5×10^{-2}	h ⁻¹
Amm_{cr}	5	mmole L ⁻¹
K_{Ala}	7	mmole L ⁻¹
K_{Amm_Gln}	2×10^{-4}	mmole 10 ⁻⁶ cell ⁻¹ h ⁻¹
$K_{Amm_HisSerAsn}$	7×10^{-4}	mmole 10 ⁻⁶ cell ⁻¹ h ⁻¹
K_{Arg}	11	mmole L ⁻¹
K_{Asn}	0.71	mmole L ⁻¹
K_{Asp}	0.55	mmole L ⁻¹
K_{Cys}	14	mmole L ⁻¹
$k_{d,Lac}$	42	mmole L ⁻¹
$k_{d,NH3}$	2×10^{-4}	mmole L ⁻¹
$K_{g,Arg}$	3×10^{-9}	mmole 10 ⁻⁶ cell ⁻¹ h ⁻¹
$K_{g,Cys}$	3×10^{-9}	mmole 10 ⁻⁶ cell ⁻¹ h ⁻¹
$K_{g,Glc}$	4.2×10^{-7}	mmole 10 ⁻⁶ cell ⁻¹ h ⁻¹
$K_{g,Gln}$	4.2×10^{-7}	mmole 10 ⁻⁶ cell ⁻¹ h ⁻¹
$K_{g,His}$	2.8×10^{-7}	mmole 10 ⁻⁶ cell ⁻¹ h ⁻¹
$K_{g,Ile}$	2.8×10^{-7}	mmole 10 ⁻⁶ cell ⁻¹ h ⁻¹
$K_{g,Leu}$	2.8×10^{-7}	mmole 10 ⁻⁶ cell ⁻¹ h ⁻¹
$K_{g,Lys}$	2.4×10^{-7}	mmole 10 ⁻⁶ cell ⁻¹ h ⁻¹
$K_{g,Met}$	2.8×10^{-7}	mmole 10 ⁻⁶ cell ⁻¹ h ⁻¹
$K_{g,Phe}$	2.8×10^{-7}	mmole 10 ⁻⁶ cell ⁻¹ h ⁻¹
$K_{g,Thr}$	2.8×10^{-7}	mmole 10 ⁻⁶ cell ⁻¹ h ⁻¹
$K_{g,Trp}$	2.8×10^{-7}	mmole 10 ⁻⁶ cell ⁻¹ h ⁻¹
$K_{g,Tyr}$	3×10^{-9}	mmole 10 ⁻⁶ cell ⁻¹ h ⁻¹
$K_{g,Val}$	2.8×10^{-7}	mmole 10 ⁻⁶ cell ⁻¹ h ⁻¹
K_{Glc}	6.3	mmole L ⁻¹
K_{Gln}	8.5	mmole L ⁻¹
K_{Glu}	2.8	mmole L ⁻¹
K_{Gly}	0.5	mmole L ⁻¹
K_{His}	0.75	mmole L ⁻¹
K_{Ile}	1.2	mmole L ⁻¹
$K_{inh,Glc}$	14	mmole L ⁻¹
$k_{inh,Lac}$	25	mmole L ⁻¹
$k_{inh,NH3}$	2×10^{-3}	mmole L ⁻¹
$K_{Lac,rev}$	2	mmole L ⁻¹
K_{Lac_Glc}	1×10^{-4}	mmole 10 ⁻⁶ cell ⁻¹ h ⁻¹
K_{Lac_Gln}	1.5×10^{-3}	mmole 10 ⁻⁶ cell ⁻¹ h ⁻¹
K_{Leu}	1	mmole L ⁻¹
K_{Lys}	1.1	mmole L ⁻¹
K_{Met}	0.7	mmole L ⁻¹
K_{Phe}	0.9	mmole L ⁻¹
K_{Pro}	7	mmole L ⁻¹
K_{scale}	2×10^{-6}	mmole 10 ⁻⁶ cell ⁻¹ h ⁻¹
K_{Ser}	0.39	mmole L ⁻¹
K_{Thr}	0.077	mmole L ⁻¹
K_{Thy}	0.76	mmole L ⁻¹

K_{Trp}	0.9	mmole L ⁻¹
K_{Val}	0.8	mmole L ⁻¹
Lac_{cr}	20	mmole L ⁻¹
m	3	-
pH	7	-
$q_{Ala,min}$	2×10^{-5}	mmole 10 ⁻⁶ cell ⁻¹ h ⁻¹
$q_{Gly,min}$	2×10^{-5}	mmole 10 ⁻⁶ cell ⁻¹ h ⁻¹
$q_{Pro,min}$	7.8×10^{-5}	mmole 10 ⁻⁶ cell ⁻¹ h ⁻¹
$r_{d,Gln}$	5×10^{-3}	h ⁻¹
r_{frag}	8.4×10^{-3}	h ⁻¹
$rmax_{res,Ala_Glc}$	-1	-
$rmax_{res,Arg_Glc}$	0	-
$rmax_{res,Asn_Glc}$	0	-
$rmax_{res,Asp_Glc}$	0	-
$rmax_{res,Cys_Glc}$	0	-
$rmax_{res,Gln_Glc}$	0	-
$rmax_{res,Glu_Glc}$	0	-
$rmax_{res,Gly_Glc}$	-1	-
$rmax_{res,His_Glc}$	0	-
$rmax_{res,Ile_Glc}$	0	-
$rmax_{res,Leu_Glc}$	0	-
$rmax_{res,Lys_Glc}$	0	-
$rmax_{res,Met_Glc}$	0	-
$rmax_{res,Phe_Glc}$	0	-
$rmax_{res,Pro_Glc}$	-1	-
$rmax_{res,Ser_Glc}$	1	-
$rmax_{res,Thr_Glc}$	0	-
$rmax_{res,Trp_Glc}$	0	-
$rmax_{res,Tyr_Glc}$	0	-
$rmax_{res,Val_Glc}$	0	-
$rmax_{Ala}$	0	mmole 10 ⁻⁶ cell ⁻¹ h ⁻¹
$rmax_{Ala_Glc}$	5×10^{-2}	mmole mmole ⁻¹
$rmax_{Ala_Gln}$	1×10^{-2}	mmole mmole ⁻¹
$rmax_{Amm_Gln}$	2	-
$rmax_{Amm_His,Ser,Asn}$	4	-
$rmax_{Arg}$	4.4×10^{-5}	mmole 10 ⁻⁶ cell ⁻¹ h ⁻¹
$rmax_{Asn}$	2.9×10^{-5}	mmole 10 ⁻⁶ cell ⁻¹ h ⁻¹
$rmax_{Asp}$	7.9×10^{-5}	mmole 10 ⁻⁶ cell ⁻¹ h ⁻¹
$rmax_{Cys}$	2.5×10^{-4}	mmole 10 ⁻⁶ cell ⁻¹ h ⁻¹
$rmax_{Cys_Ser}$	5×10^{-5}	mmole mmole ⁻¹
$rmax_{Glc}$	8×10^{-4}	mmole 10 ⁻⁶ cell ⁻¹ h ⁻¹
$rmax_{Gln}$	9×10^{-4}	mmole 10 ⁻⁶ cell ⁻¹ h ⁻¹
$rmax_{Glu}$	2.1×10^{-4}	mmole 10 ⁻⁶ cell ⁻¹ h ⁻¹
$rmax_{Gly}$	1.1×10^{-4}	mmole 10 ⁻⁶ cell ⁻¹ h ⁻¹
$rmax_{Gly_Ser}$	2×10^{-1}	mmole mmole ⁻¹
$rmax_{His}$	2.5×10^{-5}	mmole 10 ⁻⁶ cell ⁻¹ h ⁻¹
$rmax_{IFN\gamma}$	1.5×10^{-5}	mg 10 ⁻⁶ cell ⁻¹ h ⁻¹
$rmax_{Ile}$	3.5×10^{-5}	mmole 10 ⁻⁶ cell ⁻¹ h ⁻¹
$rmax_{Lac,rev}$	5.4×10^{-5}	mmole 10 ⁻⁶ cell ⁻¹ h ⁻¹
$rmax_{Lac_Glc}$	2	-
$rmax_{Lac_Gln}$	1	-
$rmax_{Leu}$	4×10^{-5}	mmole 10 ⁻⁶ cell ⁻¹ h ⁻¹
$rmax_{Lys}$	3.2×10^{-5}	mmole 10 ⁻⁶ cell ⁻¹ h ⁻¹
$rmax_{Met}$	2.1×10^{-5}	mmole 10 ⁻⁶ cell ⁻¹ h ⁻¹
$rmax_{Phe}$	2.1×10^{-5}	mmole 10 ⁻⁶ cell ⁻¹ h ⁻¹
$rmax_{Pro}$	1.6×10^{-3}	mmole 10 ⁻⁶ cell ⁻¹ h ⁻¹
$rmax_{Pro_Arg}$	4×10^{-1}	mmole mmole ⁻¹
$rmax_{Pro_Glu}$	4×10^{-1}	mmole mmole ⁻¹
$rmax_{res,Ala_Gln}$	-1	-
$rmax_{res,Arg_Gln}$	0	-

r_{res,Asn_Gln}	0	-
r_{res,Asp_Gln}	0	-
r_{res,Cys_Gln}	-1	-
$r_{res,Glc}$	1	h^{-1}
r_{res,Glc_Gln}	0	-
$r_{res,Gln}$	1	h^{-1}
r_{res,Glu_Gln}	1	-
r_{res,Gly_Gln}	-1	-
r_{res,His_Gln}	-1	-
r_{res,IFN_Glc}	-1	-
r_{res,IFN_Gln}	9	-
r_{res,Ile_Gln}	-1	-
r_{res,Leu_Gln}	-1	-
r_{res,Lys_Gln}	-1	-
r_{res,Met_Gln}	-1	-
r_{res,Phe_Gln}	-1	-
r_{res,Pro_Gln}	-1	-
r_{res,Ser_Gln}	-1	-
r_{res,Thr_Gln}	-1	-
r_{res,Trp_Gln}	-1 (as Phe)	-
r_{res,Tyr_Gln}	-1	-
r_{res,Val_Gln}	-1	-
$r_{res,Ser}$	2×10^{-5}	$mmole\ 10^{-6}cell^{-1}\ h^{-1}$
$r_{res,Thr}$	2×10^{-5}	$mmole\ 10^{-6}cell^{-1}\ h^{-1}$
$r_{res,Trp}$	2.1×10^{-5}	$mmole\ 10^{-6}cell^{-1}\ h^{-1}$
$r_{res,Tyr}$	2×10^{-5}	$mmole\ 10^{-6}cell^{-1}\ h^{-1}$
r_{res,Tyr_Phe}	2×10^{-1}	$mmole\ mmole^{-1}$
$r_{res,Val}$	3×10^{-5}	$mmole\ 10^{-6}cell^{-1}\ h^{-1}$
$r_{min,Amm}$	1.1×10^{-5}	$mmole\ 10^{-6}cell^{-1}\ h^{-1}$
$r_{min,Amm,rev}$	2×10^{-8}	$mmole^{(1-m)}\ L^m\ 10^{-6}cell^{-1}\ h^{-1}$
$x_{res,Glc}$	1.2	h^{-1}
$x_{res,Gln}$	1.2	h^{-1}
ρ_{Ala_Glc}	0.1	-
ρ_{Ala_Gln}	0.1	-
ρ_{Amm_Gln}	1	-
ρ_{Arg_Glc}	1	-
ρ_{Arg_Gln}	1	-
ρ_{Asn_Glc}	1	-
ρ_{Asn_Gln}	1	-
ρ_{Asp_Glc}	1	-
ρ_{Asp_Gln}	1	-
ρ_{Cys_Glc}	1	-
ρ_{Cys_Gln}	0.01	-
$\rho_{d,Glc}$	2	-
$\rho_{d,Gln}$	5×10^{-2}	-
ρ_g	7×10^{-2}	-
ρ_{Glc_Gln}	1	-
ρ_{Gln_Glc}	1	-
ρ_{Glu_Glc}	1	-
ρ_{Glu_Gln}	1	-
ρ_{Gly_Glc}	1	-
ρ_{Gly_Gln}	0.1	-
ρ_{His_Glc}	1	-
ρ_{His_Gln}	0.05	-
ρ_{IFN_Glc}	0.03	-
ρ_{IFN_Gln}	1	-
ρ_{Ile_Glc}	1	-
ρ_{Ile_Gln}	0.1	-

ρ_{Lac_Glc}	30	-
ρ_{Lac_Gln}	40	-
ρ_{Leu_Glc}	1	-
ρ_{Leu_Gln}	0.1	-
ρ_{Lys_Glc}	1	-
ρ_{Lys_Gln}	0.1	-
ρ_{Met_Glc}	1	-
ρ_{Met_Gln}	0.05	-
ρ_{Phe_Glc}	1	-
ρ_{Phe_Gln}	0.1	-
ρ_{Pro_Glc}	1	-
ρ_{Pro_Gln}	0.5	-
ρ_{Ser_Glc}	0.01	-
ρ_{Ser_Gln}	0.01	-
ρ_{Thr_Glc}	1	-
ρ_{Thr_Gln}	0.05	-
ρ_{Trp_Glc}	1	-
ρ_{Trp_Gln}	1	-
ρ_{Tyr_Glc}	1	-
ρ_{Tyr_Gln}	0.01	-
ρ_{Val_Glc}	1	-
ρ_{Val_Gln}	0.5	-

Table 5.4: List of degrees of freedom in the CHO-IFN γ cell cultures.

Degrees of Freedom	Value (2 sig. fig.)	Units
Glc_{in}	500	mmole L ⁻¹
Glc'_{in}	220 (40g/L)	mmole L ⁻¹
Gln_{in}	100	mmole L ⁻¹
Val_{in} (valine)	4.5	mmole L ⁻¹
Leu_{in} (leucine)	4.5	mmole L ⁻¹
Ile_{in} (isoleucine)	4.2	mmole L ⁻¹
Met_{in} (methionine)	2.3	mmole L ⁻¹
Phe_{in} (phenylalanine)	2.2	mmole L ⁻¹
Trp_{in} (tryptophan)	0.44	mmole L ⁻¹
Thr_{in} (threonine)	4.5	mmole L ⁻¹
Lys_{in} (lysine)	5.0	mmole L ⁻¹
His_{in} (histidine)	1.5	mmole L ⁻¹
Ala_{in} (alanine)	0.5	mmole L ⁻¹
Gly_{in} (glycine)	2.5	mmole L ⁻¹
Pro_{in} (proline)	1.5	mmole L ⁻¹
Asp_{in} (aspartic acid)	2	mmole L ⁻¹
Glu_{in} (glutamic acid)	1	mmole L ⁻¹
Asn_{in} (asparagine)	2	mmole L ⁻¹
Ser_{in} (serine)	5	mmole L ⁻¹
Tyr_{in} (tyrosine)	2.1	mmole L ⁻¹
Cys_{in} (cysteine)	2	mmole L ⁻¹
Arg_{in} (arginine)	7.0	mmole L ⁻¹
$F_{in}(t)$	varying	L h ⁻¹
$F_{in_etc}(t)$	varying	L h ⁻¹

5.3 R-Square Analysis of Model Performance

5.3.1 Analysis of Experiment Data

In this section, the performance of the complex CHO-IFN γ model is analysed for batch and fed-batch cultures where the nutrient supplementation time-profiles are available. The quality of model predictions is partly quantified using R-square:

$$R^2 = 1 - \frac{\sum (x_{sim} - x)^2}{\sum (x - \bar{x})^2} \quad (5.1)$$

where x_{sim} : simulated value from model

x : data from experiment

\bar{x} : mean value of x

However, when the value of x is controlled at constant levels that $\sum (x - \bar{x})^2$ tends to zero or the measurement error, θ_{err} , of x is comparable with $(x - \bar{x})^2$, the standard R-square analysis may fail to reflect the closeness of model prediction. This is the case for many measured variables in the fed-batch cultures. Therefore, a modified R-square equation (R_{mod}^2) is developed as follow:

$$R_{mod}^2 = 1 - \frac{\sum_{\forall |x_{sim} - x| > \theta_{err}} (x_{sim} - x)^2}{\sum (x - \bar{x})^2} \quad (5.2)$$

where the condition $\forall |x_{sim} - x| > \theta_{err}$ would reject any $|x_{sim} - x|$ term if it is less than θ_{err} .

For the cases that R_{mod}^2 is used instead of R^2 , the percentage of data points lying within a narrow range of simulation results would be used to identify variables that remain nearly constant throughout the cell culture time.

Estimation of θ_{err}

The measurement error for amino acids was estimated from the glutamine data which were analysed by both biochemical analyser and HPLC (Wong et al., 2005). The average value of θ_{err} for glutamine for fed-batch cultures was 0.05mM (Appendix 6).

This was assumed to be the measurement error for all other amino acids in fed-batch cultures. The measurement error for glucose is assumed to be 0.1mM because the variation of glucose concentration in fed-batch cultures was larger than that of amino acids.

Identification of Outlying Initial Amino Acid Concentrations in Fed-Batch Data

Some of the measured values of initial concentration of amino acids in fed-batch cultures were found to be problematic when subjected to mass balance analysis. Test simulations were done with the specific growth rate set to 0 and viable cell concentration set to 0^+ (X_v cannot be exactly zero as it is the denominator of many specific consumption quantities in the model). As the virtual system was set not to consume amino acids, those amino acids that the cell *cannot* produce (Table 4.1) must show a higher concentration than the real experiment data. Any initial concentrations that violate this, or when the first experimental measurement was significantly lower than subsequent measurements to an extent that cannot be compensated by production of non-essential amino acids by the cells, were classified as inaccurate and were assigned new postulated values with the help of simulations of the real system. Those inaccurate initial amino acid concentrations are highlighted in Appendix 6.

Remarks for Simulation Diagrams

Simulation results of all the 27 variables in the CHO-IFN γ batch and fed-batch cell cultures are shown in Figure 5.18a – 5.24e. The uncertainties of batch data are based on Wong et al. (2005). Fed-batch duplicate experiments are treated individually because the nutrient supplementation time-profiles were *not* identical despite the set-points of the feedback controllers were the same. Thus, uncertainties of the fed-batch data are not depicted in the corresponding diagrams.

5.3.2 Model Performance

A list of R-square and modified-R-square values for all 26 measured variables is shown in Table 5.5. The simulation performance in CHO-IFN γ batch culture is compared against six sets of fed-batch cultures with the glutamine and/or glucose feedback controller being set at five different values. For the ease of reference to each of the six fed-batch cultures, the following notations are used in this section:

- ‘0.1mM Fed-batch’ refers to the low-glutamine fed-batch culture with glutamine feedback controller set-point at 0.1mM.
- ‘1st 0.3mM Fed-batch’ refers to the 1st duplicate experiment of the low-glutamine fed-batch culture with glutamine feedback controller set-point at 0.3mM.
- ‘2nd 0.3mM Fed-batch’ refers to the 2nd duplicate experiment of the low-glutamine fed-batch culture with glutamine feedback controller set-point at 0.3mM.
- ‘0.5mM Fed-batch’ refers to the low-glutamine fed-batch culture with glutamine feedback controller set-point at 0.5mM.
- ‘0.3,0.7mM Fed-batch’ refers to the low-glutamine and low-glucose fed-batch culture with glutamine feedback controller set-point at 0.3mM and glucose feedback controller set-point at 0.7mM.
- ‘0.3,0.35mM Fed-batch’ refers to the low-glutamine and low-glucose fed-batch culture with glutamine feedback controller set-point at 0.3mM and glucose feedback controller set-point at 0.35mM.

It should be noted that the concentration of the controlled variables in the fed-batch cultures may not stay constant at the set-point values throughout the cell culture. The concentration of tryptophan was not able to be measured in the CHO-IFN γ cell culture experiment but the simulation results of tryptophan concentration would be discussed towards the end of this section.

Table 5.5: Summary of R-square and modified-R-square values for batch and fed-batch CHO-IFN γ cell cultures. (Refer to p.175 for notations of fed-batch cultures)

	Batch	0.1mM Fed-batch		1 st 0.3mM Fed-batch		2 nd 0.3mM Fed-batch		0.5mM Fed-batch		0.3,0.7mM Fed-batch		0.3,0.35mM Fed-batch	
	R ²	R ² or R ² _{mod}	% in ± 0.2 mM	R ² or R ² _{mod}	% in ± 0.2 mM	R ² or R ² _{mod}	% in ± 0.2 mM	R ² or R ² _{mod}	% in ± 0.2 mM	R ² or R ² _{mod}	% in ± 0.2 mM	R ² or R ² _{mod}	% in ± 0.2 mM
IFN γ	0.94	0.85	/	0.87	/	0.98	/	0.87	/	0.78	/	0.84	/
Viable cell	0.95	0.70	/	0.52	/	0.87	/	0.81	/	0.66	/	0.54	/
Total cell	0.98	0.46	/	0.93	/	0.98	/	0.94	/	0.92	/	0.95	/
Dead cell	0.80	-1.04	/	0.66	/	-0.07	/	-0.03	/	0.11	/	0.13	/
Glutamine	0.99	-1.36	55%	0.24	82%	-4.86	57%	-1.54	67%	-1.43	57%	-0.18	83%
Glucose	0.98	-0.64	8%	-0.75	56%	-1.07	71%	-0.16	60%	0.66	73%	0.83	73%
Ammonium	0.92	0.65	/	0.54	/	0.42	/	-0.48	/	0.07	/	0.62	/
Lactate	0.93	-21.0	/	0.41	/	-0.54	/	0.70	/	0.64	/	0.85	/
Isoleucine	0.24	0.87	92%	-0.27	88%	-0.39	100%	0.93	93%	0.92	93%	0.89	67%
Leucine	0.39	0.93	82%	0.15	88%	0.90	100%	0.95	87%	0.94	86%	0.83	50%
Methionine	0.56	0.91	100%	0.99	100%	-0.51	69%	0.60	100%	0.89	100%	0.89	100%
Valine	0.42	-3.90	18%	-0.48	88%	0.03	100%	-1.69	36%	0.46	92%	0.79	92%
Phenylalanine	0.24	-0.46	91%	-0.38	88%	0.11	100%	0.80	100%	0.33	93%	0.98	100%
Threonine	0.79	-16.0	55%	-1.09	73%	-0.74	79%	-2.53	50%	-2.10	62%	-1.56	73%
Lysine	-0.12	0.78	82%	-0.73	75%	-1.71	85%	0.83	80%	0.51	29%	0.88	67%
Histidine	0.29	-2.57	91%	-0.20	100%	1.00	100%	0.39	100%	-1.34	79%	0.97	100%
Arginine	-0.18	-10.7	17%	-11.8	27%	-30.1	69%	-6.40	29%	-10.0	50%	-17.0	42%
Tyrosine	0.10	0.43	91%	0.21	75%	0.62	100%	0.20	67%	0.42	38%	0.31	18%
Cysteine	0.47	0.89	73%	0.37	n/a	0.91	100%	0.55	36%	0.23	62%	n/a	n/a
Alanine	0.44	0.74	25%	0.93	53%	0.85	29%	0.70	33%	0.43	21%	-0.92	17%
Aspartic acid	0.99	1.00	100%	1.00	100%	1.00	100%	1.00	100%	0.90	100%	0.84	100%
Glutamic acid	0.44	0.96	100%	0.34	93%	0.92	100%	0.85	93%	0.99	100%	1.00	100%
Asparagine	0.65	0.95	100%	0.52	93%	0.77	100%	1.00	100%	0.85	93%	0.80	92%
Serine	-0.60	-29.9	55%	0.21	93%	0.96	100%	0.33	67%	-0.27	64%	-4.61	17%
Glycine	0.49	0.63	50%	-4.65	18%	-4.19	21%	-0.50	60%	0.54	36%	0.89	50%
Proline	-0.12	0.44	42%	0.31	29%	0.52	29%	-0.40	27%	0.37	21%	-3.78	17%

Remark:

- (1) n/a: data not available or incomplete data for the corresponding analysis.
- (2) *: for glucose, ‘% in ± 1 mM’ was analysed instead of 0.2mM due to larger fluctuations in glucose concentration compared to amino acids.
- (3) R² (or R²_{mod}) values < 0.40 and ‘% in ± 0.2 mM’ (or ± 1 mM for glucose) values < 50% are underlined.

IFN γ and Cell Concentrations

The model predictions of IFN γ concentration in batch and fed-batch cultures are shown in Figure 5.18a – 5.24a. The R-square values range from 0.78 to 0.98, indicating that the simulation is generally in good agreement with experiment data.

The cell concentrations are also shown in Figure 5.18a – 5.24a. The total cell concentrations (X_t) are closely predicted with R-square > 0.9 in batch and most fed-batch cultures except in '0.1mM Fed-batch' culture where X_t was over-predicted towards the end of the cell culture time with an R-square value of 0.46 (Figure 5.19a). The R-squares for viable cell concentration (X_v) vary between 0.52 and 0.95. The values of X_v in some fed-batch cultures are over-predicted near the end and are more significant in '1st 0.3mM Fed-batch' and '0.3,0.35mM Fed-batch' cultures where the R-square values are 0.52 and 0.54 respectively. Deviations in X_t and X_v are reflected in the dead cell concentration (X_d) which has R-square values of 0.80 and 0.66 in batch and '1st 0.3mM Fed-batch' cultures respectively but the R-square values for X_d are -1.04 – 0.13 in other fed-batch cultures.

Glutamine

The glutamine concentration is well simulated in batch culture with R-square equals to 0.99 (Figure 5.18a). The modified-R-square values for glutamine in fed-batch cultures range from -4.86 to 0.24 with 55 – 83% of data lying within ± 0.2 mM of the simulation (Figure 5.19a – 5.24a). Most of the deviations in fed-batch cultures take place near the end of the cell culture time when the glutamine levels increased beyond the set-point values. Only in '0.1mM Fed-batch' culture there is significant underestimation in specific glutamine consumption in the early culture time leading to significant over-prediction of glutamine concentration during the first 50 h (Figure 5.19a).

Glucose

Glucose concentration is closely simulated in batch culture with R-square equals to 0.98 (Figure 5.18a). In fed-batch cultures, most of the modified-R-square values are in between -0.75 – 0.83 with 56 – 73% data lying within ± 1 mM of the simulation (Figure 5.20a – 5.24a). There are major deviations during about 30 – 100 h of the ‘1st 0.3mM Fed-batch’ and ‘2nd 0.3mM Fed-batch’ cultures where glucose concentration was over-predicted by about 2mM but model predictions during subsequent cell culture time are in agreement with experiment data (Figure 5.20a & 5.21a). In the ‘0.1mM Fed-batch’ culture, significant over-prediction of glucose level occurred at 20 – 90 h, giving a modified-R-square value of -0.64 with only 8% of data lying within ± 1 mM of the simulation (Figure 5.19a). Such over-predictions in the model might be caused by the assumption that the byproduct inhibition constants for the specific consumption rate of all nutrients are the same (Section 4.2.1.2: Equation M6). It may be necessary to assign separate byproduct inhibition constants for glucose consumption. But a larger set of model parameters with the same small number of measured variables would further increase the amount of multiple solutions that could match the experiment data.

Ammonium

The R-square value for ammonium is 0.92 in batch culture (Figure 5.18b) and 0.42 – 0.65 in most fed-batch cultures (Figure 5.19b – 5.21b & 5.24b), except being -0.48 and 0.07 in ‘0.5mM Fed-batch’ and ‘0.3,0.7mM Fed-batch’ cultures respectively (Figure 5.22b & 5.23b). The initial accumulation rate of ammonium in all fed-batch cultures appeared to be higher than the model predictions (Figure 5.19b – 5.24b). The subsequent trend of ammonium time-profiles in ‘0.1mM Fed-batch’, ‘2nd 0.3mM Fed-batch’, and ‘0.3,0.35mM Fed-batch’ cultures are correctly followed by the model (Figure 5.19b, 5.21b, 5.24b). But the ammonium concentration in ‘1st 0.3mM Fed-batch’, ‘0.5mM Fed-batch’, and ‘0.3,0.7mM Fed-batch’ cultures showed a decreasing trend after mid-culture time and then gradually increased again near the end of the cell cultures (Figure 5.20b, 5.22b, 5.23b).

Only the initial under-prediction of ammonium accumulation in ‘0.1mM Fed-batch’ culture (Figure 5.9b) could be explained by the deviation in the corresponding

initial glutamine concentration (Figure 5.19a). The simulations of glutamine concentration in all other fed-batched cultures are mostly within ± 0.2 mM of the experimental measurement until the late exponential growth phase (Figure 5.19a – 5.24a). It is suspected that spontaneous degradation of glutamine in the medium before it was used for the fed-batch cultures might have caused the actual initial ammonium concentration to be higher than the measured values. The unexpected decrease of ammonium concentration in some of the fed-batch cultures cannot be explained by any known mechanism in the literature. In general, the model is able to capture the increase in ammonium concentration in batch and fed-batch cultures, though there are certain detailed dynamics of ammonium production revealed in some of the fed-batch cultures (transient decrease in ammonium concentration) that would require further knowledge to understand the underlying mechanisms.

Lactate

Lactate concentration is well predicted in the batch culture with R-square value equals to 0.93 (Figure 5.18b). The R-square values in most fed-batch cultures are 0.41 – 0.85 (Figure 5.20b & 5.22b – 5.24b) but are -0.54 and -21.0 in ‘2nd 0.3mM Fed-batch’ and ‘0.1mM Fed-batch’ cultures respectively (Figure 5.19b & 5.21b) which are caused by deviations in glucose prediction in the corresponding exponential growth phase. The reduction in lactate concentration in the glucose-controlled fed-batch cultures are well simulated by the model in Figure 5.23b and 5.24b. The over-prediction of lactate concentration in certain fed-batch cultures did not have significant effect on cell growth or IFN γ productivity since lactate is much less toxic than ammonium to the cells.

Isoleucine

Isoleucine appeared to be over-predicted between 20 – 70 h in the batch culture, giving an R-square value of 0.24 in batch (Figure 5.18b). The modified-R-square values in most fed-batch cultures are 0.87 – 0.93 with 67 – 93% data lying within ± 0.2 mM of the simulation (Figure 5.19b & 5.22b – 5.24b). Although the modified-R-squares in ‘1st 0.3mM Fed-batch’ and ‘2nd 0.3mM Fed-batch’ are -0.27 and -0.39 respectively, 88 – 100% data are lying within ± 0.2 mM of the simulation which indicates most of the

experiment data in those culture do not show much variation with respect to time (Figure 5.20b – 5.21b).

Leucine

The model performance for leucine is similar to isoleucine that the R-square in batch culture is 0.39 with over-prediction by 0.5 – 1 mM during mid-culture time (Figure 5.18b). The modified-R-squares are 0.83 – 0.95 in most fed-batch cultures with 50 – 100% data lying within ± 0.2 mM of the simulation (Figure 5.19b & 5.21b – 5.24b). The modified-R-square of the '1st 0.3mM Fed-batch' culture is 0.15 but 88% of data are lying within ± 0.2 mM of the simulation (Figure 5.20b).

Methionine

The R-square for methionine in batch culture is 0.56 (Figure 5.18b). The modified-R-squares in most fed-batch cultures are 0.60 – 0.99 with 100% of data within ± 0.2 mM of the simulation (Figure 5.19b, 5.20b & 5.22b – 5.24b) except in '2nd 0.3mM Fed-batch' culture where the methionine level was under-predicted by up to 0.4mM after mid-culture time, causing the modified-R-square to drop to -0.51 in 69% data lying within ± 0.2 mM of the simulation (Figure 5.21b).

Valine

Valine has an R-square value of 0.42 in batch culture (Figure 5.18b). In most fed-batch cultures, the modified-R-square values are -0.48 – 0.79 with most data (88 – 100%) lying within ± 0.2 mM of the simulation (Figure 5.20b, 5.21b, 5.23b, 5.24b). But in '0.1mM Fed-batch' and '0.5mM Fed-batch', valine concentrations are under-predicted during most of the cell-culture time by up to ~ 0.3 mM (Figure 5.19b, 5.22b). It is not certain why such fluctuation in model performance occurs in the case of valine.

Phenylalanine

The R-square value for phenylalanine in batch culture is 0.24 due to over-prediction of up to 0.5mM during mid culture time (Figure 5.18c). The phenylalanine levels in fed-batch cultures are closely predicted until the death phase where the measured concentrations become higher than the simulation (Figure 5.19c – 5.24c). The modified R-square values for all fed-batch cultures are -0.46 – 0.98 with most of the data (88 – 100%) lying within $\pm 0.2\text{mM}$ of the simulation (Figure 5.19c – 5.24c).

Threonine

The R-square value for threonine in batch culture is 0.79 (Figure 5.18c). Only three fed-batch cultures have high percentage of data lying close to the simulation: the modified-R-squares are -1.56 – -0.74 in '1st 0.3mM Fed-batch', '2nd 0.3mM Fed-batch', and '0.3,0.35mM Fed-batch' cultures with 73 – 79% data within $\pm 0.2\text{mM}$ of the simulation (Figure 5.20c, 5.21c, 5.24c). In the '0.1mM Fed-batch' culture, 55% of data are within $\pm 0.2\text{mM}$ of the simulation and the modified-R-square value is -16.0 (Figure 5.19c). In '0.5mM Fed-batch' and '0.3,0.7mM Fed-batch' cultures, the modified-R-squares are -2.53 and -2.10 respectively with 50 – 62% data within $\pm 0.2\text{mM}$ of the simulation (Figure 5.5.22c & 5.23c). Threonine concentrations are significantly under-predicted during the death phase of all fed-batch cultures, suggesting its maintenance consumption might be insignificant relative to other nutrients.

Lysine

The lysine concentration in batch culture was over-predicted in batch culture by up to about 1mM, causing the R-square value to be -0.12 (Figure 5.18c). The lysine concentration in the experimental measurement decreased rapidly during the first 50 h and then fluctuated around 1mM until the end of cell culture time. It is doubtful that lysine, being one of the essential amino acids for cell growth (Table 4.1), showed no significant consumption during the exponential growth phase at 50 – 90 h. This also occurs to the experimental data of isoleucine, valine, phenylalanine, and histidine.

In fed-batch cultures, most of the modified-R-squares are $-1.71 - 0.88$ with $67 - 85\%$ of data lying within $\pm 0.2\text{mM}$ of the simulation (Figure 5.19c – 5.22c & 5.24c) except in ‘0.3,0.7mM Fed-batch’ culture where the modified-R-square is 0.51 with 29% of data lying within $\pm 0.2\text{mM}$ of the simulation (Figure 5.23c).

Histidine

The R-square value for histidine in batch culture is 0.29 (Figure 5.18c). The modified-R-squares for all fed-batch cultures are between $-2.57 - 1.00$ with $79 - 100\%$ of data lying within $\pm 0.2\text{mM}$ of the simulation (Figure 5.19c – 5.24c). There are under-predictions in concentration of histidine in ‘0.1mM Fed-batch’, ‘1st 0.3mM Fed-batch’, and ‘0.5mM Fed-batch’ cultures in the death phase by up to 1mM (Figure 5.19c, 5.20c, 5.22c); and in ‘0.3,0.7mM Fed-batch’ culture in the death phase by up to 0.2mM (Figure 5.23c). But in ‘2nd 0.3mM Fed-batch’ the histidine level was well simulated throughout the cell culture (Figure 5.21c) and there is no significant deviation in the ‘0.3,0.35mM Fed-batch’ culture (Figure 5.24c). Thus, it is inconclusive regarding the maintenance consumption of glutamine.

Arginine

The wave-like trend of arginine in batch culture is not able to be captured by the model, resulting in an R-square value of -0.18 (Figure 5.18c). Arginine is one of the non-essential amino acids that can be produced from several other amino acids (Figure 4.10). The modified-R-square values in fed-batch cultures are all negative in the range of $-30.1 - -6.4$ with only $17 - 69\%$ of data lying within $\pm 0.2\text{mM}$ of the simulation (Figure 5.19c – 5.24c). There are under-predictions in arginine concentration in the death phase of fed-batch cultures by up to $\sim 1\text{mM}$, suggesting that the maintenance consumption of arginine might be negligible. Arginine is also a growth-stimulating amino acid (together with tyrosine and cysteine) that its absence would cause specific growth rate to drop significantly (Table 4.1). Although there are deviations in the predicted arginine levels in the death phase, the predicted values remain positive in all batch and fed-batch cultures. Thus, the effect of such deviations on cell growth prediction should be insignificant.

Tyrosine

The R-square value of tyrosine in batch culture is 0.10 due to overprediction by up to 0.5mM during mid-culture time (Figure 5.18c). Half of the fed-batch cultures are well simulated with 75 – 100% of data lying within ± 0.2 mM of the simulation and modified-R-square values being 0.21 – 0.62 in ‘0.1mM Fed-batch’, ‘1st 0.3mM Fed-batch’, and ‘2nd 0.3mM Fed-batch’ cultures (Figure 5.19c – 5.21c). But in ‘0.5mM Fed-batch’, ‘0.3,0.7mM Fed-batch’, and ‘0.3,0.35mM Fed-batch’ cultures, only 18 – 67% of data are within ± 0.2 mM of the simulation (Figure 5.22c – 5.24c). The modified-R-square values of these three fed-batch cultures are 0.20 – 0.42 due to over-predictions by up to ~ 0.5 mM during mid-culture time or towards the end of the cell culture.

Cysteine

The R-square value for cysteine in batch culture is 0.47 (Figure 5.18d). In the fed-batch cultures, 2 out of 6 data sets are incomplete (Figure 5.20d & 5.24d). Among the complete fed-batch data, the ‘0.1mM Fed-batch’ and ‘2nd 0.3mM Fed-batch’ are closely simulated with modified-R-squares being 0.89 and 0.91 respectively with 73% and 100% of data lying within ± 0.2 mM of the simulation (Figure 5.19d & 5.21d). The modified-R-squares of ‘0.5mM Fed-batch’ and ‘0.3,0.7mM Fed-batch’ cultures are lower (0.55 and 0.23 respectively) with only 36% - 62% of data lying within ± 0.2 mM of the simulation due to over-predictions by up to ~ 0.5 mM (Figure 5.22d – 5.23d).

Alanine

Alanine is one of the amino acids being actively produced by the CHO-IFN γ cells. Its R-square value in batch culture is 0.44 due to over-prediction during mid-culture time by up to ~1.5mM and under-prediction near the end of the cell culture by up to ~2mM (Figure 5.18d). The modified-R-square values for most fed-batch cultures are in the high range of 0.7 – 0.93 though only 25 – 53% of data are within ± 0.2 mM of the simulation (Figure 5.19d – 5.22d). The modified-R-squares in ‘0.3,0.7mM Fed-batch’ and ‘0.3,0.35mM Fed-batch’ cultures are in the low range of 0.43 and -0.92 respectively with only 21% and 17% data lying within ± 0.2 mM of the simulation (Figure 5.23d & 5.24d). However, the major variation in the patterns of alanine in various fed-batch cultures is already captured by the model.

Aspartic acid

The aspartic acid concentration is very well simulated in all batch and fed-batch cultures. The R-square value for batch culture is 0.99 and the modified-R-squares for fed-batch cultures are 0.84 – 1.00 with 100% of data lying within ± 0.2 mM of the simulation (Figure 5.18d – 5.24d). The consumption pattern of aspartic acid appeared to be very stable in batch and fed-batch conditions.

Glutamic acid

The R-square value for glutamic acid in batch culture is 0.44 due to the time-profile being very close to zero throughout the cell culture (Figure 5.18d). The glutamic acid levels in fed-batch cultures are well simulated with 93 – 100% of data lying within ± 0.2 mM of the simulation and modified-R-square values of 0.34 – 1.00 (Figure 5.19d – 5.24d). The pattern of glutamic acid consumption for CHO-IFN γ cells is very similar to aspartic acid.

Asparagine

The R-square value for asparagine in batch culture is 0.65 due to over-prediction during mid-culture time by up to ~0.5mM (Figure 5.18d). In the fed-batch cultures, 92 – 100% of data are within ± 0.2 mM of the simulation and the modified-R-square values are in between 0.52 – 1.00 (Figure 5.19d – 5.24d). There are under-predictions in asparagine concentration in the death phase of most fed-batch culture by up to ~0.1mM.

Serine

Serine has an R-square value of -0.60 in batch culture due to over-prediction during mid-culture time by up to ~1mM and under-prediction near the end of the cell culture by up to ~1mM (Figure 5.18d). The levels of serine in '1st 0.3mM Fed-batch' and '2nd 0.3mM Fed-batch' cultures are well simulated with 93% and 100% of data respectively within ± 0.2 mM of the simulation and modified-R-square values of 0.21 and 0.96 respectively (Figure 5.20d & 5.21d). But in '0.1mM Fed-batch' culture, only 55% of data are within ± 0.2 mM of the simulation and the modified-R-square is -29.9 due to under-prediction in the death phase by up to ~1mM (Figure 5.19d). In '0.5mM Fed-batch', '0.3,0.7mM Fed-batch', and '0.3,0.35mM Fed-batch', there is over-prediction of serine concentration during mid-culture time by up to ~0.7mM, causing the modified-R-square values to be -4.61 – 0.33 with 17 – 67% of data lying within ± 0.2 mM of the simulation (Figure 5.22d – 5.24d). The consumption pattern of serine appeared to be highly dynamic. Because it is a non-essential amino acid, such deviation has no significant effect on cell growth and IFN γ productivity.

Glycine

Glycine, together with proline, are the other two non-essential amino acids being significantly produced by the CHO-IFN γ cells. The R-square for glycine in batch culture is 0.49 (Figure 5.18e). The modified-R-squares in fed-batch culture are generally low in the range of -4.65 – 0.63 with only 18 – 60% of data lying within ± 0.2 mM of the simulation (Figure 5.19e – 5.23e). The deviations are in the form of either under-predictions during the death phase ('0.1mM Fed-batch', '0.5mM Fed-batch', and

'0.3,0.7mM Fed-batch') or over-predictions throughout most of the cell culture time ('1st 0.3mM Fed-batch' and '2nd 0.3mM Fed-batch'). But in '0.3,0.35mM Fed-batch' culture, the glycine level was well simulated with modified-R-square being 0.89 and 50% of data lying within ± 0.2 mM of the simulation (Figure 5.24e).

Proline

The model performance for proline is similar to glycine. The R-square for proline in batch culture is -0.12 due to under-prediction during mid-culture by up to 0.2mM and over-prediction in the death phase by up to -0.6 mM (Figure 5.18e). In fed-batch cultures, only 17 – 42% of data are within ± 0.2 mM of the simulation and the modified-R-square values are in the range of -3.78 – 0.52 (Figure 5.19e – 5.24e). The proline concentrations are over-predicted during mid-culture time in '1st 0.3mM Fed-batch', '2nd 0.3mM Fed-batch', and '0.3,0.35mM Fed-batch' cultures and under-predicted in the death phase in '0.1mM Fed-batch', '1st 0.3mM Fed-batch', '2nd 0.3mM Fed-batch', '0.5mM Fed-batch', and '0.3,0.7mM Fed-batch' cultures. The model is unable to capture the variations in proline production and consumption. But as a non-essential amino acid, this did not have significant effect on the major output variables of the model.

Tryptophan (experiment data not available)

The model simulations of possible tryptophan time-profiles for batch and fed-batch cultures are shown in Figure 5.18e – 5.24e. The initial tryptophan concentration is an average value of the initial concentration of other amino acids. The time-profiles of tryptophan are generally similar to other essential amino acids in the corresponding batch/fed-batch cultures. The unavailability of tryptophan data led to an uncertainty regarding its contribution to cell death during the death phase of the batch/fed-batch cultures. Tryptophan is an essential amino acid (Table 4.1) so a lack of it would cause growth rate to cease and may trigger cell death. In the simulations, tryptophan is still available at the end of the batch CHO-IFN γ culture but reaches a low but non-zero level in all fed-batch cultures in the death phase. It is recommended to improve measurement capability in future experiments so that all essential amino acids are monitored.

Hypothetical response variables ($x_{res,Gln}$ & $x_{res,Glc}$)

There are two hypothetical response variables in the model: $x_{res,Gln}$ (Figure 5.25(i)-(vii)) and $x_{res,Glc}$ (Figure 5.26(i)-(vii)) which respond to the concentration of glutamine and glucose respectively. The two variables do not directly represent any signalling molecules in the mammalian cell but serve as ‘soft sensors’ for the assumptions (that the cell culture ‘switches’ to a different metabolic pattern when the concentration of the two dominating nutrients is low; and the ‘switch’ is step-like) made in this CHO-IFN γ model. The values of $x_{res,Gln}$ are positive in most of the fed-batch cultures but $x_{res,Glc}$ is only active in two fed-batch cultures when the glucose feedback controller set-point was set at 0.7mM and 0.35mM respectively. The overall behaviour of these ‘sensors’ is up to expectation as they are able to activate metabolic changes in the mathematical model based on model assumptions.

Conclusions

In general, the model is able to simulate the main trends of key variables including IFN γ , viable and total cell, glutamine, glucose, ammonium, essential amino acids, and growth-stimulating amino acids in the batch and fed-batch CHO-IFN γ cell cultures. Though some of the fine details of dynamic responses may not be well followed in the simulations, e.g. the unexpected decreasing trend in ammonium concentration in some of the fed-batch cultures, and the lack of maintenance consumption of certain amino acids during the death phase in fed-batch cultures etc., the major cell culture responses in low-glutamine and/or low-glucose conditions are able to be captured by the model.

In the next chapter, dynamic model-based optimisation is applied to optimise the IFN γ productivity. The possible effects of parameter uncertainty are evaluated using statistical analysis and the results are discussed.

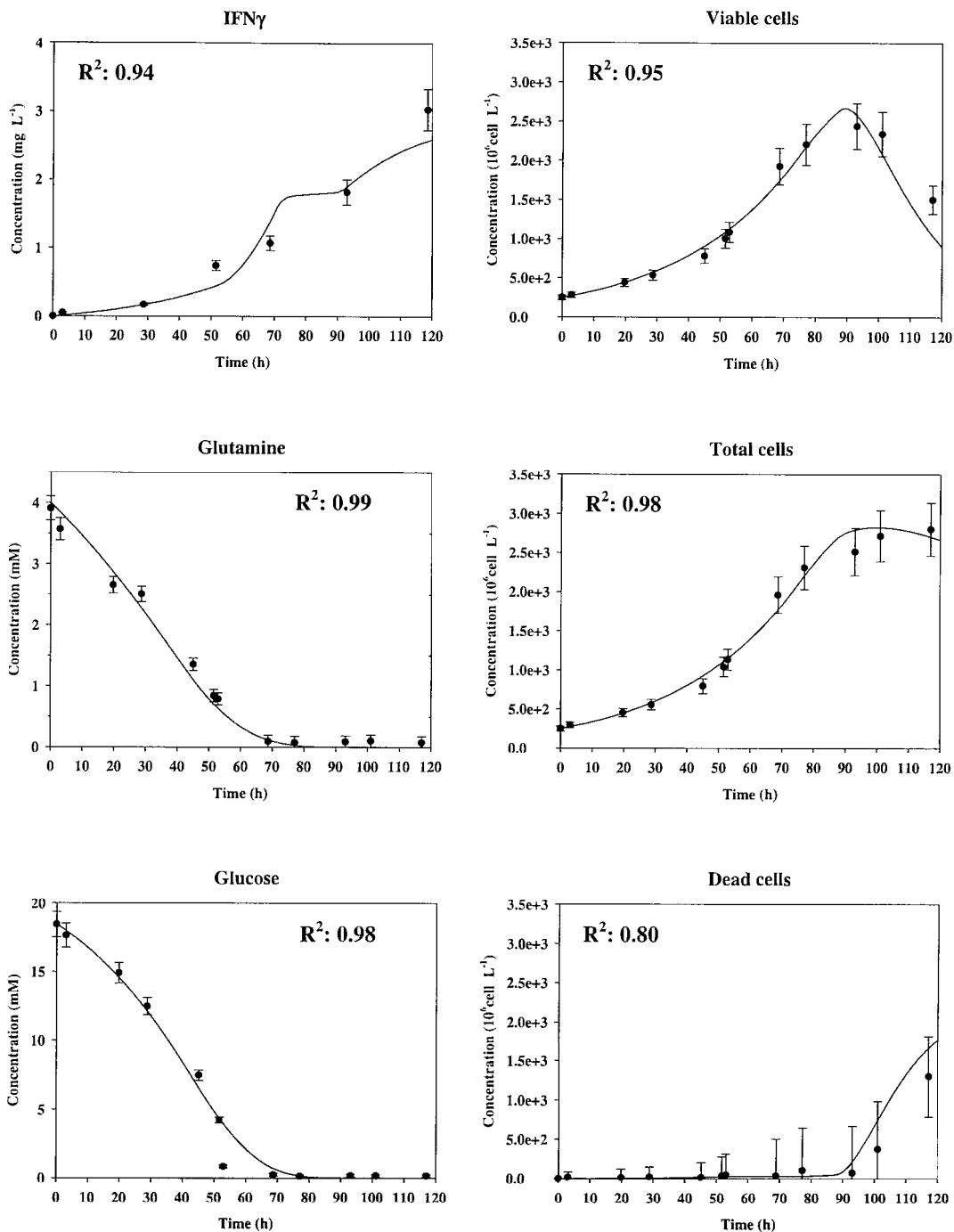


Figure 5.18a: Simulation of IFN γ , glutamine, glucose, and cell concentrations of CHO-IFN γ batch culture and comparison with corresponding experiment data.

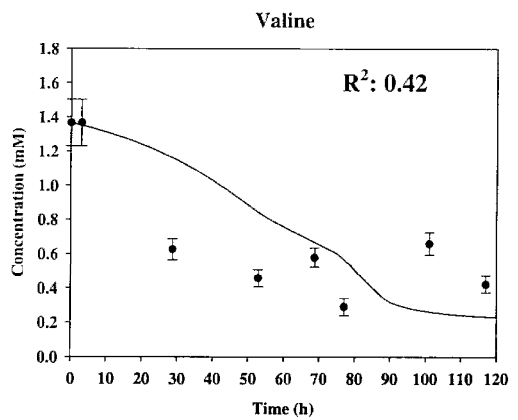
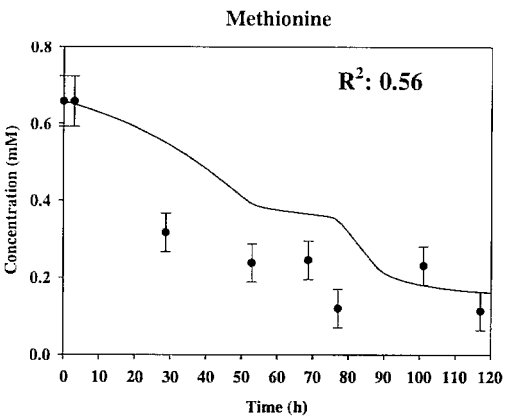
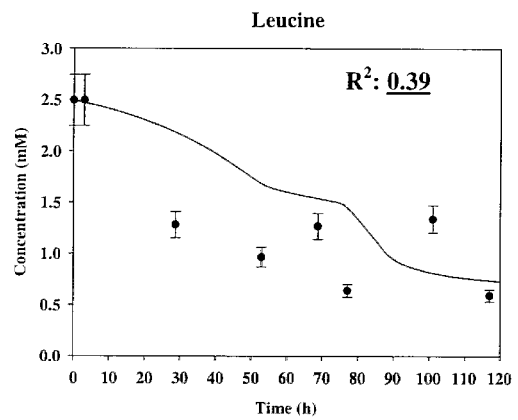
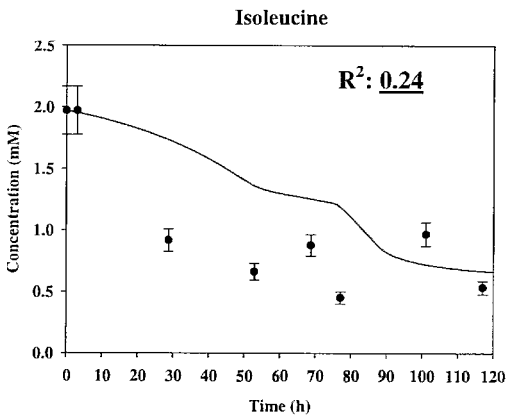
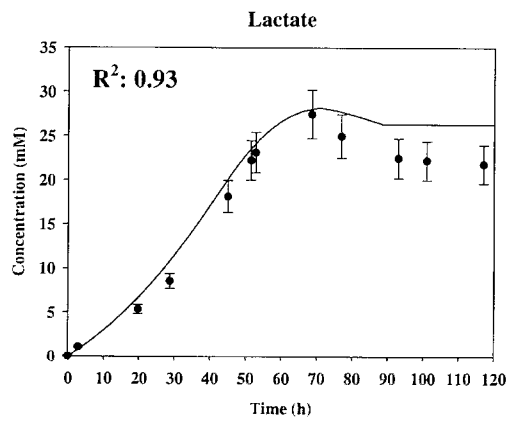
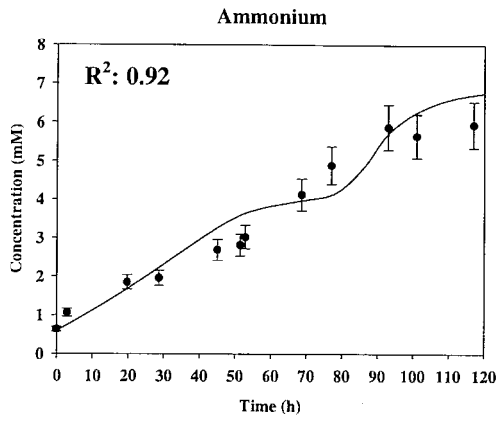


Figure 5.18b: Simulation of ammonium, lactate, isoleucine, leucine, methionine, and valine concentrations of CHO-IFN γ batch cultures and comparison with corresponding experiment data. R^2 values < 0.40 are underlined.

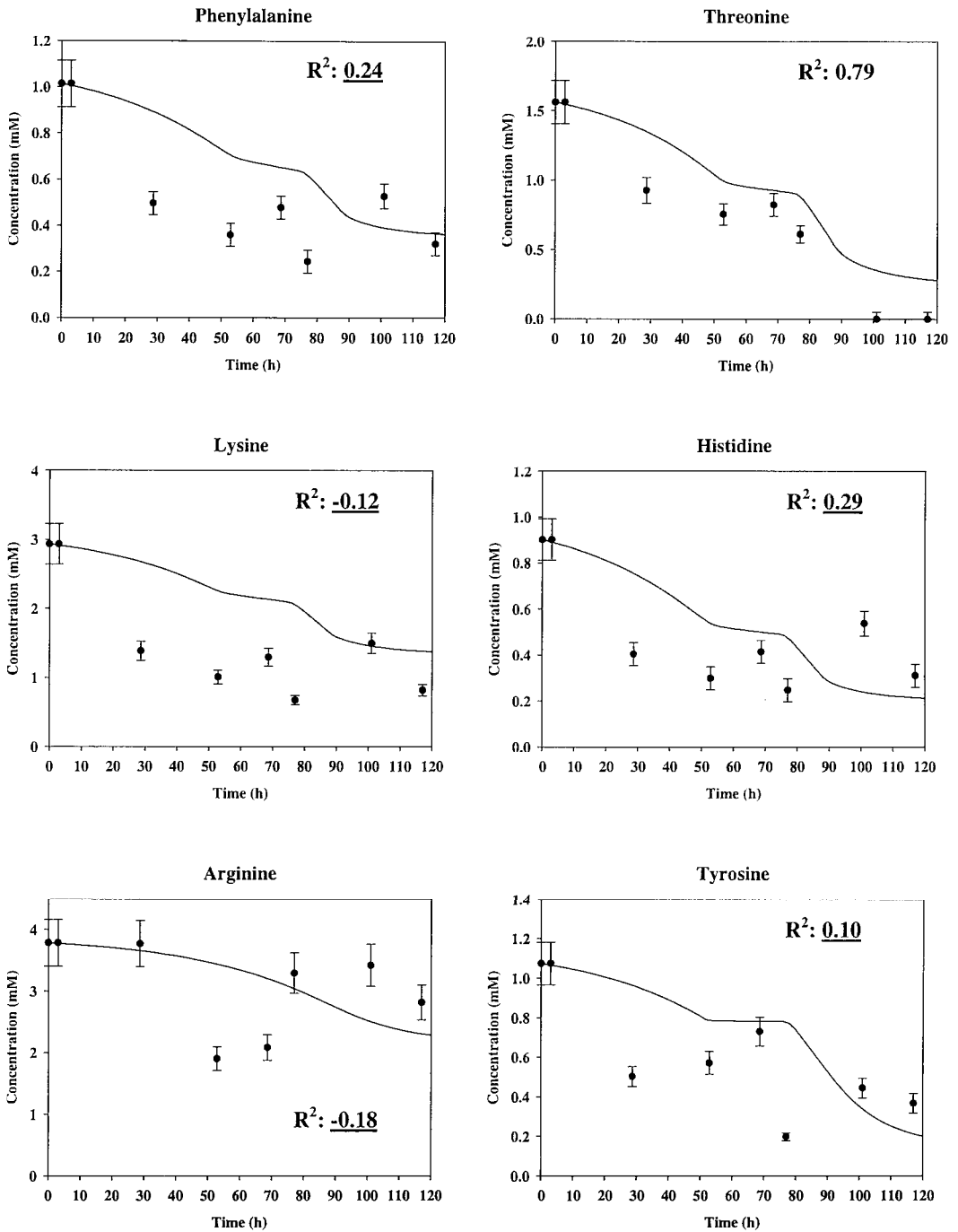


Figure 5.18c: Simulation of phenylalanine, threonine, lysine, histidine, arginine, and tyrosine concentrations of CHO-IFN γ batch cultures and comparison with corresponding experiment data. R^2 values < 0.40 are underlined.

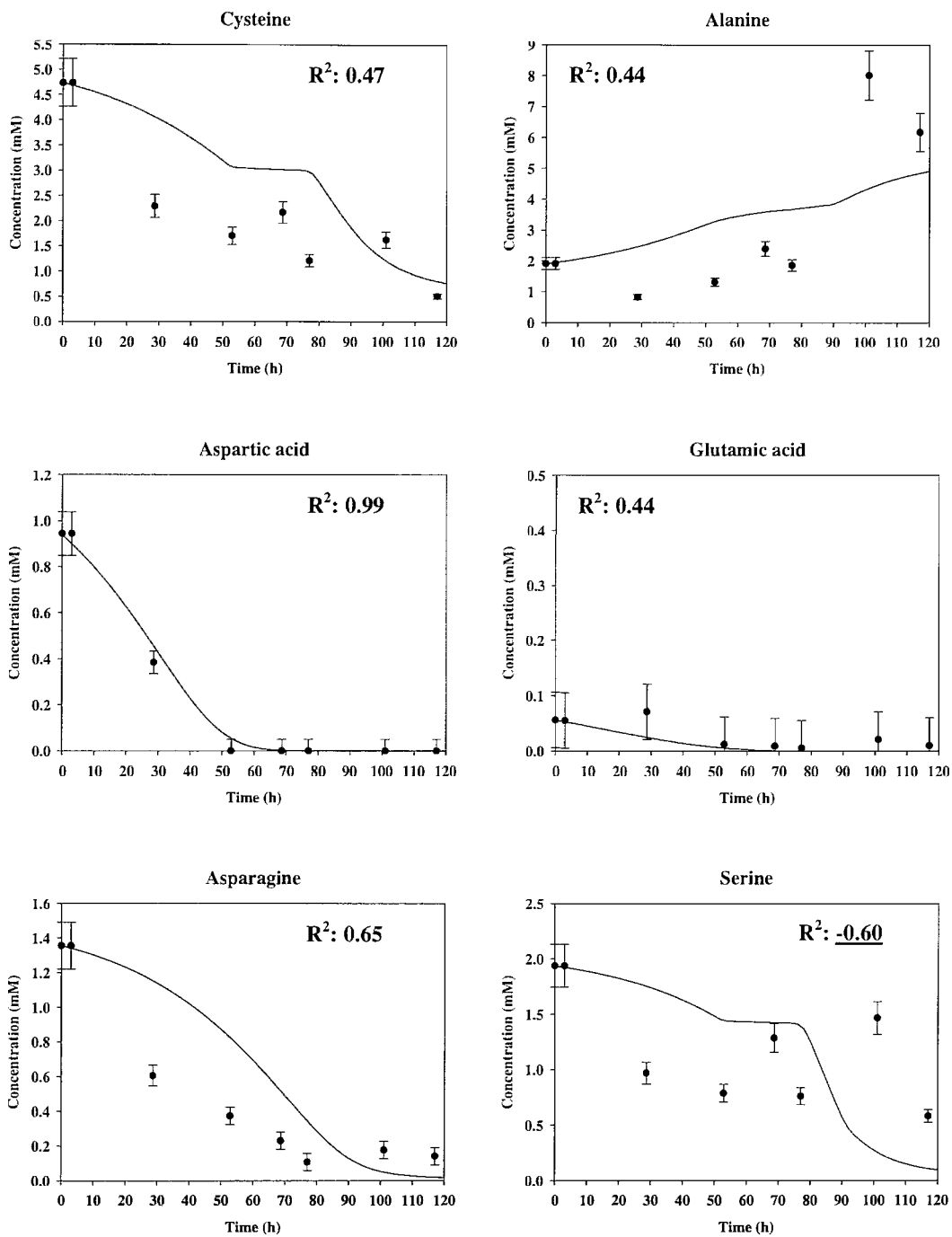


Figure 5.18d: Simulation of cysteine, alanine, aspartic acid, glutamic acid, asparagine, and serine concentrations of CHO-IFN γ batch cultures and comparison with corresponding experiment data. R^2 values < 0.40 are underlined.

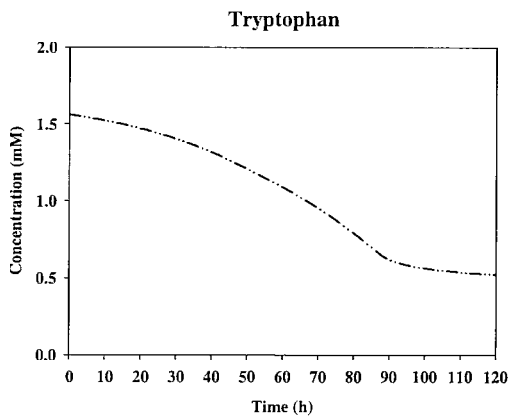
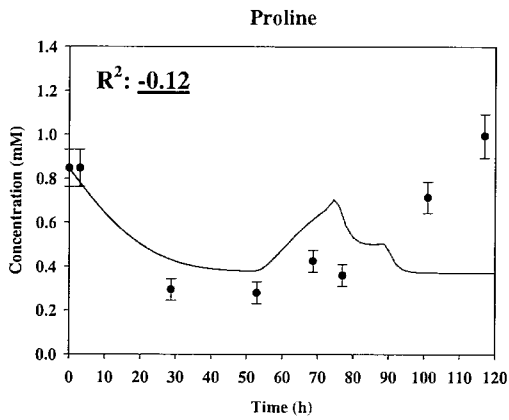
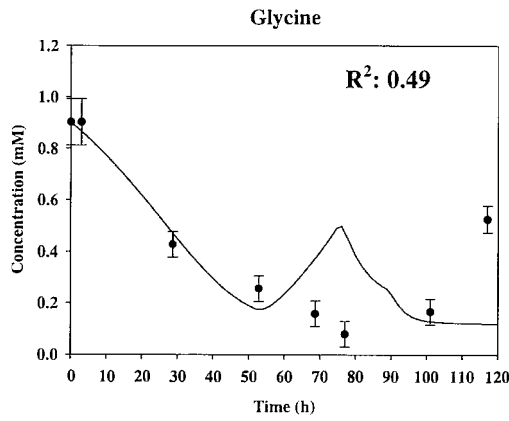


Figure 5.18e: Simulation of glycine, proline, and tryptophan concentrations of CHO-IFN γ batch cultures and comparison with corresponding experiment data. Tryptophan data was not available due to problems with HPLC analysis (initial condition of tryptophan concentration was chosen similar to threonine which had an average initial concentration among other amino acids in batch cultures). R^2 values < 0.40 are underlined.

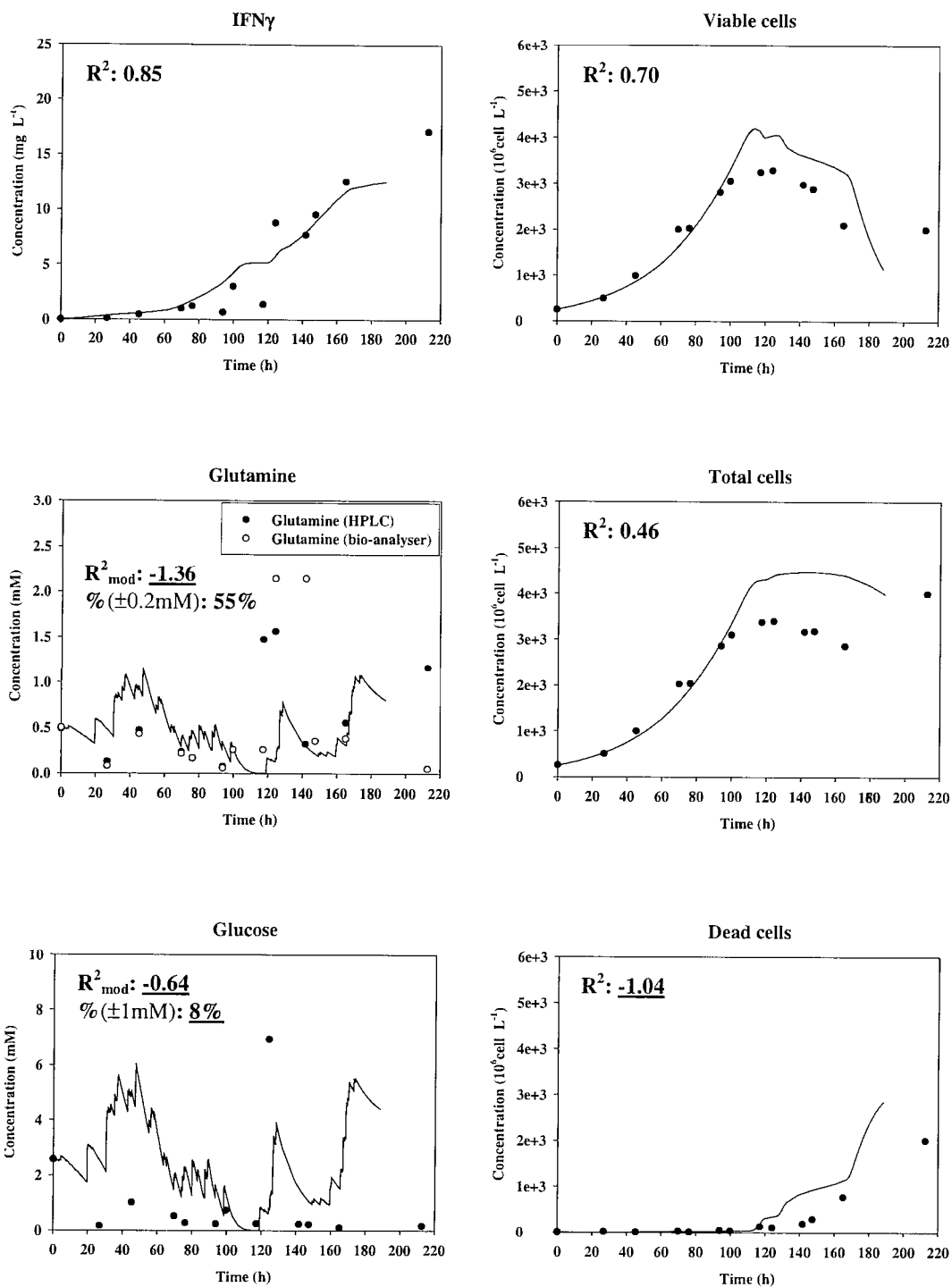


Figure 5.19a: Simulation of IFN γ , glutamine, glucose, and cell concentrations of CHO-IFN γ fed-batch culture with **glutamine set-point at 0.1mM** and comparison with corresponding experimental data. R^2 (or R^2_{mod}) values < 0.40 and '% in $\pm 0.2\text{mM}$ ' (or $\pm 1\text{mM}$ for glucose) values $< 50\%$ are underlined.

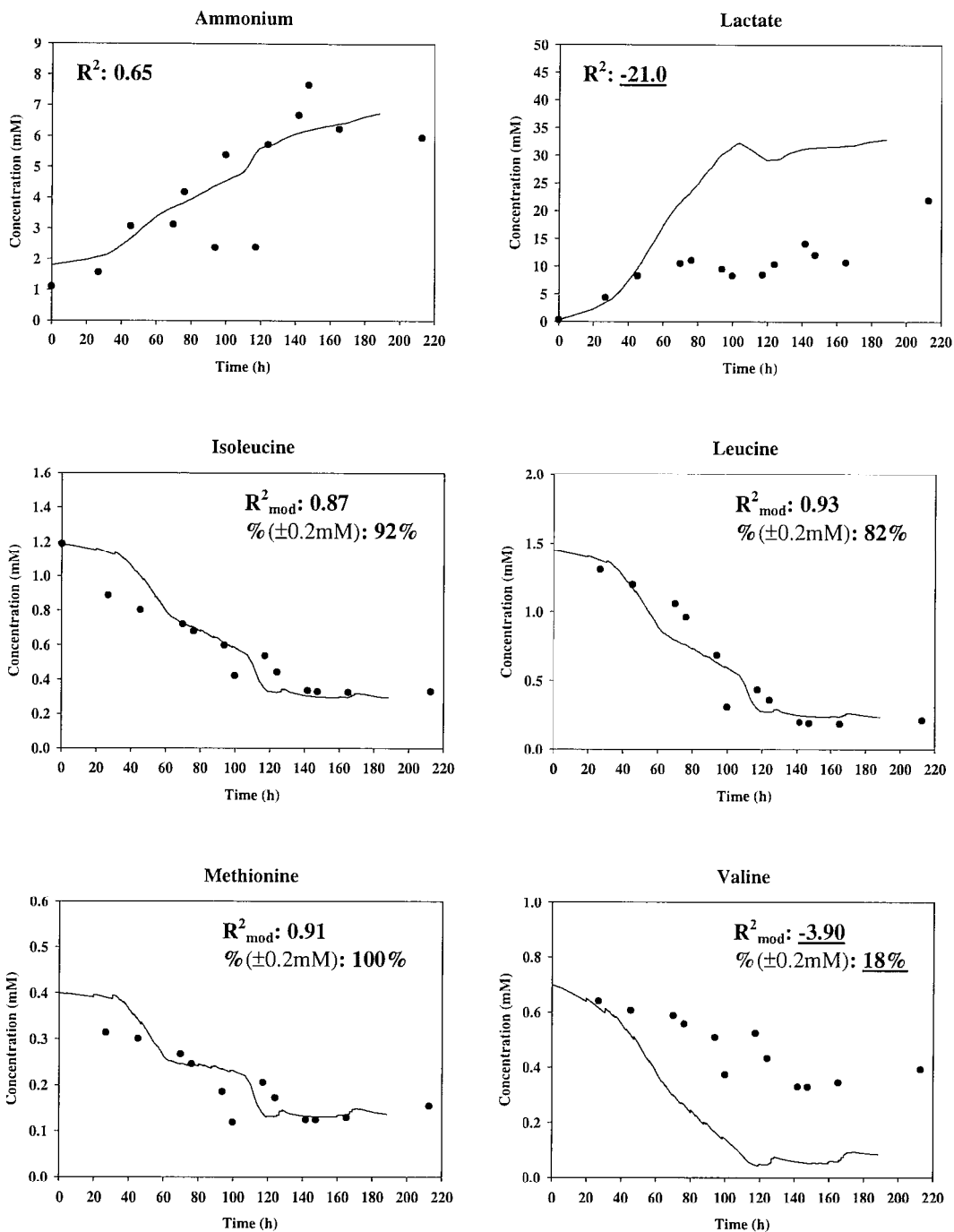


Figure 5.19b: Simulation of ammonium, lactate, isoleucine, leucine, methionine, and valine concentrations of CHO-IFN γ fed-batch culture with **glutamine set-point at 0.1mM** and comparison with corresponding experiment data. R^2 (or R^2_{mod}) values < 0.40 and ‘% in $\pm 0.2\text{mM}$ ’ values $< 50\%$ are underlined. (Refer to text and Appendix 6 for discussion of initial concentration of ammonium and amino acids respectively.)

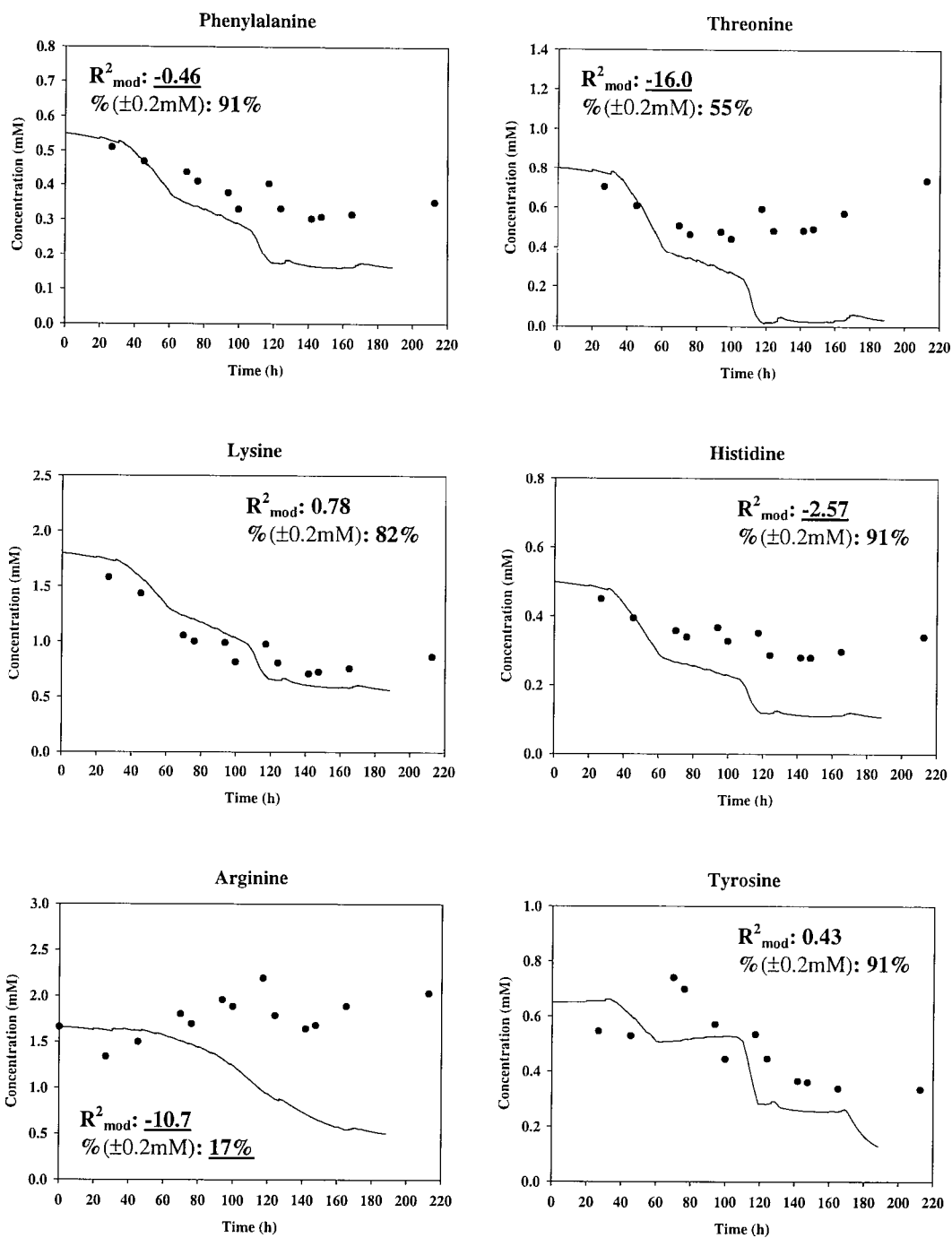


Figure 5.19c: Simulation of phenylalanine, threonine, lysine, histidine, arginine, and tyrosine concentrations of CHO-IFN γ fed-batch culture with **glutamine set-point at 0.1mM** and comparison with corresponding experiment data. R^2_{mod} values < 0.40 and '% in $\pm 0.2\text{mM}$ ' values $< 50\%$ are underlined. (Refer to Appendix 6 for discussion of initial concentration of amino acids.)

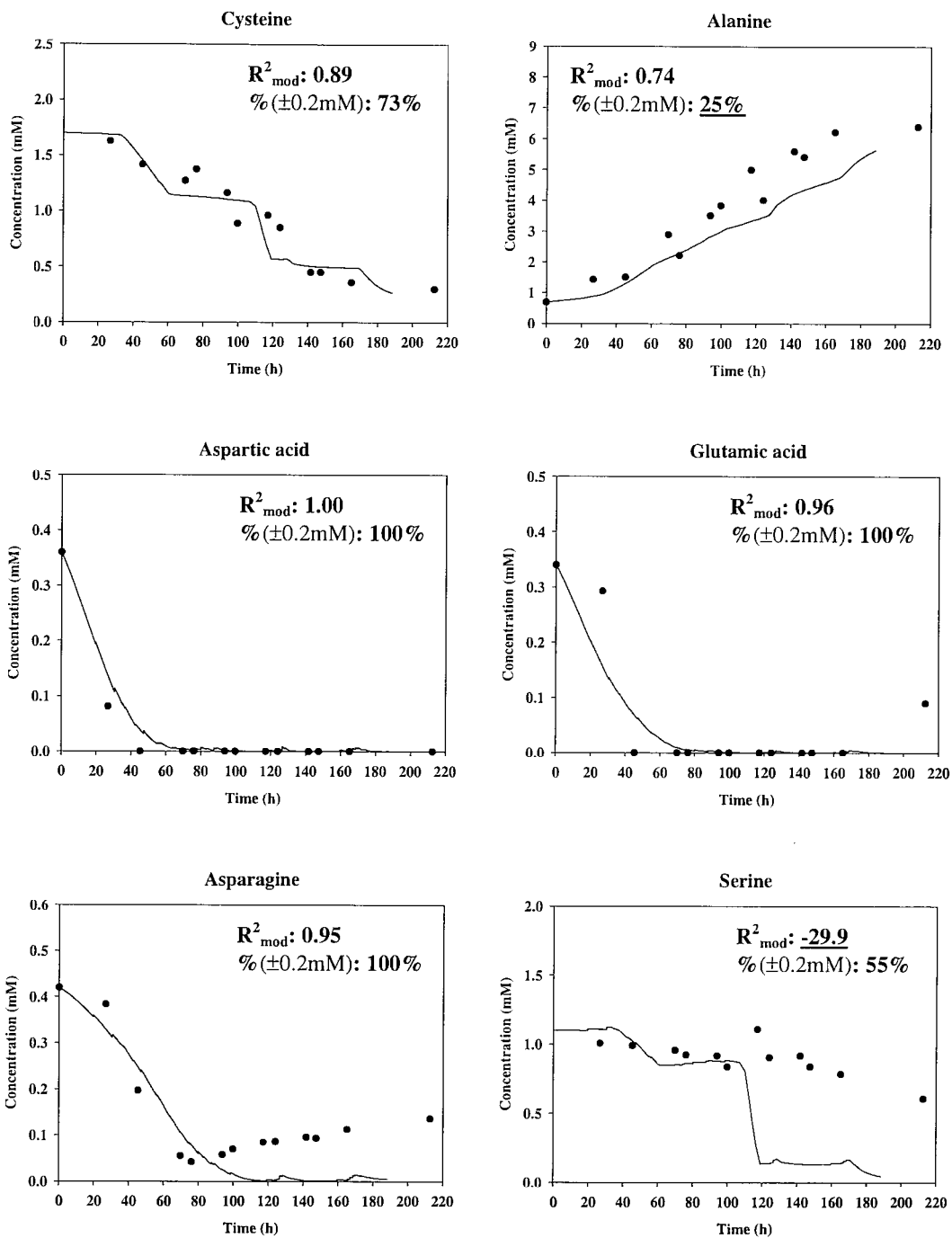


Figure 5.19d: Simulation of cysteine, alanine, aspartic acid, glutamic acid, asparagine, and serine concentrations of CHO-IFN γ fed-batch culture with **glutamine set-point at 0.1mM** and with comparison with corresponding experiment data. R^2_{mod} values < 0.40 and ' $\%$ in $\pm 0.2\text{mM}$ ' values $< 50\%$ are underlined. (Refer to Appendix 6 for discussion of initial concentration of amino acids.)

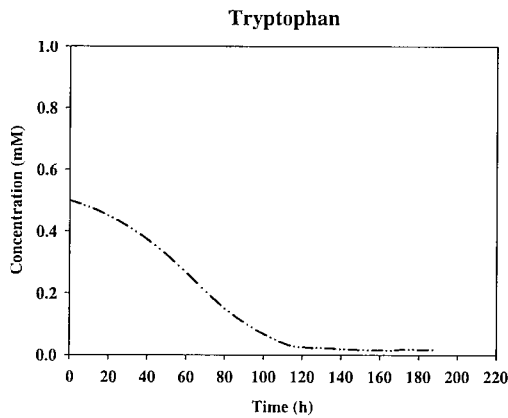
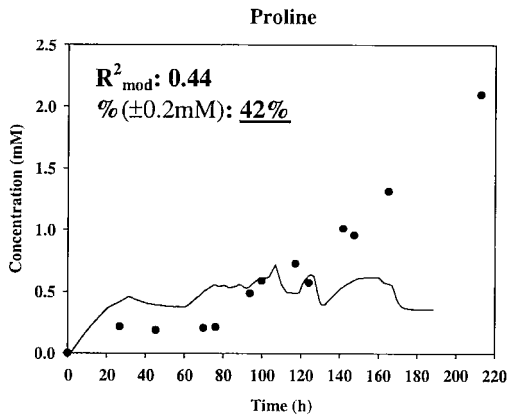
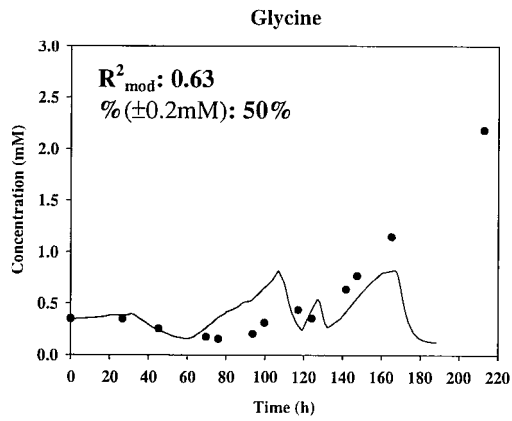


Figure 5.19e: Simulation of glycine, proline, and tryptophan concentrations of CHO-IFN γ fed-batch culture with **glutamine set-point at 0.1mM** and comparison with corresponding experiment data. Tryptophan data was not available due to problems with HPLC analysis (an initial concentration of 0.5mM was used which was an average among other amino acids in fed-batch cultures). R^2_{mod} values < 0.40 and ‘% in $\pm 0.2\text{mM}$ ’ values $< 50\%$ are underlined.

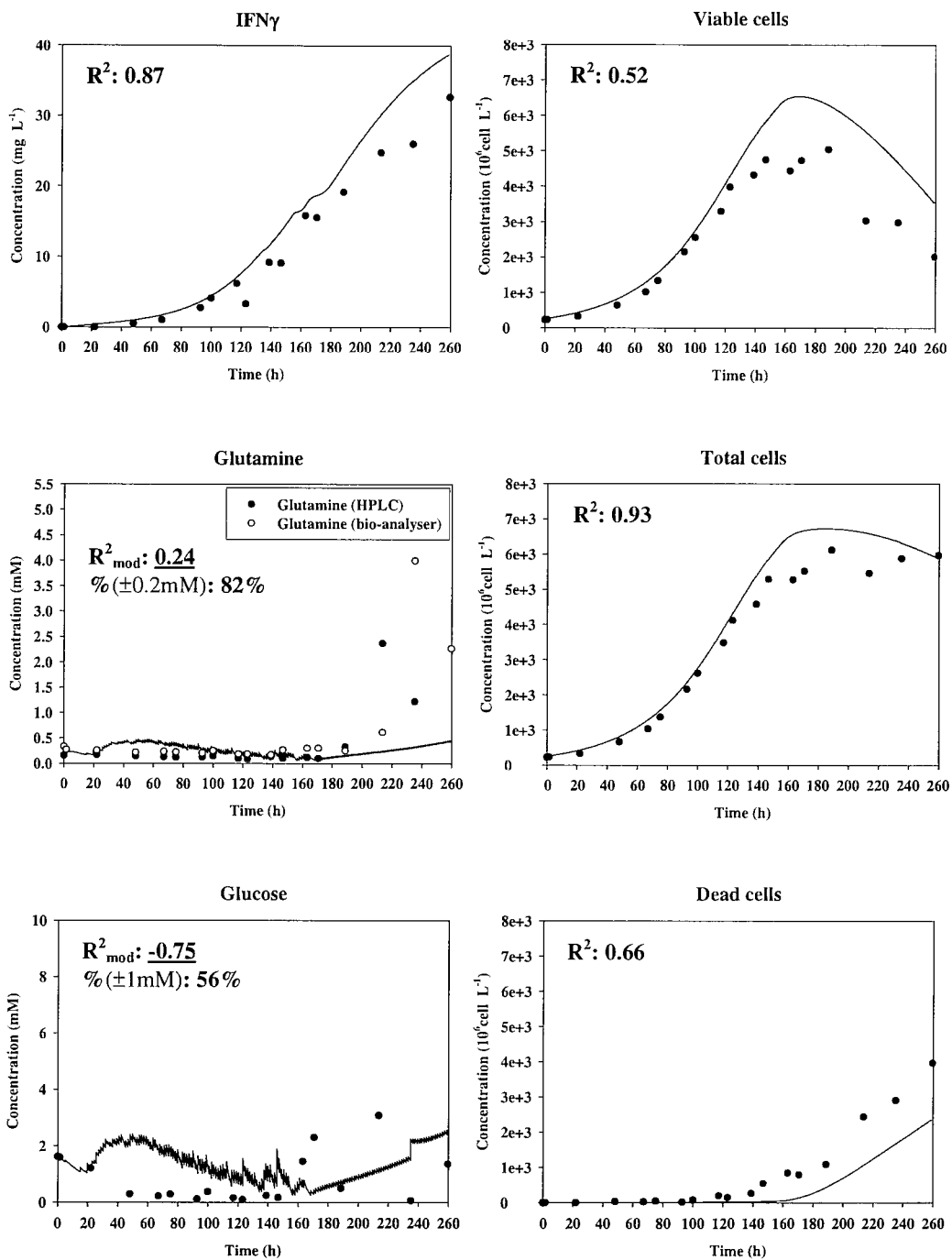


Figure 5.20a: Simulation of IFN γ , glutamine, glucose, and cell concentrations of CHO-IFN γ fed-batch culture with **glutamine set-point at 0.3mM (1st experiment)** and comparison with corresponding experiment data. R^2 (or R^2_{mod}) values < 0.40 and ‘% in $\pm 0.2\text{mM}$ ’ (or $\pm 1\text{mM}$ for glucose) values < 50% are underlined.

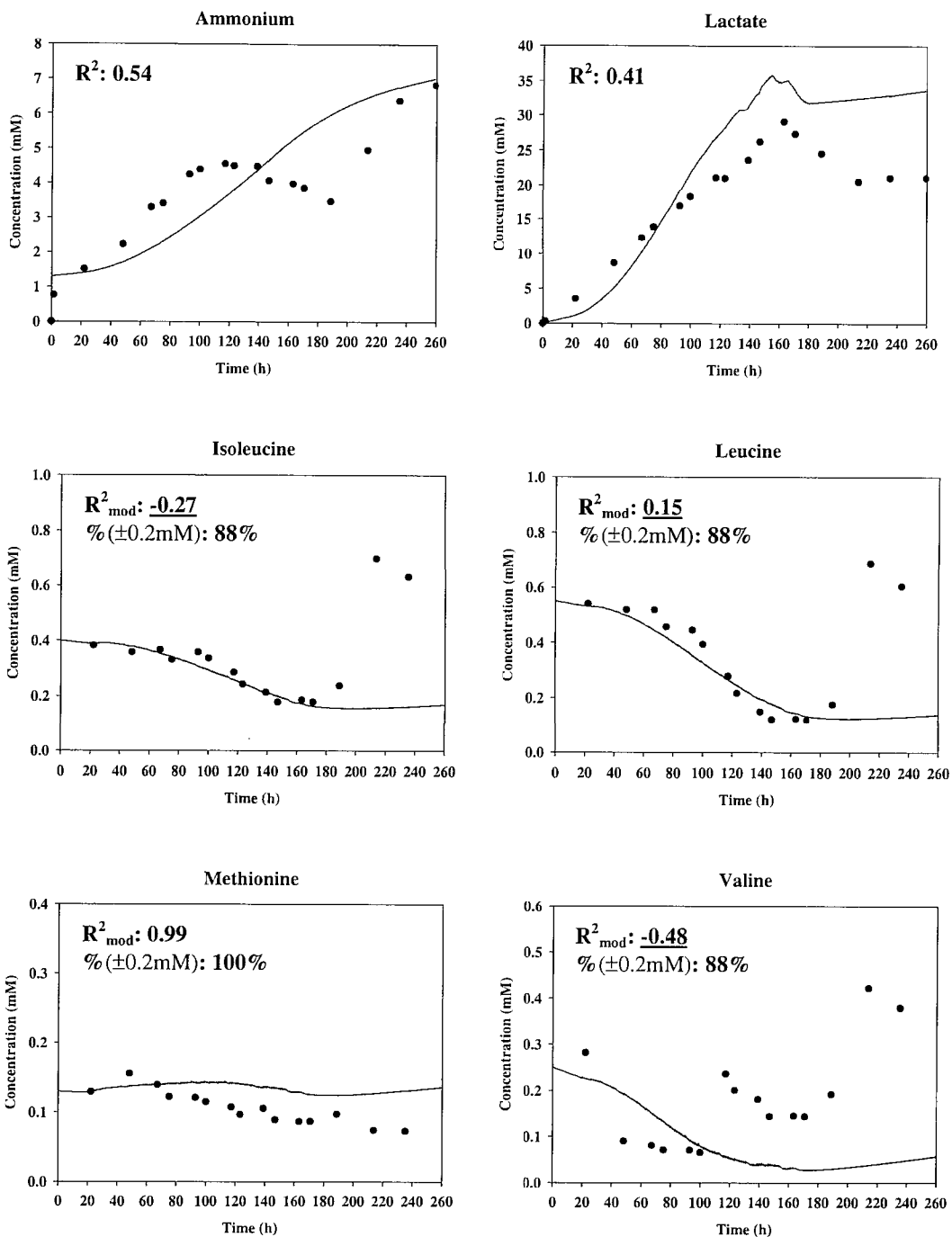


Figure 5.20b: Simulation of ammonium, lactate, isoleucine, leucine, methionine, and valine concentrations of CHO-IFN γ fed-batch culture with **glutamine set-point at 0.3mM (1st experiment)** and comparison with corresponding experiment data. R^2 (or R^2_{mod}) values < 0.40 and ‘% in $\pm 0.2\text{mM}$ ’ values $< 50\%$ are underlined. (Refer to text and Appendix 6 for discussion of initial concentration of ammonium and amino acids respectively.)

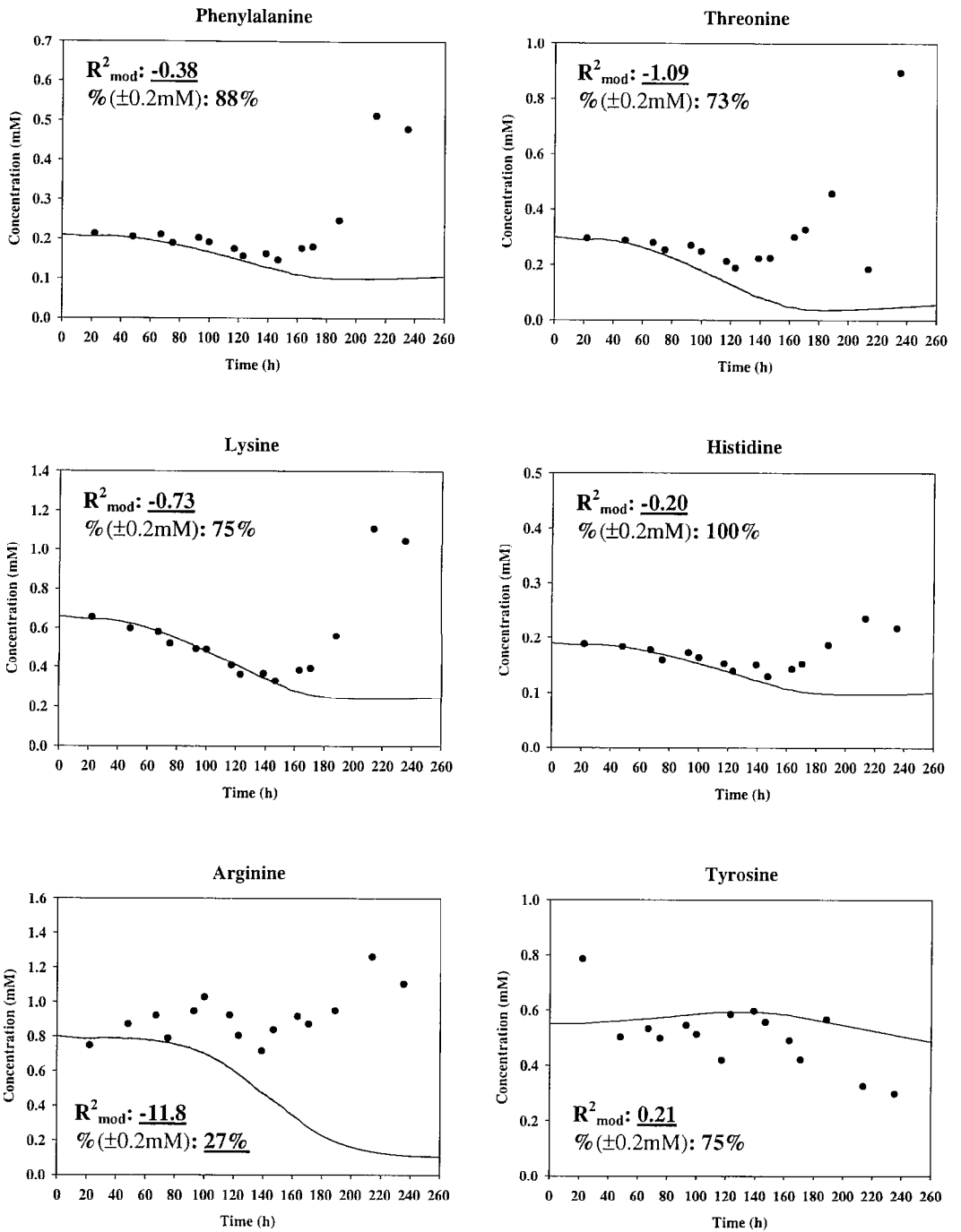


Figure 5.20c: Simulation of phenylalanine, threonine, lysine, histidine, arginine, and tyrosine concentrations of CHO-IFN γ fed-batch culture with **glutamine set-point at 0.3mM (1st experiment)** and comparison with corresponding experiment data. R^2_{mod} values < 0.40 and ‘% in $\pm 0.2\text{mM}$ ’ values $< 50\%$ are underlined. (Refer to Appendix 6 for discussion of initial concentration of amino acids.)

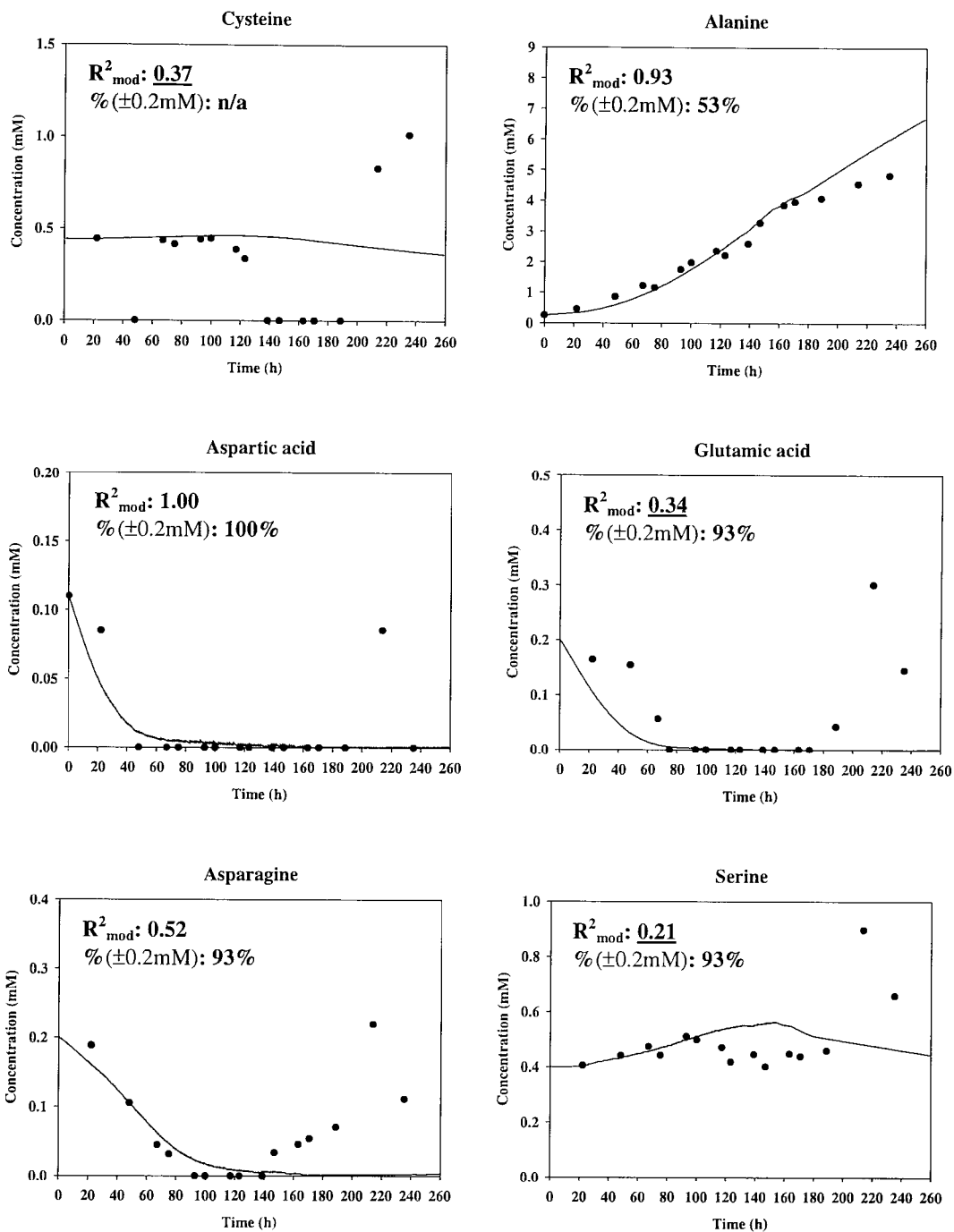


Figure 5.20d: Simulation of cysteine, alanine, aspartic acid, glutamic acid, asparagine, and serine concentrations of CHO-IFN γ fed-batch culture with **glutamine set-point at 0.3mM (1st experiment)** and comparison with corresponding experiment data. or R^2_{mod} values < 0.40 and ‘% in $\pm 0.2\text{mM}$ ’ values < 50% are underlined. (Refer to Appendix 6 for discussion of initial concentration of amino acids.)

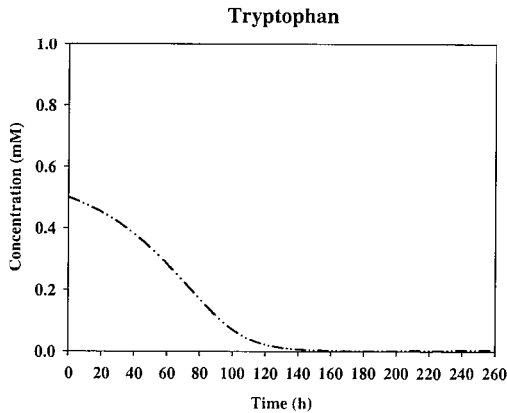
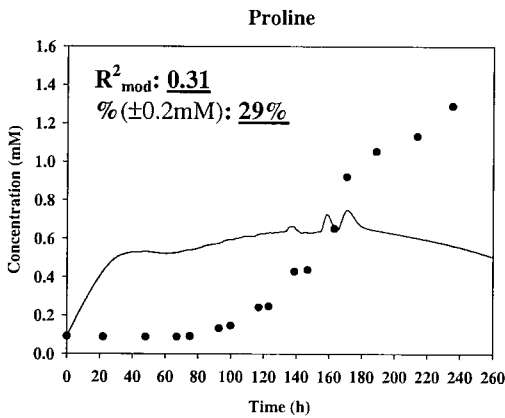
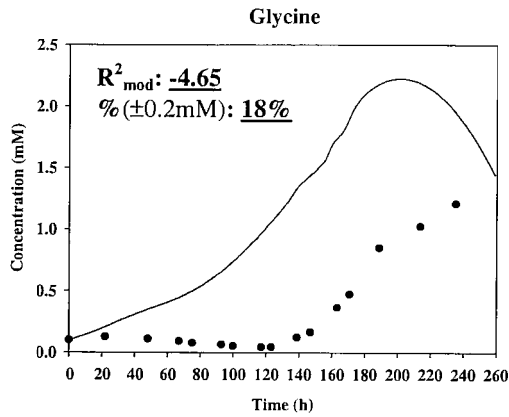


Figure 5.20e: Simulation of glycine, proline, and tryptophan concentrations of CHO-IFN γ fed-batch culture with **glutamine set-point at 0.3mM (1st experiment)** and comparison with corresponding experiment data. Tryptophan data was not available due to problems with HPLC analysis (an initial concentration of 0.5mM was used which was an average among other amino acids in fed-batch cultures). R^2_{mod} values < 0.40 and ‘% in $\pm 0.2\text{mM}$ ’ values < 50% are underlined.

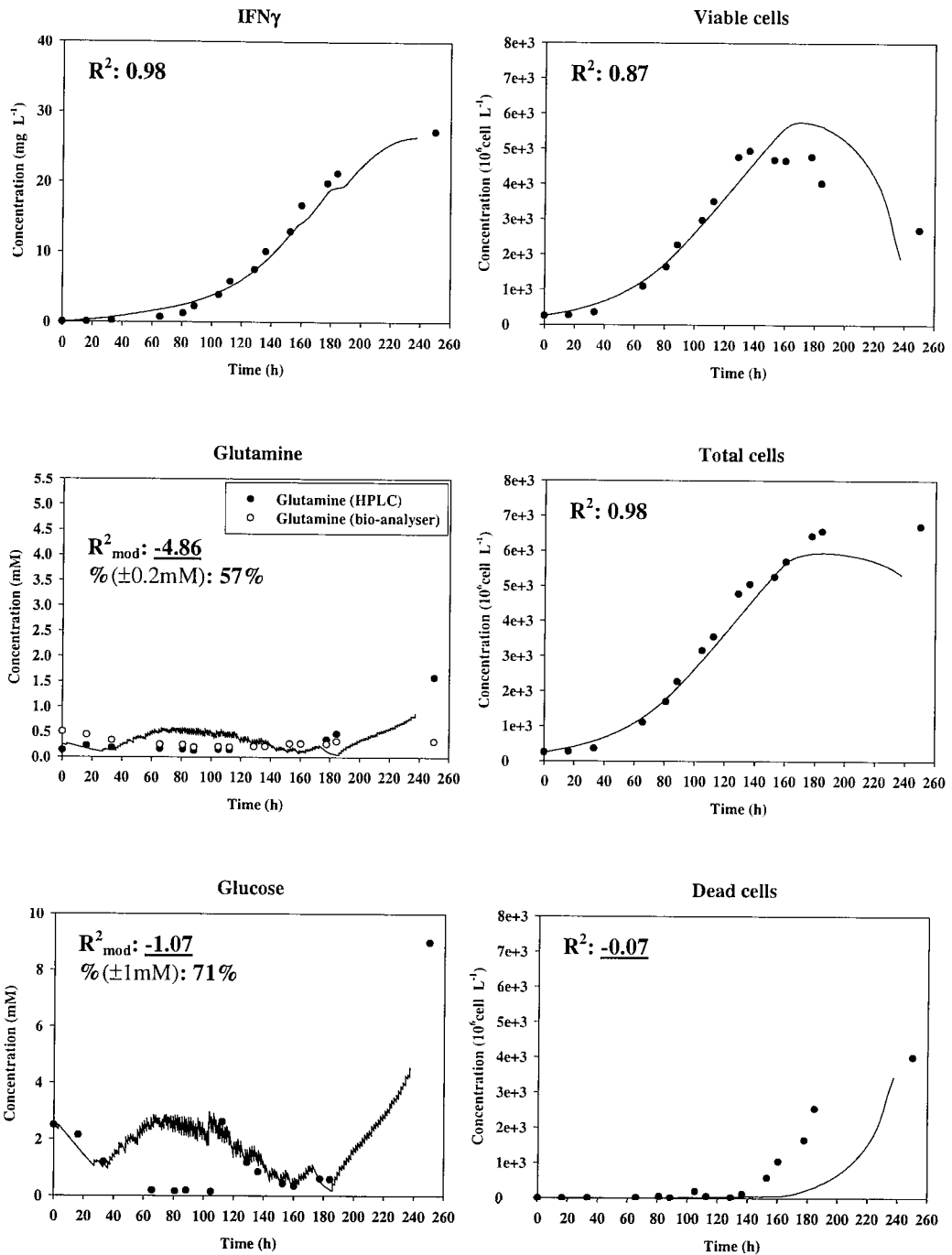


Figure 5.21a: Simulation of IFN γ , glutamine, glucose, and cell concentrations of CHO-IFN γ fed-batch culture with **glutamine set-point at 0.3mM (2nd experiment)** and comparison with corresponding experiment data. R^2 (or R^2_{mod}) values < 0.40 and ‘% in $\pm 0.2\text{mM}$ ’ (or $\pm 1\text{mM}$ for glucose) values $< 50\%$ are underlined.

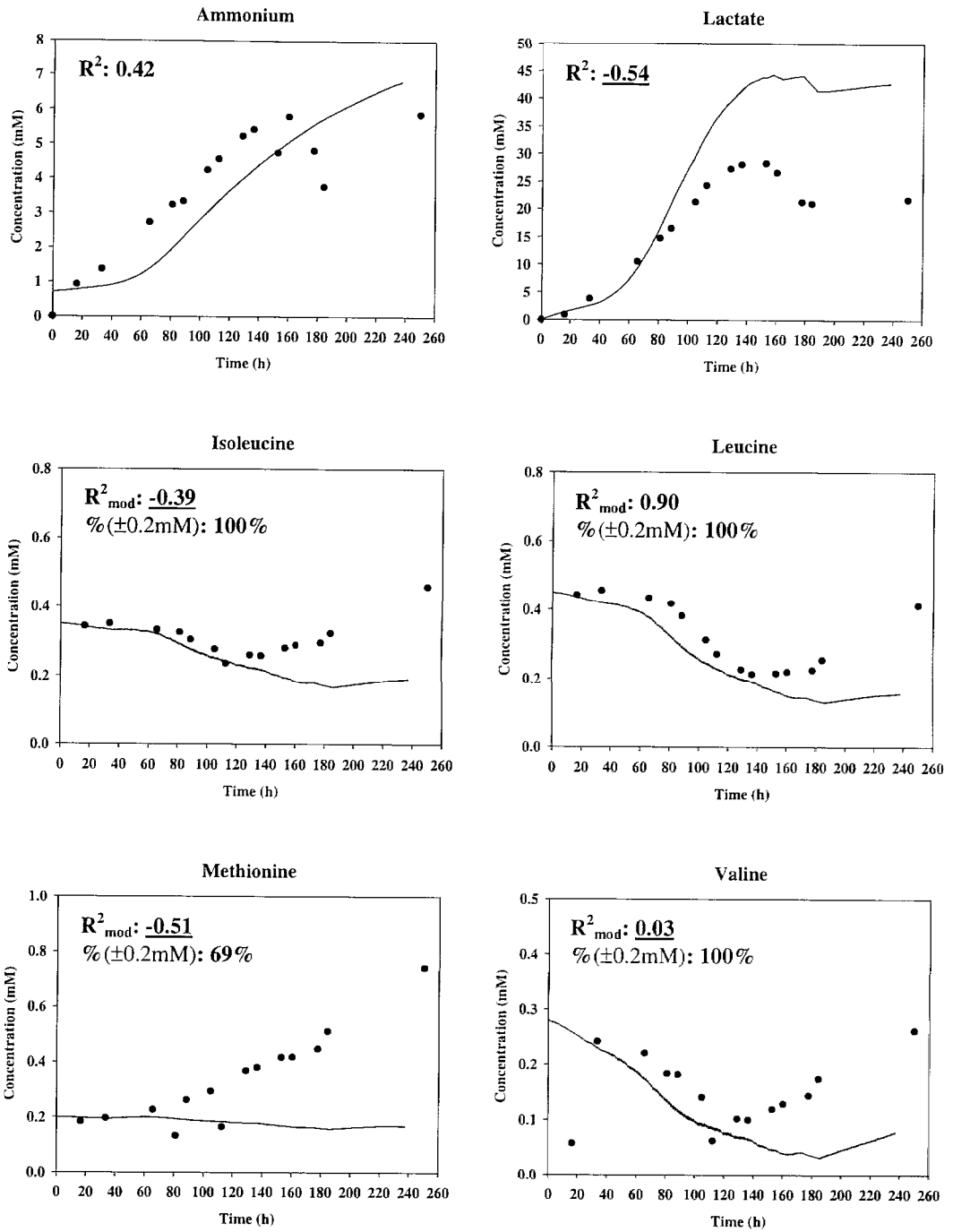


Figure 5.21b: Simulation of ammonium, lactate, isoleucine, leucine, methionine, and valine concentrations of CHO-IFN γ fed-batch culture with **glutamine set-point at 0.3mM (2nd experiment)** and comparison with corresponding experiment data. R^2 (or R^2_{mod}) values < 0.40 and '% in $\pm 0.2\text{mM}$ ' values < 50% are underlined. (Refer to text and Appendix 6 for discussion of initial concentration of ammonium and amino acids respectively.)

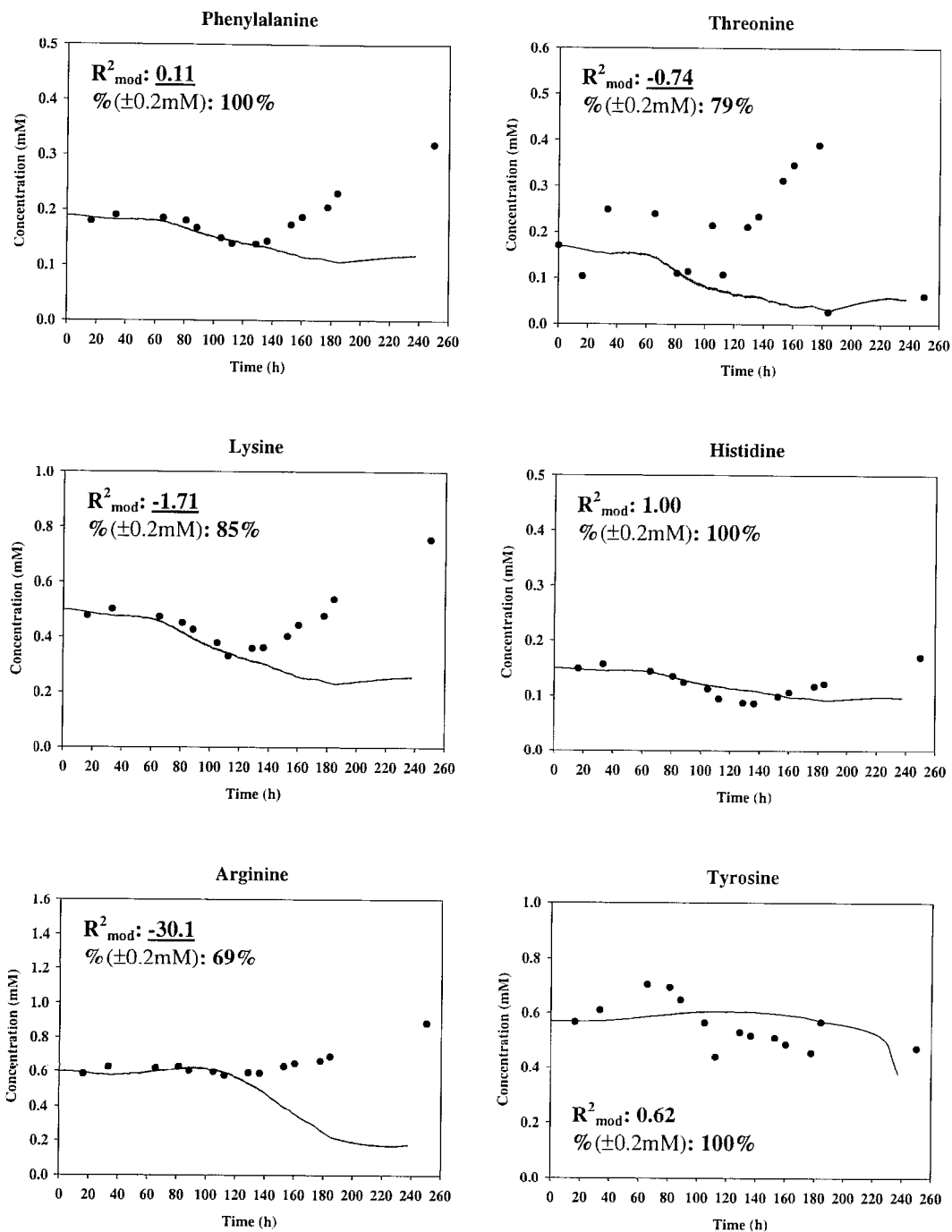


Figure 5.21c: Simulation of phenylalanine, threonine, lysine, histidine, arginine, and tyrosine concentrations of CHO-IFN γ fed-batch culture with **glutamine set-point at 0.3mM (2nd experiment)** and comparison with corresponding experiment data. R^2_{mod} values < 0.40 and ‘% in $\pm 0.2\text{mM}$ ’ values $< 50\%$ are underlined. (Refer to Appendix 6 for discussion of initial concentration of amino acids.)

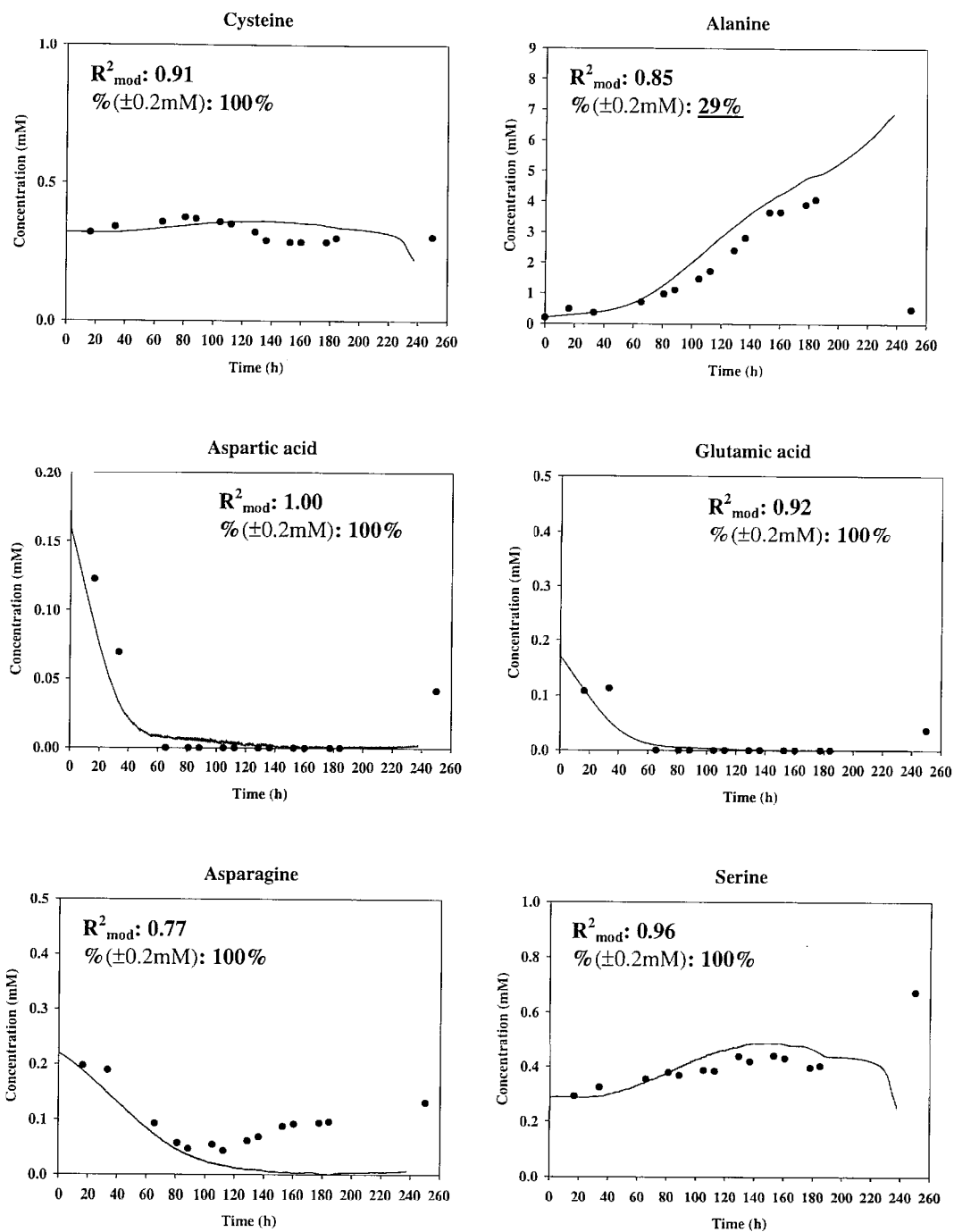


Figure 5.21d: Simulation of cysteine, alanine, aspartic acid, glutamic acid, asparagine, and serine concentrations of CHO-IFN γ fed-batch culture with **glutamine set-point at 0.3mM (2nd experiment)** and comparison with corresponding experiment data. R^2_{mod} values < 0.40 and ‘% in $\pm 0.2\text{mM}$ ’ values < 50% are underlined. (Refer to Appendix 6 for discussion of initial concentration of amino acids.)

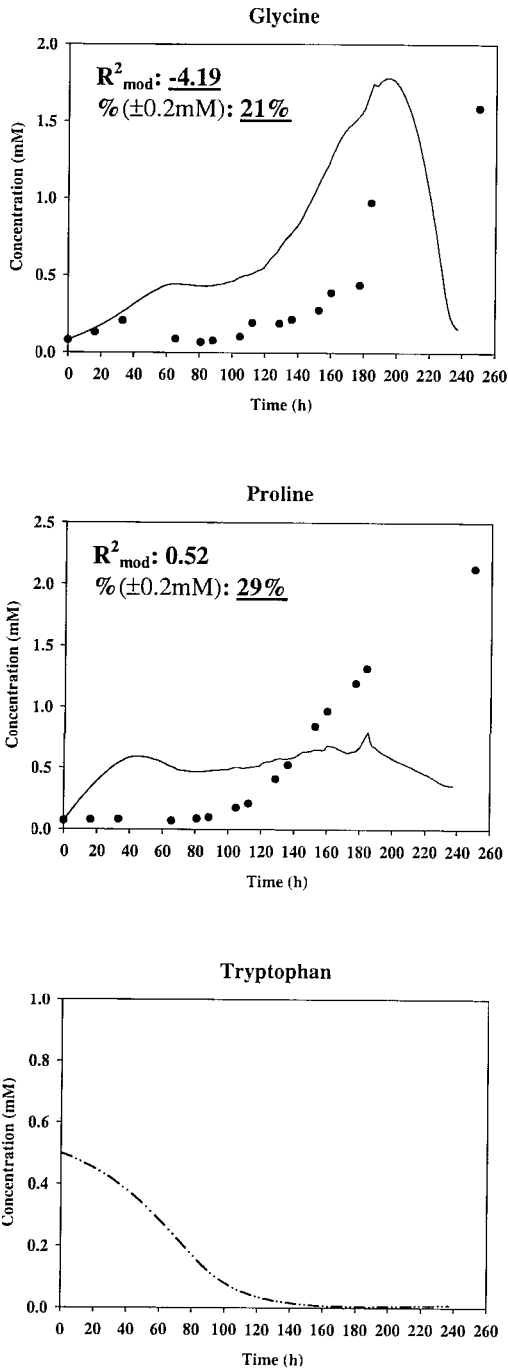


Figure 5.21e: Simulation of glycine, proline, and tryptophan concentrations of CHO-IFN γ fed-batch culture with **glutamine set-point at 0.3mM (2nd experiment)** and comparison with corresponding experiment data. Tryptophan data was not available due to problems with HPLC analysis (an initial concentration of 0.5mM was used which was an average among other amino acids in fed-batch cultures). R^2_{mod} values < 0.40 and ‘% in $\pm 0.2\text{mM}$ ’ values < 50% are underlined.

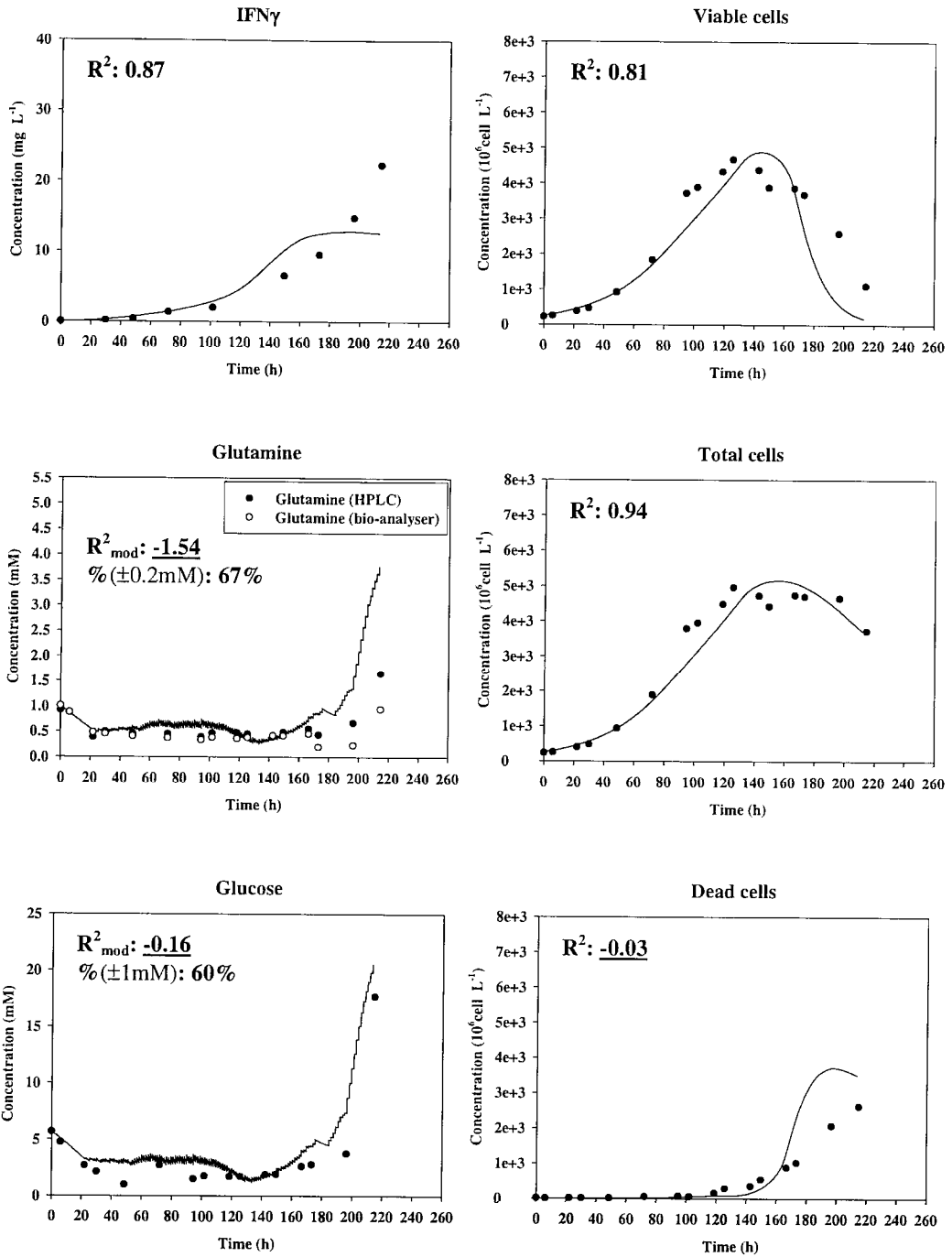


Figure 5.22a: Simulation of IFN γ , glutamine, glucose, and cell concentrations of CHO-IFN γ fed-batch culture with **glutamine set-point at 0.5mM** and comparison with corresponding experiment data. R^2 (or R^2_{mod}) values < 0.40 and ‘% in $\pm 0.2\text{mM}$ ’ (or $\pm 1\text{mM}$ for glucose) values $< 50\%$ are underlined.

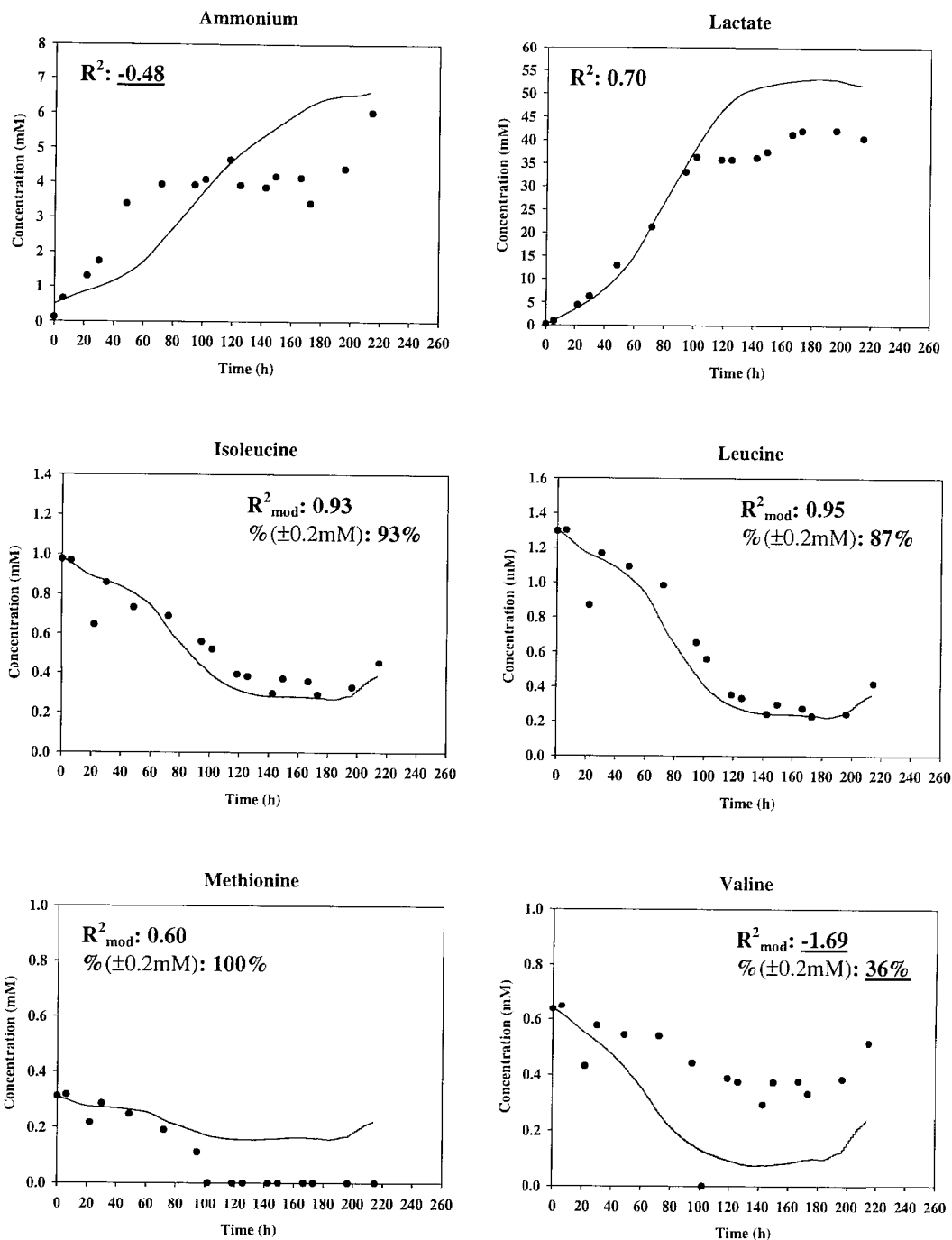


Figure 5.22b: Simulation of ammonium, lactate, isoleucine, leucine, methionine, and valine concentrations of CHO-IFN γ fed-batch culture with **glutamine set-point at 0.5mM** and comparison with corresponding experiment data. R^2 (or R^2_{mod}) values < 0.40 and '% in $\pm 0.2\text{mM}$ ' values $< 50\%$ are underlined. (Refer to text and Appendix 6 for discussion of initial concentration of ammonium and amino acids respectively.)

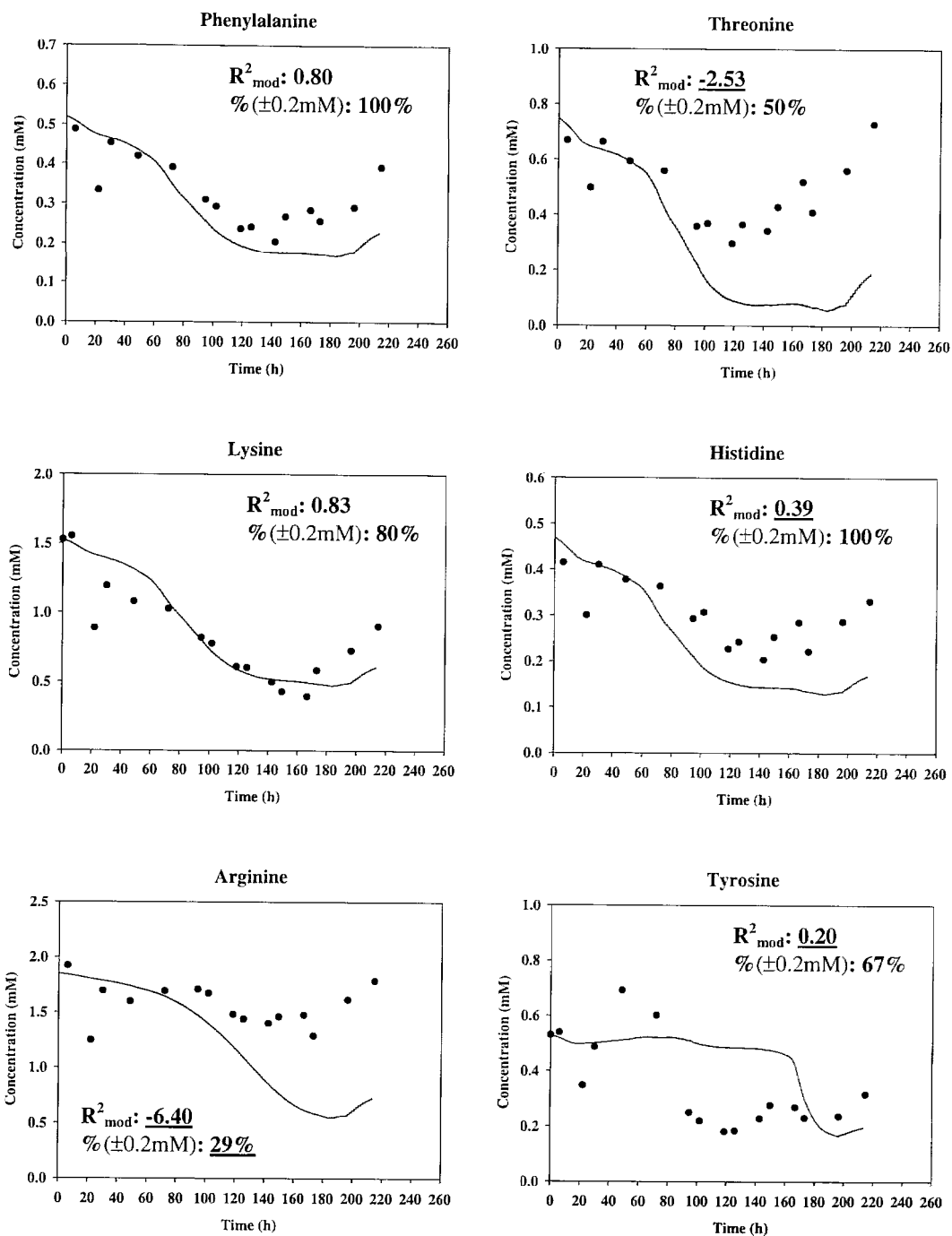


Figure 5.22c: Simulation of phenylalanine, threonine, lysine, histidine, arginine, and tyrosine concentrations of CHO-IFN γ fed-batch culture with **glutamine set-point at 0.5mM** and comparison with corresponding experiment data. R^2_{mod} values < 0.40 and '% in $\pm 0.2\text{mM}$ ' values < 50% are underlined. (Refer to Appendix 6 for discussion of initial concentration of amino acids.)

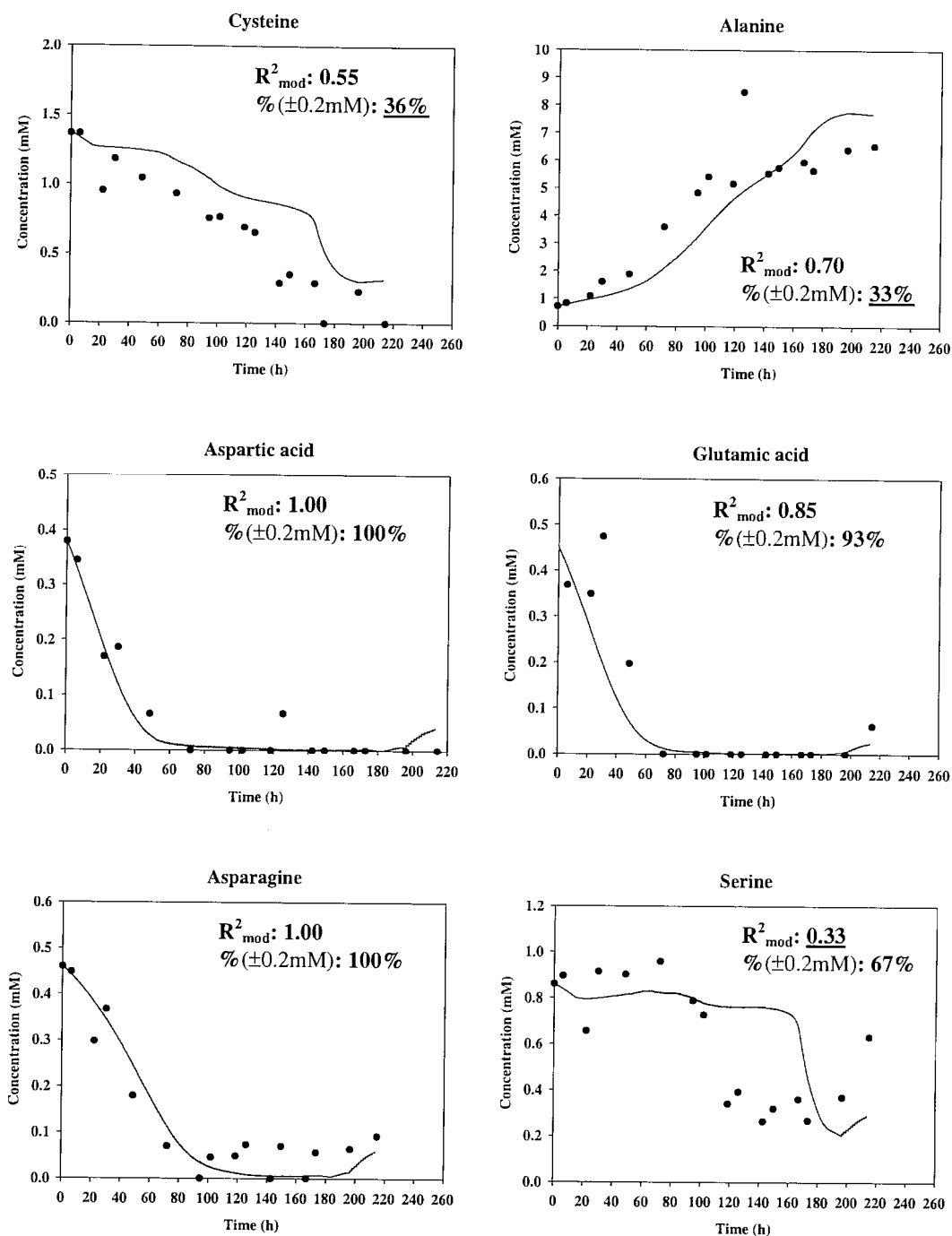


Figure 5.22d: Simulation of cysteine, alanine, aspartic acid, glutamic acid, asparagine, and serine concentrations of CHO-IFN γ fed-batch culture with **glutamine set-point at 0.5mM** and comparison with corresponding experiment data. R^2_{mod} values < 0.40 and ‘% in $\pm 0.2\text{mM}$ ’ values < 50% are underlined. (Refer to Appendix 6 for discussion of initial concentration of amino acids.)

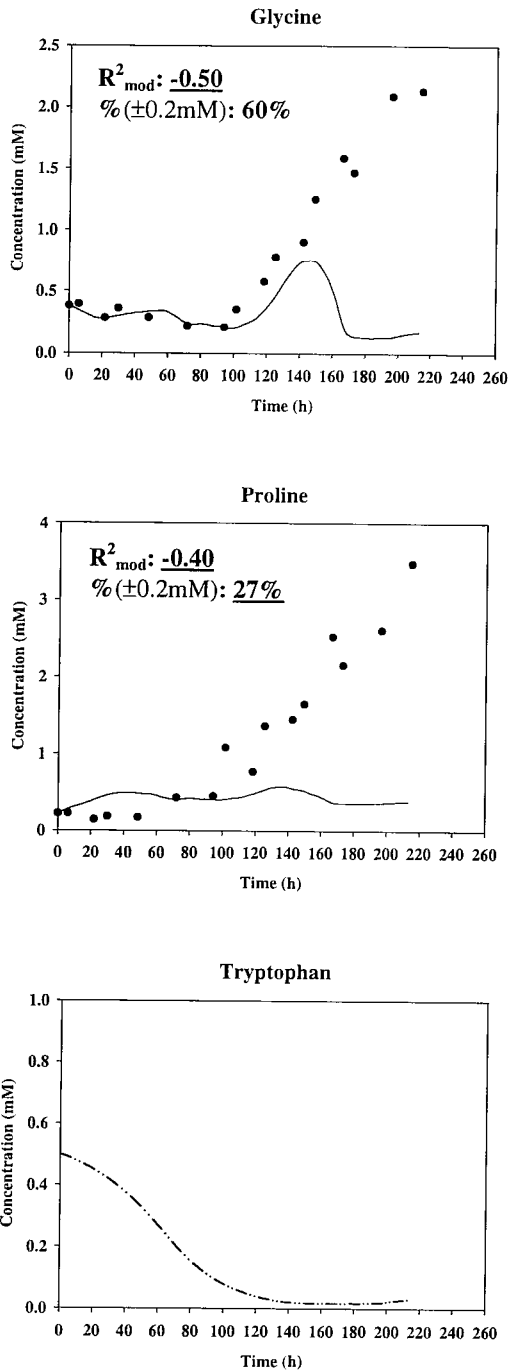


Figure 5.22e: Simulation of glycine, proline, and tryptophan concentrations of CHO-IFN γ fed-batch culture with **glutamine set-point at 0.5mM** and comparison with corresponding experiment data. Tryptophan data was not available due to problems with HPLC analysis (an initial concentration of 0.5mM was used which was an average among other amino acids in fed-batch cultures). R^2_{mod} values < 0.40 and '% in $\pm 0.2\text{mM}$ ' values < 50% are underlined.

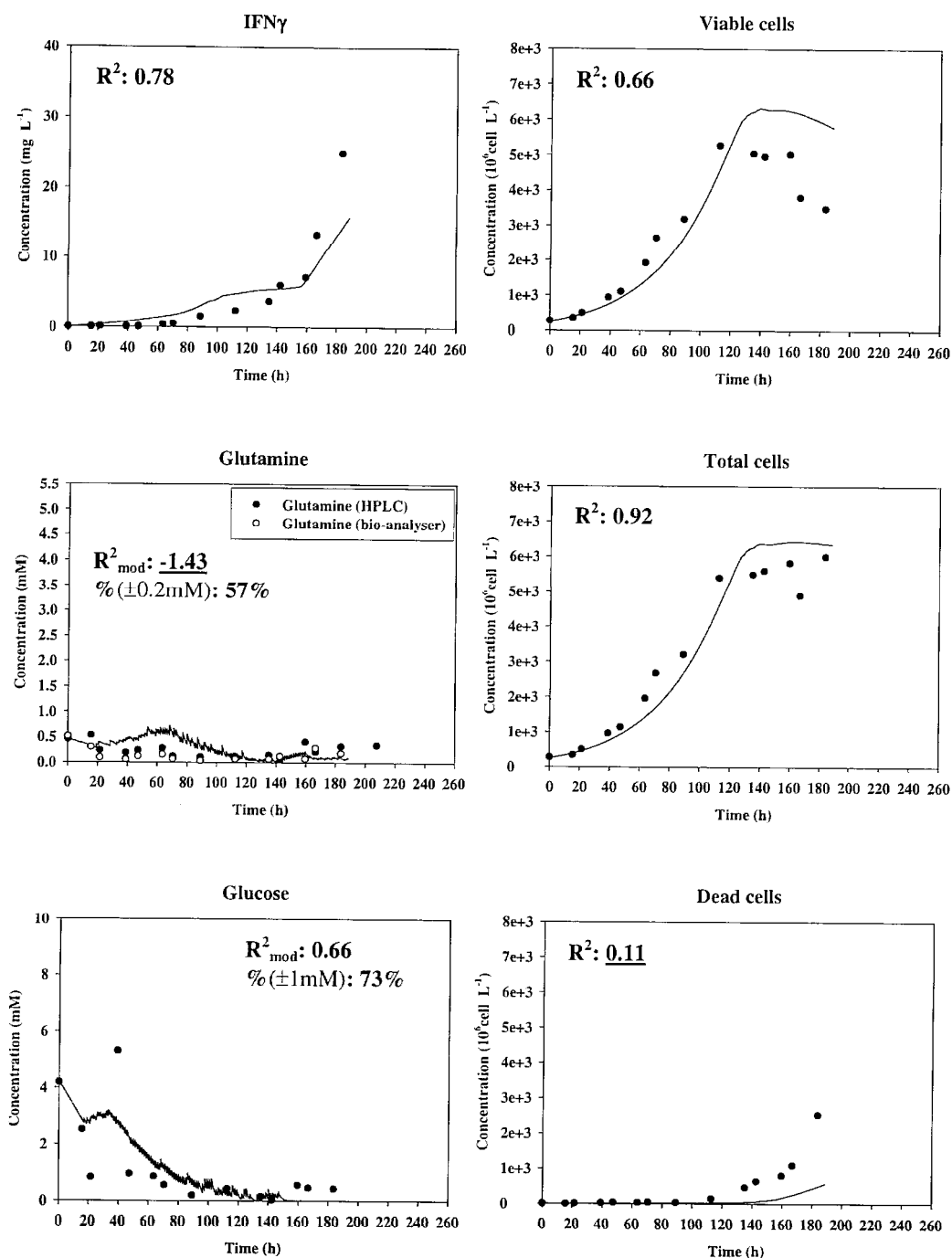


Figure 5.23a: Simulation of IFN γ , glutamine, glucose, and cell concentrations of CHO-IFN γ fed-batch culture with **glutamine set-point at 0.3mM** and **glucose set-point at 0.7mM** and comparison with corresponding experiment data. R^2_{mod} values < 0.40 and '% in $\pm 0.2\text{mM}$ ' values < 50% are underlined.

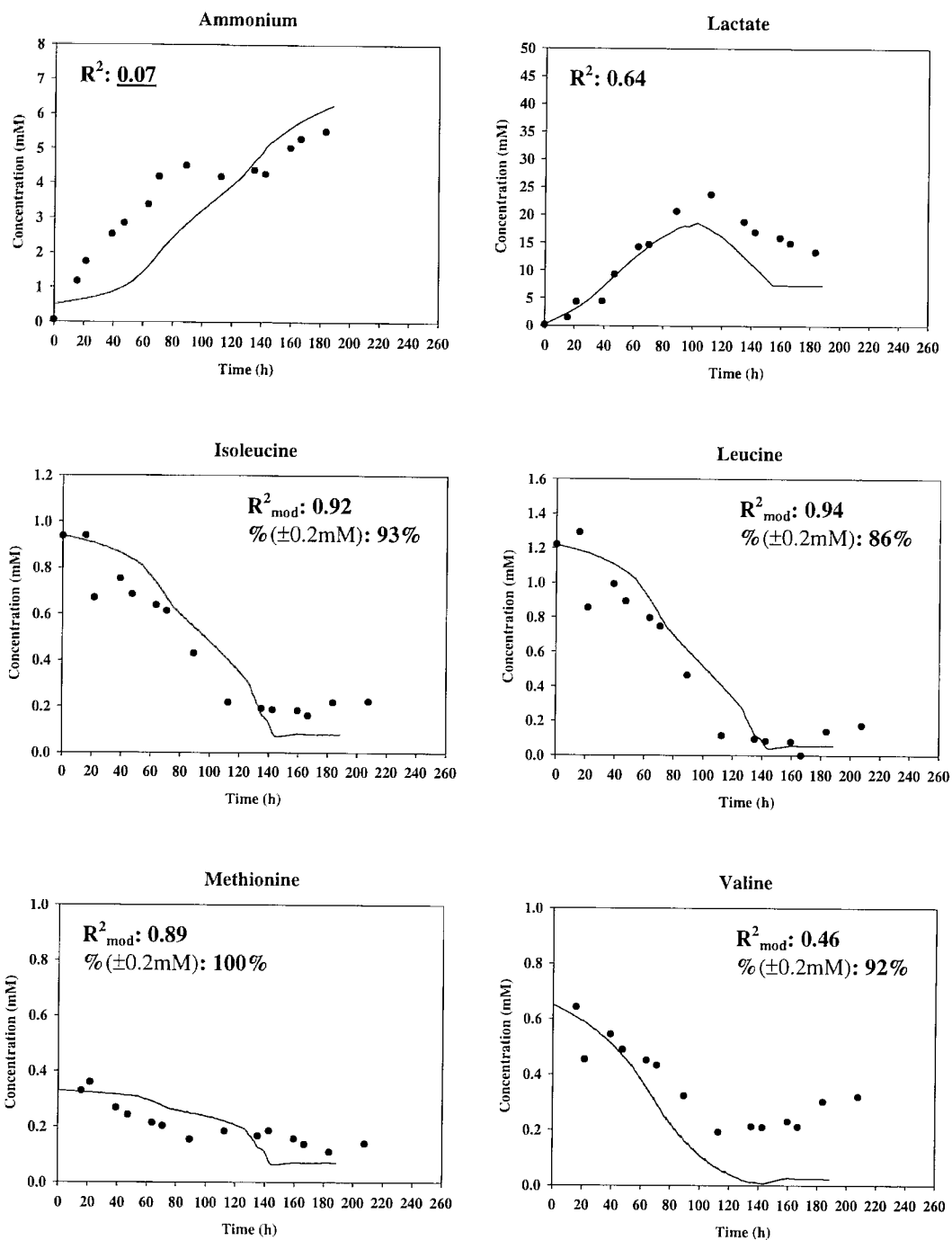


Figure 5.23b: Simulation of ammonium, lactate, isoleucine, leucine, methionine, and valine concentrations of CHO-IFN γ fed-batch culture with **glutamine set-point at 0.3mM and glucose set-point at 0.7mM** and comparison with corresponding experiment data. R^2 (or R^2_{mod}) values < 0.40 and ‘% in $\pm 0.2\text{mM}$ ’ values $< 50\%$ are underlined. (Refer to text and Appendix 6 for discussion of initial concentration of ammonium and amino acids respectively.)

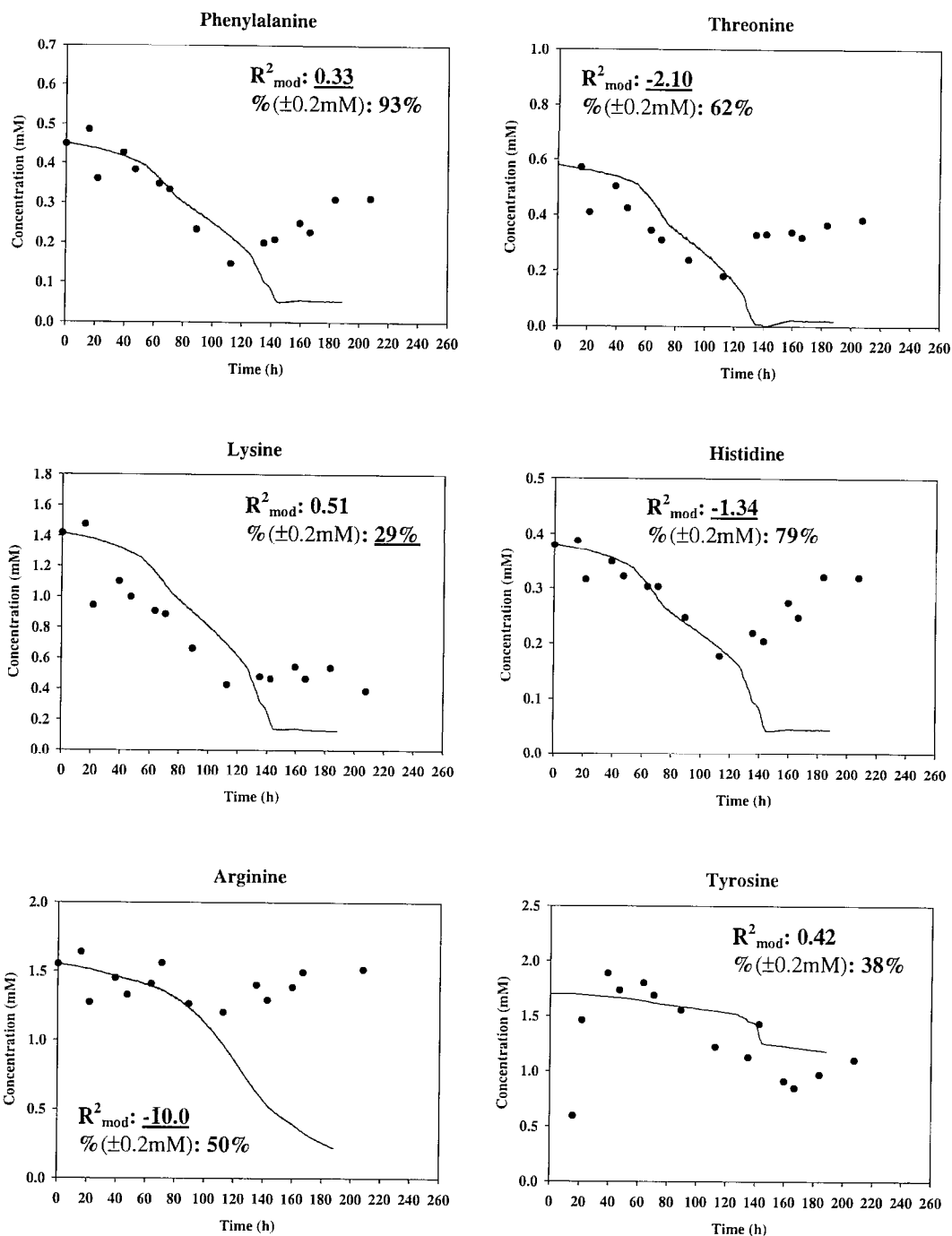


Figure 5.23c: Simulation of phenylalanine, threonine, lysine, histidine, arginine, and tyrosine concentrations of CHO-IFN γ fed-batch culture with **glutamine set-point at 0.3mM and glucose set-point at 0.7mM** and comparison with corresponding experiment data. R^2_{mod} values < 0.40 and '% in $\pm 0.2\text{mM}$ ' values < 50% are underlined. (Refer to Appendix 6 for discussion of initial concentration of amino acids.)

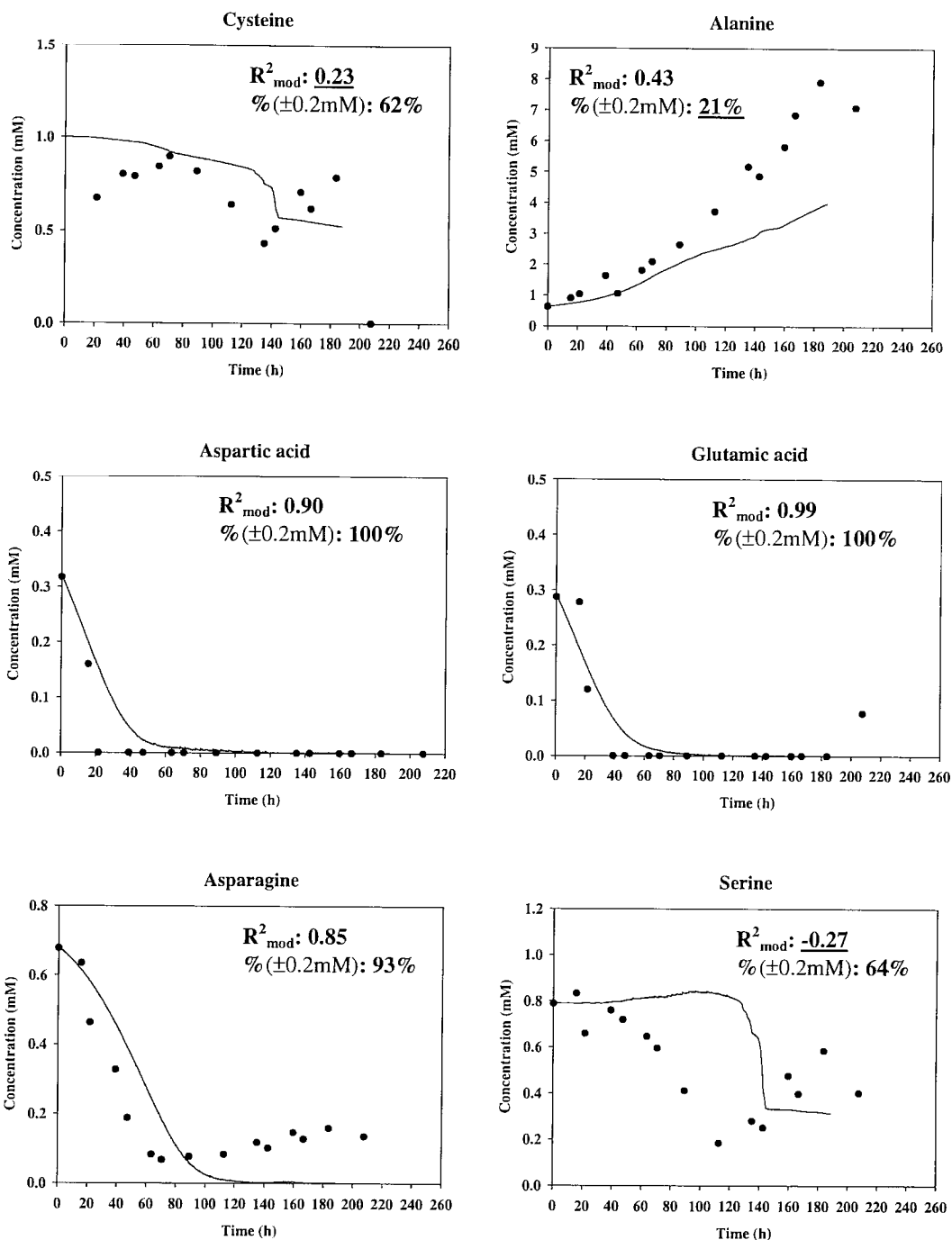


Figure 5.23d: Simulation of cysteine, alanine, aspartic acid, glutamic acid, asparagine, and serine concentrations of CHO-IFN γ fed-batch culture with **glutamine set-point at 0.3mM and glucose set-point at 0.7mM** and comparison with corresponding experiment data. R^2_{mod} values < 0.40 and '% in $\pm 0.2\text{mM}$ ' values < 50% are underlined. (Refer to Appendix 6 for discussion of initial concentration of amino acids.)

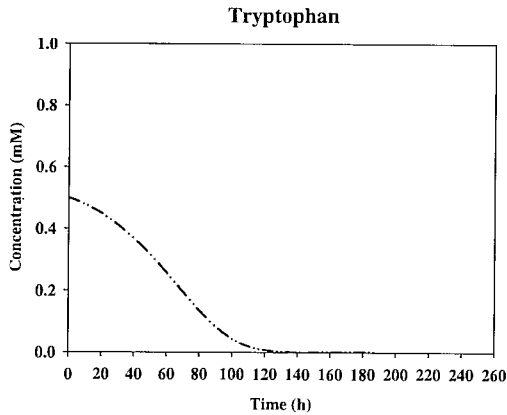
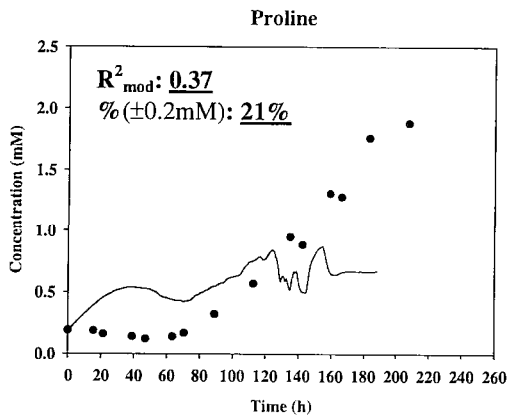
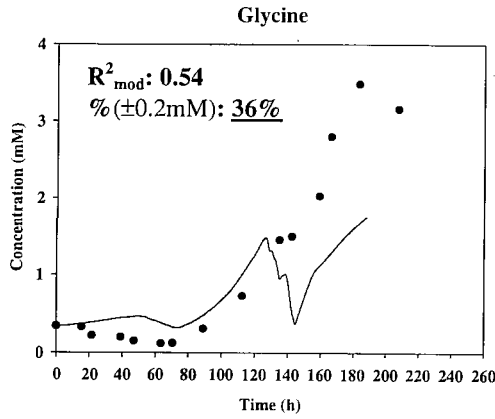


Figure 5.23e: Simulation of glycine, proline, and tryptophan concentrations of CHO-IFN γ fed-batch culture with **glutamine set-point at 0.3mM** and **glucose set-point at 0.7mM** and comparison with corresponding experiment data. Tryptophan data was not available due to problems with HPLC analysis (an initial concentration of 0.5mM was used which was an average among other amino acids in fed-batch cultures). R^2_{mod} values < 0.40 and ‘% in $\pm 0.2\text{mM}$ ’ values < 50% are underlined.

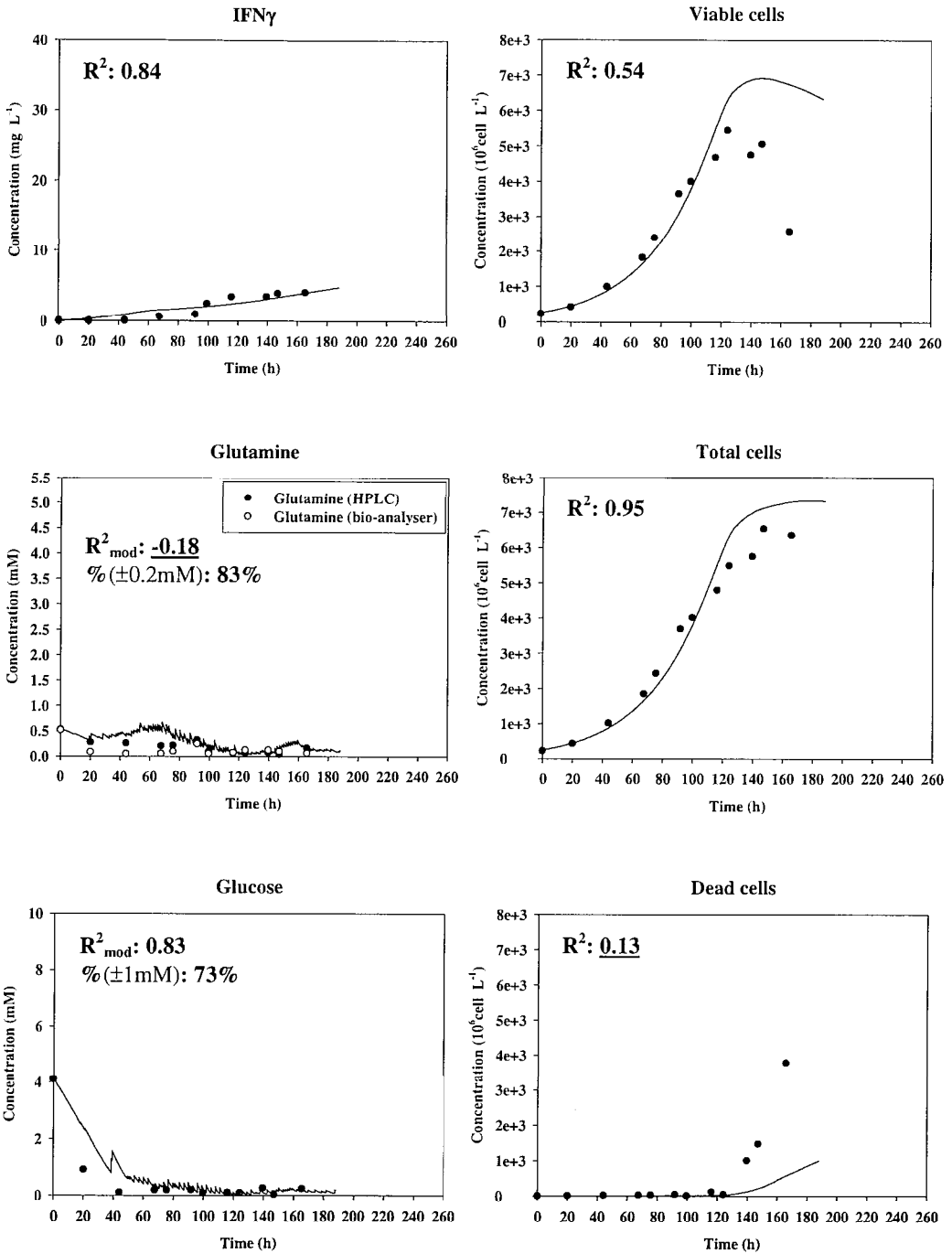


Figure 5.24a: Simulation of IFN γ , glutamine, glucose, and cell concentrations of CHO-IFN γ fed-batch culture with **glutamine set-point at 0.3mM** and **glucose set-point at 0.35mM** and comparison with corresponding experiment data. R^2 (or R^2_{mod}) values < 0.40 and ‘% in $\pm 0.2\text{mM}$ ’ (or $\pm 1\text{mM}$ for glucose) values $< 50\%$ are underlined.

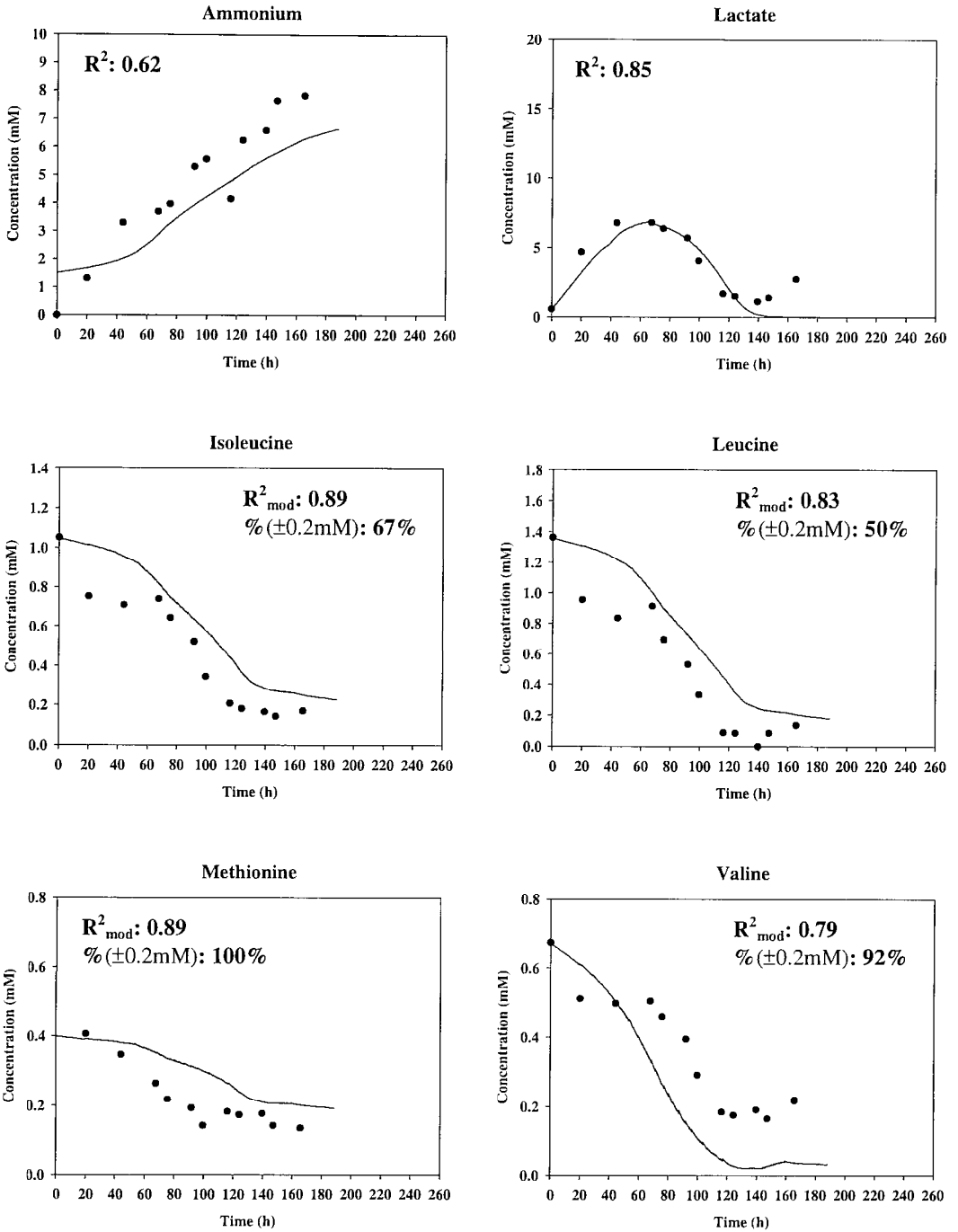


Figure 5.24b: Simulation of ammonium, lactate, isoleucine, leucine, methionine, and valine concentrations of CHO-IFN γ fed-batch culture with **glutamine set-point at 0.3mM and glucose set-point at 0.35mM** and comparison with corresponding experiment data. R^2 (or R^2_{mod}) values < 0.40 and '% in $\pm 0.2\text{mM}$ ' (or $\pm 1\text{mM}$ for glucose) values < 50% are underlined. (Refer to text and Appendix 6 for discussion of initial concentration of ammonium and amino acids respectively.)

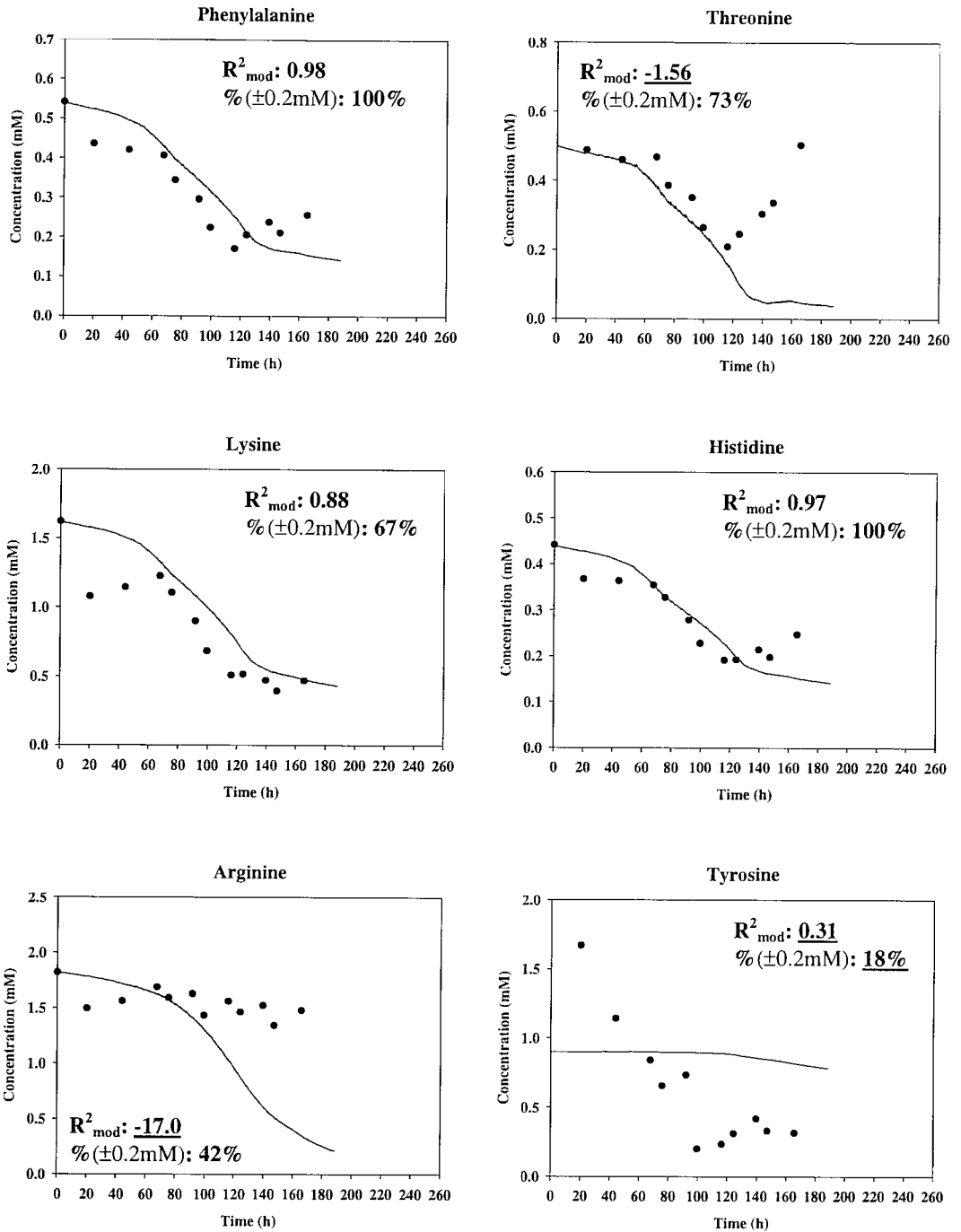


Figure 5.24c: Simulation of phenylalanine, threonine, lysine, histidine, arginine, and tyrosine concentrations of CHO-IFN γ fed-batch culture with **glutamine set-point at 0.3mM and glucose set-point at 0.35mM** and comparison with corresponding experiment data. R^2_{mod} values < 0.40 and ‘% in $\pm 0.2\text{mM}$ ’ values < 50% are underlined. (Refer to Appendix 6 for discussion of initial concentration of amino acids.)

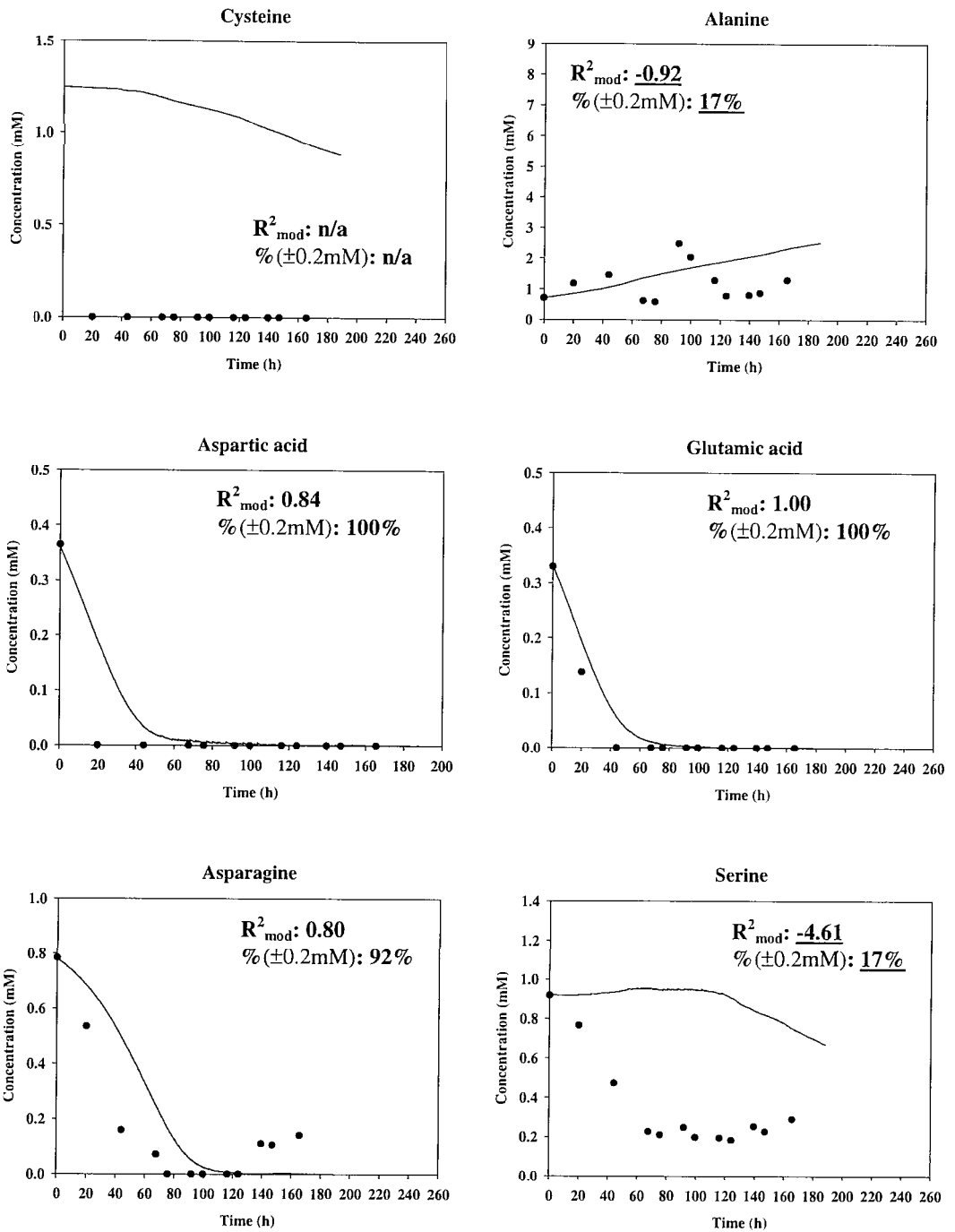


Figure 5.24d: Simulation of cysteine, alanine, aspartic acid, glutamic acid, asparagine, and serine concentrations of CHO-IFN γ fed-batch culture with **glutamine set-point at 0.3mM** and **glucose set-point at 0.35mM** and comparison with corresponding experiment data. R^2_{mod} values < 0.40 and $\% (\pm 0.2mM)$ values < 50% are underlined. (Refer to Appendix 6 for discussion of initial concentration of amino acids.)

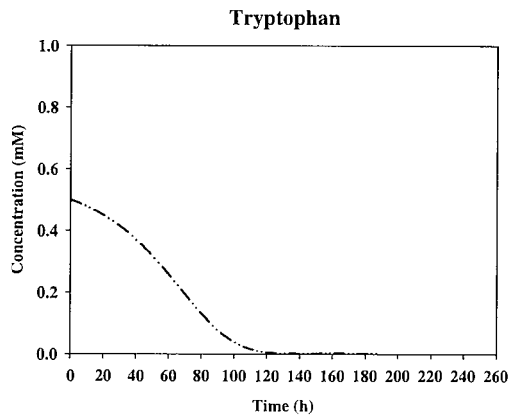
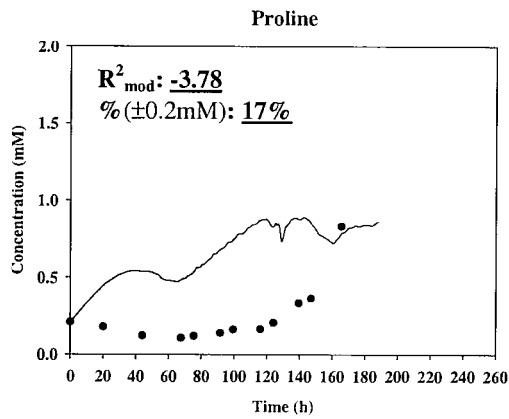
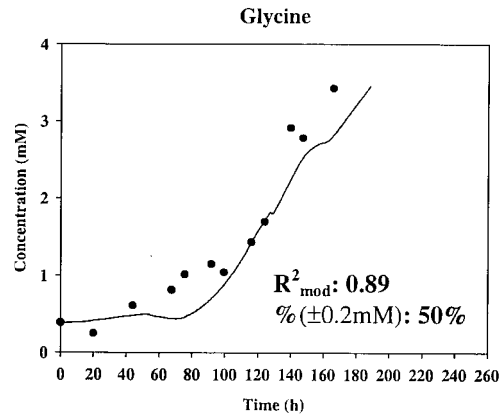
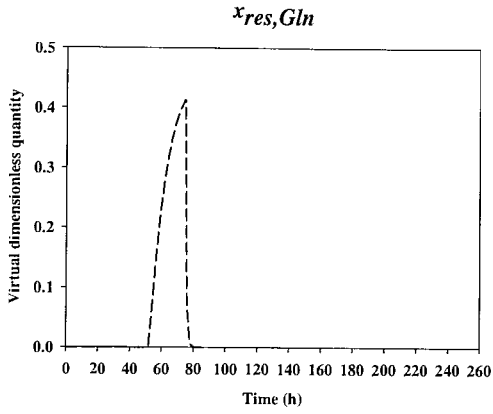
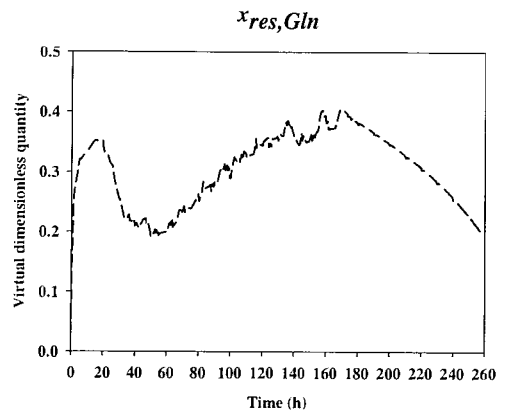


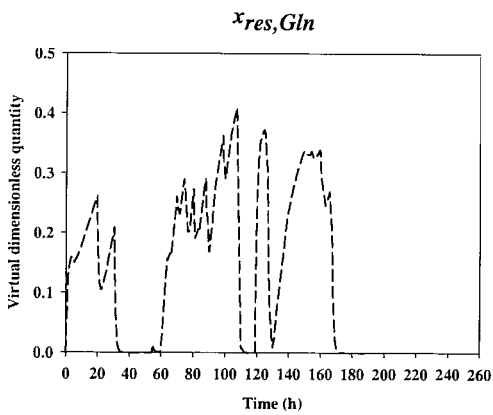
Figure 5.24e: Simulation of glycine, proline, and tryptophan concentrations of CHO-IFN γ fed-batch culture with **glutamine set-point at 0.3mM and glucose set-point at 0.35mM** and comparison with corresponding experiment data. Tryptophan data was not available due to problems with HPLC analysis (an initial concentration of 0.5mM was used which was an average among other amino acids in fed-batch cultures). R^2_{mod} values < 0.40 and ‘% in $\pm 0.2\text{mM}$ ’ values $< 50\%$ are underlined.



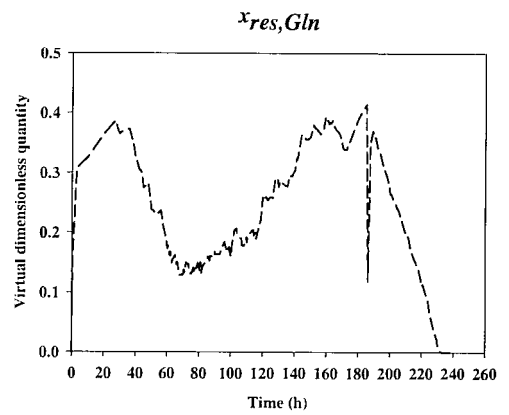
(i) Batch culture



(iii) Fed-batch culture with glutamine set-point at 0.3mM (1st experiment)

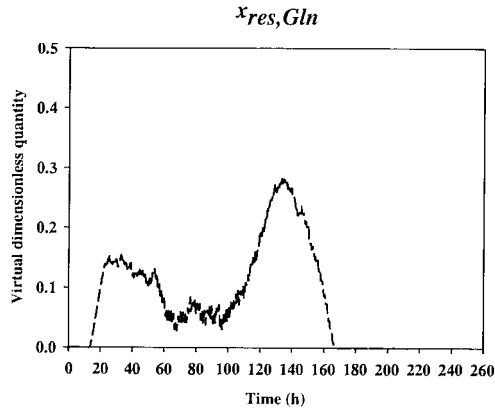


(ii) Fed-batch culture with glutamine set-point at 0.1mM

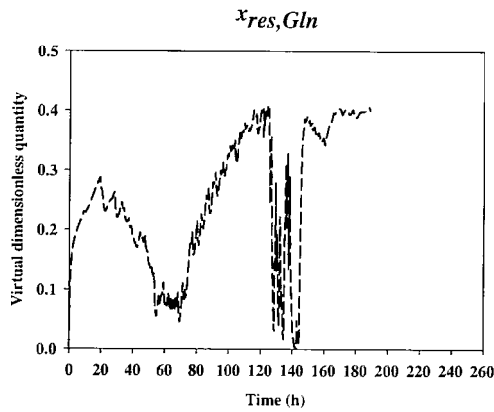


(iv) Fed-batch culture with glutamine set-point at 0.3mM (2nd experiment)

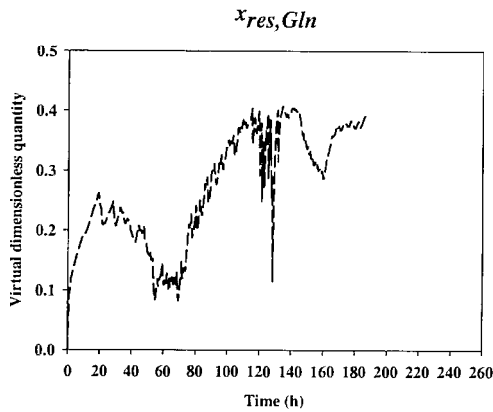
Figure 5.25(i)-(iv): Time-profiles of the hypothetical response variable for glutamine concentration ($x_{res,Gln}$) for (i) Batch, (ii) '0.1mM Fed-batch', (iii) '1st 0.3mM Fed-batch', and (iv) '2nd 0.3mM Fed-batch' cell cultures. (Notations can be found in Section 5.3.2)



(v) Fed-batch culture with glutamine set-point at 0.5mM

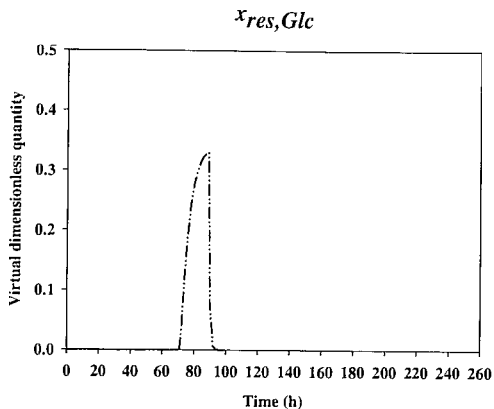


(vi) Fed-batch culture with glutamine set-point at 0.3mM and glucose set-point at 0.7mM

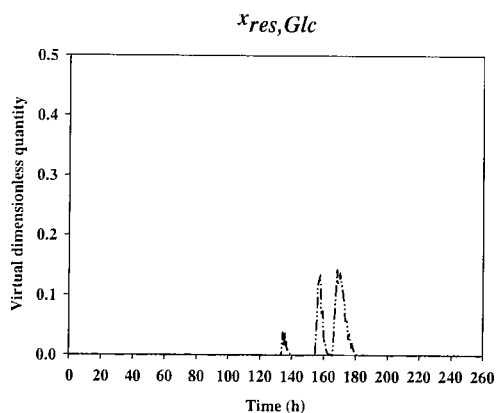


(vii) Fed-batch culture with glutamine set-point at 0.3mM and glucose set-point at 0.35mM

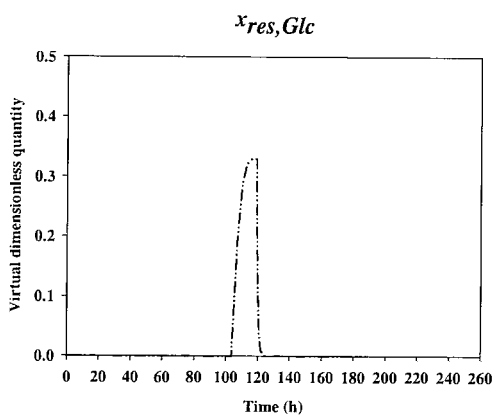
Figure 5.25(v)-(vii): Time-profiles of the hypothetical response variable for glutamine concentration ($x_{res,Gln}$) for (v) '0.5mM Fed-batch', (vi) '0.3,0.7mM Fed-batch', and (vii) '0.3,0.35mM Fed-batch' cell cultures. (Notations can be found in Section 5.3.2)



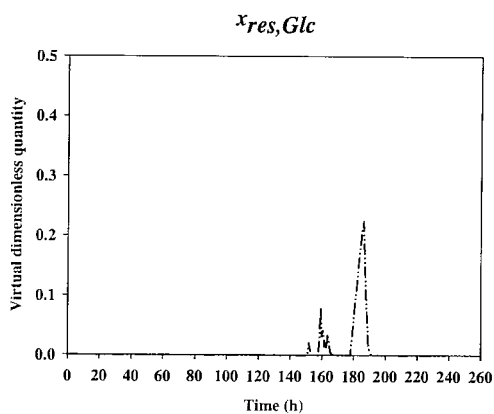
(i) Batch culture



(iii) Fed-batch culture with glutamine set-point at 0.3mM (1st experiment)

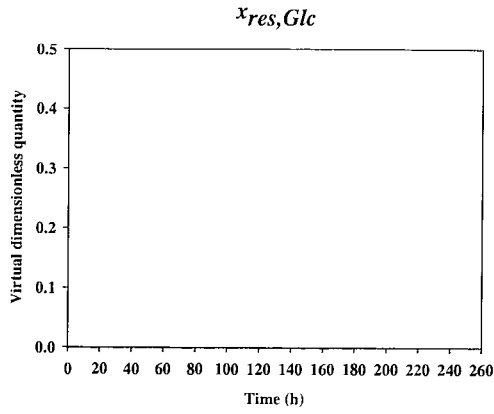


(ii) Fed-batch culture with glutamine set-point at 0.1mM

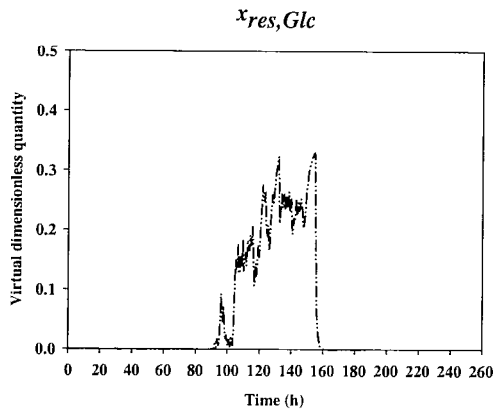


(iv) Fed-batch culture with glutamine set-point at 0.3mM (2nd experiment)

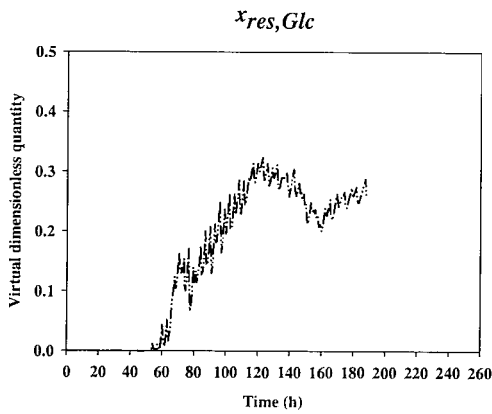
Figure 5.26(i)-(iv): Time-profiles of the hypothetical response variable for glucose concentration ($x_{res, Glc}$) for (i) Batch, (ii) '0.1mM Fed-batch', (iii) '1st 0.3mM Fed-batch', and (iv) '2nd 0.3mM Fed-batch' cell cultures. (Notations can be found in Section 5.3.2)



(v) Fed-batch culture with glutamine set-point at 0.5mM



(vi) Fed-batch culture with glutamine set-point at 0.3mM and glucose set-point at 0.7mM



(vii) Fed-batch culture with glutamine set-point at 0.3mM and glucose set-point at 0.35mM

Figure 5.26(v)-(vii): Time-profiles of the hypothetical response variable for glucose concentration ($x_{res, Glc}$) for (v) ‘0.5mM Fed-batch’, (vi) ‘0.3,0.7mM Fed-batch’, and (vii) ‘0.3,0.35mM Fed-batch’ cell cultures. (Notations can be found in Section 5.3.2)

Chapter 6

— Optimisation of the Nonlinear CHO Model with Secondary-binary Variables

In Chapter 5, a strategy was presented for estimation of parameter values of the complex CHO cell model that involved 192 parameters and 29 ordinary differential equations. With the selected parameter values, the model could then be subjected to model-based optimisation of the dynamic system.

6.1 Dynamic Optimisation Methods

The topic of dynamic optimisation encompasses all systems in which the variable of interest is time dependent and the optimisation involves transient state. The focus of this chapter is non-linear dynamic biological systems. Thus, only dynamic optimisation methods applicable to non-linear models are discussed. In the following sections, several popular dynamic optimisation approaches are introduced. The incorporation of integer variables in dynamic optimisation is briefly presented as mixed-integer dynamic optimisation (MIDO) was applied in Chapter 3 to optimise a simple hybridoma cell culture model. All the dynamic optimisations carried out in this work were done in gPROMS (Process Systems Enterprise Ltd., 2008). Thus, the dynamic optimisation algorithms available in gPROMS are also discussed.

6.1.1 Common Approaches for Continuous Dynamic Optimisation

There are numerous methods being developed in the literature to solve dynamic optimisation problems. Generally these methods can be grouped into two main categories: variational approach and variable discretisation.

The variational approach (also known as indirect method) involves finding a solution of a classical necessary conditions for optimality obtained from the Pontryagin's maximum principle (Cervantes and Biegler 1999; Schlegel et al., 2005) which is quoted below from Pontryagin et al. (1962) and Wolfram MathWorld (2008):

Let $u(t)$, $t_0 \leq t \leq t_f$, be an admissible control such that the corresponding trajectory $\mathbf{x}(t)$ which begins at the point \mathbf{x}_0 at the time t_0 passes, at some time t_f , through a point on the line Π^* . In order that $u(t)$ and $\mathbf{x}(t)$ be optimal it is necessary that there exist a nonzero continuous vector function $\boldsymbol{\psi}(t) = (\psi_0(t), \psi_1(t), \dots, \psi_n(t))$ corresponding to $u(t)$ and $\mathbf{x}(t)$, such that:

(1) For every t , $t_0 \leq t \leq t_f$, the function $H(\boldsymbol{\psi}(t), x(t), u)$ of the variable $u \in U$ attains its maximum at the point $u = u(t)$:

$$H(\boldsymbol{\psi}(t), x(t), u(t)) = \max_{u \in U} H(\boldsymbol{\psi}(t), x(t), u)$$

(2) At the terminal time t_f the relations $\psi_0(t_f) \leq 0$ and $H(\boldsymbol{\psi}(t_f), x(t_f), u(t_f)) = 0$ are satisfied.

*Line Π : In a vector space \mathbf{X} that contains state variable $\mathbf{x}(t)$, let Π be a line in \mathbf{X} passing through the point $\mathbf{x} = (0, x_f)$ and parallel to the axis made up of all the points (ξ, x_f) where ξ is arbitrary.

The differential algebraic equations formulated from the optimality conditions can be solved with different methods: single shooting, multiple shooting, collocation on finite elements and finite differences etc. (Cervantes and Biegler 1999). But it can be difficult to find a solution when there are inequality constraints and other complexities (Banga et al., 1997; Cervantes and Biegler 1999; Biegler et al., 2002). The Single shooting method requires input of initial conditions for forward numerical integration of the DAE system to obtain time profiles of the state variables (Schlegel et al., 2005). The term 'single-shooting' arises from the single integration of the dynamic model over the entire horizon. The discretisation of the control profiles is often piecewise polynomial approximation (Schlegel et al., 2005). Multiple shooting and collocation methods are also used to explicitly discretise the state variables in some of the discretisation approaches (Cervantes and Biegler 1999) so they are discussed later on in this section.

The discretisation approach can be further classified into partial discretisation and full discretisation. Sometimes the partial/full discretisation approaches are categorised according to the solution strategy: single shooting, multiple shooting, and collocation (Schlegel et al., 2005) instead of the treatment of the variables. Partial discretisation

only discretise the control profiles. It is used in dynamic programming and sequential approach (Cervantes and Biegler 1999). Dynamic programming is a mathematical theory of multi-stage decision processes for solving problems exhibiting the properties of *overlapping subproblems* (problems that can be broken down into smaller parts which are reused multiple times) and *optimal substructure* (problems of which the globally optimal solution can be constructed from locally optimal solutions of subproblems) (Bellman, 1957; Wikipedia, 2008). Some literature would classify dynamic programming separately from sequential approach due to their different solution strategies (Barton et al., 1998). Iterative dynamic programming (IDP) is often used for the solution of dynamic optimisation problems (Luus 1993a,b,c; Dadebo and McAuley 1995; Cervantes and Biegler 1999). There is a high dimensionality problem associated with the IDP algorithm though it is useful to cross-check the results of small problems when the global optimum is unknown (Cervantes and Biegler 1999). Stochastic search algorithm has also been used to find the optimal solution in non-linear optimisation (Banga et al., 1997; Rodriguez-Acosta, et al., 1999).

Sequential approach is also known as control parameterisation method (Sargent and Sullivan, 1978; Kraft, 1985). In sequential approach, only the control variables are discretised. The control variables are represented by piecewise polynomials and optimisation is done with respect to the polynomial coefficients (Biegler et al., 2002; Barton et al., 1998). The differential algebraic equation (DAE) system is solved using a DAE solver, e.g. single shooting method (Schlegel et al., 2005), in every iteration and the optimal control parameters are found using a nonlinear programming (NLP) solver (Cervantes and Biegler 1999; Vassiliadis et al., 1994a,b).

Full discretisation approach discretises both the state and control profiles which generate a large scale nonlinear programming (NLP) problem. The resulting large-scale NLP is often solved using successive quadratic programming (SQP) algorithm (Cervantes and Biegler 1998; Cervantes and Biegler 1999; Biegler et al., 2002) which uses Newton's method for unconstrained minimisation. Full discretisation is used in simultaneous approach. Both sequential approach and simultaneous approach are sometimes called direct methods as the discretisations directly transform the infinite dimensional dynamic optimisation problem into a finite dimensional nonlinear program (NLP) (Barton et al., 1998). In the simultaneous approach, the DAE system is only solved at the optimum point instead of every iteration in the sequential approach. There are two types of SQP methods to solve the NLP in simultaneous approach: full space SQP for problems with many degrees of freedom and reduced space SQP for problems when the number of state variables is much larger than number of control variables (Cervantes and Biegler 1999; Cervantes and Biegler 2000).

There are mainly two methods to discretise the state variables explicitly in the simultaneous approach: multiple shooting and collocation. Multiple shooting method is similar to single shooting method except the time horizon in multiple shooting is divided into subintervals and the DAE system is integrated separately in each subinterval so the state variables are also guessed at several intermediate time points (Cervantes and Biegler 1999; Biegler et al., 2002; Leineweber et al., 2003a,b). In collocation method, spline functions (piecewise polynomial curves) are used to approximate the state and control variables (Neuman and Sen, 1973; Birkhoff and de Boor, 1965; Ahlberg et al., 1967). The continuous time problem is converted into an NLP by approximating the continuous profiles as a family of polynomials on finite elements and the coefficients of these polynomials and element sizes become decision variables in a large-scale NLP. (Tsang et al., 1975; Biegler 1984; Cuthrell and Biegler 1987; Tieu et al., 1995; Barton et al., 1998; Cervantes and Biegler 1999).

The dynamic optimisation approaches described above are to provide a general idea of some of the many different strategies that have been used to solve non-linear dynamic optimisation problems. The aim of this work is to apply and adapt one of these existing algorithms to optimise a biological cell culture. Thus, next section will focus on the optimisation software used for this study and the available algorithms.

6.1.2 Dynamic Optimisation with/without Integer Variables in *gPROMS*

Mixed-Integer Dynamic Optimisation

The presence of binary degrees of freedom in an otherwise continuous dynamic optimisation process introduces more challenges to the optimisation strategy. A detailed review of existing solution approaches for mixed-integer dynamic optimisation (MIDO) can be found in Bansal et al. (2003). Below is a brief description of methods used to solve MIDO problems in the literature including the one used in *gPROMS*.

The binary variables can be approximated by variable space partitioning or functions which remove the discrete property of the optimisation problem (Samsatli et al., 1998). For example, the binary variables can be treated as switching parameters which take discrete values in different variable regions defined by inequality constraints (Bhatia and Biegler, 1997). Alternatively, smooth approximation functions can be applied to represent the binary variable, y , with a function in terms of continuous variable x .

E.g. in the following function,

$$y = \frac{1}{2}[\tanh((\beta \cdot x) + 1)]$$

the binary variable is defined to be 1 for any positive values of x except when $x = 0$. But the switching parameter method could result in large model size; and the smooth approximation method does not always lead to integral values of the binary variable (Samsatli et al., 1998; Bansal et al., 2003).

A Branch and Bound framework was proposed by Androulakis (2000) which defines families of solution algorithms that operate within a search tree and perform an enumeration of the alternatives without examining all the 0/1 combinations of the binary variables. This technique typically involves solving a large number of dynamic optimisation problems, making its application limited to small MIDO problems (Bansal et al., 2003).

The MIDO problem can also be handled using generalised Benders decomposition (GBD) where it is decomposed into a series of primal and master problems that the master problems decide new binary configurations for subsequent primal problems where the binary variables are fixed. The dynamic optimisation in the primal problems can be solved with reduced space approach to give an upper bound of the solution while the lower bound is obtained from the master problems (Mohideen et al., 1997a; Sharif et al., 1998; Schweiger and Floudas, 1998; Bansal et al., 2002). Bansal et al. (2003) developed a new algorithm based on GBD and outer approximation (OA)/ equality relaxation (EA) for solving general MIDO problem and can also handle time dependent binary variables. The original binary variables are relaxed but are still forced to take integral values by an addition of new binary variables. It shares a limitation of most GBD methods that when the optimisation problem is non-convex or highly non-linear, the algorithm may exclude potentially feasible choices of binary variables from the solution set (Bansal et al., 2003). Many other numerical solution approaches for MIDO in the literature are based on decomposition principles, but differ in the treatment of the differential algebraic equation system (Bansal et al., 2003; Barton 1998; Floudas, 1995; Chachuat et al., 2005). The method by Bansal et al. (2003) is the basis for the mixed-integer non-linear programming (MINLP) solver in *gPROMS* and is further discussed in next section.

***gPROMS* Optimisation Algorithms**

The dynamic optimisation was carried out in *gPROMS* version 3.0.3 (Process Systems Enterprise Ltd., 2008). There are two mathematical solvers for dynamic optimisation in *gPROMS*: CVP_SS and CVP_MS. Both solvers are based on control vector parameterisation approach which discretises the time-varying control variables and

assumes that they are piecewise constant or piecewise linear functions of time over a specified number of control intervals (Process Systems Enterprise Ltd., 2004). The CVP_SS solver uses a single-shooting method which requires initial guesses of the control variables. The CVP_MS solver implements a multiple-shooting method which requires both initial guesses of the control variables and the values of the differential variables at the start of each subsequent control interval. The choice between the CVP_SS and CVP_MS solvers for any dynamic optimisation problem depends primarily on the number of optimisation decision parameters that the algorithm has to deal with in computing the sensitivities of the model variables. CVP_SS is more suited for problems with large number of state variables but relatively few time-varying control variables and control intervals. On the other hand, CVP_MS is more appropriate for the opposite situation of CVP_SS (Process Systems Enterprise Ltd., 2004). CVP_SS was chosen for the dynamic optimisation of both the cell-cycle model in Chapter 3 and the CHO-IFN γ cell culture model in this chapter due to the relatively larger number of state variables than time-varying control variables.

The nonlinear programming problems resulting from the dynamic optimisation solvers are solved with SRQPD by default which is a sequential quadratic programming (SQP) method. When mixed-integer control variables are involved, such as in the cell-cycle model dynamic optimisation in Chapter 3, the standard mixed-integer non-linear programming (MINLP) solver is OAERAP which is similar to the algorithm developed by Bansal et al. (2003). The OAERAP solver employs an outer approximation (OA) algorithm to solve the MINLP. Any end-point equality constraints would be handled by an equality relaxation (ER) scheme. As most engineering problems are non-convex and highly non-linear, an augmented penalty (AP) strategy is also involved to increase the chance of obtaining the global solution.

In next section, the dynamic optimisation problem for CHO-IFN γ cell culture is defined and the initial guesses of the time-varying control variables are explained. The optimisation was solved with CVP_SS and the NLP was solved using SRQPD.

6.2 Model-Based Optimisation of CHO-IFN γ Culture

6.2.1 Formulation of the Optimisation Problem

In Chapter 3, dynamic optimisation with binary variable as an explicit degree of freedom has been demonstrated for simultaneous optimisation of nutrient supplementation time-profile, $F_{in}(t)$, and cell-cycle arresting time, t_a for a simple hybridoma cell culture model. In that situation, mixed-integer dynamic optimisation (MIDO) algorithm was used because the binary variable was independent of all other variables. However, for the CHO-IFN γ non-linear dynamic model with secondary-binary variables dependent on glutamine and glucose concentrations, the binary variables were not freely adjustable. The optimisation of such model was done via dynamic optimisation with inequality constraints confining the concentration of glutamine and glucose in either the active or inactive domains of the secondary-binary variables if necessary.

The dynamic optimisation objective was defined in Equation 6.1 which was to maximise the yield of IFN γ at the end-point, t_f , of the fed-batch suspension CHO culture. The degrees of freedom to be optimised were the time profiles of a glucose feed stream, $F_{in_glc}(t)$, and a glutamine-rich feed stream, $F_{in}(t)$. Both variables are continuous and could take any non-negative real values. The patterns of $F_{in_glc}(t)$ and $F_{in}(t)$ were decided to be pulses with constant time intervals, Δt , due to the small volume of concentrated nutrients required at any particular time. Though theoretically a continuous feeding pattern is also possible, in this case the volumetric flow rate involved would be extremely small which is beyond practical consideration. The choice of Δt should be less than the doubling time of the cells which is roughly a day for mammalian cultures and larger than the time required for sampling which is several minutes. It was tested computationally that when Δt was reduced from 2 h to 1 h, the optimised culture had smoother time-profiles of nutrient concentrations but there was no significant increase in IFN γ yield. Thus, Δt was fixed at 1 h for all optimisations. The duration of each feed stream pulse was assumed to be 0.001 h (3.6 s). Any slight deviation of the pulse duration in reality would not affect the product yield.

$$\text{Optimisation objective: } \max_{u(t)} IFN(t_f) \quad (6.1)$$

$$\begin{aligned} \text{subject to } \quad & \dot{x}_i(t) = f_i(x_m(t), u_j(t), t) & i = 1..29, j = 1..2, m \in [1,29] \\ & x_i(0) = x_{i,0} \\ & f_k(x_l(t), u_j(t), t) = 0 & k \in K \\ & g_l(x_m(t), u_j(t), t) \leq 0 & l \in L \end{aligned}$$

Control variables:

$$u_1(t) = F_{in_glc}(t) \quad , F_{in_glc} \geq 0 \quad (6.2)$$

$$u_2(t) = F_{in}(t) \quad , F_{in} \geq 0 \quad (6.3)$$

Inequality constraints:

$$V \leq 1.5 \cdot V_0 \quad (6.4)$$

$$\text{Viability} \geq 50\% \quad (6.5)$$

$$F_{in_glc} \leq 10 \text{ L h}^{-1} \quad (6.6)$$

$$F_{in} \leq 10 \text{ L h}^{-1} \quad (6.7)$$

$$Glc \leq 6 \text{ mM} \quad (6.8)$$

$$Gln \leq 0.65 \text{ mM} \quad (6.9)$$

The objective function above was subjected to all the differential equations, $\dot{x}_i(t)$, algebraic equations, f_k , and inequality constraints, g_l . The inequality constraints were based on the limit of the reactor volume (Equation 6.4), product degradation at low viability (Equation 6.5), amount of feed streams required by experience (Equation 6.6 – 6.7), concern of high lactate formation at high glucose concentration (Equation 6.8), and a need to restrain glutamine concentration within the active domain of secondary-binary variable y_2 (Equation 6.9). It was found that when the upper bound of glutamine concentration was set to include both active and inactive domains of y_2 (Equation 6.11), the optimisation iteration would get stuck at the inactive domain, even though previous iterations in the active domain yielded a better optimum, and was not able to recover. But setting the upper bound of glucose concentration to include both active and inactive domains did not cause any problem to the dynamic optimisation.

Secondary-binary variables:

$$y_1 = \begin{cases} 0, & Glc \geq \tau_{Glc} \\ 1, & 0 < Glc < \tau_{Glc} \\ 0, & Glc = 0 \end{cases} \quad (6.10)$$

$$y_2 = \begin{cases} 0, & Gln \geq \tau_{Gln} \\ 1, & 0 < Gln < \tau_{Gln} \\ 0, & Gln = 0 \end{cases} \quad (6.11)$$

where y represents binary variables, Glc is glucose concentration, Gln is glutamine concentration, τ_{Glc} and τ_{Gln} are the threshold concentration of glucose and glutamine respectively between the active and inactive domains of y_1 and y_2 .

Fixed variables:

- (1) All initial conditions: fixed at the initial condition of one of the fed-batch experiments with 0.3mM glutamine level control (all fed-batch experiments have similar initial conditions).
- (2) Compositions of the feed streams: 100 mM glutamine in F_{in} , 40 g L⁻¹ (220 mM) glucose in F_{in_glc} .
- (3) Nutrient supplementation time interval: 1 h

Dynamic optimisation algorithm:

The optimisation was solved using control vector parameterisation approach with single-shooting method (CVP_SS). The control profiles were piecewise-constant. The nonlinear programming solver was a sequential quadratic programming method (SRQPD).

The dynamic optimisation results were sensitive to initial guesses of the control profiles. Thus, several different modes of initial conditions were considered: constant pulses, random pulses, and progressive pulses. For the last two modes, the cell culture time was divided into only three time periods for simplicity. A total of 100 initial conditions were used and their values are listed in Table 6.1.

Table 6.1: Initial guesses of control profiles of $F_{in}(t)$ and $F_{in_glc}(t)$ used in dynamic optimisation of fed-batch CHO-IFN γ cell culture.

Control Profiles	Mode	F_{in}^* (L h ⁻¹)			$F_{in_glc}^*$ (L h ⁻¹)		
		0-80h	81-160h	161-245h	0-80h	81-160h	161-245h
1	<i>Constant</i>	0.1			0.1		
2		0.3			0.1		
3		0.3			0.3		
4		0.5			0.5		
5		0.3			0.5		
6		0.3			0.2		
7		0.2			0.2		
8		0.4			0.4		
9		0.6			0.6		
10		0.5			0.05		
11		0.1			0.6		
12		0.05			0.05		
13		0.6			0.3		
14		0.7			0.7		
15		0.8			0.8		
16		0.5			0.8		
17		0.7			0.2		
18		1			1		
19		1			2		
20		2			3		
21		2			4		
22		3			3		
23		3			4		
24		4			5		
25		2			1		
26		3			1		
27		4			3		
28		4			2		
29		2			5		
30		4			4		
31		1			3		
32		2			2		
33		1			4		
34		3			5		
		0-80h	81-160h	161-245h	0-80h	81-160h	161-245h
35	<i>Random</i>	0.1	0.4	0.2	0.2	0.8	0.4
36		0.2	0.1	0.3	0.4	0.2	0.6
37		0.4	0.3	0.2	0.8	0.6	0.4
38		0.1	0.3	0.2	0.1	0.2	0.1
39		0.2	0.4	0.3	0.1	0.2	0.05
40		0.3	0.5	0.2	0.2	0.6	0.3
41		0.4	0.1	0.3	0.3	0.7	0.5
42		0.5	0.3	0.1	0.2	0.6	0.4
43		0.6	0.4	0.2	0.3	0.5	0.1
44		0.7	0.3	0.5	0.1	0.4	0.3
45		0.8	0.6	0.4	0.2	0.3	0.1
46		0.2	0.5	0.3	0.3	0.2	0.1
47		0.3	0.4	0.1	0.6	0.1	0.4
48		0.4	0.8	0.2	0.5	0.05	0.2
49		0.5	0.1	0.6	0.3	0.5	0.3
50		0.6	0.2	0.7	0.2	0.4	0.1
51		0.7	0.3	0.1	0.1	0.3	0.2
52		1	3	2	2	1	4
53		2	4	1	1	5	3
54		3	4	2	3	2	4
55		1	4	1	4	1	2
56		4	3	4	2	5	4
57		2	1	4	1	3	2
58		3	1	2	2	4	3
59		1	2	1	3	5	3

(continue)

Control Profiles	Mode	F_{in}^* (L h ⁻¹)			$F_{in_glc}^*$ (L h ⁻¹)		
60	Random (continue)	2	3	2	1	2	1
61		3	4	1	2	1	3
62		4	2	3	5	2	3
63		2	1	3	2	5	2
64		1	4	2	4	2	3
65		3	1	4	1	4	2
66		1	4	3	2	4	1
67		2	3	1	5	1	5
68		Progressive	0.1	0.2	0.3	0.2	0.4
69	0.2		0.3	0.4	0.4	0.6	0.8
70	0.3		0.4	0.5	0.5	0.6	0.7
71	0.4		0.5	0.6	0.1	0.2	0.3
72	0.5		0.6	0.7	0.2	0.3	0.4
73	0.6		0.7	0.8	0.3	0.4	0.5
74	0.7		0.8	0.9	0.4	0.5	0.6
75	0.1		0.3	0.5	0.5	0.7	0.9
76	0.2		0.4	0.6	0.6	0.7	0.8
77	0.3		0.5	0.7	0.7	0.8	0.9
78	0.4		0.6	0.8	0.1	0.4	0.7
79	0.5		0.7	0.9	0.2	0.5	0.8
80	0.1		0.4	0.7	0.3	0.6	0.9
81	0.2		0.5	0.8	0.1	0.6	0.7
82	0.3		0.6	0.9	0.2	0.7	0.8
83	0.2		0.4	0.8	0.1	0.8	0.9
84	0.3		0.7	0.9	0.2	0.3	0.7
85	1		2	3	3	4	5
86	2		3	4	1	2	3
87	1		2	4	2	3	4
88	2		2.5	3	1	3	5
89	2.5		3	3.5	2	4	5
90	3		3.5	4	1	2	4
91	1		1.5	2	1.5	2.5	3.5
92	1.5		2	2.5	2.5	3.5	4.5
93	1		2	2.5	1	2.5	4.5
94	1.5		3	3.5	3.5	4.5	5
95	2.5		3.5	4	1	1.5	2
96	1		2.5	4	2	2.5	3
97	1.5		2	3.5	3	3.5	4
98	1		3	3.5	1	3.5	5
99	1.5		2.5	3.5	1.5	4	5
100	2	3.5	4	4	4.5	5	

*The time-width of each pulse was made such that the height of each pulse in L h⁻¹ is equivalent to volume in ml.

6.2.2 Dynamic Optimisation Results and Discussion

The best dynamic optimisation result was simulated and the profiles of IFN γ , cell concentrations, glutamine, glucose, F_{in} , F_{in_glc} , ammonium, and lactate are shown in Figure 6.1 – 6.8. The result indicated a potential for the fed-batch culture to produce IFN γ at about 60 mg L⁻¹ at the end of the culture time and the viable cell concentration could reach 9 x 10⁶ cell ml⁻¹. Experiment results of the CHO-IFN γ fed-batch cultures can be found in Chapter 5. The highest IFN γ yield and viable cell concentration achieved in the fed-batch experiment was about 35 mg L⁻¹ and 6 x 10⁶ cell ml⁻¹ respectively. The higher product yield (Figure 6.1) and cell yield (Figure 6.2) in the optimised result was due to a low concentration of toxic ammonium and a better controlled concentration of glucose and glutamine in the cell culture. The lactate concentration in the optimised result (Figure 6.8) was within the same range of the fed-batch experiments which was 7 – 50 mM. The concentration of ammonium in the fed-batch experiments reached 6 – 8 mM, some of which was at 7 mM at 150 h, but in the optimisation result the ammonium level was 7 mM at 250 h (Figure 6.7). Most of the ammonium produced in the culture came from glutamine as it was the dominating amino acid in the medium. Thus, the ammonium time-profile was closely related to $F_{in}(t)$. In the fed-batch experiments, glucose concentration was mostly below 0.5 mM or above 3 mM. The optimised glucose profile stayed between 1 – 2.5 mM (Figure 6.4) which appeared to be a balance between too low or too high glucose concentrations. The glutamine levels in the fed-batch experiments were set at various values using a feed-back controller and it was concluded by Wong et al (2005) that 0.3 mM was the best concentration. The glutamine concentration in the computational optimisation result was similar in the range of 0.1 – 0.2 mM with a low level of ~0.1mM around the exponential growth phase (80 – 160 h) and then increased towards 0.2mM near the end of the cell culture time (Figure 6.3). The optimised time-profiles of the stream containing glutamine (F_{in}) and glucose (F_{in_glc}) gradually increased in the exponential growth phase and then decreased in the death phase of the cell culture (Figure 6.5 – 6.6). The time-profiles of the hypothetical response variables ($x_{res,Gln}$ and $x_{res,Glc}$) of the optimal solution are shown in Figure 6.9. The ‘low-glutamine’ response was activated throughout the whole fed-batch culture but the ‘low-glucose’ response was not activated at all which suggested that the negative effect of low glucose concentration on productivity is more significant than its positive effect on reducing lactate formation.

The result of the optimisation is affected by the estimated values of the model parameters. In Chapter 5, the relative significance of the parameters that were active in batch cultures was analysed using Global Sensitivity Analysis (GSA). In the next section, most of the parameters that are active and sensitive in either batch or fed-batch cultures were varied and their effects upon the optimisation of the time-profiles of $F_{in}(t)$ and $F_{in_glc}(t)$ were studied.

IFN γ

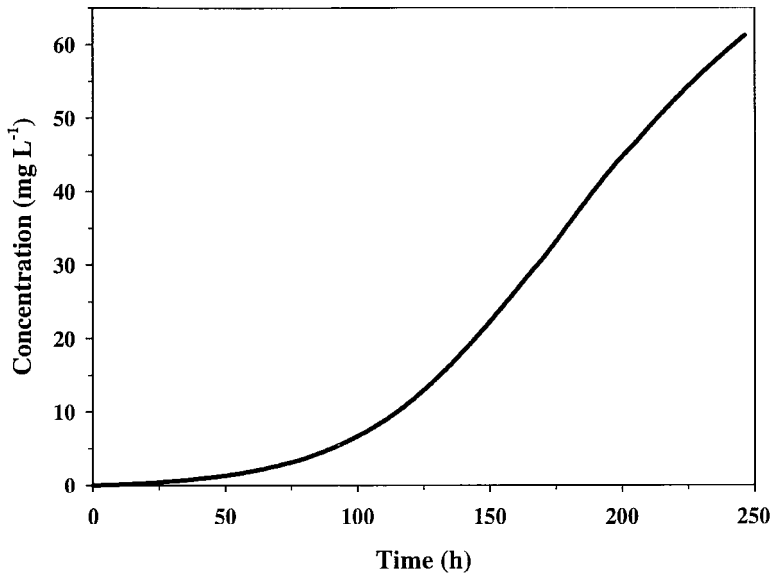


Figure 6.1: IFN γ concentration profile of the optimised fed-batch CHO-IFN γ cell culture.

Viable & Total cell

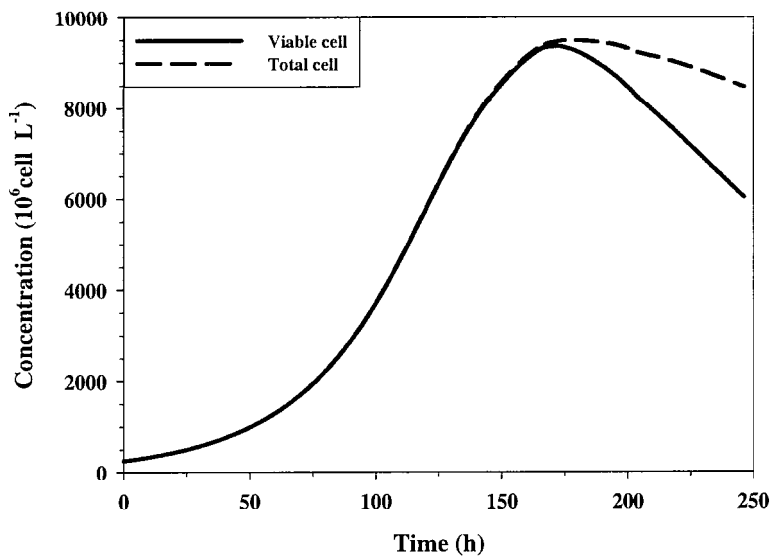


Figure 6.2: Viable and total cell concentration profiles of the optimised fed-batch CHO-IFN γ cell culture.

Glutamine

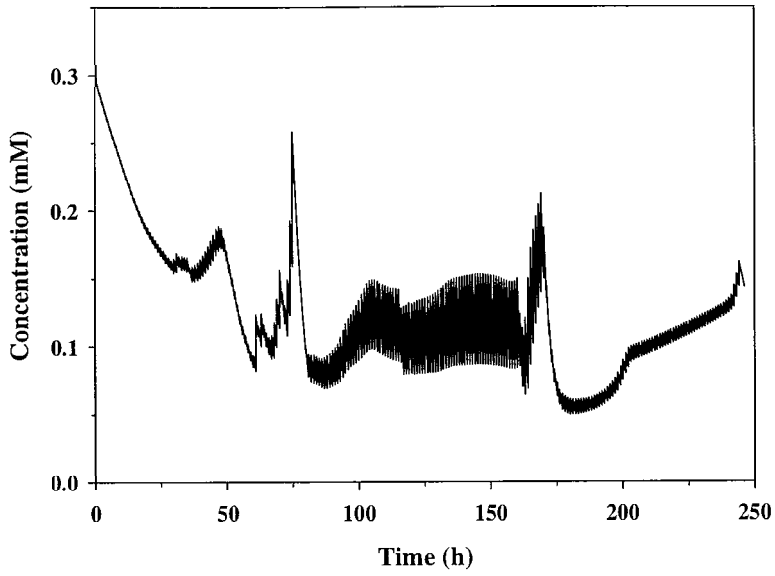


Figure 6.3: Glutamine concentration profile of the optimised fed-batch CHO-IFN γ cell culture.

Glucose

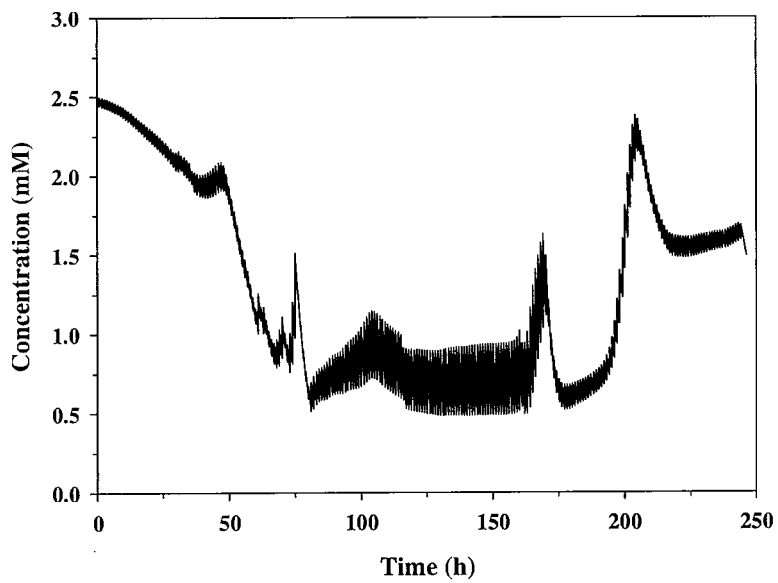


Figure 6.4: Glucose concentration profile of the optimised fed-batch CHO-IFN γ cell culture.

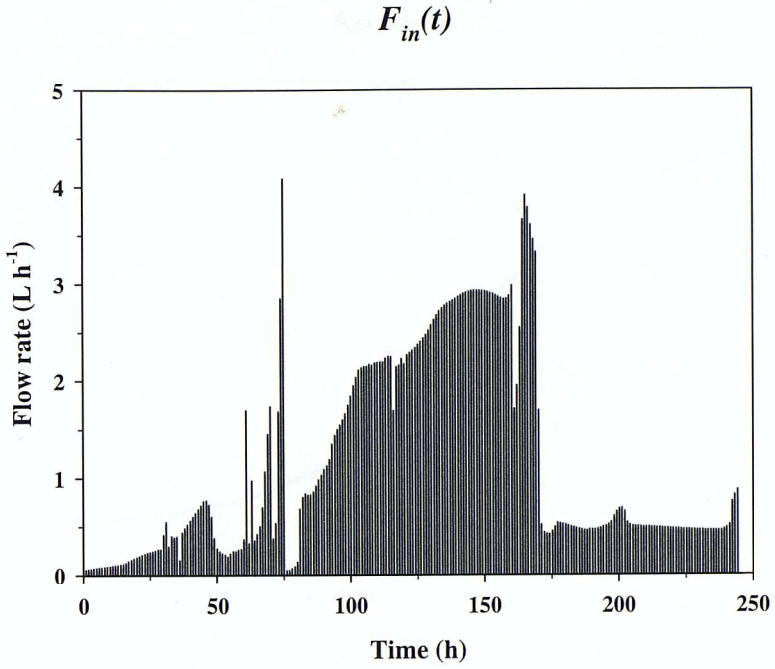


Figure 6.5: $F_{in}(t)$ supplementation profile of the optimised fed-batch CHO-IFN γ cell culture with $\Delta t = 1h$. The stream contained 100mM glutamine, other amino acids, and basic components of the DMEM medium. The height of each pulse in $L h^{-1}$ is equivalent to volume in ml.

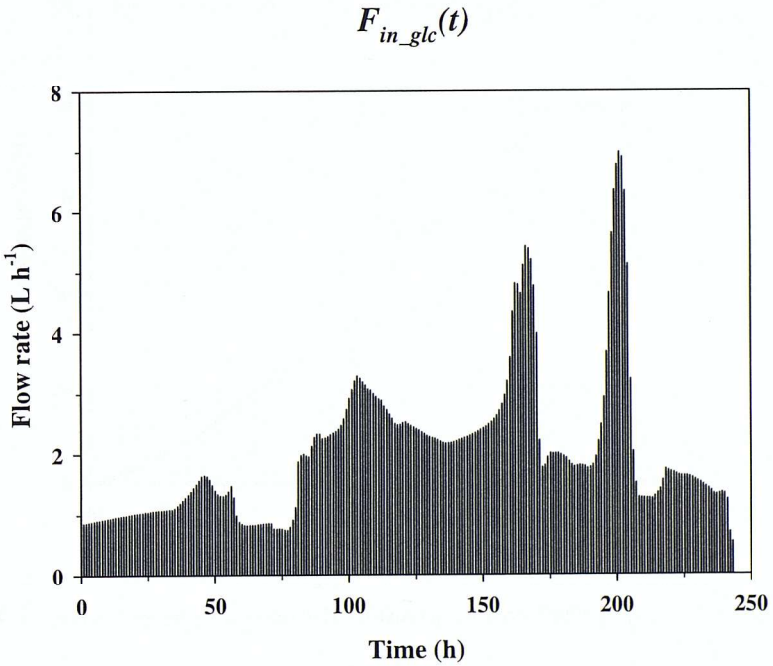


Figure 6.6: Glucose supplementation profile of the optimised fed-batch CHO-IFN γ cell culture with $\Delta t = 1h$. The stream contained 40g/L(222mM) glucose. The height of each pulse in $L h^{-1}$ is equivalent to volume in ml.

Ammonium

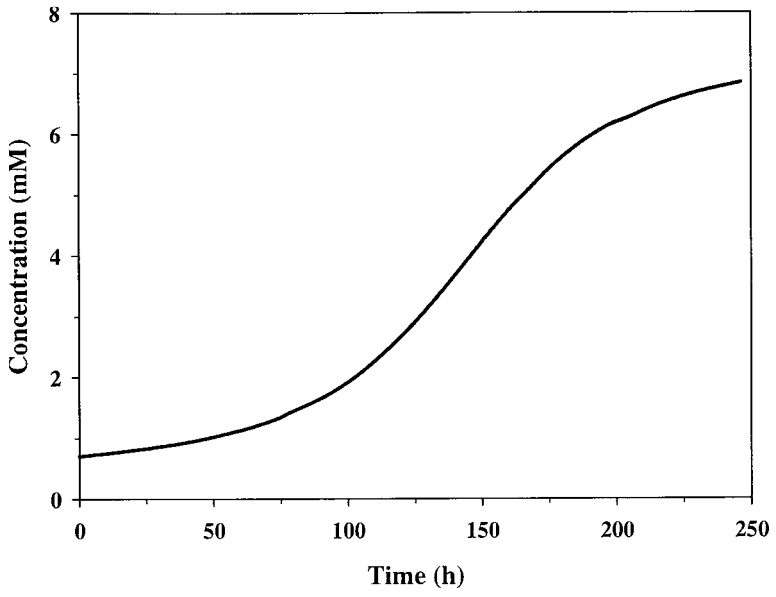


Figure 6.7: Ammonium concentration profile of the optimised fed-batch CHO-IFN γ cell culture.

Lactate

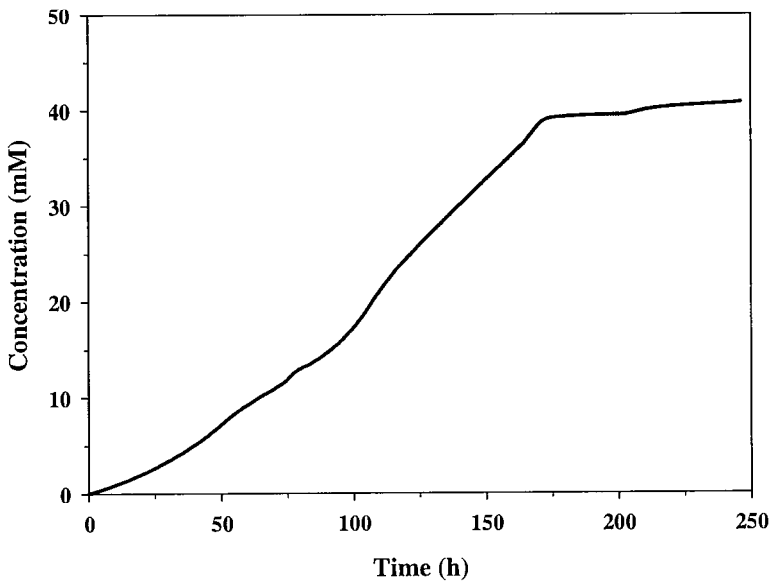


Figure 6.8: Lactate concentration profile of the optimised fed-batch CHO-IFN γ cell culture.

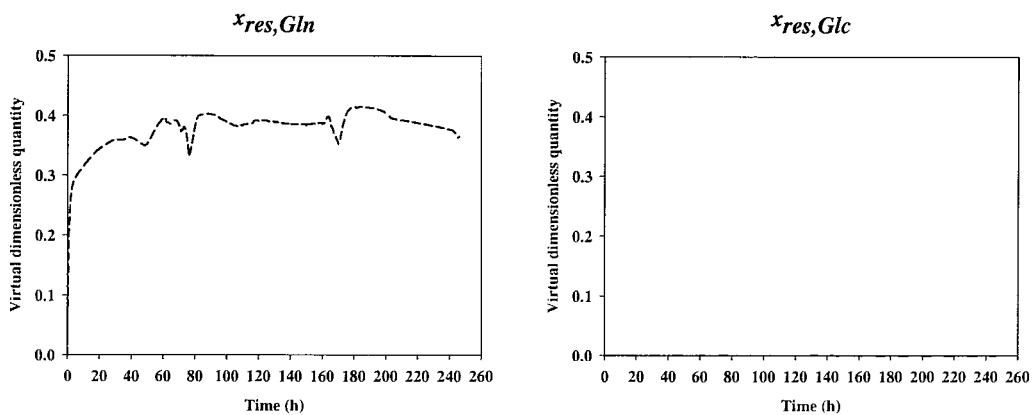


Figure 6.9: Optimised profiles of the hypothetical response variables for glutamine ($x_{res,Gln}$) and glucose ($x_{res,Glc}$) concentrations.

6.3 Evaluation of Effects of Parameter Uncertainty

6.3.1 Numerical Uncertainty Analysis Using Random Sampling

Among all the sensitive parameters that were identified in Chapter 5, those that could be isolated from the whole model and had their values estimated from individual experiment data, i.e. $r_{max_{IFN\gamma}}$, $\mu_{d,min}$, μ_{max} , and μ_{max2} , were fixed in this section because their accuracy was higher than that in bulk parameter estimation. The remaining sensitive parameters and certain significant parameters which were only active in fed-batch conditions (Table 6.2) were varied and the impact on the dynamic optimisation result was evaluated. Although some fed-batch parameters (ρ_g , $r_{max_{res,IFN_Gln}}$, ρ_{IFN_Gln} , $r_{max_{res,IFN_Glc}}$, ρ_{IFN_Glc}) could have their sensitivity determined by the Global Sensitivity Analysis (GSA) method, most fed-batch parameters are only active when the glutamine and glucose concentrations are controlled at low levels by adding an inlet feed stream. The GSA did not take into account any inlet stream because that would have introduced more complication into the analysis before identifying the sensitive batch culture parameters. The significance of those parameters that were only active in fed-batch conditions was judged based on their estimated values and biological relations in the CHO-IFN γ cell culture. For example, fed-batch parameters which had a value of zero or were set at a theoretical limit were regarded as insensitive. Any fed-batch parameters related to non-essential amino acids which affect neither the growth of the CHO-IFN γ cells nor the productivity, e.g. glutamate and alanine, were also fixed at their estimated values. A list of the insensitive/fixed fed-batch parameters are shown in Table 6.3.

The sensitive parameters in Table 6.2 were varied by different extents ($\pm 10\%$, $\pm 25\%$, $\pm 50\%$) based on the possible uncertainty range for a biological cell culture. For each tested uncertainty range, the parameters were changed randomly using a Sobol' sequence generator available from BRODA (2006). Each set of randomly selected parameters within an uncertainty range of interest was subjected to the dynamic optimisation similar to Section 6.1 but only 9 – 12 different initial guesses for control profiles (Table 6.4) were done due to the large number parameter sets involved in the uncertainty evaluation. 60 parameter sets were tested for each uncertainty range until convergence of the mean and standard deviation of the IFN γ yield was observed (Figure 6.10 – 6.11).

Table 6.2: List of parameters that were varied to test the effect of parameter value uncertainty on dynamic optimisation output.

	Parameters	Units	Value (1–2 sig. fig.)
1	Amm_{cr}	mmole L ⁻¹	5
2	$K_{Amm\ Gln}$	mmole 10 ⁻⁶ cell ⁻¹ h ⁻¹	2 x 10 ⁻⁴
3	$K_{Amm\ HisSerAsn}$	mmole 10 ⁻⁶ cell ⁻¹ h ⁻¹	7 x 10 ⁻⁴
4	$K_{d,NH3}$	mmole L ⁻¹	2 x 10 ⁻⁴
5	$K_{g,His}$	mmole 10 ⁻⁶ cell ⁻¹ h ⁻¹	2.8 x 10 ⁻⁷
6	$K_{g,Met}$	mmole 10 ⁻⁶ cell ⁻¹ h ⁻¹	2.8 x 10 ⁻⁷
7	$K_{g,Phe}$	mmole 10 ⁻⁶ cell ⁻¹ h ⁻¹	2.8 x 10 ⁻⁷
8	K_{Glc}	mmole L ⁻¹	6.3
9	K_{Gln}	mmole L ⁻¹	8.5
10	K_{His}	mmole L ⁻¹	0.75
11	K_{Ile}	mmole L ⁻¹	1.2
12	$K_{inh,Glc}$	mmole L ⁻¹	14
13	K_{Leu}	mmole L ⁻¹	1
14	K_{Met}	mmole L ⁻¹	0.7
15	K_{Phe}	mmole L ⁻¹	0.9
16	K_{scale}	mmole 10 ⁻⁶ cell ⁻¹ h ⁻¹	2 x 10 ⁻⁶
17	K_{Trp}	mmole L ⁻¹	0.9
18	K_{Val}	mmole L ⁻¹	0.8
19	ρ_g	-	7 x 10 ⁻²
20	m	-	3
21	$rmax_{Glc}$	mmole 10 ⁻⁶ cell ⁻¹ h ⁻¹	8 x 10 ⁻⁴
22	$rmax_{Gln}$	mmole 10 ⁻⁶ cell ⁻¹ h ⁻¹	9 x 10 ⁻⁴
23	$rmax_{His}$	mmole 10 ⁻⁶ cell ⁻¹ h ⁻¹	2.5 x 10 ⁻⁵
24	$rmax_{Ile}$	mmole 10 ⁻⁶ cell ⁻¹ h ⁻¹	3.5 x 10 ⁻⁵
25	$rmax_{Leu}$	mmole 10 ⁻⁶ cell ⁻¹ h ⁻¹	4 x 10 ⁻⁵
26	$rmax_{Met}$	mmole 10 ⁻⁶ cell ⁻¹ h ⁻¹	2.1 x 10 ⁻⁵
27	$rmax_{Phe}$	mmole 10 ⁻⁶ cell ⁻¹ h ⁻¹	2.1 x 10 ⁻⁵
28	$rmax_{Thr}$	mmole 10 ⁻⁶ cell ⁻¹ h ⁻¹	2 x 10 ⁻⁵
29	$rmax_{Trp}$	mmole 10 ⁻⁶ cell ⁻¹ h ⁻¹	2.1 x 10 ⁻⁵
30	$rmax_{Val}$	mmole 10 ⁻⁶ cell ⁻¹ h ⁻¹	3 x 10 ⁻⁵
31	$rmax_{res.,IFN\ Gln}$	-	9
32	$rmin_{Amm}$	mmole 10 ⁻⁶ cell ⁻¹ h ⁻¹	1.1 x 10 ⁻⁵
33	$rmin_{Amm,rev}$	mmole ^(1-m) L ^m 10 ⁻⁶ cell ⁻¹ h ⁻¹	2 x 10 ⁻⁸
34	$\rho_{Ala\ Gln}$	-	0.1
35	$\rho_{Cys\ Gln}$	-	0.01
36	$\rho_{Glu\ Gln}$	-	1
37	$\rho_{Gly\ Gln}$	-	0.1
38	$\rho_{His\ Gln}$	-	0.05
39	$\rho_{IFN\ Gln}$	-	1
40	$\rho_{Ile\ Gln}$	-	0.1
41	$\rho_{Leu\ Gln}$	-	0.1
42	$\rho_{Lys\ Gln}$	-	0.1
43	$\rho_{Met\ Gln}$	-	0.05
44	$\rho_{Phe\ Gln}$	-	0.1
45	$\rho_{Pro\ Gln}$	-	0.5
46	$\rho_{Ser\ Gln}$	-	0.01
47	$\rho_{Thr\ Gln}$	-	0.05
48	$\rho_{Trp\ Gln}$	-	1
49	$\rho_{Tyr\ Gln}$	-	0.01
50	$\rho_{Val\ Gln}$	-	0.5

Table 6.3: List of fed-batch parameters of which the values were fixed due to insensitivity, inactive (zero value), not affecting growth or productivity, or being at theoretical limit.

Fixed FB Parameters	Value	Units	Remark
$rmax_{res,IFN_Glc}$	-1	-	Insensitive from GSA
ρ_{IFN_Glc}	0.03	-	Insensitive from GSA
$\rho_{d,Gln}$	0.05	-	Insensitive from GSA
$\rho_{d,Glc}$	2	-	Insensitive from GSA
$rmax_{res,Glc_Gln}$	0	-	-
$rmax_{res,Val_Gln}$	-1	-	Theoretical limit
$rmax_{res,Leu_Gln}$	-1	-	Theoretical limit
$rmax_{res,Ile_Gln}$	-1	-	Theoretical limit
$rmax_{res,Met_Gln}$	-1	-	Theoretical limit
$rmax_{res,Phe_Gln}$	-1	-	Theoretical limit
$rmax_{res,Trp_Gln}$	-1	-	Theoretical limit
$rmax_{res,Thr_Gln}$	-1	-	Theoretical limit
$rmax_{res,Lys_Gln}$	-1	-	Theoretical limit
$rmax_{res,His_Gln}$	-1	-	Theoretical limit
$rmax_{res,Ala_Gln}$	-1	-	Theoretical limit
$rmax_{res,Gly_Gln}$	-1	-	Theoretical limit
$rmax_{res,Pro_Gln}$	-1	-	Theoretical limit
$rmax_{res,Asp_Gln}$	0	-	-
$rmax_{res,Glu_Gln}$	1	-	Not affecting growth/productivity
$rmax_{res,Asn_Gln}$	0	-	-
$rmax_{res,Ser_Gln}$	-1	-	Theoretical limit
$rmax_{res,Tyr_Gln}$	-1	-	Theoretical limit
$rmax_{res,Cys_Gln}$	-1	-	Theoretical limit
$rmax_{res,Arg_Gln}$	0	-	-
$rmax_{res,Gln_Glc}$	0	-	-
$rmax_{res,Val_Glc}$	0	-	-
$rmax_{res,Leu_Glc}$	0	-	-
$rmax_{res,Ile_Glc}$	0	-	-
$rmax_{res,Met_Glc}$	0	-	-
$rmax_{res,Phe_Glc}$	0	-	-
$rmax_{res,Trp_Glc}$	0	-	-
$rmax_{res,Thr_Glc}$	0	-	-
$rmax_{res,Lys_Glc}$	0	-	-
$rmax_{res,His_Glc}$	0	-	-
$rmax_{res,Ala_Glc}$	-1	-	Theoretical limit
$rmax_{res,Gly_Glc}$	-1	-	Theoretical limit
$rmax_{res,Pro_Glc}$	-1	-	Theoretical limit
$rmax_{res,Asp_Glc}$	0	-	-
$rmax_{res,Gln_Glc}$	0	-	-
$rmax_{res,Asn_Glc}$	0	-	-
$rmax_{res,Ser_Glc}$	1	-	Not affecting growth/productivity
$rmax_{res,Tyr_Glc}$	0	-	-
$rmax_{res,Cys_Glc}$	0	-	-
$rmax_{res,Arg_Glc}$	0	-	-
ρ_{Ile_Gln}	1	-	$rmax_{res,Glc_Gln} = 0$
ρ_{Gln_Glc}	1	-	$rmax_{res,Gln_Glc} = 0$
ρ_{Val_Glc}	1	-	$rmax_{res,Val_Glc} = 0$
ρ_{Leu_Glc}	1	-	$rmax_{res,Leu_Glc} = 0$
ρ_{Ile_Glc}	1	-	$rmax_{res,Ile_Glc} = 0$
ρ_{Met_Glc}	1	-	$rmax_{res,Met_Glc} = 0$

ρ_{Phe_Glc}	1	-	$rmax_{res,Phe_Glc} = 0$
ρ_{Trp_Glc}	1	-	$rmax_{res,Trp_Glc} = 0$
ρ_{Thr_Glc}	1	-	$rmax_{res,Thr_Glc} = 0$
ρ_{Lys_Glc}	1	-	$rmax_{res,Lys_Glc} = 0$
ρ_{His_Glc}	1	-	$rmax_{res,His_Glc} = 0$
ρ_{Ala_Glc}	0.1	-	Not affecting growth/productivity
ρ_{Gly_Glc}	1	-	Not affecting growth/productivity
ρ_{Pro_Glc}	1	-	Not affecting growth/productivity
ρ_{Asp_Glc}	1	-	$rmax_{res,Asp_Glc} = 0$
ρ_{Glu_Glc}	1	-	$rmax_{res,Glu_Glc} = 0$
ρ_{Asn_Glc}	1	-	$rmax_{res,Asn_Glc} = 0$
ρ_{Ser_Glc}	0.01	-	Not affecting growth/productivity
ρ_{Tyr_Glc}	1	-	$rmax_{res,Tyr_Glc} = 0$
ρ_{Cys_Glc}	1	-	$rmax_{res,Cys_Glc} = 0$
ρ_{Arg_Glc}	1	-	$rmax_{res,Arg_Glc} = 0$
ρ_{Asp_Gln}	1	-	$rmax_{res,Asp_Gln} = 0$
ρ_{Asn_Gln}	1	-	$rmax_{res,Asn_Gln} = 0$
ρ_{Arg_Gln}	1	-	$rmax_{res,Arg_Gln} = 0$

Table 6.4: 12 Initial guesses of control profiles of $F_{in}(t)$ and $F_{in_glc}(t)$ used in evaluation of the effects of uncertainty of sensitive model parameters. Sometimes only 3 out of 6 of the constant feeding modes were tested unless optimisation failures were encountered with certain initial guesses.

	Mode	F_{in}^\dagger (L h ⁻¹)			$F_{in_glc}^\dagger$ (L h ⁻¹)		
		0-80h	81-160h	161-245h	0-80h	81-160h	161-245h
1	Constant	0.1			0.1		
2		0.3			0.1		
3		0.3			0.3		
4		0.5			0.5		
5		0.3			0.5		
6		0.3			0.2		
7	Random	0.1	0.4	0.2	0.2	0.8	0.4
8		0.2	0.1	0.3	0.4	0.2	0.6
9		0.4	0.3	0.2	0.8	0.6	0.4
10	Progressive	0.1	0.2	0.3	0.2	0.4	0.6
11		0.2	0.3	0.4	0.4	0.6	0.8
12		0.3	0.4	0.5	0.5	0.6	0.7

Remark:

[†]The time-width of each pulse was made such that the height of each pulse in L h⁻¹ is equivalent to volume in ml.

Table 6.5: Computational time spent on dynamic optimisation of the original parameter set of the CHO model and evaluation of the effects of uncertainty of sensitive parameters.

	Original set	10%	25%	50%
Avg CPU time per optimisation (h)	0.53	0.56	0.61	0.59
Total no. of optimisation	100	621 [‡]	706 [‡]	708 [‡]
No. of different parameter sets tested	1	60	76	81
No. of ill-conditioned parameter sets	0	0	16	21
Total CPU time (h)	57	348	428	416

Remark:

[‡] Not including ill-conditioned parameter sets causing failure in initial iteration.

6.3.2 Statistical Results

The histograms of IFN γ yield distribution of 60 samples (each sample represents a different parameter set) for each tested uncertainty range are shown in Figure 6.12 – 6.14. In the histogram, the data are sorted into 50bins of equal width between the minimum and maximum sample values. Comparing with the optimised IFN γ yield of 61 mg L⁻¹ from the original set of parameter values, the mean IFN γ yield of $\pm 10\%$, $\pm 25\%$, and $\pm 50\%$ uncertainty followed a decreasing trend of 56 mg L⁻¹, 54 mg L⁻¹, and 48 mg L⁻¹ respectively. The standard deviation increased with increasing uncertainty of the sensitive parameters: 8.0 mg L⁻¹ for $\pm 10\%$, 15.2 mg L⁻¹ for $\pm 25\%$, 24.4 mg L⁻¹ for $\pm 50\%$. The distribution of the optimised IFN γ yield appeared asymmetrical around the mean values with a bias towards the lower range.

The CPU time spent on the uncertainty analysis of sensitive parameters is shown in Table 6.5. Each uncertainty range took 348 – 428 h to complete optimisation of 60 successful parameter sets. Some parameter sets generated from $\pm 25\%$ and $\pm 50\%$ of the original parameter values caused failures in initial iteration of the dynamic optimisation so a total number of 76 and 81 parameter sets were tested respectively to produce 60 optimised numerical outputs for each of the two uncertainty ranges.

**IFN γ yield optimisation mean conc.
--- effect of parameter uncertainty**

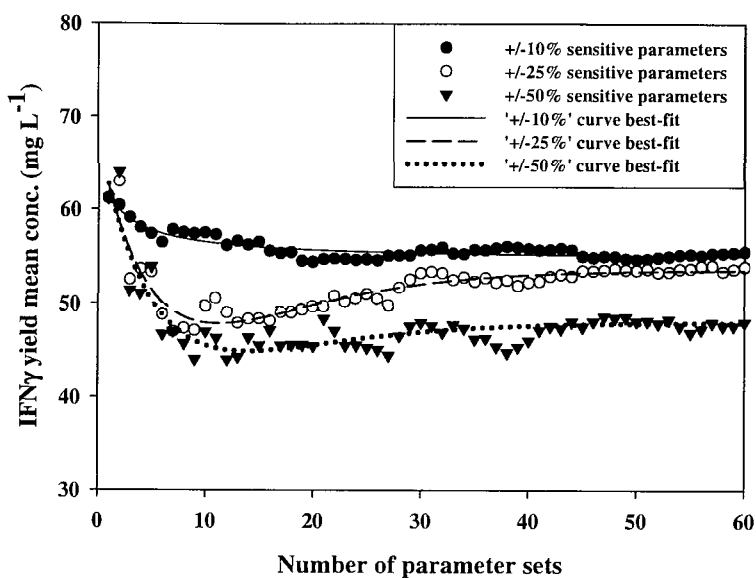


Figure 6.10: Convergence of the mean value of optimised IFN γ yield against number of parameter sets tested. The lines represent best-fit curves showing the trends of the mean values.

**IFN γ yield optimisation standard deviation
--- effect of parameter uncertainty**

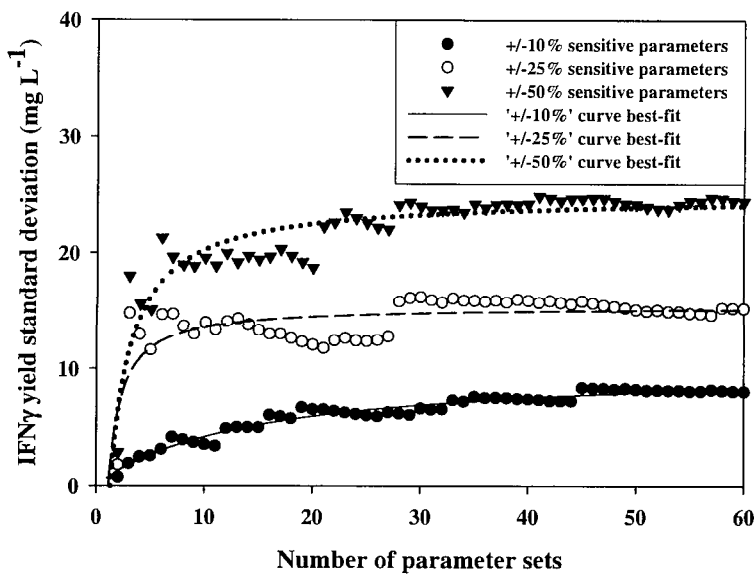


Figure 6.11: Convergence of the standard deviation of optimised IFN γ yield against number of parameter sets tested. The lines represent best-fit curves showing the trends of the standard deviation.

IFN γ yield optimisation
 — +/-10% parameter uncertainty

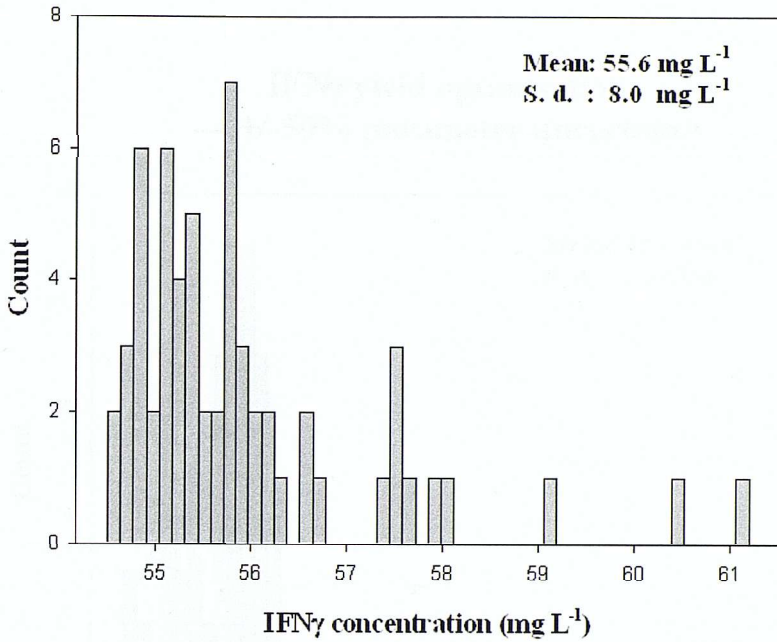


Figure 6.12: Distribution of optimised IFN γ yield among 60 different sets of parameter values when the sensitive parameters were varied $\pm 10\%$.

IFN γ yield optimisation
 — +/-25% parameter uncertainty

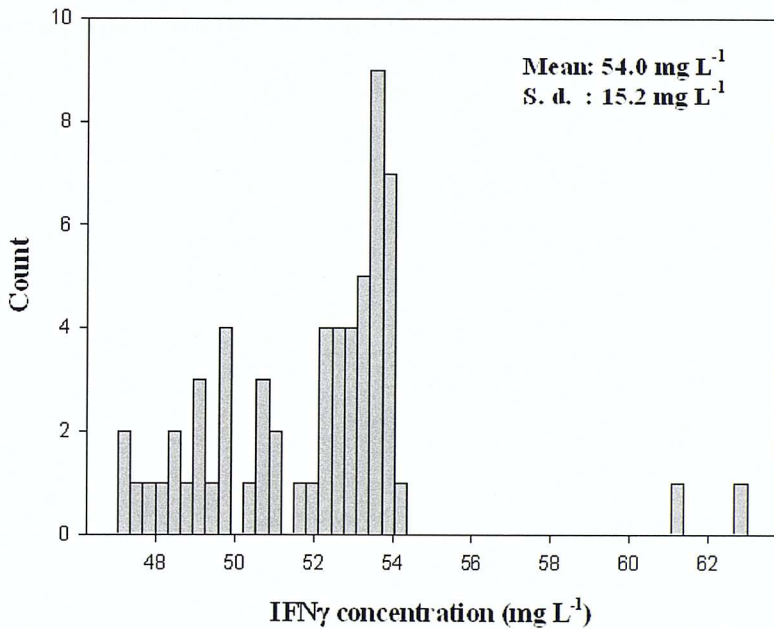


Figure 6.13: Distribution of optimised IFN γ yield among 60 different sets of parameter values when the sensitive parameters were varied $\pm 25\%$.

IFN γ yield optimisation
— +/-50% parameter uncertainty

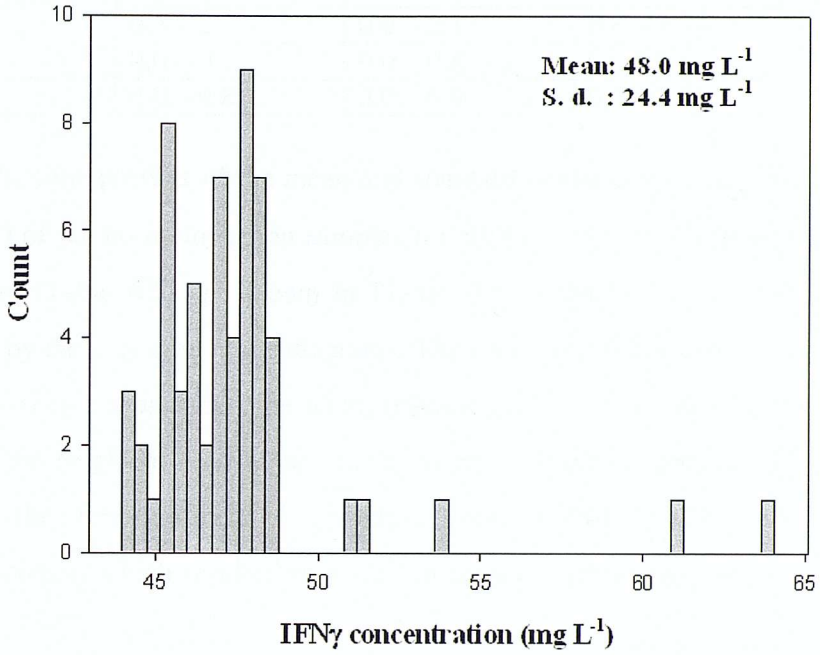


Figure 6.14: Distribution of optimised IFN γ yield among 60 different sets of parameter values when the sensitive parameters were varied $\pm 50\%$.

Uncertainty in Time-Profiles of the Controlled Variables

Table 6.6: Lower and upper ranges of the ratio of standard deviation versus mean values of $F_{in}(t)$, $F_{in_glc}(t)$, $Gln(t)$, and $Glc(t)$.

Variables	Ratio of standard deviation vs. mean value		
	±10%	±25%	±50%
$F_{in}(t)$	0.3-2.0	0.4 – 4.0	0.5 – 3.0
$F_{in_glc}(t)$	0.5 – 2.7	0.6 – 2.1	0.8 – 2.7
$Gln(t)$	0.0 – 0.7	0.0 – 0.8	0.0 – 0.8
$Glc(t)$	0.0 – 0.8	0.0 – 0.9	0.0 – 1.2

The time-profiles of the mean and standard deviation of $F_{in}(t)$, $F_{in_glc}(t)$, $Gln(t)$, and $Glc(t)$ of the 60 optimisation samples for $\pm 10\%$, $\pm 25\%$, and $\pm 50\%$ of the sensitive parameters (Table 6.2) are shown in Figure 6.15 – 6.17. The standard deviation is indicated by the grey area in the diagrams. The time interval between each pulse in $F_{in}(t)$ and $F_{in_glc}(t)$ is 1 h and the time-width of each pulse in $F_{in}(t)$ and $F_{in_glc}(t)$ was made such that the height of each pulse in $L\ h^{-1}$ is equivalent to volume in ml. The double-lines in the time-profiles of glutamine and glucose are caused by nutrient supplementation which resulted in a step increase in glutamine/glucose concentration every 1 h.

The trends of the mean values of $F_{in}(t)$, $F_{in_glc}(t)$, $Gln(t)$, and $Glc(t)$ are similar among various extent of uncertainty of the sensitive parameters. But the standard deviation widens upon increasing the uncertainty from $\pm 10\%$ to $\pm 50\%$ (Figure 6.15 – 6.17). This is also reflected in the ratios of standard deviations versus mean values of $F_{in}(t)$, $F_{in_glc}(t)$, $Gln(t)$, and $Glc(t)$ which generally increase when the uncertainty of the sensitive parameters is increased from $\pm 10\%$ to $\pm 50\%$ (Table 6.6). With the standard deviations reaching about the same order of magnitude as the mean values of glutamine/glucose concentration and up to 3 or 4 times the mean values of $F_{in_glc}(t)$ and $F_{in}(t)$, the off-line model-based optimisation results need to be combined with on-line measurements of several major cell culture variables, e.g. concentration of viable cells, total cells, glutamine, and glucose, to compensate for the uncertainties of both model parameters and experimental variations of the real cell culture system. In that case, the off-line optimisation results would provide an optimal dynamic working range for the system; the on-line measurements would enable fine adjustment of the degrees of freedom (e.g. $F_{in}(t)$ and $F_{in_glc}(t)$) when variations occur in the cell cultures.

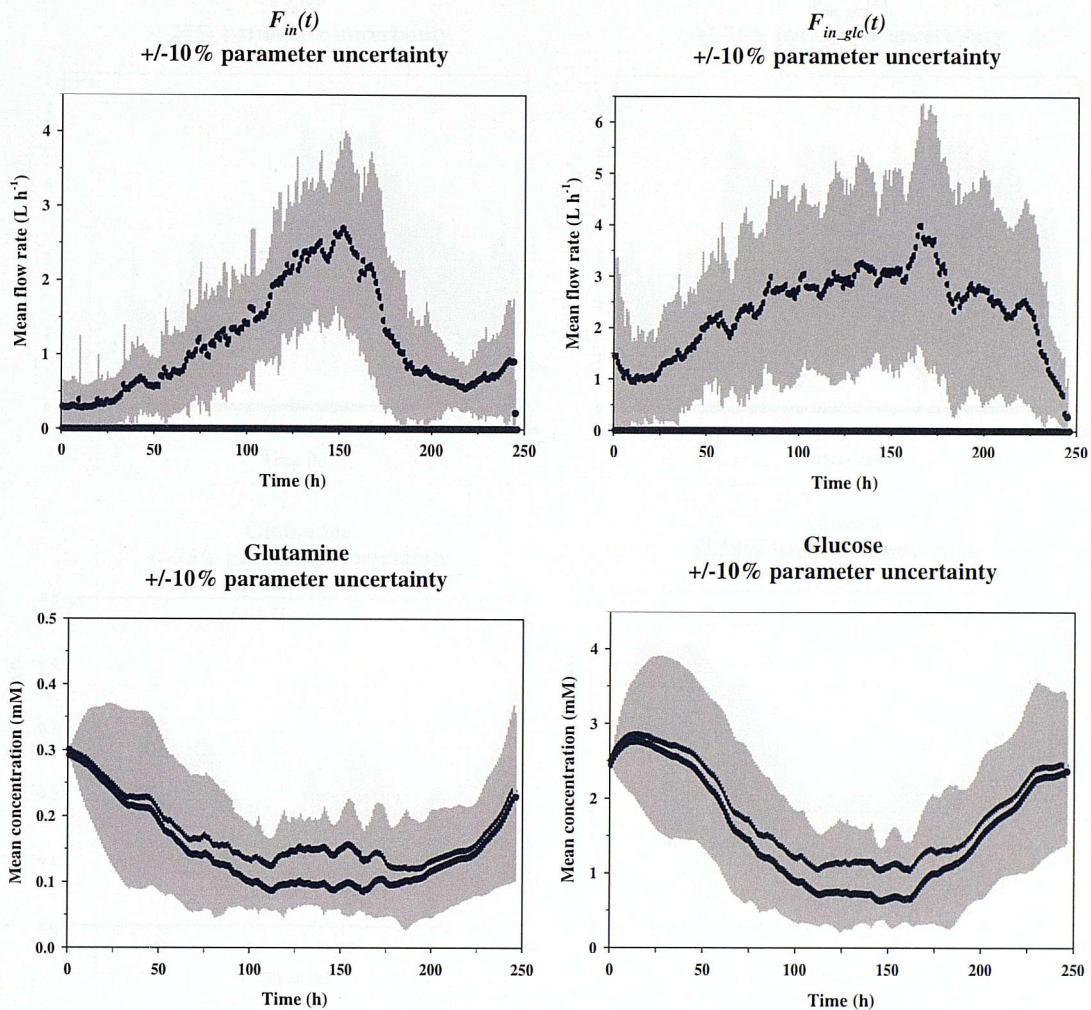


Figure 6.15: Mean (black circle) and standard deviation (grey area) of $F_{in}(t)$, $F_{in_glc}(t)$, glutamine, and glucose concentrations among the 60 optimised results of $\pm 10\%$ sensitive parameters. (The time-width of each pulse in $F_{in}(t)$ and $F_{in_glc}(t)$ was made such that the height of each pulse in $L h^{-1}$ is equivalent to volume in ml.)

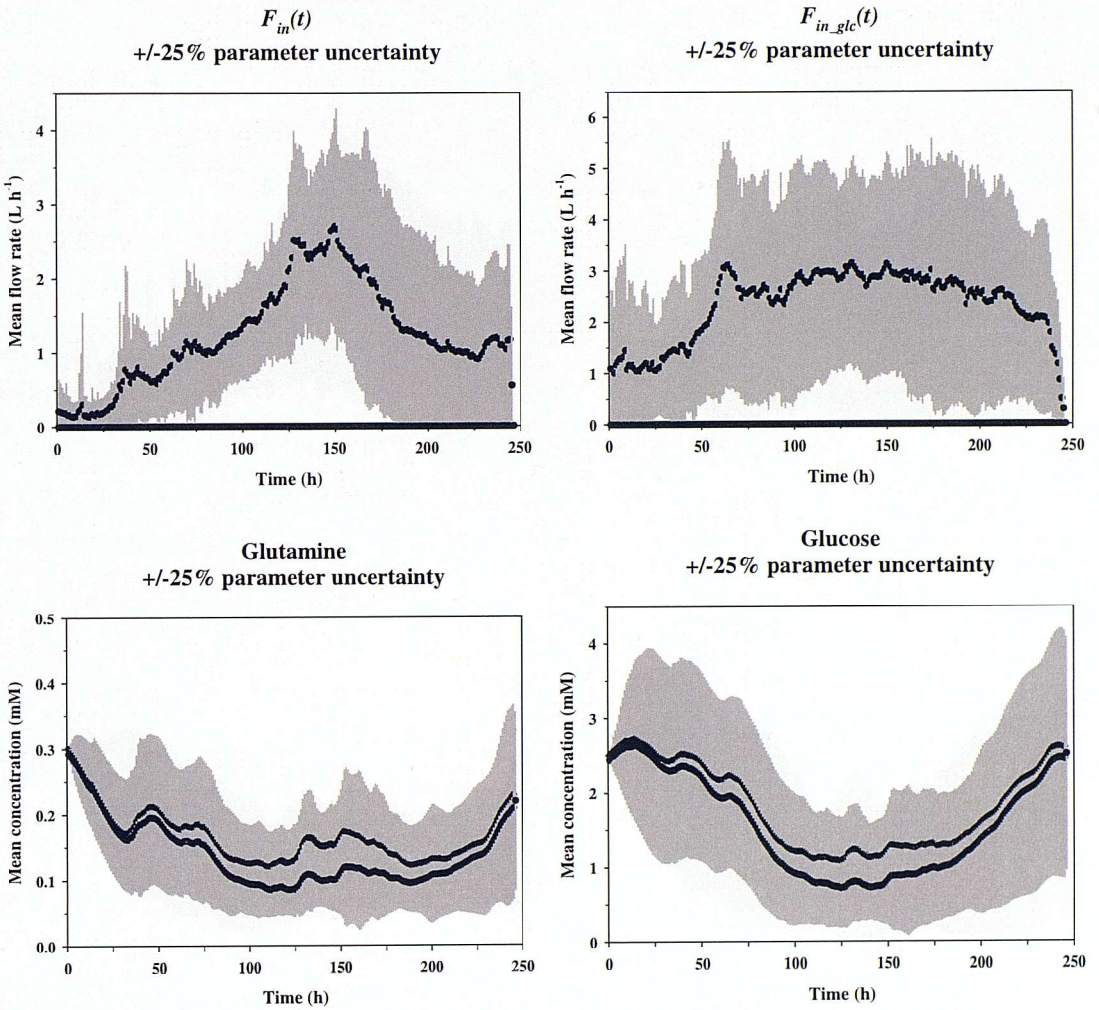


Figure 6.16: Mean (black circle) and standard deviation (grey area) of $F_{in}(t)$, $F_{in_glc}(t)$, glutamine, and glucose concentrations among the 60 optimised results of $\pm 25\%$ sensitive parameters. (The time-width of each pulse in $F_{in}(t)$ and $F_{in_glc}(t)$ was made such that the height of each pulse in L h⁻¹ is equivalent to volume in ml.)

In this chapter, it has been shown that the model can be used to predict the mean and standard deviation of the flow rate and concentration of glucose and glutamine in the blood. The model is able to predict the mean and standard deviation of the flow rate and concentration of glucose and glutamine in the blood.

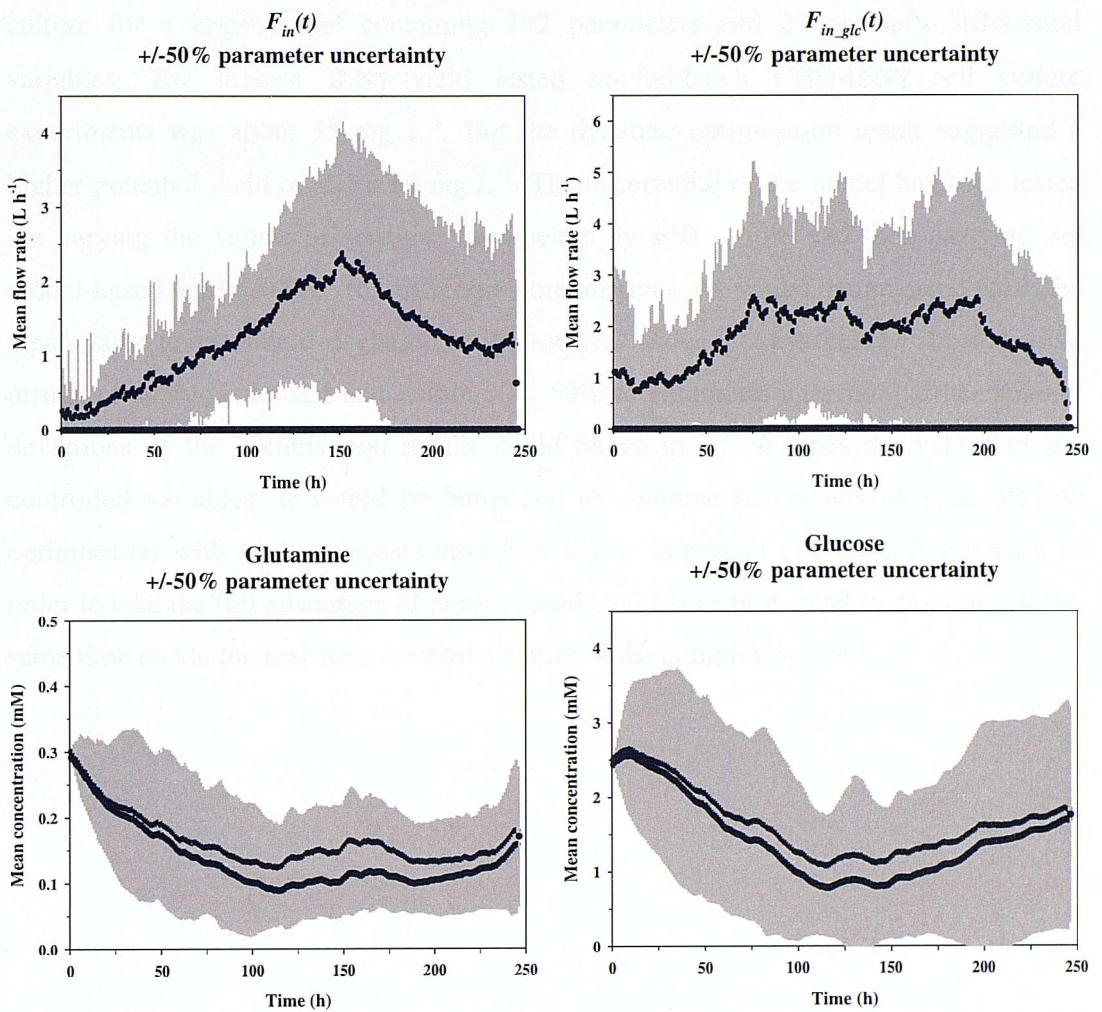


Figure 6.17: Mean (black circle) and standard deviation (grey area) of $F_{in}(t)$, $F_{in_glc}(t)$, glutamine, and glucose concentrations among the 60 optimised results of $\pm 50\%$ sensitive parameters. (The time-width of each pulse in $F_{in}(t)$ and $F_{in_glc}(t)$ was made such that the height of each pulse in $L h^{-1}$ is equivalent to volume in ml.)

Conclusions

In this chapter, it has been shown that model-based optimisation can provide useful information regarding the best operating region of a dynamic mammalian cell culture for a large model containing 192 parameters and 29 ordinary differential variables. The highest IFN γ yield tested in fed-batch CHO-IFN γ cell culture experiments was about 35 mg L⁻¹. But the dynamic optimisation result suggested a higher potential yield of about 60 mg L⁻¹. The uncertainty of the model has been tested via varying the values of sensitive parameters by $\pm 10 - 50\%$ and then carrying out model-based optimisation for different combinations of varied parameters until the mean value and standard deviation of the samples showed convergence. The statistical results of analysis showed that within 10 – 50% of parameter uncertainty, the standard deviations of the optimisation results could be up to 1 – 4 times the values of the controlled variables. It would be beneficial to combine the results of such off-line optimisation with on-line measurements of a few important cell culture variables in order to take the full advantage of model-based analysis of biological systems and at the same time tackle the real-time uncertain nature of the complex systems.

Chapter 7

— Conclusions & Future Work

7.1 Overall Conclusions

Design and optimisation of mammalian cell culture processes can become more efficient with the help of cell culture modelling. In this study, it has been demonstrated that an explicit on/off-type biological degree of freedom, e.g. cell-cycle arrest, that is step-like and irreversible with respect to time can be modelled as binary variable and optimised simultaneously with other continuous degrees of freedom using a standard mixed-integer dynamic optimisation (MIDO) algorithm with a transformation of the binary variable into a binary and two continuous dummy variables during optimisation (Section 3.2.3).

When modelling the growth of mammalian cells, traditionally only a few main energy sources, e.g. glucose and glutamine, were included in the growth kinetics and it was often implicitly assumed that other factors affecting growth rate were constant. However, such simplified approach for the growth kinetics appeared to be insufficient in the studied case of batch/fed-batch hybridoma cell culture modelling because other growth-limiting nutrients were likely to be exhausted towards the end of the cell cultures. Mammalian cells are known to be unable to synthesize certain amino acids which, if absent, would cause growth rate to cease. Thus, it is important to include amino acids that are essential/stimulating for growth in the growth kinetics when modelling the stationary/death phases of batch/fed-batch cultures or fed-batch cultures with nutrients controlled at low levels because in those situations the amino acids concentration could become significantly low. A model has been developed with the incorporation of essential and growth-stimulating amino acids in the growth kinetics for

a Chinese hamster ovary (CHO) cell culture where amino acids data are available. Mammalian cells (as well as other cellular organisms such as yeasts) respond to their surroundings by changing their gene expressions which may affect the patterns of growth, metabolism, and productivity. It is important that a model aiming at optimising a biological system of which the range of the degrees of freedom would cause a change in the cellular responses take such 'change' into account. Failure to do so would result in a model of which the parameter values are different for different experiment conditions of interest. The CHO interferon- γ (CHO-IFN γ) cell culture studied in this work was cultivated under a wide range of concentrations of glutamine and glucose in batch and fed-batch conditions. The specific growth rate and specific IFN γ production rate were observed to increase significantly when glutamine concentration was controlled at roughly 0.1 – 0.5mM in fed-batch cultures as opposed to ~4mM initial concentration in batch cultures; and both the specific lactate (byproduct) production rate and specific IFN γ production rate decreased when glucose concentration was controlled at roughly < 0.5 mM in fed-batch cultures as opposed to ~30mM in batch cultures. A 'step-like' approximation has been used to model the changes in cell growth and metabolic patterns when the concentration of major nutrients (glutamine, glucose) are shifted from high to low concentrations with an assumption that the intermediate range of nutrient concentration is less significant for the optimisation. The developed model for CHO-IFN γ cell culture contains 192 parameters and 29 ordinary differential equations (ODEs). Among the ODEs, 27 are measured variables (practically 26 since Tryptophan could not be quantified in the analysis) and 2 are hypothetical variables relating changes in glutamine/glucose concentrations to cellular responses.

The model parameters were estimated based on data of batch and fed-batch CHO-IFN γ cell cultures. The relative significance of most of the parameters were quantified using Global sensitivity analysis (GSA) in order to identify parameters that are sensitive for the specific production rate of IFN γ . GSA is a valuable tool for interpretation of higher-order interactions among model parameters throughout the whole range of the possible parameter values. The insensitive parameters were fixed at their initially estimated values and the sensitive parameters were re-estimated. The model is able to capture the time-profiles of the measured variables in batch culture and most of the fed-batch cultures. The model was then subjected to dynamic optimisation using gPROMS (Process Systems Enterprise Ltd.) to determine the optimal

supplementation time-profiles of a glutamine-containing stream and a glucose stream for maximising IFN γ yield in fed-batch CHO-IFN γ cultures. The optimisation result suggested a potential of higher IFN γ yield than the yield obtained in the tested fed-batch cultures. But a statistical analysis of the optimisation output taking into account the possible uncertainties of the sensitive parameters indicated non-negligible variations in the optimised nutrient supplementation time-profiles when the values of the sensitive parameters were changed by $\pm 10\%$, $\pm 25\%$, or $\pm 50\%$. It is recommended that a few major cell culture variables, e.g. cell concentrations, glutamine and glucose concentrations, are measured online to allow fine adjustments of the off-line optimised nutrient supplementation time-profiles.

In general, the main challenge in model-based optimisation of dynamic mammalian suspension cell cultures is in the determination of an appropriate mathematical model structure for the biological system of interest. Once a correct model structure is found, the values of the model parameters can be estimated from experiments and the predictions from the model can assist in understanding and optimisation of the system, which can save future experimentation time. This study has highlighted the importance of including essential and growth-stimulating amino acids in the growth kinetics of mammalian cell cultures. It has also been demonstrated that it is possible to simultaneously optimise binary-irreversible and continuous degrees of freedom using a standard mixed-integer dynamic optimisation (MIDO) algorithm which was not designed to handle the irreversibility encountered in biological systems; and to approximate the observed changes in cellular activities between high and low nutrients concentration by a step-like function when the intermediate range of the concentration is less significant for product yield maximisation. But the intrinsic complexity and uncertainty of the mammalian cell cultures have caused variations in the model-based off-line optimisation results. This can be improved by adjusting the optimisation results using online measurements of a few major cell culture variables. Computational simulation and wet-lab experimentation are complementary tools for the optimisation of biological processes. As the cultivation and analysis of cell cultures are often lengthy and expensive, mathematical models can help to construct relationships among process variables to propose further beneficial experiments if necessary. The use of model-based optimisation for biological systems is still a developing field. It is believed that this will be more widely applied in the bioindustry in the future when the mathematical and engineering tools for biological system simulation and optimisation are more

readily available to people who are not familiar with the relevant theoretical and technical knowledge.

7.2 Recommended Future Work

The developed framework of using ‘response’ variables to model step-like changes in cellular activities can be applied to model step changes of other controllable process variables, e.g. osmotic shift, temperature shift, pH shift etc. Depending on the reversibility of the controlled variables, the ‘response’ variables should be constrained to be activated only once or for unlimited times. For example, an increase in osmotic pressure is irreversible in batch/fed-batch cell cultures but reversible in continuous cell cultures.

The dynamics of biological cell cultures and the values of model parameters are dependent on the cell-lines due to genetic variations across different cell types. It is therefore beneficial to develop a library of general models for different mammalian cell-lines catering for each one’s unique features of nutrients requirement, death kinetics, metabolic patterns, nutrient transport mechanisms, and antibody/recombinant-protein production mechanism. Such a model library would facilitate applications of mammalian cell culture simulations by experimentalists who may have limited knowledge of cell culture model development. It would be useful that cell culture modellers and experimentalists interact more closely with each other as the task of cell culture optimisation involves cross-disciplinary skills which can become more synergetic with better mutual understanding of the strength and limitation in modelling and experimentation.

In addition to the identification of sensitive model parameters using global sensitivity analysis in Chapter 5, it is also interesting to investigate the possibility of linear dependency between sensitive model parameters. When two parameters are linearly dependent, only their ratio (instead of their individual values) can be identified from the experimental data. Such analysis can be carried out using Fisher information matrix (Zografos, 1998) to provide an additional layer of insight into the property of the parameters.

The study of low concentration of glutamine and glucose in this work has revealed a metabolic change in CHO cells which can be further explored using ^{13}C metabolic flux analysis with steady-state CHO cell culture subjected to high and low substrate concentrations. The results can indicate how the major metabolism has been affected by low extracellular nutrient concentration and may suggest useful targets for metabolic engineering to increase productivity.

Bibliography

- Abravaya, K., Phillips, B. and Morimoto, R. (1991) Attenuation of the Heat Shock Response in HeLa Cells Is Mediated by the Release of Bound Heat Shock Transcription Factor and is Modulated by Changes in Growth and in Heat Shock Temperatures. *Gene Dev*, 5, 2117-2127.
- Aguda, B. D. and Tang, Y. (1999) The Kinetic Origins of the Restriction Point in the Mammalian Cell Cycle. *Cell Prolif*, 32, 321-335.
- Ahlberg, J. H., Nilson, E. N. and Walsh, J. L. (1967) *The Theory of Splines and Their Applications*, Academic Press, New York.
- Aiba, S., Shoda, M. and Nagatani, M. (1968) Kinetics of Product Inhibition in Alcohol Fermentation. *Biotechnol Bioeng*, 10, 845-864.
- Akesson, M., Forster, J. and Nielsen, J. (2004) Integration of Gene Expression Data into Genome-Scale Metabolic Models. *Metab Eng*, 6, 285-293.
- Alberts, B., Johnson, A., Lewis, J., Raff, M., Roberts, K. and Walter, P. (2002) *Molecular Biology of the Cell*, 4th edition, Garland Science, New York, USA.
- Allen, T. E. and Palsson, B. O. (2003) Sequence-Based Analysis of Metabolic Demands for Protein Synthesis in Prokaryotes. *J Theor Biol*, 220, 1-18.
- Al-Rubeai, M. and Emery, A. N. (1990) Mechanisms and Kinetics of Monoclonal Antibody Synthesis and Secretion in Synchronous and Asynchronous Hybridoma Cell Cultures. *J Biotechnol*, 16, 67-85.
- Al-Rubeai, M., Emery, A., Chalder, S. and Jan, D. (1992) Specific Monoclonal Antibody Productivity and the Cell Cycle-Comparisons of Batch, Continuous and Perfusion Cultures. *Cytotechnology*, 9, 85-97.
- Altamirano, C., Illanes, A., Casablancas, A., Gamez, X., Cairo, J. J. and Godia, C. (2001) Analysis of CHO Cells Metabolic Redistribution in a Glutamate-Based Defined Medium in Continuous Culture. *Biotechnol Prog*, 17, 1032-1041.
- Alter, O., Brown, P. O. and Botstein, D. (2000) Singular Value Decomposition for Genome-Wide Expression Data Processing and Modeling. *Proc Natl Acad Sci Unit States Am*, 97, 10101-10106.

- Alvarez-Vasquez, F., González-Alcón, C. and Torres, N. V. (2000) Metabolism of Citric Acid Production by *Aspergillus Niger*: Model Definition, Steady-State Analysis and Constrained Optimization of Citric Acid Production Rate. *Biotechnol Bioeng*, 70, 82-108.
- Alvarez-Vasquez, F., Canovas, M., Iborra, J. L. and Torres, N. V. (2002) Modeling, Optimization and Experimental Assessment of Continuous L-(-)-Carnitine Production by *Escherichia Coli* Cultures. *Biotechnol Bioeng*, 80, 794-805.
- Andersen, D. C. and Krummen, L. (2002) Recombinant Protein Expression for Therapeutic Applications. *Curr Opin Biotechnol*, 13, 117-123.
- Ando, S., Sakamoto, E. and Iba, H. (2002) Evolutionary Modeling and Inference of Gene Network. *Inf Sci*, 145, 237-259.
- Andrews, J. F. (1968) A Mathematical Model for the Continuous Culture of Microorganisms Utilizing Inhibitory Substrates. *Biotechnol Bioeng*, 10, 707-723.
- Androulakis, I. P. (2000) Kinetic Mechanism Reduction Based on an Integer Programming Approach. *AIChE J*, 46, 361-371.
- Ardawi, M. S. and Newsholme, E. A. (1982) Maximum Activities of Some Enzymes of Glycolysis, the Tricarboxylic Acid Cycle and Ketone-Body and Glutamine Utilization Pathways in Lymphocytes of the Rat. *Biochem J*, 208, 743-748.
- Arkin, A., Ross, J. and McAdams, H. H. (1998) Stochastic Kinetic Analysis of Developmental Pathway Bifurcation in Phage λ -Infected *Escherichia coli* Cells. *Genetics*, 149, 1633-1648.
- Arrigo, A.-P., Firdaus, W. J. J., Mellier, G., Moulin, M., Paul, C., Diaz-latoud, C. and Kretz-remy, C. (2005) Cytotoxic Effects Induced by Oxidative Stress in Cultured Mammalian Cells and Protection Provided by Hsp27 Expression. *Methods*, 35, 126-138.
- Axe, D. D. and Bailey, J. E. (1994) Modeling the Regulation of Bacterial Genes Producing Proteins That Strongly Influence Growth. *Biotechnol Bioeng*, 43, 242-257.
- Bailey, J. E. (1998) Mathematical Modeling and Analysis in Biochemical Engineering: Past Accomplishments and Future Opportunities. *Biotechnol Prog*, 14, 8-20.
- Bailey, J. E. and Ollis, D. F. (1986) *Biochemical Engineering Fundamentals*, 2nd edition, McGraw-Hill, Inc., Singapore.
- Bakker, W. A. M., Schäfer, T., Beeftink, H. H., Tramper, J. and Gooijer, C. D. (1996) Hybridomas in a Bioreactor Cascade: Modeling and Determination of Growth and Death Kinetics. *Cytotechnology*, 21, 263-277.
- Banga, J. R., Alonso, A. A. and Singh, R. P. (1997) Stochastic Dynamic Optimization of Batch and Semicontinuous Bioprocesses. *Biotechnol Prog*, 13, 326-335.
- Bansal, V., Perkins, J. D. and Pistikopoulos, E. N. (2002) A Case Study in Simultaneous Design and Control Using Rigorous, Mixed-Integer Dynamic Optimization Models. *Ind Eng Chem Res*, 41, 760-778.

- Bansal, V., Sakizlis, V., Ross, R., Perkins, J. D. and Pistikopoulos, E. N. (2003) New Algorithms for Mixed-Integer Dynamic Optimization. *Comput Chem Eng*, 27, 647-668.
- Barford, J. P. (1990a) A General Model for Aerobic Yeast Growth: Batch Growth. *Biotechnol Bioeng*, 35, 907-920.
- Barford, J. P. (1990b) A General Model for Aerobic Yeast Growth: Continuous Culture. *Biotechnol Bioeng*, 35, 921-927.
- Barton, P. I., Allgor, R. J., Feehery, W. F. and Galan, S. (1998) Dynamic Optimization in a Discontinuous World. *Ind Eng Chem Res*, 37, 966-981.
- Basse, B., Baguley, B. C., Marshall, E. S., Joseph, W. R., van Brunt, B., Wake, G. and Wall, D. J. N. (2003) A Mathematical Model for Analysis of the Cell Cycle in Cell Lines Derived from Human Tumors. *J Math Biol*, 47, 295-312.
- Batt, B. C. and Kompala, D. S. (1989) A Structured Kinetic Modeling Framework for the Dynamics of Hybridoma Growth and Monoclonal Antibody Production in Continuous Suspension Cultures. *Biotechnol Bioeng*, 34, 515-531.
- Battogtokh, D., Asch, D. K., Case, M. E., Arnold, J. and Schuttler, H.-B. (2002) An Ensemble Method for Identifying Regulatory Circuits with Special Reference to the Qa Gene Cluster of *Neurospora Crassa*. *Proc Natl Acad Sci Unit States Am*, 99, 16904-16909.
- Bellman, R. E. (1957) *Dynamic Programming*, Princeton University Press, New Jersey.
- Bergin, T. M. (2008) *General Biology 1*. [Online] Available from: <http://www.dmacc.cc.ia.us/instructors/tmbergin/animalcell.jpg> [Accessed April 2008].
- Beyer, J., Richard P., Bassingthwaighe, J. B. and Deussen, A. J. (2002) A Computational Model of Oxygen Transport from Red Blood Cells to Mitochondria. *Comput Methods Programs Biomed*, 67, 39-54.
- Bhatia, T. K. and Biegler, L. T. (1997) Dynamic Optimization for Batch Design and Scheduling with Process Model Uncertainty. *Ind Eng Chem Res*, 36, 3708 -3717.
- Bibila, T. A. and Flickinger, M. C. (1991a) A Structured Model for Monoclonal Antibody Synthesis in Exponentially Growing and Stationary Phase Hybridoma Cells. *Biotechnol Bioeng*, 37, 210-226.
- Bibila, T. A. and Flickinger, M. C. (1991b) A Model of Interorganelle Monoclonal Antibody Transport and Secretion in Mouse Hybridoma Cells. *Biotechnol Bioeng*, 38, 767-780.
- Bibila, T. A. and Flickinger, M. C. (1992a) Use of a Structured Kinetic Model of Antibody Synthesis and Secretion for Optimization of Antibody Production Systems: I. Steady-State Analysis. *Biotechnol Bioeng*, 39, 251-261.
- Bibila, T. A. and Flickinger, M. C. (1992b) Use of a Structured Kinetic Model of Antibody Synthesis and Secretion for Optimization of Antibody Production Systems: II. Transient Analysis. *Biotechnol Bioeng*, 39, 262-272.
- Bibila, T. A. and Robinson, D. K. (1995) In Pursuit of the Optimal Fed-Batch Process for Monoclonal Antibody Production. *Biotechnol Prog*, 11, 1-13.

- Biegler, L. T. (1984) Solution of Dynamic Optimization Problems by Successive Quadratic Programming and Orthogonal Collocation. *Comput Chem Eng*, 8, 243-247.
- Biegler, L. T., Cervantes, A. M. and Wächter, A. (2002) Advances in Simultaneous Strategies for Dynamic Process Optimization. *Chem Eng Sci*, 57, 575-593.
- Birch, J. R. and Racher, A. J. (2006) Antibody Production. *Adv Drug Deliv Rev*, 58, 671-685.
- Birkhoff, G. and de Boor, C. R. (1965) Piecewise Polynomial Interpolation and Approximation. In: *Approximation of Functions* (Ed, Garabedian, H. L.) Elsevier, New York, pp. 164-190.
- Bittner, M., Meltzer, P. and Trent, J. (1999) Data Analysis and Integration: Of Steps and Arrows. *Nat Genet*, 22, 213-215.
- Blake, W. J., Kærn, M., Cantor, C. R. and Collins, J. J. (2003) Noise in Eukaryotic Gene Expression. *Nature*, 422, 633-637.
- Bollati-Fogolín, M., Forno, G., Nimtz, M., Conradt, H. S., Etcheverrigaray, M. and Kratje, R. (2005) Temperature Reduction in Cultures of Hgm-Csf-Expressing Cho Cells: Effect on Productivity and Product Quality. *Biotechnology Progress*, 21, 17-21.
- Borth, N., Strutzenberger, K., Donalies, U., Kunert, R. and Katinger, H. (1996) Comparison of the Production of a Human Monoclonal Antibody against HIV-1 by Teherohybridoma Cells and Recombinant CHO Cells: A Flow Cytometric Study. *Cytotechnology*, 22, 129-138.
- Bray, H. G., James, S. P., Raffan, I. M. and Thorpe, W. V. (1949) The Enzymic Hydrolysis of Glutamine and its Spontaneous Decomposition in Buffer Solutions. *Biochem J*, 44, 625-627.
- Bree, M. A. and Dhurjati, P. (1988) Kinetic Modelling of Hybridoma Cell Growth and Immunoglobulin Production in a Large-Scale Suspension Culture. *Biotechnol Bioeng*, 32, 1067-1072.
- BRODA Ltd. (2006) URL: <http://www.broda.co.uk>
- Cain, S. J. and Chau, P. C. (1998) Transition Probability Cell Cycle Model with Product Formation. *Biotechnol Bioeng*, 58, 387-399.
- Campbell, P. N. and Smith, A. D. (2000) *Biochemistry Illustrated*, Churchill Livingstone, Edinburgh, UK.
- Campolongo, F., Kleijnen, J. and Andres, T. (2000) Screening Methods. In: *Sensitivity Analysis* (Eds, Saltelli, A., Chan, K. and Scott, E. M.), John Wiley & Sons Ltd., Chichester, England, pp. 65-80.
- Canovas, M., Maiquez, J. R., Obón, J. M. and Iborra, J. L. (2002) Modeling of the Biotransformation of Crotonobetaine into L-(-)-Carnitine by *Escherichia Coli* Strains. *Biotechnol Bioeng*, 77, 764-775.

- Carling, D., Aguan, K., Woods, A., Verhoeven, A., Beri, R., Brennan, C., Sidebottom, C., Davison, M. and Scott, J. (1994) Mammalian AMP-Activated Protein Kinase Is Homologous to Yeast and Plant Protein Kinases Involved in the Regulation of Carbon Metabolism. *J Biol Chem*, 269, 11442-11448.
- Castellanos, M., Wilson, D. B. and Shuler, M. L. (2004) A Modular Minimal Cell Model: Purine and Pyrimidine Transport and Metabolism. *Proc Natl Acad Sci Unit States Am*, 101, 6681-6686.
- Cervantes, A. and Biegler, L. T. (1998) Large-Scale DAE Optimization Using a Simultaneous NLP Formulation. *AIChE J*, 44, 1038-1050.
- Cervantes, A. and Biegler, L. T. (1999) Optimization Strategies for Dynamic Systems. In: *Encyclopedia of Optimization*, Vol. IV (Eds, Floudas, C. and Pardalos, P.) Kluwer Academic Publishers, Dordrecht, Netherlands, pp. 216-227.
- Cervantes, A. M. and Biegler, L. T. (2000) A Stable Elemental Decomposition for Dynamic Process Optimization. *J Comput Appl Math*, 120, 41-57.
- Chachuat, B., Singer, A. B. and Barton, P. I. (2005) Global Mixed Integer Dynamic Optimization. *AIChE J*, 51, 2235-2253.
- Chan, K., Tarantola, S., Saltelli, A. and Sobol', I. M. (2000) Variance-Based Methods. In: *Sensitivity Analysis* (Eds, Saltelli, A., Chan, K. and Scott, E. M.), John Wiley & Sons Ltd., Chichester, England, pp. 167-197.
- Chang, Y.-H. D., Grodzinsky, A. J. and Wang, D. I. C. (1995) In-Situ Removal of Ammonium and Lactate through Electrical Means for Hybridoma Cultures. *Biotechnol Bioeng*, 47, 308-318.
- Cheema, J. J. S., Sankpal, N. V., Tambe, S. S. and Kulkarni, B. D. (2002) Genetic Programming Assisted Stochastic Optimization Strategies for Optimization of Glucose to Gluconic Acid Fermentation. *Biotechnol Prog*, 18, 1356-1365.
- Chemfinder (2005) [Online] Available from: <http://chemfinder.cambridgesoft.com/result.asp> [Accessed August 2005].
- Chen, C. T. and Hwang, C. (1990) Optimal on-Off Control for Fed-Batch Fermentation Processes. *Ind Eng Chem Res*, 29, 1869-1875.
- Chen, K. C., Csikasz-Nagy, A., Gyorfyy, B., Val, J., Novak, B. and Tyson, J. J. (2000) Kinetic Analysis of a Molecular Model of the Budding Yeast Cell Cycle. *Mol Biol Cell*, 11, 369-391.
- Cheng, C., Huang, Y. L. and Yang, S.-T. (1997) A Novel Feeding Strategy for Enhanced Plasmid Stability and Protein Production in Recombinant Yeast Fedbatch Fermentation. *Biotechnol Bioeng*, 56, 23-31.
- Cherlet, M. and Marc, A. (1999) Hybridoma Cell Behaviour in Continuous Culture under Hyperosmotic Stress. *Cytotechnology*, 29, 71-84.

- Cherlet, M., Kromenaker, S. J. and Srienc, F. (1995) Surface IgG Content of Murine Hybridomas: Direct Evidence for Variation of Antibody Secretion Rates During the Cell Cycle. *Biotechnol Bioeng*, 47, 535-540.
- Cho, R. J., Campbell, M. J., Winzeler, E. A., Steinmetz, L., Conway, A., Wodicka, L., Wolfsberg, T. G., Gabrielian, A. E., Landsman, D., Lockhart, D. J. and Davis, R. W. (1998) A Genome-Wide Transcriptional Analysis of the Mitotic Cell Cycle. *Mol Cell*, 2, 65-73.
- Christensen, B. and Nielsen, J. (1999) Metabolic Network Analysis: A Powerful Tool in Metabolic Engineering. *Advances in Biochemical Engineering and Biotechnology*, 66, 209-231.
- Chu, L. and Robinson, D. K. (2001) Industrial Choices for Protein Production by Large-Scale Cell Culture. *Curr Opin Biotechnol*, 12, 180-187.
- Chuppa, S., Tsai, Y.-S., Yoon, S., Shackleford, S., Rozales, C., Bhat, R., Tsay, G., Matanguihan, C., Konstantinov, K. and Naveh, D. (1997) Fermentor Temperature as a Tool for Control of High-Density Perfusion Cultures of Mammalian Cells. *Biotechnol Bioeng*, 55, 328-338.
- Chung, J. D. and Stephanopoulos, G. (1996) On Physiological Multiplicity and Population Heterogeneity of Biological Systems. *Chem Eng Sci*, 51, 1509-1521.
- Clark, J. M. and Hirtenstein, M. D. (1981) Optimizing Culture Conditions for the Production of Animal Cells in Microcarrier Culture. *Ann New York Acad Sci*, 369, 33-46.
- Collado-Vides, J. (1989) A Transformational-Grammar Approach to the Study of the Regulation of Gene Expression. *J Theor Biol*, 136, 403-425.
- Covert, M. W., Schilling, C. H., Famili, I., Edwards, J. S., Goryanin, I. I., Selkov, E. and Palsson, B. O. (2001) Metabolic Modeling of Microbial Strains *in Silico*. *Trends Biochem Sci*, 26, 179-186.
- Cross, F. R., Archambault, V., Miller, M. and Klovstad, M. (2002) Testing a Mathematical Model of the Yeast Cell Cycle. *Mol Biol Cell*, 13, 52-70.
- Cukier, R. I., Levine, H. B. and Shuler, K. E. (1978) Nonlinear Sensitivity Analysis of Multiparameter Model Systems. *J Comput Phys*, 26, 1-42.
- Cuthrell, J. E. and Biegler, L. T. (1987) On the Optimization of Differential-Algebraic Process Systems. *AIChE J*, 33, 1257-1270.
- Dadebo, S. A. and Mcauley, K. B. (1995) Dynamic Optimization of Constrained Chemical Engineering Problems Using Dynamic Programming. *Comput Chem Eng*, 19, 513-525.
- Dalili, M., Sayles, G. D. and Ollis, D. F. (1990) Glutamine-Limited Batch Hybridoma Growth and Antibody Production: Experiment and Model. *Biotechnol Bioeng*, 36, 74-82.
- da Silva, A. L., Marc, A., Engasser, J. M. and Goergen, J. L. (1996) Kinetic Model of Hybridoma Cultures for the Identification of Rate Limiting Factors and Process Optimisation. *Math Comput Simulat*, 42, 197-205.

- Deineko, I. V., Kel, A. E., Kel-Margoulis, O. V., Wingender, E. and Ratner, V. A. (2003) Simulation of the Dynamics of Gene Networks Regulating the Cell Cycle in Mammalian Cells. *Russ J Genet*, 39, 1085-1091.
- de Tremblay, M., Perrier, M., Chavarie, C. and Archambault, J. (1993) Fed-Batch Culture of Hybridoma Cells: Comparison of Optimal Control Approach and Closed Loop Strategies. *Bioproc Biosyst Eng*, 9, 13-21.
- D'haeseleer, P., Liang, S. and Somogyi, R. (2000) Genetic Network Inference: From Co-Expression Clustering to Reverse Engineering. *Bioinformatics*, 16, 707-726.
- Dhir, S., Morrow Jr., K. J., Rhinehart, R. R. and Wiesner, T. (2000) Dynamic Optimization of Hybridoma Growth in a Fed-Batch Bioreactor. *Biotechnol Bioeng*, 67, 197-205.
- Diderich, J. A., Schepper, M., van Hoek, P., Luttkik, M. A. H., van Dijken, J. P., Pronk, J. T., Klaassen, P., Boelens, H. F. M., de Mattos, M. J. T., van Dam, K. and Kruckeberg, A. L. (1999) Glucose Uptake Kinetics and Transcription of HXT Genes in Chemostat Cultures of *Saccharomyces cerevisiae*. *J Biol Chem*, 274, 15350-15359.
- DiMasi, D. and Swartz, R. W. (1995) An Energetically Structured Model of Mammalian Cell Metabolism. 1. Model Development and Application to Steady-State Hybridoma Cell Growth in Continuous Culture. *Biotechnol Progr*, 11, 664-676.
- Domach, M. M., Leung, S. K., Cahn, R. E., Cocks, G. G. and Shuler, M. L. (1984) Computer Model for Glucose-Limited Growth of a Single Cell of *Escherichia coli* B/R-A. *Biotechnol Bioeng*, 26, 203-216.
- Duarte, N. C., Herrgard, M. J. and Palsson, B. O. (2004) Reconstruction and Validation of *Saccharomyces cerevisiae* iND750, a Fully Compartmentalized Genome-Scale Metabolic Model. *Genome Res*, 14, 1298-1309.
- Dublanche, Y. (2006) *Smartcell: A Cell Network Simulation Program*. [Online] Available from: <http://smartcell.embl.de/> [Accessed Nov 2008].
- Duval, D., Demangel, C., Munier-Jolain, K., Moisse, S. and Geahel, I. (1991) Factors Controlling Cell Proliferation and Antibody Production in Mouse Hybridoma Cells: I. Influence of the Amino Acid Supply. *Biotechnol Bioeng*, 38, 561-570.
- Eagle, H. (1955a) The specific amino acid requirements of a mammalian cell (Strain L) in tissue culture. *J Biol Chem*, 214, 839-853.
- Eagle, H. (1955b) The specific amino acid requirements of a human carcinoma cell (Strain HeLa) in tissue culture. *J Exptl Med*, 102, 37-48.
- Eagle, H., Oyama, V. I., Levy, M., Horton, C. L. and Fleischman, R. (1956) The growth response of mammalian cells in tissue culture to L-glutamine and L-glutamic acid. *J Biol Chem*, 218, 607-617.
- Echelard, Y. and Meade, H. M. (2003) Protein Production in Transgenic Animals. In: *Gene Transfer and Expression in Mammalian Cells* (Eds, Makrides, S. C.), Elsevier Science B.V., Hungary, pp. 625-639.

- Edwards, T. J., Newman, J. and Prausnitz, J. M. (1975) Thermodynamics of Aqueous Solutions Containing Volatile Weak Electrolytes. *AIChE J*, 21, 248-259.
- Edwards, J. S. and Palsson, B. O. (2000) The Escherichia Coli MG1655 *in silico* Metabolic Genotype: Its Definition, Characteristics, and Capabilities. *Proc Natl Acad Sci Unit States Am*, 97, 5528-5533.
- Edwards, J. S., Ibarra, R. U. and Palsson, B. O. (2001) In Silico Predictions of Escherichia Coli Metabolic Capabilities Are Consistent with Experimental Data. *Nat Biotechnol*, 19, 125-130.
- Eisen, M. B., Spellman, P. T., Brown, P. O. and Botstein, D. (1998) Cluster Analysis and Display of Genome-Wide Expression Patterns. *Proc Natl Acad Sci Unit States Am*, 95, 14863-14868.
- Ekholm, S. V. and Reed, S. I. (2000) Regulation of G1 Cyclin-Dependent Kinases in the Mammalian Cell Cycle. *Curr Opin Cell Biol*, 12, 676-684.
- Electricwala, A. (1992) Can Milk Replace Serum in Mammalian Cell Culture? *Cytotechnology*, 8, 1-4.
- Elowitz, M. B., Levine, A. J., Siggia, E. D. and Swain, P. S. (2002) Stochastic Gene Expression in a Single Cell. *Science*, 297, 1183-1186.
- Europa, A. F., Gambhir, A., Fu, P. C. and Hu, W. S. (2000) Multiple Steady States with Distinct Cellular Metabolism in Continuous Culture of Mammalian Cells. *Biotechnol Bioeng*, 67, 25-34.
- Famili, I. and Palsson, B. O. (2003) Systemic Metabolic Reactions Are Obtained by Singular Value Decomposition of Genome-Scale Stoichiometric Matrices. *J Theor Biol*, 224, 87-96.
- Faraday, D. B. F., Hayter, P. and Kirkby, N. F. (2001) A Mathematical Model of the Cell Cycle of a Hybridoma Cell Line. *Biochem Eng J*, 7, 49-68.
- Floudas, C. A. (1995) *Nonlinear and Mixed-Integer Optimization Fundamentals and Applications*, Oxford University Press, Oxford, UK.
- Follstad, B. D., Balcarcel, R. R., Stephanopoulos, G. and Wang, D. I. C. (1999) Metabolic Flux Analysis of Hybridoma Continuous Culture Steady State Multiplicity. *Biotechnol Bioeng*, 63, 675-683.
- Fong, S. S., Marciniak, J. Y. and Palsson, B. O. (2003) Description and Interpretation of Adaptive Evolution of *Escherichia Coli* K-12 Mg1655 by Using a Genome-Scale *in Silico* Metabolic Model. *J Bacteriol*, 185, 6400-6408.
- Forster, J., Famili, I., Fu, P., Palsson, B. O. and Nielsen, J. (2003) Genome-Scale Reconstruction of the *Saccharomyces Cerevisiae* Metabolic Network. *Genome Res.*, 13, 244-253.

- Fox, S. R., Patel, U. A., Yap, M. G. S. and Wang, D. I. C. (2004) Maximizing Interferon- γ Production by Chinese Hamster Ovary Cells through Temperature Shift Optimization: Experimental and Modeling. *Biotechnol Bioeng*, 85, 177-184.
- Frahm, B., Lane, P., Atzert, H., Munack, A., Hoffmann, M., Hass, V. C. and Portner, R. (2002) Adaptive, Model-Based Control by the Open-Loop-Feedback-Optimal (OLFO) Controller for the Effective Fed-Batch Cultivation of Hybridoma Cells. *Biotechnol Prog*, 18, 1095-1103.
- Frahm, B., Lane, P., Markl, H. and Portner, R. (2003) Improvement of a Mammalian Cell Culture Process by Adaptive, Model-Based Dialysis Fed-Batch Cultivation and Suppression of Apoptosis. *Bioproc Biosystems Eng*, 26, 1-10.
- Frangos, J. A., McIntire, L. V. and Eskin, S. G. (1988) Shear Stress Induced Stimulation of Mammalian Cell Metabolism. *Biotechnol Bioeng*, 32, 1053-1060.
- Fraser, C. M., Gocayne, J. D., White, O., Adams, M. D., Clayton, R. A., Fleischmann, R. D., Bult, C. J., Kerlavage, A. R., Sutton, G., Kelley, J. M., Fritchman, J. L., Weidman, J. F., Small, K. V., Sandusky, M., Furhmann, J., Nguyen, D., Utterback, T. R., Saudek, D. M., Phillips, C. A., Merrick, J. M., Tomb, J.-F., Dougherty, B. A., Bott, K. F., Hu, P. C., Lucier, T. S., Peterson, S. N., Smith, H. O., Hutchison III, C. A. and Venter, J. C. (1995) The Minimal Gene Complement of Mycoplasma Genitalium. *Science*, 270, 397-403.
- Fu, P. and Barford, J. P. (1994) Methods and Strategies Available for the Process Control and Optimization of Monoclonal Antibody Production. *Cytotechnology*, 14, 219-232.
- Funahashi, A., Tanimura, N., Morohashi, M. and Kitano, H. (2003) CellDesigner: A Process Diagram Editor for Gene-Regulatory and Biochemical Networks. *BioSilico*, 1, 159-162.
- Fussenegger, M. and Bailey, J. E. (1998) Molecular Regulation of Cell-Cycle Progression and Apoptosis in Mammalian Cells: Implications for Biotechnology. *Biotechnol Prog*, 14, 807-833.
- Fussenegger, M., Bailey, J. E. and Varner, J. (2000) A Mathematical Model of Caspase Function in Apoptosis. *Nat Biotechnol*, 18, 768-774.
- Gadkar, K. G., Doyle, F. J., Crowley, T. J. and Varner, J. D. (2003) Cybernetic Model Predictive Control of a Continuous Bioreactor with Cell Recycle. *Biotechnol Prog*, 19, 1487-1497.
- Gardner, T. S., di Bernardo, D., Lorenz, D. and Collins, J. J. (2003) Inferring Genetic Networks and Identifying Compound Mode of Action Via Expression Profiling. *Science*, 301, 102-105.
- Geladé, R., Van de Velde, S., Van Dijck, P. and Thevelein, J. M. (2003) Multi-Level Response of the Yeast Genome to Glucose. *Genome Biol*, 4, 233.
- Gilman, A. and Ross, J. (1995) Genetic-wAlgorithm Selection of a Regulatory Structure That Directs Flux in a Simple Metabolic Model. *Biophys J*, 69, 1321-1333.

- Glacken, M. W., Fleischaker, R. J. and Sinskey, A. J. (1986) Reduction of Waste Product Excretion Via Nutrient Control: Possible Strategies for Maximizing Product and Cell Yields on Serum in Cultures of Mammalian Cells. *Biotechnol Bioeng*, 28, 1376-1389.
- Glacken, M. W., Adema, E. and Sinskey, A. J. (1988) Mathematical Descriptions of Hybridoma Culture Kinetics: I. Initial Metabolic Rates. *Biotechnol Bioeng*, 32, 491-506.
- Glacken, M. W., Huang, C. and Sinskey, A. J. (1989) Mathematical Descriptions of Hybridoma Culture Kinetics. III. Simulation of Fed-Batch Bioreactors. *J Biotechnol*, 10, 39-65.
- Gmunder, F. K., Nordau, C.-G., Tschopp, A., Huber, B. and Cogoli, A. (1988) Dynamic Cell Culture System: A New Cell Cultivation Instrument for Biological Experiments in Space. *J Biotechnol*, 7, 217-227.
- Goergen, J. L., Marc, A. and Engasser, J. M. (1993) Determination of Cell Lysis and Death Kinetics in Continuous Hybridoma Cultures from the Measurement of Lactate Dehydrogenase Release. *Cytotechnology*, 11, 189-195.
- Goldman, M. H., James, D. C., Ison, A. P. and Bull, A. T. (1997) Monitoring Proteolysis of Recombinant Human Interferon- γ During Batch Culture of Chinese Hamster Ovary Cells. *Cytotechnology*, 23, 103-111.
- Gorfien, S. F., Paul, W., Judd, D., Tescione, L. and Jayme, D. W. (2003) Optimized Nutrient Additives for Fed-Batch Cultures. *BioPharm Int*, April 15, 34-40.
- Goswami, J., Sinskey, A. J., Steller, H., Stephanopoulos, G. N. and Wang, D. I. C. (1999) Apoptosis in Batch Cultures of Chinese Hamster Ovary Cells. *Biotechnol Bioeng*, 62, 632-640.
- Gu, Y., Rosenblatt, J. and Morgan, D. O. (1992) Cell Cycle Regulation of CDK2 Activity by Phosphorylation of Thr160 and Tyr15. *EMBO J*, 11, 3995-4005.
- Guan, Y. H. and Kemp, R. B. (1999) On-Line Heat Flux Measurements Improve the Culture Medium for the Growth and Productivity of Genetically Engineered CHO Cells. *Cytotechnology*, 30, 107-120.
- Guardia, M. J., Gambhir, A., Europa, A. F., Ramkrishna, D. and Hu, W. S. (2000) Cybernetic Modeling and Regulation of Metabolic Pathways in Multiple Steady States of Hybridoma Cells. *Biotechnol Prog*, 16, 847-853.
- Guelzim, N., Bottani, S., Bourguin, P. and Képès, F. (2002) Topological and Causal Structure of the Yeast Transcriptional Regulatory Network. *Nat Genet*, 31, 60-63.
- Haag, J. E., Wouwer, A. V. and Bogaerts, P. (2003) From Dynamic Metabolic Modeling to Unstructured Model Identification of Complex Biosystems. *Proc 13th IFAC Symp on Syst Ident*, 144-149.
- Haaker, M. P. R. and Verheijen, P. J. T. (2004) Local and Global Sensitivity Analysis for a Reactor Design with Parameter Uncertainty. *Chem Eng Res Des*, 82, 591-598.

- Haff, R. F., Swim, H. E. and Parker, R. F. (1956) Amino Acid Requirements of Rabbit Fibroblasts and Their Relation to Vaccinia Virus Multiplication. *Bacteriol Proc*, 1956, 76-77.
- Hahn, G. M. and Shiu, E. C. (1985) Protein Synthesis, Thermotolerance and Step Down Heating. *Int J Radiat Oncol Biol Phys*, 11, 159-164.
- Hammond, T. G. and Hammond, J. M. (2001) Optimized Suspension Culture: The Rotating-Wall Vessel. *Am J Physiol Renal Physiol*, 281, F12-25.
- Hansen, H. A. and Emborg, C. (1994a) Extra- and Intracellular Amino Acid Concentrations in Continuous Chinese Hamster Ovary Cell Culture. *Appl Microbiol Biotechnol*, 41, 560-564.
- Hassell, T., Gleave, S. and Butler, M. (1991) Growth Inhibition in Animal Cell Culture. The Effect of Lactate and Ammonia. *Appl Biochem Biotechnol*, 30, 29-41.
- Hasty, J., McMillen, D., Isaacs, F. and Collins, J. J. (2001) Computational Studies of Gene Regulatory Networks: In Numero Molecular Biology. *Nat Rev Genet*, 2, 268-279.
- Hatakeyama, M., Kimura, S., Naka, T., Kawasaki, T., Yumoto, N., Ichikawa, M., Kim, J.-H., Saito, K., Saeki, M., Shirouzu, M., Yokoyama, S. and Konagaya, A. (2003) A Computational Model on the Modulation of Mitogen-Activated Protein Kinase (MAPK) and Akt Pathways in Heregulin-Induced ErbB Signalling. *Biochem J*, 373, 451-463.
- Hatzimanikatis, V., Floudas, C. A. and Bailey, J. E. (1996a) Optimization of Regulatory Architectures in Metabolic Reaction Networks. *Biotechnol Bioeng*, 52, 485-500.
- Hatzimanikatis, V., Floudas, C. A. and Bailey, J. E. (1996b) Analysis and Design of Metabolic Reaction Networks Via Mixed-Integer Linear Optimization. *AIChE J*, 42, 1277-1292.
- Hatzimanikatis, V., Lee, K. H. and Bailey, J. E. (1999) A Mathematical Description of Regulation of the G1-S Transition of the Mammalian Cell Cycle. *Biotechnol Bioeng*, 65, 631-637.
- Hayter, P. M., Curling, E. M. A., Baines, A. J., Jenkins, N., Salmon, I., Strange, P. G. and Bull, A. T. (1991) Chinese Hamster Ovary Cell Growth and Interferon Production Kinetics in Stirred Batch Culture. *Appl Microbiol Biotechnol*, 34, 559-564.
- Hayter, P. M., Curling, E. M. A., Baines, A. J., Jenkins, N., Salmon, I., Strange, P. G., Tong, J. M. and Bull, A. T. (1992) Glucose-Limited Chemostat Culture of Chinese Hamster Ovary Cells Producing Recombinant Human Interferon- γ . *Biotechnol Bioeng*, 39, 327-335.
- Heal, R. D. and McGivan, J. D. (1997) Induction of the Stress Protein Grp75 by Amino Acid Deprivation in CHO Cells does not Involve an Increase in Grp75 mRNA Levels. *Biochim Biophys Acta Mol Cell Res*, 1357, 31-40.

- Heidemann, R., Lutkemeyer, D., Bunttemeyer and Lehmann, J. (1998) Effects of Dissolved Oxygen Levels and the Role of Extra- and Intracellular Amino Acid Concentrations Upon the Metabolism of Mammalian Cell Lines During Batch and Continuous Cultures. *Cytotechnology*, 26, 185-197.
- Helton, J. C. and Davis, F. J. (2000) Sampling-Based Methods. In: *Sensitivity Analysis* (Eds, Saltelli, A., Chan, K. and Scott, E. M.), John Wiley & Sons Ltd., Chichester, England, pp. 101-153.
- Henson, M. A. (2005) Cell Ensemble Modeling of Metabolic Oscillations in Continuous Yeast Cultures. *Comput Chem Eng*, 29, 645-661.
- Henzler, H.-J. (2000) Particle Stress in Bioreactors. *Adv Biochem Eng Biotechnol*, 67, 35-82.
- Herrero, J., Diaz-Uriarte, R. and Dopazo, J. (2003) An Approach to Inferring Transcriptional Regulation among Genes from Large-Scale Expression Data. *Comp Funct Genom*, 4, 148-154.
- Herrgard, M. J., Covert, M. W. and Palsson, B. O. (2004) Reconstruction of Microbial Transcriptional Regulatory Networks. *Curr Opin Biotechnol*, 15, 70-77.
- Ho, Y. (2007) *PhD Thesis: The Effects of Hyperosmotic Culture Conditions on the GS-NS0 Antibody Production Process: A Combined Experimental and Modelling Study*. Imperial College London, UK.
- Hoffmann, F. and Rinas, U. (2004) Stress Induced by Recombinant Protein Production in *Escherichia coli*. *Adv Biochem Eng Biotechnol*, 89, 73-92.
- Holter, N. S., Maritan, A., Cieplak, M., Fedoroff, N. V. and Banavar, J. R. (2001) Dynamic Modeling of Gene Expression Data. *Proc Natl Acad Sci Unit States Am*, 98, 1693-1698.
- Hong, S.-P., Leiper, F. C., Woods, A., Carling, D. and Carlson, M. (2003) Activation of Yeast Snf1 and Mammalian AMP-activated Protein Kinase by Upstream Kinases. *Proc Natl Acad Sci Unit States Am*, 100, 8839-8843.
- Hoon, M. d., Imoto, S. and Miyano, S. (2002) Inferring Gene Regulatory Networks from Time-Ordered Gene Expression Data Using Differential Equations. *Lect Notes Comput Sci*, 2534, 267-274.
- Iba, H. and Mimura, A. (2002) Inference of a Gene Regulatory Network by Means of Interactive Evolutionary Computing. *Inf Sci*, 145, 225-236.
- Ishii, N., Robert, M., Nakayama, Y., Kanai, A. and Tomita, M. (2004) Toward Large-Scale Modeling of the Microbial Cell for Computer Simulation. *J Biotechnol*, 113, 281-294.
- Jackson, J. V. and Edwards, V. H. (1975) Kinetics of Substrate Inhibition of Exponential Yeast Growth. *Biotechnol Bioeng*, 17, 943-964.
- James, K. and Bell, G. T. (1987) Human Monoclonal Antibody Production : Current Status and Future Prospects. *J Immunol Methods*, 100, 5-40.

- Jamshidi, N., Edwards, J. S., Fahland, T., Church, G. M. and Palsson, B. O. (2001) Dynamic Simulation of the Human Red Blood Cell Metabolic Network. *Bioinformatics*, 17, 286-287.
- Jang, J. D. and Barford, J. P. (2000a) Effect of Feed Rate on Growth Rate and Antibody Production in the Fed-Batch Culture of Murine Hybridoma Cells. *Cytotechnology*, 32, 229-242.
- Jang, J. D. and Barford, J. P. (2000b) An Unstructured Kinetic Model of Macromolecular Metabolism in Batch and Fed-Batch Cultures of Hybridoma Cells Producing Monoclonal Antibody. *Biochem Eng J*, 4, 153-168.
- Jayme, D. W. and Smith, S. R. (2000) Media Formulation Options and Manufacturing Process Controls to Safeguard against Introduction of Animal Origin Contaminants in Animal Cell Culture. *Cytotechnology*, 33, 27-36.
- Jeong, J. and Ataai, M. M. (1990) A Highly Structured Model for Simulation of Batch and Continuous Cultures of *B. subtilis* and Examination of Cellular Differentiation. *Ann N Y Acad Sci*, 589, 82-90.
- Jeong, J. W., Snay, J. and Ataai, M. M. (1990) A Mathematical Model for Examining Growth and Sporulation Processes of *Bacillus subtilis*. *Biotechnol Bioeng*, 35, 160-184.
- Joosten, V., Lokman, C., van den Hondel, C. and Punt, P. (2003) The Production of Antibody Fragments and Antibody Fusion Proteins by Yeasts and Filamentous Fungi. *Microb Cell Fact*, 2, 1.
- Julien, C. and Whitford, W. (2007) Bioreactor Monitoring, Modeling, and Simulation. In *BioProcess International Supplements*, Vol. 5, pp. 10-17.
- Kaern, M., Elston, T. C., Blake, W. J. and Collins, J. J. (2005) Stochasticity in Gene Expression: From Theories to Phenotypes. *Nat Rev Genet*, 6, 451-464.
- Kauffman, S. (1974) The Large Scale Structure and Dynamics of Gene Control Circuits: An Ensemble Approach. *J Theor Biol*, 44, 167-190.
- Kaufmann, H. and Fussenegger, M. (2003) Metabolic Engineering of Mammalian Cells for Higher Protein Yield. In: *Gene Transfer and Expression in Mammalian Cells* (Eds, Makrides, S. C.), Elsevier Science B.V., Hungary, pp. 457-469.
- Keay, L. (1978) The Cultivation of Animal Cells and Production of Viruses in Serum-Free Systems. *Methods Cell Biol*, 20, 169-209.
- Kel, A. E., Kel-Margoulis, O. V., Farnham, P. J., Bartley, S. M., Wingender, E. and Zhang, M. Q. (2001) Computer-Assisted Identification of Cell Cycle-Related Genes: New Targets for E2F Transcription Factors. *J Mol Biol*, 309, 99-120.
- Kepler, T. B. and Elston, T. C. (2001) Stochasticity in Transcriptional Regulation: Origins, Consequences, and Mathematical Representations. *Biophys J*, 81, 3116-3136.
- Kidder, G. W. and Dewey, V. C. (1945) Studies on the biochemistry of *Tetrahymena*. III. Strain differences. *Physiol Zool*, 18, 136-157.

- Kierzek, A. M., Zaim, J. and Zielenkiewicz, P. (2001) The Effect of Transcription and Translation Initiation Frequencies on the Stochastic Fluctuations in Prokaryotic Gene Expression. *J Biol Chem*, 276, 8165-8172.
- Kikuchi, S., Tominaga, D., Arita, M., Takahashi, K. and Tomita, M. (2003) Dynamic Modeling of Genetic Networks Using Genetic Algorithm and S-System. *Bioinformatics*, 19, 643-650.
- Kimura, R. and Miller, W. M. (1996) Effects of Elevated pCO₂ and/or Osmolality on the Growth and Recombinant tPA Production of CHO Cells. *Biotechnol Bioeng*, 52, 152-160.
- Kitayama, T., Kinoshita, A., Sugimoto, M., Nakayama, Y. and Tomita, M. (2006) A Simplified Method for Power-Law Modelling of Metabolic Pathways from Time-Course Data and Steady-State Flux Profiles. *Theor Biol Med Modell*, 3, 24.
- Köhler, G. and Milstein, C. (1975) Continuous Cultures of Fused Cells Secreting Antibody of Predefined Specificity. *Nature*, 256, 495-497.
- Kohn, K. W. (1999) Molecular Interaction Map of the Mammalian Cell Cycle Control and DNA Repair Systems. *Mol Biol Cell*, 10, 2703-2734.
- Kompala, D. S., Ramkrishna, D. and Tsao, G. T. (1984) Cybernetic Modeling of Microbial Growth on Multiple Substrates. *Biotechnol Bioeng*, 26, 1272-1281.
- Kompala, D. S., Ramkrishna, D., Jansen, N. B. and Tsao, G. T. (1986) Investigation of Bacterial Growth on Mixed Substrates: Experimental Evaluation of Cybernetic Models. *Biotechnol Bioeng*, 28, 1044-1055.
- Kontoravdi, C. (2007) *PhD Thesis: An Integrated Modelling/ Experimental Framework for Protein-Producing Cell Cultures*, Imperial College London.
- Kontoravdi, C., Asprey, S. P., Pistikopoulos, E. N. and Mantalaris, A. (2005) Application of Global Sensitivity Analysis to Determine Goals for Design of Experiments: An Example Study on Antibody-Producing Cell Cultures. *Biotechnology Progress*, 21, 1128 -1135.
- Kontoravdi, C., Asprey, S. P., Pistikopoulos, E. N. and Mantalaris, A. (2007) Development of a Dynamic Model of Monoclonal Antibody Production and Glycosylation for Product Quality Monitoring. *Comput Chem Eng*, 31, 392-400.
- Korke, R., Gatti, M. d. L., Lau, A. L. Y., Lim, J. W. E., Seow, T. K., Chung, M. C. M. and Hu, W.-S. (2004) Large Scale Gene Expression Profiling of Metabolic Shift of Mammalian Cells in Culture. *J Biotechnol*, 107, 1-17.
- Kovarova-Kovar, K. and Egli, T. (1998) Growth Kinetics of Suspended Microbial Cells: From Single-Substrate-Controlled Growth to Mixed-Substrate Kinetics. *Microbiol Mol Biol Rev*, 62, 646-666.
- Koza, J. R. (1994) *Genetic Programming II : Automatic Discovery of Reusable Programs*, MIT Press, Cambridge, MA.

- Kraft, D. (1985) On Converting Optimal Control Problems into Nonlinear Programming Problems. In: *Computational Mathematical Programming*, Vol. 15 (Ed, Schittkowski, K.) Springer-Verlag, Berlin, pp. 261-280.
- Kremling, A., Jahreis, K., Lengeler, J. W. and Gilles, E. D. (2000) The Organization of Metabolic Reaction Networks: A Signal-Oriented Approach to Cellular Models. *Metab Eng*, 2, 190-200.
- Kremling, A. and Gilles, E. D. (2001a) The Organization of Metabolic Reaction Networks: II. Signal Processing in Hierarchical Structured Functional Units. *Metab Eng*, 3, 138-150.
- Kremling, A., Bettenbrock, K., Laube, B., Jahreis, K., Lengeler, J. W. and Gilles, E. D. (2001b) The Organization of Metabolic Reaction Networks III. Application for Diauxic Growth on Glucose and Lactose. *Metab Eng*, 3, 362-379.
- Kretzmer, G. and Schugerl, K. (1991) Response of Mammalian Cells to Shear Stress. *Appl Microbiol Biotechnol*, 34, 613-616.
- Kromenaker, S. J. and Srienc, F. (1991) Cell-Cycle-Dependent Protein Accumulation by Producer and Nonproducer Murine Hybridoma Cell Lines: A Population Analysis. *Biotechnol Bioeng*, 38, 665-677.
- Kromenaker, S. J. and Srienc, F. (1994a) Effect of Lactic Acid on the Kinetics of Growth and Antibody Production in a Murine Hybridoma: Secretion Patterns During the Cell Cycle. *J Biotechnol*, 34, 13-34.
- Kromenaker, S. J. and Srienc, F. (1994b) Cell Cycle Kinetics of the Accumulation of Heavy and Light Chain Immunoglobulin Proteins in a Mouse Hybridoma Cell Line. *Cytotechnology*, 14, 205-218.
- Kuchel, P. W. (2004) Current Status and Challenges in Connecting Models of Erythrocyte Metabolism to Experimental Reality. *Progr Biophys Mol Biol*, 85, 325-342.
- Kukuruzinska, M. A., Bergh, M. L. E. and Kackson, B. J. (1987) Protein Glycosylation in Yeast. *Annu Rev Biochem*, 56, 915-944.
- Kurano, N., Leist, C., Messi, F., Kurano, S. and Fiechter, A. (1990a) Growth Behavior of Chinese Hamster Ovary Cells in a Compact Loop Bioreactor: 1. Effects of Physical and Chemical Environments. *J Biotechnol*, 15, 101-111.
- Kurano, N., Leist, C., Messi, F., Kurano, S. and Fiechter, A. (1990b) Growth Behavior of Chinese Hamster Ovary Cells in a Compact Loop Bioreactor: 2. Effects of Medium Components and Waste Products. *J Biotechnol*, 15, 113-128.
- Kuroda, K., Hauser, C., Rott, R., Klenk, H.-D. and Doerfler, W. (1986) Expression of the Influenza Virus Haemagglutinin in Insect Cells by a Baculovirus Vector. *EMBO J*, 5, 1359-1365.
- Kutalik, Z., Cho, K.-H. and Wolkenhauer, O. (2004) Optimal Sampling Time Selection for Parameter Estimation in Dynamic Pathway Modeling. *Biosystems*, 75, 43-55.

- Laffend, L. and Shuler, M. L. (1994a) Ribosomal Protein Limitations in *Escherichia Coli* under Conditions of High Translational Activity. *Biotechnol Bioeng*, 43, 388-398.
- Laszlo, A. and Li, G. C. (1985) Heat-Resistant Variants of Chinese Hamster Fibroblasts Altered in Expression of Heat Shock Protein. *Proc Natl Acad Sci Unit States Am*, 82, 8029-8033.
- Lavric, V., Ofiteru, I. D. and Woinaroschy, A. (2006) Continuous Hybridoma Bioreactor: Sensitivity Analysis and Optimal Control. *Biotechnol Appl Biochem*, 44, 81-92.
- Lee, S. B. and Bailey, J. E. (1984a) Genetically Structured Models for *lac* Promoter-Operator Function in the *Escherichia Coli* Chromosome and in Multicopy Plasmids: *lac* Operator Function. *Biotechnol Bioeng*, 26, 1372-1382.
- Lee, S. B. and Bailey, J. E. (1984b) Genetically Structures Models for *lac* Promoter-Operator Function in the Chromosome and in Multicopy Plasmids: *lac* Promoter Function. *Biotechnol Bioeng*, 26, 1383-1389.
- Lee, I.-D. and Palsson, B. O. (1992) A Macintosh Software Package for Simulation of Human Red Blood Cell Metabolism. *Comput Methods Programs Biomed*, 38, 195-226.
- Lee, J. and Ramirez, W. F. (1994) Optimal Fed-Batch Control of Induced Foreign Protein Production by Recombinant Bacteria. *AIChE J*, 40, 899-907.
- Lee, T. I., Rinaldi, N. J., Robert, F., Odom, D. T., Bar-Joseph, Z., Gerber, G. K., Hannett, N. M., Harbison, C. T., Thompson, C. M., Simon, I., Zeitlinger, J., Jennings, E. G., Murray, H. L., Gordon, D. B., Ren, B., Wyrick, J. J., Tagne, J.-B., Volkert, T. L., Fraenkel, E., Gifford, D. K. and Young, R. A. (2002) Transcriptional Regulatory Networks in *Saccharomyces cerevisiae*. *Science*, 298, 799-804.
- Leineweber, D. B., Bauer, I., Bock, H. G. and Schlöder, J. P. (2003a) An Efficient Multiple Shooting Based Reduced Sqp Strategy for Large-Scale Dynamic Process Optimization. Part I: Theoretical Aspects. *Comput Chem Eng*, 27, 157-166.
- Leineweber, D. B., Schäfer, A., Bock, H. G. and Schlöder, J. P. (2003b) An Efficient Multiple Shooting Based Reduced Sqp Strategy for Large-Scale Dynamic Process Optimization: Part II: Software Aspects and Applications. *Comput Chem Eng*, 27, 167-174.
- Lenas, P., Kitade, T., Watanabe, H., Honda, H. and Kobayashi, T. (1997) Adaptive Fuzzy Control of Nutrients Concentration in Fed-Batch Culture of Mammalian Cells. *Cytotechnology*, 25, 9-15.
- Leroy, F. and De Vuyst, L. (2003) A Combined Model to Predict the Functionality of the Bacteriocin-Producing *Lactobacillus Sakei* Strain Ctc 494. *Appl Environ Microbiol*, 69, 1093-1099.
- Lew, D. and Reed, S. (1993) Morphogenesis in the Yeast Cell Cycle: Regulation by Cdc28 and Cyclins. *J Cell Biol*, 120, 1305-1320.
- Lievense, J. C., Modak, J. M. and Lim, H. C. (1989) A Mathematical Model for the Asymmetric Dynamic Response in Microbial Systems. *J Biotechnol*, 11, 49-66.

- Lim, H. C., Tayeb, Y. J., Modak, J. M. and Bonte, P. (1986) Computational Algorithms for Optimal Feed Rates for a Class of Fed-Batch Fermentation: Numerical Results for Penicillin and Cell Mass Production. *Biotechnol Bioeng*, 28, 1408-1420.
- Ljunggren, J. and Häggström, L. (1994) Catabolic Control of Hybridoma Cells by Glucose and Glutamine Limited Fed Batch Cultures. *Biotechnol Bioeng*, 44, 808-818.
- Lloyd, D. R., Leelavatcharamas, V., Emery, A. N. and Al-Rubeai, M. (1999) The Role of the Cell Cycle in Determining Gene Expression and Productivity in CHO Cells. *Cytotechnology*, 30, 49-57.
- Lloyd, D. R., Holmes, P., Jackson, L. P., Emery, A. N. and Al-Rubeai, M. (2000) Relationship between Cell Size, Cell Cycle and Specific Recombinant Protein Productivity. *Cytotechnology*, 34, 59-70.
- Ludemann, I., Portner, R. and Markl, H. (1994) Effect of NH₃ on the Cell Growth of a Hybridoma Cell Line. *Cytotechnology*, 14, 11-20.
- Luttmann, R., Munack, A. and Thoma, M. (1985) Mathematical Modelling, Parameter Identification and Adaptive Control of Single Cell Protein Processes in Tower Loop Bioreactors. *Adv Biochem Eng Biotechnol*, 32, 95-205.
- Luus, R. (1993a) Application of Dynamic Programming to Differential-Algebraic Process Systems. *Comput Chem Eng*, 17, 373-377.
- Luus, R. (1993b) Piecewise Linear Continuous Optimal Control by Iterative Dynamic Programming. *Ind Eng Chem Res*, 32, 859-865.
- Luus, R. (1993c) Optimization of Fed-Batch Fermentors by Iterative Dynamic Programming. *Biotechnol Bioeng*, 41, 599-602.
- Ma, J. K.-C., Drake, P. M. W. and Christou, P. (2003) The Production of Recombinant Pharmaceutical Proteins in Plants. *Nat Rev Genet*, 4, 794-805.
- MacCarthy, T., Pomiankowski, A. and Seymour, R. (2005) Using Large-Scale Perturbations in Gene Network Reconstruction. *BMC Bioinformatics*, 6, 11.
- Maeda, S. (1989) Expression of Foreign Genes in Insects Using Baculovirus Vectors. *Annu Rev Entomol*, 34, 351-372.
- Makrides, S. C. (2003) Vectors for Gene Expression in Mammalian Cells. In: *Gene Transfer and Expression in Mammalian Cells* (Eds, Makrides, S. C.), Elsevier Science B.V., Hungary, pp. 9-26.
- Makrides, S. C. and Prentice, H. L. (2003) Why Choose Mammalian Cells for Protein Production? In: *Gene Transfer and Expression in Mammalian Cells* (Eds, Makrides, S. C.), Elsevier Science B.V., Hungary, pp. 1-8.
- Mancuso, A., Sharfstein, S. T., Fernandez, E. J., Clark, D. S. and Blanch, H. W. (1998) Effect of Extracellular Glutamine Concentration on Primary and Secondary Metabolism of a Murine Hybridoma: An in Vivo ¹³C Nuclear Magnetic Resonance Study. *Biotechnol Bioeng*, 57, 172-186.

- Mantzaris, N. V. (2005) Single-Cell Gene-Switching Networks and Heterogeneous Cell Population Phenotypes. *Comput Chem Eng*, 29, 631-643.
- Mantzaris, N. V., Liou, J.-J., Daoutidis, P. and Srienc, F. (1999) Numerical Solution of a Mass Structured Cell Population Balance Model in an Environment of Changing Substrate Concentration. *J Biotechnol*, 71, 157-174.
- Mantzaris, N. V., Daoutidis, P. and Srienc, F. (2001a) Numerical Solution of Multi-Variable Cell Population Balance Models: I. Finite Difference Methods. *Comput Chem Eng*, 25, 1411-1440.
- Mantzaris, N. V., Daoutidis, P. and Srienc, F. (2001b) Numerical Solution of Multi-Variable Cell Population Balance Models. II. Spectral Methods. *Comput Chem Eng*, 25, 1441-1462.
- Mantzaris, N. V., Daoutidis, P. and Srienc, F. (2001c) Numerical Solution of Multi-Variable Cell Population Balance Models. III. Finite Element Methods. *Comput Chem Eng*, 25, 1463-1481.
- Marino, M. H. (1989) Expression Systems for Heterologous Protein Production. *BioPharm*, July/August 1989, 18-33.
- Marin-Sanguino, A. and Torres, N. V. (2000) Optimization of Tryptophan Production in Bacteria. Design of a Strategy for Genetic Manipulation of the Tryptophan Operon for Tryptophan Flux Maximization. *Biotechnol Prog*, 16, 133-145.
- Marques, S., Holtel, A., Timmis, K. N. and Ramos, J. L. (1994) Transcriptional Induction Kinetics from the Promoters of the Catabolic Pathways of TOL Plasmid pWW0 of *Pseudomonas putida* for Metabolism of Aromatics. *J Bacteriol*, 176, 2517-2524.
- Masson, C., Escriou, V., Bessodes, M. and Scherman, D. (2003) Lipid Reagents for DNA Transfer into Mammalian Cells. In: *Gene Transfer and Expression in Mammalian Cells* (Eds, Makrides, S. C.), Elsevier Science B.V., Hungary, pp. 279-289.
- Mazur, X., Fussenegger, M., Renner, W. A. and Bailey, J. E. (1998) Higher Productivity of Growth-Arrested Chinese Hamster Ovary Cells Expressing the Cyclin-Dependent Kinase Inhibitor p27. *Biotechnol Prog*, 14, 705-713.
- McAdams, H. H. and Shapiro, L. (1995) Circuit Simulation of Genetic Networks. *Science*, 269, 650-656.
- McAdams, H. H. and Arkin, A. (1997) Stochastic Mechanisms in Gene Expression. *Proc Natl Acad Sci Unit States Am*, 94, 814-819.
- McAdams, H. H. and Arkin, A. (1998) Simulation of Prokaryotic Gene Circuits. *Annu Rev Biophys Biomol Struct*, 27, 199-224.
- McCoy, T. A., Maxwell, M. and Neuman, R. E. (1956) The Amino Acid Requirements of the Walker Carcinoma 256 *in Vitro*. *Canc Res*, 16, 979-984.
- McKinney, K. L., Dilwith, R. and Belfort, G. (1995) Optimizing Antibody Production in Batch Hybridoma Cell Culture. *J Biotechnol*, 40, 31-48.

- McRae, G. J., Tilden, J. W. and Seinfeld, J. H. (1982) Global Sensitivity Analysis --- A Computational Implementation of the Fourier Amplitude Sensitivity Test (FAST). *Comput Chem Eng*, 6, 15-25.
- Meijer, M. M. C., Boonstra, J., Verkleij, A. J. and Verrips, C. T. (1998) Glucose Repression in *Saccharomyces cerevisiae* is Related to the Glucose Concentration Rather Than the Glucose Flux. *J Biol Chem*, 273, 24102-24107.
- Mendes, P. and Kell, D. (1998) Non-Linear Optimization of Biochemical Pathways: Applications to Metabolic Engineering and Parameter Estimation. *Bioinformatics*, 14, 869-883.
- Mikolajczyk, M., Awotunde, O. S., Muszynska, G., Klessig, D. F. and Dobrowolska, G. (2000) Osmotic Stress Induces Rapid Activation of a Salicylic Acid-Induced Protein Kinase and a Homolog of Protein Kinase *ASK1* in Tobacco Cells. *The Plant Cell*, 12, 165-178.
- Miller, W. M., Blanch, H. W. and Wilke, C. R. (1988) A Kinetic Analysis of Hybridoma Growth and Metabolism in Batch and Continuous Suspension Culture: Effect of Nutrient Concentration, Dilution Rate, and pH. *Biotechnol Bioeng*, 32, 947-965.
- Mitchelhill, K., Stapleton, D., Gao, G., House, C., Michell, B., Katsis, F., Witters, L. and Kemp, B. (1994) Mammalian Amp-Activated Protein Kinase Shares Structural and Functional Homology with the Catalytic Domain of Yeast Snf1 Protein Kinase. *J Biol Chem*, 269, 2361-2364.
- Moat, A. G., Foster, J. W. and Spector, M. P. (2002) *Microbial Physiology*, 4th edition, Wiley-Liss, Inc., New York, USA.
- Modak, J. M., Lim, H. C. and Tayeb, Y. J. (1986) General Characteristics of Optimal Feed Rate Profiles for Various Fed-Batch Fermentation Processes. *Biotechnol Bioeng*, 28, 1396-1407.
- Mohideen, M. J., Perkins, J. D. and Pistikopoulos, E. N. (1997a) Towards an Efficient Numerical Procedure for Mixed Integer Optimal Control. *Comput Chem Eng*, 21, S457-S462.
- Moles, C. G., Mendes, P. and Banga, J. R. (2003) Parameter Estimation in Biochemical Pathways: A Comparison of Global Optimization Methods. *Genome Res*, 13, 2467-2474.
- Monod, J. (1949) The Growth of Bacterial Cultures. *Annu Rev Microbiol*, 3, 371-394.
- Moore, A., Donahue, C. J., Hooley, J., Stocks, D. L., Bauer, K. D. and Mather, J. P. (1995) Apoptosis in CHO Cell Batch Cultures: Examination by Flow Cytometry. *Cytotechnology*, 17, 1-11.
- Moreadith, R. and Lehninger, A. (1984) The Pathways of Glutamate and Glutamine Oxidation by Tumor Cell Mitochondria --- Role of Mitochondrial NAD(P)⁺-Dependent Malic Enzyme. *J Biol Chem*, 259, 6215-6221.
- Morgan, J. F. (1958) Tissue Culture Nutrition. *Bacteriol Rev*, 22, 20-45.

- Namjoshi, A. A. and Ramkrishna, D. (2005) A Cybernetic Modeling Framework for Analysis of Metabolic Systems. *Comput Chem Eng*, 29, 487-498.
- Namjoshi, A. A., Hu, W. S. and Ramkrishna, D. (2003) Unveiling Steady-State Multiplicity in Hybridoma Cultures: The Cybernetic Approach. *Biotechnol Bioeng*, 81, 80-91.
- NCBI (2007) *The NCBI Taxonomy Homepage*. [Online] Available from: <http://www.ncbi.nlm.nih.gov/Taxonomy/> [Accessed November 2007].
- Neidhardt, F. C., Ingraham, J. L. and Schaechter, M. (1990) *Physiology of the Bacterial Cell: A Molecular Approach*, Sinauer Associates, MA, USA.
- Neuman, C. P. and Sen, A. (1973) A Suboptimal Control Algorithm for Constrained Problems Using Cubic Splines. *Automatica*, 9, 601-613.
- Nielsen, L. K., Reid, S. and Greenfield, P. F. (1997) Cell Cycle Model to Describe Animal Cell Size Variation and Lag between Cell Number and Biomass Dynamics. *Biotechnol Bioeng*, 56, 372-379.
- Norbury, C. and Nurse, P. (1992) Animal Cell Cycles and Their Control. *Annu Rev Biochem*, 61, 441-468.
- Novak, B. and Tyson, J. J. (1997) Modeling the Control of DNA Replication in Fission yeast. *Proc Natl Acad Sci Unit States Am*, 94, 9147-9152.
- Novak, B. and Tyson, J. J. (2004) A Model for Restriction Point Control of the Mammalian Cell Cycle. *J Theor Biol*, 230, 563-579.
- Novak, B., Csikasz-Nagy, A., Gyorffy, B., Chen, K. and Tyson, J. J. (1998) Mathematical Model of the Fission Yeast Cell Cycle with Checkpoint Controls at the G₁/S, G₂/M and Metaphase/Anaphase Transitions. *Biophys Chem*, 72, 185-200.
- Obeyesekere, M. N., Knudsen, E. S., Wang, J. Y. J. and Zimmerman, S. O. (1997) A Mathematical Model of the Regulation of the G₁ Phase of Rb^{+/+} and Rb^{-/-} Mouse Embryonic Fibroblasts and an Osteosarcoma Cell Line. *Cell Prolif*, 30, 171-194.
- Ogawa, N., DeRisi, J. and Brown, P. O. (2000) New Components of a System for Phosphate Accumulation and Polyphosphate Metabolism in *Saccharomyces cerevisiae* Revealed by Genomic Expression Analysis. *Mol Biol Cell*, 11, 4309-4321.
- Oh, S. K. W., Vig, P., Chua, F., Teo, W. K. and Yap, M. G. S. (1993) Substantial Overproduction of Antibodies by Applying Osmotic Pressure and Sodium Butyrate. *Biotechnol Bioeng*, 42, 601-610.
- Omasa, T., Higashiyama, K.-I., Shioya, S. and Suga, K.-I. (1992) Effects of Lactate Concentration on Hybridoma Culture in Lactate-Controlled Fed-Batch Operation. *Biotechnol Bioeng*, 39, 556-564.
- O'Neil, D. G. and Lyberatos, G. (1990) Dynamic Model Development for a Continuous Culture of *Saccharomyces cerevisiae*. *Biotechnol Bioeng*, 36, 437-445.
- Osman, J. J., Birch, J. and Varley, J. (2001) The Response of GS-NS0 Myeloma Cells to pH Shifts and pH Perturbations. *Biotechnol Bioeng*, 75, 63-73.

- Ozcan, S. and Johnston, M. (1995) Three Different Regulatory Mechanisms Enable Yeast Hexose Transporter (HXT) Genes to Be Induced by Different Levels of Glucose. *Mol Cell Biol*, 15, 1564-1572.
- Ozcan, S., Dover, J. and Johnston, M. (1998) Glucose Sensing and Signaling by Two Glucose Receptors in the Yeast *Saccharomyces cerevisiae*. *EMBO J*, 17, 2566-2573.
- Ozturk, S. S. and Palsson, B. O. (1990) Chemical Decomposition of Glutamine in Cell Culture Media: Effect of Media Type, pH, and Serum Concentration. *Biotechnol Prog*, 6, 121-128.
- Pan, K.-H., Lih, C.-J. and Cohen, S. N. (2002) Analysis of DNA Microarrays Using Algorithms That Employ Rule-Based Expert Knowledge. *Proc Natl Acad Sci Unit States Am*, 99, 2118-2123.
- Papin, J. A. and Palsson, B. O. (2004) Topological Analysis of Mass-Balanced Signaling Networks: A Framework to Obtain Network Properties Including Crosstalk. *J Theor Biol*, 227, 283-297.
- Papin, J. A., Price, N. D., Edwards, J. S. and Palsson, B. O. (2002) The Genome-Scale Metabolic Extreme Pathway Structure in *Haemophilus influenzae* Shows Significant Network Redundancy. *J Theor Biol*, 215, 67-82.
- Papin, J. A., Reed, J. L. and Palsson, B. O. (2004a) Hierarchical Thinking in Network Biology: The Unbiased Modularization of Biochemical Networks. *Trends Biochem Sci*, 29, 641-647.
- Papin, J. A., Stelling, J., Price, N. D., Klant, S., Schuster, S. and Palsson, B. O. (2004b) Comparison of Network-Based Pathway Analysis Methods. *Trends Biotechnol*, 22, 400-405.
- Pardee, A. B. (1974) A Restriction Point for Control of Normal Animal Cell Proliferation. *Proc Natl Acad Sci Unit States Am*, 71, 1286-1290.
- Park, S. and Ramirez, W. F. (1988) Optimal Production of Secreted Protein in Fed-Batch Reactors. *AIChE J*, 34, 1550-1558.
- Park, L. J., Park, C. H., Park, C. and Lee, T. (1997) Application of Genetic Algorithms to Parameter Estimation of Bioprocesses. *Med Biol Eng Comput*, 35, 47-49.
- Parulekar, S. J. and Lim, H. C. (1985) Modeling, Optimization and Control of Semi-Batch Bioreactors. *Adv Biochem Eng Biotechnol*, 32, 207-258.
- Pavlou, A. K. and Reichert, J. M. (2004) Recombinant Protein Therapeutics --- Success Rates, Market Trends and Values to 2010. *Nat Biotechnol*, 22, 1513-1519.
- Pavlou, A. K. and Belsey, M. J. (2005) The Therapeutic Antibodies Market to 2008. *Eur J Pharm Biopharm*, 59, 389-396.
- Peretti, S. W. and Bailey, J. E. (1986) Mechanistically Detailed Model of Cellular Metabolism for Glucose-Limited Growth of *Escherichia coli* B/R-A. *Biotechnol Bioeng*, 28, 1672-1689.

- Phue, J.-N., Noronha, S. B., Hattacharyya, R., Wolfe, A. J. and Shiloach, J. (2005) Glucose Metabolism at High Density Growth of E. Coli B and E. Coli K: Differences in Metabolic Pathways Are Responsible for Efficient Glucose Utilization in E. Coli B as Determined by Microarrays and Northern Blot Analyses. *Biotechnol Bioeng*, 90, 805-820.
- Pinchuk, R. J., Brown, W. A., Hughes, S. M. and Cooper, D. G. (2000) Modeling of Biological Processes Using Self-Cycling Fermentation and Genetic Algorithms. *Biotechnol Bioeng*, 67, 19-24.
- Pines, J. and Hunter, T. (1989) Isolation of a Human Cyclin cDNA: Evidence for Cyclin mRNA and Protein Regulation in the Cell Cycle and for Interaction with p34^{cdc2}. *Cell*, 58, 833-846.
- Pontryagin, L. S., Boltyanskii, V. G., Gamkrelidze, R. V. and Mishchenko, E. F. (1962) *The Mathematical Theory of Optimal Processes*, John Wiley & Sons, Inc., New York.
- Portner, R. and Schafer, T. (1996) Modelling Hybridoma Cell Growth and Metabolism -- a pComparison of Selected Models and Data. *J Biotechnol*, 49, 119-135.
- Portner, R., Bohmann, A., Ludemann, I. and Markl, H. (1994) Estimation of Specific Glucose Uptake Rates in Cultures of Hybridoma Cells. *J Biotechnol*, 34, 237-246.
- Portner, R., Schilling, A., Ludemann, I. and Markl, H. (1996) High Density Fed-Batch Cultures for Hybridoma Cells Performed with the Aid of a Kinetic Model. *Bioproc Biosyst Eng*, V15, 117-124.
- Portner, R., Schwabe, J.-O. and Frahm, B. (2004) Evaluation of Selected Control Strategies for Fed-Batch Cultures of a Hybridoma Cell Line. *Biotechnol. Appl. Biochem.*, 40, 47-55.
- Pramanik, J. and Keasling, J. D. (1997) Stoichiometric Model of *Escherichia coli* Metabolism: Incorporation of Growth-Rate Dependent Biomass Composition and Mechanistic Energy Requirements. *Biotechnol Bioeng*, 56, 398-421.
- Price, N. D., Papin, J. A., Schilling, C. H. and Palsson, B. O. (2003) Genome-Scale Microbial in Silico Models: The Constraints-Based Approach. *Trends Biotechnol*, 21, 162-169.
- Process Systems Enterprise Ltd. (2004) *gPROMS Introductory User Guide*.
- Process Systems Enterprise Ltd. (2008) URL: <http://www.psenterprise.com>
- Prokudina, E. I., Valeev, R. Y. and Tchuraev, R. N. (1991) A New Method for the Analysis of the Dynamics of the Molecular Genetic Control Systems. II: Application of the Method of Generalized Threshold Models in the Investigation of Concrete Genetic Systems. *J Theor Biol*, 151, 89-110.
- Provost, A. and Bastin, G. (2004) Dynamic Metabolic Modelling under the Balanced Growth Condition. *J Process Control*, 14, 717-728.
- Puchalka, J. and Kierzek, A. M. (2004) Bridging the Gap between Stochastic and Deterministic Regimes in the Kinetic Simulations of the Biochemical Reaction Networks. *Biophys J*, 86, 1357-1372.

- Puchalka, J., Oberhardt, M. A., Godinho, M., Bielecka, A., Regenhardt, D., Timmis, K. N., Papin, J. A. and Martins dos Santos, V. A. P. (2008) Genome-Scale Reconstruction and Analysis of the *Pseudomonas putida* KT2440 Metabolic Network Facilitates Applications in Biotechnology. *PLoS Comput Biol*, 4, e1000210.
- Qu, Z., Weiss, J. N. and MacLellan, W. R. (2003) Regulation of the Mammalian Cell Cycle: A Model of the G1-to-S Transition. *Am J Physiol Cell Physiol*, 284, C349-364.
- Ramakrishna, R. and Ramkrishna, D. (1996) Cybernetic Modeling of Growth in Mixed, Substitutable Substrate Environments: Preferential and Simultaneous Utilization. *Biotechnol Bioeng*, 52, 141-151.
- Reichert, J. M. and Pavlou, A. K. (2004) Monoclonal Antibodies Market. *Nat Rev Drug Discov*, 3, 383-384.
- Reinitz, J. and Vaisnys, J. R. (1990) Theoretical and Experimental Analysis of the Phage Lambda Genetic Switch Implies Missing Levels of Co-Operativity. *J Theor Biol*, 145, 295-318.
- Rensing, L., Olomski, R. and Drescher, K. (1982) Kinetics and Models of the Drosophila Heat-Shock System. *Biosystems*, 15, 341-356.
- Reuveny, S., Velez, D., Macmillan, J. D. and Miller, L. (1986) Factors Affecting Cell Growth and Monoclonal Antibody Production in Stirred Reactors. *J Immunol Methods*, 86, 53-59.
- Riascos, C. A. M., Gombert, A. K. and Pinto, J. M. (2005) A Global Optimization Approach for Metabolic Flux Analysis Based on Labeling Balances. *Comput Chem Eng*, 29, 447-458.
- Rinas, U., Hellmuth, K., Kang, R., Seeger, A. and Schliecker, H. (1995) Entry of *Escherichia coli* into stationary phase is indicated by endogenous and exogenous accumulation of nucleobases. *Appl Environ Microbiol*, 61, 4147-4151.
- Rizzi, M., Baltés, M., Theobald, U. and Reuss, M. (1997) In Vivo Analysis of Metabolic Dynamics in *Saccharomyces Cerevisiae*: II. Mathematical Model. *Biotechnol Bioeng*, 55, 592-608.
- Rodriguez-Acosta, F., Regalado, C. M. and Torres, N. V. (1999) Non-Linear Optimization of Biotechnological Processes by Stochastic Algorithms: Application to the Maximization of the Production Rate of Ethanol, Glycerol and Carbohydrates by *Saccharomyces Cerevisiae*. *J Biotechnol*, 68, 15-28.
- Rolland, F., Winderickx, J. and Thevelein, J. M. (2001) Glucose-Sensing Mechanisms in Eukaryotic Cells. *Trends Biochem Sci*, 26, 310-317.
- Rose, W. C., Haines, W. J. and Warner, D. T. (1954) The Amino Acid Requirements of Man. V. The Role of Lysine, Arginine, and Tryptophan. *J Biol Chem*, 206, 421-430.
- Roubos, J. A., de Gooijer, C. D., van Straten, G. and van Boxtel, A. J. B. (1997) Comparison of Optimization Methods for Fed-Batch Cultures of Hybridoma Cells. *Bioproc Biosyst Eng*, 17, 99-102.

- Rowe, M. K. and Chuang, D.-M. (2004) Lithium Neuroprotection: Molecular Mechanisms and Clinical Implications. *Expert Rev Mol Med*, 6, 1-18.
- Ryll, T., Valley, U. and Wagner, R. (1994) Biochemistry of Growth Inhibition by Ammonium Ions in Mammalian Cells. *Biotechnol Bioeng*, 40, 184-193.
- Salis, H. and Kaznessis, Y. (2005) Numerical Simulation of Stochastic Gene Circuits. *Comput Chem Eng*, 29, 577-588.
- Saltelli, A., Tarantola, S. and Chan, K. P.-S. (1999) A Quantitative Model-Independent Method for Global Sensitivity Analysis of Model Output. *Technometrics*, 41, 39-56.
- Saltelli, A., Chan, K. and Scott, E. M. (2000) *Sensitivity Analysis*, John Wiley & Sons Ltd., Chichester, England.
- Samsatli, N. J., Papageorgiou, L. G. and Shah, N. (1998) Robustness Metrics for Dynamic Optimization Models under Parameter Uncertainty. *AIChE J*, 44, 1993-2006.
- San, K.-Y. and Stephanopoulos, G. (1989) Optimization of Fed-Batch Penicillin Fermentation: A Case of Singular Optimal Control with State Constraints. *Biotechnol Bioeng*, 34, 72-78.
- Sanderson, C. (1997) *The Development and Application of a Structured Model for Animal Cell Metabolism*, PhD Thesis, University of Sydney.
- Sanderson, C. S., Barton, G. W. and Barford, J. P. (1995) Optimisation of Animal Cell Culture Media Using Dynamic Simulation. *Comput Chem Eng*, 19, 681-686.
- Sanderson, C. S., Barford, J. P. and Barton, G. W. (1997) Simulation and Dynamic Optimisation of Animal Cell Culture. *Cytotechnology*, 23, 13-17.
- Sanderson, C. S., Barford, J. P. and Barton, G. W. (1999) A Structured, Dynamic Model for Animal Cell Culture Systems. *Biochem Eng J*, 3, 203-211.
- Sargent, R. W. H. and Sullivan, G. R. (1978) The Development of an Efficient Optimal Control Package. In: *Lecture Notes in Control and Information Sciences --- Optimization Techniques Part 2 (Proceedings of the 8th IFIP Conference on Optimization Techniques)*, Vol. 7 (Ed, Stoer, J.) Springer-Verlag, Berlin/Heidelberg, pp. 158-168.
- Schaff, J. C., Fink, C. C., Slepchenko, B., Carson, J. H. and Loew, L. M. (1997) A General Computational Framework for Modeling Cellular Structure and Function. *Biophys J*, 73, 1135-1146.
- Schilling, C. H. and Palsson, B. O. (2000) Assessment of the Metabolic Capabilities of *Haemophilus Influenzae* Rd through a Genome-Scale Pathway Analysis. *J Theor Biol*, 203, 249-283.
- Schilling, C. H., Edwards, J. S. and Palsson, B. O. (1999) Toward Metabolic Phenomics: Analysis of Genomic Data Using Flux Balances. *Biotechnol Prog*, 15, 288-295.
- Schlegel, M., Stockmann, K., Binder, T. and Marquardt, W. (2005) Dynamic Optimization Using Adaptive Control Vector Parameterization. *Comput Chem Eng*, 29, 1731-1751.

- Schmid, G. and Keller, T. (1992) Monitoring Hybridoma Metabolism in Continuous Suspension Culture at the Intracellular Level. *Cytotechnology*, 9, 217-229.
- Schmid, J. W., Mauch, K., Reuss, M., Gilles, E. D. and Kremling, A. (2004) Metabolic Design Based on a Coupled Gene Expression—Metabolic Network Model of Tryptophan Production in *Escherichia Coli*. *Metab Eng*, 6, 364-377.
- Schneider, M., Marison, I. W. and von Stockar, U. (1996) The Importance of Ammonia in Mammalian Cell Culture. *J Biotechnol*, 46, 161-185.
- Schroder, M., Korner, C. and Friedl, P. (1999) Quantitative Analysis of Transcription and Translation in Gene Amplified Chinese Hamster Ovary Cells on the Basis of a Kinetic Model. *Cytotechnology*, 29, 93-102.
- Schuster, S., Hilgetag, C., Woods, J. H. and Fell, D. A. (2002) Reaction Routes in Biochemical Reaction Systems: Algebraic Properties, Validated Calculation Procedure and Example from Nucleotide Metabolism. *J Math Biol*, 45, 153-181.
- Schwabe, J. O., Portner, R. and Markl, H. (1999) Improving an on-Line Feeding Strategy for Fed-Batch Cultures of Hybridoma Cells by Dialysis and 'Nutrient-Split'-Feeding. *Bioproc Biosyst Eng*, 20, 475-484.
- Schweiger, C. A. and Floudas, C. A. (1998) Interaction of Design and Control: Optimization with Dynamic Models. In: *Optimal Control: Theory, Algorithms and Applications*(Eds, Hager, W. H. and Pardalos, P. M.) Kluwer Academic Publishers, Dordrecht, Netherlands, pp. 388-435.
- Seifert, D. B. and Phillips, J. A. (1999) The Production of Monoclonal Antibody in Growth-Arrested Hybridomas Cultivated in Suspension and Immobilized Modes. *Biotechnol Prog*, 15, 655-666.
- Semones, G. B. and Lim, H. C. (1989) Experimental Multivariable Adaptive Optimization of the Steady-State Cellular Productivity of a Continuous Baker's Yeast Culture. *Biotechnol Bioeng*, 33, 16-25.
- Sharif, M., Shah, N. and Pantelides, C. C. (1998) On the Design of Multicomponent Batch Distillation Columns. *Comput Chem Eng*, 22, S69-S76.
- Sheikh, K., Forster, J. and Nielsen, L. K. (2005) Modeling Hybridoma Cell Metabolism Using a Generic Genome-Scale Metabolic Model of *Mus Musculus*. *Biotechnol Prog*, 21, 112-121.
- Shimizu, K. (2004) Metabolic Flux Analysis Based on ¹³C-Labeling Experiments and Integration of the Information with Gene and Protein Expression Patterns. *Advances in Biochemical Engineering and Biotechnology*, 91, 1-49.
- Shuler, M. L., Leung, S. and Dick, C. C. (1979) A Mathematical Model for the Growth of a Single Bacterial Cell. *Ann New York Acad Sci*, 326, 35-52.
- Sidoli, F. R., Mantalaris, A. and Asprey, S. P. (2004) Modelling of Mammalian Cells and Cell Culture Processes. *Cytotechnology*, 44, 27-46.

- Sidoli, F. R., Mantalaris, A. and Asprey, S. P. (2005) Toward Global Parametric Estimability of a Large-Scale Kinetic Single-Cell Model for Mammalian Cell Cultures. *Ind Eng Chem Res*, 44, 868 - 878.
- Simon, I., Barnett, J., Hannett, N., Harbison, C. T., Rinaldi, N. J., Volkert, T. L., Wyrick, J. J., Zeitlinger, J., Gifford, D. K., Jaakkola, T. S. and Young, R. A. (2001) Serial Regulation of Transcriptional Regulators in the Yeast Cell Cycle. *Cell*, 106, 697-708.
- Simon, L. and Karim, M. N. (2002) Control of Starvation-Induced Apoptosis in Chinese Hamster Ovary Cell Cultures. *Biotechnol Bioeng*, 78, 645-657.
- Simpson, N. H., Singh, R. P., Perani, A., Goldenzon, C. and Al-Rubeai, M. (1998) In Hybridoma Cultures, Deprivation of Any Single Amino Acid Leads to Apoptotic Death, which is Suppressed by the Expression of the bcl-2 Gene. *Biotechnol Bioeng*, 59, 90-98.
- Slater, M. L., Sharrow, S. O. and Gart, J. J. (1977) Cell Cycle of *Saccharomyces cerevisiae* in Populations Growing at Different Rates. *Proc Natl Acad Sci Unit States Am*, 74, 3850-3854.
- Slepchenko, B. M., Schaff, J. C., Macara, I. and Loew, L. M. (2003) Quantitative Cell Biology with the Virtual Cell. *Trends Cell Biol*, 13, 570-576.
- Smolen, P., Baxter, D. A. and Byrne, J. H. (1998) Frequency Selectivity, Multistability, and Oscillations Emerge from Models of Genetic Regulatory Systems. *Am J Physiol Cell Physiol*, 274, C531-C542.
- Sobol', I. M. (1967) On the Distribution of Points in a Cube and the Approximate Evaluation of Integrals. *USSR Comput Math Math Phys*, 7, 86-112.
- Sobol', I. M. (1976) Uniformly Distributed Sequences with an Additional Uniform Property. *USSR Comput Math Math Phys*, 16, 236-242.
- Sobol', I. M. (2001) Global Sensitivity Indices for Nonlinear Mathematical Models and Their Monte Carlo Estimates. *Math Comput Simulat*, 55, 271-280.
- Spellman, P. T., Sherlock, G., Zhang, M. Q., Iyer, V. R., Anders, K., Eisen, M. B., Brown, P. O., Botstein, D. and Futcher, B. (1998) Comprehensive Identification of Cell Cycle-Regulated Genes of the Yeast *Saccharomyces cerevisiae* by Microarray Hybridization. *Mol Biol Cell*, 9, 3273-3297.
- Spier, R. E. (1997) Factors Limiting the Commercial Application of Animal Cells in Culture. *Cytotechnology*, 23, 113-117.
- Stoger, E., Schillberg, S., Twyman, R. M., Fischer, R. and Christou, P. (2003) Antibody Production in Transgenic Plants. In: *Methods in Molecular Biology, Vol.248: Antibody Engineering: Methods and Protocols* (Eds, Lo, B. K. C.), Humana Press Inc., Totowa, NJ, USA, pp. 301-318.
- Stoll, T., Perregaux, C., von Stockar, U. and Marison, I. W. (1995) Production of Immunoglobulin a in Different Reactor Configurations. *Cytotechnology*, 17, 53-63.

- Straight, J. V. and Ramkrishna, D. (1991) Complex Growth Dynamics in Batch Cultures: Experiments and Cybernetic Models. *Biotechnol Bioeng*, 37, 895-909.
- Styczynski, M. P. and Stephanopoulos, G. (2005) Overview of Computational Methods for the Inference of Gene Regulatory Networks. *Comput Chem Eng*, 29, 519-534.
- Sugimoto, M., Kikuchi, S. and Tomita, M. (2005) Reverse Engineering of Biochemical Equations from Time-Course Data by Means of Genetic Programming. *Biosystems*, 80, 155-164.
- Suzuki, E. and Ollis, D. F. (1989) Cell Cycle Model for Antibody Production Kinetics. *Biotechnol Bioeng*, 34, 1398-1402.
- Suzuki, E. and Ollis, D. F. (1990) Enhanced Antibody Production at Slowed Growth Rates: Experimental Demonstration and a Simple Structured Model. *Biotechnol Prog*, 6, 231-236.
- Svetlov, V. V. and Cooper, T. G. (1995) Compilation and Characteristics of Dedicated Transcription Factors in *Saccharomyces cerevisiae*. *Yeast*, 11, 1439-1484.
- Takahashi, K., Yugi, K., Hashimoto, K., Yamada, Y., Pickett, C. J. F. and Tomita, M. (2002) Computational Challenges in Cell Simulation: A Software Engineering Approach. *IEEE Intelligent Systems*, 17, 64-71.
- Takahashi, K., Ishikawa, N., Sadamoto, Y., Sasamoto, H., Ohta, S., Shiozawa, A., Miyoshi, F., Naito, Y., Nakayama, Y. and Tomita, M. (2003) E-Cell 2: Multi-Platform E-Cell Simulation System. *Bioinformatics*, 19, 1727-1729.
- Takahashi, K., Kaizu, K., Hu, B. and Tomita, M. (2004) A Multi-Algorithm, Multi-Timescale Method for Cell Simulation. *Bioinformatics*, 20, 538-546.
- Tamayo, P., Slonim, D., Mesirov, J., Zhu, Q., Kitareewan, S., Dmitrovsky, E., Lander, E. S. and Golub, T. R. (1999) Interpreting Patterns of Gene Expression with Self-Organizing Maps: Methods and Application to Hematopoietic Differentiation. *Proc Natl Acad Sci Unit States Am*, 96, 2907-2912.
- Tan, Y., Wang, Z.-X. and Marshall, K. C. (1996) Modeling Substrate Inhibition of Microbial Growth. *Biotechnol Bioeng*, 52, 602-608.
- Tatiraju, S., Soroush, M. and Mutharasan, R. (1999) Multi-Rate Nonlinear State and Parameter Estimation in a Bioreactor. *Biotechnol Bioeng*, 63, 22-32.
- Tavazoie, S., Hughes, J. D., Campbell, M. J., Cho, R. J. and Church, G. M. (1999) Systematic Determination of Genetic Network Architecture. *Nat Genet*, 22, 281-285.
- Tchuraev, R. N. (1991) A New Method for the Analysis of the Dynamics of the Molecular Genetic Control Systems. I: Description of the Method of Generalized Threshold Models. *J Theor Biol*, 151, 71-88.
- Tegner, J., Yeung, M. K. S., Hasty, J. and Collins, J. J. (2003) Reverse Engineering Gene Networks: Integrating Genetic Perturbations with Dynamical Modeling. *Proc Natl Acad Sci Unit States Am*, 100, 5944-5949.

- Teich, A., Meyer, S., Lin, H. Y., Andersson, L., Enfors, S.-O. and Neubauer, P. (1999) Growth Rate Related Concentration Changes of the Starvation Response Regulators σ^S and ppGpp in Glucose-Limited Fed-Batch and Continuous Cultures of *Escherichia coli*. *Biotechnol Prog*, 15, 123-129.
- Teixeira, A., Cunha, A. E., Clemente, J. J., Moreira, J. L., Cruz, H. J., Alves, P. M., Carrondo, M. J. T. and Oliveira, R. (2005) Modelling and Optimization of a Recombinant Bhk-21 Cultivation Process Using Hybrid Grey-Box Systems. *J Biotechnol*, 118, 290-303.
- Thieffry, D. and Thomas, R. (1995) Dynamical Behaviour of Biological Regulatory Networks. II: Immunity Control in Bacteriophage Lambda. *Bull Math Biol*, 57, 277-297.
- Thomas, R. (1973) Boolean Formalization of Genetic Control Circuits. *J Theor Biol*, 42, 563-585.
- Thomas, R. (1991) Regulatory Networks Seen as Asynchronous Automata: A Logical Description. *J Theor Biol*, 153, 1-23.
- Thomas, R., Thieffry, D. and Kaufman, M. (1995) Dynamical Behaviour of Biological Regulatory Networks. I: Biological Role of Feedback Loops and Practical Use of the Concept of the Loop-Characteristic State. *Math Biol*, 57, 247-276.
- Tieu, D., Cluett, W. R. and Penlidis, A. (1995) A Comparison of Collocation Methods for Solving Dynamic Optimization Problems. *Comput Chem Eng*, 19, 375-381.
- Tomita, M. (2001a) Towards Computer Aided Design (Cad) of Useful Microorganisms. *Bioinformatics*, 17, 1091-1092.
- Tomita, M. (2001b) Whole-Cell Simulation: A Grand Challenge of the 21st Century. *Trends Biotechnol*, 19, 205-210.
- Tomita, M., Hashimoto, K., Takahashi, K., Shimizu, T., Matsuzaki, Y., Miyoshi, F., Saito, K., Tanida, S., Yugi, K., Venter, J. and Hutchison, C., 3rd (1999) E-Cell: Software Environment for Whole-Cell Simulation. *Bioinformatics*, 15, 72-84.
- Torres, N. V., Voit, E. O., Glez-Alcón, C. and Rodríguez, F. (1997) An Indirect Optimization Method for Biochemical Systems: Description of Method and Application to the Maximization of the Rate of Ethanol, Glycerol, and Carbohydrate Production in *Saccharomyces Cerevisiae*. *Biotechnol Bioeng*, 55, 758-772.
- Tritsch, G. L. and Moore, G. E. (1962) Spontaneous Decomposition of Glutamine in Cell Culture Media. *Exp Cell Res*, 28, 360-364.
- Tsang, T. H., Himmelblau, D. M. and Edgar, T. F. (1975) Optimal Control via Collocation and Non-Linear Programming. *International Journal of Control*, 21, 763 - 768.
- Tsuchiya, H. M., Fredrickson, A. G. and Aris, R. (1966) Dynamics of Microbial Cell Populations. *Adv Chem Eng*, 6, 125-206.
- Turanyi, T. and Rabitz, H. (2000) Local Methods. In: *Sensitivity Analysis* (Eds, Saltelli, A., Chan, K. and Scott, E. M.), John Wiley & Sons Ltd., Chichester, England, pp. 81-99.

- Tweeddale, H., Notley-McRobb, L. and Ferenci, T. (1998) Effect of Slow Growth on Metabolism of *Escherichia Coli*, as Revealed by Global Metabolite Pool ("Metabolome") Analysis. *J Bacteriol*, 180, 5109-5116.
- Tyson, J. J., Chen, K. C. and Novak, B. (2003) Sniffers, Buzzers, Toggles and Blinkers: Dynamics of Regulatory and Signaling Pathways in the Cell. *Curr Opin Cell Biol*, 15, 221-231.
- Tziampazis, E. and Sambanis, A. (1994) Modeling of Cell Culture Processes. *Cytotechnology*, 14, 191-204.
- Uchiyama, K. and Shioya, S. (1999) Modeling and Optimization of α -Amylase Production in a Recombinant Yeast Fed-Batch Culture Taking Account of the Cell Cycle Population Distribution. *J Biotechnol*, 71, 133-141.
- Varner, J. and Ramkrishna, D. (1998) Application of Cybernetic Models to Metabolic Engineering: Investigation of Storage Pathways. *Biotechnol Bioeng*, 58, 282-291.
- Varner, J. and Ramkrishna, D. (1999a) Metabolic Engineering from a Cybernetic Perspective. 1. Theoretical Preliminaries. *Biotechnol Prog*, 15, 407-425.
- Varner, J. and Ramkrishna, D. (1999b) Metabolic Engineering from a Cybernetic Perspective. 2. Qualitative Investigation of Nodal Architectures and Their Response to Genetic Perturbation. *Biotechnol Prog*, 15, 426-438.
- Vassiliadis, V. S., Sargent, R. W. H. and Pantelides, C. C. (1994a) Solution of a Class of Multistage Dynamic Optimization Problems. 1. Problems without Path Constraints. *Ind Eng Chem Res*, 33, 2111-2122.
- Vassiliadis, V. S., Sargent, R. W. H. and Pantelides, C. C. (1994b) Solution of a Class of Multistage Dynamic Optimization Problems. 2. Problems with Path Constraints. *Ind Eng Chem Res*, 33, 2123-2133.
- Venkatesh, K. V., Doshi, P. and Rengaswamy, R. (1997) An Optimal Strategy to Model Microbial Growth in a Multiple Substrate Environment. *Biotechnol Bioeng*, 56, 635-644.
- Verma, R., Boleti, E. and George, A. J. T. (1998) Antibody Engineering: Comparison of Bacterial, Yeast, Insect and Mammalian Expression Systems. *J Immunol Methods*, 216, 165-181.
- Visek, W., Kolodny, G. and Gross, P. (1972) Ammonia Effects in Cultures of Normal and Transformed 3T3 Cells. *J Cell Physiol*, 80, 373-381.
- Volpe, P. and Eremenko, T. (1973) A Method for Measuring Cell Cycle Phases in Suspension Cultures. In: *Methods in Cell Biology*, Vol. VI (Ed, Prescott, D. M.) London, pp. 113-126.
- Vriezen, N. and van Dijken, J. P. (1998) Fluxes and Enzyme Activities in Central Metabolism of Myeloma Cells Grown in Chemostat Culture. *Biotechnol Bioeng*, 59, 28-39.

- Wang, J., Gillesa, E. D., Lengelerb, J. W. and Jahre, K. (2001) Modeling of Inducer Exclusion and Catabolite Repression Based on a PTS-Dependent Sucrose and Non-PTS-Dependent Glycerol Transport Systems in *Escherichia Coli* K-12 and Its Experimental Verification. *J Biotechnol*, 92, 133-158.
- Wang, W., Cherry, J. M., Botstein, D. and Li, H. (2002a) A Systematic Approach to Reconstructing Transcription Networks in *Saccharomyces cerevisiae*. *Proc Natl Acad Sci Unit States Am*, 99, 16893-16898.
- Wang, X., He, S., Zhang, Y., Xu, J., Feng, Q., Li, L., Mi, L. and Chen, Z. (2004) DMSO Arrested Hybridoma Cells for Enhanced Antibody Production. *Chin J Biotechnol*, 20, 568-571.
- Watanabe, S., Shuttleworth, J. and Al-Rubeai, M. (2002) Regulation of Cell Cycle and Productivity in NS0 Cells by the over-Expression of p21^{CIP1}. *Biotechnol Bioeng*, 77, 1-7.
- Werner, R. G., Walz, F., Noe, W. and Konrad, A. (1992) Safety and Economic Aspects of Continuous Mammalian Cell Culture. *J Biotechnol*, 22, 51-68.
- Whitford, W. G. (2006) Fed-Batch Mammalian Cell Culture in Bioproduction. *Bioproc Int*, 4, 30-40.
- Wick, L. M. and Egli, T. (2004) Molecular Components of Physiological Stress Responses in *Escherichia coli*. *Adv Biochem Eng Biotechnol*, 89, 1-45.
- Wiechert, W. (2002) Modeling and Simulation: Tools for Metabolic Engineering. *J Biotechnol*, 94, 37-63.
- Wikipedia (2008) *Dynamic Programming*. URL: http://en.wikipedia.org/wiki/Dynamic_programming
- Wolfram MathWorld (2008) *Pontryagin Maximum Principle*. URL: <http://mathworld.wolfram.com/PontryaginMaximumPrinciple.html>
- Wong, D. C. F., Wong, K. T. K., Goh, L. T., Heng, C. K. and Yap, M. G. S. (2005) Impact of Dynamic Online Fed-Batch Strategies on Metabolism, Productivity and N-Glycosylation Quality in CHO Cell Cultures. *Biotechnol Bioeng*, 89, 164-177.
- Woods, A., Munday, M., Scott, J., Yang, X., Carlson, M. and Carling, D. (1994) Yeast SNF1 Is Functionally Related to Mammalian AMP-activated Protein Kinase and Regulates Acetyl-CoA Carboxylase *in Vivo*. *J Biol Chem*, 269, 19509-19515.
- Wu, M.-H., Dimopoulos, G., Mantalaris, A. and Varley, J. (2004) The Effect of Hyperosmotic Pressure on Antibody Production and Gene Expression in the GS-NS0 Cell Line. *Biotechnol Appl Biochem*, 40, 41-46.
- Wu, P., Ray, N. G. and Shuler, M. L. (1992) A Single-Cell Model for CHO Cells. *Annals of New York Academy of Science*, 665, 152-187.
- Wurm, F. M. (2004) Production of Recombinant Protein Therapeutics in Cultivated Mammalian Cells. *Nat Biotechnol*, 22, 1393-1398.

- Xie, L. and Wang, D. I. C. (1994) Fed-Batch Cultivation of Animal Cells Using Different Medium Design Concepts and Feeding Strategies. *Biotechnol Bioeng*, 43, 1175-1189.
- Xie, L. and Wang, D. I. C. (1997) Integrated Approaches to the Design of Media and Feeding Strategies for Fed-Batch Cultures of Animal Cells. *Trends Biotechnol*, 15, 109-113.
- Yang, J.-D., Angelillo, Y., Chaudhry, M., Goldenberg, C. and Goldenberg, D. (2000) Achievement of High Cell Density and High Antibody Productivity by a Controlled-Fed Perfusion Bioreactor Process. *Biotechnol Bioeng*, 69, 74-82.
- Yeung, M. K. S., Tegner, J. and Collins, J. J. (2002) Reverse Engineering Gene Networks Using Singular Value Decomposition and Robust Regression. *Proc Natl Acad Sci Unit States Am*, 99, 6163-6168.
- Yin, Z., Wilson, S., Hauser, N. C., Tourneu, H., Hoheisel, J. D. and Brown, A. J. P. (2003) Glucose Triggers Different Global Responses in Yeast, Depending on the Strength of the Signal, and Transiently Stabilizes Ribosomal Protein mRNAs. *Mol Microbiol*, 48, 713-724.
- Yuk, I. H. Y. and Wang, D. I. C. (2002) Changes in the Overall Extent of Protein Glycosylation by Chinese Hamster Ovary Cells over the Course of Batch Culture. *Biotechnol Appl Biochem*, 36, 133-140.
- Zeng, A. P. (1996) Mathematical Modeling and Analysis of Monoclonal Antibody Production by Hybridoma Cells. *Biotechnol Bioeng*, 50, 238-247.
- Zeng, A.-P. and Deckwer, W.-D. (1999) Model Simulation and Analysis of Perfusion Culture of Mammalian Cells at High Cell Density. *Biotechnol Prog*, 15, 373-382.
- Zeng, A. P., Deckwer, W.-D. and Hu, W. S. (1998a) Determinants and Rate Laws of Growth and Death of Hybridoma Cells in Continuous Culture. *Biotechnol Bioeng*, 57, 642-654.
- Zeng, A.-P., Hu, W.-S. and Deckwer, W.-D. (1998b) Variation of Stoichiometric Ratios and Their Correlation for Monitoring and Control of Animal Cell Cultures. *Biotechnol Prog*, 14, 434-441.
- Zhou, W., Rehm, J. and Hu, W.-S. (1995) High Viable Cell Concentration Fed-Batch Cultures of Hybridoma Cells through on-Line Nutrient Feeding. *Biotechnol Bioeng*, 46, 579-587.
- Zhou, W., Rehm, J., Europa, A. and Hu, W.-S. (1997a) Alteration of Mammalian Cell Metabolism by Dynamic Nutrient Feeding. *Cytotechnology*, 24, 99-108.
- Zhou, W., Chen, C.-C., Buckland, B. and Aunins, J. (1997b) Fed-Batch Culture of Recombinant NS0 Myeloma Cells with High Monoclonal Antibody Production. *Biotechnol Bioeng*, 55, 783-792.
- Zografos, Z. (1998) On a Measure of Dependence Based on Fisher's Information Matrix. *Commun Statist – Theory Meth*, 27, 1715-1728.
- Zupke, C. and Stephanopoulos, G. (1995) Intracellular Flux Analysis in Hybridomas Using Mass Balances and in Vitro ¹³C NMR. *Biotechnol Bioeng*, 45, 292-303.
- zu Putlitz, J., Kubasek, W. L., Duchene, M., Marget, M., Von Specht, B.-U. and Domdey, H. (1990) Antibody Production in Baculovirus Infected Insect Cells. *Nat Biotechnol*, 8, 651-654.

Appendix 1

— ELISA Protocol for Hybridoma CRL-1606 Antibody Analysis

Antibody concentration was measured using an enzyme-linked immunosorbent assay (ELISA) modified from Kontoravdi (2007).

Protocol:

- (1) Prepare 96 wellplates (Corning or MaxiSorp [flat-bottom clear])
- (2) Dilute 10 µg of anti-human fibronectin antibody from rabbit (Sigma-Aldrich F3648) to 10ml in coating buffer (0.05M carbonate-bicarbonate buffer, pH 9.6). Add 100µl to each well. Seal plate with thin film and incubate overnight (16-20h) at ~4°C on flat surface.
- (3) Empty the plate and rinse 3 times with 250-300µl washing buffer per well (PBS (GIBCO) with 0.05% v/v Tween (Sigma)).
- (4) Block non-specific binding with 250-300µl blocking buffer (coating buffer with 0.5% w/v casein (BDH)) for 1 h.
- (5) Empty the plate and rinse 4 times with washing buffer.
- (6) Dilute 2µg of human fibronectin (Chemicon FC010) to 10ml in PBS solution. Add 100µl to each well. Seal plate and incubate at room temperature for 1 h on a shaker.
- (7) Empty the plate and rinse 4 times with washing buffer
- (8) Dilute standards (anti-human fibronectin antibody from mouse, Sigma-Aldrich F0791) and samples to suitable ranges using sample conjugate buffer (PBS solution with 0.2% w/v casein and 0.02% v/v Tween). Add 100µl of standards/ samples to each well in duplicates/ triplicates respectively. Seal plate and incubate at room temperature for 2 h on a shaker.
- (9) Empty the plate and rinse 4 times with washing buffer.

- (10) Dilute 6.4 μg of anti-mouse Fc antibody from goat (Sigma-Aldrich A0168) to 10ml with sample-conjugate buffer. Add 100 μl to each well. Seal plate and incubate at room temperature on a shaker.
- (11) Empty the plate and rinse 4 times with washing buffer.
- (12) Dissolve one tablet of 3,3',3,3'-tetramethylbenzidine (TMB, Sigma-Aldrich T-3405) in 10ml of 0.05M phosphate-citrate buffer at pH 5.0 (citric acid, BDH; dibasic sodium phosphate Na_2HPO_4 (Sigma), in the dark). Add 2 μl of fresh 30% H_2O_2 (Sigma) just before use. Add 100 μl of the mixture to each well. Seal plate and incubate in the dark at room temperature for 10-60mins on a shaker. Check every 10mins for colour development.
- (13) Stop the reaction with 50 μl of 2.5M sulphuric acid (BDH) for each well.
- (14) Analyse absorbance at 450 nm with an ELX 808 Ultra Microplate Reader (Bio-Tek Instruments, Inc., Vermont, U.S.A.)

Buffers:

(i) Coating buffer (0.05M carbonate-bicarbonate buffer, pH 9.6)

- Sodium carbonate, Na_2CO_3 (Sigma)
- Sodium hydrogencarbonate, NaHCO_3 (Sigma)

E.g. To make 500ml ---

Dissolve 0.846g Na_2CO_3 and 1.439g NaHCO_3 in 500ml water. The resulting pH should be slightly higher than 9.6. Then add a small amount of NaHCO_3 (each time the order of 0.01g) until the pH is 9.6.

(ii) 0.05M Phosphate-citrate buffer (pH 5.0)

- Citric acid, $\text{C}_6\text{H}_8\text{O}_7 \cdot \text{H}_2\text{O}$ (BDH)
- Dibasic sodium phosphate, Na_2HPO_4 (Sigma)

E.g. To make 100ml ---

Dissolve 0.864g Na_2HPO_4 in 30ml water and 0.638g citric acid in 30ml water separately. Then put 24ml citric acid solution into a container with 100ml capacity. Add 20ml Na_2HPO_4 solution and mix well. The pH should be below 5.0. Then slowly add small amounts of Na_2HPO_4 solution (starting with 1–2ml and gradually decrease to 0.25–0.5ml) until the pH is 5.0. Keep a record of how much Na_2HPO_4 solution is added. Finally add more water until the total volume is 100ml.

Appendix 2

— Protocol for Cell-Cycle Analysis

Cell fixing:

- (1) Spin cell culture sample at 800rpm for 5 min.
- (2) Remove supernatant.
- (3) Add ~0.5ml PBS solution to re-suspend cells.
- (4) Then add equal volume of ethanol drop by drop and mix well.
- (5) Store at -4°C and analyse within 1 month.

Propidium iodide (PI) staining:

- (1) Staining solution contains 50 $\mu\text{g}/\text{ml}$ propidium-iodide (Sigma-Aldrich P4864; stock 1mg/ml), 25 $\mu\text{g}/\text{ml}$ RNase Type I-A (Sigma) in PBS (GIBCO). (E.g. for 40ml staining solution, add 2ml PI stock, 1ml RNase stock, and 37ml PBS solution)
- (2) Store in dark container and keep at -4°C .

Cell-cycle flow cytometry analysis:

- (1) Check flow cytometer performance using Flow-CheckTM fluorospheres (Beckman Coulter Inc.)
- (2) Set-up software protocol to analyse cell cycle distribution. Prepare the following analysis:
 - (i) Forward scatter (FS) linear versus side scatter (SS) log [gate A]
 - (ii) PMT4 (605 – 615 nm) peak versus PMT4 integral (linear) [gate B]
Explanations: Single particles fall along the diagonal of peak versus integral diagram. The doublets lie on the right hand side of the diagonal.
 - (iii) Ratio of peak/integral of PMT4 versus PMT4 integral (linear) [gate C]
Explanation: The ratio of peak/integral for single particles is higher than doublets.

(iv) PMT4 integral (linear) versus time of flight [gate D]

Explanation: time of flight is proportional to the pulse width. Single particles have shorter TOF than doublets.

(v) Plot a histogram for gate A+B

(vi) Plot a histogram for gate A+C

(vii) Plot a histogram for gate A+D

All the 3 histograms should agree with each other

(3) Pellet $0.5 - 1 \times 10^6$ cells per sample. Then gently decant and blot away the ethanol solution. [Final sample concentration $\sim 1 - 2 \times 10^6$ cell/ml]

(4) Add 0.5ml PI-RNase solution. Then mix well and incubate at room temperature in the dark for at least 30mins.

(5) Acquire at least 10,000 – 20,000 data in the histogram.

Cell-cycle distribution histogram analysis:

- Cylchred software (Cytonet UK)

Appendix 3

— Lineage Relationship between the Animal Sources of
CHO and Hybridoma Cells

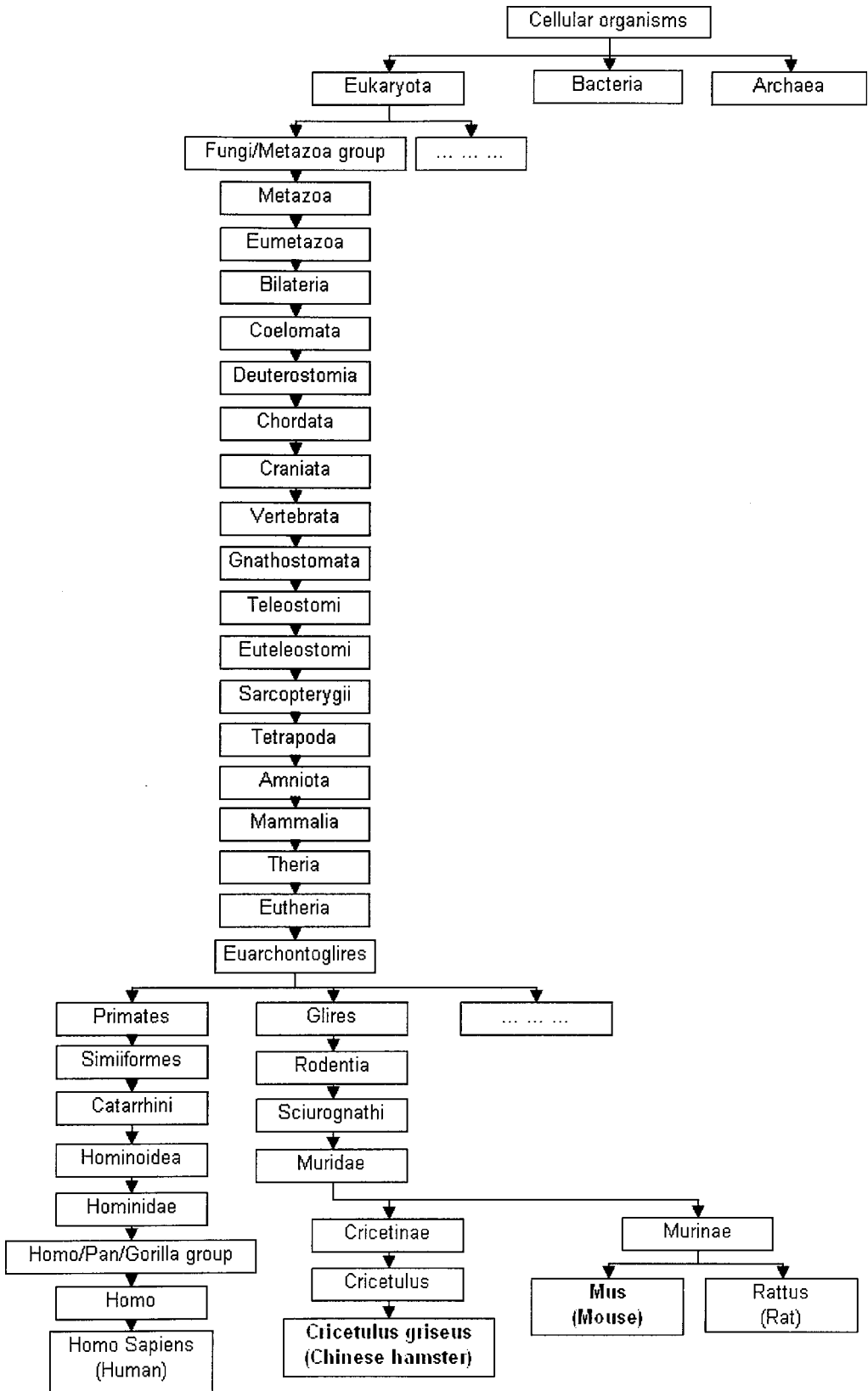
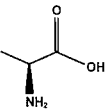
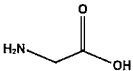
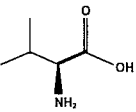
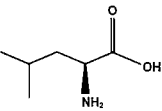
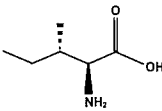
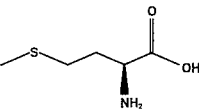
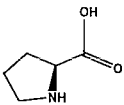
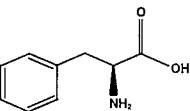
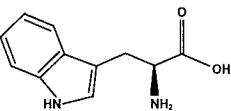


Figure A3.1: Lineage relationship between Chinese hamster and mouse which are sources of CHO and hybridoma cells respectively. (Source: NCBI 2007)

Appendix 4

— Molecular Structure of the 20 Amino Acids Modelled in CHO

Table A4.1: Amino acid structure of the 20 amino acids. Essential amino acids are highlighted in bold. (Campbell and Smith, 2000; ChemFinder 2005)

Amino acid	Structure (at pH 6-7)	Formula	MW (g/mole)
L-Alanine (Ala) [CAS: 56-41-7]		C ₃ H ₇ NO ₂	89
Glycine (Gly) [CAS: 56-40-6]		C ₂ H ₅ NO ₂	75
L-Valine (Val) [CAS: 72-18-4]		C₅H₁₁NO₂	117
L-Leucine (Leu) [CAS: 61-90-5]		C₆H₁₃NO₂	131
L-Isoleucine (Ile) [CAS: 73-32-5]		C₆H₁₃NO₂	131
L-Methionine (Met) [CAS: 63-68-3]		C₅H₁₁NO₂S	149
L-Proline (Pro) [CAS: 147-85-3]		C ₅ H ₉ NO ₂	115
L-Phenylalanine (Phe) [CAS: 63-91-2]		C₉H₁₁NO₂	165
L-Tryptophan (Trp) [CAS: 73-22-3]		C₁₁H₁₂N₂O₂	204

L-Aspartic acid (Asp) [CAS: 56-84-8]		$C_4H_7NO_4$ (at acidic pH)	133
		$C_4H_6NO_4$ (at neutral pH)	132
L-Glutamic acid (Glu) [CAS: 56-86-0]		$C_5H_9NO_4$ (at acidic pH)	147
		$C_5H_8NO_4$ (at neutral pH)	146
L-Asparagine (Asn) [CAS: 70-47-3]		$C_4H_8N_2O_3$	132
L-Glutamine (Gln) [CAS: 56-85-9]		$C_5H_{10}N_2O_3$	146
L-Serine (Ser) [CAS: 56-45-1]		$C_3H_7NO_3$	105
L-Threonine (Thr) [CAS: 72-19-5]		$C_4H_9NO_3$	119
L-Tyrosine (Tyr) [CAS: 60-18-4]		$C_9H_{11}NO_3$	181
L-Cysteine (Cys) [CAS: 52-90-4]		$C_3H_7NO_2S$	121
L-Lysine (Lys) [CAS: 56-87-1]		$C_6H_{14}N_2O_2$ (basic pH)	146
		$C_6H_{15}N_2O_2$ (neutral)	147
L-Arginine (Arg) [CAS: 74-79-3]		$C_6H_{14}N_4O_2$ (basic pH)	174
		$C_6H_{15}N_2O_2$ (neutral)	175
L-Histidine (His) [CAS: 71-00-1]		$C_6H_9N_3O_2$ (basic pH)	155
		$C_6H_{10}N_3O_2$ (neutral)	156

Appendix 5

— Calculation of Glutamine Degradation Rate, Maximum Specific Growth Rates, and Minimum Specific Death Rate

Glutamine Degradation Rate

DMEM medium was incubated at 37°C in a humidified incubator and the concentration of glutamine was monitored for about 2 days.

Table A5.1: Calculation of the average glutamine degradation rate in DMEM medium.

Time (h)	Avg. time (h)	Glutamine conc. (mM)	Avg. degradation rate (h ⁻¹)	Relative uncertainty (±%)	Absolute uncertainty	
					(- h ⁻¹)	(+ h ⁻¹)
0	-	4.37	-			
31.5	15.75	3.5	0.0063	25	0.0015	0.0016
55.5	43.5	3.19	0.0037	67	0.0024	0.0026
			Avg.: 0.005			

Glutamine

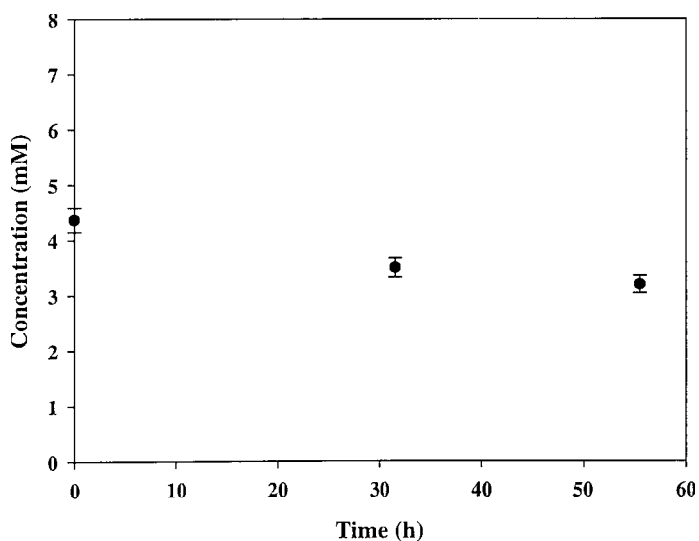


Figure A5.1: Glutamine concentration data for degradation rate estimation.

Gln degradation rate

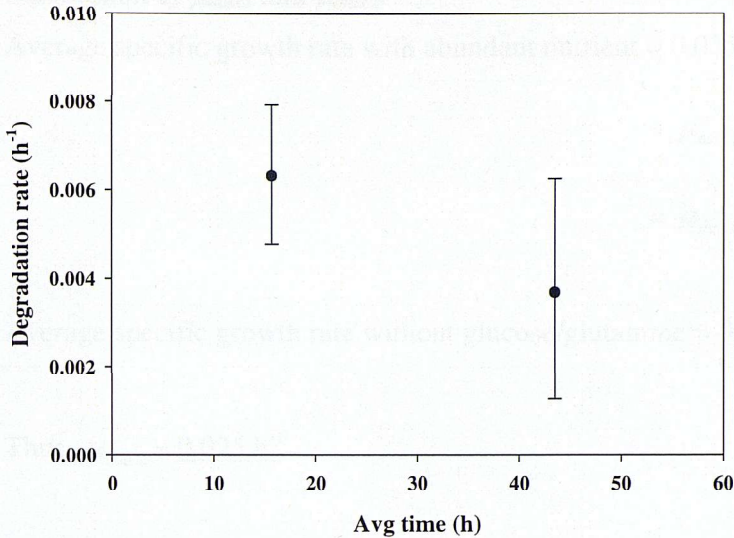


Figure A5.2: Estimation of glutamine degradation rate in DMEM medium.

Intrinsic Specific Growth Rate

The rate of change of viable cell concentration is affected by both growth, death rate and any possible lysis of viable cells. The rate of change of total cell concentration is affected by growth rate and any possible fragmentation of dead cells. Assuming the lysis of viable cells and fragmentation of dead cells are negligible, the rate of change of total cell concentration is used to estimate the intrinsic specific growth rate for CHO-IFN γ batch culture.

Table A5.2: Calculation of the average specific growth rate before and after exhaustion of glucose and glutamine in CHO-IFN γ batch culture.

Avg time (h)	Rate of change of X_t (h^{-1})	Relative uncertainty ($\pm\%$)	Absolute uncertainty		Remark	Avg rate of change of X_t (h^{-1})
			($- h^{-1}$)	($+ h^{-1}$)		
1.51	0.060	183	0.096	0.128	Abs uncertainty too high (not used)	<u>0.035</u>
11.40	0.0320	80	0.0225	0.0298		
24.23	0.0255	151	0.0338	0.0448		
36.85	0.0263	93	0.0215	0.0285		
48.27	0.0474	119	0.0494	0.0655		
52.19	0.0685	311	0.187	0.248	Abs uncertainty too high (not used)	
60.77	0.0459	57	0.0234	0.0297	Glucose and glutamine exhausted	<u>0.01</u>
72.85	0.0214	160	0.0303	0.0386		
85.02	0.00552	283	0.0140	0.0178		
97.02	0.00999	412	0.0280	0.0349		

Calculation of μ_{max1} and μ_{max2} :

Average specific growth rate with abundant nutrient = 0.035 h^{-1}

$$\sim \mu_{max1} \cdot \left(1 + \frac{\mu_{max2}}{\mu_{max1}} \right)$$

$$= \mu_{max1} + \mu_{max2}$$

Average specific growth rate without glucose/glutamine = $0.01 \text{ h}^{-1} \sim \mu_{max1}$

Thus, $\mu_{max2} \sim 0.025 \text{ h}^{-1}$

Minimum Specific Death Rate

Table A5.3: Calculation of the minimum specific death rate in CHO-IFN γ batch culture.

Time (h)	Viable cell		Total cell		Dead cell conc. (cell ml ⁻¹)	<u>Linearised dead cell conc.</u>		Viability (%)	<u>Specific death rate (h⁻¹)</u>
	conc. (cell ml ⁻¹)	(±%)	conc. (cell ml ⁻¹)	(±%)		conc. (cell ml ⁻¹)	(±%)		
0.02	0.25		0.25		0	0		100.00	0
3.02	0.28	12	0.295	12	0.015	0.001539	0.069	94.92	0.001936
19.77	0.441	12	0.453	12	0.012	0.010074	0.107	97.35	0.001413
28.69	0.536	12	0.556	12	0.02	0.014618	0.131	96.40	0.001043
45.02	0.78	14	0.795	14	0.015	0.02294	0.221	98.11	0.000774
51.52	1.005	14	1.04	14	0.035	0.026253	0.286	96.63	0.000571
									Avg: 0.001

Appendix 6

— Estimation of Measurement Error for Amino Acids & Identification of Outlying Initial Amino Acid Concentrations Using Fed-Batch Culture Simulation with Zero Growth Rate

A6.1 Estimation of Measurement Error for Amino Acids

Table A6.1: Estimation of measurement error of glutamine in CHO-IFN γ fed-batch cultures.

	<i>a</i>	<i>b</i>	Average of ‘b’ (mM)
	Average difference between glutamine measurement in HPLC and biochemical analyser (mM)	$\frac{a}{2}$ (mM)	
‘0.1mM Fed-batch’	0.089	0.0447	<u>0.05</u>
‘1 st 0.3mM Fed-batch’	0.113	0.0565	
‘2 nd 0.3mM Fed-batch’	0.076	0.0485	
‘0.5mM Fed-batch’	0.104	0.0520	
‘0.3,0.7mM Fed-batch’	0.117	0.0586	
‘0.3,0.35mM Fed-batch’	0.089	0.0447	

Remark: Refer to section 5.3.2 for notations of the glutamine- and glucose-controlled fed-batch CHO-IFN γ cultures.

A6.2 Identification of Outlying Initial Amino Acid Concentrations Using Fed-Batch Culture Simulation with Zero Growth Rate

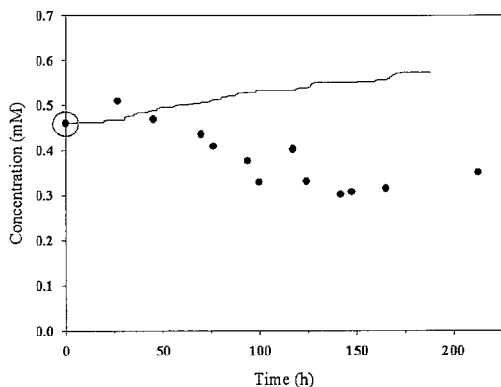
The validity of the initial conditions of amino acids in fed-batch cultures was tested using virtual simulations where the specific growth rate was set to 0 and the viable cell concentration was set to 0^+ . The viable cell concentration cannot be exactly zero due to the fact that it is used in the denominator of certain quantities in the model. Since there would be no cellular consumption in this virtual simulation, all essential amino acids (Table 4.1) must show a higher concentration than the experiment data. When this is not satisfied, or when the first experimental measurement is significantly lower than subsequent measurements in a way that cannot be explained by the cells' production of non-essential amino acids, are indicated by a ***black circle*** at time zero in the corresponding diagrams in this section.

A6.2.1 Initial Amino Acid Concentration Testing Under Zero Consumption for Fed-Batch CHO-IFN γ Data with Glutamine Set-Point at 0.1mM

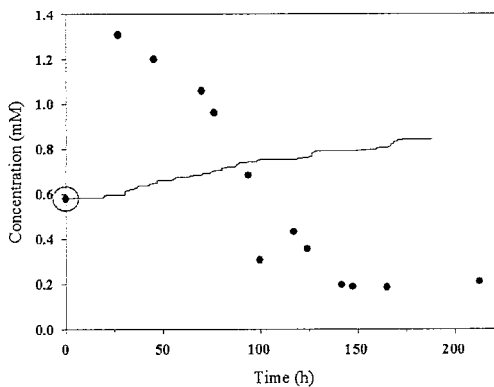
Symbols —

- : Amino acid concentration measured from high-performance liquid chromatography (HPLC) (Wong et al., 2005).
- : Glutamine concentration measured from bio-analyser (Wong et al., 2005).

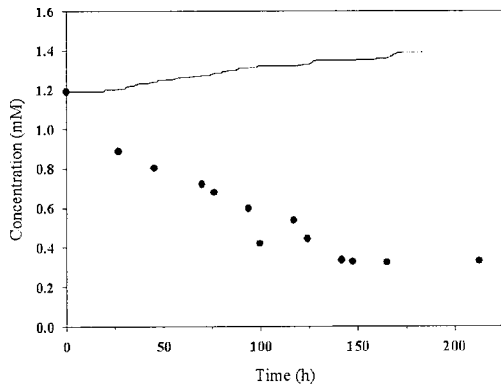
Phenylalanine (FB 0.1mM Gln)



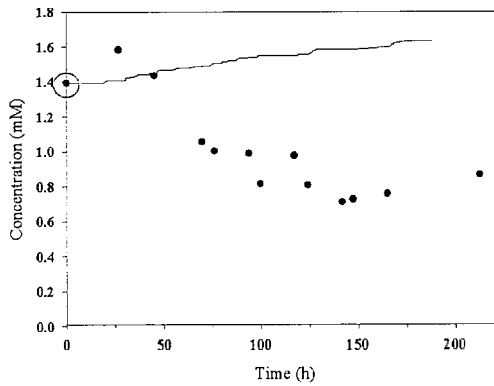
Leucine (FB 0.1mM Gln)



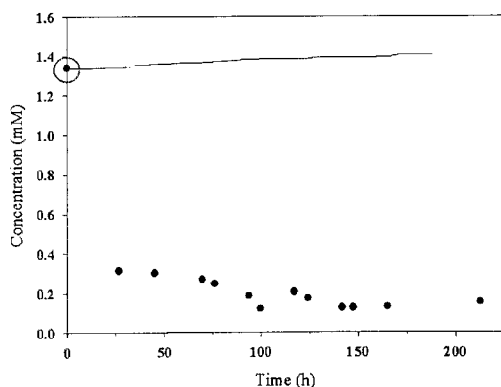
Isoleucine (FB 0.1mM Gln)



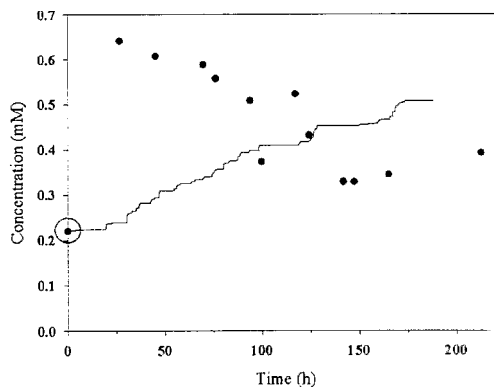
Lysine (FB 0.1mM Gln)



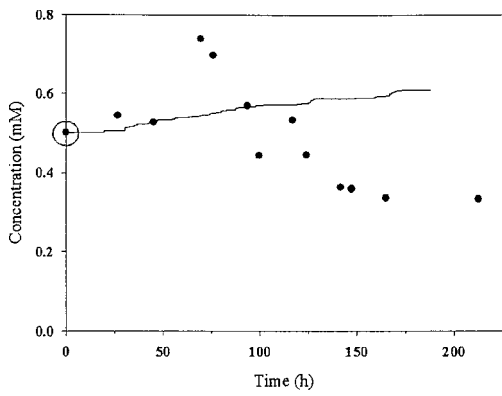
Methionine (FB 0.1mM Gln)



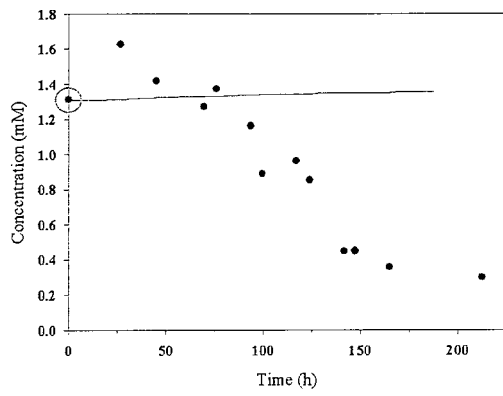
Valine (FB 0.1mM Gln)



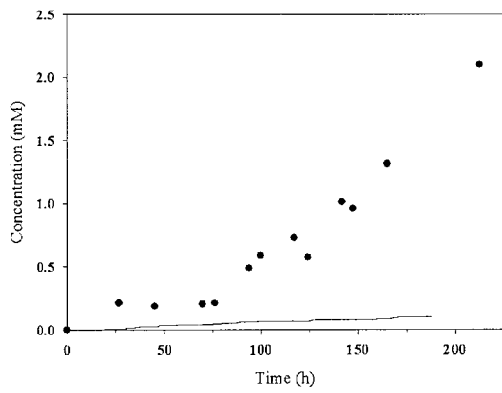
Tyrosine (FB 0.1mM Gln)



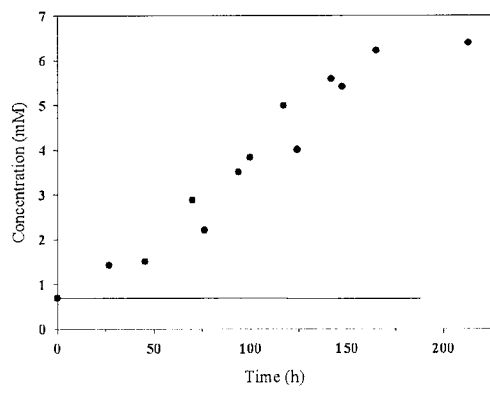
Cysteine (FB 0.1mM Gln)



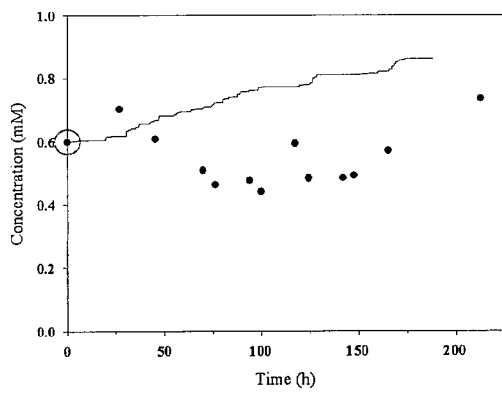
Proline (FB 0.1mM Gln)



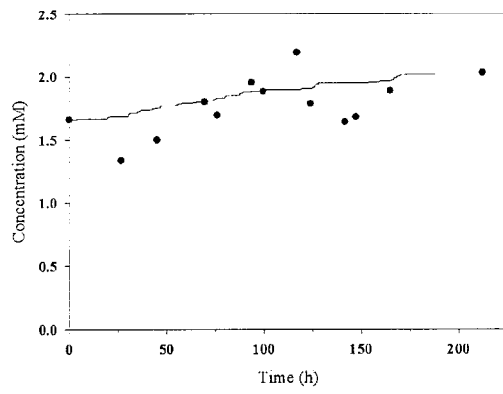
Alanine (FB 0.1mM Gln)



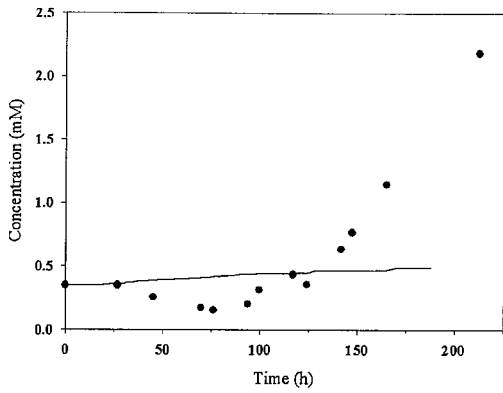
Threonine (FB 0.1mM Gln)



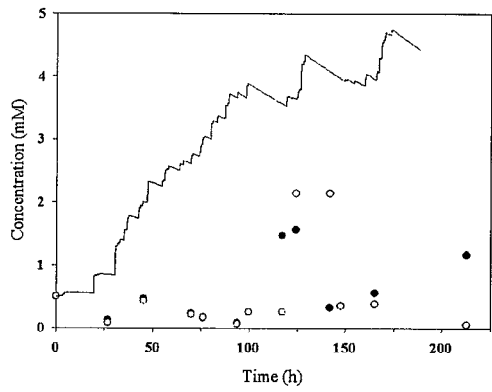
Arginine (FB 0.1mM Gln)



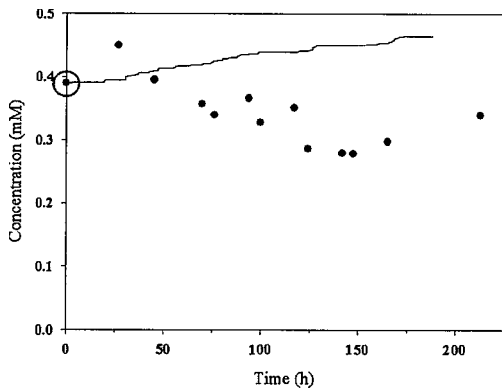
Glycine (FB 0.1mM Gln)



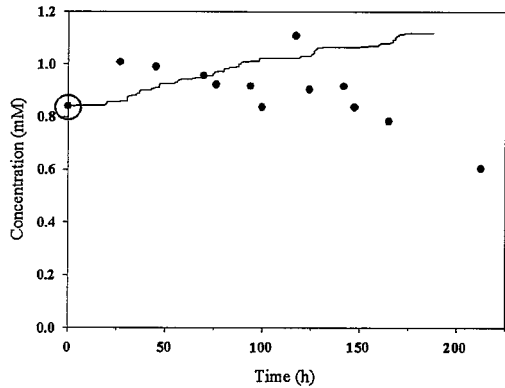
Glutamine (FB 0.1mM Gln)



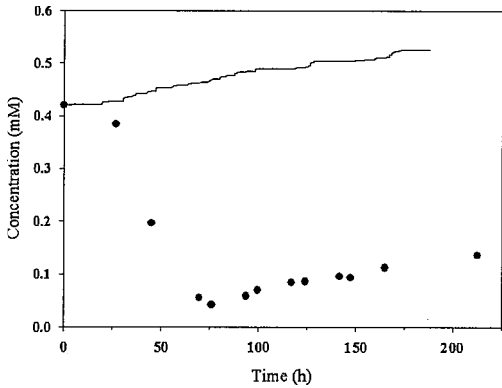
Histidine (FB 0.1mM Gln)



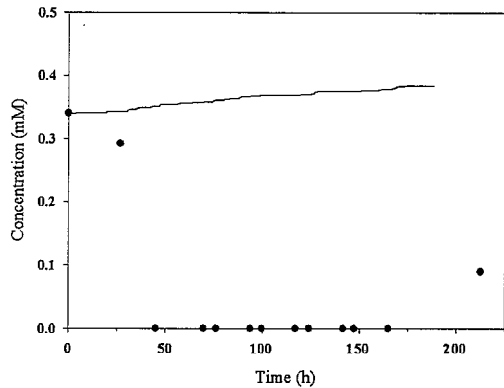
Serine (FB 0.1mM Gln)



Asparagine (FB 0.1mM Gln)



Glutamic acid (FB 0.1mM Gln)



Aspartic acid (FB 0.1mM Gln)

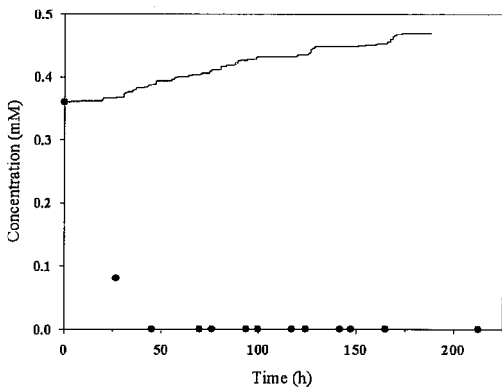


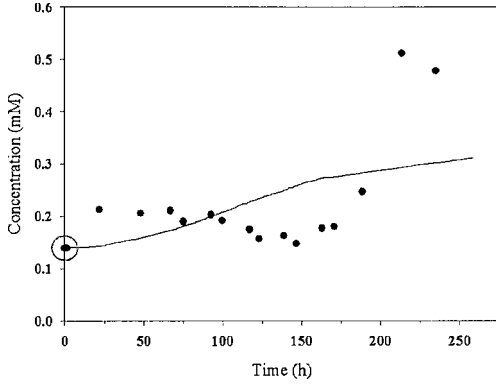
Figure A6.1: Mass balance testing of amino acids data in fed-batch CHO-IFN γ culture with glutamine set-point at 0.1mM.

A6.2.2 Initial Amino Acid Concentration Testing Under Zero Consumption for Fed-Batch CHO-IFN γ Data with Glutamine Set-Point at 0.3mM (1st experiment)

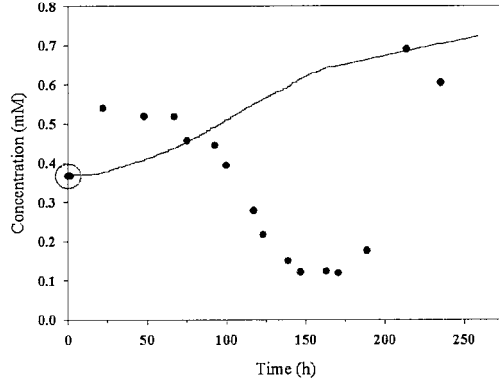
Symbols —

- : Amino acid concentration measured from high-performance liquid chromatography (HPLC) (Wong et al., 2005).
- : Glutamine concentration measured from bio-analyser (Wong et al., 2005).

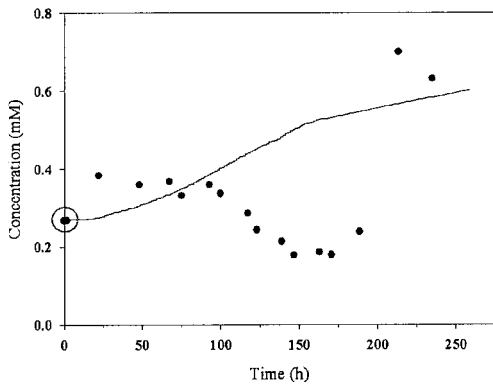
Phenylalanine (FB 0.3mM Gln(1))



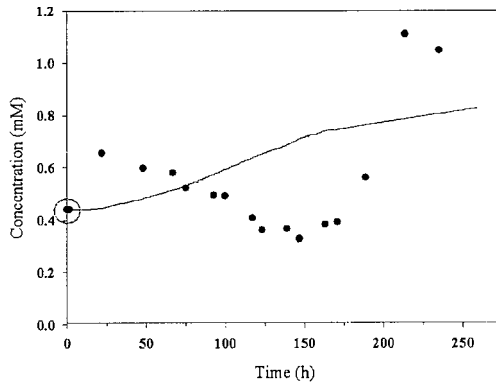
Leucine (FB 0.3mM Gln(1))



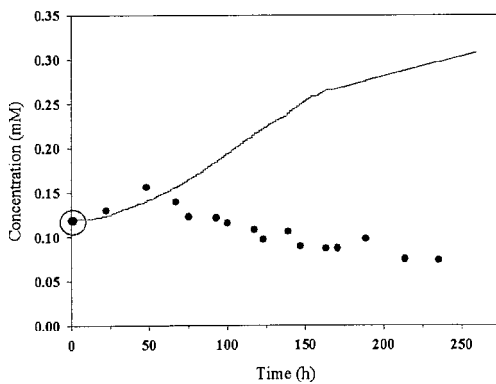
Isoleucine (FB 0.3mM Gln(1))



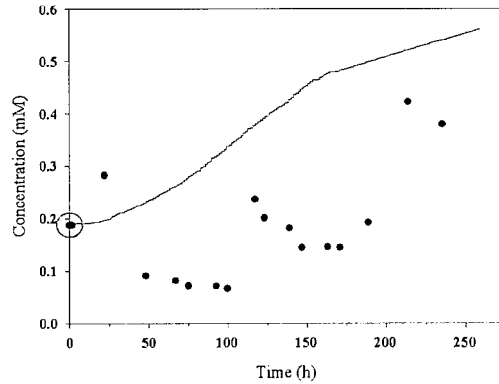
Lysine (FB 0.3mM Gln(1))



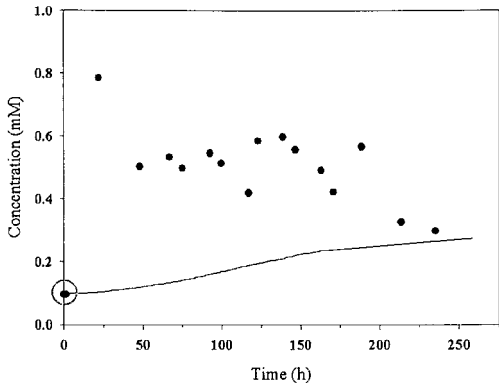
Methionine (FB 0.3mM Gln(1))



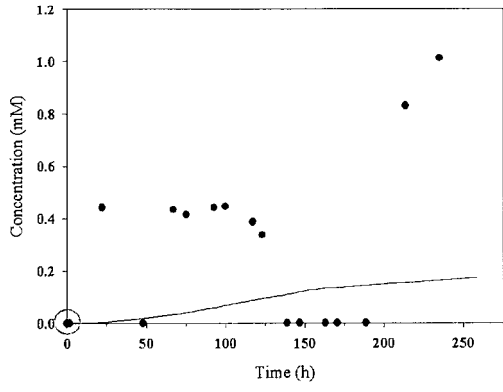
Valine (FB 0.3mM Gln(1))



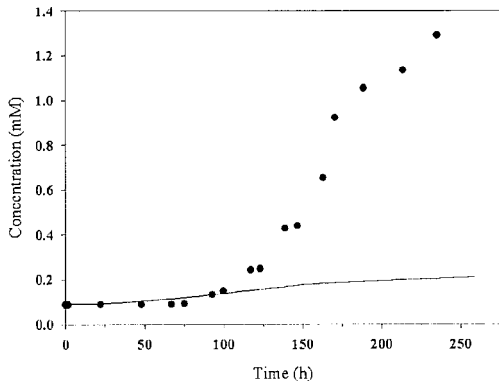
Tyrosine (FB 0.3mM Gln(1))



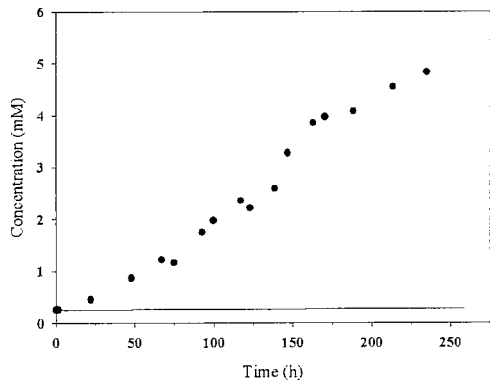
Cysteine (FB 0.3mM Gln(1))



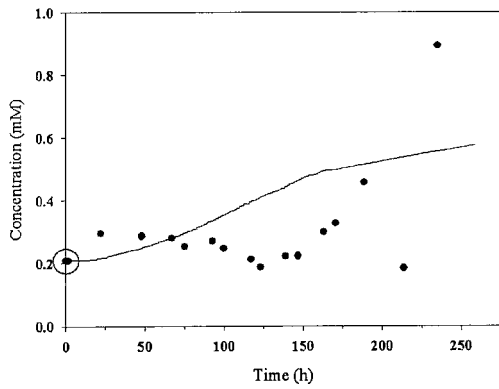
Proline (FB 0.3mM Gln(1))



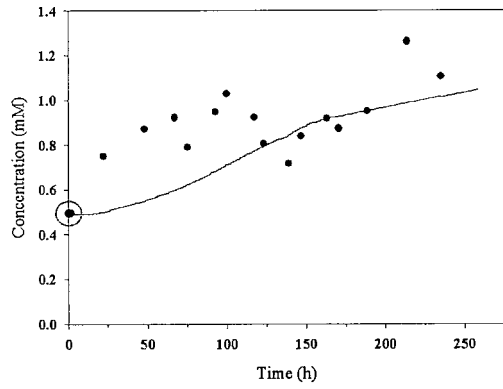
Alanine (FB 0.3mM Gln(1))



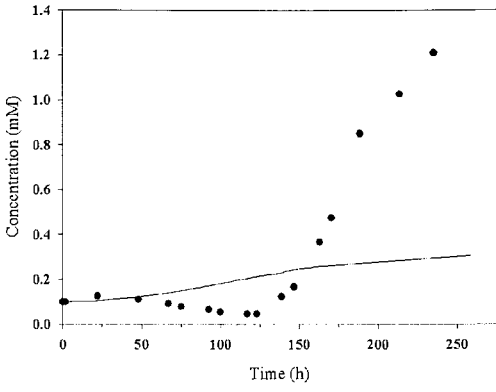
Threonine (FB 0.3mM Gln(1))



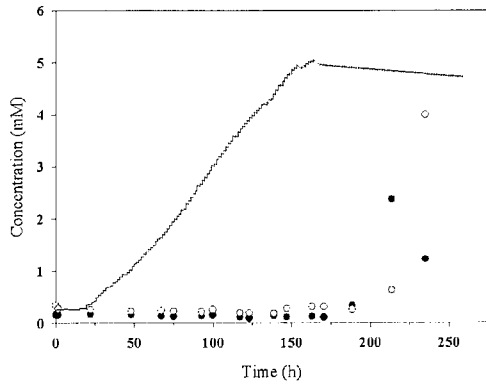
Arginine (FB 0.3mM Gln(1))



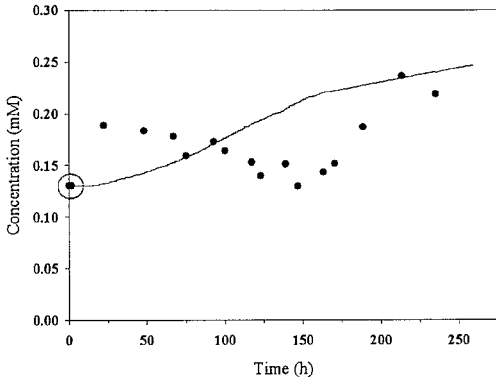
Glycine (FB 0.3mM Gln(1))



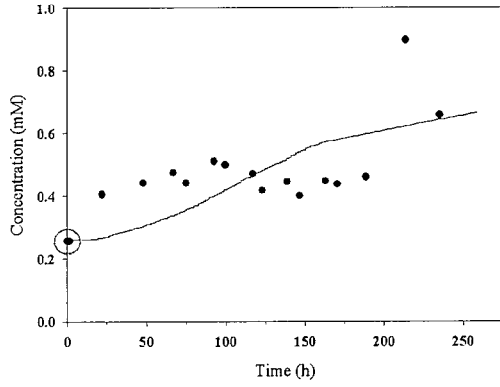
Glutamine (FB 0.3mM Gln(1))



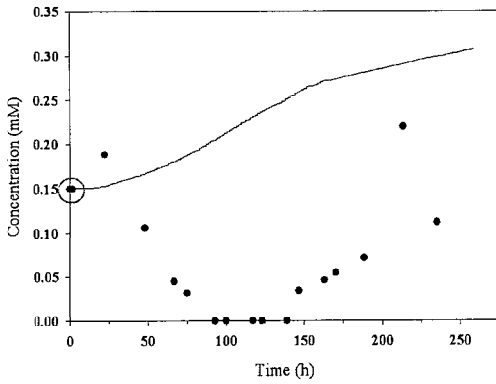
Histidine (FB 0.3mM Gln(1))



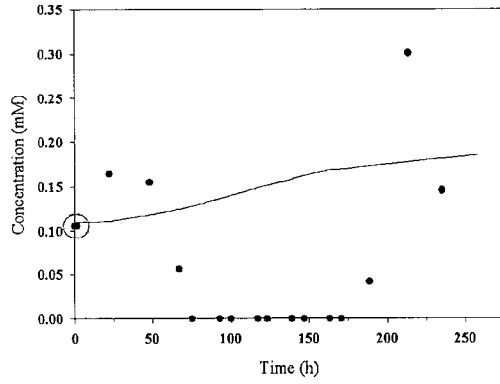
Serine (FB 0.3mM Gln(1))



Asparagine (FB 0.3mM Gln(1))



Glutamic acid (FB 0.3mM Gln(1))



Aspartic acid (FB 0.3mM Gln(1))

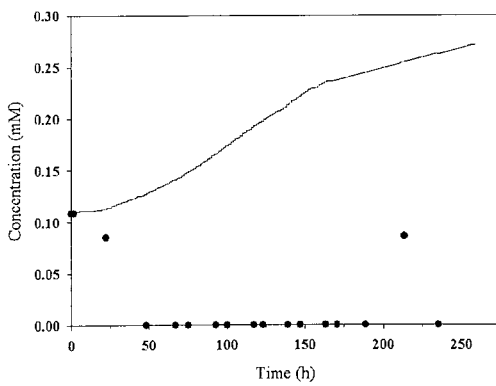


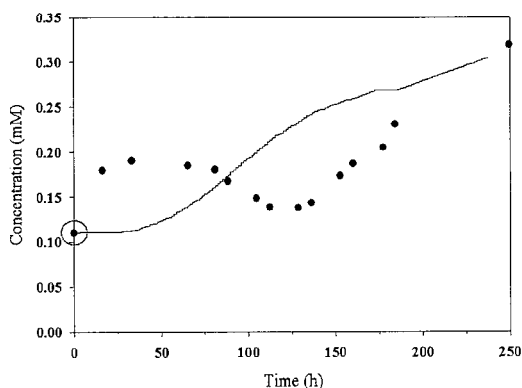
Figure A6.2: Mass balance testing of amino acids data in fed-batch CHO-IFN γ culture with glutamine set-point at 0.3mM (1st experiment).

A6.2.3 Initial Amino Acid Concentration Testing Under Zero Consumption for Fed-Batch CHO-IFN γ Data with Glutamine Set-Point at 0.3mM (2nd experiment)

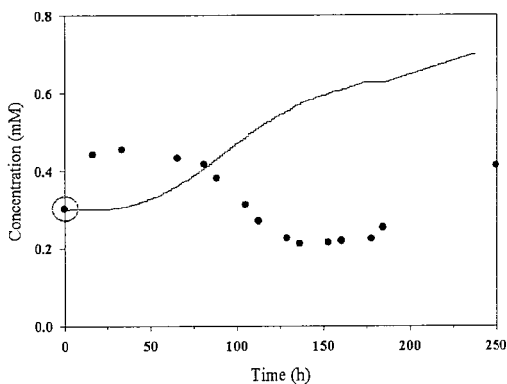
Symbols —

- : Amino acid concentration measured from high-performance liquid chromatography (HPLC) (Wong et al., 2005).
- : Glutamine concentration measured from bio-analyser (Wong et al., 2005).

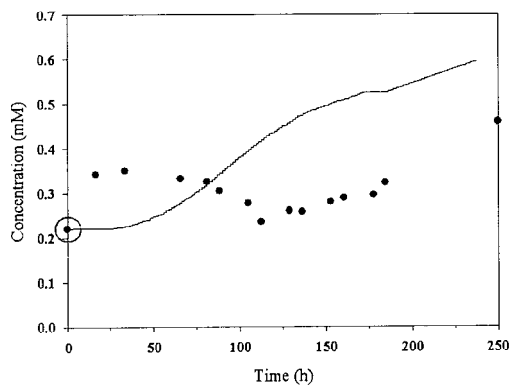
Phenylalanine (FB 0.3mM Gln(2))



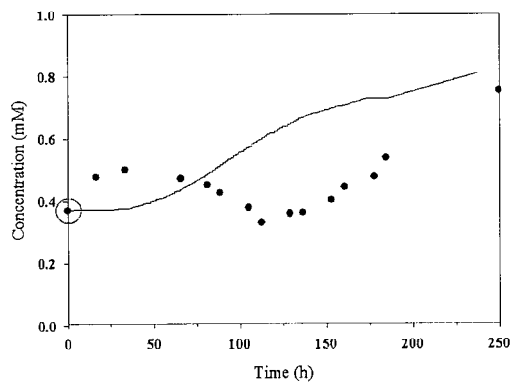
Leucine (FB 0.3mM Gln(2))



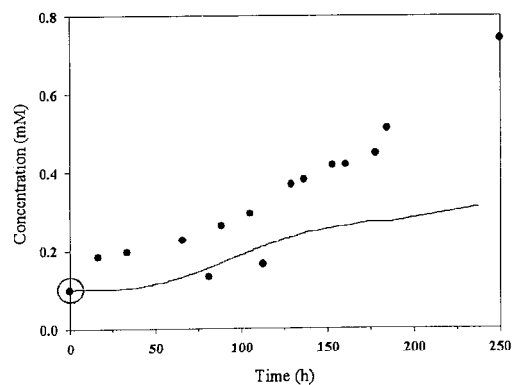
Isoleucine (FB 0.3mM Gln(2))



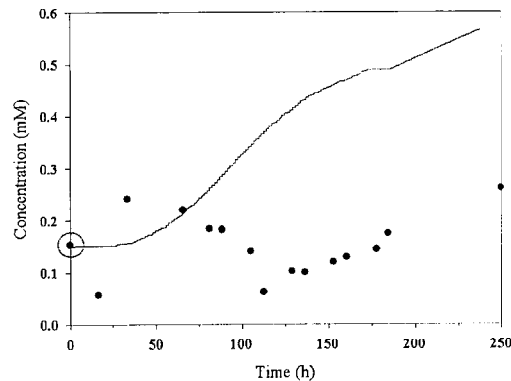
Lysine (FB 0.3mM Gln(2))



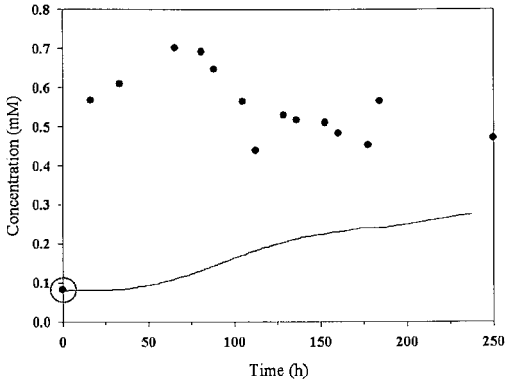
Methionine (FB 0.3mM Gln(2))



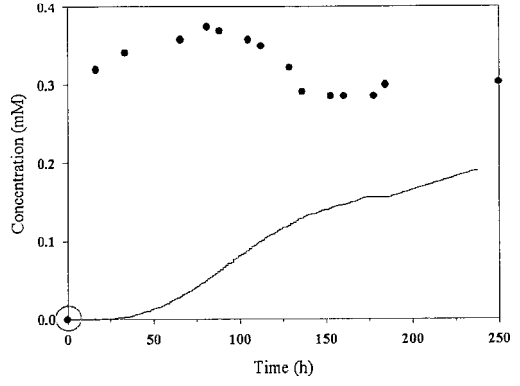
Valine (FB 0.3mM Gln(2))



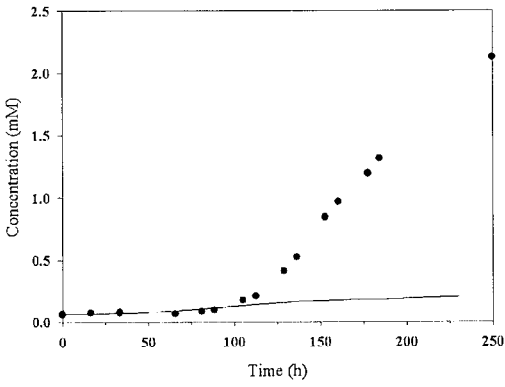
Tyrosine (FB 0.3mM Gln(2))



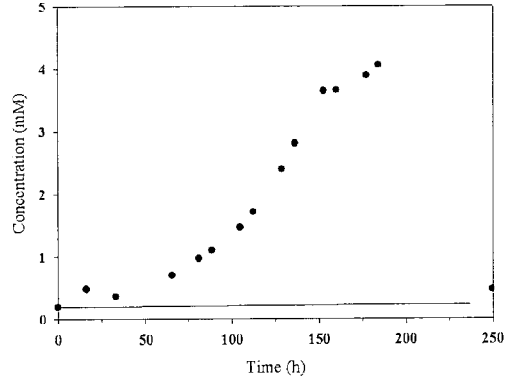
Cysteine (FB 0.3mM Gln(2))



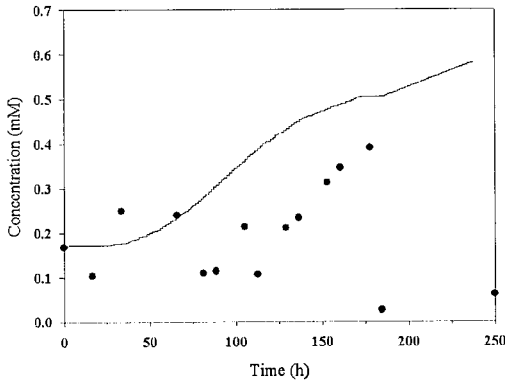
Proline (FB 0.3mM Gln(2))



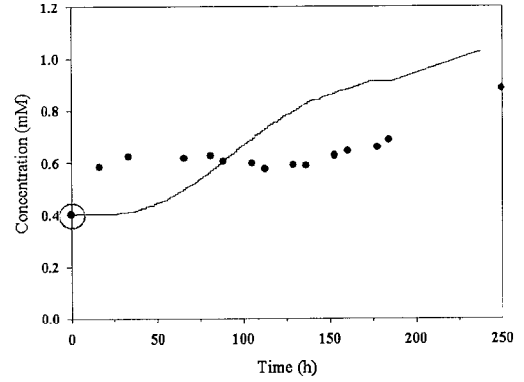
Alanine (FB 0.3mM Gln(2))



Threonine (FB 0.3mM Gln(2))



Arginine (FB 0.3mM Gln(2))



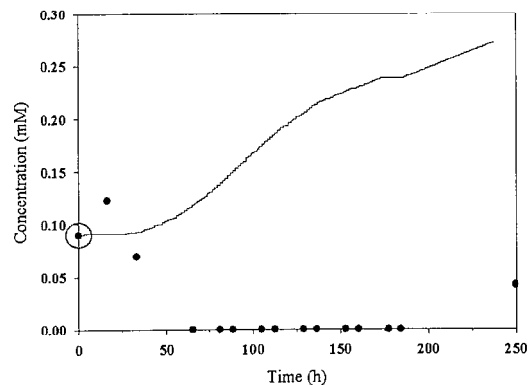
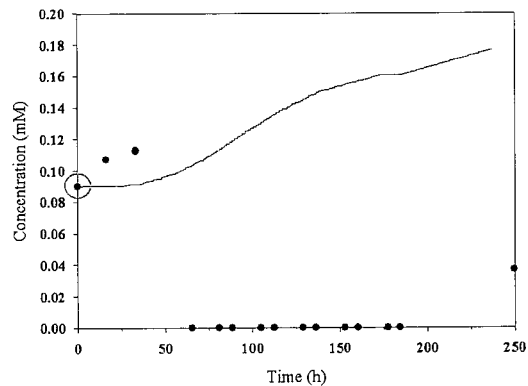
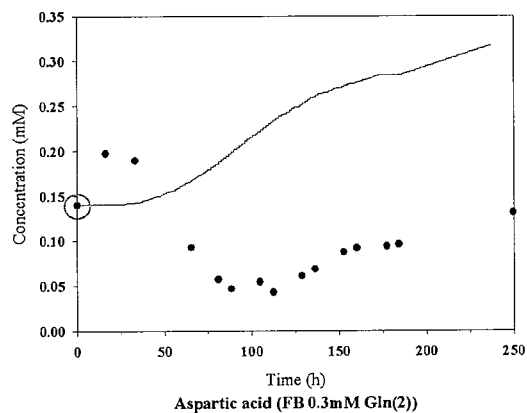
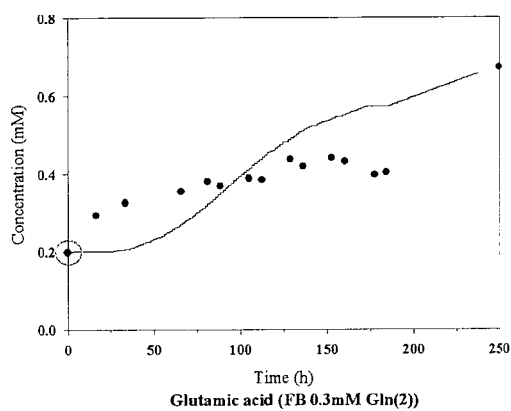
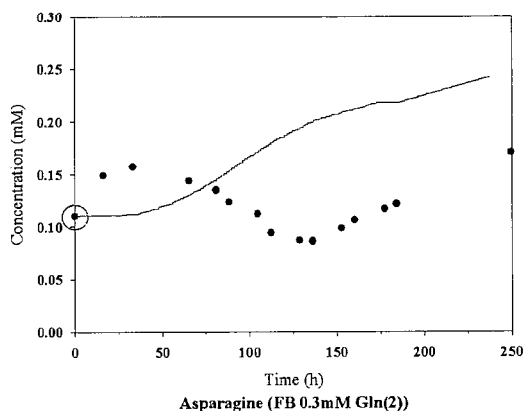
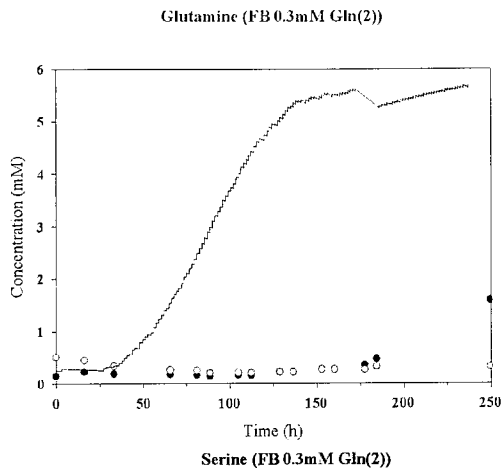
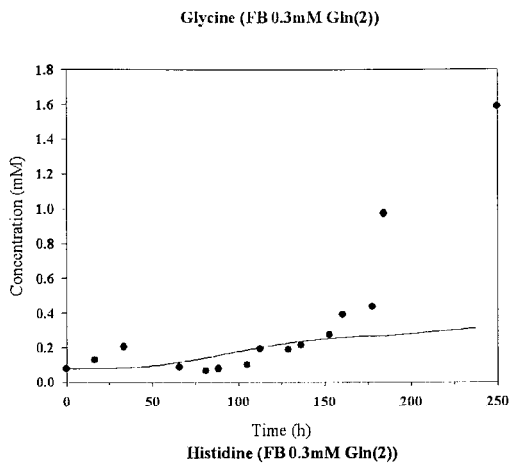


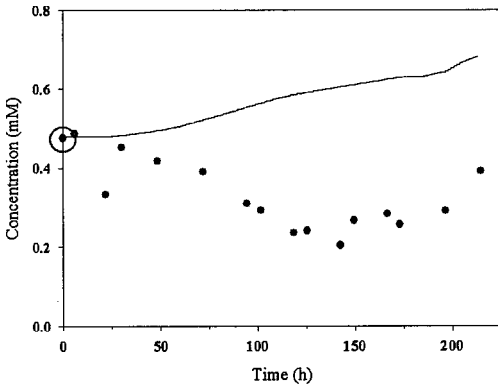
Figure A6.3: Mass balance testing of amino acids data in fed-batch CHO-IFN γ culture with glutamine set-point at 0.3mM (2nd experiment).

A6.2.4 Initial Amino Acid Concentration Testing Under Zero Consumption for Fed-Batch CHO-IFN γ Data with Glutamine Set-Point at 0.5mM

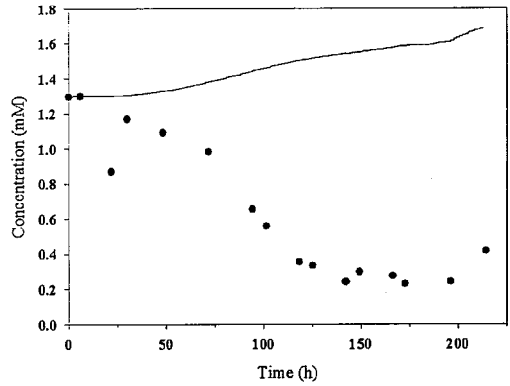
Symbols —

- : Amino acid concentration measured from high-performance liquid chromatography (HPLC) (Wong et al., 2005).
- : Glutamine concentration measured from bio-analyser (Wong et al., 2005).

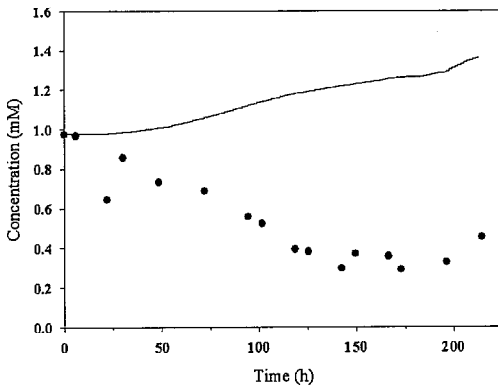
Phenylalanine (FB 0.5mM Gln(2))



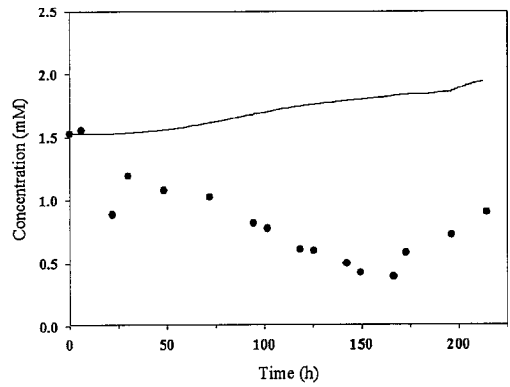
Leucine (FB 0.5mM Gln(2))



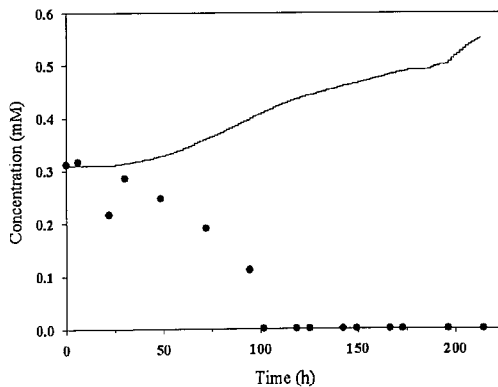
Isoleucine (FB 0.5mM Gln(2))



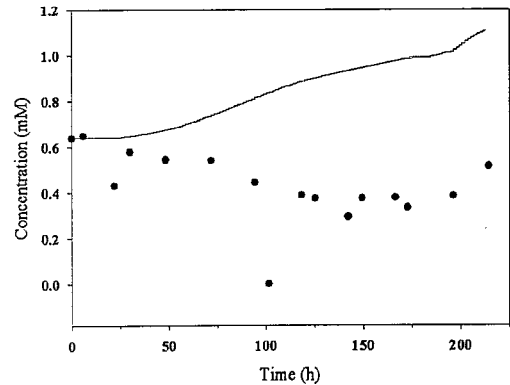
Lysine (FB 0.5mM Gln(2))



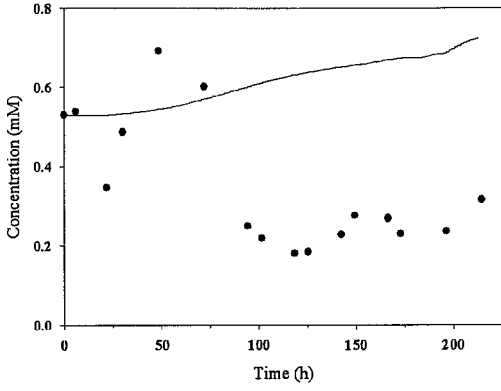
Methionine (FB 0.5mM Gln(2))



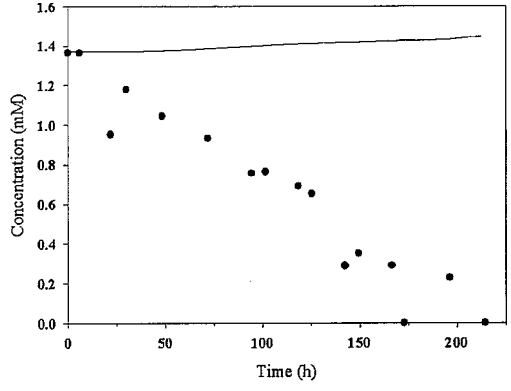
Valine (FB 0.5mM Gln(2))



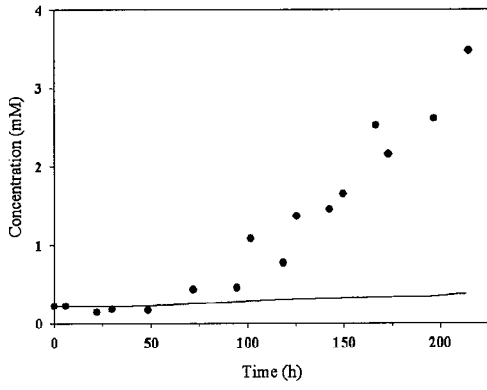
Tyrosine (FB 0.5mM Gln(2))



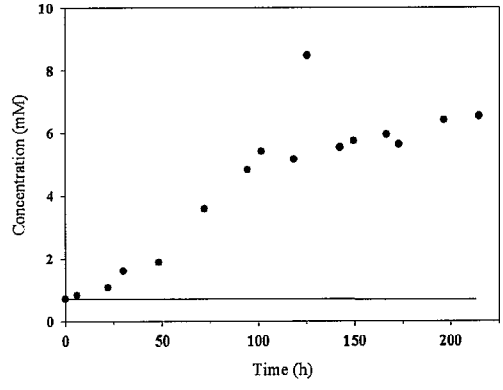
Cysteine (FB 0.5mM Gln(2))



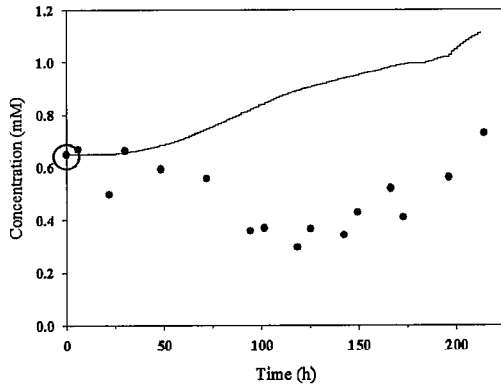
Proline (FB 0.5mM Gln(2))



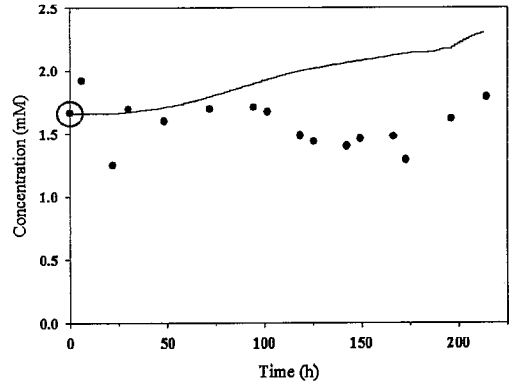
Alanine (FB 0.5mM Gln(2))



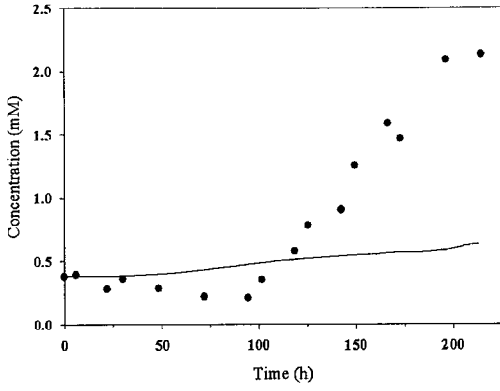
Threonine (FB 0.5mM Gln(2))



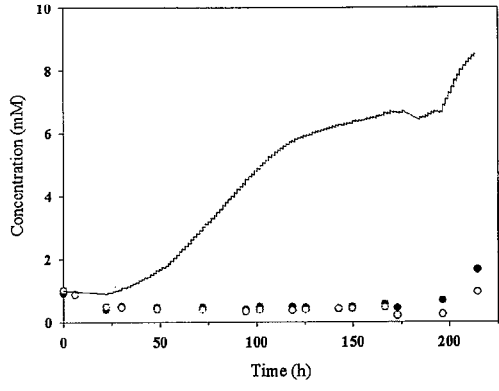
Arginine (FB 0.5mM Gln(2))



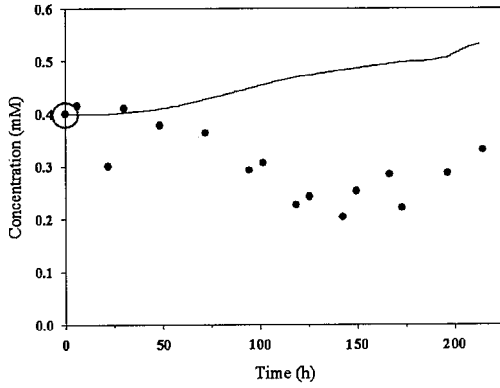
Glycine (FB 0.5mM Gln(2))



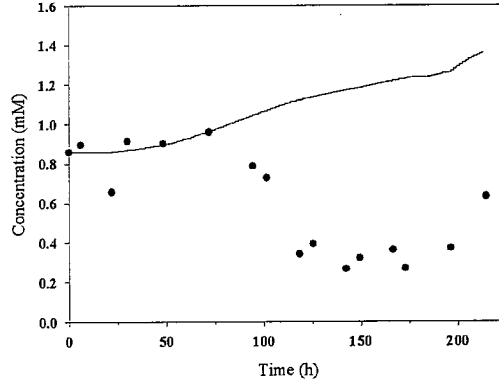
Glutamine (FB 0.5mM Gln(2))



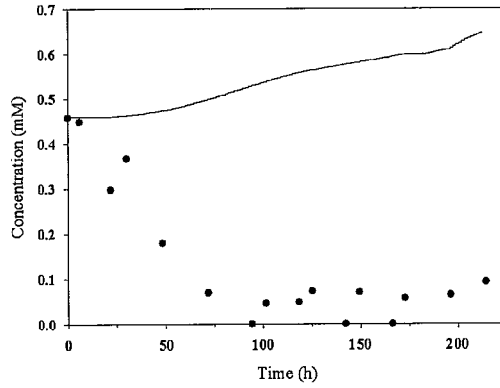
Histidine (FB 0.5mM Gln(2))



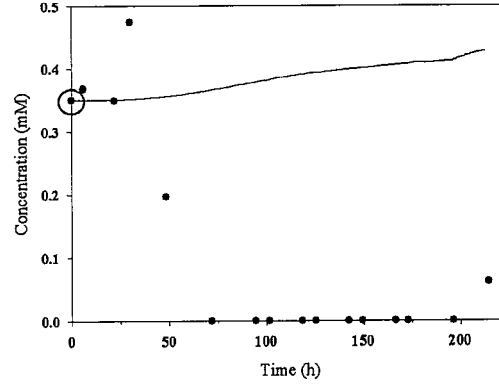
Serine (FB 0.5mM Gln(2))



Asparagine (FB 0.5mM Gln(2))



Glutamic acid (FB 0.5mM Gln(2))



Aspartic acid (FB 0.5mM Gln(2))

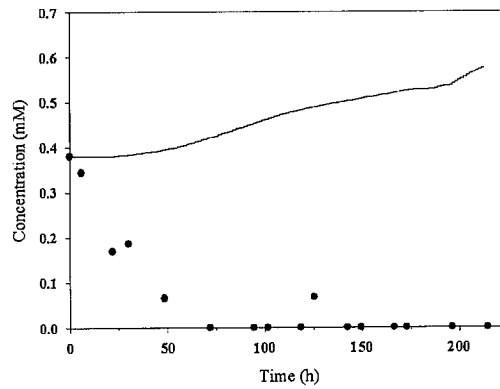


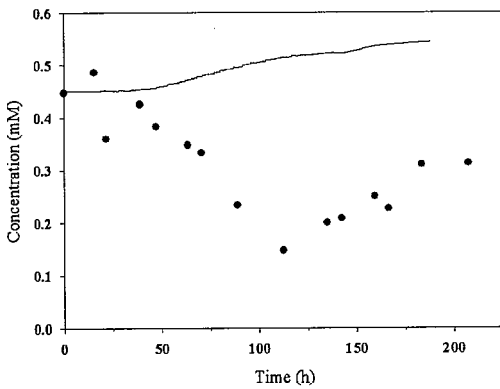
Figure A6.4: Mass balance testing of amino acids data in fed-batch CHO-IFN γ culture with glutamine set-point at 0.5mM.

A6.2.5 Initial Amino Acid Concentration Testing Under Zero Consumption for Fed-Batch CHO-IFN γ Data with Glutamine Set-Point at 0.3mM and glucose set-point at 0.7mM

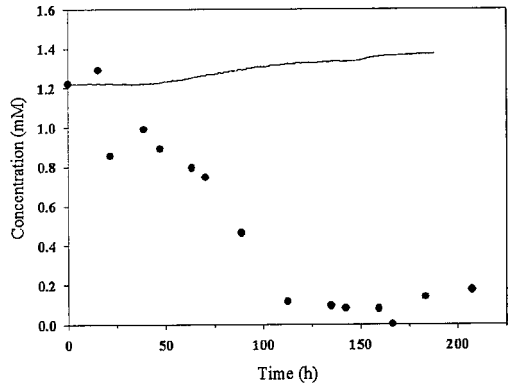
Symbols —

- : Amino acid concentration measured from high-performance liquid chromatography (HPLC) (Wong et al., 2005).
- : Glutamine concentration measured from bio-analyser (Wong et al., 2005).

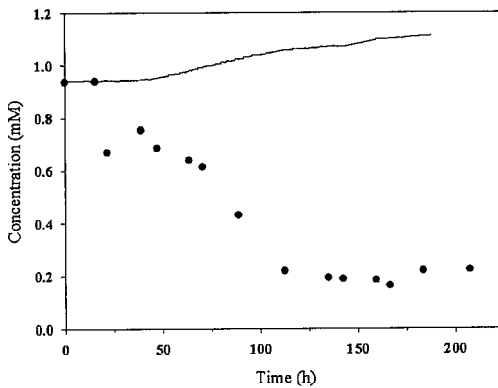
Phenylalanine (FB 0.3mM Gln, 0.7mM Glc)



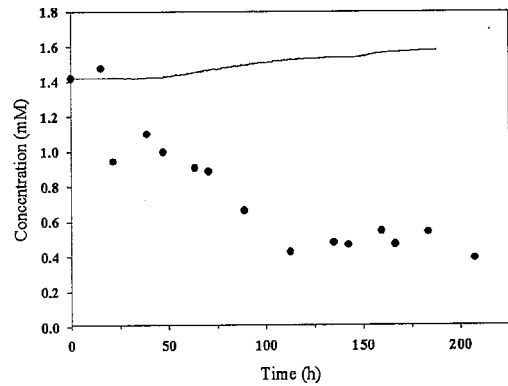
Leucine (FB 0.3mM Gln, 0.7mM Glc)



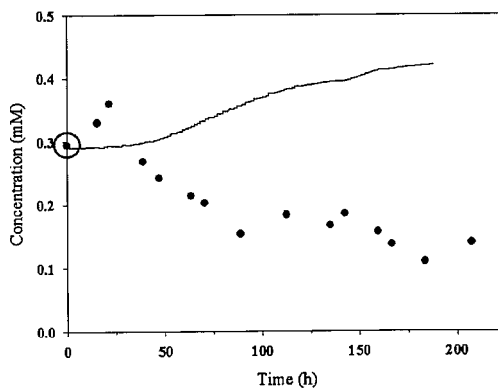
Isoleucine (FB 0.3mM Gln, 0.7mM Glc)



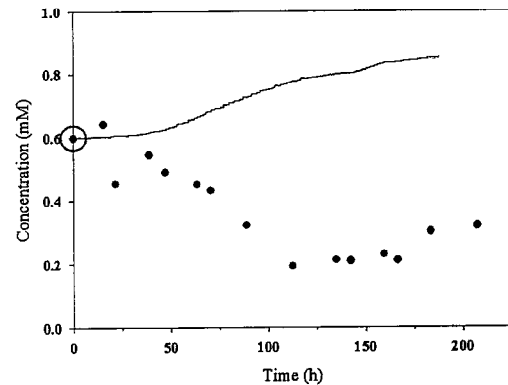
Lysine (FB 0.3mM Gln, 0.7mM Glc)



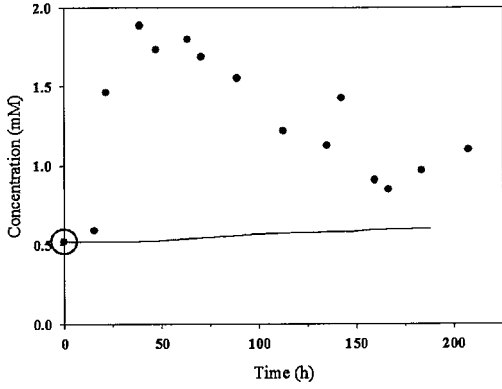
Methionine (FB 0.3mM Gln, 0.7mM Glc)



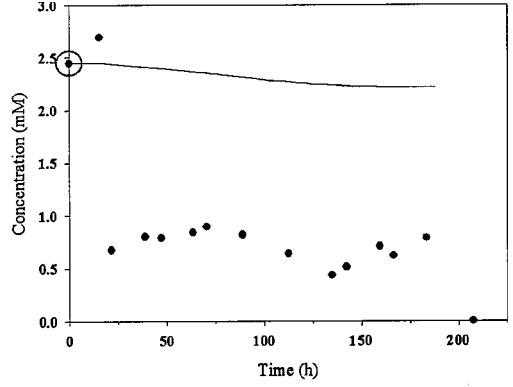
Valine (FB 0.3mM Gln, 0.7mM Glc)



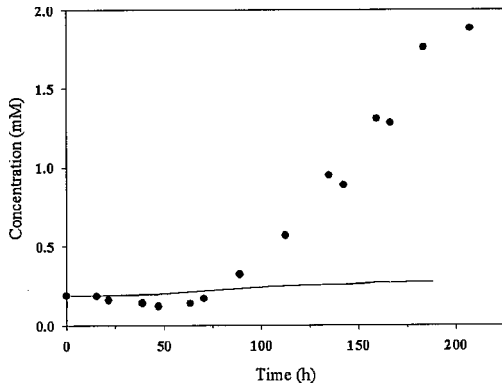
Tyrosine (FB 0.3mM Gln, 0.7mM Glc)



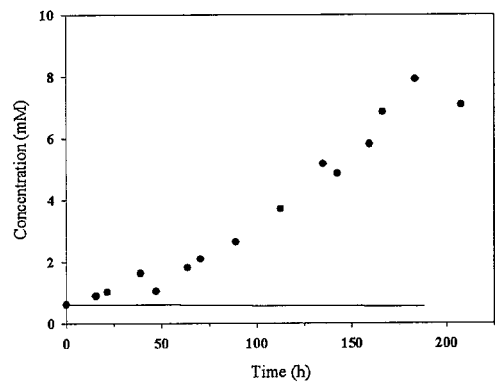
Cysteine (FB 0.3mM Gln, 0.7mM Glc)



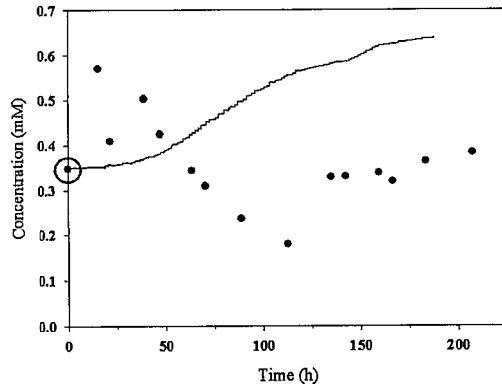
Proline (FB 0.3mM Gln, 0.7mM Glc)



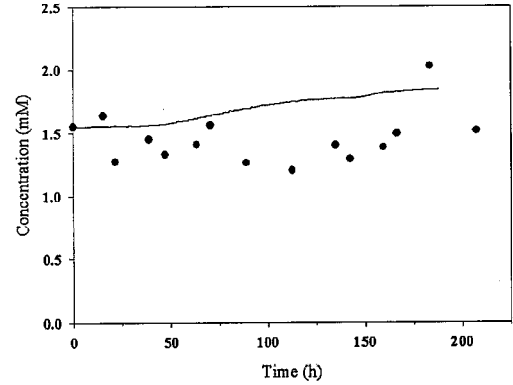
Alanine (FB 0.3mM Gln, 0.7mM Glc)



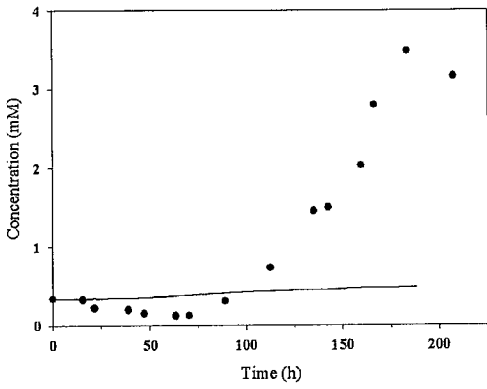
Threonine (FB 0.3mM Gln, 0.7mM Glc)



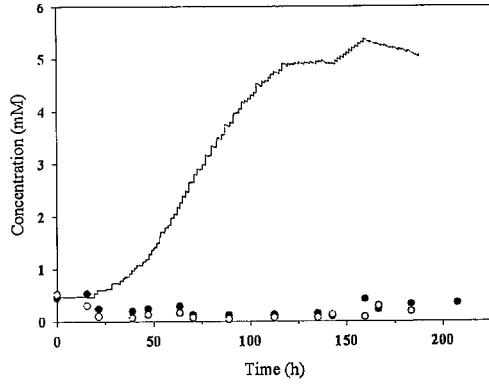
Arginine (FB 0.3mM Gln, 0.7mM Glc)



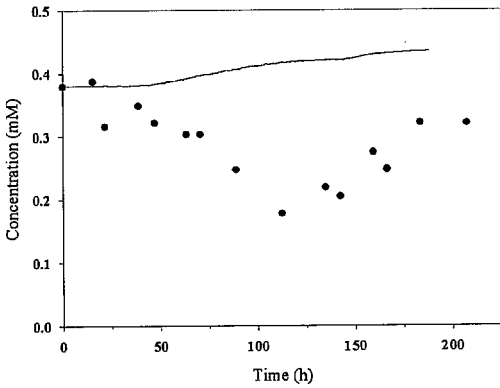
Glycine (FB 0.3mM Gln, 0.7mM Glc)



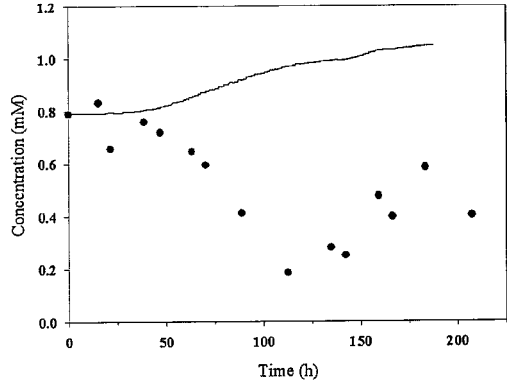
Glutamine (FB 0.3mM Gln, 0.7mM Glc)



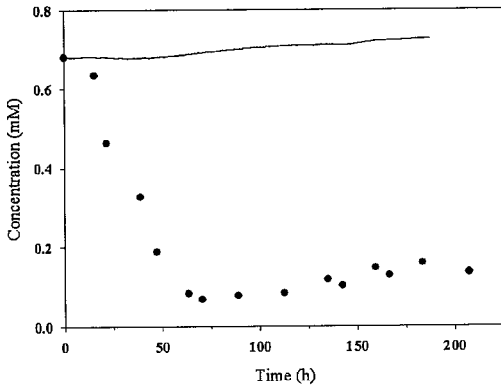
Histidine (FB 0.3mM Gln, 0.7mM Glc)



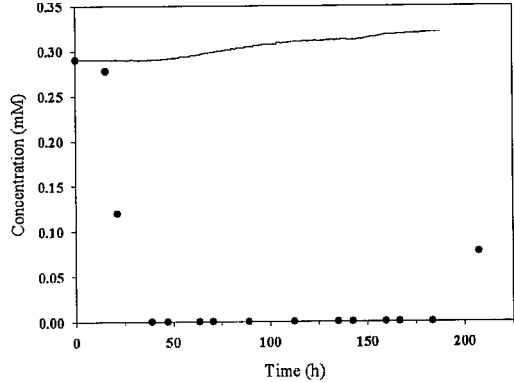
Serine (FB 0.3mM Gln, 0.7mM Glc)



Asparagine (FB 0.3mM Gln, 0.7mM Glc)



Glutamic acid (FB 0.3mM Gln, 0.7mM Glc)



Aspartic acid (FB 0.3mM Gln, 0.7mM Glc)

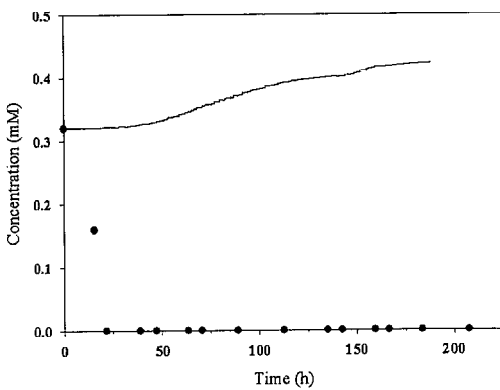


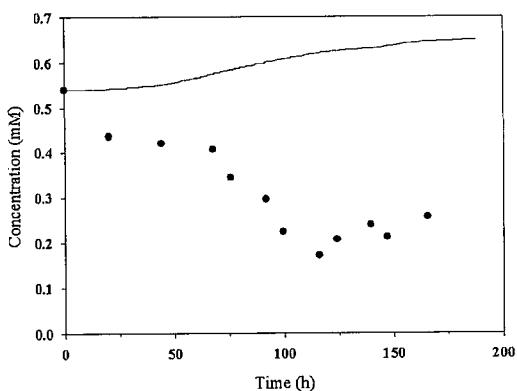
Figure A6.5: Mass balance testing of amino acids data in fed-batch CHO-IFN γ culture with glutamine set-point at 0.3mM and glucose set point at 0.7mM.

A6.2.6 Initial Amino Acid Concentration Testing Under Zero Consumption for Fed-Batch CHO-IFN γ Data with Glutamine Set-Point at 0.3mM and glucose set-point at 0.35mM

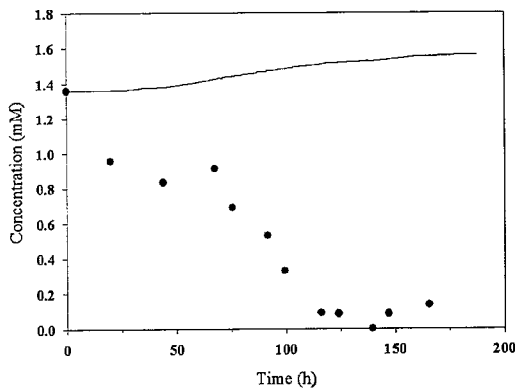
Symbols —

- : Amino acid concentration measured from high-performance liquid chromatography (HPLC) (Wong et al., 2005).
- : Glutamine concentration measured from bio-analyser (Wong et al., 2005).

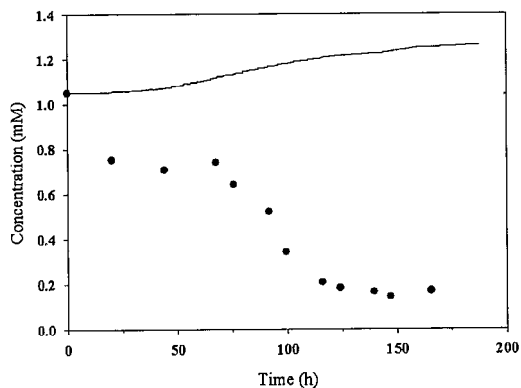
Phenylalanine (FB 0.3mM Gln, 0.35mM Glc)



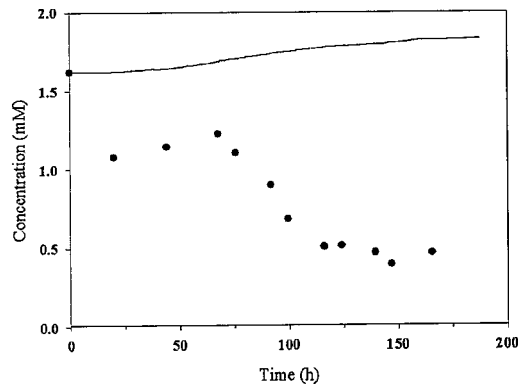
Leucine (FB 0.3mM Gln, 0.35mM Glc)



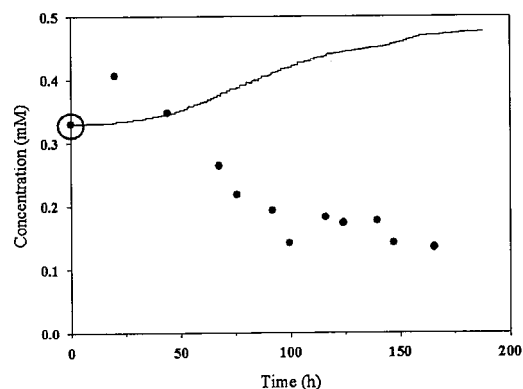
Isoleucine (FB 0.3mM Gln, 0.35mM Glc)



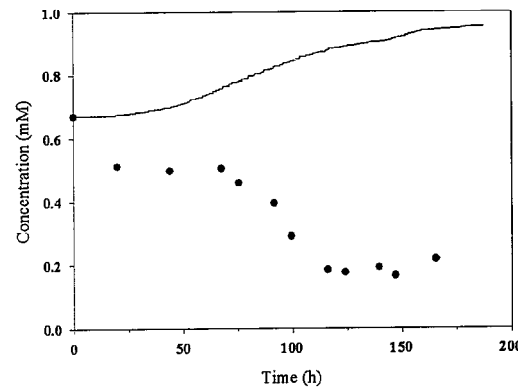
Lysine (FB 0.3mM Gln, 0.35mM Glc)



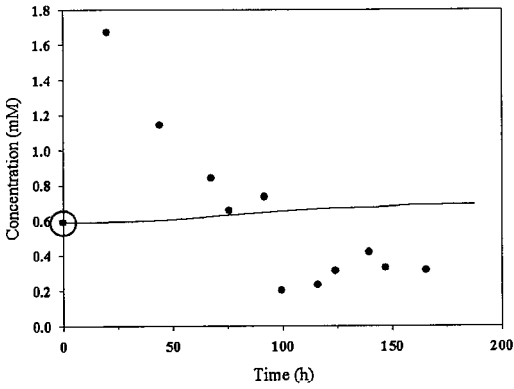
Methionine (FB 0.3mM Gln, 0.35mM Glc)



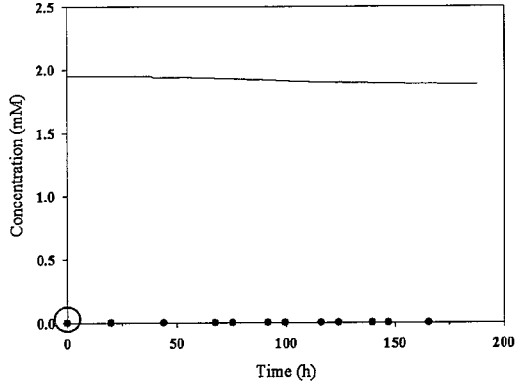
Valine (FB 0.3mM Gln, 0.35mM Glc)



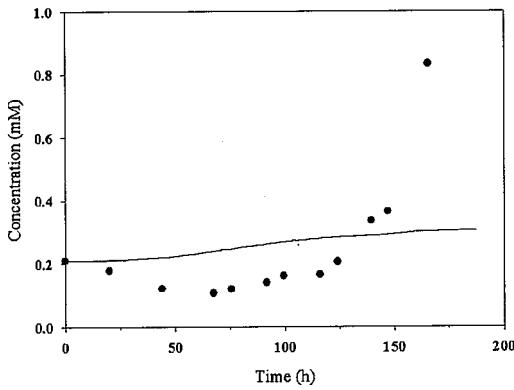
Tyrosine (FB 0.3mM Gln, 0.35mM Glc)



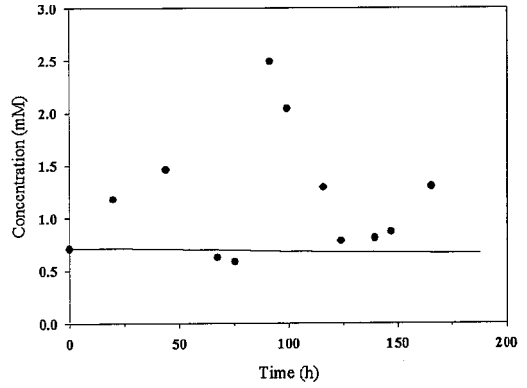
Cysteine (FB 0.3mM Gln, 0.35mM Glc)



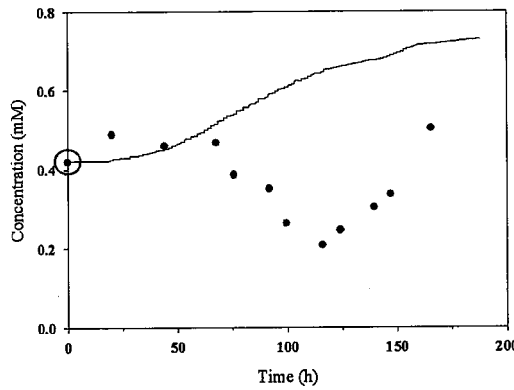
Proline (FB 0.3mM Gln, 0.35mM Glc)



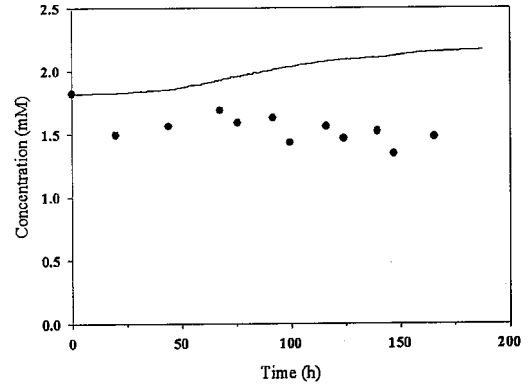
Alanine (FB 0.3mM Gln, 0.35mM Glc)



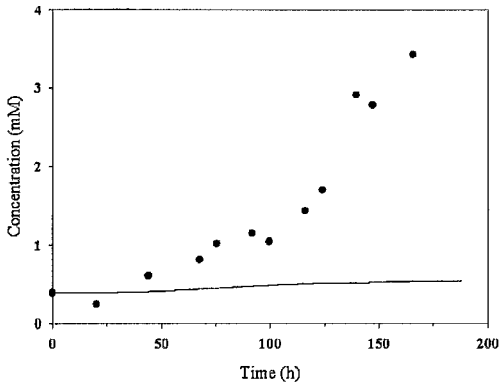
Threonine (FB 0.3mM Gln, 0.35mM Glc)



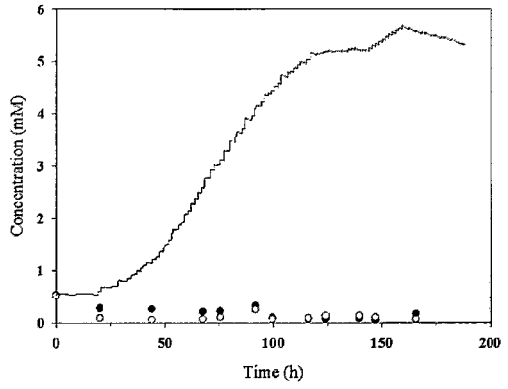
Arginine (FB 0.3mM Gln, 0.35mM Glc)



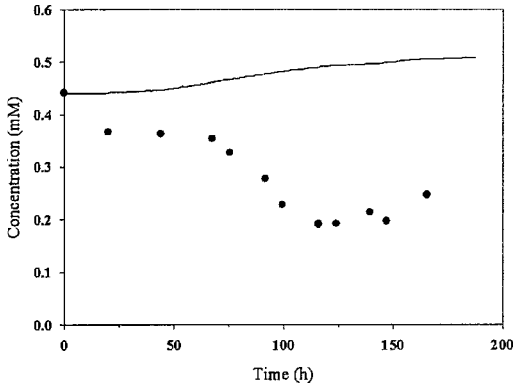
Glycine (FB 0.3mM Gln, 0.35mM Glc)



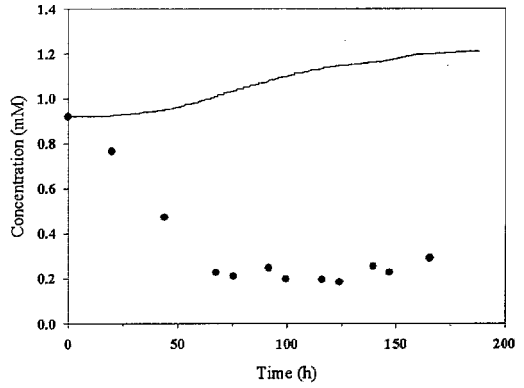
Glutamine (FB 0.3mM Gln, 0.35mM Glc)



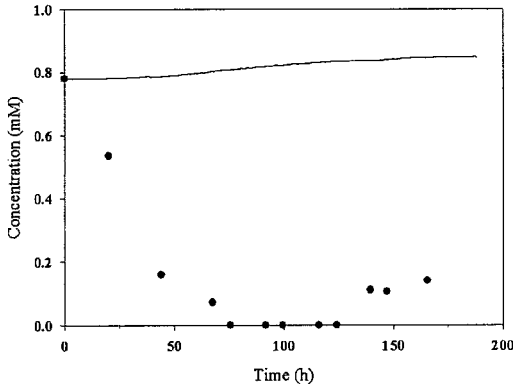
Histidine (FB 0.3mM Gln, 0.35mM Glc)



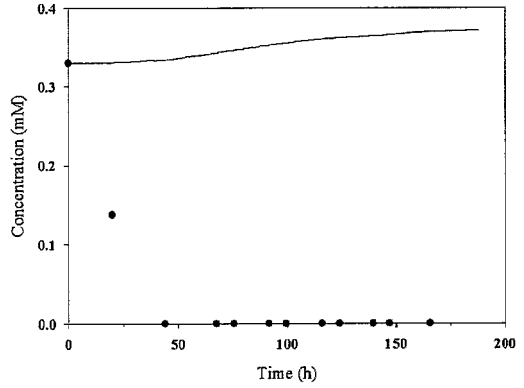
Serine (FB 0.3mM Gln, 0.35mM Glc)



Asparagine (FB 0.3mM Gln, 0.35mM Glc)



Glutamic acid (FB 0.3mM Gln, 0.35mM Glc)



Aspartic acid (FB 0.3mM Gln, 0.35mM Glc)

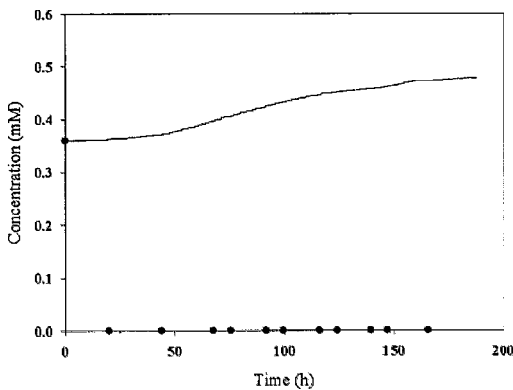


Figure A6.6: Mass balance testing of amino acids data in fed-batch CHO-IFN γ culture with glutamine set-point at 0.3mM and glucose set point at 0.35mM.